

NISTIR 8271 DRAFT SUPPLEMENT

Face Recognition Vendor Test (FRVT) Part 2: Identification

Patrick Grother
Mei Ngan
Kayee Hanaoka
*Information Access Division
Information Technology Laboratory*

This document is a draft supplement of [NIST Interagency Report 8271](#)

2022/11/09



NISTIR 8271 DRAFT SUPPLEMENT

Face Recognition Vendor Test (FRVT) Part 2: Identification

Patrick Grother
Mei Ngan
Kayee Hanaoka
*Information Access Division
Information Technology Laboratory*

This document is a draft supplement of [NIST Interagency Report 8271](#)

November 2022



U.S. Department of Commerce
Gina M. Raimondo, Secretary

National Institute of Standards and Technology
Laurie E. Locascio, NIST Director and Undersecretary of Commerce for Standards and Technology

RELEASE NOTES

2022-11-09: The 1:N track of the FRVT remains open.

- ▷ This document is the nineteenth draft update to [NIST Interagency Report 8271](#). It contains results for four first-time participant: Mukh, Turing Technology VIP, Verijelas and Verihubs Inteligensia
- ▷ The document also includes results for algorithms from two returning developers: Maxvision and Samsung S1.

2022-09-23: The 1:N track of the FRVT remains open.

- ▷ This document is the eighteenth draft update to [NIST Interagency Report 8271](#). It contains results for two first-time participants: Intema-LGL Group and T4iSB.
- ▷ The document also includes results for algorithms from two returning developers: Cloudwalk - Moon-time Smart Technology, Dermalog, Griaule, Hangzhuo Allu Network Information Technology, Intellivision, Line Corporation, NEC, Sensetime Group, Realnetworks Inc and Vietnam Posts and Telecommunications Group.

2022-07-28: The 1:N track of the FRVT remains open.

- ▷ This document is the seventeenth draft update to [NIST Interagency Report 8271](#). It contains results for one first-time participant: Maxvision.
- ▷ The document also includes results for algorithms from two returning developers: Rank One Computing, and Viettel Group.
- ▷ We have replaced the probe set used in the visa-border benchmark. It was previously comprised of 80 000 images; it now has size 1 212 892 - see amended entries in Table 1. False negative identification rates have increased.
- ▷ We have added images to the probe set used in the visa-kiosk benchmark. It was previously comprised of 21 016 mates and the same number of non-mates; it now has 31 579 mates and 45 460 non-mates - see amended and entries in Table 1. False negative identification rates are improved (reduced) slightly.

2022-06-08: The 1:N track of the FRVT remains open.

- ▷ This document is the seventeenth draft update to [NIST Interagency Report 8271](#). It includes results for algorithms submitted by three first-time participants: Digidata, DiluSense Technology, and Vietnam Posts and Telecommunications Group.
- ▷ The document also includes results for algorithms from five returning developers: Canon Inc, Imagus Technology, Neurotechnology, Thales, and Samsung S1.

2022-04-28: The 1:N track of the FRVT remains open.

- ▷ This document is the sixteenth draft update to [NIST Interagency Report 8271](#). It includes results for algorithms submitted by one first-time participants: Hangzhuo Allu Network Information Technology.
- ▷ The document also includes results for algorithms from three returning developers: HyperVerge Inc, Qnap Security, and Realnetworks Inc.
- ▷ The [1:N results page](#) has been updated.

2022-03-30: The 1:N track of the FRVT remains open.

- ▷ This document is the sixteenth draft update to [NIST Interagency Report 8271](#). It includes results for algorithms submitted by two first-time participants: Intellivision, and Pangiam.
- ▷ The document also includes results for algorithms from three returning developers: Fujitsu Research and Development Center, Idemia, and Gorilla Technology.

- ▷ The [1:N results page](#) has been updated.

2022-02-23: The 1:N track of the FRVT remains open.

- ▷ This document is the fifteenth draft update to [NIST Interagency Report 8271](#). It includes results for algorithms submitted by four first-time participants: Cloudwalk - Moontime Smart Technology, Decatur Industries Inc, NotionTag Technologies Private Limited, and Reveal Media Ltd.
- ▷ The document also includes results for algorithms from three returning developers: Cognitec Systems GmbH, Sensetime Group, and Viettel Group
- ▷ The [1:N results page](#) has been updated.

2022-01-20: The 1:N track of the FRVT remains open.

- ▷ This document is the fourteenth draft update to [NIST Interagency Report 8271](#). It includes results for algorithms recently submitted by two first-time participants: Daon and SQIsoft.
- ▷ The document also includes results for algorithms from five returning developers: Cyberlink Corp, NEC, Neurotechnology, Paravision, and Rank One Computing.
- ▷ The [1:N results page](#) has been updated.

2021-12-16: The 1:N track of the FRVT remains open.

- ▷ This document is the thirteenth draft update to [NIST Interagency Report 8271](#). It includes results for algorithms from six returning developers: Dahua Technology, Imagus Technology, Line Corporation, N-Tech Lab, Qnap Security, and Realnetworks Inc.
- ▷ The [1:N results page](#) has been updated.

2021-11-22: The 1:N track of the FRVT remains open.

- ▷ This document is the twelfth draft update to [NIST Interagency Report 8271](#). It includes results for algorithms recently submitted by three first-time participants Clearview AI, Griaule, and Mantra Softech India.
- ▷ This document and the [1:N results page](#) also include results for algorithms from six returning developers: Acer Incorporated, Canon, Dermalog, Samsung S1, VisionLabs, and Veridas Digital Authentication.

2021-10-28: The 1:N track of the FRVT remains open.

- ▷ This document is the eleventh draft update to [NIST Interagency Report 8271](#). It includes results for algorithms recently submitted by three first-time participants (20Face, Fujitsu Research and Development Center, and Vision-Box), and five returning participants (Alchera, Gorilla Technology, Tevian, Thales-Cogent, and Visidon). Visidon
- ▷ Both the main [1:N results page](#) and the small-gallery [paperless travel page](#) have been updated.

2021-09-21: The 1:N track of the FRVT remains open. Three news items:

- ▷ This document is the tenth draft update to [NIST Interagency Report 8271](#). It includes results for algorithms recently submitted by six first-time developers: Cubox, Fincore, HyperVerge, Qnap Security, Staqu Technologies, and Tripleize (Aize, 3-ize).
- ▷ It includes results also for four returning developers: Cognitec Systems, Incode Technologies, Innovatrics, Neurotechnology, and Rank One Computing.

2021-08-02: The 1:N track of the FRVT remains open. Three news items:

- ▷ This document is the ninth draft update to [NIST Interagency Report 8271](#). It includes results for algorithms recently submitted by eight participants: Cyberlink Corp, NEC Corp, N-Tech Lab, Realnetworks Inc., Sensetime Group, Veridas Digital, Viettel Group, and Vigilant Solutions.
- ▷ Algorithms submitted since July 24 will be included in the next update scheduled for September 9, 2021.
- ▷ A new report, NIST Interagency Report 8381 - FRVT Part 7: Identification for Paperless Travel and Immigration, has been released [[PDF](#), [webpage](#)]. It documents the use of FRVT 1:N algorithms in positive access control and immigration status update travel applications where the enrolled population size is as low as 420 people for aircraft boarding, and 42 000 for an airport security line. These population sizes are much smaller than those used in the main [1:N evaluation](#). Going forward, we will update the report and webpage with results for new algorithms.

2021-07-07: The 1:N track of the FRVT remains open. One update:

- ▷ This document is the eighth draft update to [NIST Interagency Report 8271](#). It include results for an algorithm from one participant: Kakao Enterprises.

2021-06-22: The 1:N track of the FRVT remains open. Three updates:

- ▷ This is the seventh draft of the update to [NIST Interagency Report 8271](#). It includes results for algorithms from three new participants: Line Corporation, Rendip, and Samsung S1 Corp.
- ▷ We have also added results for algorithms from five returning developers: Imagus Technology, Kneron, Tevian, Visidon, and Xforward AI Technology.
- ▷ The algorithm-specific report cards (examples: [1](#), [2](#), and [3](#)) now include figures showing how low threshold values can be used to reduce candidate list lengths for human review, while (usually) elevating miss rates (FNIR) only modestly. The reports also feature some minor additions and clarifications.

2021-03-26: The 1:N track of the FRVT remains open. Three updates:

- ▷ This is the sixth draft of the update to [NIST Interagency Report 8271](#). It includes results for algorithms from three returning developers: Neurotechnology, Guangzhou Pixel Solutions, and Tech5 SA.
- ▷ We have added results on the webpage and in the report for a new ageing dataset in which border crossing photos are searched against a gallery of border crossing photos collected between 10 and 15 years prior to the mated search photos. See section [2](#) for a description of the images. Table [1](#) has a new entry describing the experiment.
- ▷ We will mostly discontinue running the mugshot ageing test, reserving it for algorithms that show high accuracy on the new border-crossing set.

2021-03-26: Regarding the fifth draft of the update to [NIST Interagency Report 8271](#):

- ▷ In addition have added results for first algorithms from two new participants: Viettel Group and Veridas Digital Authentication Solutions.
- ▷ We have added results for algorithms from two returning developers: Idemia and Cognitec Systems.
- ▷ In addition to the report, the [results page](#) and its hyperlinked [report cards](#) have been updated.

2021-02-08: Regarding the fourth draft of the update to [NIST Interagency Report 8271](#):

- ▷ We have added results for eight algorithms submitted by eight developers: Cyberlink, Dermalog, Imagus, Paravision, Sensetime, Trueface, Vigilant Solutions, and X-Forward AI. With the exception of Trueface, all of these developers have participated previously.
- ▷ We anticipate updating this report again in the first week of March 2021.

- ▷ The main [results page](#) has been revised with tabs for the investigative and lights-out identification tables, and a new tab dedicated to speed and resource consumption.
- ▷ The report cards (example [here](#)) hyperlinked from the [results page](#) have been revised to improve content and format.

2020-12-14: Regarding third draft of the update to [NIST Interagency Report 8271](#):

- ▷ We have added results for fifteen algorithms submitted by thirteen developers. The four first-time participants are: Acer, Akurat Satu Indonesia, Canon, and Xforward AI Technology. The ten returning developers are: AllGoVision, Cyberlink Corp, Dahua Technology, Deepglint, Guangzhou Pixel Solutions, IIT Vision, Innovatrics, Rank One Computing, Scanovate, Sensetime Group, Synesis, and VisionLabs.
- ▷ We have added two new datasets to the evaluation: First a set of “visa-border” photos, representing search of an airport immigration lane photo against a database of closely ISO standard portraits; second a “visa-kiosk” set representing search of a photo collected in a registered traveller kiosk against the same ISO portrait gallery. The images are described in section [2.1](#).
- ▷ As in previous reports, we include results for searching mugshots against a mugshot gallery containing a single image of each of 12 million people. However we have suspending running searches against a gallery in which multiple lifetime photos per person are present, because this is computationally expensive. We retain a $N = 3$ million search test dedicated to ageing in which mugshots taken up to 18 years after the first photograph are searched - see Table [7](#).
- ▷ Tables containing computational resource information, Table [2](#) . . . , now include duration of the finalization step, in which search algorithms can, at their option, build fast-search data structures.
- ▷ We have linked revised per-algorithm PDF report cards from the main [results page](#).
- ▷ We have regenerated all figures and tables to drop algorithms submitted before June 2018. Results for prior algorithms appear in [archived editions](#) of this report.
- ▷ Going forward, we anticipate producing more frequent updates to this report. Developers may submit one algorithm to this evaluation every four calendar months.

2020-03-24: Regarding the second draft of the update to [NIST Interagency Report 8271](#):

- ▷ Adds results for three algorithms from three developers, Dermalog, Innovatrics, and Synesis.
- ▷ Adds Table [7](#) on ageing showing the increase in false negative rates with time elapsed between two photos. Some of the results were contained in graphs in prior editions of this report, but the table adds results for some newly submitted algorithms.
- ▷ Adjusts frontal mugshot results (for recent and lifetime consolidated galleries) to include the effect of removing some images that should not have been included in image test sets. These images were mostly profile views, images of tattoos containing faces, images of faces on tee shirts, and images of photographs on walls behind the intended subject. This affects many tables and reduces false negative identification rates for all algorithms. The reduction is larger for “recent” enrollments than for “lifetime consolidated” ones with the consequence that accuracy on recent images is now superior.

2020-02-26: Regarding the first draft of the update to [NIST Interagency Report 8271](#):

- ▷ Adds results for 38 algorithms from 31 different developers, eleven of whom are entirely new to the 1:N track of FRVT. These are Allgovision, Cyberlink, Deepsea Tencent, Farbar F8, Imperial College London, Intsys MSU, Kedacom, Kneron, Pixelall, and Scanovate.

DISCLAIMER

Specific hardware and software products identified in this report were used in order to perform the evaluations described in this document. In no case does identification of any commercial product, trade name, or vendor, imply recommendation or endorsement by the National Institute of Standards and Technology, nor does it imply that the products and equipment identified are necessarily the best available for the purpose.

INSTITUTIONAL REVIEW BOARD

The National Institute of Standards and Technology's Research Protections Office reviewed the protocol for this project and determined it is not human subjects research as defined in Department of Commerce Regulations, 15 CFR 27, also known as the Common Rule for the Protection of Human Subjects (45 CFR 46, Subpart A).

ACKNOWLEDGMENTS

The authors are grateful for the support and collaboration of the the Department of Homeland Security's Science & Technology Directorate (S&T), Office of Biometric Identity Management (OBIM), and Customs and Border Protection (CBP).

Additionally, the authors are grateful to staff in the NIST Biometrics Research Laboratory for infrastructure supporting rapid evaluation of algorithms.

Executive Summary

This document is a draft revision of the September 2019 report [NIST Interagency Report 8271](#). That report gave extensive documentation of face recognition applied to mugshots. This report extends that by adding more two more challenging datasets containing images with serious departures from canonical frontal image standards. The report also adds results for algorithms submitted to NIST since in 2019 and 2020. The algorithms, which implement one-to-many identification of faces appearing in two-dimensional images, are prototypes from the research and development laboratories of mostly commercial suppliers, and are submitted to NIST as compiled black-box libraries implementing a NIST-specified C++ test interface. The report therefore does not describe how algorithms operate. The report lists accuracy results alongside developer names and will therefore be useful for comparison of face recognition algorithms and assessment of absolute capability. The report is accompanied by a [webpage](#) with sortable results.

The evaluation uses six datasets: frontal mugshots, profile view mugshots, desktop webcam photos, visa-like immigration application photos, immigration lane photos, and registered traveler kiosk photos. These datasets are sequestered at NIST, meaning that developers do not have access to them for training or testing. This aspect is important because face recognition algorithms are very often deployed without the developer having access to the customers image data. A possible exception to this would be in a cloud-based application where the operational image data is uploaded to a cloud operated by a face recognition developer.

The major result in NIST IR 8271 was that massive gains in accuracy have been achieved in the years 2013 to 2018 and these far exceed improvements made in the prior period, 2010 to 2013. While the industry gains were broad - at least 30 developers' algorithms outperformed the most accurate algorithm from late 2013, there remains a wide range of capability. While this report shows accuracy gains only over the period 2018-2020, the most accurate algorithm reported here is substantially more accurate than anything reported in NIST IR 8271. This is evidence that face recognition development continues apace, and that FRVT reports are but a snapshot of contemporary capability.

From discussion with developers, the accuracy gains stem from the adoption of deep convolutional neural networks. As such, face recognition has undergone an industrial revolution, with algorithms increasingly tolerant of poorly illuminated and other low quality images, and poorly posed subjects. One related result is that a few algorithms correctly match side-view photographs to galleries of frontal photos, with search accuracy approaching that of the best c. 2010 algorithms operating on purely frontal images. The capability to recognize under a 90-degree change in viewpoint - pose invariance - has been a long-sought milestone in face recognition research.

With good quality portrait photos, the most accurate algorithms will find matching entries, when present, in galleries containing 12 million individuals, with rank one miss rates of approaching 0.1%. The remaining errors are in large part attributable to long-run ageing, facial injury and poor image quality. Given this impressive achievement - close to perfect recognition - an advocate might claim that cooperative face recognition is a solved problem, a statement that can be refuted with the following context and caveats:

- ▷ **Mugshots vs. less constrained captures:** The low error rates reported here are attained using mostly excellent cooperative live-capture mugshot images collected with an attendant present. Recognition in other circumstances, particularly those without a dedicated photographic environment and human or automated quality control checks, will lead to declines in accuracy. This is documented here for side-view images, poorer quality webcam images, and, particularly, for newly introduced ATM-style kiosk photos that were not originally intended for automated face recognition. In this case, recognition error rates are much higher, often in excess of 20% even with the more accurate algorithms which variously remain intolerant of face cropping (at image edge) and of large downward head pitch.
- ▷ **Algorithm accuracy spectrum:** Recognition accuracy is very strongly dependent on the algorithm and, more

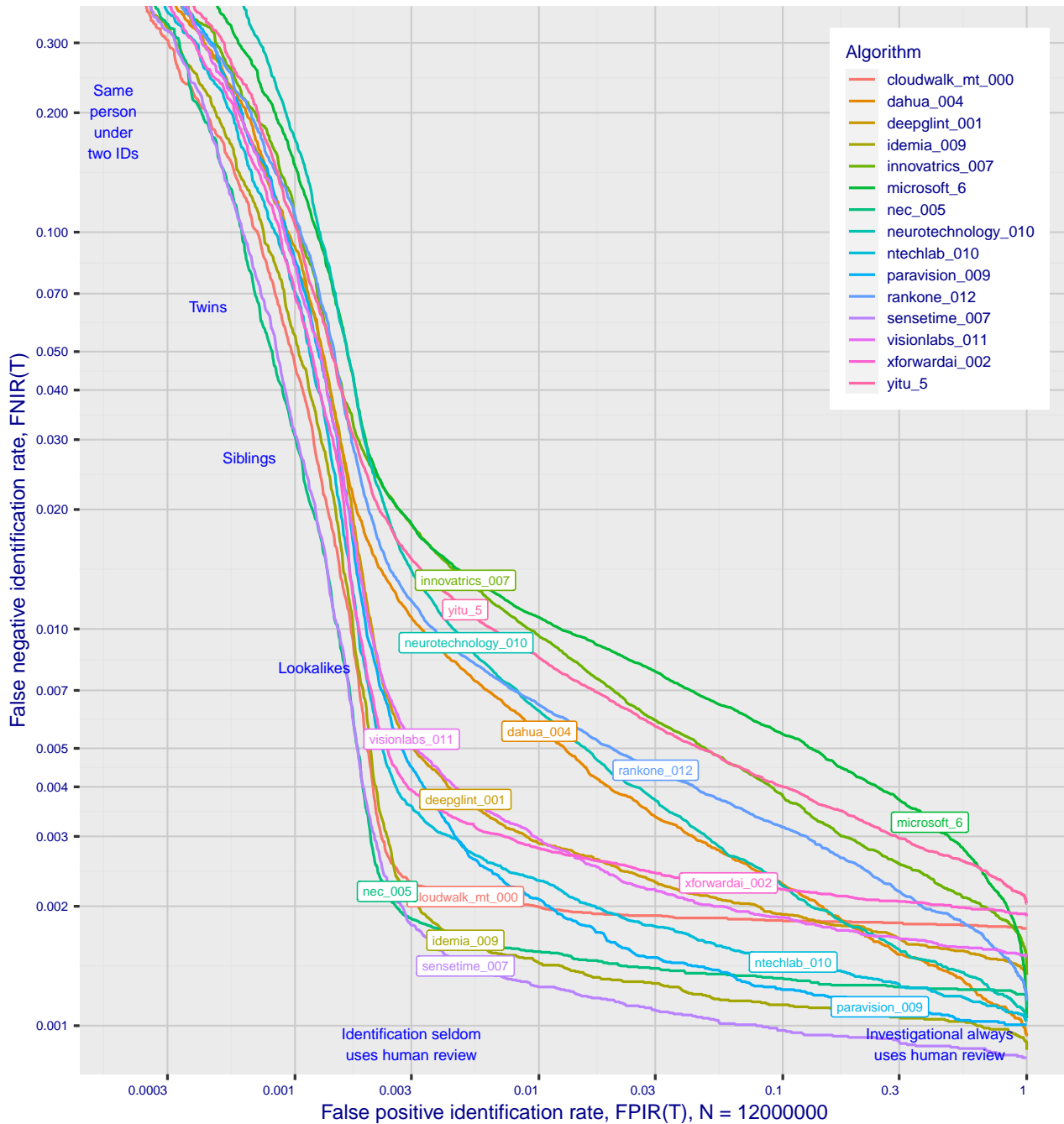


Figure 1: Identification miss rates across the false positive range. $N = 12$ million individuals are enrolled with one recent image.

generally, on the developer of the algorithm. False negative error rates in a particular scenario range from a few tenths of one percent to beyond fifty percent. This is tabulated exhaustively later: For example Table 11 shows accuracy across datasets. Figure 1 here compares algorithms on mugshot searches in a consolidated gallery of 12 million subjects and 12 million photos. Many algorithms do not achieve the low error rates noted above, and while many of those may still be useful and valuable to end-users, only the most accurate excel on poor quality images and those collected long after the initial enrollment sample.

▷ **Versioning:** While results for up to ten algorithms from each developer are reported here, the intra-provider

accuracy variations are usually smaller than the inter-provider variations. That said different versions give an order of magnitude fewer misses. Some developers demonstrate speed-accuracy tradeoffs¹. See Figs. 18, 19.

- ▷ **Low similarity scores:** In thousands of mugshot cases the correct gallery image is returned at rank 1 but its similarity score is nevertheless low, below some operationally required score threshold. This is not so important when face recognition is used for “lead generation” in investigational applications because human reviewers are specifically required to review potentially long candidate lists and the threshold is effectively 0. In applications where search volumes are higher and labor is not available to review the results from searches, a higher threshold must be applied. This reduces the length of candidate lists and false positive identification rates at the expense of increased false negative miss rates. The tradeoff between the two error rates is reported extensively later.
- ▷ **Population size:** As the number of enrolled subjects grows, some mates are displaced from rank one, decreasing accuracy. As tabulated later for N up to 12 million, false negative rates generally rise slowly with population size. This enables use of face recognition in very large populations. However in most positive and negative identification applications², a score threshold is set to limit the rate at which non-mate searches produce false positives. This has the consequence that some mated searches will report the mate below threshold, i.e. a miss, even if it is at rank 1. The utility of this is that many non-mated searches will return no candidate identities at all. As the error-tradeoff characteristic shows, investigational miss rates on the right side are very low but then rise steadily (in the center region) as threshold is increased to support “lights-out” applications, and ultimately rise quickly (left side) as discussed below. Thus, if we demand that just one in one thousand non-mate searches produce any false positives, the most accurate algorithms there (Sensetime-004 and NEC-3) would fail on between 3 and 5% of mated searches. Even though the graph shows results for the most accurate algorithms, all but two would fail to find the mate in more than 8% of mated searches. While the two most accurate algorithms produce a relatively flat error tradeoff until the threshold is raised to limit false positives to about 1 in 400 non-mated searches³.

Thereafter, as the threshold is raised to further reduce false positives, miss rates rise rapidly. This means that low false positive identification rates are inaccessible with these algorithms, a result that does not apply for ten-finger identification algorithms. The rapid rise occurs because the lower mate scores are mixed with very high non-mate scores, the low scores from poor image quality and ageing, the high non-mates from the presence of lookalikes persons (doppelgangers), twins (discussed next) and, ultimately, the presence of a few unconsolidated subjects i.e. persons present under multiple IDs.

- ▷ **False negatives from ageing:** A large source of error in long-run applications where subjects are not re-enrolled on a set schedule is ageing. Changes in facial appearance increase with the time elapsed between photographs. These will depress similarity scores and eventually cause false negatives. All faces age and while this usually proceeds in a graceful and progressive manner, drug use can accelerate this [28]. Elective surgery may be effective in delaying it although this has not been formally quantified with face recognition. As ageing is essentially unavoidable, it can only be mitigated by scheduled re-capture, as in passport re-issuance. To quantify ageing effects, we used the more accurate algorithms to enroll the earliest image of 3.1 million adults and then search

¹For example, NEC-0 prepares templates much faster than NEC-2 but gives twenty times more misses. Dermalog-5 executes a template search much more quickly than Dermalog-6 but is also much less accurate.

²In a positive identification application such as a registered traveler system, a user is making an implicit claim to be enrolled in the system - most users will be. In a negative application, such as with deportees, the implicit claim is that the subject is not enrolled - most will not be.

³The gallery size here is 12 million people, one image per person. Given 331 201 non-mated searches, an exhaustive implementation of one-too-many search would execute almost 4 trillion comparisons. At a false positive identification rate of 0.0025 the number of false positives is, to first order, 828 corresponding to single-comparison false match rate of $828 / 4 \text{ trillion} = 2.1 \times 10^{-10}$ i.e. about 1 in 5 billion. Strictly this FMR computation is meaningful only for algorithms that implement 1:N search using N 1:1 comparisons, which is not always the case.

with 10.3 million newer photos taken up to 18 years after the initial enrollment photo. Figure 2 puts ageing into context by contrasting it with the increase in false negatives that occurs when the number of individuals in an enrollment database becomes larger and the chance of a false positive increases such that higher thresholds may become necessary⁴.

The Figure shows, from top to bottom, increases in false negative identification rates (FNIR) with the algorithm being tested. This applies to increases due to N on the left side, and increases due to ageing on the right side. The relative spacing of the dots shows that for all algorithms the dependency of FNIR on N (up to 12 million) is considerably less than on ΔT (up to 18 years).

In the inset table, accuracy is seen to degrade progressively with time, as mate scores decline and non-mates displace mates from rank 1 position. More accurate algorithms tend to be less sensitive to ageing. The more accurate algorithms give fewer errors after 18 years of ageing than middle tier algorithms give after four. Note also we do not quantify an ageing rate - more formal methods [2] borrowed from the longitudinal analysis literature have been published for doing so (given suitable repeated measures data). See Figures 60, 88 and 101.

⁴Some algorithms implement strategies to automatically adjust scores to account for increased population size. This relieves the system owner of having to increase thresholds as N increases.

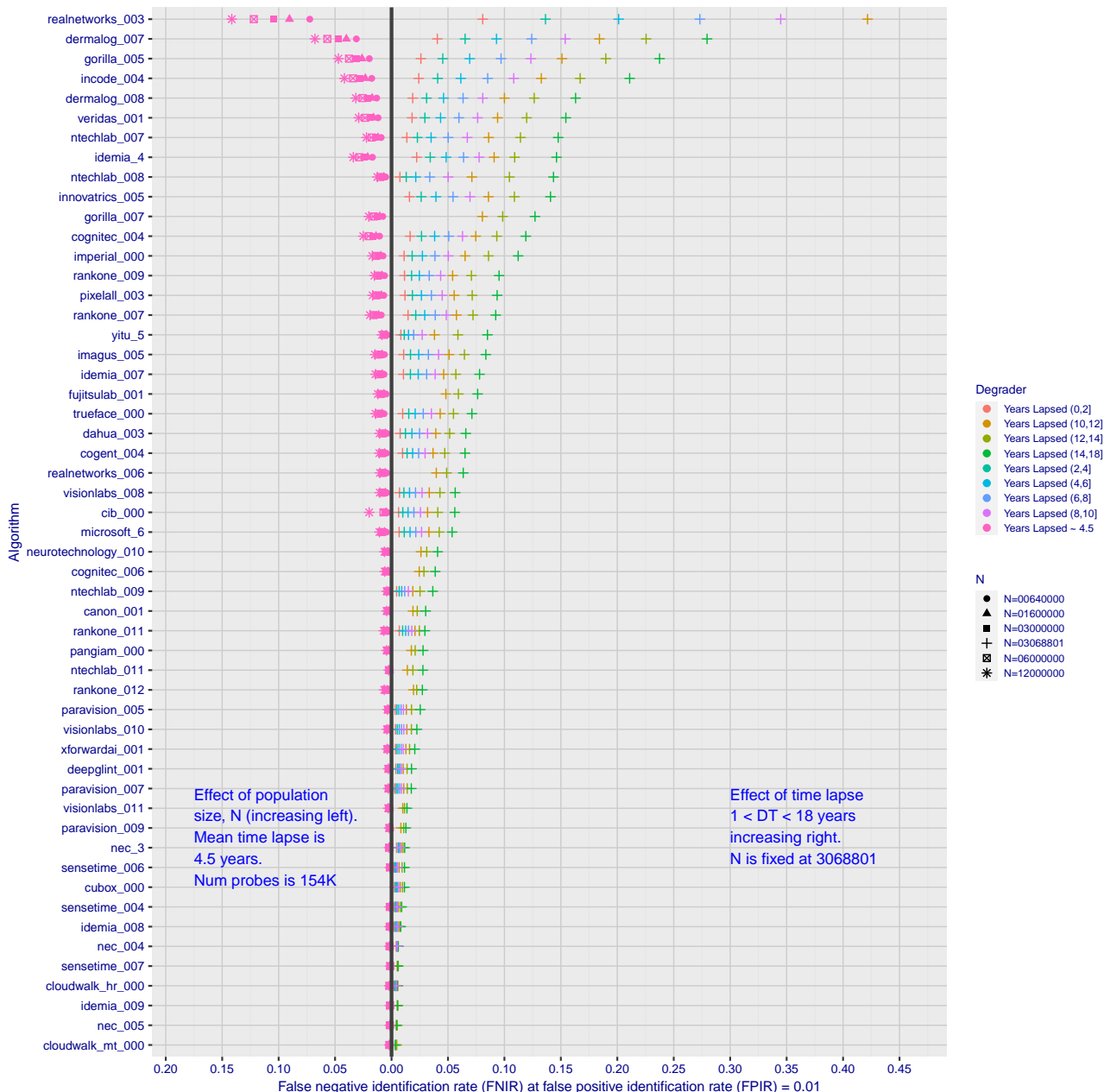


Figure 2: Identification miss rates as a function of enrolled population size, N , and time-lapse, ΔT .

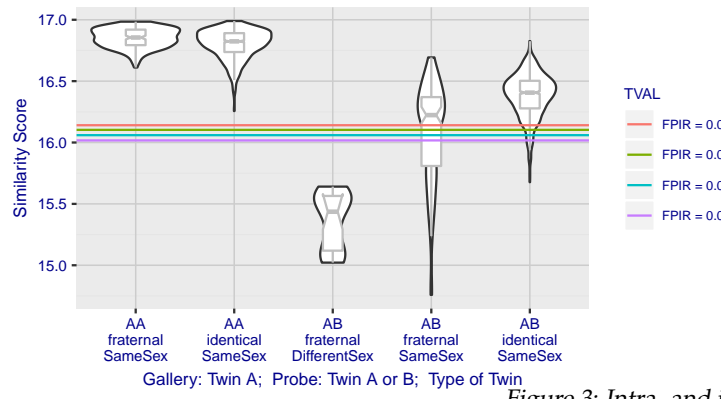


Figure 3: Intra- and inter-twin scores

▷ **False positives from twins:** By enrolling 640 000 mugshots, adding photos of one twin, and then searching photos of those subjects and their twin the inset figure shows, for one typical algorithm, the similarity is generally greater when searching twins against themselves (A) than when searching twins against their sibling (B) but very often still above even stringent thresholds i.e. those corresponding to one in one thousand searches producing a false positive. Thus twins will very often produce a high-scoring non-match on a candidate list and a false alarm in an online identification system. The plot of Fig. 3 shows that fraternal twins are sometimes correctly rejected at those thresholds - including most different sex twins (at center). Figure ?? shows substantially similar behavior for all algorithms tested. In an investigative search, a twin would typically appear at rank 1, or rank 2 if their sibling happened to also be the gallery. Twins (and triplets etc.) constituted 3.3% of all live births [17] in recent years⁵, and because that number is higher today than when the individuals in current adult databases were born, the false positives that arise from twins are now, and will increasingly be, an operational problem. Relative to the United States, twins are born with considerable regional variation. For example they are much less common in East Asia, and much more common in Sub-Saharan Africa [21].

The presence of twins in the mugshot database is inevitable given its size, around 12.3 million people. As this is not an insignificant sample of the domestic United States population, people with other familial ties will be present also. The data was collected over an extended period and because location information is not available, we are unable to estimate the proportion of the domestic population that is present in the dataset. However, if we assume twins are neither more or less disposed to arrest than the general population, we can estimate that hundreds of thousands of individuals in the dataset are twins. This will affect false positive rates because we randomly set aside 331 201 individuals for nonmate searches, and some proportion of those will be twins with siblings in the gallery.

▷ **Database integrity:** An operational error rate should be added to all false negative rates in this report reflecting the proportion of images in a real database that are un-matchable. Such anomalies arise from images that: do not contain a face; include multiple persons; cannot be decoded; are rotated by 90° or 180°; depict a face on clothing; and others introduced by a long tail of various clerical errors. While the mugshot trials in this report have been constructed to minimize such effects, they are a real problem in actual operations.

This report is being updated continuously as new algorithms are submitted to FRVT, and run on new datasets. Participation in the [one-to-many identification track](#) is independent of participation in the [one-to-one verification track](#) of FRVT.

⁵See the CDC's National Vital Statistics Report for 2017: https://www.cdc.gov/nchs/data/nvsr/nvsr67/nvsr67_08-508.pdf

Scope and Context

Audience: This report is intended for developers, integrators, end users, policy makers and others who have some familiarity with biometrics applications. The methods and metrics documented here will be of interest to organizations engaged in tests of face recognition algorithms. Some of these have been incorporated in the ISO/IEC 19795 Part 1 Biometric Testing and Reporting Framework standard, now nearing publication.

Prior benchmarks: Automated face recognition accuracy has improved massively in the two decades since initial commercialization of the various technologies. NIST has tracked that improvement through its conduct of regular independent, free, open, and public evaluations. These have fostered improvements in the state of the art. This report serves as an update to the [NIST Interagency Report 8271](#) on performance of face identification algorithms, published in September 2019.

Demographics: In December 2019, NIST published a first report on demographic dependencies in face recognition, [NIST Interagency Report 8280](#) that documented age, sex and race differentials in one-to-one and one-to-many false positive and false negative rates.

Scope: NIST IR 8271 documented recognition results for four databases containing in excess of 30.2 million still photographs of 14.4 million individuals. That constituted the largest public and independent evaluation of face recognition ever conducted. It includes results for accuracy, speed, investigative vs. identification applications, scalability to large populations, use of multiple images per person, images of cooperative and non-cooperative subjects.

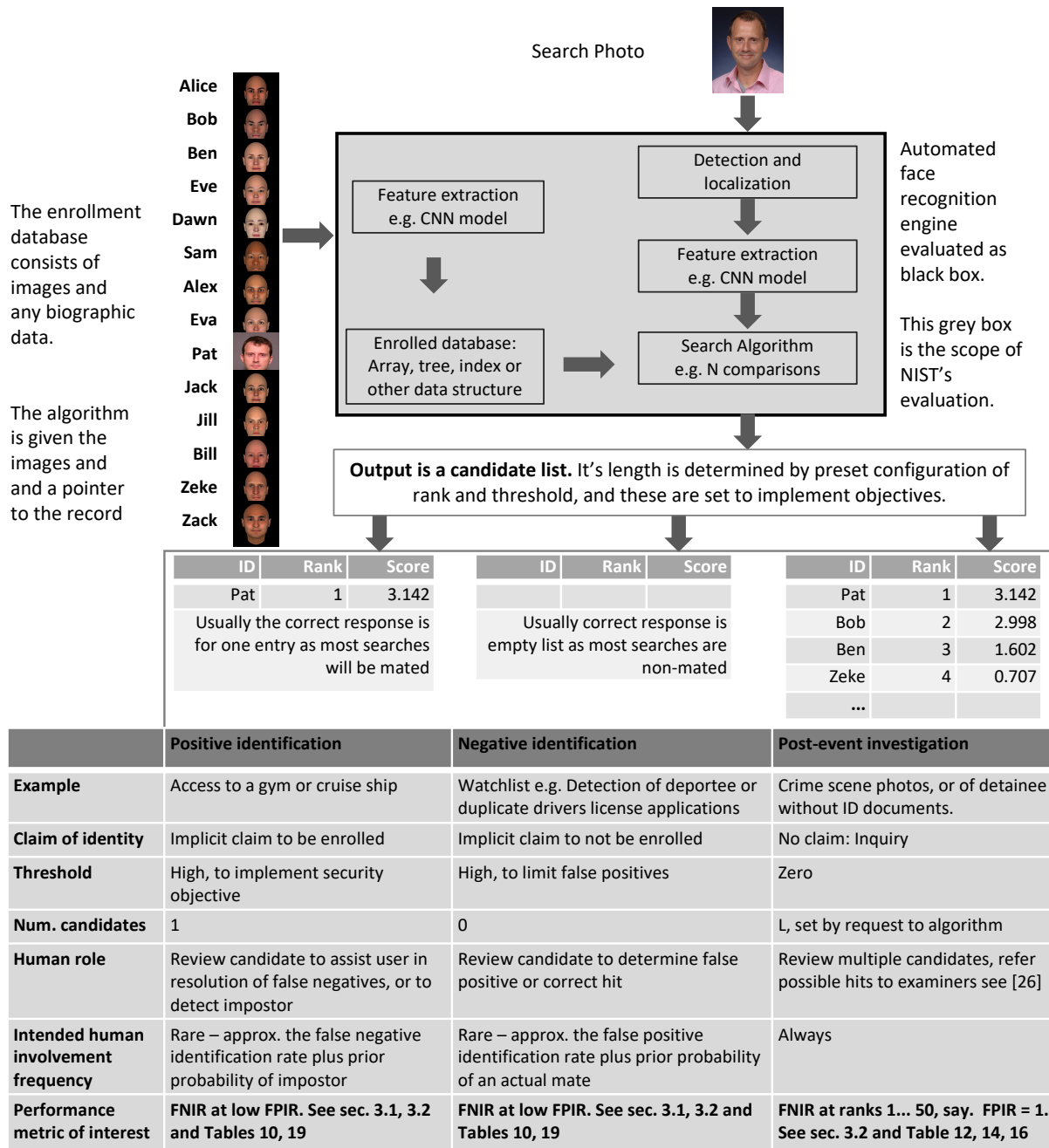
The report also includes results for ageing, recognition of twins, and recognition of profile-view images against frontal galleries. It otherwise does not address causes of recognition failure, neither image-specific problems nor subject-specific factors including demographics. Separate reports on demographic dependencies in face recognition will be published in the future. Additionally out of scope are: performance of live [human-in-the-loop transactional systems](#) like automated border control gates; human recognition accuracy as used in forensic applications; and recognition of persons in video sequences (which NIST evaluated separately [9]). Some of those applications share core matching technologies that *are* tested in this report.

Images: Five kinds of images are employed; these are either compared with images of the same kind, or against others from different capture environments as follows. The primary dataset is a set of law enforcement mugshot images (Fig. 5) which are enrolled and then searched with three kinds of images: other mugshots (i.e. within-domain); profile-view photographs (90 degree cross-view); and lower quality webcam images (Fig. 6) collected in similar detention operations (cross-domain). Additionally we compare high quality visa-like photos collected in immigration offices, with: medium quality border crossing images collected in primary immigration lanes; poor quality images collected in ATM-like registered traveller kiosks.

Participation and industry coverage: The report includes performance figures for prototype algorithms from the research laboratories of commercial developers and a few universities. This represents a substantial majority of the face recognition industry, but only a tiny minority of the academic community. Participation was open worldwide. While there is no charge for participation, developers incur some software engineering expense in implementing their algorithms behind the NIST application programming interface (API). The test is a black-box test where the function of the algorithm, and the intellectual property associated with it, is hidden inside pre-compiled libraries.

Recent technology development: Most face recognition research with deep convolutional neural networks (CNNs) has been aimed at achieving invariance to pose, illumination and expression variations that characterize photojournalism and social media images. The initial research [18, 22] employed large numbers of images of relatively few ($\sim 10^4$) individuals to learn invariance. Inevitably much larger populations ($\sim 10^7$) were employed for training [11, 20] but the benchmark, Labeled Faces in the Wild with (essentially) an equal error rate metric [12], represents an easy task,

one-to-one verification at very high false match rates. While a larger scale identification benchmark duly followed, Megaface [15], its primary metric, rank one hit rate, contrasts with the high threshold discrimination task required in most large-population applications of face recognition, namely credential de-duplication, and background checks. There, identification in galleries containing up to 10^8 individuals must be performed using a) very few images per individual and b) stringent thresholds to afford very low false positive identification rates. This track of FRVT was launched to measure the capability of the new technologies, including in these two cases. FRVT has included open-set identification tests since 2002, reporting both false negative and positive identification rates [7].



Performance metrics for applications: This report documents the performance of one-to-many face recognition algorithms. The word "performance" here refers to recognition accuracy and computational resource usage, as measured

by executing those algorithms on massive sequestered datasets.

This report includes extensive tabulation of recognition error rates germane to the main use-cases for face search technology. The Figure below, inspired by the Figure 1 in [23] differentiates different applications of the technolgy. The last row directs readers to the main tables relevant to those applications, respectively threshold-based and rank-based metrics that are special cases of the metrics given in section 3. The terms negative identification and positive identification are taken from the ISO/IEC 2382-37:2017 standardized biometrics vocabulary.

The algorithms are specifically configured for these applications by setting thresholds and candidate list lengths. Both rank-based metrics and threshold-based metrics include tradeoffs. In investigation, overall accuracy will be reduced if labor is only available to review a few candidates from the automated system. Note that when a fixed number of candidates are returned, the false positive identification rate of the automated face recognition engine will be 100%, because a probe image of anyone not enrolled will still return candidates. In identification applications where false positives must be limited to satisfy reviewer labor availability or a security objective, higher false negative rates are implied. This report includes extensive quantification of this threshold-based tradeoff.

See Sec. 3

Template diversity: The FRVT is designed to evaluate black-box technologies with the consequence that the templates that hold features extracted from face images are entirely proprietary opaque binary data that embed considerable intellectual property of the developer. Despite migration to CNN-based technologies there is no consensus on the optimal feature vector dimension. This is evidenced by template sizes ranging from below 100 bytes to more than four kilobytes. This diversity of approaches, suggests there is no prospect of a standard template something that would require a common feature set to be extracted from faces. Interoperability in automated face recognition remains solidly based on images and documentary standards for those, in particular the ICAO portrait [27] specification deriving from the ISO/IEC 19794-5 Token frontal [24] standard, which are similar to certain ANSI/NIST Type 10 [26] formats.

Training: The algorithms submitted to NIST have been developed using image datasets that developers do not disclose. The development will often include application of machine learning techniques and will additionally involve iterative training and testing cycles. NIST itself does not perform any training and does not refine or alter the algorithm in any way. Thus the model, data files, and libraries that define an algorithm are fixed for the duration of the tests. This reflects typical operational reality where recognition software, once installed, is fixed and constant until upgraded. This situation persists because on-site training of algorithms on customer data is atypical essentially because training is not a turnkey process.

Automated search and human review: Virtually all applications using automated face search require human review of the outputs at some frequency: Always for investigational applications; rarely in positive identification applications, after rejection (false or otherwise); and rarely in negative identification applications, after an alarm (false or otherwise). The human role is usually to compare a reference image with the query image or the live-subject if present, to render either a definitive decision on “exclusion” (different subjects), or “identification” (same subject), or a declaration that one or both images have “no value” and that no decision can be made. Note that automated face recognition algorithms are not built to do exclusion - low scores from a face comparison arise from different faces *and* poor quality images of the same face.

Human reviewers make recognition errors [5, 19, 25] and are sensitive to image acquisition and quality. Accurate human review is supported by high resolution - as specified in the Type 50, 51 acquisition profiles of the ANSI/NIST Type 10 record [26], and by multiple non-frontal views as specified in the same standard. These often afford views of the ear. Organizations involved in image collection should consider supporting human adjudication by collecting high-resolution frontal and non-frontal views, preparing low resolution versions for automated face recognition [24], and retaining both for any subsequent resolution of candidate matches. Along these lines, the ISO/IEC Joint Technical

Committee 1 subcommittee 37 on biometrics has just initiated projects on image quality assessment and face-aware capture.

Release Notes

FRVT Activities: Since February 2017, NIST has been evaluating one-to-one verification algorithms on an ongoing basis. NIST then restarted FRVT's one-to-many track in February 2018, inviting participants to send up to prototype algorithms. Both tracks allows developers to submit updated algorithms to NIST at any time but no more frequently than four calendar months. This more closely aligns development and evaluation schedules. Results are posted to the web within a few weeks of submission. Details and full report are linked from the [Ongoing FRVT site](#).

FRVT Reports: The results of the FRVT appear in the series NIST Interagency Reports tabulated below. The reports were developed separately and released on different schedules. In prior years NIST has mostly reported FRVT results as a single report; this had the disadvantage that results from completed sub-studies were not published until all other studies were complete.

Date	Link	Title	No.
2014-03-20	PDF	FRVT Performance of Automated Age Estimation Algorithms	7995
2015-04-20	PDF	Face Recognition Vendor Test (FRVT) Performance of Automated Gender Classification Algorithms	8052
2014-05-21	PDF	FRVT Performance of face identification algorithms	8009
2017-03-07	PDF	Face In Video Evaluation (FIVE) Face Recognition of Non-Cooperative Subjects	8173
2017-11-23	PDF	The 2017 IARPA Face Recognition Prize Challenge (FRPC)	8197
2018-11-27	PDF	Face Recognition Vendor Test - Part 2: Identification	8271
2019-09-11	PDF	Face Recognition Vendor Test - Part 2: Identification	8271
2019-12-11	PDF	Face Recognition Vendor Test - Part 3: Demographic Effects	8280
2020-01-03	WWW	Face Recognition Vendor Test (FRVT) - Part 1 Verification	Draft

Details appear on pages linked from <https://www.nist.gov/programs-projects/face-projects>.

Appendices: This report is accompanied by appendices which present exhaustive results on a per-algorithm basis. These are machine-generated and are included because the authors believe that visualization of such data is broadly informative and vital to understanding the context of the report.

Typesetting: Virtually all of the tabulated content in this report was produced automatically. This involved the use of scripting tools to generate directly type-settable L^AT_EX content. This improves timeliness, flexibility, maintainability, and reduces transcription errors.

Graphics: Many of the Figures in this report were produced using the **ggplot2** package running under **R**, the capabilities of which extend beyond those evident in this document.

Contents

Release Notes	1
Disclaimer	5
Institutional Review Board	5
Acknowledgments	5
Executive Summary	6
Scope and Context	12
Release Notes	16
1 Introduction	18
2 Evaluation datasets	19
3 Performance metrics	25
4 Results	41
Appendices	82
A Accuracy on large-population FRVT 2018 mugshots	82
B Effect of time-lapse: Accuracy after face ageing	127
C Effect of enrolling multiple images	199
D Accuracy with poor quality webcam images	206
E Accuracy for profile-view to frontal recognition	216
F Search duration	220
G Gallery Insertion Timing	230

1 Introduction

One-to-many identification represents the largest market for face recognition technology. Algorithms are used across the world in a diverse range of biometric applications: detection of duplicates in databases, detection of fraudulent applications for credentials such as passports and driving licenses, token-less access control, surveillance, social media tagging, lookalike discovery, criminal investigation, and forensic clustering.

This report contains a breadth of performance measurements relevant to many applications. Performance here refers to accuracy and resource consumption. In most applications, the core accuracy of a facial recognition algorithm is the most important performance variable. Resource consumption will be important also as it drives the amount of hardware, power, and cooling necessary to accommodate high volume workflows. Algorithms consume processing time, they require computer memory, and their static template data requires storage space. This report documents these variables.

1.1 Open-set searches

FRVT tested open-set identification algorithms. Real-world applications are almost always “open-set”, meaning that some searches have an enrolled mate, but some do not. For example, some subjects have truly not been issued a visa or drivers license before; some law enforcement searches are from first-time arrestees⁶. In an “open-set” application, algorithms make no prior assumption about whether or not to return a high-scoring result, and for a mated search, the ideal behaviour is that the search produces the correct mate at high score and first rank. For a non-mate search, the ideal behavior is that the search produces zero high-scoring candidates.

Many academic benchmarks execute only closed-set searches. The proportion of mates found in the rank one position is the default accuracy metric. This hit rate metric ignores the score with which a mate is found; weak hits count as much as strong hits. This ignores the real-world imperative that in many applications it is necessary to elevate a threshold to reduce the number of false positives.

⁶Operationally closed-set applications are rare because it is usually not the case that all searches have an enrolled mate. One counter-example, however, is a cruise ship in which all passengers are enrolled and all searches should produce exactly one identity. Another example is forensic identification of dental records from an aircraft crash.

2 Evaluation datasets

This report documents accuracy for four kinds of images - mugshots, webcam, profiles and wild - as described in the following sections.

2.1 Immigration-related images

This report includes benchmark tests sharing a common enrollment of high quality frontal portrait images collected while subject make applications for various immigration benefits. We then search that with two kinds of images, webcam images collected during in-bound immigration and also images collected from registered travelers using a ATM-style kiosk. These are described below and depicted in Figure 4.



Figure 4: Example photos.

- ▷ **Application reference photos:** The images are collected in an attended interview setting using dedicated capture equipment and lighting. The images, at size 300x300 pixels, are smaller than normally indicated by ISO. The images are all high-quality frontal portraits collected in immigration offices and with a white background. As such, potential quality related drivers of high false match rates (such as blur) can be expected to be absent. The images are encoded as ISO/IEC 10918-1 i.e. JPEG. Older images had a compression ration of about 16:1, while newer images, since 2010, are more lightly compressed at 4:1. When these images are provided as input into the algorithm, they are labeled with the type "iso". This report enrols 1 600 000 application images, one per person.
- ▷ **Border crossing photos:** Most images are have width 320 and height 240 pixels. They are JPEG compressed at 16:1 i.e. filesize just below 15KB. The images present challenges for face recognition in that subjects often exhibit non-zero yaw and pitch (associated with the rotational degrees of freedom of the camera mount), low contrast (due to varying and intense background lights), and poor spatial resolution (due to inexpensive cameras). There are often subjects standing in the background, usually at very low resolution (see Figure 4b). In such cases, algorithms should detect all faces and determine which is the largest and most centered. When these images are provided as input into the algorithm, they are labeled with the type "wild".
- ▷ **Kiosk photos:** These photos were collected from subjects whose attention was focused on interaction with an immigration kiosk. They images were not intended for use with automated face recognition. The camera is situated above a display which the user touches, and is triggered either without directing the subject to look at it, or without waiting for the subject to comply. The images are therefore characterized by pitch-down pose, sometimes exceeding 45 degrees, as in Figure 4c. Yaw-angle variation is mild, with most images close to frontal. The images

have width 320 pixels and height 240 pixels and therefore tall individuals are sometimes cropped. This is often just above the eyes and can occur at the nose or mouth. Conversely, short individuals are sometimes cropped such that only the top part of the face is visible. In a quite small number of cases, there other subjects standing just behind the primary subject such that algorithms should detect all faces and determine which is the largest and most centered. Background ceiling lighting is often visible and this sometimes leads to under-exposure of the face. When these images are provided as input into the algorithm, they are labeled with the type "wild".

2.2 Law enforcement images

The main mugshot dataset used is referred to as the FRVT 2018 set. This set was collected over the period 2002 to 2017 in routine United States law enforcement operations. This set yields three subsets

- ▷ **Mugshots:** Mugshots comprise about 86% of the database. They have reasonable compliance with the ANSI/NIST ITL1-2011 Type 10 standard's subject acquisition profiles levels 10-20 for frontal images [26]. The most common departure from the standard's requirements is the presence of mild pose variations around frontal - the images of Figure 5 are typical. The images vary in size, with many being 480x600 pixels with JPEG compression applied to produce filesizes of between 18 and 36KB with many images outside this range, implying that about 0.5 bits are being encoded per pixel. When these images are provided as input into the algorithm, they are labeled with the type "mugshot".

Example images appear in Fig. 5

[NIST Interagency Report 8238](#) includes a comparison of this set of mugshots with the smaller and easier sets of mugshots used in tests run in 2010 and 2014.

- ▷ **Profile images:** Profile-view images have been collected in law enforcement for more than 100 years, as human capability is improved with orthogonal information. The profile images used in this report were collected during the same session as the frontal mugshot photograph, in the same standardized photographic setup. These would not therefore be used with automated face recognition. A small subset, 200 000 images, were set aside for testing. When these images are provided as input into the algorithm, they are labeled with the type "wild".

Example images appear in Fig. 7

- ▷ **Webcam images:** The remaining 14% of the images were collected using an inexpensive webcam attached to a flexible operator-directed mount. These images are all of size 240x240 pixels, that are in considerable violation of most quality-related clauses of all face recognition standards. As evident in the figure, the most common defects are non-frontal pose (associated with the rotational degrees of freedom of the camera mount), low contrast (due to varying and intense background lights), and poor spatial resolution (due to inexpensive camera optics) - see examples in Fig 6. The images are overly JPEG compressed, to between 4 and 7KB, implying that only 0.5 to 1 bits are being encoded per color pixel. When these images are provided as input into the algorithm, they are labeled with the type "wild".

Example images appear in Fig. 6

These are drawn from NIST Special Database 32 which may be downloaded [here](#).

These images were partitioned in galleries and probesets for the various experiment listed in Table 1.

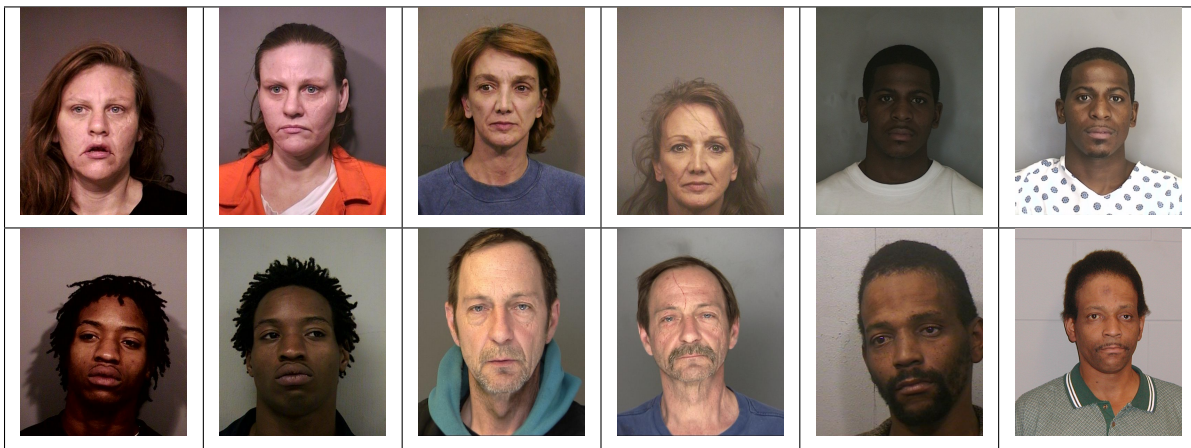


Figure 5: Six mated mugshot pairs representative of the FRVT-2014 (LEO) and FRVT-2018 datasets. The images are collected live, i.e. not scanned from paper. Image source: NIST Special Database 32 the Multiple Encounter Deceased Subjects dataset.



Figure 6: Twelve webcam images representative of probes against the FRVT-2018 mugshot gallery. The first eight images are four mated pairs. Such images present challenges to recognition including pose, non-uniform illumination, low contrast, compression, cropping, and low spatial sampling rate. Image source: NIST Special Database 32 the Multiple Encounter Deceased Subjects dataset.



Figure 7: **[Profile views]** The three images are a frontal enrollment, subsequent frontal probe, and same-session ninety degree profile view. While collection of both frontal and profile views has been typical in law enforcement for more than a century, the recognition of profile to frontal views has essentially been impossible. However, reasonably high accuracy results is now possible - see section E.

Image				
Encounter	1	...	$K_i - 1$	K_i
Capture Time	T_1	...	T_{K_i-1}	T_{K_i}
Role RECENT	Not used	Not used	Enrolled	Search
Role LIFETIME	Enrolled	Enrolled	Enrolled	Search

Figure 8: Depiction of the “recent” and “lifetime” enrollment types. Image source: NIST Special Database 32

2.3 Enrollment strategies

Many operational applications include collection and enrollment of biometric data from subjects on more than one occasion. This might be done on a regular basis, as might occur in credential (re-)issuance, or irregularly, as might happen in a criminal recidivist situation [4]. The number of images per person will depend on the application area. In civil identity credentialing (e.g. passports, driver’s licenses), the images will be acquired approximately uniformly over time (e.g. ten years for a passport). While the distribution of dates for such images of a person might be assumed uniform, a number of factors might undermine this assumption⁷. In criminal applications, the number of images would depend on the number of arrests. The distribution of dates for arrest records for a person (i.e. the recidivism distribution) has been modeled using the exponential distribution but is recognized to be more complicated⁸.

In any case, the 2010 NIST evaluation of face recognition showed that considerable accuracy benefits accrue with retention and use of *all* historical images [6].

To this end, the FRVT API document provides $K \geq 1$ images of an individual to the enrollment software. The software is tasked with producing a single proprietary undocumented “black-box” template⁹ from the K images. This affords the algorithm an ability to generate a *model* of the individual, rather than to simply extract features from each image on a sequential basis.

As depicted in Figure 8, the i -th individual in the FRVT 2018 dataset has K_i images. These are labelled as x_k for $k = 1 \dots K_i$ in chronological order of capture date. To measure the utility of having multiple enrollment images, this report evaluates three kinds of enrollment:

- ▷ **Recent:** Only the second most recent image, x_{K_i-1} is enrolled. This strategy of enrollment mimics the operational policy of retaining the imagery from the most recent encounter. This might be done operationally to ameliorate the effects of face ageing. Obviously retaining only the most recent image should only be done if the identity of the person is trusted to be correct. For example, in an access control situation retention of the most recent successful *authentication* image would be hazardous if it could be a false positive.
- ▷ **Lifetime-consolidated:** All but the most recent image are enrolled, $x_1 \dots x_{K_i-1}$. This subject-centric strategy might be adopted if quality variations exist where an older image might be more suitable for matching, despite the ageing effect.

⁷For example, a person might skip applying for a passport for one cycle, letting it expire. In addition, a person might submit identical images (from the same photography session) to consecutive passport applications at five year intervals.

⁸A number of distributions have been considered to model recidivism, see for example [3].

⁹There are no formal face template standards. Template standards only exist for fingerprint minutiae - see ISO/IEC 19794-2:2011.

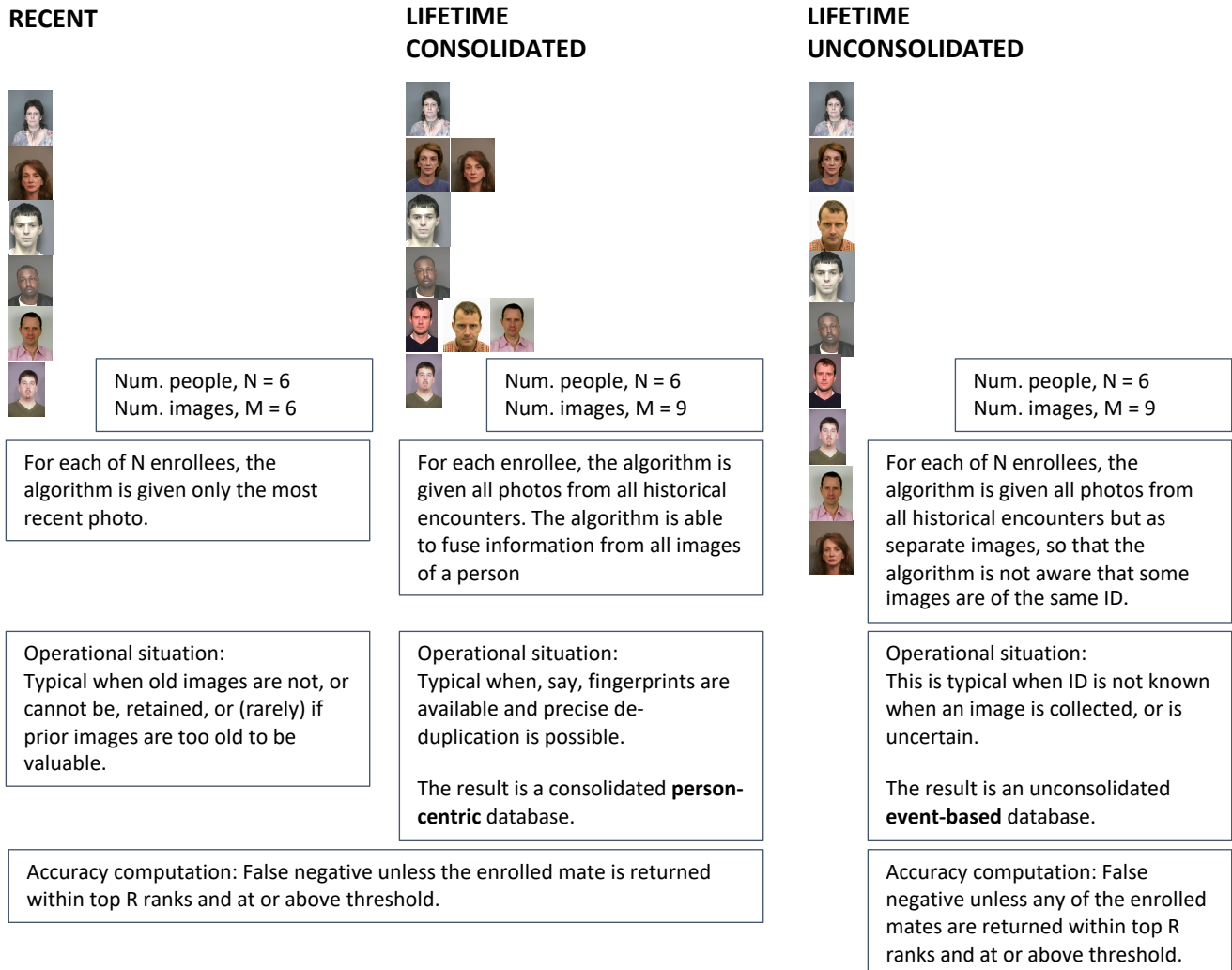


Figure 9: Enrollment strategies. The figure shows the three kinds of enrollment databases examined in this report. Image source: NIST Special Database 32

	ENROLLMENT				SEARCH			
	TYPE SEE SECTION 2.3	POPULATION FILTER	N-SUBJECTS	N-IMAGES	MATE N-SUBJECTS	NON-MATE N-IMAGES	N-SUBJECTS	N-IMAGES
Mugshot trials from enrollment of single images								
1	RECENT	NATURAL	640 000	640 000	154 549	154 549	331 254	331 254
2	RECENT	NATURAL	1 600 000	1 600 000				
3	RECENT	NATURAL	3 000 000	3 000 000				
4	RECENT	NATURAL	6 000 000	6 000 000				
5	RECENT	NATURAL	12 000 000	12 000 000				
Cross-domain								
13	MUGSHOTS AS ON ROW 2				82 106 WEBCAM	82 106 WEBCAM	331 254 WEBCAM	331 254 WEBCAM
Cross-view								
14	MUGSHOTS AS ON ROW 2				100 000 PROFILE	100 000 PROFILE	100 000 PROFILE	100 000 PROFILE
Mugshot ageing								
17	OLDEST	NATURAL	3 068 801	3 068 801	2 853 221	10 951 064	0	0
Border crossing ageing								
18	OLDEST	NATURAL	1 600 000	1 600 000	903 655	1 922 393	1 393 076	1 680 000
Visa-border								
19	PRIOR	NATURAL	1 600 000 VISA	1 600 000 VISA	577 444 BORDER	1 212 892 BORDER	79 769 BORDER	80 000 BORDER
20	VISA AS ON ROW 18				14 004 BORDER	31 579 BORDER	42 474 BORDER	45 460 BORDER

Table 1: Enrollment and search sets. Each row summarizes one identification trial. Unless stated otherwise, all entries refer to mugshot images. The term “natural” means that subjects were selected without heed to demographics, i.e. in the distribution native to this dataset. The probe images were collected in a different calendar year to the enrollment image. Missing values in rows 2-12 are the same as in row 1.

▷ **Lifetime-unconsolidated:** Again all but the most recent image are enrolled $x_1 \dots x_{K_i-1}$ but now separately, with different identifiers, such that the algorithm is not aware that the images are from the same face. This kind of event- or encounter-centric enrollment is very common when operational constraints preclude reliable consolidation of the historical encounters into a single identity. This aspect also prevents the recognition algorithm from a) building a holistic model of identity (as is common in speaker recognition systems) and b) implementing fusion, for example template-level fusion of feature vectors, or post-search score-level fusion. The result is that searches will typically yield more than one image of a person in the top ranks. This has consequences for appropriate metrics, as detailed in section 3.2.1

NIST first evaluated this kind of enrollment in mid 2018, and the results tables include some comparison of accuracy available from all three enrollment styles.

In all cases, the most recent image, x_{K_i} , is reserved as the search image. For the 1.6 million subject enrollment partition of the FRVT 2018 data, $1 \leq K_i \leq 33$ with $K_i = 1$ in 80.1% of the individuals, $K_i = 2$ in 13.4%, $K_i = 3$ in 3.7%, $K_i = 4$ in 1.4%, $K_i = 5$ in 0.6%, $K_i = 6$ in 0.3%, and $K_i > 6$ is 0.2% for everyone else. This distribution is substantially dependent on United States recidivism rates.

We did not evaluate the case of retaining only the highest quality image, since automated quality assessment is out of scope for this report. We do not anticipate that such strategies will prove beneficial when the quality assessment apparatus is imperfect and unvalidated.

3 Performance metrics

This section gives specific definitions for accuracy and timing metrics. Tests of open-set biometric algorithms must quantify frequency of two error conditions:

- ▷ **False positives:** Type I errors occur when search data from a person who has never been seen before is incorrectly associated with one or more enrollees' data.
- ▷ **Misses:** Type II errors arise when a search of an enrolled person's biometric does not return the correct identity.

Many practitioners prefer to talk about "hit rates" instead of "miss rates" - the first is simply one minus the other as detailed below. Sections 3.1 and 3.2 define metrics for the Type I and Type II performance variables.

Additionally, because recognition algorithms sometimes fail to produce a template from an image, or fail to execute a one-to-many search, the occurrence of such events must be recorded. Further because algorithms might elect to not produce a template from, for example, a poor quality image, these failure rates must be combined with the recognition error rates to support algorithm comparison. This is addressed in section 3.5.

Finally, section 3.7 discusses measurement of computation duration, and section 3.8 addresses the uncertainty associated with various measurements. Template size measurement is included with the results.

3.1 Quantifying false positives

It is typical for a search to be conducted into an enrolled population of N identities, and for the algorithm to be configured to return the closest L candidate identities. These candidates are ranked by their score, in descending order, with all scores required to be greater than or equal to zero. A human analyst might examine either all L candidates, or just the top $R \leq L$ identities, or only those with score greater than threshold, T . The workload associated with such examination is discussed later, in 3.6.

False alarm performance is quantified in two related ways. These express how many searches produces false positives, and then, how many false positives are produced in a search.

False positive identification rate: The first quantity, FPIR, is the proportion of non-mate searches that produce an adverse outcome:

$$\text{FPIR}(N, T) = \frac{\text{Num. non-mate searches where one or more enrolled candidates are returned with score at or above threshold}}{\text{Num. non-mate searches attempted.}} \quad (1)$$

Under this definition, FPIR can be computed from the highest non-mate candidate produced in a search - it is not necessary to consider candidates at rank 2 and above. FPIR is the primary measure of Type I errors in this report.

Selectivity: However, note that in any given search, several non-mate may be returned above threshold. In order to quantify such events, a second quantity, selectivity (SEL), is defined as the *number* of non-mates returned on a candidate list, averaged over all searches.

$$\text{SEL}(N, T) = \frac{\text{Num. non-mate enrolled candidates returned with score at or above threshold}}{\text{Num. non-mate searches attempted.}} \quad (2)$$

where $0 \leq \text{SEL}(N, T) \leq L$. Both of these metrics are useful operationally. FPIR is useful for targeting how often an

adverse false positive outcome can occur, while SEL as a number is related to workload associated with adjudicating candidate lists. The relationship between the two quantities is complicated - it depends on whether an algorithm concentrates the false alarms in the results of a few searches or whether it disburses them across many. This was detailed in FRVT 2014, NISTIR 8009. It has not yet been detailed in FRVT 2018.

3.2 Quantifying hits and misses

If L candidates are returned in a search, a shorter candidate list can be prepared by taking the top $R \leq L$ candidates for which the score is above some threshold, $T \geq 0$. This reduction of the candidate list is done because thresholds may be applied, and only short lists might be reviewed (according to policy or labor availability, for example). It is useful then to state accuracy in terms of R and T , so we define a “miss rate” with the general name **false negative identification rate** (FNIR), as follows:

$$\text{FNIR}(N, R, T) = \frac{\text{Num. mate searches with enrolled mate found outside top } R \text{ ranks or score below threshold}}{\text{Num. mate searches attempted.}} \quad (3)$$

This formulation is simple for evaluation in that it does not distinguish between causes of misses. Thus a mate that is not reported on a candidate list is treated the same as a miss arising from face finding failure, algorithm intolerance of poor quality, or software crashes. Thus if the algorithm fails to produce a candidate list, either because the search failed, or because a search template was not made, the result is regarded as a miss, adding to FNIR.

Hit rates, and true positive identification rates: While FNIR states the “miss rate” as how often the correct candidate is either not above threshold or not at good rank, many communities prefer to talk of “hit rates”. This is simply the **true positive identification rate**(TPIR) which is the complement of FNIR giving a positive statement of how often mated searches are successful:

$$\text{TPIR}(N, R, T) = 1 - \text{FNIR}(N, R, T) \quad (4)$$

This report does not report true positive “hit” rates, preferring false negative miss rates for two reasons. First, costs rise linearly with error rates. For example, if we double FNIR in an access control system, then we double user inconvenience and delay. If we express that as decrease of TPIR from, say 98.5% to 97%, then we mentally have to invert the scale to see a doubling in costs. More subtly, readers don’t perceive differences in numbers near 100% well, becoming inured to the “high nineties” effect where numbers close to 100 are perceived indifferently.

Reliability is a corresponding term, typically being identical to TPIR, and often cited in automated (fingerprint) identification system (AFIS) evaluations.

An important special case is the **cumulative match characteristic**(CMC) which summarizes accuracy of mated-searches only. It ignores similarity scores by relaxing the threshold requirement, and just reports the fraction of mated searches returning the mate at rank R or better.

$$\text{CMC}(N, R) = 1 - \text{FNIR}(N, R, 0) \quad (5)$$

We primarily cite the complement of this quantity, $\text{FNIR}(N, R, 0)$, the fraction of mates *not* in the top R ranks.

The **rank one hit rate** is the fraction of mated searches yielding the correct candidate at best rank, i.e. $\text{CMC}(N, 1)$. While this quantity is the most common summary indicator of an algorithm’s efficacy, it is not dependent on similarity scores, so it does not distinguish between strong (high scoring) and weak hits. It also ignores that an adjudicating reviewer is often willing to look at many candidates.

3.2.1 False negative rates for unconsolidated galleries

As detailed in section 2.3 a common type of gallery, here referred to as the lifetime unconsolidate type, is populated with all images of an individual without any association between them. That is, the gallery construction algorithm is not provided with any ID labels that would support processing of a person's images jointly. This contrasts with the lifetime consolidate type where an algorithm may explicitly fuse features from multiple images of a person, or select a best image. In such cases, where the number of enrolled images is a random variable, we define two false negative rates as follows.

The first demands that the algorithm place any of the K_i mates in the top $R \geq 1$ ranks. The proportion of searches for which this does not occur forms a false negative identification rate:

$$\text{FNIR}_{\text{any}}(N, R, T) = 1 - \frac{\text{Num. mate searches where any enrolled mate is found in the top } R \text{ ranks and at-or-above threshold}}{\text{Num. mate searches attempted.}} \quad (6)$$

The second demands that the algorithm place all K_i mates in the top $R \geq K_i$ ranks. The proportion of searches for which this does not occur forms a false negative identification rate:

$$\text{FNIR}_{\text{all}}(N, R, T) = 1 - \frac{\text{Num. mate searches where all enrolled mates are found in the top } R \text{ ranks and at-or-above threshold}}{\text{Num. mate searches attempted.}} \quad (7)$$

Placing all mates in the top ranks is a more difficult task than correctly retrieving any image, so it holds that: $\text{FNIR}_{\text{all}} \geq \text{FNIR}_{\text{any}}$. This is evident in the results presented for November 2018 algorithms in Tables starting at ??.

The information retrieval community might prefer to compute and plot *precision* and *recall*; this is a valid approach, but we advance the two metrics above because they relate to our normal definition of consolidated FNIR, and they cover the two extreme use-cases of wanting any hit vs. all hits.

3.3 DET interpretation

In biometrics, a false negative occurs when an algorithm fails to match two samples of one person – a Type II error. Correspondingly, a false positive occurs when samples from two persons are improperly associated – a Type I error.

Matches are declared by a biometric system when the native comparison score from the recognition algorithm meets some threshold. Comparison scores can be either similarity scores, in which case higher values indicate that the samples are more likely to come from the same person, or dissimilarity scores, in which case higher values indicate different people. Similarity scores are traditionally computed by fingerprint and face recognition algorithms, while dissimilarities are used in iris recognition. In some cases, the dissimilarity score is a distance possessing metric properties. In any case, scores can be either mate scores, coming from a comparison of one person's samples, or nonmate scores, coming from comparison of different persons' samples.

The words "genuine" or "authentic" are synonyms for mate, and the word "impostor" is used as a synonym for non-mate. The words "mate" and "nonmate" are traditionally used in identification applications (such as law enforcement search, or background checks) while genuine and impostor are used in verification applications (such as access control).

An error tradeoff characteristic represents the tradeoff between Type II and Type I classification errors. For identification this plots false negative vs. false positive identification rates i.e. FNIR vs. FPIR parametrically with T. Such plots

are often called detection error tradeoff (DET) characteristics or receiver operating characteristic (ROC). These serve the same function – to show error tradeoff – but differ, for example, in plotting the complement of an error rate (e.g. $TPIR = 1 - FNIR$) and in transforming the axes, most commonly using logarithms, to show multiple decades of FPIR. More rarely, the function might be the inverse of the Gaussian cumulative distribution function.

The slides of Figures 10 through 15 discuss presentation and interpretation of DETs used in this document for reporting face identification accuracy. Further detail is provided in formal biometrics testing standards, see the various parts of ISO/IEC 19795 Biometrics Testing and Reporting. More terms, including and beyond those to do with accuracy, appear in ISO/IEC 2382-37 Information technology – Vocabulary – Part 37: Harmonized biometric vocabulary.

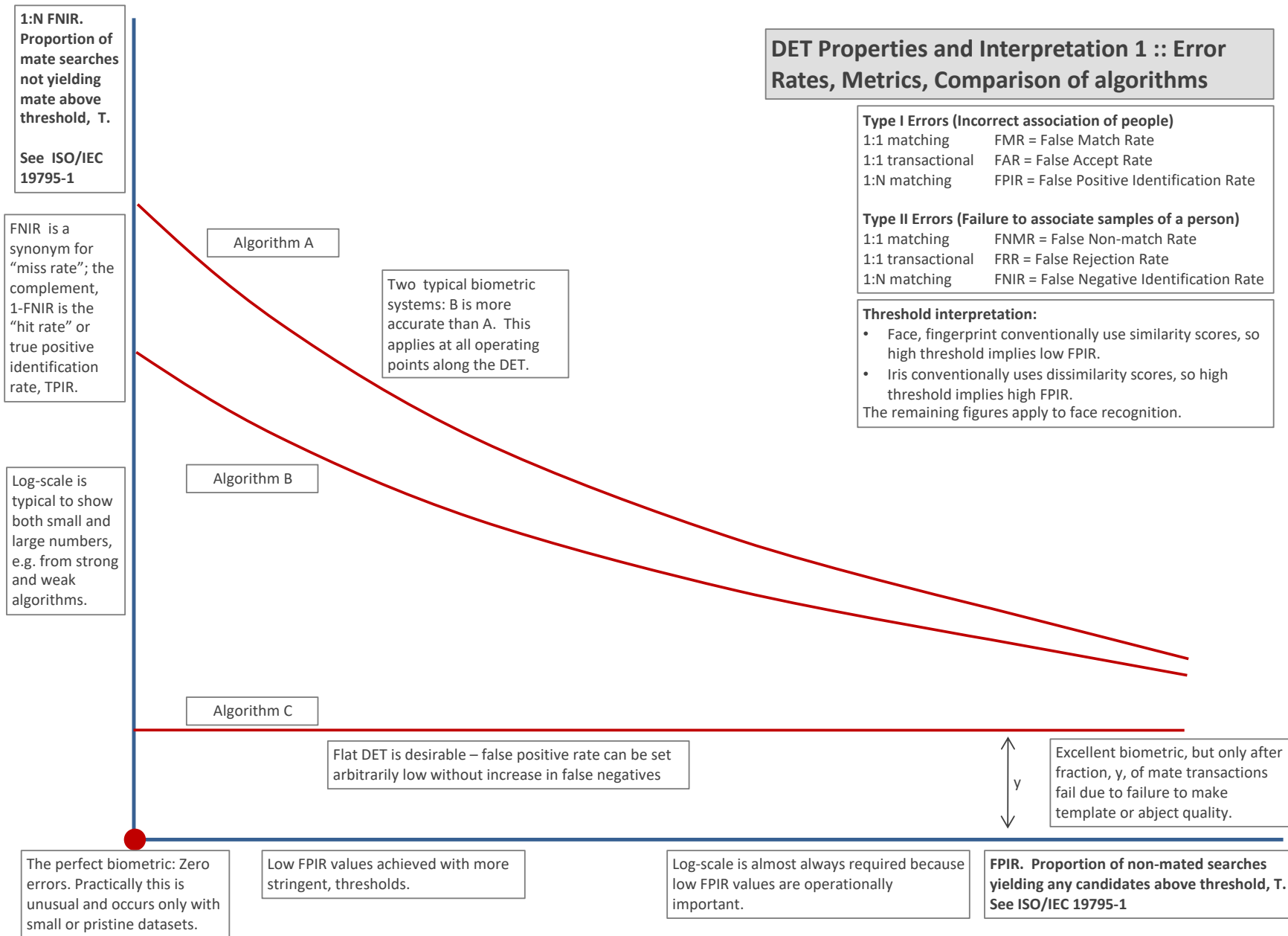


Figure 10: DET as the primary performance reporting mechanism.

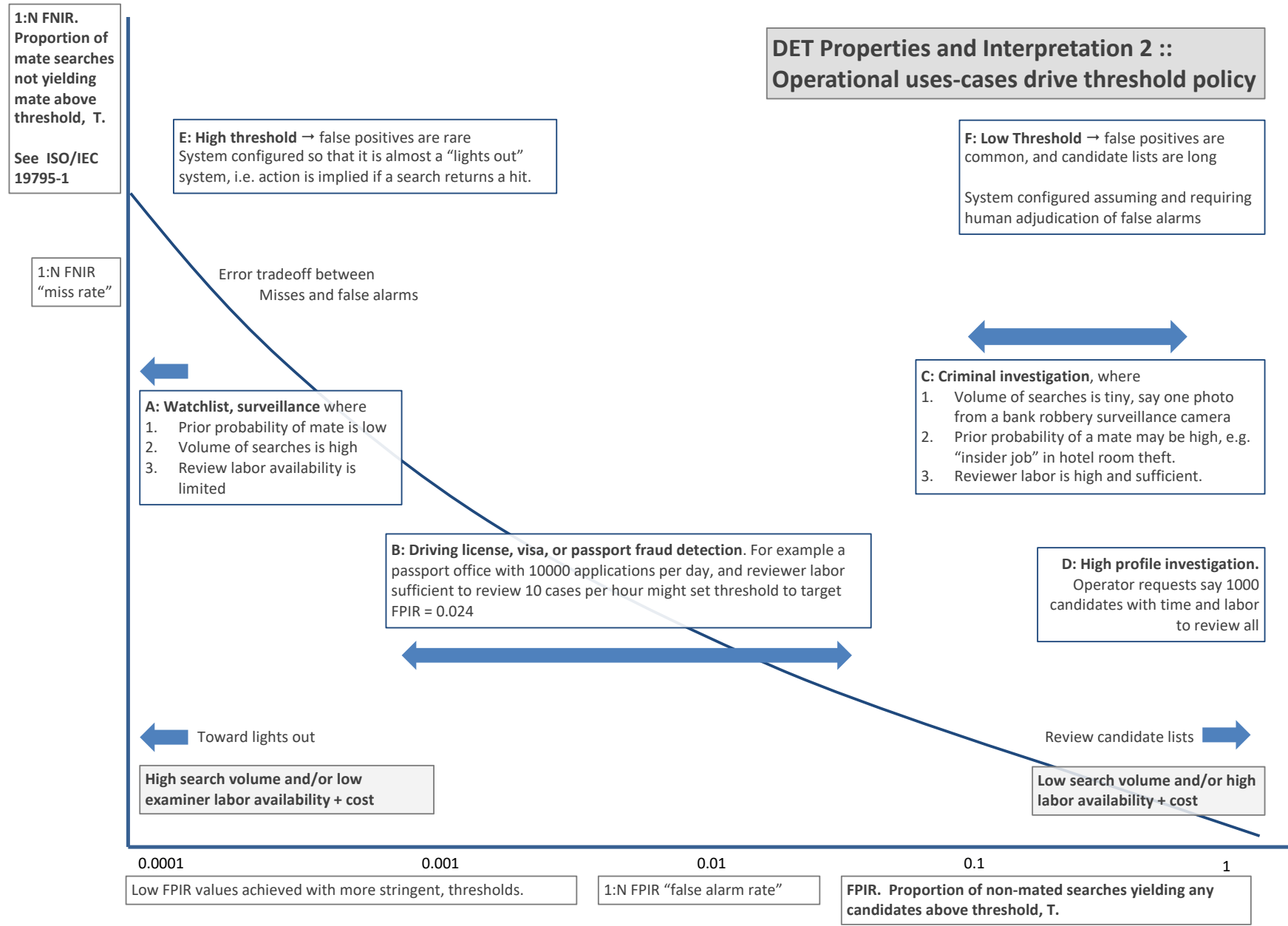
2022/11/09
18:02:21FNIR(N, R, T) = False neg. identification rate
FPIR(N, T) = False pos. identification rate
N = Num. enrolled subjects
R = Num. candidates examinedT = Threshold
T = 0 → Investigation
T > 0 → Identification

Figure 11: DET as the primary performance reporting mechanism.

2022/11/09
18:02:21

$\text{FNIR}(N, R, T) =$ False neg. identification rate
 $\text{FPIR}(N, T) =$ False pos. identification rate

N = Num. enrolled subjects
 R = Num. candidates examined

T = Threshold

$T = 0 \rightarrow$ Investigation
 $T > 0 \rightarrow$ Identification

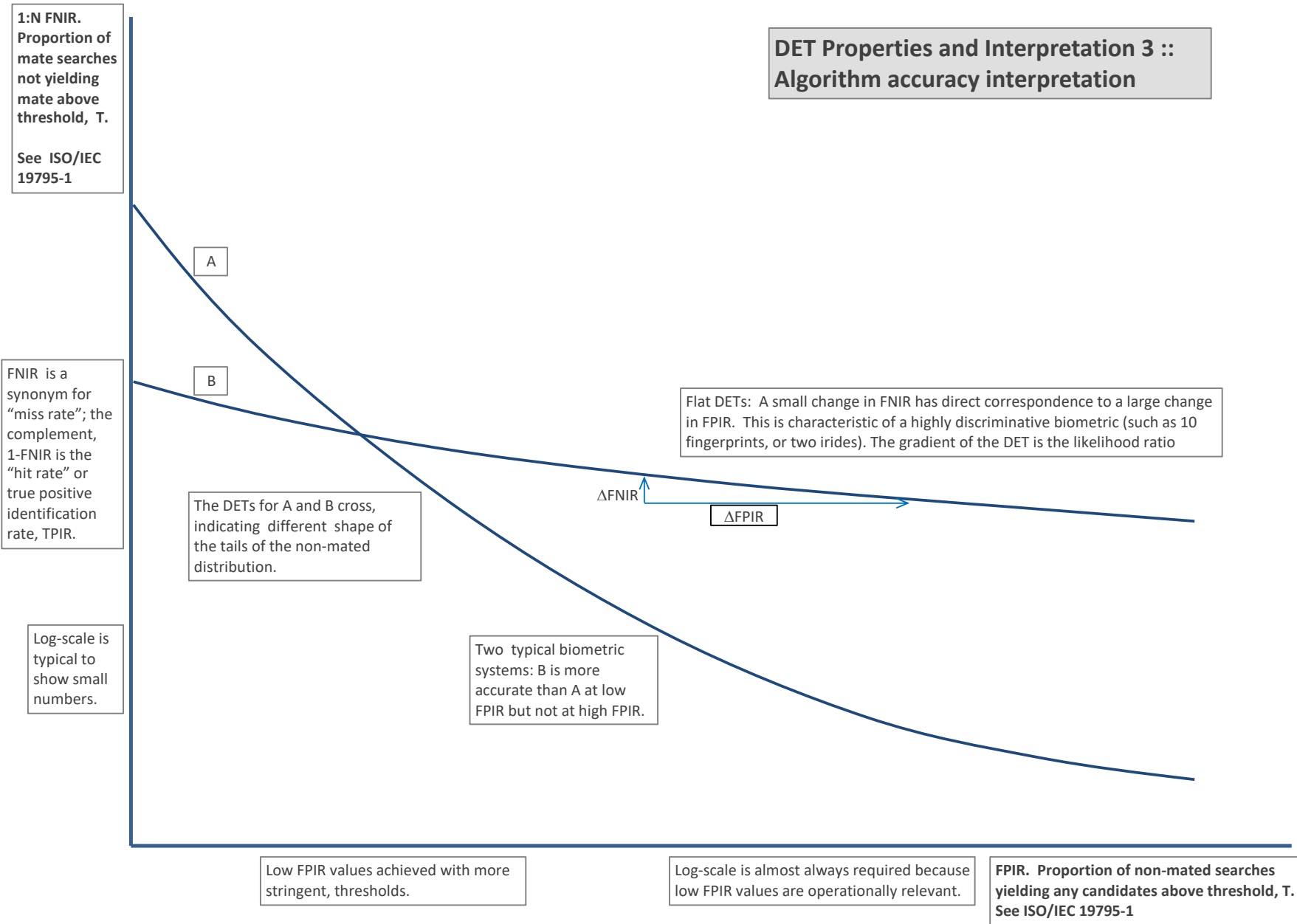


Figure 12: DET as the primary performance reporting mechanism.

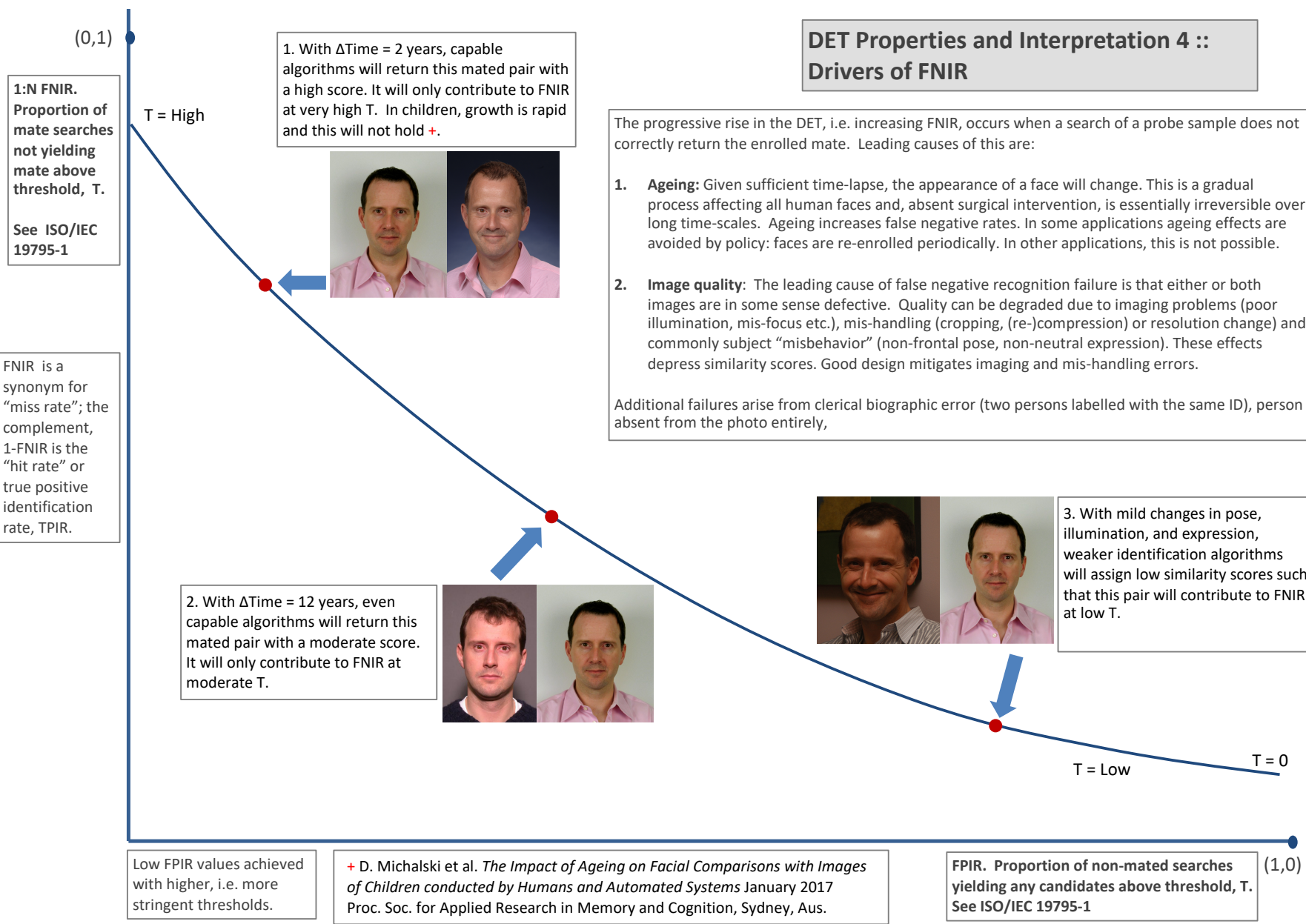


Figure 13: DET as the primary performance reporting mechanism.

2022/11/09
18:02:21

$\text{FNIR}(N, R, T) =$ False neg. identification rate
 $\text{FPIR}(N, T) =$ False pos. identification rate

$N =$ Num. enrolled subjects
 $R =$ Num. candidates examined

$T =$ Threshold
 $T = 0 \rightarrow$ Investigation
 $T > 0 \rightarrow$ Identification

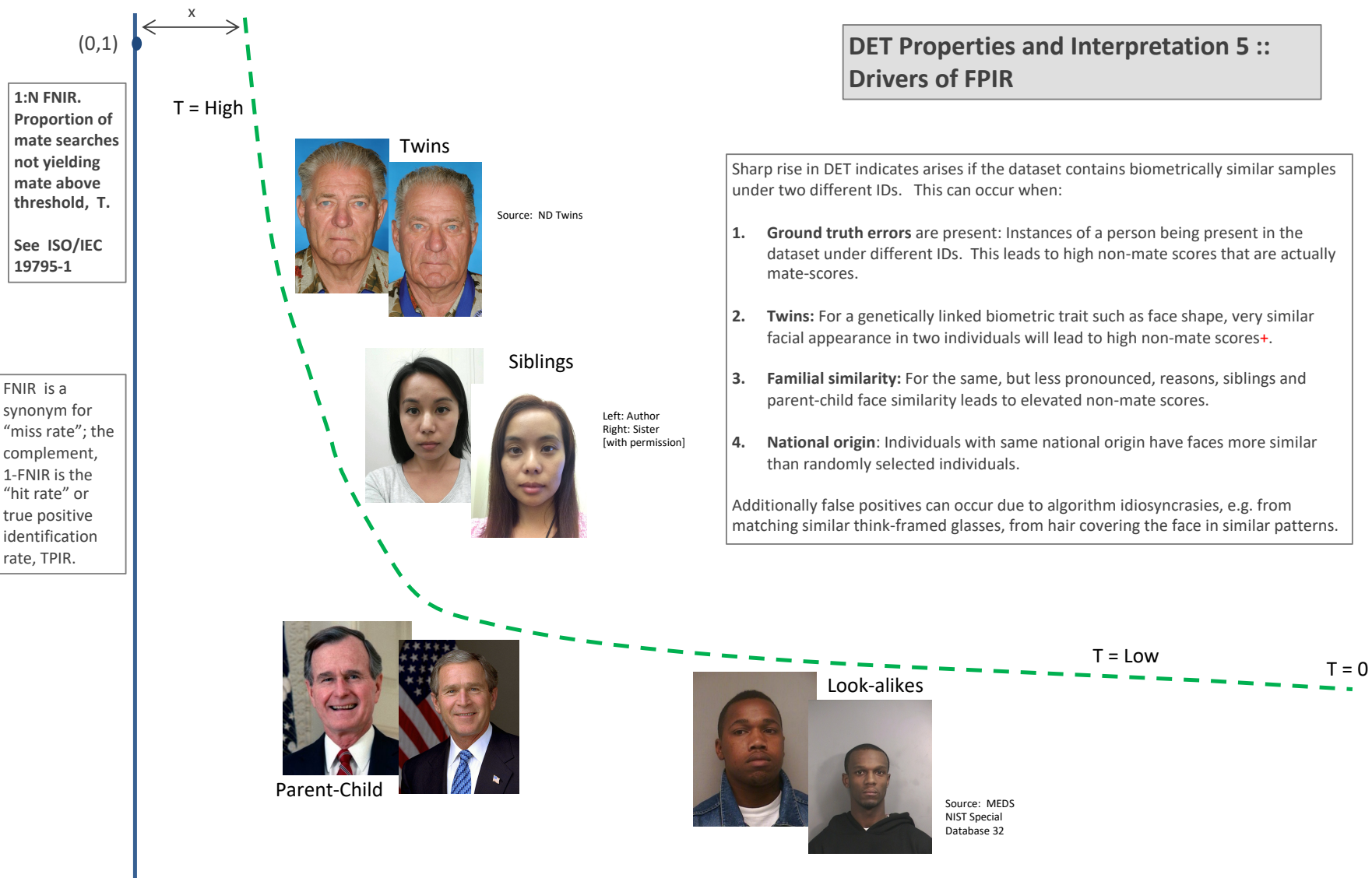


Figure 14: DET as the primary performance reporting mechanism.

2022/11/09
18:02:21

$\text{FNIR}(N, R, T) =$
False neg. identification rate
 $\text{FPIR}(N, T) =$
False pos. identification rate

$N = \text{Num. enrolled subjects}$
 $R = \text{Num. candidates examined}$

$T = \text{Threshold}$

$T = 0 \rightarrow \text{Investigation}$
 $T > 0 \rightarrow \text{Identification}$

1:N FNIR.
Proportion of mate searches not yielding mate above threshold, T .
See ISO/IEC 19795-1

Algorithm X,
Condition 1

Algorithm X,
Condition 2

FNIR is a synonym for "miss rate"; the complement, 1-FNIR is the "hit rate" or true positive identification rate, TPIR.

Log-scale is typical to show small numbers.

If system X is used with images of different properties, say from different imaging systems, or from different populations, generally both FNIR and FPIR will change. The dotted line joins points of the same threshold. Horizontal (vertical) lines indicate change in FPIR (FNIR) only. Two cases concerning population size are shown below (A and B), for the blue curves.

Algorithm Y,
Condition 1

Algorithm Y,
Condition 2

If DETs are computed for two categories (men and women) or (cameras A and B) or (indoor vs. outdoor), generally the Type I and Type II errors will differ and the line of constant threshold will be neither horizontal nor vertical.

The ideal situation in most applications is that a fixed threshold yields a fixed FPIR so that system owners see no change in false alarms across populations or conditions.

Low FPIR values achieved with higher, i.e. more stringent, thresholds.

Log-scale is often required because low FPIR values are operationally relevant.

FPIR. Proportion of non-mated searches yielding any candidates above threshold, T . See ISO/IEC 19795-1

Figure 15: DET as the primary performance reporting mechanism.

1:N FNIR.
Proportion of mate searches not yielding mate above threshold, T.
See ISO/IEC 19795-1

FNIR is a synonym for "miss rate"; the complement, 1-FNIR is the "hit rate" or true positive identification rate, TPIR.

Log-scale is typical to show small numbers.

A: Typical case: In theory, and often in practice, a 1:N search is implemented by executing N 1:1 comparisons independently and then sorting by similarity score:

Mate scores: A mate comparison score is independent of the rest of enrollment data, and so independent of N. This implies the horizontal line above $\text{FNIR}(T, N) = \text{FNMR}(T, 1)$.

Non-mate scores: FPIR increases linearly with N from binomial theory: $\text{FPIR}(N, T) = 1 - (1 - \text{FMR}(T))^N \rightarrow N \text{ FMR}(T)$ for small FPIR.

Pop. N1



Pop. N2 > N1



B: Special case: An enrollment database is not just a linear data structure, it could be an index, or tree, then search is not simply N 1:1 comparisons and a sort. In that case:

Mate scores become dependent on the enrollment data, either its size or actual content, then generally $\text{FNIR}(T, N) \neq \text{FNIR}(T, 1)$.

Non-mate scores are normally no longer just the highest 1:1 comparison score. Instead, for example, scores may be normalized as the implementation attempts to make FPIR independent of N will yield the vertical line linking points of equal threshold.

Low FPIR values achieved with higher, i.e. more stringent, thresholds.

Log-scale is often required because low FPIR values are operationally important.

DET Properties and Interpretation 7 :: Effect of enrolled population size.

DET Properties and Interpretation 8 :: Non-ideal tests, datasets or systems

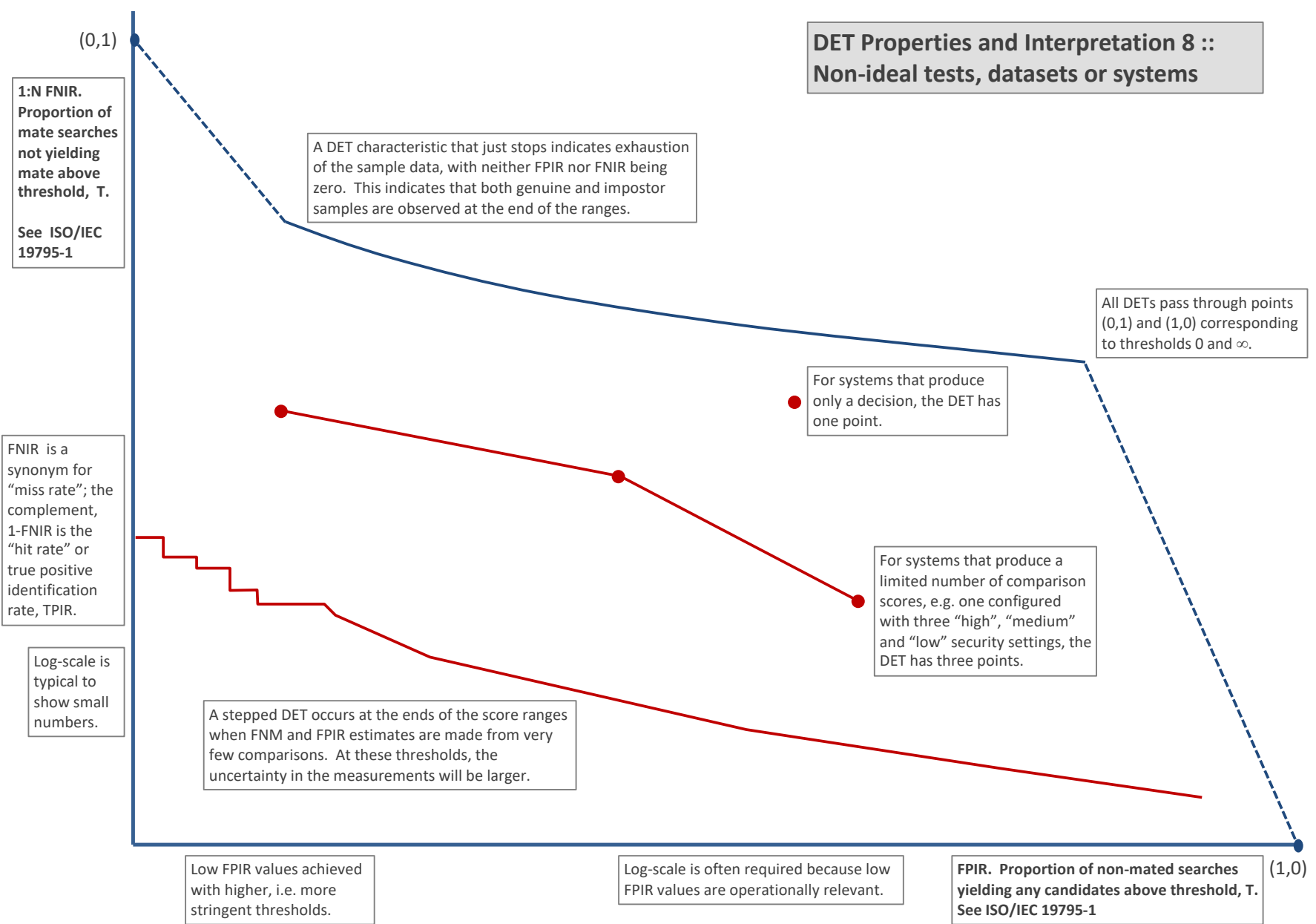


Figure 17: DET as the primary performance reporting mechanism.

3.4 Best practice testing requires execution of searches with and without mates

FRVT embeds 1:N searches of two kinds: Those for which there is an enrolled mate, and those for which there is not. The respective numbers for these types of searches appear in Table 1. However, it is common to conduct only mated searches¹⁰. The cumulative match characteristic is computed from candidate lists produced in mated searches. Even if the CMC is the only metric of interest, the actual trials executed in a test should nevertheless include searches for which no mate exists. As detailed in Table 1 the FRVT reserved disjoint populations of subjects for executing true non-mate searches.

3.5 Failure to extract features

During enrollment some algorithms fail to convert a face image to a template. The proportion of failures is the failure-to-enroll rate, denoted by FTE. Similarly, some search images are not converted to templates. The corresponding proportion is termed failure-to-extract, denoted by FTX.

We do not report FTX because we assume that the same underlying algorithm is used for template generation for enrollment and search.

Failure to extract rates are incorporated into FNIR and FPIR measurements as follows.

- ▷ **Enrollment templates:** Any failed enrollment is regarded as producing a zero length template. Algorithms are required by the API [10] to transparently process zero length templates. The effect of template generation failure on search accuracy depends on whether subsequent searches are mated, or non-mated: Mated searches will fail giving elevated FNIR; non-mated searches will not produce false positives so, to first order, FPIR will be reduced by a factor of $1 - \text{FTE}$.
- ▷ **Search templates and 1:N search:** In cases where the algorithm fails to produce a search template from input imagery, the result is taken to be a candidate list whose entries have no hypothesized identities and zero score. The effect of template generation failure on search accuracy depends on whether searches are mated, or non-mated: Mated searches will fail giving elevated FNIR; Non-mated searches will not produce false positives, so FPIR will be reduced. Thus given a measurement of false negative and positive rates made over only those where failures-to-extract did not occur, those rates - call them FNIR^\dagger and FPIR^\dagger - could be adjusted by an explicit measurement of FTX as follows

$$\text{FNIR} = \text{FTX} + (1 - \text{FTX})\text{FNIR}^\dagger \quad (8)$$

$$\text{FPIR} = (1 - \text{FTX})\text{FPIR}^\dagger \quad (9)$$

This approach is the correct treatment for positive-identification applications such as access control where cooperative users are enrolled and make attempts at recognition. This approach is not appropriate to negative identification applications, such as visa fraud detection, in which hostile individuals may attempt to evade detection by submitting poor quality samples. In those cases, template generation failures should be investigated as though a false alarm had occurred.

¹⁰For example, the [Megaface benchmark](#). This is bad practice for several reasons: First, if a developer knows, or can reasonably assume, that a mate always exists, then unrealistic gaming of the test is possible. A second reason is that it does not put FPIR on equal footing with FNIR and that matters because in most applications, not all searches have mates - not everyone has been previously enrolled in a driving license issuance or a criminal justice system - so addressing between-class separation becomes necessary.

3.6 Fixed length candidate lists, threshold independent workload

Suppose an automated face identification algorithm returns L candidates, and a human reviewer is retained to examine up to R candidates, where $R \leq L$ might be set by policy, preference or labor availability. For now, assume also that the reviewer is not provided with, or ignores, similarity scores, and thresholds are not applied. Given the algorithm typically places mates at low (good) ranks, the number of candidates a reviewer can be expected to review can be derived as follows. Note that the reviewer will:

- ▷ Always inspect the first ranked image Frac. reviewed = 1
- ▷ Then inspect those candidates where mate not confirmed at rank 1 Frac. reviewed = 1-CMC(1)
- ▷ Then inspect those candidates where mate not confirmed at rank 1 or 2 Frac. reviewed = 1-CMC(2)

etc. Thus if the reviewer will stop after a maximum of R candidates, the expected number of candidate reviews is

$$M(R) = 1 + (1 - CMC(1)) + (1 - CMC(2)) + \dots + (1 - CMC(R - 1)) \quad (10)$$

$$= R - \sum_{r=1}^{R-1} CMC(r) \quad (11)$$

A recognition algorithm that front-loads the cumulative match characteristic will offer reduced workload for the reviewer. This workload is defined only over the searches for which a mate exists. In the cases where there truly is no mate, the reviewer would review all R candidates. Thus, if the proportion of searches for which a mate does exist is β , which in the law enforcement context would be the recidivism rate [3], the full expression for workload becomes:

$$M(R) = \beta \left(R - \sum_{r=1}^{R-1} CMC(r) \right) + (1 - \beta)R \quad (12)$$

$$= R - \beta \sum_{r=1}^{R-1} CMC(r) \quad (13)$$

3.7 Timing measurement

Algorithms were submitted to NIST as implementations of the application programming interface(API) specified by NIST in the Evaluation Plan [10]. The API includes functions for initialization, template generation, finalization, search, gallery insert, and gallery delete. Two template generation functions are required, one for the preparation of an enrollment template, and one for a search template.

In NIST's test harness, all functions were wrapped by calls to the C++ std::chrono::high_resolution_clock which on the dedicated timing machine counts 1ns clock ticks. Precision is somewhat worse than that however.

3.8 Uncertainty estimation

3.8.1 Random error

This study leverages operational datasets for measurement of recognition error rates. This affords several advantages. First, large numbers of searches are conducted (see Table 1) giving precision to the measurements. Moreover, for the two mugshot datasets, these do not involve reuse of individuals so binomial statistics can be expected to apply to recognition error counts. In that case, an observed count of a particular recognition outcome (i.e. a false negative or false positive) in M trials will sustain 95% confidence that the actual error rate is no larger than some value.

As an example, the minimum number of mugshot searches conducted in this report is $M = 154\,549$, and for an observed FNIR around 0.002, the measurement supports a conclusion that the actual FNIR is no higher than 0.00228 at 99% confidence level. On the false positive side, we tabulate FNIR at FPIR values as low as 0.001. Given estimates based on 331 254 non-mate trials, the actual FPIR values will be below 0.00115 at 99% confidence. In conclusion, large scale evaluation, without reuse of subjects, supports tight uncertainty bounds on the measured error rates.

3.8.2 Systematic error

The FRVT 2018 dataset includes anomalies discovered as a result of inspecting images involved in recognition failures from the most accurate algorithms. Two kinds of failure occur: False negatives (which, for the purpose here, include failures to make templates) and false positives.

False negative errors: We reviewed 600 false negative pairs for which either or both of the leading two algorithms did not put the correct mate in the top 50 candidates. Given 154 549 searches, this number represents 0.39% of the total, resulting in $\text{FNIR} \sim 0.0039$. Of the 600 pairs:

- ▷ **A: Poor quality:** About 20% of the pairs included images of very low quality, often greyscale, low resolution, blurred, low contrast, partially cropped, interlaced, or noisy scans of paper images. Additionally, in a few cases, the face is injured or occluded by bandages or heavy cosmetics.
- ▷ **B: Ground truth identity label bugs:** About 15% of the pairs are not actually mated. We only assigned this outcome when a pair is clearly not mated.
- ▷ **C: Profile views:** About 35% included an image of a profile (side) view of the face, or, more rarely, an image that was rotated 90 degrees in-plane (roll).
- ▷ **D: Tattoos:** About 30% included an image of a tattoo that contained a face image. These arise from mis-labelling in the parent dataset metadata.
- ▷ **E: Ageing:** There is considerable time-lapse between the two captures.

All these estimates are approximate. Of these, the tattoo and mislabelled images can never be matched. These constitute an accuracy floor in the sample implying that FNIR cannot be below 0.0018¹¹. The profile-views, low-quality images, and images with considerable ageing can, in principle, be successfully matched - indeed some algorithms do so - so are not part of the accuracy floor.

¹¹This value is the sum of two partial false negative rates: $\text{FNIR}_B = 0.15 * 0.0039$ plus $\text{FNIR}_D = 0.3 * 0.0039$

For the microsoft-4 algorithm the lowest miss rate from (recent entry in Table 26) is $\text{FNIR}(640\,000, 50, 0) = 0.0018$. This is close to the value estimated from the inspection of misses. It is below the 0.0039 figure because the algorithm does match some profile and poor quality images, that the yitu-2 algorithm does not.

For many tables (e.g. Table 26), the FNIR values obtained for the FRVT-2018 mugshots could be corrected by reducing them by 0.0018. The best values would then be indistinct from zero. The results in this report *were not* adjusted to account for this systematic error.

False positive errors: As shown in Figure 1 and discussed in Figure 14 many of the DET characteristics in this report exhibit a pronounced turn upward at low false positive rates. The shape can be caused by identity labelling errors in the ground truth of a dataset, specifically persons present in the database under two IDs such that some proportion of non-mate pairs are actually mated. To look for such possibilities, we merged the highest 1000 non-mate pairs produced by three different algorithms which resulted in 1839 unique pairs. This constitutes 0.56% of all non-mate searches. We assert that it is *very* difficult for human reviewers to assign the pairs into the following three categories: twins; doppelgangers; or ground-truth errors (instances of the same person under two IDs). Given this difficulty we made no attempt to correct any possible ground truth errors except by removing 57 pairs in the following categories:

- ▷ **A: Profile views:** Thirteen pairs included one or two profile-view images. As described in Figure 144, these can cause false positives.
- ▷ **B: Same-session photographs:** For twelve pairs, the images were identical or trivially altered (e.g. cropped) versions of the same photo. These were present under a different ID likely due to some clerical or procedural mistake.
- ▷ **C: Tattoos of faces:** There were fourteen instances of tattoo photographs that contained faces causing false matches.
- ▷ **D: T-shirt faces:** There were six instances of T-shirt photographs (of Bob Marley and Che Guevara) being detected instead of the face and causing false positives.
- ▷ **E: Background faces:** There were twelve instances of one subject appearing in the background of two otherwise correct portrait photos.

Note we did not remove any images where there was a chance that the pair was actually a different person.

In any case, the results in this report have not been adjusted for this systematic error.

4 Results

This section gives extensive results for algorithms submitted to FRVT 2018. Three page “report cards” for each algorithm are contained in a [separate supplement](#). Performance metrics were described in section 3. The main results are summarized in tabular form with more exhaustive data included as DET, CMC and related graphs in appendices as follows:

- ▷ The three tables 2-4 list algorithms alongside full developer names, acceptance date, size of the provided configuration data, template size and generation time, and search duration data.
 - The **template generation duration** is most important to applications that require fast response. For example, an eGate taking more than two seconds to produce a template might be unacceptable. Note that GPUs may be of utility in expediting this operation for some algorithms, though at additional expense. Two additional factors should be considered¹²¹³.
 - The **search duration** is the time taken for a search of a search template into a gallery of N enrollment templates. This performance variable, together with the volume of searches, is influential on the amount of hardware needed to sustain an operational deployment. This is measured here with the algorithm running on a single core of a contemporary CPU. Search is most simply implemented as N computations of a distance metric followed by a sort operation to find the closest enrollments. However, considerable optimization of this process is possible, up to and including fast-search algorithms that, by various means, avoid computation of all N distances.
 - The **template size** is the size of the extracted feature vector (or vectors) and any needed header information. Large template sizes may be influential on bus or network bandwidth, storage requirements, and on search duration. While the template itself is an opaque data blob, the feature dimensionality might be estimated by assuming a four-bytes-per-float encoding. There is a wide range of encodings. For the more accurate algorithm, sizes range from 256 bytes to about 2KB bytes, indicating essentially no consensus on face modeling and template design.
 - The **template size multiplier** column shows how, given k input images, the size of the template grows. Most implementations internally extract features from each image and concatenate them, and implement some score-level fusion logic during search. Other implementations, including many of the most accurate algorithms, produce templates whose size does not grow with k . This could be achieved via selection of the best quality image - but this is not optimal in handling ageing where the oldest image could be the best quality. Another mechanism would be feature-level fusion where information is fused from all k inputs. In any case, as a black-box test, the fusion scheme is proprietary and unknown.
 - The size of the **configuration data** is the total size of all files resident in a vendor-provided directory that contains arbitrary read-only files such as parameters, recognition models (e.g caffe). Generally a large value for this quantity may prohibit the use of the algorithm on a resource-constrained device.

¹²The FRVT 2018 API prohibited threading, so some gains from parallelism may be available on multiple-cores or multiple processors, if the feature extraction code could be distributed across them.

¹³Note also that factors of two or more may be realizable by exploiting modern vector processing instructions on CPUs. It is not clear in our measurements whether all developers exploited Intel’s AVX2 instructions, for example. Our machine was so equipped, but we insisted that the same compiled library should also run on older machines lacking that instruction. The more sophisticated implementations may have detected AVX2 presence and branched accordingly. The less sophisticated may be defaulted to the reduced instruction set. Readers should see the FRVT 2018 API document for the specific chip details.

▷ Tables 26-27 report core rank-based accuracy for mugshot images. The population size is limited to $N = 1.6$ million identities because this is the largest gallery size on which all algorithms were executed. Notable observations from these tables are as follows:

- **Accuracy gains since 2018:** NIST Interagency Report 8238 documented massive gains over those reported in the FRVT 2014 report, NIST Interagency Report 8009. Further gains are documented in this report. Comparing the most accurate algorithm in November 2018, NEC-3, the value of $\text{FNIR}(N, L, T)$ reduced from 0.0031 to 0.0024 for the Sensetime-004 algorithm with $N = 12$ million recent images. The tables show broader gains: many developers have made advances since 2018 with between two and five-fold reduction in errors.
- **Wide range in accuracy:** The rank-1 miss rates vary from $\text{FNIR}(N, 1, 0) = 0.0012$ for sensetime-004 up to about 0.5 for the very fast but inaccurate microfocus-x algorithms. Among the developers who are superior to NEC in 2013, the range is from 0.002 to 0.035 for camvi-3. This large accuracy range is consistent with the buyer-beware maxim, and indicates that face recognition software is far from being commoditized.

▷ Tables 31-32 report threshold-based error rates, $\text{FNIR}(N, L, T)$, for $N = 1.6$ million for mugshot-mugshot accuracy on FRVT 2014, FRVT 2018, and also (in pink) mugshot-webcam accuracy using FRVT 2018 enrollments. Notable observations from these tables are as follows:

- **Order of magnitude accuracy gains since 2014:** As with rank-based results, the gains in accuracy are substantial, though somewhat reduced. At $\text{FPIR} = 0.01$, the best improvement over NEC in 2014 is a 27 fold reduction in FNIR using the NEC_2 algorithm. At $\text{FPIR} = 0.001$, the largest gain is a six-fold reduction in FNIR via the NEC_3 algorithm.
- **Broad gains across the industry:** About 19 companies realize accuracy better than the NEC benchmark from 2014. This is somewhat lower than the 28 developers who succeeded on the rank-1 metric. This may be due to the ubiquity of, and emphasis on, the rank-1 metric in many published algorithm development papers.
- **Webcam images:** Searches of webcam images give $\text{FNIR}(N, T)$ values around 2 to 3 times higher than mugshot searches. Notably the leading developers with mugshots are approximately the same with poorer quality webcams. But some developers e.g. Camvi, Megvii, TongYi, and Neurotechnology do improve their relative rankings on webcams, perhaps indicating their algorithms were tailored to less constrained images.

▷ Tables 18, 22, 23 and show, respectively, high-threshold, rank 1, and rank 50 FNIR values for all algorithms performing searches into five different gallery sizes, $N = 640\,000$, $N = 1\,600\,000$, $N = 3\,000\,000$, $N = 6\,000\,000$ and $12\,000\,000$. The $\text{FPIR} = 0.001$ table is included to inform high-volume duplicate detection applications. The Rank-1 table is included as a primary accuracy indicator. The Rank-50 table is included to inform agencies who routinely produce 50 candidates for human-review. The notable results are:

- **Slow growth in rank-based miss rates:** $\text{FNIR}(N, R)$ generally grows as a power law, aN^b . From the straight lines of many graphs of Figure 20 this is clearly a reasonable model for most, but not all, algorithms. The coefficient a can be interpreted as FNIR in a gallery of size 1. The more important coefficient b indicates scalability, and often, $b \ll 1$, implies very benign growth in FNIR. The coefficients of the models appear in the Tables 22 and 23.
- **Slow growth in threshold-based miss rates:** $\text{FNIR}(N, T)$ also generally grows as a power law, aN^b except at the high threshold values corresponding to low FPIR values. This is visible in the plots of Figure 36 which

show straight lines except for $FPIR = 0.001$, which increase more rapidly with N above 3 000 000. Each trace in those figures shows $FNIR(N, T)$ at fixed $FPIR$ with both N and T varying. Thus at large N , it is usually necessary to elevate T to maintain fixed $FPIR$. This causes increased $FNIR$. Why that would no-longer obey a power-law is not known. However, if we expect large galleries to contain individuals with familial relations to the non-mate search images - in the most extreme case, twins - then suppression of false positives becomes more difficult. This is discussed in the Figures starting at Fig. 10

▷ Figure ?? shows false positives from twins against their enrolled siblings, broken out by type of twin: fraternal or identical. The Figure is based on the enrollment of 104 single images on one of a pair of twins, and then the search of 2354 second images. Note that the dataset is heavily skewed towards identical twins which is not representative of the true population. There is also a skew towards same sex fraternal twin pairs compared to different sex fraternal twin pairs again not representative of the true population.

The notable results are:

- For all algorithms tested, the 1087 mated searches (Twin A vs. Twin A) produce scores almost always above typical operational thresholds, with (not shown) matches at rank 1. The images are of good quality, so this is the result expected from the rest of this report.
- For the 1066 identical twin searches (AB), almost all produce the twin at rank 1, with a few producing the mate at further down the candidate lists rank and low score.
- For the 169 fraternal searches (AB) from same sex pairs, most algorithms give a large number of very high scores, implying false positives at all thresholds. However, there are long tails containing lower scores that are correctly below threshold. In general, scores that are higher in this distribution are all rank 1 whereas the lower scores have much higher ranks.
- (Not shown) Of the 169, there are 24 fraternal searches (AB) involving different sex twins. Here most algorithms correctly report scores well below the lowest threshold, and usually not on the candidate list at all.

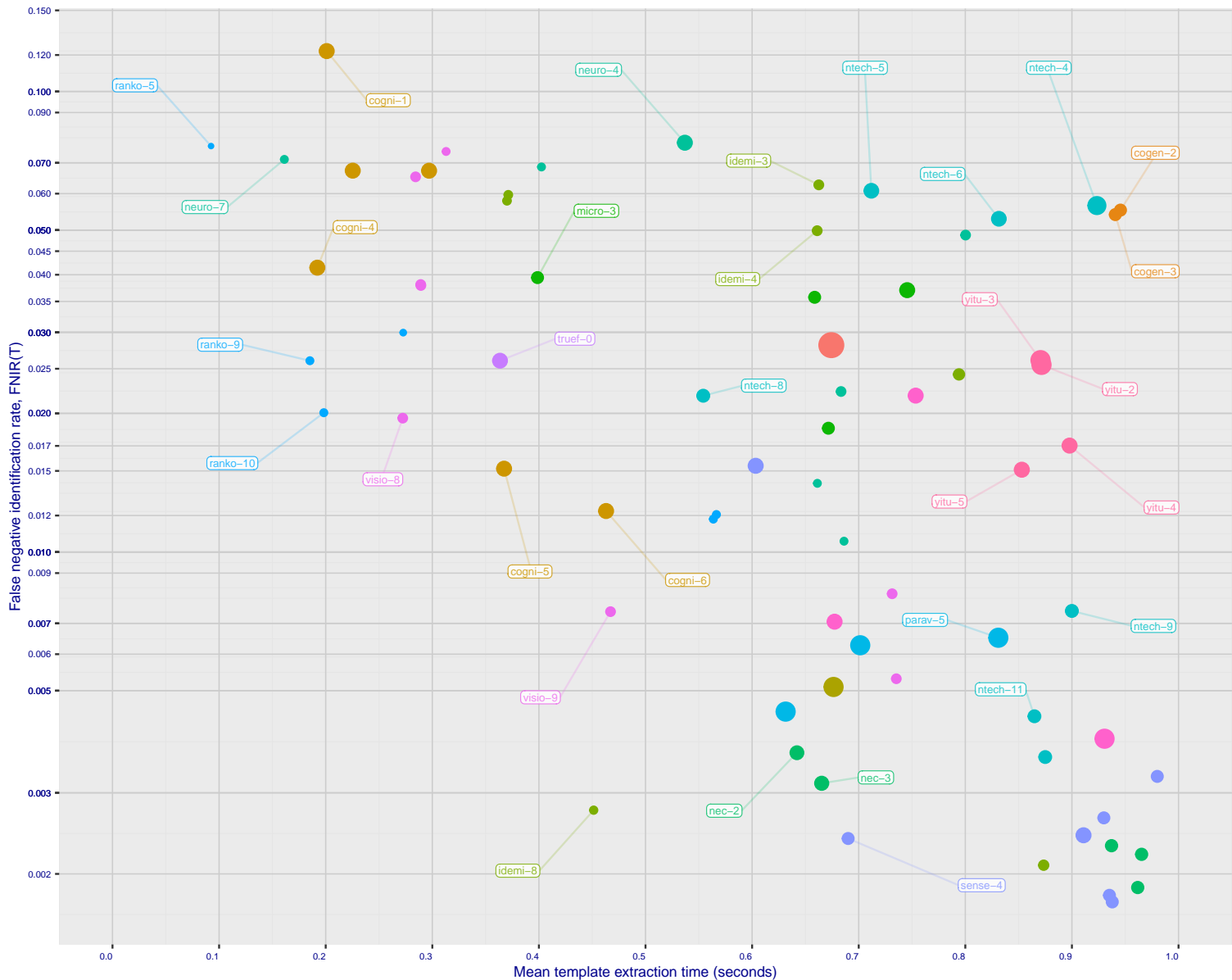
2022/11/09
18:02:21

Figure 18: [Mugshot Dataset] Speed-accuracy tradeoff. For developers of the more accurate algorithms the plot shows the tradeoff of high-threshold recognition miss-rates, $\text{FNIR}(N, N, T)$ for $\text{FPIR}(N, T) = 0.003$, and template generation time. Developers are coded by color. Template size is encoded by the size of the circle. Some labels are quite distant from the respective point, to avoid superposing text. Without any other influences, the assumption would be that taking time to localize the face, and extract features, would lead to better accuracy. The most notable result, for NEC, is that their slower algorithms are much more accurate than the version that extract features in fewer than 90 milliseconds.

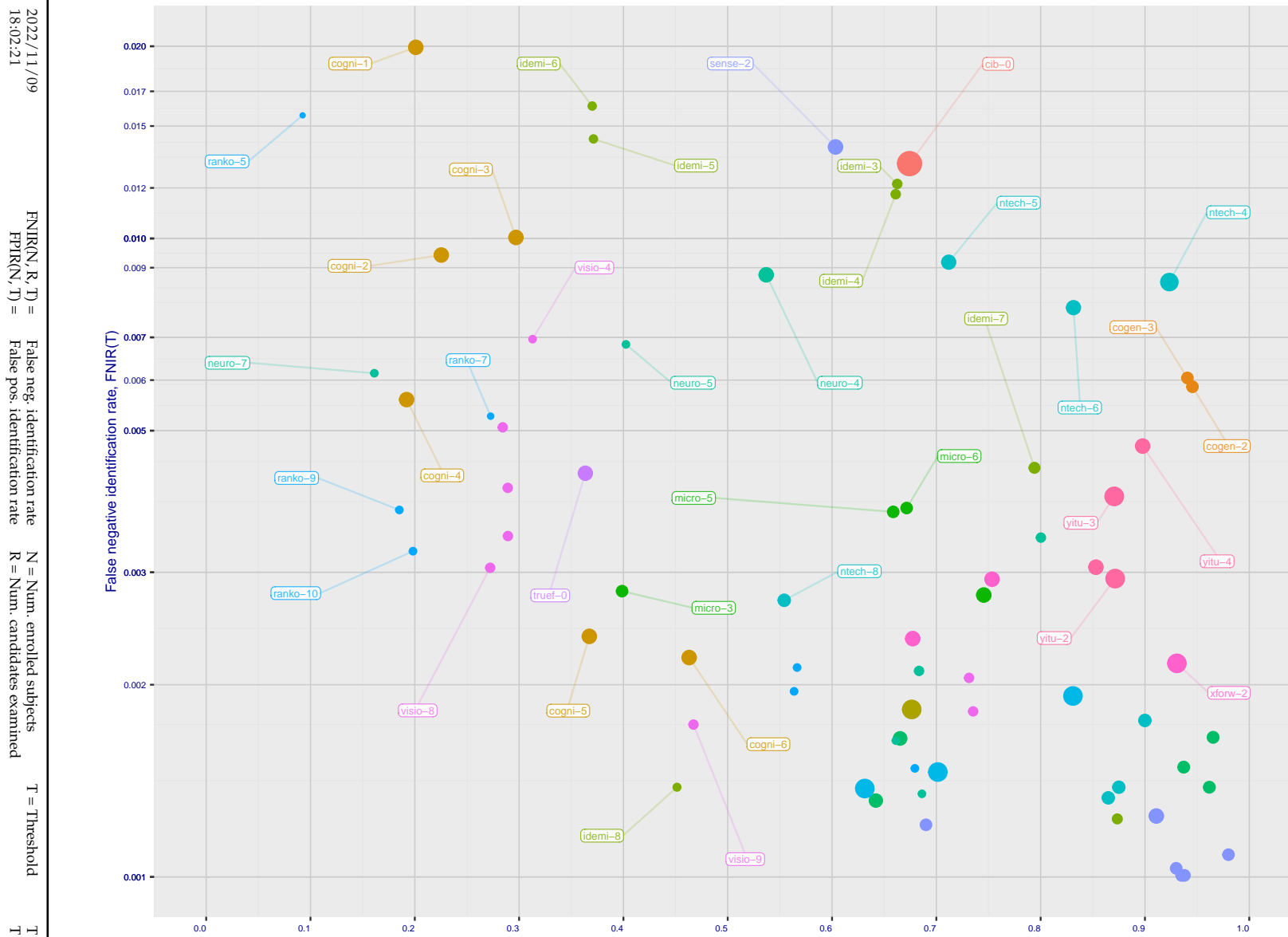


Figure 19: [Mugshot Dataset] Speed-accuracy tradeoff. For developers of the more accurate algorithms the plot shows the tradeoff of rank-one recognition miss-rates, FNIR($N, 1, 0$), and template generation time. Developers are coded by color. Template size is encoded by the size of the circle. Some labels are quite distant from the respective point, to avoid superposing text. Without any other influences, the assumption would be that taking time to localize the face, and extract features, would lead to better accuracy. This occurs for NEC with their slower algorithm being much accurate than the version that extract features in fewer than 90 milliseconds.

	DEVELOPER	SHORT	SEQ.	VALIDATION	CONFIG ¹	LIB ²	TEMPLATE GENERATION			FINALIZE ²	SEARCH DURATION ⁵ MILLISEC														
							DATA (MB)	DATA (MB)	SIZE (B)		N=1.6M	N=1.6M	N=3M	N=6M	N=12M	(μs)									
	FULL NAME	NAME	NUM.	DATE																					
1	20Face	20face	000	2021-10-01	112	319	126	2048	-	21	236	71	9	(231)	6355	6341	-	-	-	-					
2	3Divi	3divi	5	2018-10-26	186	51	223	4096	k	19	638	194	28	(103)	538	(103)	537	(96)	1377	(92)	2614	(87)	5530	169	0.07 N ^{1.1}
3	3Divi	3divi	6	2018-10-26	187	51	41	528	k	120	640	29	5	(16)	33	(15)	33	-	-	-	-	-	-	-	
4	Acer Incorporated	acer	000	2020-08-12	35	67	34	512	-	16	198	19	4	(67)	295	(66)	295	(56)	623	(86)	2302	(79)	4915	200	0.00 N ^{1.3}
5	Acer Incorporated	acer	001	2021-11-08	42	610	115	2048	-	12	184	68	9	(11)	619	(112)	575	-	-	-	-	-	-	-	
6	Akurat Satu Indonesia	ptakuratsatu	000	2020-10-23	0	572	44	538	-	226	905	248	28633	(8)	15	(6)	16	(6)	17	(5)	17	(4)	17	3	6827.74 N ^{0.1}
7	Alchera Inc	alchera	2	2018-10-30	7	14	122	2048	k	6	114	223	63	(206)	2923	(209)	2929	-	-	-	-	-	-	-	
8	Alchera Inc	alchera	3	2018-10-30	251	14	139	2048	k	93	531	226	63	(207)	2955	(210)	2956	(181)	6546	(182)	15013	(182)	35262	195	0.10 N ^{1.2}
9	Alchera Inc	alchera	004	2021-09-17	476	24	140	2048	-	201	853	207	35	(232)	6657	(239)	6851	-	-	-	-	-	-	-	
10	Alivia / Innovation Sys	isystems	3	2018-10-30	350	784	144	2048	1	191	825	157	16	(80)	385	(83)	389	(76)	979	(73)	1822	(118)	9348	201	0.00 N ^{1.3}
11	AllGoVision	allgovidision	000	2019-07-30	168	150	174	2048	k	56	404	102	12	(210)	3226	(213)	3193	(179)	6129	(179)	12449	(178)	25835	101	1.40 N ^{1.0}
12	AllGoVision	allgovidision	001	2020-07-14	283	126	168	2048	-	175	777	108	13	(209)	3174	(212)	3183	(178)	6073	(177)	12284	(177)	25701	99	1.42 N ^{1.0}
13	Anke Investments	anke	0	2018-10-30	779	27	211	2072	k	64	429	154	16	(120)	675	(126)	748	(103)	1483	(101)	2968	(96)	6148	133	0.21 N ^{1.1}
14	Anke Investments	anke	1	2018-10-30	779	27	212	2072	k	65	430	147	15	(125)	707	(129)	769	-	-	-	-	-	-	-	
15	Anke Investments	anke	002	2019-06-27	341	401	204	2056	k	111	623	123	13	(118)	624	(120)	682	(93)	1306	(88)	2403	(84)	5082	91	0.30 N ^{1.0}
16	Aware	aware	5	2018-10-30	368	27	221	3100	k	180	792	206	34	(20)	95	(25)	98	(23)	203	(20)	371	(14)	252	15	4.13 N ^{0.7}
17	Aware	aware	6	2018-10-30	368	27	2	124	k	179	789	42	2	(37)	158	(37)	162	-	-	-	-	-	-	-	
18	Ayonix	ayonix	1	2018-10-29	74	2	67	1036	k	2	12	94	11	(65)	279	(63)	279	-	-	-	-	-	-	-	
19	Ayonix	ayonix	2	2018-10-30	74	2	68	1036	1	1	11	130	14	(66)	279	(61)	276	(45)	535	(45)	1087	(45)	2284	111	0.11 N ^{1.0}
20	Camvi Technologies	camvitech	4	2018-10-30	233	220	56	1024	1	139	686	204	31	(17)	33	(14)	32	(12)	38	(10)	40	(7)	48	4	8492.66 N ^{0.1}
21	Camvi Technologies	camvitech	5	2018-10-30	257	220	51	1024	1	164	751	202	31	(15)	31	(11)	30	-	-	-	-	-	-	-	
22	Canon Inc	cib	000	2020-10-19	426	127	249	8196	-	131	674	232	113	(211)	3589	(215)	3604	(182)	6738	(180)	13495	(179)	27114	34	2.33 N ^{1.0}
23	Canon Inc	canon	001	2021-10-27	1139	91	224	4096	-	216	885	180	21	(234)	6804	(237)	6789	(200)	12741	(196)	25650	(193)	51922	67	3.82 N ^{1.0}
24	Canon Inc	canon	002	2022-04-26	1231	111	243	6200	-	221	897	227	58	(236)	7673	(240)	7559	(202)	14216	(198)	28503	(196)	57633	65	4.35 N ^{1.0}
25	Clearview AI Inc	clearviewai	000	2021-11-12	358	316	228	4096	-	169	765	199	30	(131)	802	(117)	657	(84)	1134	(77)	1939	(71)	3889	21	1.59 N ^{0.9}
26	Cloudwalk - Hengrui AI Technology	hr	000	2021-02-10	501	392	161	2048	-	227	905	140	15	(64)	282	(60)	276	(47)	539	(54)	1268	(63)	3177	173	0.03 N ^{1.1}
27	Cloudwalk - Moontime Smart Technology	cloudwalk	000	2022-01-31	716	573	104	2048	-	208	869	86	10	(91)	440	(79)	371	(49)	547	(44)	1065	(57)	2902	25	0.53 N ^{0.9}
28	Cloudwalk - Moontime Smart Technology	cloudwalk	mtt	2022-07-27	797	574	105	2048	-	242	953	135	14	(58)	273	(90)	427	(65)	784	(65)	1601	(65)	3341	81	0.21 N ^{1.0}
29	Cognitec Systems GmbH	cognitec	2	2018-10-30	463	26	183	2052	k	20	225	189	27	(181)	1733	(183)	1763	(163)	3660	(156)	7279	(152)	13895	96	0.83 N ^{1.0}
30	Cognitec Systems GmbH	cognitec	3	2018-10-30	465	26	191	2052	k	32	297	152	16	(180)	1719	(184)	1791	(159)	3638	(155)	7277	(159)	14904	122	0.66 N ^{1.0}
31	Cognitec Systems GmbH	cognitec	004	2021-03-08	384	60	184	2052	-	15	192	119	13	(179)	1673	(181)	1727	(143)	2904	(143)	5801	(141)	11707	29	1.15 N ^{1.0}
32	Cognitec Systems GmbH	cognitec	005	2021-07-30	460	61	177	2052	-	43	367	73	9	(170)	1556	(172)	1551	(147)	2916	(152)	6561	(153)	13958	139	0.38 N ^{1.1}
33	Cognitec Systems GmbH	cognitec	006	2022-02-10	689	61	185	2052	-	76	463	81	10	(146)	1006	(145)	1002	(121)	2097	(117)	4312	(107)	7624	131	0.30 N ^{1.1}
34	Cubox	cubox	000	2021-08-24	529	298	165	2048	-	230	917	82	10	(212)	3646	(217)	4076	(184)	7605	(183)	15871	-	-	132	1.16 N ^{1.1}
35	Cyberlink Corp	cyberlink	000	2019-06-12	217	93	182	2052	1	124	654	198	30	(122)	696	(122)	701	(97)	1379	(93)	2639	(98)	6214	115	0.28 N ^{1.0}
36	Cyberlink Corp	cyberlink	001	2019-10-07	459	102	180	2052	1	62	423	195	28	(123)	698	(121)	700	(99)	1350	(141)	5524	(144)	12031	199	0.00 N ^{1.3}
37	Cyberlink Corp	cyberlink	002	2020-07-31	333	109	241	4140	-	155	724	238	6875	(167)	1353	(214)	3198	(180)	6138	(176)	12205	(150)	13106	19	16.71 N ^{0.8}
38	Cyberlink Corp	cyberlink	003	2021-01-05	333	100	244	6212	-	142	691	211	35	(95)	488	(123)	723	(100)	1415	(99)	2886	(89)	5643	153	0.12 N ^{1.1}
39	Cyberlink Corp	cyberlink	004	2021-07-16	371	100	246	6212	-	157	728	184	23	(97)	492	(100)	504	(74)	923	(61)	1448	(66)	3350	24	0.73 N ^{0.9}
40	Cyberlink Corp	cyberlink	005	2022-01-07	371	100	245	6212	-	159	733	201	30	(99)	501	(96)	498	(89)	1193	(94)	2672	(91)	5693	190	0.03 N ^{1.2}
41	DAON	daon	000	2021-12-23	274	2	208	2069	-	101	583	51	8	(102)	524	(116)	625	(101)	1454	(104)	3097	(100)	6316	191	0.03 N ^{1.2}
42	Dahua Technology Co Ltd	dahua	0	2018-10-29	276	167	160	2048	k	48	374	182	22	-	(58)	258	-	-	-	-	-	-	-		
43	Dahua Technology Co Ltd	dahua	1	2018-10-29	276	167	135	2048	k	44	369	191	28	-	(56)	257	(54)	602	(51)	1202	(60)	3007	180	0.02 N ^{1.2}	
44	Dahua Technology Co Ltd	dahua	002	2019-12-02	607	137	113	2048	k	137	685	171	19	(50)	243	(50)	269	(87)	1189	(100)	2950	(104)	6732	205	0.00 N ^{1.5}
45	Dahua Technology Co Ltd	dahua	003	2020-11-18	889	154	163	2048	-	154	723	168	16	(65)	283	(54)	249	(41)	468	(41)	935	(39)	1871	36	0.16 N ^{1.0}
46	Dahua Technology Co Ltd	dahua	004	2021-11-18	812	116	166	2048	-	167	758	88	11	(88)	423	(87)	411	(71)	871	(64)	1568	(62)	3174	103	0.17 N ^{1.0}
47	Decatur Industries Inc	decatur	000	2022-02-09	411	383	187	2052	-	204	863	75	182	(182)	1761	(191)	2023	(154)	3361	(157)</					

	DEVELOPER	SHORT	SEQ.	VALIDATION	CONFIG ¹	LIB ¹	TEMPLATE GENERATION			FINALIZE ²	SEARCH DURATION ³ MILLISEC						
							DATA (MB)	DATA (MB)	SIZE (B)		N=1.6M	N=1.6M	N=1.6M	N=3M	N=6M	N=12M	
	FULL NAME	NAME	NUM.	DATE	DATA (MB)	SIZE (B)	MULT	TIME (MS)	TIME (S)	N=1.6M	N=1.6M	N=1.6M	N=3M	N=6M	N=12M	(μs)	
53	Dermalog	dermalog	009	2021-11-09	0	318	32512	-	39347	153	(55) 253	(51) 246	(39) 461	(39) 923	(37) 1846	³⁸ 0.16 N ^{1.0}	
54	Dermalog	dermalog	010	2022-07-25	0	514	35512	-	115633	173	(49) 241	(49) 242	(38) 454	(38) 910	(36) 1823	⁴¹ 0.15 N ^{1.0}	
55	Digidata	digidata	000	2022-06-03	248	33	1302048	-	96560	235	2444	(2) 0	(20) 95	-	-	-	
56	DiluSense Technology	dilusense	000	2022-05-26	311	56	1412048	-	24247	188	26	(186) 1904	(186) 1898	(158) 3597	(154) 7256	(157) 14689	⁹⁰ 0.88 N ^{1.0}
57	FarBar Inc	f8	001	2019-10-03	266	19	1612048	k	18810	12	14	-	-	-	-	-	
58	Fincore Ltd	fincore	000	2021-08-18	250	224	1082048	-	79475	62	9	(111) 562	(108) 560	-	-	-	
59	Fujitsu Research and Development Center	fujitsulab	000	2021-10-12	497	337	641032	-	23945	31	5	(178) 1668	(176) 1657	(151) 3140	(148) 6320	(147) 12723	⁸⁸ 0.78 N ^{1.0}
60	Fujitsu Research and Development Center	fujitsulab	001	2022-03-15	675	386	621032	-	215882	63	9	(184) 1854	(185) 1817	(155) 3451	(153) 6986	(154) 14166	¹⁰⁷ 0.72 N ^{1.0}
61	Gorilla Technology	gorilla	2	2018-10-29	91	1252	761132	k	38338	186	24	(35) 145	(35) 146	(29) 293	(28) 612	(30) 1509	¹⁵⁹ 0.02 N ^{1.1}
62	Gorilla Technology	gorilla	3	2018-10-26	94	1252	2142156	k	95559	242	12020	-	(192) 2047	-	-	-	
63	Gorilla Technology	gorilla	004	2020-01-06	182	1244	2152192	k	51388	213	41	(66) 286	(65) 285	(88) 1191	(89) 2416	(83) 5036	¹⁹⁸ 0.00 N ^{1.3}
64	Gorilla Technology	gorilla	005	2021-02-22	306	1420	2476288	-	83483	228	78	(130) 802	(130) 799	(105) 1514	(120) 4454	(114) 8820	¹⁸³ 0.05 N ^{1.2}
65	Gorilla Technology	gorilla	006	2021-09-30	377	691	2508336	-	170767	231	99	(174) 1626	(173) 1612	(131) 2422	(119) 4422	(119) 9363	⁸⁷ 0.59 N ^{1.0}
66	Gorilla Technology	gorilla	007	2022-02-16	392	322	2486290	-	91526	230	89	(128) 765	(125) 745	(99) 1408	(98) 2823	(92) 5764	⁶⁸ 0.42 N ^{1.0}
67	Griaule	griaule	000	2021-11-01	0	584	1812052	-	61417	45	8	(226) 5827	(230) 6150	(192) 11473	(190) 22952	(187) 46700	³⁵ 3.89 N ^{1.0}
68	Griaule	griaule	001	2022-07-26	0	615	1942052	-	2501102	97	12	(227) 5866	(231) 6181	(194) 11629	(191) 23175	(188) 46504	⁵⁷ 3.74 N ^{1.0}
69	Guangzhou Pixel Solutions Co Ltd	pixelall	002	2019-07-01	0	165	2102560	k	14190	144	15	(164) 1296	(166) 1334	(138) 2526	(133) 5136	(137) 11045	¹¹² 0.52 N ^{1.0}
70	Guangzhou Pixel Solutions Co Ltd	pixelall	003	2019-11-05	0	690	2172560	k	148703	185	22	(161) 1273	(162) 1307	(135) 2474	(134) 5198	(138) 11141	¹²² 0.46 N ^{1.0}
71	Guangzhou Pixel Solutions Co Ltd	pixelall	004	2020-07-02	0	538	2192560	k	67449	165	17	(160) 1259	(161) 1300	(134) 2465	(139) 5492	(139) 11443	¹³⁸ 0.34 N ^{1.1}
72	Guangzhou Pixel Solutions Co Ltd	pixelall	005	2021-03-23	0	717	2182560	-	197840	92	11	(172) 1606	(171) 1528	(140) 2609	(130) 4926	(142) 11770	⁷⁰ 0.73 N ^{1.0}
73	Hangzhou Allu Network Information Technology	hzailu	000	2022-03-18	855	97	531024	-	122649	93	11	(203) 2609	(207) 2551	(176) 4813	(174) 9702	(173) 19338	⁶⁰ 1.50 N ^{1.0}
74	Hangzhou Allu Network Information Technology	hzailu	001	2022-08-18	273	162	1022048	-	172777	99	12	(215) 4537	(221) 4637	(187) 8666	(185) 17109	(184) 39805	¹¹⁴ 1.79 N ^{1.0}
75	Hikvision Research Institute	hikvision	5	2018-10-29	593	9	811408	1	106607	150	16	(139) 883	(140) 895	(116) 1908	(110) 3792	(121) 9387	¹⁷⁰ 0.10 N ^{1.1}
76	Hikvision Research Institute	hikvision	6	2018-10-29	593	9	821408	1	108598	153	16	(137) 871	(139) 877	-	-	-	-
77	HyperVerge Inc	hyperverge	001	2021-08-11	1791	212	571024	-	200845	27	5	(124) 705	(119) 681	(94) 1346	(95) 2681	(90) 5680	⁹⁸ 0.32 N ^{1.0}
78	HyperVerge Inc	hyperverge	002	2022-04-13	1140	1118	521024	-	233934	67	9	(119) 661	(118) 659	(92) 1292	(82) 2188	(43) 2181	¹⁷ 11.29 N ^{0.8}
79	Idemia	idemia	5	2018-10-29	417	48	24352	1	47371	25	5	(31) 137	(32) 138	(39) 437	(33) 724	(32) 1630	¹⁹⁷ 0.01 N ^{1.2}
80	Idemia	idemia	6	2018-10-29	417	48	25352	1	45370	25	4	(32) 137	(31) 138	(36) 442	(36) 827	(33) 1646	¹⁹⁴ 0.01 N ^{1.2}
81	Idemia	idemia	007	2020-01-17	738	113	50860	1	181794	128	14	(36) 151	(36) 152	(60) 683	(63) 1481	(61) 3022	²⁰³ 0.00 N ^{1.4}
82	Idemia	idemia	008	2021-03-15	378	65	23300	-	69451	16	3	(30) 132	(30) 131	(26) 247	(25) 501	(24) 1013	⁷¹ 0.07 N ^{1.0}
83	Idemia	idemia	009	2022-03-01	735	68	48636	-	210873	39	7	(45) 211	(44) 205	(34) 389	(35) 787	(31) 1615	⁹³ 0.10 N ^{1.0}
84	Imagus Technology Pty Ltd	imagus	005	2021-01-15	222	311	1282048	-	178786	126	14	(48) 236	(69) 313	(57) 651	(58) 1361	(48) 2461	¹⁶⁸ 0.03 N ^{1.1}
85	Imagus Technology Pty Ltd	imagus	006	2021-05-27	248	369	1662048	-	229904	76	9	(71) 317	(47) 234	(43) 499	(55) 1273	(52) 2727	¹⁸⁹ 0.01 N ^{1.2}
86	Imagus Technology Pty Ltd	imagus	007	2021-11-16	248	366	1712048	-	102609	57	9	(47) 234	(48) 238	(37) 442	(37) 881	(35) 1765	³⁰ 0.16 N ^{1.0}
87	Imagus Technology Pty Ltd	imagus	008	2022-05-26	204	335	1592048	-	66445	163	17	(109) 560	(111) 565	-	-	-	-
88	Imperial College London	imperial	000	2019-08-28	461	15	1162048	1	100577	107	13	(77) 360	(82) 379	(109) 1626	(114) 4057	(135) 10291	²⁰⁶ 0.00 N ^{1.5}
89	Incode Technologies Inc	incode	2	2018-10-29	71	31	1342048	1	31289	149	15	(86) 411	(84) 404	-	-	-	-
90	Incode Technologies Inc	incode	3	2018-10-29	133	31	1362048	1	145697	139	15	(88) 408	(88) 412	(67) 847	(66) 1608	(77) 4486	¹⁶³ 0.05 N ^{1.1}
91	Incode Technologies Inc	incode	004	2019-06-24	254	50	1492048	1	80475	98	12	(78) 365	(81) 378	(102) 1482	(68) 1660	(59) 2954	¹³⁶ 0.12 N ^{1.1}
92	Incode Technologies Inc	incode	005	2021-07-29	259	21	1272048	-	85500	81	10	(70) 316	(93) 454	(72) 890	(74) 1843	(69) 3640	¹⁵³ 0.07 N ^{1.1}
93	Innovatrics	innovatrics	4	2018-10-30	0	400	721076	k	52399	239	10902	(7) 8	(4) 8	(4) 11	(2) 9	(3) 13	⁹ 668.38 N ^{0.2}
94	Innovatrics	innovatrics	005	2019-09-30	0	455	43538	1	193827	241	11897	(6) 8	(5) 8	(3) 9	(3) 9	(2) 9	¹ 4055.65 N ^{0.1}
95	Innovatrics	innovatrics	007	2021-08-16	175	58	42538	-	173777	129	14	(25) 97	(27) 100	(20) 188	(22) 378	(21) 788	²⁶ 0.09 N ^{1.0}
96	Intellivision	intellivision	001	2022-03-08	62	130	1992056	-	58406	177	20	(81) 388	(80) 377	-	-	-	-
97	Intellivision	intellivision	002	2022-07-28	114	128	2052056	-	34331	113	13	(242) 20542	(247) 20448	-	-	-	-
98	Intema-LGL Group	intema	000	2022-08-24	1042	20	28512	-	162737	246	13809	(14) 27	(12) 31	(10) 36	(12) 44	(10) 54	¹¹ 791.50 N ^{0.3}
99	IrexAI	irex	000	2021-02-09	724	46	2203080	-	198444	173	19	(116) 616	(113) 600	(83) 1120	(91) 2477	(93) 5863	¹⁴⁰ 0.13 N ^{1.1}
100	Kakao Enterprise	kakao	000	2021-06-23	404	124	1882052	-	196835	42	8	(46) 213	(45) 215	(44) 510	(42) 971	(40) 1955	¹⁴⁷ 0.05 N ^{1.1}
101	Kakao Enterprise	kakao	001	2022-06-08	615	102	1382048	-	245961	167	18	(93) 469	(94) 471	(75) 952	(76) 1887	(70) 3870	¹⁴⁰ 0.11 N ^{1.1}
102	Kedacom International Pte	kedacom	001	2019-09-16	239	36	22292	1	88507	6	2	(127) 764	(127) 760	(117) 1940	(102) 2983	(103) 6623	¹¹⁸ 0.31 N ^{1.0}
103	Kneron	kneron	000	2020-03-03	366	13	1432048	k	90523	112	13	(202) 2535	(205) 2506	(175) 4752	(173) 9696	(175) 20926	¹¹⁹ 0.95 N ^{1.0}
104	Kneron	kneron	001	2021-06-10	270	69	1172048	-	78472	64	9	(204) 2690	(208) 2642	-	-	-	-

|
<td data-cs="17" data-kind="parent
| |

DEVELOPER	SHORT NAME	SEQ. NUM.	VALIDATION DATE	CONFIG ¹	LIB ¹	TEMPLATE GENERATION TIME (MS) ⁴	FINALIZE ² TIME (S)	SEARCH DURATION ⁵ MILLISEC													
								L=1	L=50	L=50	L=50	L=50	POWER LAW								
								N=1.6M	N=1.6M	N=1.6M	N=3M	N=6M	N=12M								
105	Line Corporation	line	000	2021-06-02	138	397	173	2048	-	82	481	52	8	(221) 5433	(225) 5418	(190) 10144	-	-	33	3.65N ^{1.0}	
106	Line Corporation	line	001	2021-11-21	471	396	175	2048	-	228	907	53	8	(185) 1872	(189) 1934	(160) 3647	(161) 7675	-	126	0.64N ^{1.0}	
107	Line Corporation	lineclova	002	2022-07-29	560	72	107	2048	-	190	824	115	13	(56) 262	(57) 257	(42) 488	(43) 977	(41) 1963	61	0.15N ^{1.0}	
108	Lomonosov Moscow State University	intsysmsu	000	2019-08-19	375	168	147	2048	1	109	614	118	13	(89) 430	(91) 431	(70) 860	(69) 1730	(86) 5353	178	0.03N ^{1.1}	
109	Lookman Electoplast Industries	lookman	3	2018-10-28	203	24	21	292	1	37	336	14	3	(126) 739	(124) 745	(98) 1394	(97) 2817	(109) 8286	156	0.13N ^{1.1}	
110	Lookman Electoplast Industries	lookman	4	2018-10-28	184	24	48	548	1	33	320	24	4	(144) 981	(144) 998	-	-	-	-	-	
111	Lookman Electoplast Industries	lookman	005	2019-09-16	239	36	45	548	1	86	506	20	4	(145) 1005	(146) 1008	(139) 2597	(138) 5446	(115) 8939	154	0.19N ^{1.1}	
112	Mantra Softech India	mantra	000	2021-10-28	460	61	192	2052	-	60	412	80	10	(141) 916	(141) 910	(111) 1714	(109) 3411	(105) 6841	39	0.57N ^{1.0}	
113	Maxvision	maxvision	000	2022-06-17	167	60	167	2048	-	11	183	1	-	(220) 5044	(224) 5188	(189) 9663	(188) 19358	(183) 39552	89	2.41N ^{1.0}	
114	Maxvision	maxvision	001	2022-10-28	228	63	114	2048	-	71	457	114	13	(155) 1173	(155) 1177	(125) 2233	(124) 4589	(120) 9371	72	0.65N ^{1.0}	
115	Megvii/Face++	megvii	1	2018-10-28	1703	41	231	4096	1	113	631	205	32	(106) 552	(109) 561	(91) 1222	(87) 2321	(94) 5968	162	0.08N ^{1.1}	
116	Megvii/Face++	megvii	2	2018-10-28	1735	42	229	4096	1	117	635	203	31	(107) 553	(106) 558	-	-	-	-	-	
117	MicroFocus	microfocus	5	2018-10-29	94	26	7	256	k	25	262	9	2	(42) 182	(41) 186	(32) 354	(32) 708	(28) 1425	63	0.11N ^{1.0}	
118	MicroFocus	microfocus	6	2018-10-29	94	26	14	256	k	26	262	11	2	(43) 183	(40) 186	-	-	-	-	-	
119	Microsoft	microsoft	5	2018-10-29	381	155	54	1024	1	125	658	95	11	(171) 1606	(177) 1673	(150) 3076	(147) 6302	(151) 13160	85	0.79N ^{1.0}	
120	Microsoft	microsoft	6	2018-10-29	478	155	55	1024	1	129	671	143	15	(175) 1642	(175) 1618	(162) 3710	(150) 6401	(149) 12892	106	0.68N ^{1.0}	
121	N-Tech Lab	ntech	5	2018-10-30	1685	113	93	1940	k	152	711	225	55	(52) 243	(53) 246	(46) 538	(46) 1100	(59) 2867	174	0.05N ^{1.1}	
122	N-Tech Lab	ntech	6	2018-10-30	1686	117	94	1940	k	195	831	224	63	(51) 243	(52) 246	(48) 546	(47) 1104	(56) 2873	176	0.02N ^{1.1}	
123	N-Tech Lab	ntechlab	007	2019-06-25	2450	51	222	3348	k	182	795	227	73	(82) 393	(89) 427	(64) 780	(72) 1768	(68) 3499	116	0.16N ^{1.0}	
124	N-Tech Lab	ntechlab	008	2020-01-06	1111	51	79	1300	k	94	554	212	36	(41) 179	(38) 184	(31) 341	(31) 683	(27) 1395	54	0.11N ^{1.0}	
125	N-Tech Lab	ntechlab	009	2021-03-01	1208	42	80	1300	-	223	899	210	35	(40) 178	(39) 184	(30) 336	(30) 676	(34) 1704	137	0.05N ^{1.1}	
126	N-Tech Lab	ntechlab	010	2021-06-24	351	213	78	1280	-	211	874	32	6	(90) 440	(92) 435	(66) 821	(67) 1645	(64) 3337	79	0.22N ^{1.0}	
127	N-Tech Lab	ntechlab	011	2021-12-07	679	208	77	1280	-	205	864	34	6	(96) 488	(95) 483	(73) 912	(75) 1869	(81) 5003	158	0.07N ^{1.1}	
128	NEC	nec	2	2018-10-30	705	35	89	1616	k	121	642	170	18	(83) 409	(86) 408	(101) 1072	(70) 1755	(76) 4255	165	0.06N ^{1.1}	
129	NEC	nec	3	2018-10-30	774	110	90	1712	k	127	665	178	21	(5)	(7)	(5)	(4)	(11) 82	184	0.00N ^{1.2}	
130	NEC	nec	004	2021-07-19	971	63	75	1104	-	246	965	35	7	(74) 349	(74) 351	(58) 662	(56) 1330	(50) 2685	66	0.20N ^{1.0}	
131	NEC	nec	005	2021-12-13	922	88	74	1104	-	244	961	36	7	(94) 473	(104) 551	(79) 1017	(80) 2091	(74) 4242	76	0.28N ^{1.0}	
132	NEC	nec	006	2022-08-10	701	54	73	1104	-	235	937	61	9	(75) 358	(75) 354	(59) 666	(57) 1331	(51) 2707	56	0.21N ^{1.0}	
133	Neurotechnology	neurotech	5	2018-10-30	266	53	12	256	k	54	402	10	2	(134) 835	(136) 839	(110) 1690	(108) 3219	(116) 8955	144	0.19N ^{1.1}	
134	Neurotechnology	neurotech	6	2018-10-30	564	53	11	256	k	156	726	8	2	(138) 839	(137) 842	-	-	-	-	-	
135	Neurotechnology	neurotech	007	2019-10-03	57	51	13	256	k	7	161	7	2	(151) 1118	(151) 1110	(123) 2143	(118) 4397	(117) 9045	84	0.55N ^{1.0}	
136	Neurotechnology	neurotechnology	008	2021-03-22	355	49	40	514	-	183	800	23	4	(154) 1167	(154) 1149	(126) 2266	(123) 4573	(129) 9586	94	0.55N ^{1.0}	
137	Neurotechnology	neurotechnology	009	2021-01-01	246	82	38	513	-	168	683	12	3	(148) 1035	(148) 1049	(119) 1977	(116) 4270	(112) 8756	130	0.32N ^{1.1}	
138	Neurotechnology	neurotechnology	010	2022-01-07	247	83	11	256	-	126	661	3	2	(144) 988	(142) 984	(114) 1897	(113) 3977	(108) 8048	121	0.36N ^{1.0}	
139	Neurotechnology	neurotechnology	012	2022-06-07	247	84	8	256	-	138	686	13	3	(149) 1036	(150) 1063	(120) 2046	(115) 4179	(111) 8624	117	0.41N ^{1.0}	
140	Newland Computer Co Ltd	newland	2	2018-10-30	96	27	112	2048	-	203	855	145	15	(238) 8741	(243) 8854	(206) 17892	(204) 39356	-	160	1.32N ^{1.1}	
141	Nobilis	noblis	1	2018-10-30	114	176	151	2048	1	18	206	141	15	(162) 1273	(159) 1272	-	-	-	-	-	
142	Nobilis	noblis	2	2018-10-30	153	176	242	6144	1	89	517	215	43	(201) 2513	(206) 2522	(177) 5649	(178) 12432	(186) 44262	196	0.04N ^{1.3}	
143	NotionTag Technologies Private Limited	notiontag	000	2022-01-14	265	945	213	2120	-	70	453	81	10	(237) 8619	(242) 8705	(165) 20652	(203) 38794	(200) 90607	164	1.15N ^{1.1}	
144	Pangiam	pangiam	000	2022-02-22	453	23	118	2048	-	118	636	164	17	(59) 276	(70) 319	(53) 601	(52) 1210	(47) 2443	64	0.18N ^{1.0}	
145	Paravision (EverAI)	everai	2	2018-10-30	224	304	123	2048	1	42	366	203	60	(61) 278	(64) 283	-	-	-	-	-	
146	Paravision (EverAI)	everai	3	2018-10-30	438	304	131	2048	1	153	717	193	28	(60) 278	(63) 281	(50) 572	(48) 1146	(44) 2278	108	0.12N ^{1.0}	
147	Paravision (EverAI)	everai-paravision	004	2019-06-19	527	128	227	4096	1	130	672	218	45	(108) 559	(107) 559	(141) 2611	(151) 6445	(155) 14519	204	0.00N ^{1.5}	
148	Paravision (EverAI)	paravision	005	2019-12-11	543	154	232	4096	1	194	830	220	48	(110) 561	(110) 564	(80) 1056	(84) 2298	(80) 4966	134	0.16N ^{1.1}	
149	Paravision (EverAI)	paravision	007	2021-02-01	529	235	225	4096	-	146	701	224	48	(112) 569	(105) 558	(82) 1086	(81) 2111	(75) 4254	23	1.11N ^{0.9}	
150	Paravision	paravision	009	2021-12-14	672	300	236	4100	-	114	631	228	213	3690	(218) 4230	(183) 8037	(184) 16532	(180) 31422	110	1.62N ^{1.0}	
151	Qnap Security	qnap	000	2021-07-28	182	15	176	2048	-	72	457	69	9	(157) 1231	(182) 1763	-	-	-	-	-	
152	Qnap Security	qnap	001	2021-12-09	191	13	100	2048	-	108	613	48	8	(177) 1666	(169) 1429	(156) 3472	(158) 7375	(161) 15159	181	0.11N ^{1.2}	
153	Qnap Security	qnap	002	2022-04-15	338	32	111	2048	-	189	822	161	17	(142) 958	(156) 1179	(128) 2312	(127) 4789	(132) 9791	146	0.24N ^{1.1}	
154	Quantasoft	quantasoft	1	2018-10-30	276	452	124	2048	k	50	385	33	6	(240) 15422	(145) 14858	(203) 14717	-	(166) 18323	-	31	0.07N ^{1.0}
155	Rank One Computing	rankone	4	2018-10-09	0	101	101	185	k	3	36	37	7	(27) 101	(28) 101	(22) 190	-	-	-	-	
156	Rank One Computing	rankone	5	2018-10-24	0	101	101	133	k	4	92	38	7								

	DEVELOPER	SHORT	SEQ.	VALIDATION	CONFIG ¹	LIB ²	TEMPLATE GENERATION			FINALIZE ³	SEARCH DURATION ⁵ MILLISEC					
							DATA (MB)	DATA (MB)	SIZE (B)	MULT ³	TIME (MS) ⁴	TIME (S)	L=1	L=50	L=50	L=50
	FULL NAME	NAME	NUM.	DATE			N=1.6M	N=1.6M	N=3M	N=6M	N=12M					
157	Rank One Computing	rankone	006	2019-06-03	0	133	⁶ 165	k	²⁵ 245	⁴⁶ 8	-	-	-	-	-	-
158	Rank One Computing	rankone	007	2019-11-12	0	137	⁷ 165	k	²⁷ 272	⁴¹ 7	⁽²⁹⁾ 116	⁽²⁹⁾ 115	⁽²⁴⁾ 215	⁽²⁴⁾ 439	⁽²²⁾ 877	⁶² 0.07N ^{1.0}
159	Rank One Computing	rankone	009	2020-06-26	0	105	¹⁶ 260	k	¹³ 185	⁹¹ 11	⁽²¹⁾ 95	⁽²⁴⁾ 96	⁽¹⁸⁾ 181	⁽¹⁸⁾ 362	⁽¹⁹⁾ 727	⁴² 0.06N ^{1.0}
160	Rank One Computing	rankone	010	2020-11-05	0	135	²⁰ 261	-	¹⁷ 198	⁸⁵ 10	⁽²²⁾ 95	⁽¹⁹⁾ 95	⁽¹⁶⁾ 178	⁽¹⁶⁾ 357	⁽¹⁷⁾ 714	³⁷ 0.06N ^{1.0}
161	Rank One Computing	rankone	011	2021-08-27	0	175	¹⁸ 261	-	⁹⁸ 566	⁵⁴ 8	⁽²⁴⁾ 96	⁽²¹⁾ 95	⁽¹⁹⁾ 183	⁽¹⁹⁾ 370	⁽¹⁶⁾ 714	⁵¹ 0.06N ^{1.0}
162	Rank One Computing	rankone	012	2021-12-27	0	257	¹⁷ 261	-	⁹⁷ 563	⁴³ 8	⁽²³⁾ 95	⁽²²⁾ 95	⁽¹⁷⁾ 179	⁽¹⁷⁾ 361	⁽¹⁸⁾ 718	⁴⁰ 0.06N ^{1.0}
163	Rank One Computing	rankone	013	2022-07-21	0	223	²¹ 261	-	¹³ 679	¹⁵⁵ 16	⁽²⁸⁾ 101	⁽²⁶⁾ 100	⁽²¹⁾ 188	⁽²¹⁾ 376	⁽²⁰⁾ 784	²² 0.20N ^{0.9}
164	Realnetworks Inc	realnetworks	2	2018-10-30	105	104	²³ 4104	k	²² 241	¹⁹² 28	⁽¹⁸⁾ 2008	⁽¹⁹⁾ 2048	⁽¹⁶⁾ 4194	⁽¹⁶⁾ 8642	⁽¹⁶⁾ 15035	⁷⁷ 1.08N ^{1.0}
165	Realnetworks Inc	realnetworks	003	2019-06-12	93	102	⁹ 1848	k	¹⁰ 173	¹⁰⁶ 13	⁽¹⁵⁾ 1145	⁽¹⁵⁾ 1132	⁽¹²⁾ 2142	⁽¹³⁾ 5241	⁽¹³⁾ 10495	¹⁵⁰ 0.21N ^{1.1}
166	Realnetworks Inc	realnetworks	004	2019-10-17	94	102	⁹¹ 1848	1	⁹ 171	⁹⁰ 11	⁽¹⁵⁾ 1143	⁽¹⁵⁾ 1137	⁽¹²⁾ 2149	⁽¹²⁾ 4740	⁽¹²⁾ 9693	¹²⁹ 0.36N ^{1.0}
167	Realnetworks Inc	realnetworks	005	2021-06-23	168	209	²⁰ 2056	-	³ 332	⁶⁹ 9	⁽¹⁷⁾ 1654	⁽¹⁷⁾ 1616	⁽¹⁴⁾ 3030	⁽¹⁴⁾ 6068	⁽¹⁴⁾ 12134	⁴⁷ 1.01N ^{1.0}
168	Realnetworks Inc	realnetworks	006	2021-12-02	250	56	²⁰ 2056	-	⁴⁰ 348	⁴⁹ 8	⁽¹⁰⁾ 543	⁽¹⁰⁾ 531	⁽⁷⁾ 996	⁽⁷⁾ 1998	⁽⁷⁾ 3991	⁴⁵ 0.33N ^{1.0}
169	Realnetworks Inc	realnetworks	007	2022-04-11	455	99	¹⁹ 2056	-	¹¹ 634	¹⁶² 17	⁽¹³⁾ 815	⁽¹³⁾ 812	⁽¹⁰⁾ 1559	⁽¹⁰⁾ 16361	⁽¹²⁾ 277N ^{1.0}	
170	Realnetworks Inc	realnetworks	008	2022-08-29	557	99	¹⁹ 2056	-	²⁴ 968	¹⁰⁰ 12	⁽¹⁰⁾ 538	⁽¹⁰⁾ 525	⁽⁷⁾ 986	⁽⁷⁾ 1967	⁽⁸⁾ 5559	¹⁵¹ 0.09N ^{1.1}
171	Remark Holdings	remarkai	000	2019-06-12	234	1092	¹³ 2048	k	¹² 650	¹⁰⁵ 12	⁽²²⁾ 5776	⁽²²⁾ 5703	⁽¹⁹⁾ 11604	⁽²⁰⁾ 31233	⁽²⁰⁾ 91436	⁹⁷ 0.05N ^{1.3}
172	Remark Holdings	remarkai	0	2018-10-30	187	847	¹³ 2048	k	¹⁰² 593	¹³³ 14	⁽²²⁾ 5685	⁽²²⁾ 5723	-	-	-	
173	Remark Holdings	remarkai	1	2018-10-30	187	847	¹⁴ 2048	-	⁶ 427	¹³⁸ 14	⁽²²⁾ 5680	⁽²²⁾ 5761	⁽¹⁹⁾ 12475	⁽¹⁹⁾ 28726	⁽¹⁹⁾ 59618	¹⁸⁶ 0.37N ^{1.2}
174	Rendip	rendip	000	2021-05-21	0	416	¹¹ 2048	-	²¹ 890	⁷² 9	⁽⁵⁾ 249	⁽⁷⁾ 368	⁽⁶⁾ 697	⁽⁵⁾ 1452	⁽⁵⁾ 2926	¹⁴¹ 0.08N ^{1.1}
175	Reveal Media Ltd	revealmedia	000	2022-02-02	287	196	¹⁷ 2052	-	⁴⁹ 383	⁷⁹ 10	⁽¹⁹⁾ 2322	⁽¹⁹⁾ 2019	⁽¹⁶⁾ 3838	⁽¹⁶⁾ 7816	⁽¹⁶⁾ 16559	¹¹³ 0.78N ^{1.0}
176	SQLsoft	sqisoft	001	2021-12-20	271	377	¹⁹ 2056	-	⁷ 462	⁷⁰ 9	⁽¹⁶⁾ 1310	⁽¹⁶⁾ 1319	⁽¹³⁾ 2456	⁽¹²⁾ 4906	⁽¹³⁾ 9755	³² 0.90N ^{1.0}
177	Samsung S1 Corp	s1	000	2021-06-03	257	196	²³ 4096	-	²⁰ 865	¹⁷⁵ 20	⁽²³⁾ 6715	⁽²³⁾ 6794	⁽²⁰⁾ 13032	⁽¹⁹⁾ 26372	⁽¹⁹⁾ 55723	¹⁰⁵ 2.82N ^{1.0}
178	Samsung S1 Corp	s1	001	2021-11-01	240	198	¹² 2048	-	¹⁸ 813	⁵⁸ 8	⁽¹⁹⁾ 2415	⁽²⁰⁾ 2491	⁽¹⁷⁾ 4718	⁽¹⁷⁾ 614	⁽¹⁶⁾ 24472	¹⁴⁵ 0.53N ^{1.1}
179	Samsung S1 Corp	s1	002	2022-05-04	244	93	¹⁵ 2048	-	²⁴ 958	¹⁵¹ 16	⁽¹⁸⁾ 1234	⁽¹⁶⁾ 1285	⁽¹³⁾ 2411	⁽¹³⁾ 4805	⁽¹³⁾ 9705	⁵⁵ 0.77N ^{1.0}
180	Samsung S1 Corp	s1	003	2022-09-27	471	93	¹⁰ 2048	-	²⁴ 877	¹²¹ 13	⁽¹⁷⁾ 1620	⁽¹⁷⁾ 1697	⁽¹⁵⁾ 3187	⁽¹⁴⁾ 6400	⁽¹⁴⁾ 12792	⁵⁹ 0.99N ^{1.0}
181	Scanovate Ltd	scanovate	000	2020-01-15	250	446	¹⁷ 2048	-	¹⁴ 705	¹³⁶ 14	⁽¹⁶⁾ 1419	⁽¹⁶⁾ 1412	⁽¹⁴⁾ 3008	⁽¹⁵⁾ 11616	⁽¹⁴⁾ 2012	¹⁸⁷ 0.10N ^{1.2}
182	Scanovate Ltd	scanovate	001	2020-09-10	250	446	¹⁶ 2048	-	¹³ 675	¹¹¹ 13	⁽¹⁶⁾ 1321	⁽¹⁶⁾ 1320	⁽¹³⁾ 2502	⁽¹³⁾ 5047	⁽¹³⁾ 10163	⁸⁰ 0.65N ^{1.0}
183	Sensetime Group	sensetime	0	2018-10-30	525	6	²³ 4104	k	¹⁴ 693	²¹⁴ 41	⁽⁹⁾ 498	⁽⁹⁾ 501	⁽⁹⁾ 1212	⁽⁸⁾ 2281	⁽⁸⁾ 5032	¹⁵⁷ 0.09N ^{1.1}
184	Sensetime Group	sensetime	1	2018-10-30	525	6	²⁴ 4104	k	¹¹ 628	²¹⁹ 48	⁽¹⁰⁾ 516	⁽⁹⁾ 502	⁽⁸⁾ 1146	⁽⁸⁾ 2301	⁽⁷⁾ 4763	¹⁵⁵ 0.09N ^{1.1}
185	Sensetime Group	sensetime	002	2019-06-03	523	6	²⁰ 2056	k	¹⁰ 603	¹⁶⁸ 18	⁽⁷⁾ 359	⁽⁷⁾ 370	⁽¹⁵⁾ 1897	⁽¹²⁾ 4508	⁽¹²⁾ 9543	²⁰⁷ 0.00N ^{1.5}
186	Sensetime Group	sensetime	003	2019-12-02	769	76	²⁰ 2056	1	²² 910	¹⁷² 19	⁽²¹⁾ 4885	⁽²³⁾ 4989	⁽¹⁶⁾ 12325	⁽¹⁹⁾ 24712	⁽¹⁹⁾ 49445	¹⁶⁷ 0.67N ^{1.1}
187	Sensetime Group	sensetime	004	2020-08-10	456	29	⁵⁸ 1032	-	¹⁴ 690	¹⁰⁴ 12	⁽²⁰⁾ 2490	⁽²⁰⁾ 2477	⁽¹⁷⁾ 4654	⁽¹⁷⁾ 4402	⁽¹⁷⁾ 19651	⁸³ 1.22N ^{1.0}
188	Sensetime Group	sensetime	005	2020-12-17	631	39	⁶⁵ 1032	-	²⁴ 980	⁸⁹ 11	⁽¹⁶⁾ 2459	⁽¹⁶⁾ 2393	⁽¹⁸⁾ 14768	⁽¹⁷⁾ 2398	⁽²⁰⁾ 19016	²⁰ 14.03N ^{0.9}
189	Sensetime Group	sensetime	006	2021-07-26	526	54	⁶⁰ 1032	-	²³ 929	⁴² 7	⁽¹⁹⁾ 2414	⁽¹⁹⁾ 2422	⁽¹⁶⁾ 4527	⁽¹⁶⁾ 9128	⁽¹⁶⁾ 18640	⁶⁹ 1.35N ^{1.0}
190	Sensetime Group	sensetime	007	2022-01-15	526	37	⁵⁹ 1032	-	²³ 935	⁵⁶ 8	⁽¹⁹⁾ 2432	⁽¹⁹⁾ 2406	⁽¹⁶⁾ 4513	⁽¹⁶⁾ 8998	⁽¹⁷⁾ 18796	⁷⁵ 1.28N ^{1.0}
191	Sensetime Group	sensetime	008	2022-08-17	567	37	⁶³ 1032	-	²³ 637	⁶⁶ 9	⁽¹⁹⁾ 2444	⁽¹⁹⁾ 2419	⁽¹⁶⁾ 4525	⁽¹⁶⁾ 9114	⁽¹⁶⁾ 18279	⁵⁸ 1.43N ^{1.0}
192	Shaman Software	shaman	6	2018-10-26	0	200	¹⁰ 2048	k	¹⁵⁰ 706	¹³⁴ 14	⁽¹⁵⁾ 603	⁽¹⁴⁾ 612	-	-	-	
193	Shaman Software	shaman	7	2018-10-26	0	200	¹⁵ 2048	k	¹⁵¹ 707	¹³⁷ 14	⁽¹⁴⁾ 602	⁽¹⁵⁾ 614	⁽⁸⁾ 1187	⁽⁹⁾ 2448	⁽⁸⁾ 5083	¹⁰⁹ 0.25N ^{1.0}
194	Shanghai Yitu Technology	yitu	4	2018-10-30	2119	136	²⁰ 2070	1	²⁰ 853	²¹⁶ 44	⁽¹⁵⁾ 1237	⁽¹⁵⁾ 1199	⁽¹³⁾ 2513	⁽¹³⁾ 5013	⁽¹²⁾ 9620	¹⁰⁰ 0.55N ^{1.0}
195	Shanghai Yitu Technology	yitu	5	2018-10-30	2043	136	²¹⁰ 2070	1	²⁰ 853	²¹⁶ 44	⁽¹⁵⁾ 1237	⁽¹⁵⁾ 1199	⁽¹³⁾ 2513	⁽¹³⁾ 5013	⁽¹²⁾ 9620	¹⁰⁰ 0.55N ^{1.0}
196	Smilart	smilart	4	2018-10-30	65	89	³⁷ 512	k	¹⁶ 17	²⁴ 4	⁽²⁴⁾ 16137	⁽²⁴⁾ 15633	-	-	-	
197	Smilart	smilart	5	2018-10-30	562	89	¹²¹ 2048	k	⁶⁸ 450	¹³¹ 14	-	-	-	-	-	
198	Stagu Technologies	stagu	000	2021-08-30	1018	690	²³ 4096	-	¹⁹ 826	¹⁸⁷ 24	⁽²¹⁾ 4950	⁽²²⁾ 4933	-	-	-	
199	Synesis	synesis	003	2019-07-04	143	17	¹⁷ 2048	k	¹⁹ 211	¹⁰¹ 12	⁽¹⁰⁾ 507	⁽⁹⁾ 502	⁽¹²⁾ 2297	⁽¹²⁾ 4564	⁽¹²⁾ 9452	²⁰² 0.00N ^{1.4}
200	Synesis	synesis	3	2018-10-30	237	150	²³ 4096	k	⁵⁹ 99	¹⁹⁶ 29	⁽¹²⁾ 789	⁽¹³⁾ 801	⁽¹⁸⁾ 1941	⁽¹¹⁾ 3888	⁽¹¹⁾ 8810	¹⁷⁵ 0.07N ^{1.1}
201	Synesis	synesis	005	2020-09-08	494	24	²³⁸ 4104	-	¹⁶⁶ 756	¹⁸⁵ 24	⁽¹⁸⁾ 877	⁽¹⁸⁾ 865	⁽¹⁵⁾ 3182	⁽¹⁵⁾ 4658	⁽¹³⁾ 9750	¹⁸⁸ 0.06N ^{1.2}
202	T4iSB	t4isb	000	2022-08-17	228	15	¹⁴² 2048	-	¹⁶³ 741	¹¹⁸ 13	⁽¹⁴⁾ 250	⁽¹⁵⁾ 250	-	-	-	
203	Tech5 SA	tech5	001	2019-08-19	1394	116	⁸³ 1536	k	²¹⁷ 887	⁷⁸ 10	⁽⁷⁹⁾ 383	⁽¹²⁾ 766	⁽¹⁴⁾ 2767	⁽¹⁴⁾ 6149	⁽⁹⁷⁾ 6178	¹⁶⁶ 0.12N ^{1.1}
204	Tech5 SA	tech5	002	2021-04-07	727	112	³⁹ 513	-	²³⁸ 940	¹⁸ 4	⁽²¹⁾ 4682	⁽²³⁾ 6689	⁽¹⁹⁾ 12541	⁽¹⁹⁾ 25145	⁽¹⁹⁾ 50239	⁴⁴ 4.18N ^{1.0}
205	Tencent Deepsea Lab	deepsea	001	2019-												

2022/11/09
18:02:21FNIR(N, R, T) = False neg. identification rate
FPIN(R, T) = False pos. identification rateN = Num. enrolled subjects
R = Num. candidates examined
T = ThresholdT = 0 → Investigation
T √ 0 → Identification

	DEVELOPER	SHORT	SEQ.	VALIDATION	CONFIG ¹	LIB ¹	TEMPLATE GENERATION	FINALIZE ²	SEARCH DURATION ³						POWER LAW (μ s)							
									TIME (S)	L=1	L=50	L=50	L=50	N=6M	N=12M							
FULL NAME	NAME	NUM.	DATE	DATA (MB)	DATA (MB)	SIZE (B)	MULT ³	TIME (MS) ⁴	N=1.6M	N=1.6M	N=1.6M	N=3M	N=6M	N=12M	(μ s)							
209	Thales	cogent	2	2018-10-30	681	39	70	1043	k	240	945	190	27	(188)	2017	(195) 2144	(166) 4298	(163) 8472	(163) 16429	82.108 N ^{1.0}		
210	Thales	cogent	3	2018-10-30	681	39	69	1043	k	237	940	79	(156)	1230	(163) 1311	(142)	2687	(137) 5398	(134) 10184	95.622 N ^{1.0}		
211	Thales	cogent	004	2021-02-10	1376	59	195	2053	-	241	947	124	14	(205)	2903	(187) 1911	(157) 3566	(159) 7498	(162) 16370	127.644 N ^{1.0}		
212	Thales	cogent	005	2021-09-13	1043	56	71	1062	-	17	769	35	5	(140)	912	(143) 996	(113) 1872	(111) 3845	(106) 7555	97.444 N ^{1.0}		
213	Thales	cogent	006	2022-05-14	508	70	47	550	-	198	843	44	8	(113)	587	(134) 820	(107) 1564	(106) 3173	(110) 8290	149.16 N ^{1.1}		
214	TigerIT Americas LLC	tiger	2	2018-10-29	416	518	186	2052	k	73	461	146	15	(183)	1816	(188) 1921	(163) 3833	(160) 7526	(158) 14820	102.083 N ^{1.0}		
215	TigerIT Americas LLC	tiger	3	2018-10-30	416	518	190	2052	k	74	461	250	37431	(44)	191	(42)	189	-	-	-		
216	Toshiba	toshiba	0	2018-10-30	961	105	88	1548	k	217	876	96	12	(220)	6153	(232) 6236	(195) 12221	(195) 25355	(191) 49448	182.036 N ^{1.2}		
217	Toshiba	toshiba	1	2018-10-30	961	105	207	2060	k	212	875	251	44701	(229)	6007	(234)	6355	-	-	-		
218	Tripleize	aize	001	2021-08-06	262	150	125	2048	-	50	402	69	9	(208)	3087	(211) 3080	-	-	-	-		
219	Trueface.ai	trueface	000	2021-01-27	247	119	95	2000	-	41	363	109	13	(57)	271	(73) 327	(55) 614	(53) 1239	(49) 2678	92.015 N ^{1.0}		
220	Veridas Digital Authentication Solutions S.L.	veridas	001	2021-03-05	347	875	152	2048	-	209	872	110	13	(222)	5493	(226) 5469	(191) 10350	(189) 20655	(185) 41264	48.340 N ^{1.0}		
221	Veridas Digital Authentication Solutions S.L.	veridas	002	2021-07-06	347	870	9	2048	-	218	877	87	10	(72)	322	(71) 325	(61) 685	(59) 1365	(53) 2730	135.09 N ^{1.1}		
222	Veridas Digital Authentication Solutions S.L.	veridas	003	2021-11-09	346	870	169	2048	-	207	867	58	9	(92)	440	(72) 327	(63) 699	(60) 1401	(72) 3954	185.022 N ^{1.2}		
223	Vietnam Posts and Telecommunications Group	vnpt	001	2022-05-05	361	235	96	2048	-	229	892	176	20	(132)	813	(132) 804	(104) 1514	(105) 3037	(95) 6128	46.050 N ^{1.0}		
224	Vietnam Posts and Telecommunications Group	vnpt	002	2022-09-08	547	235	129	2048	-	184	808	160	16	(136)	857	(135) 835	(108) 1576	(107) 3183	(102) 6412	74.044 N ^{1.0}		
225	Viettel Group	vts	000	2021-03-12	250	257	99	2048	-	84	492	234	2295	(3)	4	(2)	6	(4)	11	-	14.061 N ^{0.6}	
226	Viettel Group	vts	001	2021-07-16	352	600	101	2048	-	219	891	181	21	(197)	2477	(203) 2487	(170) 4644	(169) 9313	(169) 18713	49.153 N ^{1.0}		
227	Viettel Group	vts	002	2022-02-08	244	600	155	2048	-	224	903	197	29	(199)	2485	(205) 2485	(173) 4678	(170) 9370	(171) 18833	57.149 N ^{1.0}		
228	Viettel Group	vts	003	2022-07-14	493	468	158	2048	-	147	702	207	34	(198)	2482	(201) 2480	(171) 4649	(168) 9302	(166) 18651	50.152 N ^{1.0}		
229	Vigilant Solutions	vigilant	5	2018-10-30	335	122	86	1544	k	168	762	171	19	-	(180)	1720	-	-	-	-		
230	Vigilant Solutions	vigilant	6	2018-10-30	337	122	84	1544	k	187	816	179	21	-	(179)	1713	-	-	-	-		
231	Vigilant Solutions	vigilantsolutions	007	2021-01-08	340	51	87	1544	-	110	616	159	16	(168)	1354	(167) 1352	(146) 2911	(144) 5966	(140) 11466	148.027 N ^{1.1}		
232	Vigilant Solutions	vigilantsolutions	008	2021-07-23	340	51	85	1544	-	55	403	117	13	(150)	1062	(149) 1061	(129) 2330	(140) 5520	(123) 9499	171.011 N ^{1.1}		
233	Visidon	visidon	1	2018-10-30	166	42	179	2052	k	128	667	148	15	(214)	4370	(220) 4472	(186) 8454	(186) 17262	(181) 34288	73.240 N ^{1.0}		
234	Visidon	vd	002	2021-05-18	248	42	19	2052	-	14	687	59	9	(189)	2089	(196) 2366	-	-	-	-		
235	Visidon	vd	003	2021-10-12	497	43	189	2052	-	143	692	50	8	(190)	2095	(194) 2095	-	-	-	-		
236	VisioBox	visionbox	000	2021-09-17	252	274	20	2059	-	84	481	158	16	(87)	422	(76) 359	(69) 855	(29) 631	(42) 2096	18.246 N ^{0.8}		
237	VisionLabs	visionlabs	6	2018-10-30	360	17	29	512	1	30	289	247	20290	(18)	36	(16) 36	(13) 39	(11) 44	(9) 53	83211.93 N ^{0.2}		
238	VisionLabs	visionlabs	7	2018-10-30	360	17	27	512	1	29	289	24	34666	(19)	63	(17) 63	(14) 72	(11) 80	(12) 115	102076.32 N ^{0.2}		
239	VisionLabs	visionlabs	008	2019-06-18	348	17	30	512	1	28	272	244	12747	(12)	23	(8) 24	(7)	26	(6)	(5) 33	62539.61 N ^{0.2}	
240	VisionLabs	visionlabs	009	2020-08-04	689	20	36	512	-	77	467	24	13245	(13)	29	(10)	29	(9)	(13) 61	13.88 N ^{0.6}		
241	VisionLabs	visionlabs	010	2021-02-05	1042	20	31	512	-	158	731	240	11837	(10)	21	(13)	32	(11)	36	(6) 43	73183.79 N ^{0.2}	
242	VisionLabs	visionlabs	011	2021-10-20	1042	20	26	512	-	160	735	243	12255	(11)	21	(7)	23	(8)	26	(7) 34	(8) 51	12.301.26 N ^{0.3}
243	Vocord	vocord	5	2018-10-30	1035	185	49	768	k	176	780	40	7	(38)	158	(43) 204	(33) 383	(34)	767	(29) 1466	53.012 N ^{1.0}	
244	Vocord	vocord	6	2018-10-30	1035	185	251	10240	k	177	785	235	243	(39)	170	(46)	216	-	-	-	-	
245	Xforward AI Technology	xforwardai	000	2020-07-24	236	171	14	2048	-	161	753	120	13	(216)	4603	(241) 7647	(204)	15723	(192) 23900	(194) 53729	172.056 N ^{1.1}	
246	Xforward AI Technology	xforwardai	001	2021-01-21	332	50	150	2048	-	134	677	156	16	(228)	5887	(219) 4384	(188)	8798	(187) 18553	(189) 48993	179.032 N ^{1.1}	
247	Xforward AI Technology	xforwardai	002	2021-05-24	691	50	226	4096	-	23	930	169	18	(239)	6957	(235) 6400	(199)	12659	(200) 31077	(198) 65158	177.052 N ^{1.1}	
248	["Developer name**"]	verijelas	000	2022-10-11	248	11	145	2048	-	334	125	14	(9)	20	(9)	27	-	-	-	-		
249	["Developer name**"]	verihubs-inteligensia	000	2022-09-29	204	75	156	2048	-	97	575	132	14	(239)	9715	(241) 9670	(207)	18711	(202) 38110	(199) 79675	86.4.77 N ^{1.0}	
250	["Developer name**"]	turingtechvip	001	2022-09-29	151	161	132	2048	-	188	817	123	13	(243)	22085	(248) 22044	-	-	-	-		
251	["Developer name**"]	mukh	002	2022-09-16	693	442	154	2048	-	251	1278	237	4261	(4)	5	(18)	83	(15)	106	(15) 313	(15) 628	27.07 N ^{1.0}

Notes

- Configuration size does not capture static data present in libraries. Libraries are included but the size also includes any ancillary libraries for image processing (e.g. openCV) or numerical computation (e.g. blas).
- Finalization is the processing of converting $N = 1600000$ templates into a searchable data structure an operation which can be a simple copy, or the building of an index or tree, for example. The duration of the operation may be data dependent, and may not be linear in the number of input templates.
- This multiplier expresses the increase in template size when k images are passed to the template generation function.
- All durations are measured on Intel®Xeon®CPU E5-2630 v4 @ 2.20GHz processors. Estimates are made by wrapping the API function call in calls to std::chrono::high_resolution_clock which on the machine in (3) counts 1ns clock ticks. Precision is somewhat worse than that however.
- Search durations are measured as in the prior note. The power-law model in the final column mostly fits the empirical results in Figure 145. However in certain cases the model is not correct and should not be used numerically.

Table 6: Summary of algorithms and properties included in this report. The blue superscripts give ranking for the quantity in that column. Missing search durations, denoted by “-”, are absent because those runs were not executed, usually because we did not run on the larger galleries. Caution: The power-law model is sometimes an incorrect model. It is included here only to show broad sublinear behavior, which is flagged in green. The models should not be used for prediction.

#	ALGORITHM	INVESTIGATION _i FNIR(N, R = 1, T = 0)								IDENTIFICATION _i FNIR(N, R = L, T ≥ 0) FOR FPIR = 0.001							
		(0, 2]	(2, 4]	(4, 6]	(6, 8]	(8, 10]	(10, 12]	(12, 14]	(14, 18]	(0, 2]	(2, 4]	(4, 6]	(6, 8]	(8, 10]	(10, 12]	(12, 14]	(14, 18]
1	3DIVI-005	⁹⁷ 0.0207	⁹⁷ 0.0304	⁹⁷ 0.0415	⁹⁷ 0.0533	⁹⁷ 0.0646	¹³⁵ 0.0735	¹³⁵ 0.0884	¹³⁶ 0.1148	¹⁰⁷ 0.1580	⁹⁸ 0.2316	⁹⁸ 0.3033	⁹⁸ 0.3740	⁹⁸ 0.4285	¹³⁴ 0.4742	¹³⁴ 0.5329	¹³⁴ 0.5975
2	ANKE-000	⁹⁵ 0.0162	⁹⁵ 0.0245	⁹⁵ 0.0333	⁹⁵ 0.0428	⁹⁵ 0.0515	¹³³ 0.0615	¹³³ 0.0780	¹³² 0.1028	⁹⁶ 0.1132	⁹⁵ 0.1761	⁹⁶ 0.2402	⁹⁵ 0.3057	⁹⁵ 0.3640	¹³¹ 0.4200	¹³¹ 0.4928	¹³¹ 0.5680
3	ANKE-002	⁴⁷ 0.0055	⁵⁰ 0.0074	⁵⁰ 0.0090	⁴⁹ 0.0103	⁴⁸ 0.0116	⁸⁵ 0.0135	⁸⁴ 0.0162	⁸⁰ 0.0202	⁵⁴ 0.0329	⁵⁴ 0.0560	⁵⁶ 0.0843	⁵⁷ 0.1169	⁵⁷ 0.1481	⁹² 0.1820	⁹³ 0.2280	⁹² 0.2831
4	AWARE-005	¹⁰⁶ 0.0328	¹⁰⁶ 0.0519	¹⁰⁶ 0.0712	¹⁰⁹ 0.0910	¹⁰⁴ 0.1078	¹⁴² 0.1235	¹⁴² 0.1457	¹⁴³ 0.1831	¹⁰⁸ 0.3605	¹⁰⁷ 0.4949	¹⁰⁷ 0.5948	¹⁰⁷ 0.6783	¹⁰⁸ 0.7393	¹⁴⁴ 0.7905	¹⁴⁴ 0.8408	¹⁴⁵ 0.8831
5	AWARE-006	¹¹⁰ 0.0702	¹¹¹ 0.1110	¹¹¹ 0.1502	¹¹⁸ 0.1899	¹¹⁸ 0.2253	¹⁵¹ 0.2614	¹⁵⁰ 0.3045	¹⁵⁰ 0.3659								
6	AYONIX-002	¹¹³ 0.3360	¹¹⁴ 0.4389	¹¹⁴ 0.5144	¹¹⁴ 0.5814	¹¹⁴ 0.6340	¹⁵⁴ 0.6818	¹⁵⁴ 0.7297	¹⁵⁵ 0.7774	¹¹⁶ 0.8288	¹¹¹ 0.9013	¹¹¹ 0.9375	¹¹¹ 0.9603	¹¹¹ 0.9744	¹⁴⁹ 0.9837	¹⁴⁹ 0.9893	¹⁴⁹ 0.9927
7	CAMVI-004	¹⁰⁹ 0.0623	¹⁰⁹ 0.0944	¹⁰⁹ 0.1243	¹⁰⁸ 0.1548	¹⁰⁸ 0.1812	¹⁴⁸ 0.2056	¹⁴⁸ 0.2344	¹⁴⁶ 0.2672	⁹¹ 0.0810	⁹¹ 0.1267	⁸⁸ 0.1721	⁸⁸ 0.2203	⁸⁸ 0.2619	¹²² 0.3040	¹²¹ 0.3543	¹¹⁷ 0.4124
8	CAMVI-005	¹¹¹ 0.0849	¹¹¹ 0.1255	¹¹¹ 0.1631	¹¹¹ 0.1989	¹¹⁷ 0.2298	¹⁵⁰ 0.2585	¹⁴⁹ 0.2915	¹⁴⁹ 0.3246								
9	CANON-001						³⁶ 0.0052	²⁸ 0.0057	²⁸ 0.0042						⁴⁰ 0.0491	⁴⁰ 0.0606	⁴² 0.0826
10	CANON-002						⁴⁸ 0.0062	⁴⁷ 0.0070	⁴⁶ 0.0070						³⁸ 0.0472	³⁸ 0.0582	⁴⁰ 0.0792
11	CIB-000	¹⁴ 0.0022	¹⁴ 0.0030	¹⁵ 0.0037	¹⁵ 0.0044	¹⁷ 0.0049	⁴⁴ 0.0057	⁴⁵ 0.0069	⁴⁶ 0.0062	²⁵ 0.0139	²⁶ 0.0240	²⁷ 0.0373	²⁸ 0.0525	²⁸ 0.0689	⁵⁶ 0.0859	⁵⁷ 0.1109	⁵⁷ 0.1454
12	CLEARVIEW1-000	⁴ 0.0017	⁴ 0.0023	⁴ 0.0028	⁹ 0.0034	¹¹ 0.0039	²⁷ 0.0046	³⁴ 0.0056	³⁷ 0.0047	¹⁶ 0.0066	¹⁸ 0.0121	¹⁸ 0.0194	¹⁹ 0.0287	¹⁹ 0.0385	⁴¹ 0.0493	⁴⁵ 0.0662	⁴⁵ 0.0873
13	CLOUDWALK-HR-000	⁷ 0.0019	⁷ 0.0024	⁸ 0.0029	⁶ 0.0032	⁵ 0.0032	⁶ 0.0036	⁷ 0.0041	⁷ 0.0020	¹ 0.0029	¹ 0.0041	¹ 0.0054	¹ 0.0064	⁶ 0.0085	⁶ 0.0102	⁶ 0.0112	
14	CLOUDWALK-MT-000						³ 0.0037	² 0.0038	² 0.0013						³ 0.0065	³ 0.0072	³ 0.0075
15	CLOUDWALK-MT-001						⁷ 0.0037	⁶ 0.0037	⁶ 0.0012						² 0.0045	² 0.0051	² 0.0042
16	COGENT-000	⁹⁰ 0.0128	⁹¹ 0.0184	⁹² 0.0250	⁹³ 0.0327	⁹² 0.0407	¹²⁸ 0.0488	¹²⁸ 0.0611	¹²⁵ 0.0794	⁷⁷ 0.0559	⁷⁸ 0.0923	⁷⁶ 0.1342	⁷⁷ 0.1812	⁷⁸ 0.2243	¹¹⁰ 0.2675	¹⁰⁹ 0.3240	¹¹¹ 0.3992
17	COGENT-001	⁹¹ 0.0128	⁹¹ 0.0184	⁹³ 0.0250	⁹² 0.0327	⁹³ 0.0407	¹²⁷ 0.0488	¹²⁷ 0.0611	¹²⁶ 0.0794	⁷⁸ 0.0559	⁷⁹ 0.0923	⁷⁷ 0.1342	⁷⁶ 0.1812	⁷⁵ 0.2243	¹¹¹ 0.2675	¹¹⁰ 0.3240	¹¹¹ 0.3992
18	COGENT-002	⁶⁹ 0.0081	⁶⁶ 0.0105	⁶³ 0.0123	⁶⁴ 0.0137	⁶² 0.0157	⁹⁸ 0.0175	⁹⁶ 0.0215	⁹⁶ 0.0280	⁶⁹ 0.0499	⁶⁸ 0.0827	⁶⁷ 0.1207	⁶⁹ 0.1639	⁶⁷ 0.2037	¹⁰² 0.2432	¹⁰³ 0.2972	¹⁰³ 0.3638
19	COGENT-003	⁷¹ 0.0082	⁶⁷ 0.0108	⁶³ 0.0128	⁶⁷ 0.0145	⁶⁶ 0.0168	¹⁰⁴ 0.0191	¹⁰⁵ 0.0239	¹⁰² 0.0312	⁸⁰ 0.0582	⁸⁰ 0.0971	⁸⁰ 0.1417	⁸⁰ 0.1918	⁸⁰ 0.2380	¹¹⁷ 0.2836	¹¹⁹ 0.3440	¹²⁰ 0.4207
20	COGENT-004	⁵⁹ 0.0066	⁵³ 0.0080	⁴⁵ 0.0085	³⁹ 0.0080	³¹ 0.0083	⁶⁴ 0.0092	⁶⁵ 0.0106	⁶⁸ 0.0130	⁶³ 0.0410	⁶⁵ 0.0720	⁶⁵ 0.1099	⁶⁵ 0.1539	⁶⁴ 0.1974	¹⁰ 0.2443	¹⁰ 0.3043	¹⁰ 0.3757
21	COGENT-006						²⁵ 0.0045	²² 0.0049	²⁶ 0.0038						³² 0.0370	²⁸ 0.0448	²⁸ 0.0602
22	COGNITEC-000	¹⁰⁵ 0.0265	¹⁰³ 0.0423	¹⁰³ 0.0588	¹⁰³ 0.0757	¹⁰² 0.0894	¹⁴⁰ 0.1014	¹⁴⁰ 0.1169	¹³⁹ 0.1381	¹⁰⁶ 0.1522	⁹⁹ 0.2330	⁹⁹ 0.3051	⁹⁹ 0.3751	⁹⁹ 0.4300	¹³⁰ 0.4779	¹³⁴ 0.5307	¹³⁴ 0.5913
23	COGNITEC-001	⁹³ 0.0149	⁹⁴ 0.0228	⁹⁴ 0.0312	⁹⁴ 0.0399	⁹⁴ 0.0479	¹³⁰ 0.0546	¹²⁹ 0.0656	¹²⁷ 0.0806	⁹³ 0.0963	⁹³ 0.1562	⁹³ 0.2157	⁹³ 0.2771	⁹³ 0.3287	¹²⁹ 0.3771	¹²⁸ 0.4343	¹²⁷ 0.4959
24	COGNITEC-002	⁷ 0.0101	⁸ 0.0138	⁸¹ 0.0170	⁸¹ 0.0201	⁸¹ 0.0237	⁸¹ 0.0264	¹¹⁴ 0.0309	¹¹³ 0.0389	⁷² 0.0517	⁷¹ 0.0879	⁷¹ 0.1269	⁷¹ 0.1707	⁷¹ 0.2098	¹⁰ 0.2463	¹⁰ 0.2919	¹⁰ 0.3535
25	COGNITEC-003	⁷⁸ 0.0104	⁸¹ 0.0140	⁸² 0.0174	⁸² 0.0205	⁸² 0.0238	¹¹⁷ 0.0266	¹¹⁵ 0.0311	¹¹⁵ 0.0401	⁷¹ 0.0504	⁷⁰ 0.0855	⁶⁹ 0.1235	⁶⁹ 0.1662	⁶⁹ 0.2045	¹⁰¹ 0.2403	¹⁰¹ 0.2854	¹⁰¹ 0.3451
26	COGNITEC-004	⁶ 0.0073	⁶ 0.0099	⁶ 0.0118	⁵⁹ 0.0130	⁵⁹ 0.0147	⁹⁷ 0.0163	⁹³ 0.0189	⁹² 0.0239	⁵³ 0.0325	⁵³ 0.0548	⁵² 0.0798	⁵¹ 0.1074	⁵⁰ 0.1325	⁸⁴ 0.1591	⁸¹ 0.1952	⁸⁰ 0.2414
27	COGNITEC-006						³⁸ 0.0081	³⁶ 0.0086	³⁶ 0.0090						⁵³ 0.0777	⁵³ 0.0926	⁵³ 0.1274
28	CUBOX-000	⁷ 0.0019	⁵ 0.0024	⁵ 0.0028	⁴ 0.0031	⁴ 0.0032	⁸ 0.0037	¹⁴ 0.0044	¹⁴ 0.0027	⁶ 0.0039	⁶ 0.0059	⁷ 0.0083	⁸ 0.0111	⁸ 0.0141	¹⁸ 0.0252	¹⁸ 0.0339	
29	CYBERLINK-002	⁵⁰ 0.0055	⁴⁹ 0.0068	⁴¹ 0.0075	³⁵ 0.0078	³² 0.0084	⁶⁵ 0.0094	⁶⁶ 0.0107	⁶¹ 0.0114	³² 0.0180	³³ 0.0302	³⁰ 0.0460	³¹ 0.0643	³⁰ 0.0837	⁶⁴ 0.1058	⁶⁴ 0.1370	⁶⁴ 0.1787
30	CYBERLINK-003	³⁵ 0.0041	³⁴ 0.0052	²² 0.0057	²⁵ 0.0058	²⁵ 0.0061	³⁵ 0.0068	³² 0.0078	³⁴ 0.0078	¹⁹ 0.0109	¹⁹ 0.0175	²⁰ 0.0259	²¹ 0.0356	²¹ 0.0468	⁴⁷ 0.0594	⁴⁹ 0.0787	⁵¹ 0.1072
31	DAHUA-002	³ 0.0035	²⁸ 0.0047	²⁸ 0.0058	²⁷ 0.0067	²⁸ 0.0074	⁹⁹ 0.0082	⁶² 0.0100	⁶¹ 0.0108	³⁰ 0.0169	³² 0.0294	³¹ 0.0449	³⁰ 0.0635	³⁰ 0.0817	⁶² 0.1013	⁶¹ 0.1291	⁶⁰ 0.1638
32	DAHUA-003	¹⁹ 0.0026	¹⁹ 0.0036	¹⁹ 0.0043	²⁰ 0.0050	²⁰ 0.0062	⁵⁴ 0.0080	⁴⁹ 0.0073	²⁹ 0.0160	³⁰ 0.0280	²⁹ 0.0432	²⁹ 0.0615	²⁹ 0.0794	⁶⁰ 0.0987	⁶⁰ 0.1270	⁵⁸ 0.1587	
33	DEEPLINT-001	¹⁷ 0.0024	¹⁶ 0.0032	¹⁴ 0.0037	¹³ 0.0040	¹³ 0.0043	³² 0.0049	⁴⁰ 0.0060	³⁹ 0.0052	¹² 0.0058	¹⁰ 0.0087	¹¹ 0.0119	¹¹ 0.0155	¹¹ 0.0199	²¹ 0.0249	²¹ 0.0338	²² 0.0463
34	DEEPSEA-001	⁷⁰ 0.0081	⁷⁰ 0.0116	⁷³ 0.0149	⁷⁶ 0.0182	⁷⁶ 0.0216	¹¹² 0.0260	¹¹⁷ 0.0332	¹¹⁷ 0.0432	⁶⁶ 0.0458	⁶⁶ 0.0752	⁶⁴ 0.1086	⁶³ 0.1460	⁶³ 0.1812	⁹⁹ 0.2186	⁹⁹ 0.2663	⁹⁸ 0.3213
35	DERMALOG-006	⁸ 0.0113	⁸² 0.0142	⁷⁸ 0.0163	⁷⁷ 0.0183	⁷⁴ 0.0200	¹⁰⁹ 0.0218	¹⁰⁷ 0.0251	¹⁰⁵ 0.0329	⁷⁵ 0.0454	⁷³ 0.0889	⁷² 0.1271	⁷¹ 0.1697	⁷⁰ 0.2090	¹⁰ 0.2498	¹⁰ 0.3028	¹⁰ 0.3670
36	DERMALOG-007	⁸⁸ 0.0125	⁸⁸ 0.0170	⁸⁸ 0.0214	⁸⁸ 0.0264	⁸⁷ 0.0309	¹²² 0.0356	¹²³ 0.0432	¹²³ 0.0579	⁹² 0.0910	⁹² 0.1453	⁹² 0.2009	⁹² 0.2602	⁹³ 0.3134	¹²⁸ 0.3649	¹²⁷ 0.4289	¹²⁸ 0.5007
37	DERMALOG-008	⁵ 0.0057	⁵² 0.0077	⁵⁴ 0.0095	⁵⁴ 0.0110	⁵³ 0.0128	⁹¹ 0.0148	⁹⁰ 0.0180	⁹¹ 0.0223	⁷⁰ 0.0							

#	ALGORITHM	INVESTIGATION, FNIR($N, R = 1, T = 0$)								IDENTIFICATION, FNIR($N, R = L, T \geq 0$) FOR FPIR = 0.001							
		(0, 2]	(2, 4]	(4, 6]	(6, 8]	(8, 10]	(10, 12]	(12, 14]	(14, 18]	(0, 2]	(2, 4]	(4, 6]	(6, 8]	(8, 10]	(10, 12]	(12, 14]	(14, 18]
45	HZAILU-001																
46	IDEMIA-003	⁸¹ 0.0110	⁸⁶ 0.0151	⁸⁶ 0.0196	⁸⁵ 0.0238	⁸⁴ 0.0281	¹²⁰ 0.0313	¹²⁰ 0.0368	¹¹⁹ 0.0504	⁸² 0.0717	⁸⁶ 0.1147	⁸⁶ 0.1614	⁸⁶ 0.2113	⁸⁵ 0.2553	¹²¹ 0.2976	¹²⁰ 0.3537	¹²¹ 0.4334
47	IDEMIA-004	⁸¹ 0.0107	⁸⁴ 0.0148	⁸⁵ 0.0192	⁸⁴ 0.0233	⁸³ 0.0277	¹¹⁹ 0.0312	¹¹⁹ 0.0367	¹²⁰ 0.0512	⁸⁵ 0.0373	⁸⁵ 0.0587	⁸⁴ 0.0833	⁸⁵ 0.1100	⁵⁷ 0.1340	⁸³ 0.1580	⁸⁰ 0.1911	⁸¹ 0.2482
48	IDEMIA-005	⁸⁴ 0.0118	⁸⁷ 0.0167	⁹⁰ 0.0218	⁸⁹ 0.0270	⁸⁸ 0.0317	¹²³ 0.0357	¹²² 0.0425	¹²² 0.0579	⁶⁵ 0.0440	⁶⁴ 0.0689	⁶⁰ 0.0964	⁵⁹ 0.1254	⁵⁸ 0.1513	⁹⁰ 0.1762	⁸⁵ 0.2113	⁸⁷ 0.2698
49	IDEMIA-006	⁸¹ 0.0124	⁸⁷ 0.0171	⁸⁹ 0.0218	⁸⁷ 0.0263	⁸⁶ 0.0302	¹²¹ 0.0321	¹¹⁸ 0.0356	¹¹⁸ 0.0471	⁶² 0.0409	⁵⁹ 0.0620	⁵⁸ 0.0850	⁵⁸ 0.1097	⁴⁷ 0.1309	⁷⁸ 0.1486	⁷⁵ 0.1738	⁷⁴ 0.2200
50	IDEMIA-007	⁴⁷ 0.0050	⁴⁸ 0.0071	⁴⁸ 0.0089	⁵⁰ 0.0106	⁵¹ 0.0124	⁸⁷ 0.0142	⁸⁷ 0.0171	⁸⁰ 0.0220	³⁶ 0.0202	³⁶ 0.0335	³⁴ 0.0491	³³ 0.0663	³¹ 0.0825	⁶¹ 0.0999	⁵⁸ 0.1240	⁶¹ 0.1645
51	IDEMIA-008	³ 0.0018	⁶ 0.0024	⁶ 0.0029	⁵ 0.0032	⁷ 0.0035	¹¹ 0.0039	¹⁷ 0.0044	¹⁹ 0.0033	³ 0.0034	³ 0.0051	⁵ 0.0069	⁵ 0.0087	¹¹ 0.0123	¹⁰ 0.0146	¹⁰ 0.0186	
52	IDEMIA-009																
53	IMAGUS-005	³³ 0.0039	³³ 0.0052	³¹ 0.0061	²⁹ 0.0067	³⁰ 0.0077	⁶² 0.0088	⁶³ 0.0103	⁶² 0.0109	³⁹ 0.0212	³⁹ 0.0357	⁴⁰ 0.0539	⁴⁰ 0.0755	³⁸ 0.0967	⁷⁰ 0.1183	⁶⁹ 0.1485	⁶⁷ 0.1893
54	IMAGUS-008																
55	IMPERIAL-000	³⁴ 0.0040	³⁵ 0.0054	³⁶ 0.0067	³⁸ 0.0079	⁴⁰ 0.0093	⁷⁵ 0.0112	⁷⁴ 0.0139	⁷⁷ 0.0178	⁴⁹ 0.0286	⁵¹ 0.0503	⁵¹ 0.0779	⁵⁴ 0.1116	⁵⁶ 0.1455	⁹³ 0.1844	⁹⁶ 0.2341	⁹⁵ 0.2951
56	INCODE-003	⁹¹ 0.0155	⁹⁶ 0.0247	⁹⁶ 0.0348	⁹⁶ 0.0463	⁹⁶ 0.0571	¹³⁴ 0.0674	¹³⁴ 0.0856	¹³⁵ 0.1114	¹⁰² 0.1627	¹⁰² 0.2507	¹⁰² 0.3322	¹⁰⁰ 0.4122	¹⁰⁰ 0.4772	¹³ 0.5368	¹³ 0.6059	¹³ 0.6766
57	INCODE-004	⁵⁶ 0.0061	⁵⁹ 0.0087	⁵⁹ 0.0110	⁶¹ 0.0136	⁶⁴ 0.0161	¹⁰⁰ 0.0185	¹⁰³ 0.0236	¹⁰¹ 0.0309	⁷³ 0.0532	⁷⁴ 0.0908	⁷⁵ 0.1334	⁷⁵ 0.1809	⁷⁷ 0.2245	¹¹² 0.2675	¹¹¹ 0.3249	¹¹⁰ 0.3932
58	INNOVATRICS-004	¹¹⁴ 0.3594	¹¹³ 0.3629	¹¹² 0.3688	¹¹² 0.3754	¹¹² 0.3813	¹⁵² 0.3870	¹⁵² 0.3960	¹⁵² 0.4135	¹⁰² 0.4234	¹⁰⁶ 0.4642	¹⁰⁶ 0.5073	¹⁰⁶ 0.5522	¹⁰⁵ 0.5902	¹⁴ 0.6274	¹³ 0.6736	¹³ 0.7253
59	INNOVATRICS-005	⁴¹ 0.0046	⁴¹ 0.0063	⁴² 0.0078	⁴⁵ 0.0092	⁴⁵ 0.0106	⁷⁸ 0.0124	⁷⁹ 0.0149	⁷⁸ 0.0178	³⁵ 0.0343	⁵⁶ 0.0590	⁵⁸ 0.0886	⁵⁸ 0.1222	⁵⁷ 0.1544	⁹⁶ 0.1881	⁹⁵ 0.2321	⁹³ 0.2874
60	INTELLIVISION-002																
61	INTEMA-000																
62	IREX-000	²⁴ 0.0031	²⁴ 0.0042	²⁵ 0.0051	²⁶ 0.0060	²⁶ 0.0068	⁵⁷ 0.0080	⁵⁹ 0.0095	⁶⁰ 0.0107	⁵² 0.0313	⁵² 0.0539	⁵³ 0.0815	⁵⁶ 0.1137	⁵⁵ 0.1442	⁸⁹ 0.1755	⁹¹ 0.2181	⁸⁹ 0.2718
63	ISYSTEMS-002	⁷⁶ 0.0101	⁷⁹ 0.0135	⁸⁰ 0.0169	⁷⁹ 0.0197	⁸⁰ 0.0228	¹¹³ 0.0256	¹¹³ 0.0304	¹¹⁴ 0.0398	⁹⁰ 0.0779	⁹⁰ 0.1258	⁹¹ 0.1759	⁹⁰ 0.2299	⁹⁰ 0.2758	¹²⁵ 0.3204	¹²⁵ 0.3763	¹²³ 0.4401
64	ISYSTEMS-003	⁷⁹ 0.0089	⁶⁹ 0.0115	⁶⁹ 0.0139	⁶⁹ 0.0158	⁷⁰ 0.0177	¹⁰⁶ 0.0198	¹⁰² 0.0234	⁹⁸ 0.0303	⁸⁴ 0.0647	⁸⁴ 0.1056	⁸⁴ 0.1502	⁸¹ 0.1986	⁸³ 0.2402	¹¹⁰ 0.2819	¹¹⁵ 0.3351	¹¹⁵ 0.3976
65	KAKAO-001																
66	KEDACOM-001	⁸³ 0.0116	⁷⁵ 0.0130	⁶⁷ 0.0135	⁶⁰ 0.0133	⁵⁷ 0.0135	⁸⁶ 0.0141	⁸⁰ 0.0151	⁷⁹ 0.0176	⁴¹ 0.0241	⁴¹ 0.0360	³⁹ 0.0513	³⁴ 0.0689	³⁴ 0.0866	⁶⁶ 0.1060	⁶² 0.1327	⁶² 0.1694
67	LINECLOVA-002																
68	LOOKMAN-003	⁸⁶ 0.0123	⁸³ 0.0144	⁷⁷ 0.0158	⁷⁰ 0.0168	⁷¹ 0.0178	¹⁰² 0.0188	⁹⁵ 0.0212	⁹⁶ 0.0260	⁶⁴ 0.0438	⁶² 0.0687	⁶¹ 0.0978	⁶¹ 0.1296	⁶¹ 0.1581	⁹⁵ 0.1879	⁹⁴ 0.2294	⁹¹ 0.2756
69	LOOKMAN-005	⁸⁹ 0.0118	⁷⁷ 0.0134	⁷⁰ 0.0142	⁶⁶ 0.0144	⁶¹ 0.0150	⁹⁶ 0.0160	⁸⁸ 0.0176	⁸⁶ 0.0213	⁵¹ 0.0310	⁴⁹ 0.0480	⁴⁶ 0.0698	⁴⁶ 0.0954	⁴⁶ 0.1216	⁷⁹ 0.1491	⁷⁹ 0.1890	⁷⁹ 0.2381
70	MAXVISION-000																
71	MAXVISION-001																
72	MICROFOCUS-005	¹¹⁵ 0.4269	¹¹⁵ 0.5527	¹¹⁵ 0.6355	¹¹⁶ 0.7024	¹¹⁶ 0.7503	¹⁵⁶ 0.7876	¹⁵⁶ 0.8234	¹⁵⁷ 0.8601	¹¹¹ 0.8338	¹¹² 0.9113	¹¹² 0.9468	¹¹² 0.9667	¹¹² 0.9771	¹⁴ 0.9836	¹⁴ 0.9880	¹⁴ 0.9924
73	MICROSOFT-003	²⁸ 0.0034	³² 0.0050	³³ 0.0064	³⁶ 0.0078	³⁸ 0.0092	²¹ 0.0107	⁷³ 0.0135	⁷⁴ 0.0166	⁵⁰ 0.0288	⁵⁰ 0.0503	⁵⁰ 0.0763	⁵⁰ 0.1067	⁵⁴ 0.1359	⁸⁶ 0.1680	⁸⁶ 0.2116	⁸⁵ 0.2644
74	MICROSOFT-004	²⁹ 0.0032	²⁷ 0.0047	²⁹ 0.0060	³² 0.0075	³⁵ 0.0087	⁶⁸ 0.0103	⁷² 0.0131	⁷² 0.0159	⁴⁷ 0.0268	⁴⁸ 0.0470	⁴⁸ 0.0716	⁴⁸ 0.1007	⁴⁸ 0.1291	⁸³ 0.1610	⁸⁴ 0.2052	⁸³ 0.2590
75	MICROSOFT-005	²² 0.0031	²⁹ 0.0047	³⁵ 0.0066	⁴³ 0.0084	⁴³ 0.0103	⁸³ 0.0131	⁸⁵ 0.0164	⁸¹ 0.0185	⁴³ 0.0243	⁴⁴ 0.0432	⁴⁴ 0.0658	⁴⁴ 0.0913	⁴⁷ 0.1172	⁷⁶ 0.1476	⁷⁸ 0.1874	⁷⁶ 0.2272
76	MICROSOFT-006	²⁶ 0.0032	³¹ 0.0049	³⁴ 0.0065	⁴² 0.0081	⁴² 0.0096	⁷⁶ 0.0117	⁷⁵ 0.0144	⁷³ 0.0160	²⁴ 0.0134	²⁴ 0.0233	²⁵ 0.0346	²³ 0.0462	²² 0.0578	⁵² 0.0713	⁵² 0.0903	⁵² 0.1156
77	MUKH-002																
78	NEC-000	⁹⁷ 0.0195	⁹⁹ 0.0316	⁹⁷ 0.0445	⁹⁹ 0.0581	⁹⁸ 0.0699	¹³⁷ 0.0817	¹³⁷ 0.0998	¹³⁷ 0.1237	⁸⁹ 0.0759	⁸⁹ 0.1245	⁸⁹ 0.1729	⁸⁹ 0.2240	⁸⁹ 0.2671	¹²⁴ 0.3117	¹²² 0.3639	¹²² 0.4348
79	NEC-001	¹⁰⁴ 0.0246	¹⁰² 0.0382	¹⁰⁵ 0.0524	¹⁰⁶ 0.0672	¹⁰⁷ 0.0793	¹³⁹ 0.0904	¹³⁸ 0.1076	¹³⁸ 0.1317	⁹⁴ 0.1019	⁹⁴ 0.1623	⁹⁴ 0.2214	⁹⁴ 0.2834	⁹¹ 0.3341	¹³ 0.3844	¹³ 0.4440	¹² 0.5183
80	NEC-002	²⁷ 0.0033	²² 0.0041	¹⁸ 0.0043	¹⁶ 0.0044	¹⁵ 0.0045	³¹ 0.0059	³⁰ 0.0067	³⁰ 0.0077	⁵⁸ 0.0073	⁵⁹ 0.0056	⁵⁹ 0.0076	⁵⁹ 0.0091	⁷⁰ 0.0105	⁶⁹ 0.0119	⁶⁹ 0.0131	⁶⁹ 0.0149
81	NEC-003	³¹ 0.0036	²⁶ 0.0046	²⁴ 0.0051	²⁴ 0.0055	²⁴ 0.0055	²⁴ 0.0059	³⁰ 0.0067	³⁰ 0.0052	²⁵ 0.0036	²⁷ 0.0046	⁵ 0.0057	² 0.0063	² 0.0066	¹ 0.0069	⁴ 0.0076	⁴ 0.0090
82	NEC-004	³² 0.0039	²⁹ 0.0045	²² 0.0047	¹⁸ 0.0046	¹⁴ 0.0044	³⁰ 0.0046	³⁰ 0.0052	²⁵ 0.0036	²⁷ 0.0046	⁵ 0.0057	² 0.0063	² 0.0066	¹ 0.0069	⁴ 0.0076	⁴ 0.0105	
83	NEC-005																
84	NEC-006																
85	NEUROTECHNOLOGY-003	¹⁰¹ 0.0234	¹⁰¹ 0.0379	¹⁰² 0.0549	¹⁰¹ 0.0682	¹⁰² 0.0720	¹³⁶ 0.0747	¹³⁶ 0.0886	¹³⁴ 0.1066	¹⁰⁹ 0.6802	¹⁰⁹ 0.8187	¹¹⁰ 0.8920	¹¹⁰ 0.9355	¹¹⁰ 0.9594	¹⁴ 0.9738	¹⁴ 0.9828	¹⁴ 0.9885
86	NEUROTECHNOLOGY-004	⁷⁹ 0.0104	⁷⁹ 0.0134	⁷⁶ 0.0156	⁷³ 0.0173	⁷² 0.0195	¹⁰⁸ 0.0212	¹⁰⁶ 0.0245	¹⁰³ 0.0320	⁸³ 0.0642	⁸² 0.1015	⁸¹ 0.1426	⁷⁹ 0				

MISS RATES		INVESTIGATION, FNIR(N, R = 1, T = 0)								IDENTIFICATION, FNIR(N, R = L, T ≥ 0) FOR FPIR = 0.001									
#	ALGORITHM	(0, 2]	(2, 4]	(4, 6]	(6, 8]	(8, 10]	(10, 12]	(12, 14]	(14, 18]	(0, 2]	(2, 4]	(4, 6]	(6, 8]	(8, 10]	(10, 12]	(12, 14]	(14, 18]		
89	NEUROTECHNOLOGY-010						37.0053	41.0061	41.0053						37.00863	38.01050	39.01333		
90	NEUROTECHNOLOGY-012						22.0044	25.0051	24.0038						38.00638	40.00783	40.01027		
91	NOBLIS-002	112.0.1520	112.0.2419	112.0.3296	113.0.4114	113.0.4856	113.0.5528	113.0.6061	113.0.6532	113.0.9984	113.0.9996	113.0.9998	113.0.9999	113.0.9999	150.1.0000	150.1.0000	156.1.0000		
92	NTECHLAB-003	65.0.0078	76.0.0131	80.0.0202	96.0.0295	91.0.0405	126.0.0543	133.0.0761	133.0.1035	68.0.0491	72.0.0881	79.0.1384	83.0.1985	87.0.2594	126.0.3270	126.0.4065	126.0.4891		
93	NTECHLAB-004	62.0.0068	68.0.0110	79.0.0167	86.0.0239	89.0.0330	126.0.0447	128.0.0641	130.0.0891	60.0.0379	63.0.0688	66.0.1108	66.0.1629	73.0.2192	118.0.2846	123.0.3657	125.0.4524		
94	NTECHLAB-006	21.0.0056	62.0.0095	77.0.0148	83.0.0218	85.0.0301	124.0.0413	128.0.0591	128.0.0814	56.0.0349	60.0.0636	63.0.1023	64.0.1506	68.0.2024	108.0.2617	115.0.3374	117.0.4185		
95	NTECHLAB-007	37.0.0044	43.0.0066	49.0.0089	57.0.0118	60.0.0150	103.0.0189	108.0.0255	108.0.0342	45.0.0256	46.0.0450	48.0.0705	49.0.1012	51.0.1334	87.0.1692	88.0.2170	90.0.2752		
96	NTECHLAB-008	18.0.0025	21.0.0038	29.0.0052	31.0.0074	44.0.0104	104.0.0236	108.0.0348	108.0.0432	26.0.0143	28.0.0267	32.0.0459	37.0.0733	40.0.1062	79.0.1469	80.0.2044	86.0.2698		
97	NTECHLAB-009	13.0.0022	15.0.0031	16.0.0038	17.0.0045	19.0.0055	52.0.0067	57.0.0088	59.0.0100	18.0.0073	17.0.0117	17.0.0170	17.0.0238	18.0.0319	39.0.0419	36.0.0577	43.0.0833		
98	NTECHLAB-011									42.0.0056	43.0.0066	50.0.0073					28.0.0351	29.0.0475	34.0.0724
99	PANGIAM-000									34.0.0051	32.0.0055	33.0.0046					43.0.0503	45.0.0617	41.0.0810
100	PARAVISION-002	53.0.0058	58.0.0083	60.0.0111	63.0.0137	63.0.0162	101.0.0187	100.0.0229	98.0.0295										
101	PARAVISION-003	44.0.0048	44.0.0067	51.0.0090	52.0.0109	54.0.0128	89.0.0148	89.0.0178	87.0.0219	57.0.0354	58.0.0618	59.0.0931	60.0.1290	61.0.1625	97.0.1964	97.0.2408	99.0.2924		
102	PARAVISION-004	16.0.0024	17.0.0032	17.0.0040	19.0.0047	18.0.0053	46.0.0061	48.0.0073	48.0.0072	20.0.0118	23.0.0209	24.0.0327	24.0.0465	24.0.0613	34.0.0779	34.0.1008	34.0.1285		
103	PARAVISION-005	12.0.0021	13.0.0028	15.0.0035	14.0.0041	16.0.0046	40.0.0054	44.0.0067	47.0.0070	11.0.0057	12.0.0093	12.0.0144	14.0.0207	15.0.0278	30.0.0368	30.0.0508	33.0.0715		
104	PARAVISION-007	6.0.0019	8.0.0025	7.0.0029	8.0.0033	8.0.0036	19.0.0042	21.0.0049	17.0.0030	10.0.0057	13.0.0094	14.0.0144	13.0.0206	14.0.0275	29.0.0357	30.0.0485	30.0.0652		
105	PARAVISION-009						17.0.0041	15.0.0046	15.0.0026						23.0.0283	24.0.0371	25.0.0525		
106	PIXELALL-002	72.0.0085	73.0.0119	71.0.0147	72.0.0172	73.0.0198	116.0.0225	109.0.0270	110.0.0349	97.0.1193	97.0.1900	97.0.2601	97.0.3332	97.0.3955	133.0.4565	133.0.5268	134.0.6030		
107	PIXELALL-003	46.0.0050	42.0.0063	39.0.0072	34.0.0077	33.0.0085	66.0.0095	67.0.0113	65.0.0119	44.0.0248	43.0.0418	43.0.0622	43.0.0861	43.0.1104	72.0.1364	72.0.1723	72.0.2167		
108	PIXELALL-004	45.0.0049	40.0.0063	40.0.0072	37.0.0079	36.0.0089	70.0.0103	70.0.0127	70.0.0146	38.0.0211	40.0.0360	42.0.0553	42.0.0792	39.0.1045	71.0.1317	71.0.1700	75.0.2246		
109	PTAKURSATSU-000	54.0.0061	58.0.0082	58.0.0097	50.0.0109	49.0.0120	82.0.0131	77.0.0146	80.0.0180	59.0.0375	57.0.0596	55.0.0842	55.0.1116	53.0.1357	88.0.1553	78.0.1820	78.0.2326		
110	RANKONE-002	99.0.0212	98.0.0313	99.0.0431	98.0.0562	99.0.0712	138.0.0881	139.0.1130	140.0.1543	95.0.1111	95.0.1707	95.0.2305	95.0.2968	96.0.3646	132.0.4345	132.0.5172	135.0.6110		
111	RANKONE-004	108.0.0424	107.0.0643	107.0.0875	107.0.1127	107.0.1364	144.0.1579	149.0.1914	145.0.2378	104.0.1855	103.0.2681	103.0.3431	101.0.4155	101.0.4785	136.0.5350	136.0.5980	136.0.6722		
112	RANKONE-005	92.0.0136	93.0.0192	91.0.0246	91.0.0303	90.0.0362	124.0.0422	124.0.0521	124.0.0694	81.0.0582	75.0.0910	71.0.1260	68.0.1645	68.0.2005	100.0.2353	100.0.2816	101.0.3522		
113	RANKONE-007	67.0.0078	64.0.0099	61.0.0113	58.0.0123	58.0.0139	92.0.0156	94.0.0191	93.0.0242	42.0.0242	42.0.0376	41.0.0542	38.0.0737	37.0.0935	68.0.11130	66.0.1416	66.0.1811		
114	RANKONE-009	48.0.0054	49.0.0072	48.0.0085	47.0.0098	47.0.0113	81.0.0130	86.0.0169	90.0.0220	37.0.0208	38.0.0345	37.0.0504	36.0.0706	36.0.0930	69.0.1174	70.0.1504	69.0.2002		
115	RANKONE-010	42.0.0047	38.0.0061	38.0.0070	33.0.0076	34.0.0087	67.0.0098	68.0.0113	66.0.0120	31.0.0177	29.0.0269	26.0.0368	26.0.0479	25.0.0590	51.0.0688	50.0.0803	48.0.0991		
116	RANKONE-011	23.0.0031	23.0.0041	23.0.0047	23.0.0053	22.0.0058	53.0.0067	49.0.0077	51.0.0073	23.0.0127	20.0.0194	21.0.0265	20.0.0345	20.0.0422	42.0.0499	41.0.0611	37.0.0756		
117	RANKONE-012									49.0.0065	46.0.0069	40.0.0053					36.0.0460	34.0.0540	31.0.0672
118	RANKONE-013									35.0.0051	27.0.0051	21.0.0035					24.0.0306	23.0.0355	20.0.0405
119	REALNETWORKS-002	107.0.0381	108.0.0687	108.0.1062	108.0.1495	108.0.1963	149.0.2513	151.0.3206	151.0.3927	108.0.2153	108.0.3323	108.0.4444	105.0.5485	106.0.6355	142.0.7132	143.0.7855	145.0.8437		
120	REALNETWORKS-003	103.0.0245	105.0.0437	105.0.0686	106.0.0975	108.0.1312	147.0.1719	148.0.2294	148.0.2907	98.0.1468	100.0.2370	101.0.3313	103.0.4269	105.0.5142	140.0.5979	141.0.6815	141.0.7567		
121	REALNETWORKS-004	102.0.0244	104.0.0428	104.0.0663	105.0.0939	105.0.1251	146.0.1634	146.0.2170	147.0.2785	99.0.1484	101.0.2377	100.0.3303	102.0.4249	102.0.5106	139.0.5924	140.0.6758	140.0.7534		
122	REALNETWORKS-006									56.0.0069	51.0.0077	55.0.0080					63.0.1022	59.0.1253	59.0.1622
123	REALNETWORKS-008									33.0.0049	31.0.0054	35.0.0047					37.0.0462	37.0.0577	36.0.0745
124	S1-002									28.0.0046	26.0.0051	27.0.0038					39.0.0482	39.0.0597	38.0.0788
125	S1-003									43.0.0057	42.0.0063	43.0.0056					39.0.0681	51.0.0839	50.0.1061
126	SCANOVATE-001	68.0.0079	72.0.0117	78.0.0151	78.0.0185	78.0.0221	114.0.0259	116.0.0321	116.0.0427	88.0.0727	88.0.1169	87.0.1650	87.0.2115	88.0.2528	120.0.2925	117.0.3437	116.0.4084		
127	SENSETIME-002	90.0.0186	92.0.0191	89.0.0183	73.0.0179	68.0.0173	84.0.0133	58.0.0089	44.0.0059	40.0.0220	25.0.0236	19.0.0237	18.0.0240	17.0.0245	129.0.0219	129.0.0195	129.0.0222		
128	SENSETIME-003	11.0.0021	12.0.0028	11.0.0031	7.0.0033	6.0.0035	14.0.0040	18.0.0047	18.0.0033	8.0.0046	8.0.0064	6.0.0076	4.0.0086	4.0.0101	10.0.0122	11.0.0155	11.0.0196		
129	SENSETIME-004	3.0.0016	3.0.0022	3.0.0025	3.0.0028	3.0.0030	5.0.0035	13.0.0043	12.0.0025	4.0.0036	4.0.0052	3.0.0066	3.0.0081	3.0.0099	12.0.0126	13.0.0169	14.0.0230		
130	SENSETIME-005	2.0.0015	2.0.0020	2.0.0024	2.0.0026	2.0.0029	4.0.0035	10.0.0043	15.0.0028	5.0.0036	7.0.0059	8.0.0089	7.0.0128	10.0.0177	20.0.0240	22.0.0345	23.0.0493		
131	SENSETIME-006	1.0.0015	1.0.0019	1.0.0022	1.0.0025	1.0.0027	1.0.0033	5.0.0040	8.0.0021	2.0.0031	2.0.0049	4.0.0068	6.0.0097	7.0.0132	16.0.0184	19.0.0262	19.0.0359		
132	SENSETIME-007						3.0.0035	2.0.0038	3.0.0015						9.0.0112	9.0.0140	9.0.0176		

T = 0 → Investigation
T > 0 → Identification

MISS RATES		INVESTIGATION, FNIR(N, R = 1, T = 0)								IDENTIFICATION, FNIR(N, R = L, T ≥ 0) FOR FPIR = 0.001							
#	ALGORITHM	(0, 2]	(2, 4]	(4, 6]	(6, 8]	(8, 10]	(10, 12]	(12, 14]	(14, 18]	(0, 2]	(2, 4]	(4, 6]	(6, 8]	(8, 10]	(10, 12]	(12, 14]	(14, 18]
133	SENSETIME-008	¹¹⁷ 0.8309	¹¹⁷ 0.8310	¹¹⁷ 0.8311	¹¹⁷ 0.8306	¹¹⁷ 0.8296	¹¹⁷ 0.8302	¹¹⁷ 0.8300	¹¹⁷ 0.8301	¹¹² 0.8340	¹¹⁸ 0.8368	¹⁰⁹ 0.8404	¹⁰⁹ 0.8445	¹⁴⁵ 0.8480	¹⁴⁵ 0.8532	¹⁴⁵ 0.8595	¹⁴⁴ 0.8691
134	SIAT-002	⁸⁹ 0.0125	⁸⁸ 0.0151	⁸³ 0.0174	⁸⁰ 0.0199	⁷⁹ 0.0223	¹¹¹ 0.0240	¹¹¹ 0.0279	¹⁰⁶ 0.0311	⁸⁵ 0.0658	⁸³ 0.1052	⁸³ 0.1483	⁸² 0.1968	⁸² 0.2399	¹¹⁶ 0.2834	¹¹⁶ 0.3405	¹¹⁵ 0.4046
135	SYNESIS-003	⁴⁰ 0.0044	³⁷ 0.0058	³⁷ 0.0070	⁴⁰ 0.0080	³⁹ 0.0091	⁶⁹ 0.0103	⁶⁹ 0.0125	⁷¹ 0.0152	⁴⁸ 0.0262	⁴⁵ 0.0444	⁴⁵ 0.0666	⁴⁵ 0.0923	⁴⁴ 0.1156	⁷³ 0.1399	⁷⁴ 0.1736	⁷³ 0.2185
136	SYNESIS-005																
137	T4ISB-000																
138	TECH5-001	⁵⁷ 0.0061	⁶¹ 0.0093	⁶⁶ 0.0128	⁷¹ 0.0171	⁷⁷ 0.0221	¹¹⁸ 0.0289	¹² 0.0412	¹² 0.0560	⁸⁹ 0.0660	⁸⁷ 0.1156	⁹⁰ 0.1733	⁹¹ 0.2385	⁹¹ 0.2998	¹²⁷ 0.3629	¹²⁹ 0.4424	¹³⁰ 0.5284
139	TOSHIBA-001	⁷³ 0.0086	⁷⁴ 0.0119	⁷⁴ 0.0150	⁷⁴ 0.0178	⁷⁸ 0.0209	¹¹² 0.0241	¹¹² 0.0292	¹¹¹ 0.0365								
140	TRUEFACE-000	³⁶ 0.0043	³⁶ 0.0057	³⁰ 0.0061	²⁹ 0.0067	²⁹ 0.0073	⁶⁹ 0.0084	⁶⁰ 0.0097	⁵⁸ 0.0099	³⁶ 0.0200	³⁷ 0.0338	³⁸ 0.0504	³⁵ 0.0705	³⁵ 0.0904	⁶⁷ 0.1112	⁶⁸ 0.1401	⁶⁵ 0.1792
141	VERIDAS-001	⁵⁸ 0.0063	⁵⁶ 0.0083	⁵⁶ 0.0099	⁵⁶ 0.0113	⁵⁶ 0.0132	⁹⁰ 0.0148	⁹¹ 0.0184	⁸⁸ 0.0219	⁶¹ 0.0403	⁶¹ 0.0684	⁶² 0.1012	⁶² 0.1386	⁶² 0.1741	⁹⁸ 0.2113	⁹⁸ 0.2611	⁹⁹ 0.3233
142	VISIONLABS-004	⁴³ 0.0048	⁴⁶ 0.0069	⁵² 0.0091	⁵¹ 0.0111	⁵⁰ 0.0130	⁹⁵ 0.0152	⁹² 0.0187	⁹⁴ 0.0242	⁷¹ 0.0540	⁷⁷ 0.0916	⁷⁸ 0.1358	⁷⁸ 0.1855	⁷⁹ 0.2303	¹¹⁴ 0.2745	¹¹³ 0.3312	¹⁰⁹ 0.3913
143	VISIONLABS-005	³⁹ 0.0044	³⁹ 0.0063	⁴³ 0.0081	⁴⁶ 0.0095	⁴⁶ 0.0109	⁷⁹ 0.0125	⁸¹ 0.0151	⁸² 0.0187	⁶⁷ 0.0479	⁶⁷ 0.0812	⁶⁸ 0.1212	⁷⁰ 0.1664	⁶⁹ 0.2078	¹⁰⁵ 0.2473	¹⁰⁴ 0.2999	¹⁰³ 0.3577
144	VISIONLABS-006	²⁹ 0.0035	³⁰ 0.0048	³² 0.0061	³⁰ 0.0069	²⁹ 0.0077	⁶¹ 0.0087	⁶⁴ 0.0105	⁶⁷ 0.0120	⁴⁸ 0.0273	⁴⁷ 0.0465	⁴⁷ 0.0702	⁴⁷ 0.0970	⁴⁷ 0.1228	⁷⁷ 0.1486	⁷⁷ 0.1847	⁷⁷ 0.2295
145	VISIONLABS-008	²¹ 0.0028	²⁰ 0.0037	²¹ 0.0047	²² 0.0053	²³ 0.0058	⁵¹ 0.0067	⁵⁵ 0.0081	⁵⁶ 0.0085	²⁷ 0.0143	²⁷ 0.0241	²⁸ 0.0373	²⁷ 0.0519	²⁷ 0.0677	³⁵ 0.0850	³⁶ 0.1104	³⁶ 0.1444
146	VISIONLABS-009	¹⁰ 0.0020	¹⁰ 0.0026	¹⁰ 0.0030	¹⁰ 0.0034	¹⁰ 0.0038	²¹ 0.0044	²⁹ 0.0052	³⁴ 0.0046	¹⁴ 0.0065	¹⁵ 0.0105	¹⁵ 0.0156	¹⁵ 0.0217	¹⁶ 0.0289	³¹ 0.0368	³² 0.0499	³² 0.0681
147	VISIONLABS-010	⁹ 0.0020	⁹ 0.0025	⁹ 0.0030	¹¹ 0.0034	⁹ 0.0036	²⁹ 0.0043	²⁴ 0.0051	³⁶ 0.0047	¹⁷ 0.0069	¹⁶ 0.0113	¹⁶ 0.0170	¹⁶ 0.0238	¹⁷ 0.0316	³⁴ 0.0411	³⁵ 0.0557	³⁵ 0.0740
148	VISIONLABS-011														²² 0.0270	²⁰ 0.0337	²¹ 0.0432
149	VNPT-002														⁴⁶ 0.0534	⁴⁶ 0.0670	⁴⁶ 0.0882
150	VTS-000	¹¹⁶ 0.5878	¹¹⁶ 0.6312	¹¹⁶ 0.6602	¹¹⁵ 0.6863	¹¹⁵ 0.7073	¹⁵⁵ 0.7246	¹⁵⁵ 0.7458	¹⁵⁴ 0.7747	¹⁰⁸ 0.5929	¹⁰⁸ 0.6397	¹⁰⁸ 0.6729	¹⁰⁸ 0.7034	¹⁰⁷ 0.7279	¹⁴³ 0.7493	¹⁴² 0.7739	¹⁴² 0.8076
151	VTS-003														⁴⁸ 0.0597	⁴⁹ 0.0731	⁴⁹ 0.0950
152	XFORWARDAI-000	²⁰ 0.0027	¹⁸ 0.0034	²⁰ 0.0044	²¹ 0.0052	²¹ 0.0058	⁵¹ 0.0067	⁵¹ 0.0079	⁵³ 0.0076	²⁸ 0.0157	³¹ 0.0281	³⁰ 0.0443	³¹ 0.0635	³² 0.0834	⁶⁴ 0.1050	⁶³ 0.1330	⁶³ 0.1714
153	XFORWARDAI-001	¹⁵ 0.0023	¹¹ 0.0028	¹² 0.0034	¹² 0.0037	¹³ 0.0039	²⁴ 0.0045	²⁸ 0.0052	³¹ 0.0043	¹⁷ 0.0060	¹⁴ 0.0096	¹³ 0.0144	¹² 0.0200	¹³ 0.0260	²⁶ 0.0334	²⁶ 0.0435	²⁷ 0.0586
154	YITU-002	⁶⁰ 0.0066	⁵⁷ 0.0083	⁵³ 0.0094	⁴⁸ 0.0101	⁵⁰ 0.0121	⁹² 0.0150	⁹² 0.0223	¹⁰⁴ 0.0328	³³ 0.0189	³⁴ 0.0317	³⁵ 0.0494	³⁹ 0.0750	⁴¹ 0.1066	⁸⁹ 0.1494	⁸⁹ 0.2171	⁹⁶ 0.2958
155	YITU-003	⁶³ 0.0072	⁶⁰ 0.0089	⁵⁷ 0.0100	⁵¹ 0.0107	⁵⁷ 0.0125	⁹⁴ 0.0153	⁹⁹ 0.0226	¹⁰⁷ 0.0334	³⁶ 0.0194	³⁸ 0.0321	³⁶ 0.0500	⁴¹ 0.0756	⁴² 0.1071	⁸¹ 0.1500	⁹⁶ 0.2177	⁹⁶ 0.2964
156	YITU-004	⁵⁵ 0.0061	⁵¹ 0.0075	⁴⁴ 0.0081	⁴¹ 0.0081	³⁹ 0.0092	⁷² 0.0107	⁸³ 0.0154	⁸⁵ 0.0207	²² 0.0125	²² 0.0204	²³ 0.0314	²⁵ 0.0469	²⁶ 0.0671	⁹⁹ 0.0955	⁶⁸ 0.1421	⁷⁰ 0.2006
157	YITU-005	⁶¹ 0.0067	⁵⁴ 0.0080	⁴⁷ 0.0087	⁴⁸ 0.0094	⁷³ 0.0108	⁸² 0.0151	⁸⁴ 0.0204	²¹ 0.0124	²¹ 0.0198	²² 0.0308	²² 0.0462	²⁵ 0.0667	²⁶ 0.0953	⁶⁷ 0.1418	⁶⁷ 0.1930	

#	ALGORITHM	INVESTIGATION MODE						IDENTIFICATION MODE						FAILURE TO EXTRACT FEATURES						
		RANK ONE MISS RATE, FNIR(N, 0, 1)						HIGH T → FPIR = 0.001, FNIR(N, T, L)												
		N=1.6M						N=1.6M												
GALLERY	MUGSHOT	MUGSHOT	MUGSHOT	VISA	BORDER	BOR ₁ 10YR	KIOSK	MUGSHOT	MUGSHOT	MUGSHOT	VISA	BORDER	BOR ₁ 10YR	KIOSK	MUGSHOT	MUGSHOT	MUGSHOT	VISA	BORDER	KIOSK
PROBE	MUGSHOT	WEBCAM	PROFILE	BORDER	BOR ₁ 10YR	KIOSK		MUGSHOT	WEBCAM	PROFILE	BORDER	BOR ₁ 10YR	KIOSK		MUGSHOT	WEBCAM	PROFILE	BORDER	BOR ₁ 10YR	KIOSK
1	20FACE-000	²⁷ 0.055	²⁶ 0.085	¹⁷ 0.736	²⁰ 0.056	¹² 0.239	¹⁹ 0.243	²⁷ 0.348	²⁶ 0.450	²³ 0.100	²⁰ 0.424	¹¹ 0.772	¹⁹ 0.938	0.000	0.000	0.000	0.000	0.000	0.000	
2	3DIVI-003	²⁸ 0.083	²⁸ 0.206	²¹ 0.141	²² 0.474	²⁹ 0.400	²⁸ 0.626	²⁷ 0.605	¹⁸ 0.821	²⁰ 0.002	⁰ 0.005									
3	3DIVI-004	²⁴ 0.018	²⁵ 0.062	¹⁹ 0.035	¹⁹ 0.279	²⁴ 0.169	²⁵ 0.343	¹⁹ 0.277	¹⁵ 0.607	⁰ 0.005										
4	3DIVI-005	²⁴ 0.018	²⁵ 0.062	²² 0.930	²³ 0.821	²⁰ 0.279	²⁴ 0.166	²⁵ 0.339	¹⁶ 0.996	²² 0.864	¹⁵ 0.597	⁰ 0.002	⁰ 0.005	⁰ 0.442						
5	3DIVI-006	²⁵ 0.024	²⁵ 0.074	¹⁹ 0.047	²⁰ 0.312	²⁴ 0.168	²⁵ 0.342	¹⁹ 0.283	¹⁵ 0.615	⁰ 0.002	⁰ 0.005									
6	ACER-000	²¹ 0.011	²⁴ 0.036	²⁰ 0.827	¹⁷ 0.025	¹⁸ 0.209	²³ 0.246	¹¹ 0.981	¹⁸ 0.201	¹³ 0.490	⁰ 0.000	⁰ 0.000	⁰ 0.042							
7	ACER-001	¹⁷ 0.005	¹⁶ 0.020	¹¹ 0.422	¹⁴ 0.008	¹⁰ 0.050	⁸ 0.098	¹⁸ 0.056	¹⁶ 0.109	²⁰ 0.999	¹⁴ 0.068	¹⁰ 0.406	¹³ 0.479	⁰ 0.001	⁰ 0.001	⁰ 0.041	⁰ 0.000			
8	AIZE-001	¹⁷ 0.006	¹⁶ 0.022	¹⁶ 0.683	¹⁶ 0.016	¹⁰ 0.050	¹⁶ 0.165	²⁰ 0.077	¹⁸ 0.143	¹⁴ 0.994	¹⁵ 0.101	⁹ 0.364	¹¹ 0.387	⁰ 0.001	⁰ 0.001	⁰ 0.047				
9	ALCHERA-000	²³ 0.016	²³ 0.047	²⁰ 0.870	¹⁹ 0.046	²⁰ 0.292	²³ 0.138	²¹ 0.216	¹⁷ 0.999	¹⁸ 0.176	¹⁷ 0.803	⁰ 0.006	⁰ 0.014	⁰ 0.328						
10	ALCHERA-001	³¹ 0.987	³⁰ 1.000	²³ 1.000	³⁰ 8.000	³¹ 0.999	³⁰ 8.000	³⁰ 8.000	³⁰ 8.000	³⁰ 7.000	³⁰ 7.000	⁰ 0.006	⁰ 0.013	⁰ 0.324						
11	ALCHERA-002	²⁸ 0.095	²⁷ 0.166	²³ 0.954	²³ 0.668	²¹ 0.446	²⁶ 0.486	²⁷ 0.591	²⁰ 6.1000	²² 0.827	¹⁷ 7.811	⁰ 0.001	⁰ 0.002	⁰ 1.106						
12	ALCHERA-003	²¹ 0.010	²¹ 0.035	¹⁷ 0.741	¹⁶ 0.016	¹⁸ 0.206	²⁴ 0.155	²² 0.239	¹⁹ 0.999	¹⁸ 0.172	¹³ 0.464	⁰ 0.001	⁰ 0.002	⁰ 1.106						
13	ALCHERA-004	²² 0.011	²¹ 0.038	¹¹ 0.345	¹⁶ 0.017	¹¹ 0.088	¹⁵ 0.144	²⁷ 0.394	²⁷ 0.529	¹³ 0.991	²⁰ 4.424	¹⁰ 8.708	¹⁴ 9.546	⁰ 0.001	⁰ 0.001	⁰ 0.046	⁰ 0.000			
14	ALLGOVISION-000	²² 0.011	²⁰ 0.033	²¹ 0.894	¹⁷ 0.021	²⁰ 2.282	²¹ 0.088	²⁰ 4.166	¹³ 1.990	¹⁶ 2.117	¹⁴ 0.526	⁰ 0.002	⁰ 0.003	⁰ 1.122						
15	ALLGOVISION-001	²⁰ 5.009	²² 0.038	¹⁶ 1.661	¹⁷ 3.021	¹⁹ 3.241	²¹ 7.102	²² 1.221	¹² 0.986	¹⁷ 4.150	¹³ 9.491	⁰ 0.001	⁰ 0.001	⁰ 0.042						
16	ANKE-000	²³ 0.013	²⁰ 0.036	²² 0.931	²⁴ 1.000	²⁶ 1.000	²² 0.117	²² 0.220	¹⁴ 0.994	²⁶ 1.000	²⁵ 1.000	⁰ 0.000	⁰ 0.001	⁰ 0.080						
17	ANKE-001	²³ 0.013	²¹ 0.038	²³ 0.946	³⁰ 0.000	²⁸ 8.000	²² 0.119	²¹ 0.220	¹⁴ 0.994	²⁹ 1.000	²⁸ 5.000	⁰ 0.000	⁰ 0.001	⁰ 0.080						
18	ANKE-002	¹³ 0.003	¹³ 0.016	¹³ 0.522	¹⁰ 0.005	¹² 0.119	¹⁴ 0.032	¹² 0.079	⁸ 0.948	¹⁰ 5.034	⁸ 0.245	⁰ 0.001	⁰ 0.001	⁰ 0.049						
19	AWARE-003	²⁶ 1.031	²⁶ 0.090	²⁴ 0.966	²² 0.316	²⁰ 4.290	²³ 0.128	²⁴ 0.298	¹¹ 7.984	²⁰ 8.428	¹⁴ 7.530	⁰ 0.004	⁰ 0.003	⁰ 0.874						
20	AWARE-004	²⁷ 0.068	²⁸ 0.176	²⁵ 0.976	²¹ 2.122	²¹ 6.414	²⁶ 0.269	²⁷ 1.509	²⁰ 9.100	²⁰ 0.397	¹⁷ 8.816	⁰ 0.003	⁰ 0.003	⁰ 0.776						
21	AWARE-005	²⁶ 2.031	²³ 0.067	²⁸ 0.978	¹⁹ 0.048	²⁰ 8.308	²⁷ 0.364	²³ 0.253	²¹ 6.1000	¹⁹ 1.255	¹⁹ 2.916	⁰ 0.001	⁰ 0.002	⁰ 0.189						
22	AWARE-006	²⁸ 1.070	²⁴ 0.128	²⁶ 0.983	²¹ 1.111	²¹ 7.421	²⁶ 3.276	²⁵ 0.398	²⁰ 3.999	¹⁹ 8.368	¹⁷ 0.749	⁰ 0.001	⁰ 0.002	⁰ 1.189						
23	AYONIX-000	³⁰ 4.050	³⁰ 4.685	²⁶ 0.996	²² 0.607	²³ 0.867	²⁹ 0.811	²⁹ 0.939	¹⁷ 0.998	²² 0.954	²⁰ 8.982	⁰ 0.010	⁰ 0.031	⁰ 0.939						
24	AYONIX-001	³⁰ 0.341	²⁶ 0.527	²⁶ 0.993	²³ 0.994	²² 0.778	³⁰ 0.824	²⁹ 0.920	¹⁹ 8.999	²³ 0.999	²⁰ 3.099	⁰ 0.010	⁰ 0.031	⁰ 0.939						
25	AYONIX-002	³⁰ 0.341	²⁹ 0.527	²⁶ 0.993	²² 0.464	²² 0.778	²⁹ 0.824	²⁹ 0.920	²⁰ 0.999	²² 0.915	²⁰ 8.969	⁰ 0.010	⁰ 0.031	⁰ 0.939						
26	CAMVI-003	²⁷ 4.052	²⁶ 0.090	²¹ 9.911	²⁰ 8.093	²¹ 3.360	¹⁹ 5.071	¹⁸ 0.132	⁹ 4.970	¹⁶ 1.114	¹² 1.402	⁰ 0.006	⁰ 0.013	⁰ 0.675						
27	CAMVI-004	²⁷ 7.047	²⁶ 0.077	¹⁷ 0.744	²⁰ 0.072	²⁰ 7.296	¹⁹ 0.072	¹⁸ 2.136	¹⁹ 5.999	¹⁵ 0.100	¹⁷ 7.787	⁰ 0.000	⁰ 0.000	⁰ 0.000						
28	CAMVI-005	²⁷ 8.065	²⁷ 2.103	¹⁸ 0.746	²⁰ 0.098	²¹ 2.341	²¹ 6.099	²¹ 1.179	²⁰ 7.100	¹⁷ 5.156	²¹ 4.999	⁰ 0.000	⁰ 0.000	⁰ 0.000						
29	CANON-001	¹ 0.001	⁵ 0.006	⁴⁰ 0.088	²⁸ 0.001	²⁰ 0.007	²⁴ 0.062	⁴ 0.005	²⁰ 0.023	²¹ 0.365	²⁹ 0.008	²⁸ 0.068	³ 0.139	⁰ 0.001	⁰ 0.000	⁰ 0.042	⁰ 0.000			
30	CANON-002	²⁵ 0.001	⁶ 0.006	⁴⁸ 0.106	¹⁸ 0.001	²⁴ 0.007	²⁰ 0.059	³⁵ 0.005	²⁶ 0.020	²⁴ 0.407	⁵² 0.013	³³ 0.075	⁶⁸ 0.188	⁰ 0.001	⁰ 0.000	⁰ 0.042	⁰ 0.000			
31	CIB-000	⁵ 0.002	³¹ 0.008	⁴⁶ 0.100	⁴⁸ 0.002	⁴⁹ 0.011	³⁵ 0.069	⁷ 0.012	⁶⁷ 0.045	²² 4.1000	⁶⁷ 0.017	⁵⁹ 0.141	¹⁸ 0.894	⁰ 0.000	⁰ 0.000	⁰ 0.000				
32	CLEARVIEWAI-000	¹⁶ 0.001	¹⁴ 0.007	¹¹ 0.062	²⁴ 0.001	¹⁵ 0.006	¹³ 0.056	⁴⁴ 0.006	³⁴ 0.025	⁹⁹ 0.974	³⁶ 0.008	²³ 0.057	⁹⁵ 0.268	⁰ 0.000	⁰ 0.000	⁰ 0.037	⁰ 0.000			
33	CLOUDWALK-HR-000	⁵ 0.001	⁵² 0.010	¹⁵ 0.064	³⁶ 0.002	¹⁸ 0.006	¹⁴ 0.057	¹ 0.002	¹² 0.013	³ 0.133	¹⁵ 0.005	¹⁰ 0.033	²⁰ 0.099	⁰ 0.001	⁰ 0.000	⁰ 0.042	⁰ 0.000			
34	CLOUDWALK-MT-000	⁷ 5.002	⁷² 0.011	⁵ 0.057	⁷ 0.001	⁵ 0.004	⁵ 0.051	¹⁰ 0.002	¹¹ 0.013	² 0.109	¹ 0.002	⁴ 0.018	² 0.072	⁰ 0.001	⁰ 0.000	⁰ 0.042	⁰ 0.000			
35	CLOUDWALK-MT-001	⁷ 2.002	⁷³ 0.011	² 0.053	⁷ 0.001	⁷ 0.003	⁷ 0.042	¹⁰ 0.002	¹ 0.012	¹ 0.070	⁷ 0.001	¹ 0.015	¹ 0.056	⁰ 0.001	⁰ 0.000	⁰ 0.042	⁰ 0.000			
36	COGENT-000	²¹⁸ 0.010	²³⁷ 0.046	²⁴⁷ 0.965				¹⁷ 0.053	¹⁸⁸ 0.140	¹⁵⁴ 0.995										
37	COGENT-001	²¹⁷ 0.010	²³⁶ 0.046	²⁴⁶ 0.965				¹⁷⁰ 0.053	¹⁸⁴ 0.140	¹⁵² 0.995										
38	COGENT-002	¹⁴⁸ 0.004	¹⁶⁴ 0.020	²²⁰ 0.925				¹⁵ 0.044	¹⁸⁰ 0											

#	ALGORITHM	INVESTIGATION MODE						IDENTIFICATION MODE						FAILURE TO EXTRACT						
		RANK ONE MISS RATE, FNIR(N, 0, 1)						HIGH T → FPIR = .001, FNIR(N, T, L)						FEATURES						
		N=1.6M						N=1.6M												
	GALLERY	MUGSHOT	MUGSHOT	MUGSHOT	VISA	BORDER	VISA	MUGSHOT	MUGSHOT	MUGSHOT	VISA	BORDER	VISA	MUGSHOT	MUGSHOT	MUGSHOT	VISA	BORDER	KIOSK	
47	COGNITEC-004	141.003	135.016	199.813	158.013	113.057	153.043	140.031	148.097	128.090	144.068	92.316	97.288	0.002	0.001	0.635	0.006			
48	COGNITEC-005	63.002	89.010	172.073	175.021	104.037	122.015	61.010	63.041	261.1000	116.041	60.157	61.179	0.002	0.001	0.614	0.017			
49	COGNITEC-006	59.002	50.010	167.073	133.007	84.024	115.011	54.008	61.040	292.1000	93.030	66.171	161.081	0.002	0.001	0.568	0.003			
50	CUBOX-000	45.001	56.010	8.058	29.002	7.004	3.049	21.003	23.019	6.168	11.004	9.028	3.073	0.001	0.000	0.042	0.000			
51	CYBERLINK-000	152.004	161.020	177.0717	136.0007	146.0134	181.0056	161.0116	158.0995	142.063	111.0339	100.0001	100.0001	0.001	0.001	0.063				
52	CYBERLINK-001	146.004	149.018	174.0731	129.0007	145.0133	174.0054	161.0109	151.0995	139.062	160.0652	160.0000	160.0000	0.000	0.000	0.040				
53	CYBERLINK-002	126.003	87.012	159.0577	87.0004	102.0107	84.015	89.0053	126.0988	81.024	96.288	96.0001	96.0001	0.001	0.000	0.042				
54	CYBERLINK-003	60.002	39.009	129.0474	68.0003	50.012	62.0082	35.0008	54.0035	47.0972	49.012	41.100	111.0368	0.000	0.000	0.039	0.000			
55	CYBERLINK-004	65.002	83.011	128.0423	67.0003	47.0111	98.0104	51.0007	53.0036	239.1000	51.013	42.1009	20.0954	0.000	0.000	0.011	0.000			
56	CYBERLINK-005	77.002	66.011	75.0209	48.0002	42.010	89.0098	65.0010	62.0041	213.1000	54.014	37.089	197.0926	0.000	0.000	0.034	0.000			
57	DAHUA-000	209.009	195.026					208.086	181.0135					0.004	0.003					
58	DAHUA-001	187.007	187.024	170.0703				198.073	172.0122	103.0980				0.002	0.002	0.346				
59	DAHUA-002	81.002	86.012	99.304	63.003	64.0084	85.0015	71.0046	45.0638	60.0017	52.0159	0.001	0.000	0.099						
60	DAHUA-003	29.001	16.007	27.0206	41.0002	40.0009	41.0073	79.014	64.0041	45.0579	50.0013	35.0081	36.0134	0.000	0.000	0.000	0.000			
61	DAHUA-004	14.001	21.008	60.0144	30.0002	23.0007	33.0069	50.0007	36.0026	35.0485	36.0008	19.0051	30.0113	0.000	0.000	0.000	0.000			
62	DAON-000	155.004	143.017	141.0530	107.0005	75.0202	133.0125	114.023	99.0061	212.1000	82.025	68.0173	180.0846	0.002	0.002	0.108	0.001			
63	DECATUR-000	101.002	88.0111	82.0229	92.0004	72.019	110.0109	117.023	108.066	80.0675	86.027	67.0173	81.0239	0.001	0.000	0.044	0.001			
64	DEEPEGLINT-001	49.001	15.007	71.0200	26.0002	42.0073	25.0003	15.014	26.0100	21.006	51.0159	0.000	0.000	0.038						
65	DEEPEA-001	160.004	133.016	200.0814	145.0010	152.0140	161.0046	152.0101	118.0985	149.0077	108.0326	0.000	0.001	0.047						
66	DERMALOG-003	280.0126	283.0217		219.0296	223.0560	285.0482	286.0655		219.0677	187.0070	0.002	0.002	0.103						
67	DERMALOG-004	289.0125	282.0215	223.0930	213.0135	219.0467	284.0480	288.0657	157.0995	214.0603	188.0856	0.001	0.002	0.107						
68	DERMALOG-005	237.0015	217.037	168.0701	218.0242	215.0384	211.0088	195.0154	130.0990	194.0300	157.0614	0.001	0.002	0.102						
69	DERMALOG-006	200.0008	191.024	159.0619	146.0010	161.0155	168.0052	150.0105	112.0981	137.0059	107.0318	0.003	0.006	0.181						
70	DERMALOG-007	208.009	197.027	163.0675	162.0014	162.0170	209.086	192.0152	129.0990	157.0099	132.0557	0.001	0.002	0.102						
71	DERMALOG-008	134.003	125.015	130.0516	126.0007	98.0029	151.0139	159.0045	141.0094	24.1000	134.0057	98.0382	196.0940	0.000	0.000	0.002	0.000			
72	DERMALOG-009	132.003	120.014	67.0167	134.0007	131.0999	101.0106	107.0021	106.0066	226.0000	95.0031	123.0999	183.0840	0.001	0.001	0.018	0.003			
73	DERMALOG-010	105.002	80.011	21.066	193.038	123.0124	120.0113	49.0007	89.0055	18.0999	135.0089	123.0000	144.0522	0.001	0.001	0.018	0.003			
74	DIGIDATA-000	309.0590	298.0548	213.0895	229.0642	129.0707	231.0813	291.0610	276.0577	145.0994	217.0646	118.0789	181.0824	0.002	0.001	0.070	0.001			
75	DILUSENSE-000	107.002	91.012	97.0297	139.0008	95.0028	89.0099	138.030	124.0078	45.0655	112.0039	102.0664	73.0203	0.001	0.001	0.219	0.006			
76	EYEDEA-003	283.080	226.0148	242.0960	210.0101	214.0379	275.0388	274.0543	148.0994	212.0570	170.0792	0.001	0.003	0.161						
77	F8-001	230.012		169.0669	270.0000	238.0000	245.0166		125.0000			0.004	0.000	1.000	0.158					
78	HINCORE-000	221.0011	211.034	180.0767	186.0032	122.0117	176.0191	234.0134	218.0217	218.0000	182.0187	108.0598	131.0458	0.000	0.001	0.043	0.000			
79	FUJITSULAB-000	108.002	113.014	123.0440	91.0004	78.0023	86.0098	108.0021	92.0056	79.0024	69.0177	82.0240	0.000	0.001	0.016	0.000				
80	FUJITSULAB-001	84.002	106.013	120.0455	94.0004	82.0026	105.0106	98.0018	94.0058	136.0092	80.0024	109.00739	84.00247	0.000	0.003	0.150	0.002			
81	GLORY-000	294.0178	289.0320	268.0994	217.0228	225.0678	274.0367	273.0547	150.0995	207.0453	182.0839	0.011	0.013	0.985						
82	GLORY-001	291.0127	286.0267	266.0992	216.0178	225.0594	285.0305	273.0537	150.0993	204.0408	177.0819	0.011	0.013	0.988						
83	GORILLA-001	276.0060	268.0095	227.0936	204.0069	210.0329	280.0406	267.0453	247.0000	208.0468	248.0000	140.0000	0.001	0.001	0.069					
84	GORILLA-002	249.0020	233.0044	187.0753	180.027	187.0214	252.0188	242.0268	232.0000	190.0250	219.0000	0.001	0.001	0.069						
85	GORILLA-003	263.0036	255.0070	201.0821	197.0048	197.0265	267.0318	264.0434	271.0000	201.0407	311.0000	0.001	0.001	0.069						
86	GORILLA-004	184.0006	188.0024	166.0971	151.0012	164.0162	214.0089	201.0160	168.0959	168.0135	127.0438	0.000	0.001	0.042						
87	GORILLA-005	140.0003	150.018	72.0209	119.0006	131.0124	183.0058	187.0142	152.0700	154.0088	108.0315	0.000	0.000	0.040						
88	GORILLA-006	71.0002	89.012	53.0122	76.0003	67.0018	100.0105	130.0027	136.0089	35.0531	87.0028	64.0166	73.0218	0.000	0.000	0.041	0.000			
89	GORILLA-007	68.0002	65.011	51.0114	53.0002	65.0116	69.0088	129.0027	122.0077	30.0534	83.0026	61.0178	0.000	0.000	0.041	0.000				
90	GRIAULE-000	124.0002	107.0014	105.0327	149.0111	101.0031	133.0126	105.0020	102.0063	153.0095	102.0033	73.0185	0.000	0.002	0.090	0.001				
91	GRIAULE-001	28.0001	25.0008	57.0132	70.0001	80.0023	26.0065	36.0005	41.0028	71.0865	25.0007	122.0995	15.0099	0.000	0.000	0.000	0.000			
92	HIK-003	227.0012	200.0027	166.0689	154.0012	158.0151	219.0103	197.0158	92.0969	171.0142	129.0445	0.000	0.000	0.048						

Table 12: **Miss rates by dataset**: At left, rank 1 miss rates relevant to investigations; at right, with threshold set to target FPIR = 0.01 for higher volume, low prior, uses. Yellow indicates most accurate algorithm. Throughout blue superscripts indicate the rank of the algorithm for that column.

2022/11/0
18:02:21

FNIR(N, K, I) = False neg. identification rate
 FPIR(N, T) = False pos. identification rate

N = Num. enrolled subjects
R = Num. candidates examined

≡ 1 hreshold

$T \geq 0 \rightarrow$ Identification

#	ALGORITHM	INVESTIGATION MODE						IDENTIFICATION MODE						FAILURE TO EXTRACT					
		RANK ONE MISS RATE, FNIR(N, 0, 1)						HIGH T → FPIR = 0.001, FNIR(N, T, L)						FEATURES					
		N=1,6M						N=1,6M											
	GALLERY	MUGSHOT	MUGSHOT	MUGSHOT	VISA	BORDER	BOR ₂ 10YR	MUGSHOT	MUGSHOT	MUGSHOT	VISA	BORDER	BOR ₂ 10YR	MUGSHOT	MUGSHOT	MUGSHOT	VISA	BORDER	KIOSK
	PROBE	MUGSHOT	WEBCAM	PROFILE	BORDER	BOR ₂ 10YR	KIOSK	MUGSHOT	WEBCAM	PROFILE	BORDER	BOR ₂ 10YR	KIOSK	MUGSHOT	WEBCAM	PROFILE	BORDER	BOR ₂ 10YR	KIOSK
93	HIK-004	224.001	198.027	171.043	182.012	160.012	215.099	194.015	153.013	100.076	169.0137	126.0434	0.000	0.000	0.048				
94	HIK-005	164.005	138.017	145.055	131.007	113.011	154.044	125.077	202.099	143.068	146.0541	0.000	0.000	0.000	0.000	0.000			
95	HIK-006	165.005	137.017	145.055			163.047	135.086	247.0000			0.000	0.000	0.000	0.000	0.000			
96	HYPERVERGE-001	41.001	75.011	24.067	28.002	21.007	22.061	32.004	47.031	122.020	26.007	21.053	23.101	0.001	0.000	0.041			0.000
97	HYPERVERGE-002	38.001	71.011	15.063	18.001	17.006	19.058	26.004	36.027	10.0210	18.006	18.048	15.093	0.001	0.000	0.041			0.000
98	HZAILU-000	106.002	105.013	86.0244	69.0003	62.015	72.090	104.020	76.051	90.067	70.020	91.0316	46.0153	0.001	0.001	0.054			0.001
99	HZAILU-001	91.002	74.011	40.016	49.002	120.113	75.092	56.009	215.183	123.0986	186.0196	168.1000	16.0679	0.000	0.000	0.039			0.000
100	IDEMIA-003	190.007	209.034	239.058	170.018	183.0210	164.047	203.0165		163.0123	172.0766	0.000	0.000	0.041					
101	IDEMIA-004	186.007	207.032	239.047	171.018	184.0210	150.037	168.0118	98.0973	164.0123	177.0766	0.000	0.000	0.041					
102	IDEMIA-005	199.008	225.039	239.0954	177.021	188.0217	156.0044	192.0150	103.0978	165.0130	188.0879	0.000	0.000	0.041					
103	IDEMIA-006	213.010	257.072	251.0969	182.030	196.0253	153.043	223.0226	114.0982	172.0144	168.0733	0.000	0.000	0.041					
104	IDEMIA-007	125.003	130.015	277.1000	120.006	103.036	142.0131	97.018	89.055	263.1000	128.0052	71.0182	299.1000	0.000	0.000	0.040			0.000
105	IDEMIA-008	13.001	8.007	36.079	27.001	25.007	47.075	9.002	10.013	9.0204	14.0005	14.036	26.106	0.000	0.000	0.040			0.000
106	IDEMIA-009	5.001	7.006	18.065	8.001	11.005	6.051	3.002	2.011	1.041	5.0003	3.027	8.074	0.000	0.000	0.040			0.000
107	IMAGUS-002	297.0220	287.0301	262.0988				295.0749	289.0816	240.1000				0.004	0.008	0.550			
108	IMAGUS-003	303.0356	294.0513	269.0993				297.0807	299.0909	225.1000				0.004	0.008	0.550			
109	IMAGUS-005	90.002	88.012	107.0319	118.006	76.0022	144.0132	101.018	108.0066	69.0838	89.029	63.0161	78.0231	0.000	0.000	0.000			0.000
110	IMAGUS-006	97.002	110.014	96.0293	95.0004	74.0119	117.0112	103.019	110.0069	78.0897	88.0028	62.0161	89.0260	0.000	0.000	0.000			0.000
111	IMAGUS-007	98.002	103.013	108.0321	88.0004	77.0022	124.0117	116.0023	118.0073	76.0893	96.0031	65.0169	91.0265	0.000	0.000	0.000			0.000
112	IMAGUS-008	285.086	267.093	108.0305	176.021	118.081	122.0119	305.0974	286.0774	159.0996	210.0520	128.1000	143.0518	0.000	0.000	0.000			0.000
113	IMPERIAL-000	121.002	127.015	91.0280	103.004	82.0097	123.026	108.068	18.0999	117.0042	81.0245	0.000	0.000	0.000					
114	INCODE-000	273.049	270.100	234.0951				266.0310	263.0420	174.0998				0.001	0.004	0.173			
115	INCODE-001	240.017	238.0046	187.062				255.0212	247.0296	238.1000				0.001	0.004	0.173			
116	INCODE-002	244.018	240.048	204.0843				251.0184	243.0269	139.0993				0.000	0.001	0.066			
117	INCODE-003	232.013	227.040	187.0764				247.0167	239.0264	139.0999				0.000	0.001	0.066			
118	INCODE-004	147.004	147.017	139.0475	143.0008	148.0135	177.0054	171.0120	149.0095	141.0063	103.0313	0.000	0.001	0.066					
119	INCODE-005	64.002	81.011	63.0147	35.0002	55.013	56.079	69.011	67.0043	36.0528	62.017	54.0145	49.0155	0.000	0.000	0.042			0.000
120	INNOVATRICS-002	291.045	258.074	207.0853				260.0234	259.0310	243.1000				0.000	0.001	0.046			
121	INNOVATRICS-003	257.026	241.055	206.0845				256.0221	246.0297	210.1000				0.000	0.001	0.046			
122	INNOVATRICS-004	231.012	229.040	239.0958				232.0132	222.0222	108.0980				0.000	0.001	0.046			
123	INNOVATRICS-005	122.002	119.014	118.0407	105.0005	108.0109	143.034	135.089	70.0846	124.0047	86.0251	0.000	0.001	0.041					
124	INNOVATRICS-007	67.002	79.011	87.0248	38.0002	57.0013	50.077	75.0013	77.0051	57.043	61.017	39.0093	47.0154	0.000	0.001	0.041			0.000
125	INTELIGENSIA-000	96.002	96.012	76.0210	101.004	102.0033	130.0124	118.0024	121.0077	61.0786	132.0053	81.0235	87.0255	0.001	0.000	0.046			0.001
126	INTELLIVISION-001	264.036	270.102	259.0972	201.0057	127.022	211.0333	264.0279	266.0404	214.0000	196.0328	111.0749	165.0685	0.001	0.000	0.044			0.000
127	INTELLIVISION-002	220.011	206.031	230.0942	169.018	117.0080	178.0200	239.0154	219.0196	186.0999	167.0134	103.0437	133.0460	0.001	0.000	0.043			0.000
128	INTEMA-000	19.001	34.008	7.0058	10.0001	14.0005	4.051	16.0002	18.017	245.0000	16.0005	89.0288	8.081	0.000	0.000	0.040			0.000
129	INTSYSMSU-000	292.046	185.023	151.0562	205.072	143.0132	308.0998	303.0000	211.0000	229.0999	210.0999	0.000	0.000	0.050					
130	IREX-000	161.004	45.010	164.0681	34.0002	51.0102	60.0882	134.0288	98.060	84.0957	120.0044	90.302	58.0170	0.000	0.000	0.042			0.000
131	ISYSTEMS-002	185.006	194.026	208.0844				202.078	178.0126	167.0988				0.002	0.002	0.142			
132	ISYSTEMS-003	173.005	182.023	189.0791				186.059	159.0107	215.1000				0.002	0.002	0.142			
133	KAKAO-000	51.001	64.011	39.0119	57.0002	54.013	52.0078	87.0105	91.0056	30.0468	67.019	49.0141	59.0158	0.000	0.000	0.041			0.000
134	KAKAO-001	42.001	40.009	6.058	5.0001	9.0004	2.047	19.003	20.017	5.159	10.004	17.0042	5.074	0.000	0.000	0.040			0.000
135	KEDACOM-001	195.008	213.036	259.0972	188.0304	196.0237	115.0023	115.0072	122.0986	133.0055	103.0305	0.000	0.000	0.000					
136	KNERON-000	180.006	199.027	149.0552	181.0028	171.0195								0.000	0.000	0.000			
137	KNERON-001	260.030	303.0621	87.0237	215.0144	126.0207	201.0280							0.000	0.000	0.000			0.000
138	LINE-000	109.002	111.014	81.0223	111.0005	96.0029	103.0107	139.031	145.0095	122.046	86.0278	269.1000	0.000	0.000	0.000			0.000	

Table 13: **Miss rates by dataset**: At left, rank 1 miss rates relevant to investigations; at right, with threshold set to target FPIR = 0.01 for higher volume, low prior, uses. Yellow indicates most accurate algorithm. Throughout blue superscripts indicate the rank of the algorithm for that column.

2022/11/0
18:02:21

FNIR(N, R, T) = False neg. identification rate
FPIRN(T) = False pos. identification rate

N = Num. enrolled subjects
R = Num. candidates examined

= Threshold

$T = 0 \rightarrow$ Investigation
 $T > 0 \rightarrow$ Identification

#	ALGORITHM	INVESTIGATION MODE						IDENTIFICATION MODE						FAILURE TO EXTRACT FEATURES											
		RANK ONE MISS RATE, FNIR(N, 0, 1)						HIGH T → FPIR = 0.001, FNIR(N, T, L)						N=1.6M											
		GALLERY	MUGSHOT	MUGSHOT	WEBCAM	PROFILE	BORDER	BOR;10YR	KIOSK	MUGSHOT	WEBCAM	PROFILE	BORDER	BOR;10YR	KIOSK	MUGSHOT	MUGSHOT	WEBCAM	PROFILE	BORDER	BOR;10YR	KIOSK			
139	LINE-001	18.001	18.007	14.063	37.002	35.008	68.085	37.005	37.027	241.000	42.009	30.072	281.000	0.000	0.000	0.000	0.000	0.000	0.000	0.000	0.000	0.000	0.000	0.000	0.001
140	LINECLOVA-002	36.001	20.008	20.070	32.002	48.011	18.058	27.004	177.130	111.027	111.040	127.1000	166.700	0.000	0.000	0.001	0.040	0.000	0.000	0.000	0.000	0.000	0.000	0.000	
141	LOOKMAN-003	204.009	223.038	191.035	192.239	155.044	163.112	158.045	157.105	101.977	153.084	0.000	0.000	0.000	0.000	0.000	0.000	0.000	0.000	0.000	0.000	0.000	0.000		
142	LOOKMAN-004	206.009	226.039	258.0973	20.035	191.237	137.030	131.086	104.978	140.062	102.308	0.000	0.000	0.000	0.000	0.000	0.000	0.000	0.000	0.000	0.000	0.000	0.000		
143	LOOKMAN-005	198.008	216.036	255.0972	190.035	191.0237	137.030	131.086	104.978	140.062	102.308	0.000	0.000	0.000	0.000	0.000	0.000	0.000	0.000	0.000	0.000	0.000	0.000		
144	MANTRA-000	70.002	57.010	17.0709	128.0007	85.024	115.012	66.010	63.041	278.1000	98.029	58.0152	218.1000	0.002	0.001	0.591	0.003	0.000	0.000	0.000	0.000	0.000	0.000		
145	MAXVISION-000	119.002	123.015	105.327	98.0004	110.051	91.101	138.028	226.237	58.0767	173.149	123.097	151.557	0.000	0.000	0.042	0.000	0.000	0.000	0.000	0.000	0.000	0.000		
146	MAXVISION-001	30.001	22.008	17.064	12.001	70.018	17.057	30.004	33.025	11.219	21.007	118.051	22.100	0.000	0.000	0.042	0.000	0.000	0.000	0.000	0.000	0.000	0.000		
147	MEGVII-001	228.012	146.017	249.1000	241.000	197.072	149.097	201.077	147.096	177.098	0.000	0.000	0.000	0.000	0.000	0.002	0.000	0.000	0.000	0.000	0.000	0.000	0.033		
148	MEGVII-002	229.012	148.017	124.450	241.000	197.072	149.097	201.077	147.096	177.098	0.000	0.000	0.000	0.000	0.000	0.002	0.000	0.000	0.000	0.000	0.000	0.000	0.033		
149	MICROFOCUS-003	311.594	307.781	232.708	234.907	303.931	302.979	228.982	210.991	0.001	0.000	0.000	0.000	0.000	0.005	0.000	0.000	0.000	0.000	0.000	0.000	0.000			
150	MICROFOCUS-004	308.576	306.758	231.701	235.904	306.999	306.975	229.974	208.989	0.001	0.000	0.000	0.000	0.000	0.005	0.000	0.000	0.000	0.000	0.000	0.000	0.000			
151	MICROFOCUS-005	304.424	301.601	226.494	227.777	301.835	296.928	229.935	207.985	0.001	0.000	0.000	0.000	0.000	0.005	0.000	0.000	0.000	0.000	0.000	0.000	0.000			
152	MICROFOCUS-006	305.427	300.583	225.490	230.782	306.978	295.923	223.923	204.971	0.001	0.000	0.000	0.000	0.000	0.005	0.000	0.000	0.000	0.000	0.000	0.000	0.000			
153	MICROSOFT-003	61.002	93.012	86.0004	111.0109	132.028	139.091	108.036	80.233	0.000	0.000	0.000	0.000	0.000	0.005	0.000	0.000	0.000	0.000	0.000	0.000	0.000			
154	MICROSOFT-004	53.001	92.012	79.004	112.109	124.026	133.087	103.033	76.222	0.000	0.000	0.000	0.000	0.000	0.005	0.000	0.000	0.000	0.000	0.000	0.000	0.000			
155	MICROSOFT-005	85.002	70.011	61.144	73.003	87.099	121.026	112.070	41.587	81.027	64.180	0.000	0.000	0.000	0.049	0.000	0.000	0.000	0.000	0.000	0.000	0.000			
156	MICROSOFT-006	93.002	84.011	65.150	83.004	90.100	70.012	56.037	22.386	99.032	60.178	0.000	0.000	0.000	0.049	0.000	0.000	0.000	0.000	0.000	0.000	0.000			
157	MUKH-002	256.026	215.036	159.638	150.012	116.079	138.129	280.594	232.242	222.1000	170.170	110.741	118.389	0.000	0.000	0.042	0.000	0.000	0.000	0.000	0.000	0.000			
158	NEC-000	241.017	231.041	241.059	178.025	194.023	204.040	186.140	108.097	136.074	0.000	0.000	0.000	0.000	0.000	0.000	0.000	0.000	0.000	0.000	0.000	0.000			
159	NEC-001	250.021	244.056	249.067	18.033	198.027	221.016	215.197	121.986	166.133	0.000	0.000	0.000	0.000	0.000	0.005	0.000	0.000	0.000	0.000	0.000	0.000			
160	NEC-002	11.001	38.009	111.0363	78.0003	123.0117	18.0003	25.020	196.0999	32.008	162.076	0.000	0.000	0.000	0.000	0.000	0.041	0.000	0.000	0.000	0.000	0.000	0.000		
161	NEC-003	39.001	55.010	113.0352	82.004	55.013	129.120	15.002	19.017	66.0824	31.008	15.036	161.668	0.000	0.000	0.041	0.000	0.000	0.000	0.000	0.000	0.000			
162	NEC-004	47.001	36.009	144.0538	71.0003	31.007	46.075	6.0002	9.013	44.0622	12.0004	4.019	21.000	0.000	0.000	0.041	0.000	0.000	0.000	0.000	0.000	0.000			
163	NEC-005	25.001	23.008	38.081	36.0002	10.0005	43.073	4.0002	5.012	49.0673	7.0003	3.019	17.099	0.000	0.000	0.040	0.000	0.000	0.000	0.000	0.000	0.000			
164	NEC-006	33.001	30.008	17.063	4.0001	13.0005	15.0057	11.0002	1.018	29.0463	8.0004	7.026	14.094	0.000	0.000	0.040	0.000	0.000	0.000	0.000	0.000	0.000			
165	NEUROTECHNOLOGY-003	251.022	232.042	243.0961	0.000	293.0636	241.266	254.0000	0.000	0.000	0.000	0.000	0.000	0.000	0.000	0.000	0.000	0.000	0.000	0.000	0.000	0.131			
166	NEUROTECHNOLOGY-004	175.006	160.020	257.0970	0.000	191.063	165.117	144.0994	0.000	0.000	0.000	0.000	0.000	0.000	0.000	0.000	0.000	0.000	0.000	0.000	0.000	0.131			
167	NEUROTECHNOLOGY-005	159.004	190.024	211.0893	0.000	178.054	178.130	169.0998	0.000	0.000	0.000	0.000	0.000	0.000	0.000	0.000	0.000	0.000	0.000	0.000	0.000	0.030			
168	NEUROTECHNOLOGY-006	245.018	235.045	150.606	0.000	261.0249	261.0418	0.000	0.000	0.000	0.000	0.000	0.000	0.000	0.000	0.000	0.000	0.000	0.000	0.000	0.000	0.000			
169	NEUROTECHNOLOGY-007	151.004	168.021	192.0796	144.009	173.0180	190.062	207.0173	221.0000	197.0339	270.0000	0.000	0.000	0.000	0.000	0.000	0.041	0.000	0.000	0.000	0.000	0.000	0.000		
170	NEUROTECHNOLOGY-008	104.002	118.014	120.0457	90.004	81.0023	94.0101	172.053	127.080	231.0000	103.035	89.0293	71.203	0.000	0.000	0.052	0.000	0.000	0.000	0.000	0.000	0.000			
171	NEUROTECHNOLOGY-009	48.001	68.011	70.179	4.002	56.013	55.079	88.015	81.052	42.0588	69.020	59.0153	35.0165	0.000	0.000	0.046	0.000	0.000	0.000	0.000	0.000	0.000			
172	NEUROTECHNOLOGY-010	31.001	44.009	29.070	21.001	30.007	32.068	64.010	59.037	17.0277	45.010	34.0075	33.0126	0.000	0.000	0.041	0.000	0.000	0.000	0.000	0.000	0.000			
173	NEUROTECHNOLOGY-012	9.001	26.008	17.063	4.0001	13.0005	15.0057	48.0007	51.032	86.0595	39.0008	25.061	193.016	0.000	0.000	0.039	0.000	0.000	0.000	0.000	0.000	0.000			
174	NEWLAND-002	282.079	273.117	226.0936	0.000	282.0438	268.0466	189.0999	0.000	0.000	0.000	0.000	0.000	0.000	0.000	0.000	0.000	0.000	0.000	0.000	0.000	0.000			
175	NOBLIS-001	299.049	295.052	261.0993	0.000	311.0000	305.1000	234.0000	0.000	0.000	0.000	0.000	0.000	0.000	0.000	0.000	0.000	0.000	0.000	0.000	0.000	0.000			
176	NOBLIS-002	295.079	292.0392	259.0982	0.000	307.0997	314.1000	248.0000	0.000	0.000	0.000	0.000	0.000	0.000	0.000	0.000	0.000	0.000	0.000	0.000	0.000	0.000			
177	NOTIONTAG-000	123.002	94.012	77.0204	92.004	63.016	79.095	92.017	97.059	45.0611	74.0201	57.0150	59.0176	0.000	0.000	0.000	0.000								

Table 15: **Miss rates by dataset**: At left, rank 1 miss rates relevant to investigations; at right, with threshold set to target FPIR = 0.01 for higher volume, low prior, uses. Yellow indicates most accurate algorithm. Throughout blue superscripts indicate the rank of the algorithm for that column.

2022/11/0
18:02:21

FNIR(N, R, T) = False neg. identification rate
FPIRN(T) = False pos. identification rate

N = Num. enrolled subjects
R = Num. candidates examined

T = Threshold

$T = 0 \rightarrow$ Investigation
 $T > 0 \rightarrow$ Identification

#	ALGORITHM	INVESTIGATION MODE						IDENTIFICATION MODE						FAILURE TO EXTRACT FEATURES						
		RANK ONE MISS RATE, FNIR(N, 0, 1)						HIGH T → FPIR = 0.001, FNIR(N, T, L)												
		N=1.6M						N=1.6M												
	GALLERY	MUGSHOT	MUGSHOT	MUGSHOT	VISA	BORDER	VISA	MUGSHOT	MUGSHOT	MUGSHOT	VISA	BORDER	VISA	MUGSHOT	MUGSHOT	MUGSHOT	VISA	BORDER	KIOSK	
	PROBE	MUGSHOT	WEBCAM	PROFILE	BORDER	BOR ₂ 10YR	KIOSK	MUGSHOT	WEBCAM	PROFILE	BORDER	BOR ₂ 10YR	KIOSK	MUGSHOT	WEBCAM	PROFILE	BORDER	BOR ₂ 10YR	KIOSK	
231	S1-001	138.0003	114.0014	79.0215	65.0003	68.0018	48.0077	80.0016	80.0052	119.0985	66.0019	47.0136	44.0148	0.001	0.000	0.035		0.000		
232	S1-002	46.0001	41.0009	45.0093	11.0001	45.0010	12.0055	46.0006	46.0031	8.0196	2.0007	116.0792	184.0841	0.000	0.000	0.028		0.000		
233	S1-003	59.0001	47.0010	50.0114	25.0001	27.0007	21.0060	59.0009	57.0037	219.1000	51.0014	49.0396	315.1000	0.000	0.000	0.033		0.000		
234	SCANOVATE-000	170.0005	234.0045	150.0560	189.0035	188.0211	194.067	231.0240	75.0893	188.0215	126.0400	0.000	0.001	0.057						
235	SCANOVATE-001	17.0005	228.0040	154.0585	187.0031	172.0178	209.0081	224.0227	79.0911	187.0192	125.0404	0.000	0.001	0.044						
236	SENSETIME-000	114.0002	132.0016	140.0528				109.0221	101.0063	266.1000				0.004	0.000	0.042				
237	SENSETIME-001	118.0002	131.0016					118.0222	103.0064					0.004	0.000					
238	SENSETIME-002	238.0014	158.0020	117.0384	147.0011			97.0104	83.0015	42.0028	143.0994	98.0032		145.0523	0.009	0.000	0.040			
239	SENSETIME-003	7.0001	9.0007	64.0150	66.0003			74.0091	3.0002	6.0012	31.0477	3.0008		20.133	0.000	0.000	0.041			
240	SENSETIME-004	10.0001	12.0007	31.0072	59.0002			67.0084	3.0002	8.0013	14.0229	19.0006		29.0113	0.000	0.000	0.041			
241	SENSETIME-005	4.0001	4.0006	10.0059	51.0002	26.0007	59.0082	14.0002	14.014	7.0173	23.0007	20.0051	24.0104	0.000	0.000	0.041		0.000		
242	SENSETIME-006	3.0001	3.0006	4.0055	8.0001	4.0004	26.0064	7.0002	7.0012	175.0998	9.0004	12.0034	12.0093	0.000	0.000	0.025		0.000		
243	SENSETIME-007	2.0001	2.0006	1.0052	3.0001	3.0003	23.0062	2.0001	2.0009	197.0999	4.0003	6.0024	9.0085	0.000	0.000	0.025		0.000		
244	SENSETIME-008	1.0001	1.0006	3.0054	2.0001	2.0003	30.0067	1.0001	1.0009	23.0405	2.0002	3.0021	7.0080	0.000	0.000	0.039		0.000		
245	SHAMAN-003	297.0124	297.0172						293.0451	278.0597					0.020	0.011				
246	SHAMAN-004	29.0222	288.0319						29.0615	288.0754					0.020	0.011				
247	SHAMAN-006	26.0040	246.0058	228.0938					230.0141	227.0237	96.0972				0.020	0.011	0.869			
248	SHAMAN-007	26.0040	245.0057						234.0141	230.0240					0.020	0.010				
249	SIAT-001	76.0002	290.0333	108.0004				88.0099	99.0018	257.0365		94.0031		0.000	0.000					
250	SIAT-002	79.0002	293.0446	221.0348				95.0102	110.022	269.0478	199.0372		195.0923	0.000	0.000					
251	SMILART-004	312.0965	308.0974						304.0968	301.0976					0.011	0.013				
252	SMILART-005														0.011	0.013				
253	SQLSOFT-001	158.0004	156.0019	94.0282	110.0005	89.0027	83.0097	233.0132	234.0252	62.0797	114.0040	93.0317	125.0420	0.000	0.000	0.039		0.000		
254	STAQU-000	192.0007	163.0020	157.0613	172.0020	112.0055	163.0159	198.0062	268.0443	217.1000	211.0535	120.0961	240.1000	0.000	0.000	0.000		0.000		
255	SYNESIS-003	23.0016	183.0023	203.0827	159.0013			149.0136	198.0065	173.0123	87.0960	148.0075	104.0314	0.000	0.001	0.063				
256	SYNESIS-003	293.0170	284.0235						298.0582	281.0646					0.006	0.015				
257	SYNESIS-005	20.0009	100.0013	179.0744	75.0003			76.0092	115.0025	113.0072	116.0984	101.0032	73.0214	0.001	0.000	0.135				
258	T4ISB-000	215.0010	186.0023	127.0462	62.0003	121.0115	58.0081	90.016	83.0053	34.0510	71.0211	112.0759	53.0161	0.000	0.000	0.000		0.000		
259	TECH5-001	153.0004	139.0017	135.0584	122.0007			108.0107	188.0057	297.0935	250.1000	189.0244	212.0994	0.000	0.000	0.006				
260	TECH5-002	128.0003	67.0011	101.0312	74.0003	97.0029	70.0089	120.0027	111.0070	65.0805	113.0039	76.0205	128.0440	0.001	0.000	0.041		0.000		
261	TEVIAN-003	236.0015	241.0052						250.0177	247.0298					0.001	0.002				
262	TEVIAN-004	22.0011	221.0038						223.0117	209.0176					0.001	0.002				
263	TEVIAN-005	193.0007	203.0028	128.0467					210.0087	189.0144	88.0962				0.001	0.002	0.116			
264	TEVIAN-006	12.0002	77.0011	54.0123	66.0003	59.0013	38.0071	65.0010	49.0032	25.0425	58.0016	38.0093	200.0951	0.001	0.000	0.062		0.000		
265	TEVIAN-007	75.0002	42.0009	44.0093	42.0002	41.0009	31.0067	41.0005	27.0022	19.0301	43.0009	27.0065	31.0122	0.000	0.000	0.062		0.000		
266	TIGER-000	27.0062	269.0095						27.0390	270.0500					0.000	0.000				
267	TIGER-002	176.0006	180.0023	134.0514					206.0086	198.0158	185.0999				0.000	0.000	0.056			
268	TIGER-003	17.0006	181.0023						20.0086	199.0158					0.000	0.000				
269	TONGYITRANS-000	188.0007	177.0022						198.0074	162.0112					0.003	0.001				
270	TONGYITRANS-001	189.0007	178.0022						193.0066	153.0101					0.003	0.001				
271	TOSHIBA-000	162.0004	170.0022	185.0766					189.0062	167.0118	155.0995				0.000	0.000	0.070			
272	TOSHIBA-001	167.0005	174.0022						184.0058	140.0092					0.000	0.000				
273	TRUEFACE-000	144.0003	108.0014	83.0230	132.0007	83.0024	77.0092	99.0018	100.0062	72.0882	93.0030	74.0194	67.0188	0.001	0.001	0.047		0.003		
274	TURINGTECHVIP-001	211.0009	196.0026	37.0081	194.0045	125.0199	189.0220	268.0345	291.0850	137.0993	227.0978	187.0000	216.0999	0.001	0.003	0.044		0.000		
275	VD-000	30.0474	299.0551						304.0019	299.0946					0.011	0.013				
276	VD-001	259.0028	242.0053						254.0201	244.0281					0.005	0.001				

Table 16: **Miss rates by dataset**: At left, rank 1 miss rates relevant to investigations; at right, with threshold set to target FPIR = 0.01 for higher volume, low prior, uses. Yellow indicates most accurate algorithm. Throughout blue superscripts indicate the rank of the algorithm for that column.

2022/11/0
18:02:21

FNIR(N, K, I) = False neg. identification rate
 FPIR(N, T) = False pos. identification rate

N = Num. enrolled subjects
R = Num. candidates examined

1 = 1 threshold

$I \equiv 0 \rightarrow$ Investigation
 $T > 0 \rightarrow$ Identification

#	ALGORITHM	INVESTIGATION MODE						IDENTIFICATION MODE						FAILURE TO EXTRACT FEATURES					
		RANK ONE MISS RATE, FNIR(N, 0, 1)						HIGH T → FPIR = 0.001, FNIR(N, T, L)											
		N=1.6M						N=1.6M											
	GALLERY	MUGSHOT	MUGSHOT	MUGSHOT	VISA	BORDER	VISA	MUGSHOT	MUGSHOT	MUGSHOT	VISA	BORDER	VISA	MUGSHOT	MUGSHOT	MUGSHOT	VISA	BORDER	KIOSK
	PROBE	MUGSHOT	WEBCAM	PROFILE	BORDER	BOR ₂ 10YR	KIOSK	MUGSHOT	WEBCAM	PROFILE	BORDER	BOR ₂ 10YR	KIOSK	MUGSHOT	WEBCAM	PROFILE	BORDER	BOR ₂ 10YR	KIOSK
277	VD-002	²¹² 0.010	²⁰¹ 0.027	²¹⁰ 0.893	¹⁵⁹ 0.013	¹⁰⁸ 0.050	¹⁷⁰ 0.176	²⁰³ 0.079	¹⁹¹ 0.148	¹⁵⁸ 0.996	¹⁵⁶ 0.095	⁹⁵ 0.367	¹¹⁵ 0.372	0.004	0.003	0.156			0.002
278	VD-003	¹⁹³ 0.008	¹⁷¹ 0.022	¹⁸⁸ 0.773	¹⁴⁹ 0.008	⁹⁹ 0.030	¹⁵⁰ 0.137	¹⁶⁰ 0.046	¹⁵¹ 0.100	¹⁸⁷ 0.999	¹²² 0.051	⁹² 0.244	¹⁰⁵ 0.315	0.003	0.003	0.144			0.002
279	VERIDAS-001	¹³ 0.003	¹¹⁵ 0.014	¹⁴⁷ 0.550	¹²¹ 0.006	⁹⁴ 0.028	¹⁴¹ 0.131	¹⁴⁸ 0.037	¹²⁸ 0.082	¹²⁴ 0.987	¹¹⁹ 0.044	⁸⁴ 0.266	⁹³ 0.264	0.000	0.002	0.093			0.001
280	VERIDAS-002	¹³⁰ 0.003	¹¹⁶ 0.014	¹⁴⁸ 0.550	¹²³ 0.006	⁹³ 0.028	¹⁴⁰ 0.131	¹⁴⁹ 0.037	¹²⁹ 0.082	¹²⁵ 0.987	¹¹⁸ 0.044	⁸⁵ 0.266	⁹² 0.264	0.000	0.002	0.093			0.001
281	VERIDAS-003	⁷⁸ 0.002	⁷⁶ 0.011	⁹⁸ 0.297	⁸⁹ 0.004	⁶⁴ 0.016	¹⁰⁸ 0.108	⁹¹ 0.017	⁹⁰ 0.055	¹⁶⁴ 0.997	⁶⁸ 0.020	⁹⁶ 0.150	⁶² 0.178	0.000	0.002	0.093			0.001
282	VERIJELAS-000	³⁰² 0.355	²⁹¹ 0.369	²⁵⁹ 0.968	²⁰⁷ 0.086	¹²⁴ 0.191	²⁰⁶ 0.292	²⁹⁶ 0.799	²⁸⁸ 0.813	¹⁸² 0.999	¹⁹⁸ 0.324	¹¹⁷ 0.933	¹⁵³ 0.589	0.002	0.001	0.070			0.001
283	VIGILANTSOLUTIONS-003	²⁸ 0.069	²⁷ 0.151	²⁴⁰ 0.958				²⁸ 0.408	²⁸⁴ 0.660	¹⁸¹ 0.999				0.000	0.001	0.127			
284	VIGILANTSOLUTIONS-004	²⁹⁸ 0.125	²⁸⁵ 0.244	²⁴⁵ 0.965				²⁸⁷ 0.549	²⁹⁰ 0.817	¹⁶¹ 0.996				0.000	0.001	0.127			
285	VIGILANTSOLUTIONS-005	²⁰ 0.009	²¹⁷ 0.920					²⁷ 0.388		²⁴² 1.000				0.000	0.001	0.127			
286	VIGILANTSOLUTIONS-006	²¹⁴ 0.010	²¹⁸ 0.921					²⁷ 1.035		²³⁵ 1.000				0.000	0.001	0.127			
287	VIGILANTSOLUTIONS-007	¹⁴ 0.003	¹⁴⁴ 0.017	²²¹ 0.925	¹⁵⁷ 0.013	¹¹⁴ 0.068	¹⁶⁸ 0.175	¹³⁰ 0.028	¹³⁴ 0.088	¹⁶⁰ 0.996	¹⁵² 0.081	⁹⁷ 0.371	¹¹⁹ 0.391	0.000	0.001	0.127			0.001
288	VIGILANTSOLUTIONS-008	¹³⁶ 0.003	¹⁴⁵ 0.017	²¹⁶ 0.913	¹⁶¹ 0.014	¹¹⁵ 0.072	¹⁷¹ 0.178	¹⁰⁶ 0.021	¹²⁰ 0.077	¹⁸⁴ 0.999	¹⁶⁰ 0.104	¹⁰⁰ 0.398	¹⁴² 0.511	0.000	0.001	0.127			0.001
289	VISIONBOX-000	⁸⁹ 0.002	⁷⁸ 0.011	¹⁸¹ 0.752	¹⁰⁸ 0.005	⁶⁶ 0.017	⁵⁴ 0.078	⁹⁰ 0.018	⁹³ 0.057	¹³² 0.990	⁷⁸ 0.023	⁵⁰ 0.146	³⁴ 0.162	0.000	0.001	0.043			
290	VISIONLABS-004	¹²⁹ 0.003	¹⁵⁹ 0.020	¹¹⁰ 0.343				¹⁸³ 0.058	²⁰⁰ 0.159	⁷⁴ 0.890				0.001	0.001	0.046			
291	VISIONLABS-005	¹¹⁷ 0.002	¹⁵⁴ 0.019	¹⁰⁸ 0.334				¹⁶ 0.050	¹⁹⁰ 0.147	⁷³ 0.888				0.001	0.001	0.046			
292	VISIONLABS-006	⁸⁰ 0.002	¹²⁹ 0.015	⁷⁸ 0.211	⁸⁴ 0.004			⁸¹ 0.096	¹² 0.027	¹³⁸ 0.090	⁴⁷ 0.672			0.001	0.001	0.051			
293	VISIONLABS-007	⁷⁴ 0.002	¹²⁸ 0.015	⁷⁷ 0.211	⁸⁰ 0.004			¹²⁶ 0.027	¹³⁷ 0.090	⁴⁸ 0.672	⁹⁷ 0.031		⁶⁶ 0.185	0.001	0.001	0.051			
294	VISIONLABS-008	⁹⁷ 0.002	¹⁰⁹ 0.014	⁵⁹ 0.141	⁵⁶ 0.002			³⁷ 0.081	⁷⁰ 0.013	⁷⁹ 0.051	³² 0.481	⁵⁹ 0.017	⁴¹ 0.151	0.001	0.001	0.075			
295	VISIONLABS-009	²⁰ 0.001	³⁵ 0.008	⁴³ 0.091	²² 0.001			³⁷ 0.071	³⁴ 0.005	³⁵ 0.025	⁶³ 0.799	³⁸ 0.008	²⁸ 0.113	0.000	0.000	0.060			
296	VISIONLABS-010	⁴ 0.001	⁶² 0.010	²⁷ 0.069	¹⁹ 0.001	¹⁵ 0.006	³⁶ 0.069	⁴ 0.005	⁴⁰ 0.027		³¹ 0.008	²² 0.055	²⁰ 0.109	0.000	0.000	0.040			0.000
297	VISIONLABS-011	²⁶ 0.001	³⁷ 0.009	¹⁶ 0.064	¹⁶ 0.001	⁸ 0.004	²⁵ 0.063	²⁴ 0.003	²⁴ 0.020		¹³ 0.004	¹⁵ 0.034	¹⁰ 0.090	0.000	0.000	0.032			0.000
298	VNP7-001	¹⁰ 0.002	¹²¹ 0.014	⁶² 0.145	⁶⁶ 0.002	³² 0.023	³⁹ 0.071	⁸ 0.014	¹⁰⁹ 0.068	⁵³ 0.718	¹⁰⁶ 0.035	¹² 0.990	¹¹⁵ 0.362	0.001	0.000	0.042			0.000
299	VNP7-002	⁸⁷ 0.002	⁹⁵ 0.012	²⁶ 0.068	¹³ 0.001	¹⁹ 0.006	¹¹ 0.054	⁴⁷ 0.007	⁴⁸ 0.032	¹⁸ 0.292	²⁸ 0.007	³¹ 0.072	¹⁵ 0.096	0.001	0.000	0.042			0.000
300	VOCORD-003	¹⁸ 0.006	¹⁸⁹ 0.024	¹⁹⁶ 0.804	²⁰ 0.061			¹⁷⁵ 0.188	²² 0.122	¹⁹⁶ 0.155	¹⁷³ 0.998	¹⁷⁶ 0.157	¹²⁷ 0.404	0.001	0.011	0.425			
301	VOCORD-004	¹⁹ 0.008	¹⁶⁶ 0.021	¹⁹⁰ 0.792	¹⁵⁷ 0.012			¹³⁷ 0.127	²⁷ 0.355	²¹⁶ 0.173	²²⁰ 1.000	¹⁸⁹ 0.193	²⁹⁹ 0.991	0.000	0.000	0.000			
302	VOCORD-005	¹⁹¹ 0.007	¹⁸⁴ 0.023	¹⁸⁸ 0.812	¹⁹⁹ 0.055			¹⁷⁹ 0.206	²⁴¹ 0.158	¹⁷⁹ 0.130	¹⁶⁵ 0.997	¹⁷⁴ 0.138	¹¹⁶ 0.381	0.001	0.009	0.554			
303	VOCORD-006	³¹ 1.000	³¹⁵ 1.000	²⁹¹ 1.000	²⁶⁴ 1.000			²⁴³ 1.000	³¹¹ 1.000	³⁰⁹ 1.000	²³⁷ 1.000	²²⁷ 1.000	0.001	0.009	0.554				
304	VTS-000	³¹⁰ 0.594	³⁰² 0.608	²¹⁴ 0.909	²²⁷ 0.607	¹³⁰ 0.724	²²⁶ 0.739	²⁹⁰ 0.598	²⁹ 0.619	¹⁹⁴ 0.999	²¹⁶ 0.613	¹¹³ 0.760	¹⁷¹ 0.761	0.000	0.001	0.047			0.000
305	VTS-001	⁵ 0.002	⁵⁴ 0.010	⁶⁸ 0.167	¹¹⁷ 0.006	⁶⁹ 0.018	⁵¹ 0.077	⁷ 0.013	⁷⁸ 0.051	¹⁴² 0.994	⁷⁶ 0.022	⁵² 0.141	⁶⁹ 0.192	0.000	0.000	0.040			0.000
306	VTS-002	⁸⁹ 0.002	¹⁰¹ 0.013	⁸⁴ 0.233	¹⁶³ 0.014	¹⁰⁵ 0.038	¹³² 0.125	¹²² 0.026	¹¹⁸ 0.075	²⁰⁴ 1.000	¹²¹ 0.045	⁸⁰ 0.231	¹²⁴ 0.417	0.000	0.000	0.029			0.000
307	VTS-003	² 0.001	¹⁵ 0.007	³³ 0.074	³¹ 0.002	²⁸ 0.009	⁸ 0.053	⁵ 0.007	³² 0.033	²²⁸ 1.000	⁵⁰ 0.014	¹⁷ 0.954	¹⁵⁹ 0.635	0.000	0.001	0.029			0.000
308	XFORWARDAI-000	¹¹¹ 0.002	¹¹² 0.014	⁴² 0.089	⁸⁵ 0.004	⁶¹ 0.015	⁷⁸ 0.094	⁸⁶ 0.015	⁸⁷ 0.053	²⁷ 0.440	⁷² 0.021	⁶¹ 0.159	⁵⁷ 0.169	0.000	0.000	0.000			
309	XFORWARDAI-001	¹⁰ 0.002	⁹⁸ 0.013	²³ 0.067	⁷⁹ 0.003	³⁹ 0.009	⁶¹ 0.082	³⁰ 0.005	⁴³ 0.028	²⁸ 0.448	³⁴ 0.008	²⁰ 0.062	²⁴ 0.123	0.000	0.000	0.000			
310	XFORWARDAI-002	⁹² 0.002	⁹⁰ 0.012	⁹ 0.059	⁹⁹ 0.002	²² 0.007	⁴⁹ 0.077	²³ 0.003	¹⁷ 0.016	³⁵ 0.525	¹⁷ 0.005	¹⁶ 0.041	¹⁹ 0.099	0.000	0.000	0.000			
311	YISHENG-001	²⁵ 0.027	²⁴ 0.060	²⁰ 0.058				²⁰³ 0.287	²⁶ 0.346	²⁸ 0.808	²¹⁸ 0.666	¹⁹⁴ 0.919	0.002	0.005					
312	YITU-002	⁸² 0.002	³⁸ 0.010					⁹⁴ 0.018	⁷³ 0.049					0.000	0.000				
313	YITU-003	¹³ 0.003	¹³⁴ 0.016					¹⁰ 0.019	⁸² 0.052					0.003	0.001				
314	YITU-004	³¹ 0.001	³³ 0.008	²⁰⁸ 0.866				⁶⁰ 0.010	³⁸ 0.027	⁸² 0.936				0.000	0.000	0.000			
315	YITU-005	¹¹³ 0.002	¹²² 0.014					⁶⁷ 0.010	⁵⁰ 0.032					0.003	0.001				

Table 17: **Miss rates by dataset**: At left, rank 1 miss rates relevant to investigations; at right, with threshold set to target FPIR = 0.01 for higher volume, low prior, uses. Yellow indicates most accurate algorithm. Throughout blue superscripts indicate the rank of the algorithm for that column.

2022/11/09
18:02:21

FNIR(N, K, T)
FPIR(N, T)

False neg. identification rate
False pos. identification rate

N = Num. enrolled subjects
 R = Num. candidates examined

T = Threshold

$T = 0 \rightarrow$ Investigation
 $T > 0 \rightarrow$ Identification

FRVT - FACE RECOGNITION VENDOR TEST - IDENTIFICATION

#	ALGORITHM	MISSES BELOW THRESHOLD, T	ENROL, MOST RECENT			
		DATASET: FRVT 2018 MUGSHOTS				
		N=0.64M	N=1.6M	N=3.0M	N=6.0M	N=12.0M
1	3DIVI-005	²⁴⁶ 0.1358	²⁴⁶ 0.1664	²¹⁷ 0.1915	²⁰⁸ 0.2370	¹⁹⁹ 0.3054
2	ACER-000	²³⁹ 0.1185	²³⁸ 0.1455	²¹¹ 0.1714	²⁰¹ 0.2074	¹⁹² 0.2537
3	ALCHERA-003	²⁵ 0.1176	²⁴⁰ 0.1553	²¹⁷ 0.1853	²⁰⁹ 0.2409	²⁰ 0.3553
4	ALLGOVISION-000	²¹¹ 0.0688	²¹² 0.0881	¹⁹⁴ 0.1084	¹⁸⁶ 0.1389	¹⁷² 0.2129
5	ALLGOVISION-001	²¹⁷ 0.0785	²¹⁷ 0.1017	²⁰¹ 0.1218	¹⁹³ 0.1584	¹⁷ 0.2273
6	ANKE-000	²²⁴ 0.0942	²²² 0.1169	²⁰⁶ 0.1404	¹⁹⁸ 0.1776	¹⁹³ 0.2559
7	ANKE-002	¹⁴ 0.0229	¹⁴¹ 0.0318	¹⁴¹ 0.0406	¹³⁵ 0.0605	¹² 0.1466
8	AWARE-003	²³⁴ 0.1098	²³⁰ 0.1283	²⁰⁷ 0.1447	¹⁹⁶ 0.1768	¹⁸⁴ 0.2364
9	AWARE-005	²⁷ 0.3389	²⁷³ 0.3643	²²¹ 0.3993	²¹ 0.4526	¹⁹ 0.2531
10	AYONIX-002	²⁹⁹ 0.7862	²⁹⁹ 0.8242	²³¹ 0.8508	²²³ 0.8704	²¹⁶ 0.8939
11	CAMVI-004	¹⁶ 0.0367	¹⁹⁶ 0.0716	¹⁸⁹ 0.0983	²¹¹ 0.2508	¹⁹⁹ 0.2701
12	CANON-001	⁴² 0.0039	⁴² 0.0054	⁴² 0.0074	⁴⁰ 0.0158	⁴⁸ 0.0924
13	CANON-002	³ 0.0036	³⁵ 0.0047	³⁶ 0.0061	³¹ 0.0124	² 0.0808
14	CIB-000	⁷¹ 0.0086	⁷⁴ 0.0125	⁷⁴ 0.0160	⁷⁹ 0.0303	⁹⁴ 0.1251
15	CLEARVIEWAI-000	⁴ 0.0040	⁴⁴ 0.0058	⁴⁴ 0.0078	⁴¹ 0.0159	⁵¹ 0.0971
16	CLOUDWALK-HR-000	¹⁵ 0.0019	¹³ 0.0020	¹⁰ 0.0023	¹⁵ 0.0072	²¹ 0.0701
17	CLOUDWALK-MT-000	¹⁴ 0.0019	¹² 0.0020	⁷ 0.0022	⁶ 0.0049	¹⁸ 0.0466
18	CLOUDWALK-MT-001	¹² 0.0018	¹⁰ 0.0019	⁸ 0.0020	⁷ 0.0052	¹⁵ 0.0555
19	COGENT-000	¹⁸ 0.0430	¹⁷¹ 0.0527	¹⁷¹ 0.0695	¹⁷² 0.1133	¹⁶ 0.1960
20	COGENT-001	¹⁸⁵ 0.0430	¹⁷⁰ 0.0527	¹⁷¹ 0.0695	¹⁷¹ 0.1133	¹⁶¹ 0.1960
21	COGENT-002	¹⁵³ 0.0322	¹⁵⁷ 0.0444	¹⁵⁶ 0.0610	¹⁶⁹ 0.1116	¹⁷⁴ 0.2180
22	COGENT-003	¹⁵⁴ 0.0328	¹⁶² 0.0463	¹⁶⁸ 0.0683	¹⁷⁹ 0.1294	¹⁸ 0.2445
23	COGENT-004	¹⁵⁸ 0.0210	¹⁴² 0.0331	¹⁵¹ 0.0527	¹⁷⁴ 0.1138	¹⁷¹ 0.2119
24	COGENT-005	⁵⁹ 0.0064	⁵⁹ 0.0091	⁵⁹ 0.0123	⁷⁸ 0.0303	⁹ 0.1233
25	COGENT-006	³¹ 0.0032	³¹ 0.0044	³¹ 0.0057	²⁷ 0.0120	³³ 0.0830
26	COGNITEC-000	²⁴ 0.1377	²⁴⁴ 0.1606	²¹⁶ 0.1870	²⁰³ 0.2176	¹⁹⁹ 0.2831
27	COGNITEC-001	²¹⁹ 0.0807	²¹⁸ 0.1017	²⁰⁹ 0.1214	¹⁸⁹ 0.1513	¹⁷⁷ 0.2238
28	COGNITEC-002	¹⁷⁸ 0.0406	¹⁷³ 0.0531	¹⁶⁴ 0.0666	¹⁵⁷ 0.0935	¹⁵⁶ 0.1874
29	COGNITEC-003	¹⁷⁵ 0.0400	¹⁶⁹ 0.0526	¹⁵⁹ 0.0650	¹⁵² 0.0895	¹⁴⁹ 0.1772
30	COGNITEC-004	¹⁴⁰ 0.0222	¹⁴⁰ 0.0313	¹³⁷ 0.0388	¹²⁷ 0.0540	⁷² 0.1103
31	COGNITEC-005	⁵⁸ 0.0063	⁶¹ 0.0096	⁶⁷ 0.0144	⁷² 0.0287	⁵⁸ 0.0967
32	COGNITEC-006	⁵² 0.0053	⁵⁴ 0.0077	⁵⁸ 0.0117	⁵⁹ 0.0254	⁴⁴ 0.0919
33	CYBERLINK-000	¹⁸ 0.0414	¹⁸¹ 0.0565	¹⁷⁵ 0.0707	¹⁶⁵ 0.1031	¹⁶ 0.2050
34	CYBERLINK-001	¹⁷¹ 0.0392	¹⁷⁴ 0.0536	¹⁶⁹ 0.0695	¹⁶² 0.0973	¹⁵⁰ 0.1794
35	CYBERLINK-002	⁸¹ 0.0105	⁸⁴ 0.0148	⁸⁰ 0.0202	¹⁰⁰ 0.0399	⁹ 0.1255
36	CYBERLINK-003	⁵⁴ 0.0056	⁵⁵ 0.0077	⁵² 0.0100	⁵⁵ 0.0235	⁹¹ 0.1237
37	CYBERLINK-004	⁵⁰ 0.0051	⁵¹ 0.0071	⁵⁴ 0.0102	⁴⁷ 0.0199	⁹⁸ 0.1269
38	CYBERLINK-005	⁶² 0.0067	⁶⁵ 0.0099	⁶⁹ 0.0138	⁹⁷ 0.0394	¹³ 0.1566
39	DAHUA-001	²⁰⁰ 0.0569	¹⁹⁸ 0.0727	¹⁸³ 0.0878	¹⁷⁵ 0.1148	¹⁵⁵ 0.1867
40	DAHUA-002	⁸⁶ 0.0108	⁸⁵ 0.0151	⁸⁴ 0.0191	⁷⁴ 0.0291	⁸³ 0.1153
41	DAHUA-003	⁷⁸ 0.0100	⁷⁹ 0.0139	⁸⁰ 0.0180	⁷⁵ 0.0296	²⁷ 0.1130
42	DAHUA-004	⁴⁸ 0.0048	⁵⁰ 0.0069	⁴⁹ 0.0090	⁴³ 0.0164	³⁴ 0.0853
43	DAON-000	¹¹⁴ 0.0161	¹¹⁴ 0.0226	¹¹⁵ 0.0293	¹³⁴ 0.0562	¹⁴³ 0.1702
44	DECATUR-000	¹¹⁶ 0.0173	¹¹⁷ 0.0229	¹¹⁶ 0.0305	¹¹⁰ 0.0464	¹¹ 0.1433
45	DEEPLINT-001	²⁵ 0.0027	²⁵ 0.0033	²⁴ 0.0043	²⁹ 0.0121	⁴⁷ 0.0922
46	DEEPSA-001	¹⁶³ 0.0347	¹⁶¹ 0.0462	¹⁵⁹ 0.0586	¹⁵⁰ 0.0802	¹⁴ 0.1708
47	DERMALOG-005	²¹⁵ 0.0700	²¹¹ 0.0880	¹⁹⁶ 0.1144	¹⁹² 0.1578	¹⁸⁷ 0.2451
48	DERMALOG-006	¹⁷ 0.0395	¹⁶⁸ 0.0517	¹⁶¹ 0.0659	¹⁶¹ 0.0973	¹⁴ 0.1745
49	DERMALOG-007	²¹² 0.0691	²⁰⁹ 0.0863	¹⁹³ 0.1107	¹⁸⁸ 0.1504	¹⁸² 0.2299
50	DERMALOG-008	¹⁵⁹ 0.0338	¹⁵⁹ 0.0455	¹⁵⁸ 0.0626	¹⁶⁶ 0.1060	¹⁸⁰ 0.2276
51	DERMALOG-009	¹⁰ 0.0148	¹⁰⁷ 0.0206	¹⁰⁷ 0.0268	¹⁰⁴ 0.0416	¹¹ 0.1374
52	DERMALOG-010	⁵¹ 0.0052	⁴⁹ 0.0069	⁴⁸ 0.0088	⁴⁸ 0.0207	⁵² 0.0971
53	DILUSENSE-000	¹³⁷ 0.0208	¹³⁸ 0.0305	¹³¹ 0.0377	¹³¹ 0.0543	¹¹¹ 0.1429
54	FUJITSULAB-000	¹⁰⁸ 0.0148	¹⁰⁸ 0.0206	¹¹¹ 0.0277	¹²⁹ 0.0541	¹⁴⁷ 0.1739
55	FUJITSULAB-001	⁹¹ 0.0126	⁹⁸ 0.0182	¹⁰⁵ 0.0251	¹³⁸ 0.0646	¹⁶ 0.2079
56	GORILLA-002	²⁵² 0.1539	²⁵² 0.1880	²²⁰ 0.2184	²¹² 0.2596	²⁰⁶ 0.3398
57	GORILLA-004	²¹ 0.0699	²¹⁴ 0.0892	¹⁹⁷ 0.1048	¹⁸⁴ 0.1370	¹⁶ 0.1969
58	GORILLA-005	¹⁹⁰ 0.0453	¹⁸⁵ 0.0583	¹⁷⁴ 0.0704	¹⁶³ 0.0974	¹²¹ 0.1474
59	GORILLA-006	¹³⁰ 0.0196	¹³⁰ 0.0275	¹²² 0.0331	¹¹⁹ 0.0516	⁷⁴ 0.1113
60	GORILLA-007	¹²⁷ 0.0190	¹²⁹ 0.0271	¹²⁸ 0.0348	¹²³ 0.0520	⁷⁶ 0.1129
61	GRIAULE-000	¹⁰⁴ 0.0145	¹⁰⁵ 0.0201	¹⁰³ 0.0253	¹⁰² 0.0407	¹¹¹ 0.1440
62	GRIAULE-001	³³ 0.0033	³⁶ 0.0047	³⁸ 0.0064	³⁸ 0.0153	⁴¹ 0.0910
63	HIK-003	²²⁰ 0.0828	²¹⁹ 0.1028	¹⁹⁷ 0.1202	¹⁹¹ 0.1525	¹⁸⁹ 0.2480
64	HIK-004	²¹⁸ 0.0796	²¹⁵ 0.0988	¹⁹⁷ 0.1147	¹⁸⁷ 0.1474	¹⁹ 0.2483
65	HIK-005	¹⁵¹ 0.0312	¹⁵⁴ 0.0436	¹⁵⁴ 0.0560	¹⁵⁴ 0.0911	¹⁷³ 0.2129
66	HYPERVERGE-001	³² 0.0033	³² 0.0045	³⁸ 0.0059	²⁴ 0.0117	³⁰ 0.0872
67	HYPERVERGE-002	²⁷ 0.0028	²⁶ 0.0037	²⁶ 0.0046	¹² 0.0064	¹ 0.0064
68	HZAILU-000	¹⁰ 0.0143	¹⁰⁴ 0.0197	¹⁰¹ 0.0255	¹⁰³ 0.0411	⁸⁸ 0.1174
69	HZAILU-001	⁶¹ 0.0066	⁵⁶ 0.0086	⁵⁵ 0.0109	⁴⁹ 0.0207	⁶⁵ 0.1052
70	IDEARIA-003	¹⁶ 0.0346	¹⁶⁴ 0.0471	¹⁸¹ 0.0892	²¹⁴ 0.2789	²¹⁰ 0.4311
71	IDEARIA-004	¹⁵⁰ 0.0300	¹⁵⁰ 0.0373	¹⁴³ 0.0447	¹³⁶ 0.0617	¹⁴² 0.1635
72	IDEARIA-005	¹⁶⁸ 0.0360	¹⁵⁶ 0.0440	¹⁵⁶ 0.0537	¹⁴⁹ 0.0764	¹⁵ 0.1915

Table 18: Identification-mode: Effect of N on FNIR at high threshold. Values are threshold-based miss rates i.e. FNIR at FPIR = 0.001 for five enrollment population sizes, N. The right six columns apply for enrollment of one image. Missing entries usually apply because another algorithm from the same developer was run instead. Some developers are missing because less accurate algorithms were not run on galleries with $N \geq 3\,000\,000$. Throughout blue superscripts indicate the rank of the algorithm for that column.

#	ALGORITHM	MISSES BELOW THRESHOLD, T		ENROL MOST RECENT					
		FNIR(N, T > 0, R > L)		DATASET: FRVT 2018 MUGSHOTS					
73	IDEARIA-006	¹⁶⁴ 0.0351	¹³³ 0.0433	N=0.64M	N=1.6M	N=3.0M	N=6.0M	N=12.0M	¹⁷³ 0.2201
74	IDEARIA-007	⁹⁹ 0.0136	⁹⁷ 0.0181	⁹¹ 0.0228	⁹⁰ 0.0357	¹¹⁴ 0.1402			
75	IDEARIA-008	⁹ 0.0016	⁹ 0.0019	¹² 0.0024	⁸ 0.0053	¹¹ 0.0470			
76	IDEARIA-009	³ 0.0013	³ 0.0016	³ 0.0018	¹¹ 0.0061	¹⁴ 0.0550			
77	IMAGUS-005	¹⁰⁰ 0.0137	¹⁰¹ 0.0185	⁹⁷ 0.0237	⁹² 0.0368	⁶⁸ 0.1067			
78	IMAGUS-006	¹⁰ 0.0137	¹⁰³ 0.0190	¹⁰⁸ 0.0244	⁸⁶ 0.0396	⁸¹ 0.1159			
79	IMAGUS-007	¹¹² 0.0160	¹¹⁶ 0.0228	¹¹⁷ 0.0284	¹⁰⁷ 0.0444	⁸⁷ 0.1179			
80	IMPERIAL-000	¹²³ 0.0187	¹²⁵ 0.0259	¹³³ 0.0358	¹⁴⁵ 0.0733	¹⁵¹ 0.1794			
81	INCODE-003	²⁴⁵ 0.1324	²⁴⁷ 0.1672	²¹⁸ 0.1961	²¹⁶ 0.2345	²⁰¹ 0.3123			
82	INCODE-004	¹⁷⁶ 0.0403	¹⁷⁷ 0.0538	¹⁶³ 0.0662	¹⁵⁶ 0.0917	¹³⁹ 0.1619			
83	INCODE-005	⁶⁹ 0.0083	⁶⁹ 0.0113	⁶⁹ 0.0145	⁵⁶ 0.0247	⁴² 0.0912			
84	INNOVATRICS-007	⁷³ 0.0093	⁷⁵ 0.0125	⁷³ 0.0159	⁶¹ 0.0259	⁶⁹ 0.1092			
85	INTEMA-000	¹⁵ 0.0019	¹⁶ 0.0024	¹⁷ 0.0032	²¹ 0.0098	²⁵ 0.0745			
86	INTSYSMSU-000	³¹⁰ 0.9982	³⁰⁸ 0.9984	²³⁵ 0.9985	²²⁶ 0.9987	²²⁰ 0.9988			
87	IREX-000	¹²⁸ 0.0190	¹³⁴ 0.0280	¹³⁸ 0.0391	¹⁴¹ 0.0677	¹²⁴ 0.1479			
88	ISYSTEMS-002	²⁰² 0.0584	²⁰² 0.0783	¹⁸⁸ 0.0973	¹⁸⁵ 0.1373	¹⁸¹ 0.2295			
89	ISYSTEMS-003	¹⁸⁸ 0.0438	¹⁸⁶ 0.0590	¹⁸¹ 0.0807	¹⁷⁷ 0.1259	¹⁸³ 0.2357			
90	KAKAO-000	⁸⁷ 0.0109	⁸⁷ 0.0151	⁸⁶ 0.0196	⁸⁵ 0.0324	⁵⁶ 0.1010			
91	KAKAO-001	²⁰ 0.0021	¹⁹ 0.0026	¹⁸ 0.0032	¹⁹ 0.0085	²⁰ 0.0693			
92	KEDACOM-001	¹¹⁸ 0.0181	¹¹⁵ 0.0227	¹⁰⁵ 0.0265	¹⁰⁶ 0.0422	¹⁰⁷ 0.1340			
93	LINECLOVA-002	²⁰ 0.0028	²⁷ 0.0040	²⁷ 0.0049	²⁸ 0.0120	³¹ 0.0824			
94	LOOKMAN-003	¹⁶² 0.0346	¹⁵⁵ 0.0437	¹⁴⁸ 0.0514	¹⁴⁴ 0.0724	¹⁴⁰ 0.1620			
95	LOOKMAN-005	¹⁴ 0.0240	¹³⁷ 0.0301	¹³ 0.0356	¹¹⁸ 0.0512	¹⁰⁶ 0.1334			
96	MANTRA-000	⁶⁰ 0.0065	⁶⁶ 0.0101	⁶⁹ 0.0151	⁸⁰ 0.0308	⁶¹ 0.1035			
97	MAXVISION-000	¹⁵⁶ 0.0206	¹³⁵ 0.0282	¹²⁹ 0.0355	¹²⁰ 0.0517	¹⁰⁸ 0.1340			
98	MAXVISION-001	²⁹ 0.0031	³⁰ 0.0043	²⁸ 0.0055	³⁰ 0.0122	⁴⁰ 0.0895			
99	MEGVII-001	¹⁹⁸ 0.0562	¹⁹⁷ 0.0722	¹⁸² 0.0872	¹⁸¹ 0.1309	¹⁹ 0.2713			
100	MICROFOCUS-005	³⁰⁷ 0.9732	³⁰¹ 0.8354	²³² 0.8555	²²⁴ 0.8755	²¹⁷ 0.8954			
101	MICROSOFT-003	¹³¹ 0.0198	¹³² 0.0278	¹³¹ 0.0356	¹²⁶ 0.0538	¹³⁰ 0.1539			
102	MICROSOFT-004	¹²¹ 0.0185	¹²⁴ 0.0259	¹²³ 0.0333	¹²¹ 0.0517	¹²⁸ 0.1510			
103	MICROSOFT-005	¹¹⁹ 0.0181	¹²¹ 0.0256	¹²⁸ 0.0320	¹¹⁷ 0.0512	¹²² 0.1491			
104	MICROSOFT-006	⁷⁴ 0.0091	⁷⁰ 0.0120	⁷⁹ 0.0162	⁷⁷ 0.0301	¹²⁵ 0.1482			
105	MUKH-002	²⁸⁹ 0.5041	²⁸⁹ 0.5942	²²⁹ 0.6674	²²¹ 0.7314	²¹⁵ 0.8276			
106	NEC-000	²⁰⁶ 0.0637	²⁰⁴ 0.0789	¹⁸⁷ 0.0933	¹⁷⁶ 0.1163	¹⁵⁹ 0.1941			
107	NEC-001	²²¹ 0.0863	²²¹ 0.1055	²⁰³ 0.1249	¹⁹⁰ 0.1519	¹⁷⁸ 0.2253			
108	NEC-002	¹⁸ 0.0020	¹⁸ 0.0026	¹⁹ 0.0033	³⁴ 0.0135	¹⁸ 0.0653			
109	NEC-003	¹⁹ 0.0021	¹⁵ 0.0024	¹⁴ 0.0028	¹⁰ 0.0059	¹³ 0.0540			
110	NEC-004	¹⁰ 0.0017	⁶ 0.0018	³ 0.0020	³ 0.0037	³ 0.0329			
111	NEC-005	⁵ 0.0015	⁴ 0.0017	⁴ 0.0019	¹³ 0.0065	³ 0.0307			
112	NEC-006	¹ 0.0018	¹¹ 0.0020	¹² 0.0026	²³ 0.0103	¹⁰ 0.0573			
113	NEUROTECHNOLOGY-003	²⁹² 0.5698	²⁹³ 0.6362	²³⁰ 0.7035	²²² 0.7602	²¹⁴ 0.8224			
114	NEUROTECHNOLOGY-004	¹⁹² 0.0466	¹⁹¹ 0.0629	¹⁷⁸ 0.0779	¹⁷³ 0.1135	¹⁷² 0.2102			
115	NEUROTECHNOLOGY-005	¹⁷³ 0.0396	¹⁷⁸ 0.0538	¹⁶⁶ 0.0675	¹⁶⁰ 0.0950	¹⁶³ 0.1966			
116	NEUROTECHNOLOGY-007	¹⁸⁷ 0.0436	¹⁹⁰ 0.0623	¹⁷⁸ 0.0802	¹⁸² 0.1320	¹⁸⁵ 0.2393			
117	NEUROTECHNOLOGY-008	¹⁶ 0.0339	¹⁷² 0.0530	¹⁸⁷ 0.0893	¹⁹⁷ 0.1769	²⁰¹ 0.3288			
118	NEUROTECHNOLOGY-009	⁸⁵ 0.0108	⁸⁸ 0.0152	⁸⁷ 0.0196	⁸³ 0.0324	⁷¹ 0.1102			
119	NEUROTECHNOLOGY-010	⁶⁹ 0.0069	⁶⁴ 0.0099	⁶⁶ 0.0138	¹⁰⁹ 0.0449	¹⁴⁶ 0.1727			
120	NEUROTECHNOLOGY-012	⁴⁷ 0.0047	⁴⁸ 0.0068	⁵¹ 0.0097	⁶⁵ 0.0265	¹¹⁰ 0.1343			
121	NOTIONTAG-000	⁹² 0.0128	⁹² 0.0175	⁹² 0.0228	⁹¹ 0.0357	⁹⁹ 0.1270			
122	NTechLab-003	¹⁸² 0.0421	¹⁷⁶ 0.0537	¹⁶⁸ 0.0674	¹⁵³ 0.0907	¹⁵⁶ 0.1582			
123	NTechLab-004	¹⁵ 0.0312	¹⁵¹ 0.0405	¹⁴⁷ 0.0519	¹⁴⁵ 0.0722	¹² 0.1503			
124	NTechLab-005	¹⁵⁶ 0.0334	¹⁵² 0.0424	¹⁵³ 0.0537	¹⁴⁸ 0.0760	¹⁵³ 0.1543			
125	NTechLab-006	¹⁴⁸ 0.0288	¹⁴⁶ 0.0367	¹⁴⁶ 0.0471	¹⁴⁰ 0.0670	¹²⁹ 0.1523			
126	NTechLab-007	¹²⁴ 0.0188	¹²⁰ 0.0256	¹¹⁸ 0.0317	¹¹⁵ 0.0495	¹⁰⁵ 0.1306			
127	NTechLab-008	⁸³ 0.0107	⁸¹ 0.0145	⁸² 0.0187	⁷¹ 0.0286	⁵⁴ 0.0995			
128	NTechLab-009	³⁹ 0.0037	³⁹ 0.0049	³⁷ 0.0062	³² 0.0125	²⁴ 0.0735			
129	NTechLab-010	¹⁶ 0.0020	¹⁷ 0.0025	¹⁵ 0.0030	¹⁷ 0.0077	²³ 0.0710			
130	NTechLab-011	² 0.0022	²² 0.0030	²³ 0.0038	¹⁶ 0.0075	¹ 0.0625			
131	PANGAM-000	⁴⁵ 0.0042	⁴⁵ 0.0060	⁴⁸ 0.0080	⁴² 0.0160	³⁸ 0.0876			
132	PARAVISION-003	¹⁴² 0.0260	¹⁴⁴ 0.0351	¹⁴⁴ 0.0447	¹³⁹ 0.0657	¹⁴ 0.1630			
133	PARAVISION-004	⁶⁶ 0.0074	⁶⁸ 0.0101	⁶⁴ 0.0136	⁶⁶ 0.0267	⁶⁶ 0.1256			
134	PARAVISION-005	³⁶ 0.0032	²⁹ 0.0041	³⁶ 0.0057	⁴⁵ 0.0174	⁶² 0.1037			
135	PARAVISION-007	²⁸ 0.0030	²⁸ 0.0040	²⁹ 0.0055	³⁰ 0.0211	²⁰ 0.1097			
136	PARAVISION-009	¹⁷ 0.0020	²⁰ 0.0026	²² 0.0038	²² 0.0098	³⁵ 0.0857			
137	PIXELALL-002	²¹⁶ 0.0716	²²⁰ 0.1052	²⁰⁹ 0.1475	²¹⁰ 0.2489	²⁰⁷ 0.3904			
138	PIXELALL-003	¹¹¹ 0.0158	¹¹¹ 0.0218	¹¹⁴ 0.0288	¹¹¹ 0.0474	⁸¹ 0.1138			
139	PIXELALL-004	⁹² 0.0129	¹⁰⁰ 0.0183	¹⁰¹ 0.0245	⁹³ 0.0378	¹¹² 0.1375			
140	PIXELALL-005	⁷² 0.0087	⁷² 0.0121	⁷⁷ 0.0171	⁵⁸ 0.0250	⁶⁴ 0.1052			
141	PTAKURATSATU-000	¹⁴⁰ 0.0275	¹⁴⁵ 0.0366	¹⁴⁴ 0.0458	¹²⁴ 0.0523	¹⁴ 0.0523			
142	QNAP-001	¹⁷⁷ 0.0404	¹⁷⁵ 0.0536	¹⁶² 0.0661	¹⁵⁵ 0.0916	¹⁵⁷ 0.1595			
143	QNAP-002	¹³ 0.0200	¹²⁵ 0.0265	¹²¹ 0.0327	¹¹⁵ 0.0490	¹⁰ 0.1341			
144	QUANTASOFT-001	²⁹⁴ 0.6387	²⁹⁴ 0.6387	²²⁸ 0.6387	²¹² 0.6387				

Table 19: **Identification-mode: Effect of N on FNIR at high threshold.** Values are threshold-based miss rates i.e. FNIR at FPIR = 0.001 for five enrollment population sizes, N. The right six columns apply for enrollment of one image. Missing entries usually apply because another algorithm from the same developer was run instead. Some developers are missing because less accurate algorithms were not run on galleries with $N \geq 3\ 000\ 000$. Throughout blue superscripts indicate the rank of the algorithm for that column.

#	ALGORITHM	MISSES BELOW THRESHOLD, T FNIR(N, T > 0, R > L)		ENROL MOST RECENT DATASET: FRVT 2018 MUGSHOTS				
				N=0.64M	N=1.6M	N=3.0M	N=6.0M	N=12.0M
145	RANKONE-002	²² 0.0973	²² 0.1175	²⁰ 0.1359	¹⁹ 0.1718	¹⁹ 0.2613		
146	RANKONE-003	²³ 0.0973	²² 0.1175	²⁰ 0.1359	¹⁹ 0.1718	¹⁹ 0.2613		
147	RANKONE-005	¹⁹ 0.0473	¹⁸ 0.0592	¹⁷ 0.0700	¹⁸ 0.0944	¹⁶ 0.1998		
148	RANKONE-007	¹¹ 0.0168	¹¹ 0.0222	¹⁰ 0.0266	⁹ 0.0381	⁷ 0.1132		
149	RANKONE-009	⁹ 0.0132	⁹ 0.0177	⁹ 0.0230	⁸ 0.0344	⁴ 0.0921		
150	RANKONE-010	⁸ 0.0106	⁷ 0.0136	⁷ 0.0174	⁶ 0.0265	² 0.0785		
151	RANKONE-011	⁵ 0.0063	⁵ 0.0087	⁵ 0.0115	⁶ 0.0269	⁸ 0.1135		
152	RANKONE-012	³⁵ 0.0058	⁵³ 0.0077	⁵¹ 0.0100	⁵¹ 0.0220	⁷⁴ 0.1111		
153	RANKONE-013	³⁵ 0.0034	³³ 0.0046	³³ 0.0059	³³ 0.0127	³⁷ 0.0875		
154	REALNETWORKS-002	²⁸ 0.1943	²⁵ 0.2314	²² 0.2656	²¹ 0.3134	²⁰ 0.3208		
155	REALNETWORKS-003	²⁴ 0.1300	²⁴ 0.1594	²¹ 0.1858	²⁰ 0.2246	²⁰ 0.3076		
156	REALNETWORKS-004	²⁴ 0.1279	²⁴ 0.1581	²¹ 0.1857	²⁰ 0.2329	²⁰ 0.3179		
157	REALNETWORKS-005	¹³ 0.0202	¹³ 0.0277	¹³ 0.0355	¹³ 0.0560	¹¹ 0.1431		
158	REALNETWORKS-006	⁷ 0.0097	⁸ 0.0145	⁸ 0.0182	⁸ 0.0308	⁵³ 0.0991		
159	REALNETWORKS-007	⁶⁴ 0.0068	⁶² 0.0097	⁶⁰ 0.0125	⁵³ 0.0233	⁴³ 0.0917		
160	REALNETWORKS-008	⁴⁶ 0.0044	⁴⁶ 0.0062	⁴⁶ 0.0082	³⁵ 0.0139	³⁰ 0.0824		
161	REMARKAI-000	¹⁷ 0.0406	¹⁷ 0.0552	¹⁶ 0.0676	¹⁶ 0.1028	¹⁶ 0.2003		
162	RENDIP-000	⁷⁰ 0.0085	⁷¹ 0.0121	⁷¹ 0.0156	⁷⁰ 0.0277	⁶⁸ 0.1182		
163	REVEALMEDIA-000	⁷³ 0.0090	⁷³ 0.0122	⁷³ 0.0158	⁶⁹ 0.0277	³⁸ 0.1019		
164	S1-000	¹³ 0.0204	¹³ 0.0279	¹³ 0.0382	¹³ 0.0630	¹⁴ 0.1707		
165	S1-001	³⁸ 0.0115	⁸⁹ 0.0156	⁸⁸ 0.0199	⁹⁶ 0.0392	⁹⁷ 0.1256		
166	S1-002	⁴³ 0.0040	⁴³ 0.0056	⁴³ 0.0077	⁶³ 0.0264	¹⁰¹ 0.1285		
167	S1-003	⁵⁶ 0.0061	⁵⁸ 0.0088	⁵⁷ 0.0116	⁶⁸ 0.0277	¹⁰² 0.1298		
168	SCANOVATE-000	¹⁹ 0.0498	¹⁹ 0.0667	¹⁷ 0.0804	¹⁸ 0.1097	⁷³ 0.1109		
169	SCANOVATE-001	²⁰ 0.0630	²⁰ 0.0815	¹⁹ 0.0993	¹⁷ 0.1292	¹⁶ 0.1960		
170	SENSETIME-000	¹¹ 0.0158	¹⁰ 0.0208	¹⁰ 0.0270	⁹ 0.0398	⁸⁹ 0.1232		
171	SENSETIME-001	¹¹ 0.0161	¹¹ 0.0219	¹¹ 0.0277	¹⁰ 0.0420	¹⁰³ 0.1304		
172	SENSETIME-002	¹⁰ 0.0146	⁸³ 0.0148	⁷⁰ 0.0153	⁵⁴ 0.0234	¹⁹ 0.0657		
173	SENSETIME-003	⁷ 0.0016	⁸ 0.0018	⁸ 0.0021	⁹ 0.0054	⁸ 0.0451		
174	SENSETIME-004	⁶ 0.0015	⁵ 0.0018	⁷ 0.0021	⁴ 0.0040	⁶ 0.0354		
175	SENSETIME-005	⁸ 0.0016	¹⁴ 0.0022	¹⁶ 0.0031	²⁰ 0.0089	⁹ 0.0454		
176	SENSETIME-006	⁴ 0.0014	⁷ 0.0018	¹¹ 0.0023	⁵ 0.0047	⁷ 0.0372		
177	SENSETIME-007	² 0.0012	² 0.0014	² 0.0016	² 0.0036	⁴ 0.0316		
178	SENSETIME-008	¹ 0.0011	¹ 0.0013	¹ 0.0015	¹ 0.0031	² 0.0288		
179	SHAMAN-007	²¹ 0.1212	²³ 0.1413	²¹ 0.1587	¹⁹ 0.1879	¹⁸ 0.2460		
180	SIAT-001	⁹⁸ 0.0136	⁹³ 0.0176	⁹⁵ 0.0230	⁸⁶ 0.0344	⁶⁰ 0.1035		
181	SIAT-002	¹⁰⁹ 0.0154	¹¹⁰ 0.0216	¹¹⁰ 0.0273	¹⁰¹ 0.0404	¹⁰⁰ 0.1283		
182	SQISOFT-001	²² 0.0921	²³ 0.1322	²¹ 0.1781	²⁰ 0.2348	²¹⁸ 0.9271		
183	SYNESIS-003	¹⁹ 0.0499	¹⁹ 0.0652	¹⁸ 0.0804	¹⁶ 0.1095	¹⁵ 0.1916		
184	SYNESIS-003	²⁹ 0.5341	²⁸ 0.5821	²² 0.6113	²² 0.6479	²¹ 0.6822		
185	SYNESIS-005	¹¹ 0.0181	¹¹ 0.0248	¹¹ 0.0319	¹² 0.0518	¹⁵ 0.1580		
186	TECH5-001	¹⁸¹ 0.0420	¹⁸² 0.0574	¹⁸⁶ 0.0911	²⁰² 0.2106	²⁰⁸ 0.3725		
187	TECH5-002	¹² 0.0194	¹² 0.0269	¹² 0.0346	¹² 0.0537	¹³ 0.1607		
188	TEVIAN-005	²¹ 0.0692	²¹ 0.0873	¹⁹ 0.1066	¹⁸ 0.1301	¹⁵ 0.1840		
189	TEVIAN-006	⁶ 0.0078	⁶³ 0.0098	⁶ 0.0130	⁶² 0.0261	¹⁰ 0.1305		
190	TEVIAN-007	⁴¹ 0.0038	⁴¹ 0.0052	³⁹ 0.0065	³⁹ 0.0154	⁴⁹ 0.0957		
191	TIGER-002	²⁸ 0.0647	²⁰ 0.0861	¹⁹ 0.1036	¹⁸ 0.1332	¹⁷ 0.2231		
192	TOSHIBA-000	¹⁹ 0.0460	¹⁸ 0.0620	¹⁷ 0.0780	¹⁷ 0.1117	¹⁶ 0.2082		
193	TRUEFACE-000	⁹⁷ 0.0134	⁹⁹ 0.0182	⁹⁸ 0.0238	⁹⁴ 0.0380	¹¹³ 0.1385		
194	VD-001	²⁵ 0.1642	²⁵ 0.2015	²² 0.2351	²¹ 0.2736	²⁰ 0.3293		
195	VERIDAS-001	¹⁴ 0.0278	¹⁴ 0.0373	¹⁴ 0.0491	¹⁴ 0.0753	¹³ 0.1541		
196	VERIDAS-002	¹⁴ 0.0278	¹⁴ 0.0373	¹³ 0.0373	¹⁴ 0.0491	²⁶ 0.0753		
197	VERIDAS-003	⁸⁹ 0.0117	⁹¹ 0.0166	⁹⁰ 0.0219	¹⁰⁸ 0.0446	¹³² 0.1543		
198	VIGILANTSOLUTIONS-008	¹⁰ 0.0146	¹⁰ 0.0205	¹⁰ 0.0269	¹¹ 0.0489	⁸ 0.1164		
199	VISIONBOX-000	⁹⁰ 0.0122	⁹⁶ 0.0177	⁹⁹ 0.0239		²¹ 0.9538		
200	VISIONLABS-004	¹⁸ 0.0427	¹⁸ 0.0578	¹⁷ 0.0703	¹⁹ 0.0949	¹⁵ 0.1853		
201	VISIONLABS-005	¹⁶ 0.0369	¹⁶ 0.0502	¹⁵ 0.0626	¹⁵ 0.0847	¹⁵ 0.1815		
202	VISIONLABS-006	¹² 0.0188	¹² 0.0267	¹² 0.0336	¹³ 0.0542	¹² 0.1478		
203	VISIONLABS-007	¹² 0.0188	¹² 0.0266	¹² 0.0335	¹² 0.0540	¹² 0.1479		
204	VISIONLABS-008	⁷⁶ 0.0096	⁷⁶ 0.0131	⁷⁸ 0.0166	⁷⁵ 0.0291	⁹² 0.1247		
205	VISIONLABS-009	³⁶ 0.0034	³⁴ 0.0046	³⁴ 0.0060	³⁶ 0.0140	³⁹ 0.0881		
206	VISIONLABS-010	⁴⁰ 0.0038	⁴⁰ 0.0051	⁴¹ 0.0070	³⁷ 0.0149	⁴⁵ 0.0920		
207	VISIONLABS-011	²⁵ 0.0025	²⁴ 0.0033	²⁵ 0.0044	²⁶ 0.0120	³² 0.0825		
208	VNPT-001	⁸⁰ 0.0104	⁸⁰ 0.0143	⁸³ 0.0190	⁷⁶ 0.0296	⁵⁹ 0.1028		
209	VNPT-002	⁴⁷ 0.0051	⁴⁷ 0.0065	⁴⁷ 0.0083	⁴⁴ 0.0172	³⁹ 0.1005		
210	VCORD-005	²³⁸ 0.1179	²⁴¹ 0.1577	²¹⁹ 0.2183	²¹⁵ 0.3122	²¹¹ 0.4490		
211	VTS-001	⁷⁹ 0.0102	⁷⁷ 0.0133	⁷⁹ 0.0175	⁸² 0.0322	⁹² 0.1243		
212	VTS-002	¹²⁰ 0.0185	¹²² 0.0259	¹²⁶ 0.0344	¹³² 0.0549	¹¹⁹ 0.1447		
213	VTS-003	⁵³ 0.0053	⁵² 0.0073	⁵⁶ 0.0096	⁴⁶ 0.0188	⁵⁹ 0.1017		
214	XFORWARDAI-000	⁸⁴ 0.0107	⁸⁶ 0.0151	⁸⁵ 0.0195	⁸⁴ 0.0324	⁶⁶ 0.1057		
215	XFORWARDAI-001	³⁸ 0.0037	³⁸ 0.0049	³⁶ 0.0060	²⁵ 0.0120	²⁸ 0.0800		
216	XFORWARDAI-002	²⁴ 0.0026	²³ 0.0030	²¹ 0.0035	¹⁸ 0.0078	²² 0.0706		

Table 20: **Identification-mode: Effect of N on FNIR at high threshold.** Values are threshold-based miss rates i.e. FNIR at FPIR = 0.001 for five enrollment population sizes, N. The right six columns apply for enrollment of one image. Missing entries usually apply because another algorithm from the same developer was run instead. Some developers are missing because less accurate algorithms were not run on galleries with $N \geq 3\,000\,000$. Throughout blue superscripts indicate the rank of the algorithm for that column.

MISSES BELOW THRESHOLD, T FNIR(N, T > 0, R > L)		ENROL MOST RECENT				
#	ALGORITHM	DATASET: FRVT 2018 MUGSHOTS				
		N=0.64M	N=1.6M	N=3.0M	N=6.0M	N=12.0M
217	YITU-002	⁹⁴ 0.0129	⁹⁴ 0.0177	⁹³ 0.0228	⁸⁸ 0.0345	⁷⁹ 0.1133
218	YITU-003	¹⁰² 0.0138	¹⁰² 0.0185	⁹⁶ 0.0236	⁸⁹ 0.0353	⁸¹ 0.1148
219	YITU-004	⁶³ 0.0067	⁶⁰ 0.0096	⁶¹ 0.0129	⁵² 0.0232	⁶³ 0.1046
220	YITU-005	⁶⁷ 0.0074	⁶⁷ 0.0101	⁶⁵ 0.0135	⁶⁰ 0.0255	⁶⁷ 0.1057

Table 21: Identification-mode: Effect of N on FNIR at high threshold. Values are threshold-based miss rates i.e. FNIR at FPIR = 0.001 for five enrollment population sizes, N. The right six columns apply for enrollment of one image. Missing entries usually apply because another algorithm from the same developer was run instead. Some developers are missing because less accurate algorithms were not run on galleries with $N \geq 3\,000\,000$. Throughout blue superscripts indicate the rank of the algorithm for that column.

MISSES AT GIVEN RANK		ENROL MOST RECENT													
#	ALGORITHM	RANK 1					aN^b	RANK 50					aN^b		
		N=0.64M	N=1.6M	N=3.0M	N=6.0M	N=12.0M		N=0.64M	N=1.6M	N=3.0M	N=6.0M	N=12.0M			
1	3DIVI-005	²⁴⁵ 0.0137	²⁴³ 0.0176	²¹⁰ 0.0210	²⁰⁴ 0.0253	¹⁹⁸ 0.0302	¹⁵⁵ 0.0004 N ^{0.271} ¹⁸¹	²²⁴ 0.0040	²²⁴ 0.0049	²⁰⁰ 0.0057	¹⁹⁶ 0.0068	¹⁹⁰ 0.0081	⁴⁹ 0.0002 N ^{0.240} ¹⁸⁵		
2	ACER-000	²¹¹ 0.0081	²¹⁹ 0.0106	¹⁹⁸ 0.0128	¹⁹⁶ 0.0157	¹⁹¹ 0.0195	⁶³ 0.0001 N ^{0.299} ²⁰⁵	¹⁶⁹ 0.0020	¹⁸⁸ 0.0026	¹⁷⁷ 0.0031	¹⁷⁷ 0.0037	¹⁷² 0.0045	¹⁹ 0.0000 N ^{0.284} ¹⁹⁹		
3	ALCHERA-003	²⁰⁷ 0.0079	²¹⁶ 0.0104	¹⁹⁶ 0.0123	¹⁹⁵ 0.0147	¹⁸⁹ 0.0180	⁹⁵ 0.0002 N ^{0.278} ¹⁹²	²⁰⁵ 0.0027	²⁰³ 0.0032	¹⁸³ 0.0035	¹⁸⁸ 0.0042	¹⁷³ 0.0048	⁵⁸ 0.0002 N ^{0.199} ¹⁷⁵		
4	ALLGOVISION-000	²²⁷ 0.0101	²²⁵ 0.0114	¹⁹⁷ 0.0127	¹⁹⁴ 0.0145	¹⁸⁸ 0.0166	¹⁹⁴ 0.0010 N ^{0.171} ¹¹⁵	²⁴⁵ 0.0063	²⁴⁰ 0.0067	²⁰⁵ 0.0071	¹⁹⁹ 0.0075	¹⁸⁹ 0.0081	²⁰² 0.0020 N ^{0.086} ¹³²		
5	ALLGOVISION-001	¹⁹⁹ 0.0069	²⁰⁶ 0.0090	¹⁹¹ 0.0107	¹⁸⁹ 0.0128	¹⁸⁷ 0.0157	⁸⁰ 0.0002 N ^{0.277} ¹⁹⁰	¹⁹¹ 0.0023	¹⁹² 0.0027	¹⁷⁸ 0.0031	¹⁷⁷ 0.0036	¹⁶⁷ 0.0043	⁴ 0.0001 N ^{0.211} ¹⁸⁰		
6	ANKE-000	²³⁰ 0.0102	²³³ 0.0132	²⁰⁶ 0.0155	²⁰¹ 0.0188	¹⁹⁴ 0.0225	¹³⁴ 0.0003 N ^{0.270} ¹⁸⁰	²¹⁴ 0.0032	²¹⁶ 0.0040	¹⁹⁶ 0.0046	¹⁸⁹ 0.0056	¹⁸¹ 0.0066	⁴⁰ 0.0001 N ^{0.247} ¹⁸⁷		
7	ANKE-002	¹³² 0.0024	¹³¹ 0.0026	¹³³ 0.0032	¹²⁹ 0.0037	¹²³ 0.0043	⁷³ 0.0002 N ^{0.203} ¹³²	¹³⁸ 0.0016	¹³⁹ 0.0017	¹³² 0.0017	¹²⁴ 0.0018	¹¹⁸ 0.0019	¹¹¹ 0.0006 N ^{0.076} ¹¹⁹		
8	AWARE-003	²⁶³ 0.0238	²⁶¹ 0.0306	²²¹ 0.0361	²¹⁶ 0.0431	²¹⁵ 0.0506	¹⁹⁰ 0.0008 N ^{0.258} ¹⁷⁵	²³⁹ 0.0055	²⁴⁷ 0.0075	²¹⁶ 0.0092	²¹¹ 0.0113	²⁰⁹ 0.0143	³⁰ 0.0001 N ^{0.323} ²⁰⁹		
9	AWARE-005	²⁶⁴ 0.0245	²⁶² 0.0311	²²³ 0.0366	²¹⁷ 0.0434	²⁰³ 0.0312	²¹³ 0.0056 N ^{0.118} ⁶⁷	²⁴³ 0.0062	²⁵³ 0.0082	²¹⁸ 0.0101	²¹⁴ 0.0128	¹⁹² 0.0089	¹³⁷ 0.0007 N ^{0.169} ¹⁷⁰		
10	AYONIX-002	³⁰⁸ 0.2935	³⁰¹ 0.3414	²³¹ 0.3736	²²⁵ 0.4101	²¹⁸ 0.4465	¹⁸⁸ 0.0440 N ^{0.143} ⁸⁷	²⁵⁹ 0.0950	³⁰¹ 0.1274	²³³ 0.1524	²²⁴ 0.1828	²¹ 0.2150	²⁰⁴ 0.0023 N ^{0.279} ¹⁹⁶		
11	CAMVI-004	²³⁸ 0.0124	²²⁷ 0.0468	²²⁷ 0.0719	²²⁴ 0.2363	²¹⁷ 0.2367	¹¹⁹ 0.0001 N ^{0.055} ²¹⁹	²¹⁷ 0.0117	²⁸⁶ 0.0464	²²⁹ 0.0715	²²⁸ 0.2361	²¹⁸ 0.2364	³ 0.0000 N ^{0.371} ²¹⁹		
12	CANON-001	¹⁷ 0.0011	¹⁵ 0.0011	¹⁶ 0.0012	¹⁸ 0.0013	¹⁵ 0.0014	¹¹² 0.0002 N ^{0.113} ⁶⁰	²² 0.0009	¹¹⁰ 0.0006 N ^{0.026} ⁶²						
13	CANON-002	²³ 0.0011	²³ 0.0012	²⁹ 0.0013	³⁰ 0.0014	²⁹ 0.0016	⁷² 0.0002 N ^{0.142} ⁸⁶	²³ 0.0009	²¹ 0.0009	²⁰ 0.0009	¹⁹ 0.0009	¹⁷ 0.0009	¹³⁸ 0.0007 N ^{0.015} ³³		
14	CIB-000	⁶⁰ 0.0014	⁵⁸ 0.0015	⁵⁶ 0.0017	⁶⁰ 0.0019	¹⁷⁹ 0.0131	⁴ 0.0000 N ^{0.335} ²¹⁸	⁶⁸ 0.0012	⁶⁰ 0.0012	⁵⁹ 0.0012	⁵⁸ 0.0012	⁵⁶ 0.0012	⁴ 0.0000 N ^{0.647} ²¹⁸		
15	CLEARVIEW1-000	¹⁴ 0.0010	¹⁶ 0.0011	¹⁷ 0.0012	²⁰ 0.0013	²⁰ 0.0015	⁸⁸ 0.0002 N ^{0.129} ⁷⁸	²⁴ 0.0009	²⁰ 0.0009	²¹ 0.0009	²⁰ 0.0009	²⁰ 0.0010	¹²⁷ 0.0007 N ^{0.109} ⁴⁹		
16	CLOUDWALK-HR-000	⁶⁴ 0.0015	⁵² 0.0015	⁴⁸ 0.0015	⁴³ 0.0016	³⁶ 0.0017	¹⁸⁸ 0.0007 N ^{0.054} ¹²	¹²⁴ 0.0014	¹¹⁰ 0.0014	⁹⁹ 0.0014	⁹⁹ 0.0014	⁸⁵ 0.0014	¹⁸² 0.0012 N ^{0.102} ²³		
17	CLOUDWALK-MT-000	⁹² 0.0018	⁷³ 0.0018	⁶⁵ 0.0018	⁵⁵ 0.0019	⁴⁸ 0.0020	¹⁹⁶ 0.0011 N ^{0.036} ⁷	¹⁵⁴ 0.0018	¹⁴⁹ 0.0018	¹³⁷ 0.0018	¹²¹ 0.0018	¹⁰⁵ 0.0018	¹⁹⁸ 0.0017 N ^{0.002} ⁴		
18	CLOUDWALK-MT-001	⁹¹ 0.0018	⁷² 0.0018	⁶² 0.0018	⁵³ 0.0018	⁴⁶ 0.0019	¹⁹⁸ 0.0012 N ^{0.029} ⁴	¹⁵³ 0.0017	¹⁴⁸ 0.0018	¹³⁶ 0.0018	¹²⁸ 0.0018	¹⁰⁶ 0.0018	¹⁹⁷ 0.0017 N ^{0.003} ⁷		
19	COGENT-000	²²⁸ 0.0101	²¹⁸ 0.0105	¹⁹³ 0.0109	¹⁸⁴ 0.0115	¹⁷⁷ 0.0125	²¹⁰ 0.0038 N ^{0.071} ²³	¹⁷⁹ 0.0021	¹⁷² 0.0024	¹⁷² 0.0028	¹⁷⁴ 0.0036	¹⁶⁶ 0.0095	⁹ 0.0000 N ^{0.466} ²¹⁵		
20	COGENT-001	²²⁹ 0.0101	²¹ 0.0105	¹⁹² 0.0109	¹⁸⁵ 0.0115	¹⁷⁶ 0.0125	²¹¹ 0.0038 N ^{0.071} ²²	¹⁸⁰ 0.0021	¹⁸¹ 0.0024	¹⁷⁵ 0.0028	¹⁷⁶ 0.0036	¹⁶⁹ 0.0095	⁸ 0.0000 N ^{0.466} ²¹⁴		
21	COGENT-002	¹⁴⁵ 0.0029	¹⁴⁸ 0.0036	¹⁴⁶ 0.0041	¹⁴⁴ 0.0049	¹³⁹ 0.0059	⁴³ 0.0001 N ^{0.244} ¹⁶⁶	¹²⁰ 0.0014	¹³⁰ 0.0015	¹²⁶ 0.0017	¹³⁰ 0.0019	¹³¹ 0.0021	⁵⁴ 0.0002 N ^{0.144} ¹⁶⁴		
22	COGENT-003	¹⁵¹ 0.0031	¹⁵⁰ 0.0038	¹⁵¹ 0.0043	¹⁴⁷ 0.0051	¹⁴¹ 0.0060	⁵⁹ 0.0001 N ^{0.230} ¹⁵⁵	¹³² 0.0015	¹⁴⁰ 0.0017	¹⁴⁴ 0.0020	¹⁴⁰ 0.0020	¹³⁶ 0.0022	⁵⁶ 0.0002 N ^{0.143} ¹⁶³		
23	COGENT-004	⁹⁴ 0.0018	⁹² 0.0020	⁹² 0.0022	⁹² 0.0025	⁸⁴ 0.0028	¹⁰³ 0.0002 N ^{0.159} ¹⁰⁴	¹¹³ 0.0013	¹⁰⁸ 0.0014	⁹⁴ 0.0014	⁹⁶ 0.0015	⁸⁶ 0.0015	¹¹⁹ 0.0007 N ^{0.050} ⁹⁸		
24	COGENT-005	⁷¹ 0.0016	⁶⁹ 0.0017	⁶⁶ 0.0018	⁶³ 0.0020	⁵⁷ 0.0021	¹⁵⁶ 0.0004 N ^{0.108} ³⁵	¹¹⁴ 0.0013	⁹⁹ 0.0013	⁹² 0.0014	⁸⁷ 0.0014	⁷² 0.0014	¹⁷⁷ 0.0011 N ^{0.017} ³⁹		
25	COGENT-006	³⁴ 0.0012	³² 0.0012	³⁰ 0.0013	²⁷ 0.0014	²⁴ 0.0015	¹⁵³ 0.0004 N ^{0.088} ³⁸	⁴⁹ 0.0011	⁴⁹ 0.0011	⁴⁴ 0.0011	³⁶ 0.0011	³³ 0.0011	¹⁵³ 0.0008 N ^{0.019} ⁴⁶		
26	COGNITEC-000	²⁵⁶ 0.0195	²⁵² 0.0252	²¹⁸ 0.0297	²¹³ 0.0352	²⁰⁶ 0.0417	¹⁸¹ 0.0006 N ^{0.259} ¹⁷⁶	²³⁴ 0.0050	²³⁸ 0.0065	²¹² 0.0077	²⁰⁹ 0.0097	²⁰³ 0.0122	³⁷ 0.0001 N ^{0.305} ²⁰³		
27	COGNITEC-001	²²² 0.0090	²²⁰ 0.0117	²⁰¹ 0.0139	¹⁹⁹ 0.0166	¹⁹² 0.0199	¹²³ 0.0002 N ^{0.221} ¹⁸³	²¹⁰ 0.0030	²⁰⁹ 0.0034	¹⁹² 0.0040	¹⁸⁸ 0.0046	¹⁷⁷ 0.0054	³⁶ 0.0002 N ^{0.207} ¹⁷⁹		
28	COGNITEC-002	¹⁸¹ 0.0048	¹⁷⁹ 0.0057	¹⁷¹ 0.0067	¹⁶⁵ 0.0079	¹⁶³ 0.0094	¹⁰⁵ 0.0002 N ^{0.232} ¹⁵⁷	¹⁹³ 0.0024	¹⁸⁹ 0.0026	¹⁷⁵ 0.0028	¹⁶⁷ 0.0030	¹⁵⁷ 0.0034	⁹¹ 0.0005 N ^{0.117} ¹⁵⁰		
29	COGNITEC-003	¹⁸⁴ 0.0053	¹⁸⁶ 0.0062	¹⁷⁴ 0.0072	¹⁷¹ 0.0085	¹⁶⁶ 0.0100	¹³⁰ 0.0003 N ^{0.222} ¹⁴⁶	²⁰⁷ 0.0028	²⁰¹ 0.0030	¹⁸⁸ 0.0032	¹⁷⁸ 0.0035	¹⁶⁶ 0.0037	¹⁴⁸ 0.0008 N ^{0.097} ¹⁴⁰		
30	COGNITEC-004	¹⁴⁰ 0.0027	¹⁴¹ 0.0032	¹⁴¹ 0.0037	¹³⁹ 0.0045	¹³⁶ 0.0056	³³ 0.0001 N ^{0.253} ¹⁷²	¹⁰⁹ 0.0013	¹¹¹ 0.0014	¹⁰⁵ 0.0015	¹⁰¹ 0.0017	¹¹² 0.0019	⁶³ 0.0002 N ^{0.123} ¹⁵⁵		
31	COGNITEC-005	⁶¹ 0.0014	⁶⁰ 0.0016	⁶⁸ 0.0018	⁶⁶ 0.0021	⁶⁰ 0.0024	⁶⁴ 0.0001 N ^{0.169} ¹¹²	⁵⁶ 0.0011	⁵⁷ 0.0011	⁵⁶ 0.0012	⁵⁶ 0.0012	⁴⁶ 0.0012	¹¹⁷ 0.0007 N ^{0.037} ⁷⁶		
32	COGNITEC-006	⁵⁷ 0.0014	⁵⁹ 0.0016	⁵⁵ 0.0017	⁵⁹ 0.0019	⁵² 0.0021	¹⁷³ 0.0006 N ^{0.085} ³⁷	¹²¹ 0.0014	¹¹³ 0.0014	¹⁰³ 0.0014	⁹³ 0.0014	⁸⁰ 0.0015	¹⁷⁶ 0.0010 N ^{0.032} ⁵³		
33	CYBERLINK-000	¹⁵⁷ 0.0034	¹⁵⁴ 0.0046	¹⁵⁰ 0.0054	¹⁴⁷ 0.0063	¹⁴⁰ 0.0071	⁹⁹ 0.0002 N ^{0.209} ¹³⁹	¹⁷⁷ 0.0021	¹⁶⁷ 0.0022	¹⁶⁴ 0.0023	¹⁶⁰ 0.0027	¹⁵⁴ 0.0030	⁷⁷ 0.0002 N ^{0.107} ³⁷		
34	CYBERLINK-001	¹⁴⁸ 0.0030	¹⁴⁶ 0.0035	¹⁴⁰ 0.0042	¹⁴⁰ 0.0050	¹³⁴ 0.0060	⁴⁴ 0.0001 N ^{0.243} ¹⁶⁵	¹⁴¹ 0.0016	¹⁴⁰ 0.0016	¹³⁴ 0.0017	¹³⁹ 0.0018	¹³⁰ 0.00			

MISSES AT GIVEN RANK		ENROL MOST RECENT											
#	FNIR(N, T= 0, R)	RANK 1					RANK 50						
		N=0.64M	N=1.6M	N=3.0M	N=6.0M	N=12.0M	aN ^b	N=0.64M	N=1.6M	N=3.0M	N=6.0M	N=12.0M	aN ^b
73	IDEORIA-006	²⁰⁴ 0.0076	²¹³ 0.0096	¹⁹⁵ 0.0113	¹⁹¹ 0.0135	¹⁸⁷ 0.0161	¹¹⁹ 0.0002 N ^{0.259} ¹⁷⁷	²⁰⁶ 0.0028	²¹⁵ 0.0037	¹⁹⁵ 0.0046	¹⁹¹ 0.0059	¹⁸⁶ 0.0076	¹⁵ 0.0000 N ^{0.344} ²¹¹
74	IDEORIA-007	¹¹⁶ 0.0021	¹²⁵ 0.0026	¹² 0.0030	¹²⁵ 0.0036	¹² 0.0044	²⁵ 0.0001 N ^{0.250} ¹⁷⁰	⁵⁹ 0.0011	⁶⁴ 0.0012	⁶⁸ 0.0012	⁸⁰ 0.0014	⁸⁴ 0.0015	⁶⁴ 0.0002 N ^{0.110} ¹⁴⁷
75	IDEORIA-008	⁹ 0.0010	¹³ 0.0011	¹² 0.0011	¹² 0.0013	¹³ 0.0014	⁹² 0.0002 N ^{0.121} ⁷¹	²¹ 0.0009	¹⁹ 0.0009	¹⁶ 0.0009	¹⁸ 0.0009	¹³ 0.0009	¹³¹ 0.0007 N ^{0.116} ³⁵
76	IDEORIA-009	⁵ 0.0009	⁵ 0.0010	⁸ 0.0010	⁸ 0.0011	⁸ 0.0012	¹²⁵ 0.0003 N ^{0.097} ⁴⁶	¹⁴ 0.0008	¹⁰ 0.0009	⁹ 0.0009	⁷ 0.0009	¹⁴⁷ 0.0008 N ^{0.007} ¹³	
77	IMAGUS-005	⁹³ 0.0018	⁹⁰ 0.0019	⁹⁰ 0.0022	⁹⁰ 0.0025	⁸² 0.0028	¹⁰² 0.0002 N ^{0.158} ¹⁰³	⁹³ 0.0013	⁹⁸ 0.0013	⁹³ 0.0014	⁹¹ 0.0014	⁸⁹ 0.0016	⁹⁵ 0.0005 N ^{0.066} ¹¹⁸
78	IMAGUS-006	⁹⁵ 0.0018	⁹⁷ 0.0020	⁸⁹ 0.0022	⁸⁹ 0.0025	⁸⁹ 0.0026	¹⁰² 0.0002 N ^{0.156} ⁹⁷	¹¹⁵ 0.0014	¹¹⁵ 0.0014	¹¹¹ 0.0015	⁹⁹ 0.0015	⁹⁴ 0.0016	¹³⁰ 0.0007 N ^{0.049} ⁹⁷
79	IMAGUS-007	⁸⁷ 0.0017	⁹⁸ 0.0022	⁹⁷ 0.0026	⁹⁰ 0.0030	⁹⁷ 0.0032	⁵⁷ 0.0012 N ^{0.189} ¹²⁴	⁷⁹ 0.0012	⁷⁶ 0.0013	⁷⁴ 0.0013	⁷¹ 0.0013	⁷⁷ 0.0015	⁹⁴ 0.0005 N ^{0.064} ¹¹⁶
80	IMPERIAL-000	¹²⁵ 0.0022	¹²¹ 0.0024	¹¹⁸ 0.0027	¹¹⁸ 0.0030	¹⁰⁶ 0.0035	¹² 0.0003 N ^{0.157} ⁹⁹	¹⁴⁶ 0.0016	¹⁴² 0.0017	¹³⁴ 0.0017	¹²² 0.0018	¹¹⁰ 0.0018	¹⁶⁸ 0.0009 N ^{0.041} ⁸⁴
81	INCODE-003	²²⁶ 0.0098	²³² 0.0129	²⁰⁵ 0.0154	²⁰⁹ 0.0191	¹⁹⁵ 0.0233	⁹¹ 0.0002 N ^{0.296} ²⁰²	¹⁹⁴ 0.0024	²⁰² 0.0031	¹⁹⁰ 0.0036	¹⁸⁷ 0.0046	¹⁷⁹ 0.0056	²⁵ 0.0001 N ^{0.265} ²⁰⁰
82	INCODE-004	¹⁴⁶ 0.0029	¹⁴⁷ 0.0035	¹⁴⁴ 0.0041	¹⁴⁹ 0.0049	¹⁴⁴ 0.0061	⁴² 0.0001 N ^{0.244} ¹⁶⁷	¹⁵⁸ 0.0018	¹⁵⁴ 0.0019	¹⁵³ 0.0020	¹⁴⁸ 0.0021	¹³⁵ 0.0022	¹⁰⁹ 0.0006 N ^{0.077} ¹²⁶
83	INCODE-005	⁶⁷ 0.0015	⁶⁴ 0.0017	⁶³ 0.0018	⁶⁴ 0.0020	⁶⁵ 0.0023	¹¹⁴ 0.0002 N ^{0.140} ⁸⁴	⁸³ 0.0012	⁷⁵ 0.0013	⁷⁶ 0.0013	⁶⁸ 0.0014	¹²⁹ 0.0007 N ^{0.041} ⁸¹	
84	INNOVATRICS-007	⁷³ 0.0016	⁶⁷ 0.0017	⁷⁰ 0.0019	⁶⁷ 0.0021	⁶⁹ 0.0024	¹¹¹ 0.0002 N ^{0.143} ⁸⁹	⁸¹ 0.0012	⁷³ 0.0012	⁷¹ 0.0013	⁶⁷ 0.0013	⁶² 0.0013	¹³⁵ 0.0007 N ^{0.037} ⁷⁸
85	INTEMA-000	²⁰ 0.0011	¹⁹ 0.0011	¹⁹ 0.0012	¹⁹ 0.0013	² 0.0016	⁹⁶ 0.0002 N ^{0.124} ⁷³	⁴¹ 0.0010	⁴² 0.0010	⁴⁶ 0.0011	⁴¹ 0.0011	⁵¹ 0.0013	⁷⁴ 0.0003 N ^{0.059} ¹²⁷
86	INTSYSMSU-000	²⁹² 0.1395	²⁹² 0.1457	²²⁹ 0.1498	²²¹ 0.1544	²¹⁴ 0.1591	²²⁰ 0.0768 N ^{0.145} ⁹	³⁰¹ 0.1098	²⁹⁹ 0.1163	²³² 0.1206	²²³ 0.1252	²¹⁶ 0.1296	²²⁰ 0.0519 N ^{0.056} ¹⁰⁵
87	IREX-000	¹⁷² 0.0043	¹⁶¹ 0.0044	¹⁵² 0.0044	¹⁴⁹ 0.0046	¹³⁰ 0.0048	²⁰⁷ 0.0028 N ^{0.132} ⁶	²²⁹ 0.0043	²²⁰ 0.0043	¹⁹⁴ 0.0043	¹⁸³ 0.0043	¹⁶⁷ 0.0043	²¹⁰ 0.0042 N ^{0.002} ⁵
88	ISYSTEMS-002	¹⁸⁶ 0.0053	¹⁸⁵ 0.0064	¹⁷⁵ 0.0072	¹⁶⁹ 0.0083	¹⁶⁴ 0.0096	¹⁴⁹ 0.0003 N ^{0.204} ¹³⁴	²¹⁶ 0.0033	²¹⁰ 0.0034	¹⁸⁸ 0.0036	¹⁷⁸ 0.0038	¹⁶⁵ 0.0041	¹⁸⁷ 0.0013 N ^{0.171} ¹²¹
89	ISYSTEMS-003	¹⁷⁶ 0.0046	¹⁷³ 0.0052	¹⁶⁷ 0.0057	¹⁵⁹ 0.0066	¹⁵² 0.0076	¹⁶⁰ 0.0004 N ^{0.174} ¹¹⁷	²¹⁴ 0.0031	²⁰⁶ 0.0033	¹⁸¹ 0.0034	¹⁷¹ 0.0035	¹⁶³ 0.0037	¹⁸⁸ 0.0013 N ^{0.063} ¹¹⁵
90	KAKAO-000	⁴¹ 0.0013	⁵¹ 0.0015	⁵³ 0.0016	⁵⁸ 0.0019	⁶¹ 0.0022	³⁷ 0.0001 N ^{0.192} ¹²⁸	²⁹ 0.0009	²⁹ 0.0010	²⁸ 0.0010	³⁰ 0.0011	⁸⁰ 0.0005 N ^{0.050} ⁹⁹	
91	KAKAO-001	⁵⁰ 0.0014	⁴² 0.0014	⁴⁰ 0.0015	³⁴ 0.0015	³¹ 0.0016	¹⁷⁸ 0.0006 N ^{0.060} ¹⁶	⁹⁷ 0.0013	⁸⁷ 0.0013	⁷² 0.0013	³⁸ 0.0013	¹⁸⁰ 0.0011 N ^{0.012} ²²	
92	KEDACOM-001	²⁰⁵ 0.0076	¹⁹⁵ 0.0077	¹⁸⁰ 0.0079	¹⁶⁸ 0.0083	¹⁵⁷ 0.0087	²¹² 0.0040 N ^{0.047} ¹⁰	²⁵⁰ 0.0071	²⁴³ 0.0072	²⁰⁹ 0.0072	¹⁹⁷ 0.0073	¹⁸³ 0.0073	²¹⁵ 0.0063 N ^{0.009} ¹⁸
93	KNERON-000	¹⁸⁰ 0.0048	¹⁸⁰ 0.0059	¹⁷² 0.0067	¹⁶⁸ 0.0079	¹⁶² 0.0093	¹¹⁸ 0.0002 N ^{0.226} ¹⁵¹	²³¹ 0.0048	²³³ 0.0059	²⁰⁴ 0.0067	²⁰² 0.0079	¹⁹⁴ 0.0093	⁶² 0.0002 N ^{0.226} ¹⁸³
94	LINECLOVA-002	⁴⁰ 0.0013	³⁶ 0.0013	³³ 0.0014	³⁵ 0.0015	³⁰ 0.0016	¹⁶¹ 0.0004 N ^{0.079} ³⁰	⁷⁴ 0.0012	⁶⁵ 0.0012	⁵⁸ 0.0012	⁴³ 0.0012	¹⁷⁸ 0.0011 N ^{0.008} ¹⁴	
95	LOOKMAN-003	²¹⁵ 0.0083	²⁰⁴ 0.0088	¹⁹⁷ 0.0091	¹⁹⁵ 0.0096	¹⁸⁸ 0.0104	²⁰⁸ 0.0030 N ^{0.076} ²⁶	²⁵⁹ 0.0072	²⁴⁶ 0.0074	²¹¹ 0.0075	²⁰⁰ 0.0076	¹⁸⁷ 0.0077	²¹³ 0.0054 N ^{0.022} ⁵²
96	LOOKMAN-005	²⁰⁶ 0.0078	¹⁹⁸ 0.0080	¹⁸² 0.0083	¹⁷² 0.0086	¹⁶⁹ 0.0092	²⁰⁹ 0.0038 N ^{0.075} ¹¹	²⁵¹ 0.0072	²⁴⁴ 0.0072	²¹⁰ 0.0073	¹⁹⁸ 0.0073	¹⁸⁴ 0.0074	²¹⁴ 0.0060 N ^{0.013} ²⁹
97	MANTRA-000	⁶⁸ 0.0015	⁷⁰ 0.0017	⁷⁰ 0.0019	⁷⁵ 0.0022	⁷⁰ 0.0025	⁶⁷ 0.0002 N ^{0.171} ¹¹⁴	⁷³ 0.0012	⁶⁷ 0.0012	⁶⁵ 0.0012	⁶² 0.0013	⁵⁷ 0.0013	¹¹⁵ 0.0007 N ^{0.042} ⁸⁵
98	MAXVISION-000	¹¹⁵ 0.0021	¹¹⁹ 0.0024	¹²⁰ 0.0027	¹¹⁹ 0.0032	¹¹⁷ 0.0038	⁵⁴ 0.0001 N ^{0.206} ¹³⁷	⁹⁴ 0.0013	¹⁰⁴ 0.0014	¹⁰² 0.0014	¹⁰⁶ 0.0015	¹⁰³ 0.0017	⁷⁰ 0.0003 N ^{0.100} ¹⁴²
99	MAXVISION-001	³² 0.0012	³⁰ 0.0012	²⁹ 0.0013	²⁵ 0.0014	²⁴ 0.0015	¹⁴⁷ 0.0003 N ^{0.089} ³⁹	⁵² 0.0011	⁴⁸ 0.0011	⁴³ 0.0011	⁴⁰ 0.0011	³⁴ 0.0011	¹⁶¹ 0.0009 N ^{0.014} ³¹
100	MEGVII-001	²³³ 0.0105	²²⁸ 0.0118	¹⁹³ 0.0142	¹⁸⁶ 0.0161	²⁰² 0.0015 N ^{0.143} ⁸⁸	²⁵⁶ 0.0077	²⁵² 0.0080	²¹³ 0.0082	²⁰⁷ 0.0086	¹⁹³ 0.0089	²⁰⁹ 0.0040 N ^{0.048} ⁹⁶	
101	MICROFOCUS-005	³⁰⁴ 0.0300	³⁰⁴ 0.0424	²⁵ 0.04610	²⁵ 0.05000	²¹ 0.05391	²¹⁹ 0.0674 N ^{0.128} ⁷⁷	³⁰⁴ 0.1300	³⁰⁴ 0.1724	²³⁴ 0.2046	²²² 0.2425	²¹⁹ 0.2810	²⁰⁸ 0.0404 N ^{0.263} ¹⁹³
102	MICROSOFT-003	³⁷ 0.0013	⁶¹ 0.0016	⁶⁹ 0.0018	⁷⁷ 0.0022	⁸³ 0.0028	¹⁴ 0.0000 N ^{0.271} ¹⁸⁴	²⁰⁹ 0.0028	²⁰⁶ 0.0030	¹⁹⁶ 0.0036	¹⁹⁰ 0.0039	¹⁸⁸ 0.0040	²⁸ 0.0001 N ^{0.158} ¹⁶⁹
103	MICROSOFT-004	³⁵ 0.0012	⁵³ 0.0015	⁶¹ 0.0018	⁷² 0.0021	⁸¹ 0.0028	¹⁵ 0.0000 N ^{0.281} ¹⁹³	¹⁹ 0.0006	¹⁹ 0.0006	¹⁹ 0.0006	¹⁹ 0.0007	¹⁹ 0.0007	³⁸ 0.0001 N ^{0.139} ¹⁶¹
104	MICROSOFT-005	⁶⁶ 0.0015	⁸⁵ 0.0019	¹⁰¹ 0.0023	¹¹³ 0.0030	¹¹³ 0.0037	⁹ 0.0000 N ^{0.320} ²¹⁰	³ 0.0006	³ 0.0006	² 0.0006	² 0.0007	⁸ 0.0009	³⁹ 0.0001 N ^{0.136} ¹⁶⁰
105	MICROSOFT-006	⁷⁰ 0.0016	⁹³ 0.0020	¹¹⁴ 0.0025	¹¹⁸ 0.0030	¹¹⁸ 0.0036	¹²⁰ 0.0003 N ^{0.305} ²⁰⁶	⁴ 0.0006	⁴ 0.0006	³ 0.0007	³ 0.0007	²⁵ 0.0010	²⁴ 0.0000 N ^{0.184} ¹⁷²
106	MUKH-002	²⁶⁰ 0.0204	²¹⁸ 0.0305	²¹¹ 0.0361	²⁰⁹ 0.0430	¹⁸⁰ 0.0507	¹⁸⁰ 0.0007 N ^{0.255} ¹⁷³	²³⁸ 0.0054	²⁴⁰ 0.0070	²¹⁴ 0.0083	²¹⁰ 0.0101	¹⁹⁵ 0.0124	⁴¹ 0.0001 N ^{0.280} ¹⁹⁷
107	NEC-000	²⁴¹ 0.0131	²⁴¹ 0.0170	²⁰⁵ 0.0203	²⁰⁹ 0.0244	¹⁹⁹ 0.0294	¹⁴⁴ 0.0003 N ^{0.276} ¹⁸⁹	²⁰⁹ 0.0029	²¹⁵ 0.0038	¹⁹⁷ 0.0048	¹⁹² 0.0059	¹⁸⁵ 0.0074	¹⁶ 0.0000 N ^{0.319} ²⁰⁷
108	NEC-001	²⁵³ 0.0180	²⁵⁰ 0.0209	²¹³ 0.0233	²⁰⁹ 0.0266	¹⁹⁹ 0.0304	²⁰⁸ 0.0016 N ^{0.179} ¹¹⁹	²⁶⁹ 0.0109	²⁶² 0.0113	²¹⁹ 0.0116	²¹² 0.0121	²⁰⁶ 0.0129	²¹² 0.0051 N ^{0.056} ¹⁰³
109	NEC-002	⁶ 0.0009	¹¹ 0.0010	¹¹ 0.0011	¹¹ 0.0012	⁸ 0.0013	¹⁰¹ 0.0002 N ^{0.113} ⁶²	⁵ 0.0008	⁸⁶ 0.0005 N ^{0.038} ⁷⁹				
110	NEC-003	⁴⁴ 0.0013	³⁹ 0.0014										

MISSES AT GIVEN RANK FNIR(N, T= 0, R)		ENROL MOST RECENT													
#	ALGORITHM	RANK 1					RANK 50								
		N=0.64M	N=1.6M	N=3.0M	N=6.0M	N=12.0M	aN ^b	N=0.64M	N=1.6M	N=3.0M	N=6.0M	N=12.0M	aN ^b		
145	QUANTASOFT-001	²⁹⁹ 0.2177	²⁹⁶ 0.2177	²³² 0.2177	²¹⁵ 0.2177	²²¹ 0.2177 N ^{0.000 1}	³⁰⁵ 0.1116	²⁹⁸ 0.1116	²³¹ 0.1116	²¹⁵ 0.1116	²²¹ 0.1116 N ^{-0.000 1}				
146	RANKONE-002	²⁴⁹ 0.0155	²⁴² 0.0194	²¹¹ 0.0224	²⁰⁶ 0.0262	²⁰⁰ 0.0304	¹⁸⁸ 0.0007 N ^{-0.230 154}	²³³ 0.0048	²³⁶ 0.0060	²⁰⁷ 0.0071	²⁰⁶ 0.0085	¹⁹⁹ 0.0102	⁴⁷ 0.0002 N ^{0.254 190}		
147	RANKONE-003	²⁴⁸ 0.0155	²⁴⁸ 0.0194	²¹² 0.0224	²⁰⁹ 0.0262	²⁰¹ 0.0304	¹⁸⁷ 0.0007 N ^{-0.230 153}	²³³ 0.0048	²³⁵ 0.0060	²⁰⁶ 0.0071	²⁰⁵ 0.0085	²⁰⁰ 0.0102	⁴⁸ 0.0002 N ^{0.254 190}		
148	RANKONE-005	²⁰³ 0.0075	²¹⁰ 0.0094	¹⁹⁴ 0.0110	¹⁹⁰ 0.0132	¹⁸⁴ 0.0156	¹²⁷ 0.0003 N ^{-0.251 171}	²⁰³ 0.0026	²⁰⁴ 0.0032	¹⁸⁹ 0.0036	¹⁸² 0.0043	¹⁷⁴ 0.0050	⁴³ 0.0001 N ^{0.221 181}		
149	RANKONE-007	¹⁴⁴ 0.0028	¹⁴³ 0.0034	¹⁴² 0.0038	¹³⁸ 0.0045	¹³⁶ 0.0053	⁷⁹ 0.0002 N ^{-0.211 141}	¹³⁴ 0.0015	¹³⁷ 0.0017	¹⁴⁰ 0.0018	¹³⁴ 0.0019	¹³² 0.0021	⁶⁸ 0.0003 N ^{0.123 154}		
150	RANKONE-009	¹⁰⁸ 0.0020	¹¹⁶ 0.0024	¹¹⁸ 0.0027	¹²⁰ 0.0032	¹¹⁵ 0.0038	⁴¹ 0.0001 N ^{-0.219 144}	¹¹⁷ 0.0013	¹⁰⁸ 0.0014	¹⁰⁸ 0.0015	¹⁰² 0.0015	⁹³ 0.0016	¹⁰⁵ 0.0006 N ^{0.059 109}		
151	RANKONE-010	¹¹² 0.0020	¹¹⁰ 0.0022	¹⁰⁸ 0.0025	¹⁰⁸ 0.0029	⁹⁹ 0.0032	¹⁰⁸ 0.0002 N ^{-0.164 109}	¹²⁷ 0.0014	¹¹⁹ 0.0015	¹¹⁶ 0.0015	¹⁰⁷ 0.0016	¹⁰⁰ 0.0017	¹¹² 0.0005 N ^{-0.058 107}		
152	RANKONE-011	⁴⁹ 0.0014	⁵⁴ 0.0015	⁵⁴ 0.0017	⁵⁰ 0.0018	⁵⁰ 0.0021	⁸⁷ 0.0002 N ^{0.150 94}	⁶⁰ 0.0011	⁵⁸ 0.0012	⁵⁷ 0.0012	⁵¹ 0.0012	⁴⁵ 0.0012	¹⁵⁸ 0.0008 N ^{0.023 35}		
153	RANKONE-012	³⁹ 0.0013	⁴⁰ 0.0014	⁴⁷ 0.0015	⁴⁵ 0.0017	⁴⁷ 0.0020	⁸⁹ 0.0002 N ^{0.144 90}	⁵¹ 0.0011	⁵³ 0.0011	⁵⁰ 0.0011	⁴³ 0.0011	³⁷ 0.0012	¹⁶² 0.0009 N ^{0.016 34}		
154	RANKONE-013	¹¹ 0.0010	¹² 0.0011	¹³ 0.0012	¹⁷ 0.0013	¹⁹ 0.0015	¹⁸ 0.0009	¹⁵ 0.0009	¹⁴ 0.0009	¹⁵ 0.0009	¹¹ 0.0009	¹²¹ 0.0007 N ^{-0.017 38}			
155	REALNETWORKS-002	²⁶⁹ 0.0299	²⁶⁵ 0.0393	²²⁵ 0.0470	²¹⁹ 0.0562	²¹³ 0.0580	¹⁹⁹ 0.0013 N ^{-0.236 160}	²³⁷ 0.0054	²⁴⁸ 0.0076	²¹⁷ 0.0097	²¹³ 0.0126	²⁰⁷ 0.0132	³³ 0.0001 N ^{0.320 208}		
156	REALNETWORKS-003	²⁵⁴ 0.0183	²⁵⁴ 0.0242	²¹⁷ 0.0291	²¹⁸ 0.0352	²⁰⁸ 0.0423	¹⁵⁷ 0.0004 N ^{-0.287 197}	²²² 0.0041	²²⁸ 0.0054	²⁰³ 0.0064	²⁰³ 0.0080	¹⁹⁸ 0.0101	²⁷ 0.0000 N ^{0.307 204}		
157	REALNETWORKS-004	²⁵¹ 0.0175	²⁵² 0.0236	²¹⁶ 0.0284	²¹¹ 0.0347	²⁰⁵ 0.0416	¹⁴⁸ 0.0003 N ^{-0.295 200}	²²³ 0.0040	²²⁸ 0.0050	²⁰¹ 0.0061	²⁰¹ 0.0078	¹⁹⁷ 0.0099	²⁶ 0.0001 N ^{0.315 205}		
158	REALNETWORKS-005	¹⁰⁹ 0.0020	¹¹² 0.0023	¹¹⁷ 0.0026	¹¹² 0.0030	¹¹¹ 0.0037	⁴⁹ 0.0001 N ^{-0.207 138}	⁶⁹ 0.0012	⁷¹ 0.0012	⁸⁰ 0.0013	⁸⁴ 0.0014	⁷⁶ 0.0015	⁷⁰ 0.0004 N ^{0.081 129}		
159	REALNETWORKS-006	⁴² 0.0013	⁴³ 0.0014	⁵¹ 0.0016	⁵⁰ 0.0018	⁵⁰ 0.0021	⁶⁹ 0.0001 N ^{-0.163 108}	³⁹ 0.0010	³⁵ 0.0010	³⁸ 0.0010	³⁸ 0.0011	³⁸ 0.0012	⁸² 0.0004 N ^{0.060 111}		
160	REALNETWORKS-007	³⁸ 0.0013	³⁹ 0.0013	³⁶ 0.0014	³⁹ 0.0016	⁴⁰ 0.0018	¹¹⁷ 0.0002 N ^{0.124 72}	³³ 0.0010	³⁰ 0.0010	³⁵ 0.0010	³⁴ 0.0011	³⁴ 0.0011	⁸⁴ 0.0004 N ^{0.057 106}		
161	REALNETWORKS-008	¹⁸ 0.0011	²² 0.0011	²⁵ 0.0013	²⁹ 0.0014	²⁶ 0.0016	⁸⁸ 0.0002 N ^{0.131 79}	¹⁷ 0.0009	¹⁴ 0.0009	¹⁹ 0.0009	¹⁹ 0.0009	¹⁸ 0.0009	⁹⁸ 0.0005 N ^{0.037 77}		
162	REMARKAI-000	¹⁴¹ 0.0027	¹⁴⁵ 0.0034	¹⁴⁵ 0.0040	¹⁴³ 0.0048	¹³⁸ 0.0058	³² 0.0001 N ^{-0.260 178}	¹²⁹ 0.0014	¹²⁸ 0.0015	¹²⁵ 0.0016	¹²² 0.0018	¹²³ 0.0020	⁷¹ 0.0003 N ^{0.108 143}		
163	RENDIP-000	⁵⁸ 0.0014	⁵⁸ 0.0015	⁵⁹ 0.0017	⁶¹ 0.0019	⁶⁰ 0.0022	⁷⁹ 0.0002 N ^{0.158 101}	⁶⁷ 0.0012	⁶⁶ 0.0012	⁶² 0.0012	⁵⁵ 0.0012	⁵⁰ 0.0013	¹⁵⁷ 0.0008 N ^{0.025 58}		
164	REVEALMEDIA-000	⁸⁰ 0.0017	⁸³ 0.0019	⁷⁶ 0.0020	⁷⁸ 0.0023	⁷¹ 0.0025	¹³² 0.0003 N ^{0.134 80}	⁷⁶ 0.0012	⁷² 0.0012	⁶⁷ 0.0012	⁶¹ 0.0013	⁵⁶ 0.0013	¹⁴⁴ 0.0007 N ^{0.035 73}		
165	S1-000	¹¹⁴ 0.0021	¹¹⁸ 0.0024	¹²³ 0.0028	¹²¹ 0.0032	¹¹¹ 0.0037	⁵⁶ 0.0001 N ^{-0.203 133}	¹³¹ 0.0014	¹²⁵ 0.0015	¹¹¹ 0.0016	¹⁰² 0.0017	¹²⁰ 0.0007 N ^{0.052 102}			
166	S1-001	¹⁵² 0.0031	¹³⁸ 0.0031	¹³⁶ 0.0034	¹²⁵ 0.0036	¹²⁰ 0.0040	¹⁹¹ 0.0009 N ^{0.092 43}	¹⁸⁸ 0.0023	¹⁷⁸ 0.0023	¹⁶⁵ 0.0024	¹⁵⁷ 0.0024	¹⁴⁴ 0.0025	¹⁹⁶ 0.0017 N ^{0.023 56}		
167	S1-002	⁵² 0.0014	⁴⁶ 0.0014	⁴³ 0.0015	⁴⁵ 0.0016	³⁹ 0.0018	¹⁶² 0.0004 N ^{0.085 34}	¹⁰⁸ 0.0013	⁹⁶ 0.0013	⁸⁵ 0.0013	⁷³ 0.0013	⁶³ 0.0013	¹⁸¹ 0.0011 N ^{0.011 21}		
168	S1-003	⁵¹ 0.0014	⁵⁰ 0.0015	⁴⁹ 0.0015	⁴⁶ 0.0017	⁴⁴ 0.0019	¹⁵¹ 0.0003 N ^{0.101 50}	⁸⁴ 0.0012	⁷⁷ 0.0013	⁷² 0.0013	⁶⁵ 0.0013	⁵⁵ 0.0013	¹⁵⁹ 0.0009 N ^{0.024 57}		
169	SCANOVATE-000	¹⁶⁷ 0.0038	¹⁷⁰ 0.0050	¹⁶⁸ 0.0059	¹⁶⁷ 0.0073	¹⁵⁹ 0.0073	⁸⁸ 0.0002 N ^{-0.235 159}	¹²⁴ 0.0014	¹³¹ 0.0015	¹²⁵ 0.0020	¹²⁵ 0.0020	¹²⁶ 0.0020 N ^{0.142 162}			
170	SCANOVATE-001	¹⁷⁰ 0.0041	¹⁷⁴ 0.0053	¹⁶⁹ 0.0064	¹⁶⁷ 0.0079	¹⁶⁵ 0.0098	²⁷ 0.0001 N ^{-0.299 203}	¹¹⁶ 0.0013	¹²⁸ 0.0015	¹³⁰ 0.0017	¹⁴⁷ 0.0021	¹⁴³ 0.0024	³⁶ 0.0001 N ^{0.207 178}		
171	SENSETIME-0000	¹²² 0.0022	¹¹⁴ 0.0023	¹¹⁷ 0.0026	¹⁰⁸ 0.0028	⁹⁸ 0.0032	¹⁸⁰ 0.0003 N ^{0.135 81}	¹⁴⁷ 0.0016	¹⁴⁶ 0.0017	¹⁴¹ 0.0018	¹²⁸ 0.0018	¹¹⁹ 0.0020	¹⁴⁵ 0.0007 N ^{0.060 110}		
172	SENSETIME-001	¹²⁰ 0.0022	¹¹⁵ 0.0023	¹¹¹ 0.0025	¹¹⁹ 0.0029	¹¹¹ 0.0037	⁹² 0.0002 N ^{-0.177 118}	¹⁴⁴ 0.0016	¹³⁵ 0.0016	¹²⁹ 0.0017	¹²⁵ 0.0018	¹⁴¹ 0.0024	⁶⁷ 0.0003 N ^{0.125 156}		
173	SENSETIME-002	²⁴⁴ 0.0136	²³⁸ 0.0137	²⁰² 0.0137	¹⁹² 0.0138	¹⁸⁰ 0.0139	²¹⁶ 0.0124 N ^{0.007 2}	²⁷⁵ 0.0136	²⁶⁸ 0.0136	²²¹ 0.0136	²¹⁵ 0.0136	²⁰⁸ 0.0136	²¹⁷ 0.0135 N ^{0.001 3}		
174	SENSETIME-003	⁸ 0.0010	⁷ 0.0010	⁷ 0.0010	⁷ 0.0011	⁷ 0.0012	¹³⁸ 0.0003 N ^{0.085 36}	²⁹ 0.0009	²⁶ 0.0009	²⁶ 0.0009	²⁴ 0.0009	²⁰ 0.0010	¹⁹ 0.0010	¹⁴⁸ 0.0008 N ^{0.013 26}	
175	SENSETIME-004	⁷ 0.0010	⁶ 0.0010	⁵ 0.0010	⁶ 0.0011	⁵ 0.0012	¹⁴⁰ 0.0003 N ^{0.081 31}	¹² 0.0008	¹¹ 0.0009	¹¹ 0.0009	⁹ 0.0009	¹¹⁴ 0.0007 N ^{0.018 45}			
176	SENSETIME-005	⁴ 0.0008	⁴ 0.0009	⁴ 0.0009	⁴ 0.0010	⁴ 0.0011	¹²⁸ 0.0003 N ^{0.085 35}	¹⁶ 0.0008	⁷ 0.0008	⁷ 0.0008	⁵ 0.0008	¹⁵ 0.0008	¹⁵ 0.0008 N ^{0.002 6}		
177	SENSETIME-006	³ 0.0008	³ 0.0009	³ 0.0009	³ 0.0010	³ 0.0010	¹⁴² 0.0003 N ^{0.069 20}	⁸ 0.0008	⁸ 0.0008	⁸ 0.0008	⁸ 0.0008	⁸ 0.0008	¹²⁸ 0.0007 N ^{0.011 20}		
178	SENSETIME-007	² 0.0008	² 0.0008	¹ 0.0009	¹ 0.0009	¹ 0.0009	¹⁵² 0.0004 N ^{0.061 17}	⁷ 0.0008	⁹ 0.0008	⁹ 0.0008	⁸ 0.0008	⁸ 0.0008	¹³⁹ 0.0007 N ^{0.008 15}		
179	SENSETIME-008	¹ 0.0008	¹ 0.0008	¹ 0.0009	¹ 0.0009	¹ 0.0010	¹⁴³ 0.0003 N ^{0.067 19}	⁷ 0.0008	⁶ 0.0008	⁶ 0.0008	⁴ 0.0008	² 0.0008	¹¹⁶ 0.0007 N ^{0.013 25}		
180	SHAMAN-007	²⁷³ 0.0371	²⁶⁶ 0.0396	²²⁴ 0.0416	²¹⁸ 0.0443	²¹¹ 0.0473	²¹⁵ 0.0122 N ^{0.153 52}	²⁸⁰ 0.0314	²²⁷ 0.0319	²¹⁹ 0.0326	²¹² 0.0337	²¹⁸ 0.0207 N ^{0.029 69}			
181	SIAT-001	⁷⁸ 0.0017	⁷⁶ 0.0018	⁸⁰ 0.0020	⁸² 0.0023	⁷⁹ 0.0027	⁷¹ 0.0002 N ^{0.173 116}	⁴⁸ 0.0010	⁵² 0.0011	⁵⁵ 0.0012	⁶⁰ 0.0013	⁵⁹ 0.0013	⁷² 0.0003 N ^{0.085 131}		
182	SIAT-002	⁷⁶ 0.0016	⁷⁹ 0.0018	⁸³ 0.0020	⁸¹ 0.0023	⁷⁶ 0.0027	⁷² 0.0002 N ^{0.171 113}	⁶⁴ 0.0011	⁶⁹ 0.0012	⁷⁰ 0.0013	⁶⁹ 0.0013	⁶⁹ 0.0014	⁹³ 0.0005 N<		

#	ALGORITHM	MISSES AT GIVEN RANK FNIR(N, T= 0, R)										ENROL MOST RECENT										
		RANK 1					aN^b					RANK 50					aN^b					
		N=0.64M	N=1.6M	N=3.0M	N=6.0M	N=12.0M	N=0.64M	N=1.6M	N=3.0M	N=6.0M	N=12.0M	N=0.64M	N=1.6M	N=3.0M	N=6.0M	N=12.0M	N=0.64M	N=1.6M	N=3.0M	N=6.0M	N=12.0M	
217	XFORWARDAI-002	¹⁰⁵ 0.0019	⁹² 0.0020	⁸¹ 0.0020	⁶⁹ 0.0021	⁵⁸ 0.0022	¹⁹⁷ 0.0011 N ^{0.038} ⁸	¹⁶³ 0.0019	¹⁵⁷ 0.0019	¹⁴⁹ 0.0019	¹³² 0.0019	¹¹⁵ 0.0019	¹⁹⁹ 0.0018 N ^{0.003} ⁸									
218	YITU-002	⁷⁹ 0.0016	⁸² 0.0018	⁸⁸ 0.0021	⁸⁸ 0.0024	⁸⁹ 0.0029	³⁷ 0.0001 N ^{0.213} ¹⁴²	³⁶ 0.0009	³⁸ 0.0010	³⁶ 0.0010	³⁵ 0.0011	⁴⁰ 0.0012	⁷⁵ 0.0004 N ^{0.073} ¹²⁴									
219	YITU-003	¹³⁸ 0.0026	¹³³ 0.0029	¹³⁰ 0.0031	¹²³ 0.0035	¹¹⁸ 0.0039	¹⁵⁶ 0.0004 N ^{0.141} ⁸⁵	¹⁷⁴ 0.0020	¹⁶⁸ 0.0021	¹⁶¹ 0.0022	¹⁵³ 0.0023	¹⁴² 0.0024	¹⁷² 0.0010 N ^{0.054} ¹⁰¹									
220	YITU-004	²⁹ 0.0011	³⁴ 0.0013	⁴⁴ 0.0015	⁴⁸ 0.0017	¹²⁸ 0.0047	^{0.0000} N ^{0.438} ²¹⁵	¹⁵ 0.0008	¹² 0.0009	¹³ 0.0009	¹² 0.0009	¹⁵⁹ 0.0036	⁷ 0.0000 N ^{0.395} ²¹²									
221	YITU-005	¹²⁴ 0.0022	¹¹⁵ 0.0023	¹⁰⁹ 0.0025	⁹⁹ 0.0027	⁹³ 0.0031	¹⁷¹ 0.0005 N ^{0.113} ⁶¹	¹⁶⁷ 0.0020	¹⁶² 0.0020	¹⁵⁵ 0.0020	¹⁴³ 0.0020	¹²⁶ 0.0020	¹⁹⁵ 0.0017 N ^{0.012} ²⁴									

Table 25: Investigation-mode: Effect of N on FNIR on recent images For five enrollment population sizes, N , with $T = 0$ and $FPIR = 1$. The left five columns are rank 1 miss rates The right five columns are rank 50 miss rates Missing entries usually apply because another algorithm from the same developer was run instead. Some developers are missing because less accurate algorithms were not run on galleries with $N > 1\,600\,000$. Throughout blue superscripts indicate the rank of the algorithm for that column, and yellow highlighting indicates the most accurate value. Caution: The Power-low models are mostly intended to draw attention to the kind of behavior, not as a model to be used for prediction.

MISSES OUTSIDE RANK R		RESOURCE USAGE		ENROL MOST RECENT, N = 1.6M					
#	ALGORITHM	BYTES	MSEC	R=1	R=5	R=10	R=20	R=50	WORK-10
1	20FACE-000	¹⁵⁰ 2048	⁷⁹ 247	²⁷⁵ 0.0552	²⁶⁹ 0.0269	²⁶⁸ 0.0198	²⁶⁵ 0.0146	²⁵⁸ 0.0099	²⁷⁰ 1.275
2	3DIVI-003	⁸³ 512	¹⁸⁰ 625	²⁸⁴ 0.0833	²⁷⁹ 0.0444	²⁷⁹ 0.0349	²⁷⁵ 0.0270	²⁷⁵ 0.0191	²⁸⁰ 1.447
3	3DIVI-004	²⁸⁶ 4096	¹⁸¹ 628	²⁴⁴ 0.0175	²³³ 0.0091	²³¹ 0.0075	²²⁸ 0.0061	²²³ 0.0049	²³⁸ 1.092
4	3DIVI-005	²⁸⁶ 4096	¹⁸⁹ 653	²⁴³ 0.0176	²³⁴ 0.0091	²²⁹ 0.0074	²²⁷ 0.0061	²²⁴ 0.0049	²³⁹ 1.092
5	3DIVI-006	⁹² 528	¹⁸⁸ 653	²³⁹ 0.0240	²⁶⁰ 0.0171	²⁶⁷ 0.0160	²⁶⁵ 0.0154	²⁷¹ 0.0148	²⁹⁷ 1.162
6	ACER-000	⁸² 512	⁶⁹ 201	²¹⁹ 0.0108	²⁰¹ 0.0051	¹⁹⁷ 0.0041	¹⁹⁵ 0.0034	¹⁸⁸ 0.0026	²⁰² 1.053
7	ACER-001	²¹² 2048	⁶⁰ 184	¹⁷² 0.0051	¹⁷⁴ 0.0032	¹⁷³ 0.0028	¹⁷² 0.0025	¹⁷¹ 0.0022	¹⁷³ 1.031
8	AIZE-001	²¹¹ 2048	¹¹⁹ 403	¹⁷⁸ 0.0056	¹⁷⁸ 0.0037	¹⁸⁰ 0.0033	¹⁸⁴ 0.0030	¹⁹¹ 0.0027	¹⁷⁹ 1.035
9	ALCHERA-000	¹⁶⁸ 2048	²⁶³ 263	²³⁸ 0.0161	²⁴⁷ 0.0124	²⁵³ 0.0117	²⁵⁸ 0.0111	²⁶¹ 0.0105	²⁴⁶ 1.116
10	ALCHERA-001	¹⁷⁷ 2048	⁴⁵ 66	³¹¹ 0.9869	³¹³ 0.9782	³¹¹ 0.9735	³¹³ 0.9679	³¹² 0.9590	³¹¹ 9.811
11	ALCHERA-002	¹⁷⁰ 2048	⁵³ 115	²⁸⁶ 0.0949	²⁸⁴ 0.0555	²⁸³ 0.0443	²⁸² 0.0354	²⁷⁷ 0.0254	²⁸⁴ 1.544
12	ALCHERA-003	¹⁸⁷ 2048	¹⁶⁴ 548	²¹⁶ 0.0104	²⁰⁴ 0.0054	²⁰⁹ 0.0045	²⁰⁴ 0.0038	²⁰³ 0.0032	²⁰⁶ 1.055
13	ALCHERA-004	²¹⁶ 2048	²⁷² 854	²²² 0.0110	²⁰⁰ 0.0049	¹⁹³ 0.0038	¹⁸⁷ 0.0032	¹⁸⁴ 0.0025	²⁰⁰ 1.051
14	ALLGOVISION-000	¹⁹ 2048	¹²⁹ 425	²²⁴ 0.0114	²²⁸ 0.0084	²³⁴ 0.0078	²³⁵ 0.0073	²⁴⁰ 0.0067	²²⁸ 1.079
15	ALLGOVISION-001	²²⁶ 2048	²⁵¹ 792	²⁰⁵ 0.0090	¹⁹⁸ 0.0048	¹⁹⁶ 0.0040	¹⁹⁴ 0.0033	¹⁹² 0.0027	¹⁹⁸ 1.048
16	ANKE-000	²⁶ 2072	¹³¹ 431	²³ 0.0132	²¹⁹ 0.0073	²¹⁶ 0.0060	²¹⁷ 0.0050	²¹⁶ 0.0040	²²³ 1.072
17	ANKE-001	²⁶⁵ 2072	¹³³ 433	²³⁴ 0.0132	²²⁰ 0.0073	²²⁰ 0.0061	²¹⁸ 0.0050	²¹⁷ 0.0040	²²³ 1.073
18	ANKE-002	²⁵ 2056	¹⁸⁴ 641	¹³⁰ 0.0028	¹³² 0.0020	¹³¹ 0.0018	¹³⁷ 0.0018	¹³⁹ 0.0017	¹³⁴ 1.019
19	AWARE-003	²⁶ 2076	²²⁵ 716	²⁶¹ 0.0306	²⁵⁸ 0.0162	²⁵⁹ 0.0127	²⁵¹ 0.0100	²⁴⁷ 0.0075	²⁶⁹ 1.163
20	AWARE-004	⁴¹ 92	²²² 712	²³⁹ 0.0679	²⁷⁶ 0.0348	²⁷⁴ 0.0274	²⁷³ 0.0208	²⁷⁰ 0.0145	²⁷⁹ 1.354
21	AWARE-005	²⁷ 3100	²⁵⁹ 827	²⁶² 0.0311	²⁵⁹ 0.0167	²⁵⁴ 0.0134	²⁵³ 0.0107	²⁵³ 0.0082	²⁶¹ 1.167
22	AWARE-006	⁴² 124	²⁵⁵ 818	²⁸¹ 0.0697	²⁷⁸ 0.0369	²⁷⁴ 0.0288	²⁷⁴ 0.0223	²⁷² 0.0158	²⁷⁸ 1.371
23	AYONIX-000	¹²³ 1036	⁴⁰ 10	³⁰⁴ 0.4505	³⁰⁷ 0.3540	³⁰⁷ 0.3176	³⁰⁷ 0.2834	³⁰⁶ 0.2381	³⁰⁷ 4.288
24	AYONIX-001	¹²³ 1036	⁴² 12	³⁰⁰ 0.3414	³⁰⁰ 0.2338	³⁰⁰ 0.1977	³⁰¹ 0.1652	³⁰⁰ 0.1274	³⁰⁰ 3.226
25	AYONIX-002	¹²³ 1036	⁴¹ 11	³⁰¹ 0.3414	³⁰¹ 0.2338	³⁰¹ 0.1977	³⁰¹ 0.1652	³⁰¹ 0.1274	³⁰¹ 3.226
26	CAMVI-003	¹⁰⁹ 1024	²¹⁸ 707	²⁷⁴ 0.0520	²⁸³ 0.0517	²⁸⁴ 0.0517	²⁸⁷ 0.0517	²⁸⁷ 0.0517	²⁸² 1.466
27	CAMVI-004	¹⁰⁷ 1024	²²⁷ 718	²⁷⁴ 0.0468	²⁸¹ 0.0465	²⁸⁴ 0.0465	²⁸⁶ 0.0464	²⁷⁹ 1.419	
28	CAMVI-005	¹¹⁰ 1024	²⁴² 769	²⁷⁸ 0.0652	²⁸⁵ 0.0648	²⁸⁹ 0.0648	²⁹⁰ 0.0648	²⁹² 0.0647	²⁸¹ 1.584
29	CANON-001	²⁸ 4096	²⁸⁸ 893	¹⁵ 0.0011	²⁵ 0.0010	²⁶ 0.0010	²² 0.0009	²² 0.0009	²¹ 1.009
30	CANON-002	¹⁷ 0	³⁹ 6	²⁵ 0.0012	²¹ 0.0010	¹⁹ 0.0009	¹⁸ 0.0009	²¹ 0.0009	¹⁸ 1.009
31	CIB-000	³¹³ 8196	¹⁹⁷ 674	³⁶ 0.0015	⁵⁹ 0.0013	⁵⁷ 0.0012	⁵⁸ 0.0012	⁶⁰ 0.0012	⁶⁰ 1.012
32	CLEARVIEWAI-000	²⁹ 4096	²³⁹ 765	¹⁶ 0.0011	²⁴ 0.0010	²⁵ 0.0010	²⁰ 0.0009	²⁰ 0.0009	¹⁹ 1.009
33	CLOUDWALK-HR-000	¹⁸³ 2048	²⁹⁵ 908	³² 0.0015	⁸⁰ 0.0014	⁸⁷ 0.0014	¹⁰³ 0.0014	¹¹⁰ 0.0014	⁷³ 1.013
34	CLOUDWALK-MT-000	¹⁶⁹ 2048	²⁷⁹ 870	⁷³ 0.0018	¹¹¹ 0.0018	¹²¹ 0.0018	¹³⁴ 0.0018	¹⁴⁹ 0.0018	¹⁰⁷ 1.016
35	CLOUDWALK-MT-001	³² 0	¹⁷ 2	²² 0.0018	¹¹³ 0.0018	¹²⁴ 0.0018	¹³¹ 0.0018	¹⁴⁸ 0.0018	¹⁰⁸ 1.016
36	COGENT-000	⁹⁰ 525	¹⁶⁵ 551	²¹⁸ 0.0105	²⁴⁰ 0.0096	²⁴⁴ 0.0095	¹⁸⁸ 0.0032	¹⁸⁰ 0.0024	²³⁶ 1.088
37	COGENT-001	⁸⁹ 525	¹⁶⁶ 552	²¹⁷ 0.0105	²³⁹ 0.0096	²⁴⁴ 0.0095	¹⁸⁹ 0.0032	¹⁸¹ 0.0024	²³⁵ 1.088
38	COGENT-002	¹²³ 1043	³¹³ 987	¹⁴⁸ 0.0036	¹⁴³ 0.0022	¹⁴⁶ 0.0020	¹³⁵ 0.0018	¹³⁰ 0.0015	¹⁴⁴ 1.021
39	COGENT-003	¹²³ 1043	³¹⁰ 960	¹⁵⁰ 0.0038	¹⁵⁴ 0.0024	¹⁵⁰ 0.0021	¹⁵¹ 0.0019	¹⁴⁰ 0.0017	¹⁵² 1.023
40	COGENT-004	²⁵ 2053	³⁰⁷ 952	⁹⁸ 0.0020	⁹⁵ 0.0016	⁹⁷ 0.0015	¹⁰⁵ 0.0015	¹⁰⁸ 0.0014	⁹⁵ 1.015
41	COGENT-005	¹²⁷ 1062	²⁴⁵ 774	⁶⁶ 0.0017	⁷⁹ 0.0014	⁸¹ 0.0014	⁹¹ 0.0014	⁹⁹ 0.0013	⁷⁸ 1.013
42	COGENT-006	²⁰ 0	⁵ 0	³⁶ 0.0012	³⁸ 0.0011	³⁶ 0.0011	⁴² 0.0011	⁴⁹ 0.0011	³⁷ 1.010
43	COGNITEC-000	²⁵⁰ 2052	⁵⁸ 176	²⁵⁵ 0.0252	²⁵³ 0.0136	²⁵⁷ 0.0107	²⁴⁸ 0.0085	²³⁸ 0.0065	²⁵¹ 1.136
44	COGNITEC-001	²⁴⁸ 2052	²⁰² 202	²²⁶ 0.0117	²¹² 0.0062	²¹¹ 0.0051	²¹² 0.0042	²⁰⁹ 0.0034	²¹² 1.062
45	COGNITEC-002	²⁴¹ 2052	⁷⁵ 227	¹⁷⁰ 0.0057	¹⁷⁷ 0.0037	¹⁷⁸ 0.0032	¹⁷⁹ 0.0029	¹⁸⁹ 0.0026	¹⁷⁸ 1.035
46	COGNITEC-003	²²⁹ 2052	⁹³ 297	¹⁸³ 0.0062	¹⁸⁶ 0.0040	¹⁸⁷ 0.0036	¹⁹³ 0.0033	²⁰¹ 0.0030	¹⁸⁵ 1.039
47	COGNITEC-004	²³¹ 2052	⁶⁶ 192	¹⁴⁴ 0.0032	¹³⁵ 0.0020	¹²² 0.0018	¹¹⁵ 0.0015	¹¹¹ 0.0014	¹³⁸ 1.020
48	COGNITEC-005	²³⁰ 2052	¹⁰⁷ 367	⁶³ 0.0016	⁵⁴ 0.0013	⁵³ 0.0012	⁵³ 0.0012	⁵⁷ 0.0011	⁵⁴ 1.012
49	COGNITEC-006	²⁴¹ 2052	⁴⁶³ 463	⁵⁹ 0.0016	⁴⁹ 0.0013	⁴⁸ 0.0012	⁵¹ 0.0012	⁵¹ 0.0011	⁵¹ 1.012
50	CUBOX-000	¹⁷¹ 2048	²⁹⁹ 918	⁴⁵ 0.0014	⁶⁹ 0.0014	⁸² 0.0014	⁹² 0.0014	¹⁰³ 0.0014	⁶⁹ 1.012
51	CYBERLINK-000	²³⁹ 2052	²¹² 699	¹⁵⁰ 0.0040	¹⁶⁴ 0.0028	¹⁶⁸ 0.0026	¹⁷⁰ 0.0024	¹⁷² 0.0022	¹⁶⁷ 1.027
52	CYBERLINK-001	²⁴¹ 2052	¹³² 433	¹⁴⁶ 0.0035	¹⁴⁹ 0.0023	¹⁴⁸ 0.0021	¹⁴² 0.0018	¹⁴³ 0.0017	¹⁴⁷ 1.022
53	CYBERLINK-002	³⁰⁷ 4140	²³⁴ 738	¹²⁶ 0.0026	¹⁴⁵ 0.0023	¹⁵⁴ 0.0022	¹⁶² 0.0021	¹⁶⁶ 0.0021	¹⁴² 1.021
54	CYBERLINK-003	³¹¹ 6212	²¹¹ 696	⁶⁹ 0.0016	⁸⁸ 0.0013	⁹⁹ 0.0013	¹⁰⁰ 0.0012	⁹⁹ 0.0012	⁶³ 1.012
55	CYBERLINK-004	³⁰⁹ 6212	²³⁵ 738	⁶⁵ 0.0017	⁸⁶ 0.0015	⁹⁵ 0.0015	¹⁰¹ 0.0014	¹¹³ 0.0014	⁸² 1.014
56	CYBERLINK-005	³¹¹ 6212	²³⁶ 739	⁷⁰ 0.0018	⁹⁶ 0.0016	¹⁰⁵ 0.0015	¹⁰⁹ 0.0015	¹¹⁴ 0.0014	⁹⁶ 1.015
57	DAHUA-000	²²⁸ 2048	¹¹³ 378	²⁰⁹ 0.0093	²¹⁵ 0.0066	²¹⁹ 0.0061	²²⁵ 0.0057	²²⁹ 0.0054	²¹³ 1.062
58	DAHUA-001	¹⁹⁷ 2048	¹⁰⁹ 371	¹⁸⁶ 0.0067	¹⁸⁷ 0.0040	¹⁸⁷ 0.0036	¹⁹¹ 0.0033	¹⁹⁵ 0.0029	¹⁸⁷ 1.040
59	DAHUA-002	¹⁷⁸ 2048	²¹³ 699	⁸¹ 0.0018	⁸⁴ 0.0015	⁹² 0.0014	⁹⁶ 0.0014	¹⁰⁰ 0.0013	⁸⁴ 1.014
60	DAHUA-003	¹⁹⁶ 2048	²³⁰ 725	²⁸ 0.0012	¹⁵ 0.0010	¹⁵ 0.0009	¹⁴ 0.0009	¹³ 0.0009	¹⁶ 1.009
61	DAHUA-004	¹⁹² 2048	²³⁸ 759	¹⁴ 0.0011	¹⁴ 0.0010	¹⁶ 0.0009	¹⁷ 0.0009	¹⁸ 0.0009	¹⁴ 1.009
62	DAON-000	²⁶⁶ 2069	¹⁷¹ 584	¹⁵⁰ 0.0041	¹⁷⁹ 0.0038	¹⁹⁶ 0.0037	²⁰³ 0.0037	²¹² 0.0036	¹⁷³ 1.034
63	DECATUR-000	²⁴³ 2052	²⁸² 874	¹⁰¹ 0.0021	⁹⁷ 0.0016	⁹⁹ 0.0015	⁹⁸ 0.0014	⁹² 0.0013	⁹⁷ 1.015
64	DEEPLIGHT-001	²⁹ 4096	²⁰² 687	⁴⁹ 0.0014	⁶⁸ 0.0014	⁷² 0.0013	⁷⁷ 0.0013	⁸⁴ 0.0013	⁶⁵ 1.012
65	DEEPSEA-001	¹⁵⁸ 2048	²⁴⁸ 780	¹⁶⁰ 0.0043	¹⁴⁴ 0.0022	¹²⁸ 0.0018	¹²⁰ 0.0016	¹⁰⁵ 0.0014	

MISSES OUTSIDE RANK R		RESOURCE USAGE		ENROL MOST RECENT, N = 1.6M								
#	FNIR(N, T=0, R)	TEMPLATE		FRVT 2018 MUGSHOTS								
		BYTES	MSEC	R=1	R=5	R=10	R=20	R=50	WORK-10			
73	DERMALOG-010	110	30	105	0.0022	138	0.0021	147	0.0020	163	0.0020	
74	DIGIDATA-000	100	23	307	0.5897	310	0.5892	310	0.5891	310	0.5891	
75	DILUSENSE-000	80	28	107	0.0022	92	0.0015	86	0.0014	87	0.0013	
76	EYEDEA-003	121	1036	115	385	283	0.0800	280	0.0451	280	0.0362	
77	F8-001	215	2048	271	851	230	0.0120	242	0.0105	248	0.0102	
78	FINCORE-000	218	2048	146	477	22	0.0108	203	0.0052	197	0.0042	
79	FUJITSULAB-000	116	1032	306	950	108	0.0022	103	0.0016	103	0.0015	
80	FUJITSULAB-001	380	0	10	84	0.0019	91	0.0015	108	0.0015	106	0.0014
81	GLORY-000	71	418	54	160	294	0.1781	296	0.1391	296	0.1266	
82	GLORY-001	150	1726	122	405	29	0.1268	291	0.0967	292	0.0778	
83	GORILLA-001	270	2156	56	169	226	0.0603	271	0.0304	270	0.0230	
84	GORILLA-002	131	1132	102	341	24	0.0197	235	0.0092	229	0.0070	
85	GORILLA-003	269	2156	169	563	263	0.0361	256	0.0146	242	0.0078	
86	GORILLA-004	271	2192	117	395	184	0.0063	173	0.0032	169	0.0026	
87	GORILLA-005	312	6288	149	483	140	0.0032	120	0.0019	118	0.0017	
88	GORILLA-006	314	8336	241	768	71	0.0017	52	0.0013	51	0.0012	
89	GORILLA-007	250	0	38	6	68	0.0017	48	0.0012	41	0.0011	
90	GRIAULE-000	238	2052	128	419	124	0.0025	128	0.0020	133	0.0019	
91	GRIAULE-001	30	0	25	2	28	0.0012	29	0.0011	34	0.0011	
92	HIK-003	138	1408	182	633	227	0.0117	210	0.0060	209	0.0048	
93	HIK-004	132	1152	154	510	224	0.0113	208	0.0059	206	0.0047	
94	HIK-005	137	1408	179	619	164	0.0046	156	0.0025	142	0.0020	
95	HIK-006	139	1408	175	610	165	0.0046	157	0.0025	143	0.0020	
96	HYPERVERGE-001	106	1024	270	846	41	0.0014	56	0.0013	73	0.0013	
97	HYPERVERGE-002	40	0	11	1	38	0.0014	55	0.0013	64	0.0013	
98	HZAILU-000	310	0	7	106	0.0022	100	0.0016	108	0.0015	106	0.0014
99	HZAILU-001	30	0	32	2	91	0.0020	108	0.0017	113	0.0016	
100	IDEMIA-003	93	528	204	689	190	0.0069	194	0.0045	196	0.0034	
101	IDEMIA-004	91	528	195	669	186	0.0066	183	0.0038	179	0.0032	
102	IDEMIA-005	69	352	111	374	199	0.0081	191	0.0044	188	0.0036	
103	IDEMIA-006	70	352	110	373	213	0.0096	202	0.0052	200	0.0042	
104	IDEMIA-007	108	860	253	807	12	0.0026	98	0.0016	71	0.0013	
105	IDEMIA-008	68	300	136	451	15	0.0011	10	0.0009	19	0.0009	
106	IDEMIA-009	380	0	40	5	5	0.0010	5	0.0009	10	0.0009	
107	IMAGUS-002	81	512	46	76	297	0.2023	295	0.1342	299	0.1090	
108	IMAGUS-003	73	512	44	57	303	0.3559	302	0.2491	302	0.2132	
109	IMAGUS-005	157	2048	250	788	90	0.0019	99	0.0016	96	0.0015	
110	IMAGUS-006	198	2048	293	905	97	0.0020	104	0.0016	107	0.0015	
111	IMAGUS-007	222	2048	172	590	98	0.0020	87	0.0015	84	0.0014	
112	IMAGUS-008	360	0	152	2	285	0.0860	286	0.0701	288	0.0646	
113	IMPERIAL-000	188	2048	191	654	121	0.0024	122	0.0019	126	0.0018	
114	INCODE-000	105	1024	63	190	273	0.0489	268	0.0261	269	0.0160	
115	INCODE-001	177	2048	206	690	24	0.0166	229	0.0084	222	0.0055	
116	INCODE-002	174	2048	90	291	244	0.0178	232	0.0090	229	0.0070	
117	INCODE-003	187	2048	214	704	233	0.0129	214	0.0064	212	0.0051	
118	INCODE-004	227	2048	153	508	147	0.0035	150	0.0024	153	0.0021	
119	INCODE-005	224	2048	152	500	64	0.0017	71	0.0014	79	0.0014	
120	INNOVATRICS-002	95	530	81	255	27	0.0451	273	0.0342	277	0.0322	
121	INNOVATRICS-003	95	530	80	255	257	0.0263	248	0.0126	243	0.0095	
122	INNOVATRICS-004	128	1076	123	406	22	0.0123	213	0.0063	211	0.0050	
123	INNOVATRICS-005	96	538	268	842	122	0.0024	116	0.0018	115	0.0017	
124	INNOVATRICS-007	97	538	249	785	67	0.0017	76	0.0014	71	0.0013	
125	INTELLIGENSA-000	350	0	162	2	96	0.0020	83	0.0015	74	0.0013	
126	INTELLIVISION-001	120	0	24	2	264	0.0365	266	0.0199	261	0.0160	
127	INTELLIVISION-002	290	0	142	2	220	0.0107	206	0.0055	201	0.0044	
128	INTEMA-000	260	0	10	19	30	0.0011	33	0.0011	35	0.0010	
129	INTSYSMSU-000	223	2048	199	675	292	0.1457	294	0.1320	297	0.1272	
130	IREX-000	278	3080	315	2379	161	0.0044	188	0.0043	202	0.0043	
131	ISYSTEMS-002	167	2048	98	316	185	0.0064	189	0.0043	199	0.0039	
132	ISYSTEMS-003	172	2048	273	856	173	0.0052	184	0.0039	198	0.0036	
133	KAKAO-000	236	2052	840	91	31	0.0015	36	0.0011	34	0.0010	
134	KAKAO-001	200	0	122	2	42	0.0014	62	0.0013	81	0.0013	
135	KEDACOM-001	69	292	160	537	195	0.0077	221	0.0074	234	0.0072	
136	KNERON-000	176	2048	157	530	180	0.0059	209	0.0059	226	0.0059	
137	KNERON-001	205	2048	146	468	260	0.0295	270	0.0295	277	0.0295	
138	LINE-000	179	2048	147	482	109	0.0022	93	0.0015	83	0.0014	
139	LINE-001	186	2048	298	910	18	0.0011	23	0.0010	24	0.0009	
140	LINECLOVA-002	150	0	222	2	36	0.0013	46	0.0012	48	0.0012	
141	LOOKMAN-003	69	292	103	342	204	0.0088	225	0.0078	239	0.0075	
142	LOOKMAN-004	99	548	99	325	206	0.0091	226	0.0079	232	0.0075	
143	LOOKMAN-005	104	548	156	514	198	0.0081	223	0.0075	236	0.0074	
144	MANTRA-000	234	2052	125	412	70	0.0017	65	0.0013	63	0.0012	

Table 27: **Rank-based accuracy for the FRVT 2018 mugshot sets.** In columns 3 and 4 are template size and template generation duration. Thereafter values are rank-based FNIR with $T = 0$ and FPIR = 1. This is appropriate to investigational uses but not those with higher volumes where candidates from all searches would need review. The next column is a workload statistic, a small value shows an algorithm front-loads mates into the first 10 candidates. Throughout, blue superscripts indicate the rank of the algorithm for that column, and the best value is highlighted in yellow.

MISSES OUTSIDE RANK R			RESOURCE USAGE		ENROL MOST RECENT, N = 1.6M					
FNIR(N, T=0, R)			TEMPLATE		FRVT 2018 MUGSHOTS					
#	ALGORITHM		BYTES	MSEC	R=1	R=5	R=10	R=20	R=50	WORK-10
145	MAXVISION-000		¹⁸ 0	³⁷ 2	¹¹⁹ 0.0024	¹⁰⁸ 0.0017	¹⁰⁸ 0.0016	¹¹¹ 0.0015	¹⁰⁸ 0.0014	¹¹³ 1.016
146	MAXVISION-001		⁷ 0	²⁶ 2	³⁰ 0.0012	³⁷ 0.0011	⁴¹ 0.0011	⁴⁵ 0.0011	⁴⁸ 0.0011	³⁶ 1.010
147	MEGVII-001		²⁹³ 4096	¹⁸¹ 652	²²⁸ 0.0118	²³⁶ 0.0093	²³⁶ 0.0087	²⁴⁶ 0.0084	²⁵² 0.0080	²³² 1.086
148	MEGVII-002		²⁹⁴ 4096	¹⁹² 656	²²⁹ 0.0118	²³⁷ 0.0093	²³⁸ 0.0088	²⁴⁵ 0.0084	²⁵¹ 0.0080	²³³ 1.087
149	MICROFOCUS-003		⁵⁵ 256	⁸⁶ 269	³¹¹ 0.5942	³⁰⁵ 0.4692	³⁰⁷ 0.4204	³⁰⁹ 0.3724	³⁰⁷ 0.3095	³⁰ 5.361
150	MICROFOCUS-004		⁵³ 256	⁸⁷ 270	³⁰⁸ 0.5763	³⁰⁸ 0.4519	³⁰⁸ 0.4026	³⁰⁸ 0.3560	³⁰⁸ 0.2957	³⁰⁸ 5.199
151	MICROFOCUS-005		⁵⁷ 256	⁸⁵ 266	³⁰⁴ 0.4242	³⁰⁴ 0.3028	³⁰⁷ 0.2606	³⁰³ 0.2209	³⁰⁴ 0.1724	³⁰⁴ 3.861
152	MICROFOCUS-006		⁶¹ 256	⁸⁴ 265	³⁰⁵ 0.4268	³⁰⁵ 0.3049	³⁰⁴ 0.2623	³⁰⁵ 0.2233	³⁰⁵ 0.1746	³⁰⁵ 3.880
153	MICROSOFT-003		¹¹² 1024	¹²⁰ 404	⁶¹ 0.0016	²² 0.0010	⁷ 0.0009	³ 0.0008	⁷ 0.0006	² 1.009
154	MICROSOFT-004		²⁰⁴ 2048	²⁴⁴ 773	⁵³ 0.0015	¹² 0.0009	¹ 0.0008	¹ 0.0007	¹ 0.0006	²³ 1.009
155	MICROSOFT-005		¹⁰⁸ 1024	¹⁹⁶ 673	⁸⁸ 0.0019	¹⁷ 0.0010	⁷ 0.0008	² 0.0008	⁷ 0.0006	³¹ 1.010
156	MICROSOFT-006		¹¹¹ 1024	²⁰⁹ 695	⁹³ 0.0020	³⁹ 0.0011	²⁴ 0.0010	⁴ 0.0008	⁴ 0.0007	⁴⁵ 1.011
157	MUKH-002		¹⁴ 0	²¹ 2	²⁵⁶ 0.0258	²⁵⁴ 0.0139	²⁵² 0.0112	²⁴⁹ 0.0090	²⁴² 0.0070	²⁵⁵ 1.140
158	NEC-000		²⁷⁶ 2592	⁴⁷ 82	²⁴¹ 0.0170	²³¹ 0.0086	²²⁷ 0.0066	²¹⁹ 0.0052	²¹⁷ 0.0038	²³⁴ 1.087
159	NEC-001		²⁷⁷ 2592	⁴⁸ 88	²⁵⁰ 0.0209	²⁵³ 0.0141	²⁵⁶ 0.0128	²⁵⁹ 0.0119	²⁶² 0.0113	²⁵³ 1.135
160	NEC-002		¹⁴⁸ 1616	¹⁹⁶ 653	¹¹ 0.0010	⁷ 0.0009	⁷ 0.0008	⁶ 0.0008	⁷ 0.0008	⁶ 1.008
161	NEC-003		¹⁴⁹ 1712	²⁰⁵ 690	³⁹ 0.0014	⁵¹ 0.0012	⁵⁴ 0.0012	⁶¹ 0.0012	⁶² 0.0012	⁴⁷ 1.011
162	NEC-004		¹² 1104	³¹² 967	⁴⁷ 0.0014	⁶⁶ 0.0013	²⁸ 0.0013	⁷⁸ 0.0013	⁸⁰ 0.0013	⁶¹ 1.012
163	NEC-005		¹³⁰ 1104	³¹¹ 964	²⁵ 0.0012	³⁸ 0.0011	³⁹ 0.0011	⁴³ 0.0011	⁴⁷ 0.0011	³⁵ 1.010
164	NEC-006		²⁷ 0	⁸ 1	³³ 0.0013	⁴⁷ 0.0012	⁵⁰ 0.0012	⁵² 0.0012	⁵⁶ 0.0011	⁴² 1.011
165	NEUROTECHNOLOGY-003		¹⁵⁹ 2048	¹⁶³ 547	²⁵¹ 0.0225	²⁴⁹ 0.0126	²⁴⁶ 0.0100	²⁴³ 0.0078	²³⁸ 0.0057	²⁵⁰ 1.125
166	NEUROTECHNOLOGY-004		²²⁰ 2048	¹⁶² 543	¹⁷⁵ 0.0056	¹⁷⁶ 0.0036	¹⁸² 0.0032	¹⁸³ 0.0029	¹⁸² 0.0025	¹⁷⁷ 1.035
167	NEUROTECHNOLOGY-005		⁵² 256	¹²⁴ 412	¹⁵⁹ 0.0043	¹⁶⁶ 0.0029	¹⁷⁴ 0.0027	¹⁷¹ 0.0024	¹⁷⁶ 0.0023	¹⁶ 1.028
168	NEUROTECHNOLOGY-006		⁵⁶ 256	²³⁷ 746	²⁴⁵ 0.0180	²²⁷ 0.0079	²¹⁵ 0.0059	²¹⁵ 0.0046	²⁰⁷ 0.0033	²²⁹ 1.083
169	NEUROTECHNOLOGY-007		⁵⁸ 256	⁵⁷ 169	¹⁵¹ 0.0039	¹⁶¹ 0.0027	¹⁶⁶ 0.0025	¹⁶⁷ 0.0023	¹⁶⁶ 0.0022	¹⁵⁹ 1.026
170	NEUROTECHNOLOGY-008		⁸⁸ 514	²⁵² 804	¹⁰⁴ 0.0022	⁸⁸ 0.0015	⁹¹ 0.0014	⁹³ 0.0014	⁹³ 0.0013	⁹¹ 1.015
171	NEUROTECHNOLOGY-009		⁸⁷ 513	²⁰¹ 686	⁴⁸ 0.0014	⁴⁵ 0.0012	⁴⁹ 0.0012	⁴⁸ 0.0011	⁵¹ 0.0011	⁴⁶ 1.011
172	NEUROTECHNOLOGY-010		⁵⁴ 256	¹⁹⁴ 663	³¹ 0.0012	²⁷ 0.0011	²⁸ 0.0010	³⁰ 0.0010	³⁰ 0.0010	²⁹ 1.010
173	NEUROTECHNOLOGY-012		²⁵ 0	⁹ 0	⁹ 0.0010	¹⁹ 0.0010	²¹ 0.0010	²⁵ 0.0009	²⁵ 0.0009	¹³ 1.009
174	NEWLAND-002		¹⁹² 2048	²⁷⁸ 868	²⁸² 0.0786	²⁸² 0.0480	²⁸¹ 0.0397	²⁸¹ 0.0332	²⁷⁸ 0.0263	²⁸³ 1.468
175	NOBLIS-001		¹⁶³ 2048	⁷³ 211	²⁹⁹ 0.2492	²⁹⁹ 0.1772	²⁹⁹ 0.1542	²⁹⁹ 0.1339	²⁹⁷ 0.1112	²⁹⁹ 2.679
176	NOBLIS-002		³⁰⁸ 6144	¹⁵⁹ 535	²⁹⁵ 0.1794	²⁹² 0.1108	²⁹² 0.0903	²⁹¹ 0.0722	²⁹⁰ 0.0535	²⁹² 2.077
177	NOTIONTAG-000		²⁶⁸ 2120	¹⁴⁰ 461	¹²³ 0.0024	¹⁴⁰ 0.0021	¹⁴⁶ 0.0021	¹⁵⁷ 0.0020	¹⁶¹ 0.0019	¹³⁶ 1.019
178	NTECHLAB-003		²⁸¹ 3484	²⁶ 831	¹⁸¹ 0.0062	¹⁶⁹ 0.0029	¹⁶² 0.0023	¹⁵² 0.0019	¹³⁸ 0.0016	¹⁷² 1.030
179	NTECHLAB-004		²⁸² 3484	³⁰⁰ 929	¹⁶⁸ 0.0048	¹⁴⁷ 0.0023	¹³⁵ 0.0019	¹²³ 0.0016	⁹⁷ 0.0013	¹⁵⁵ 1.024
180	NTECHLAB-005		¹⁵⁴ 1940	²²⁶ 717	¹⁶⁶ 0.0047	¹⁴² 0.0022	¹²⁴ 0.0017	⁷⁹ 0.0013	⁴⁴ 0.0011	¹⁵⁰ 1.023
181	NTECHLAB-006		¹⁵³ 1940	²⁶⁶ 841	¹⁵⁶ 0.0041	¹²¹ 0.0019	⁹⁸ 0.0015	⁵⁵ 0.0012	²³ 0.0009	¹³⁷ 1.019
182	NTECHLAB-007		²⁸ 3348	²⁶¹ 834	¹²⁷ 0.0027	¹⁰⁵ 0.0017	⁹⁶ 0.0014	⁸⁶ 0.0013	⁶⁶ 0.0012	¹⁰ 1.016
183	NTECHLAB-008		¹³⁶ 1300	¹⁶⁷ 562	⁶⁹ 0.0017	⁴⁴ 0.0012	⁴⁵ 0.0012	⁴⁴ 0.0011	⁴⁰ 0.0010	⁵⁰ 1.012
184	NTECHLAB-009		¹³ 1300	²⁹ 900	³⁵ 0.0013	³¹ 0.0011	³⁰ 0.0010	²⁷ 0.0010	²⁸ 0.0009	³¹ 1.010
185	NTECHLAB-010		¹³⁴ 1280	²⁸ 875	¹⁷ 0.0011	²⁶ 0.0010	²⁷ 0.0010	²⁹ 0.0010	³⁶ 0.0010	²⁴ 1.009
186	NTECHLAB-011		¹³³ 1280	²⁷ 865	¹⁰ 0.0010	⁹ 0.0009	¹³ 0.0009	¹⁶ 0.0009	¹⁷ 0.0009	⁹ 1.008
187	PANGIAM-000		³⁴ 0	¹⁹ 2	²⁷ 0.0012	³³ 0.0011	³⁵ 0.0011	³³ 0.0010	³⁷ 0.0010	³² 1.010
188	PARAVISION-000		²²⁵ 2048	¹³⁵ 438	²⁴⁶ 0.0188	²⁶¹ 0.0171	²⁶⁶ 0.0167	²⁶⁹ 0.0165	²⁷⁴ 0.0164	²⁵⁷ 1.156
189	PARAVISION-001		¹⁸⁴ 2048	¹⁷⁵ 590	¹⁴⁹ 0.0038	¹⁵³ 0.0024	¹⁵⁵ 0.0022	¹⁵⁸ 0.0020	¹⁵⁷ 0.0019	¹⁵³ 1.023
190	PARAVISION-002		¹⁹⁶ 2048	¹¹² 377	¹⁵⁴ 0.0040	¹⁵⁸ 0.0025	¹⁵⁸ 0.0022	¹⁶¹ 0.0021	¹⁵⁶ 0.0019	¹⁵⁶ 1.025
191	PARAVISION-003		²¹³ 2048	²³² 735	¹³⁹ 0.0031	¹⁴¹ 0.0022	¹⁴⁸ 0.0020	¹⁴⁶ 0.0019	¹⁴⁴ 0.0017	¹⁴ 1.021
192	PARAVISION-004		²⁹² 4096	²²⁹ 720	⁶² 0.0016	⁷² 0.0014	⁷⁷ 0.0013	⁸⁴ 0.0013	⁹¹ 0.0013	⁷² 1.013
193	PARAVISION-005		²⁹¹ 4096	²⁷⁴ 858	⁵⁷ 0.0015	⁷⁰ 0.0014	⁷⁶ 0.0013	⁸⁵ 0.0013	⁹⁵ 0.0013	⁶¹ 1.013
194	PARAVISION-007		²⁸⁴ 4096	²¹⁷ 706	²⁴ 0.0012	³² 0.0011	³¹ 0.0010	³² 0.0010	³² 0.0010	²⁸ 1.010
195	PARAVISION-009		²⁹⁹ 4100	¹⁸³ 638	⁸ 0.0010	¹⁶ 0.0010	²² 0.0010	²⁶ 0.0009	²⁵ 0.0009	¹² 1.009
196	PIXELALL-002		²⁷³ 2560	⁶⁷ 198	¹⁶³ 0.0045	¹⁶⁷ 0.0029	¹⁶⁴ 0.0025	¹⁶⁴ 0.0022	¹⁶⁸ 0.0019	¹⁶⁸ 1.028
197	PIXELALL-003		²⁷³ 2560	²²⁸ 719	¹⁰² 0.0021	¹⁰¹ 0.0016	¹⁰⁴ 0.0015	¹⁰² 0.0014	¹¹² 0.0014	¹⁰¹ 1.015
198	PIXELALL-004		²⁷⁴ 2560	¹³⁷ 453	⁹⁹ 0.0020	⁹⁶ 0.0015	⁹⁹ 0.0015	⁹⁹ 0.0014	¹⁰¹ 0.0013	⁸⁹ 1.014
199	PIXELALL-005		²⁷² 2560	⁸⁶ 845	⁸⁶ 0.0019	¹⁰⁶ 0.0017	¹⁰⁹ 0.0016	¹²² 0.0016	¹³³ 0.0016	⁹⁹ 1.015
200	PTAKURATSATU-000		⁹⁸ 538	²⁹⁶ 910	¹³⁷ 0.0030	¹³⁹ 0.0021	¹³⁹ 0.0019	¹³⁰ 0.0018	¹³⁴ 0.0016	¹³⁹ 1.020
201	QNAP-000		²¹⁰ 2048	¹³⁸ 457	¹⁹⁶ 0.0078	¹⁹² 0.0044	¹⁹¹ 0.0037	¹⁹² 0.0033	¹⁹⁴ 0.0028	¹⁹² 1.043
202	QNAP-001		²⁰⁶ 2048	¹⁷⁶ 615	¹⁵⁷ 0.0041	¹⁶⁸ 0.0029	¹⁷⁷ 0.0027	¹⁷³ 0.0025	¹⁷⁴ 0.0023	¹⁶⁵ 1.028
203	QNAP-002		¹ 0	³¹ 2	¹⁶⁹ 0.0049	¹⁹⁶ 0.0044	²⁰⁵ 0.0043	²¹⁴ 0.0043	²¹⁹ 0.0042	¹⁸⁸ 1.040
204	QUANTASOFT-001		²¹⁷ 2048	¹¹⁸ 396	²⁰⁶ 0.2177	²⁰⁶ 0.1643	²⁰⁶ 0.1468	²⁰⁶ 0.1312	²⁰⁶ 0.1116	²⁰⁶ 2.539
205	RANKONE-002		⁴⁷ 133	⁵¹ 113	²⁴⁷ 0.0194	²⁴³ 0.0112	²⁴⁰ 0.0093	²⁴¹ 0.0077	²³⁶ 0.0060	²⁴³ 1.111
206	RANKONE-003		⁴⁸ 133	⁵² 114	²⁴⁸ 0.0194	²⁴⁴ 0.0112	²⁴⁴ 0.0093	²⁴⁰ 0.0077	²³⁶ 0.0060	²⁴ 1.111
207	RANKONE-004									

MISSES OUTSIDE RANK R			RESOURCE USAGE		ENROL MOST RECENT, N = 1.6M					
FNIR(N, T=0, R)			TEMPLATE		R=1	R=5	R=10	R=20	R=50	WORK-10
#	ALGORITHM		BYTES	MSEC						
217	REALNETWORKS-001		³⁰⁴ 4104	⁷⁸ 243	²⁶⁵ 0.0402	²⁶⁴ 0.0195	²⁶¹ 0.0149	²⁵⁹ 0.0111	²⁴⁹ 0.0077	²⁶⁵ 1.201
218	REALNETWORKS-002		³⁰⁴ 4104	⁷⁸ 245	²⁶⁵ 0.0393	²⁶³ 0.0189	²⁵⁹ 0.0142	²⁵⁹ 0.0108	²⁴⁸ 0.0076	²⁶³ 1.195
219	REALNETWORKS-003		¹⁵² 1848	⁵⁹ 178	²⁵⁴ 0.0242	²⁴⁶ 0.0117	²³⁹ 0.0090	²³³ 0.0070	²²⁸ 0.0054	²⁴⁸ 1.120
220	REALNETWORKS-004		¹⁵¹ 1848	⁶¹ 185	²⁵² 0.0236	²⁴⁸ 0.0112	²³⁷ 0.0087	²³¹ 0.0068	²²² 0.0050	²⁴⁵ 1.116
221	REALNETWORKS-005		²⁵⁷ 2056	¹⁰¹ 337	¹¹² 0.0023	⁹⁴ 0.0016	⁸⁵ 0.0014	⁸⁸ 0.0013	⁷¹ 0.0012	⁹⁶ 1.015
222	REALNETWORKS-006		²⁵⁷ 2056	¹⁰⁵ 350	⁴³ 0.0014	⁴² 0.0012	⁴² 0.0011	³⁸ 0.0011	³⁵ 0.0010	⁴¹ 1.011
223	REALNETWORKS-007		⁹ 0	²⁹ 2	³⁷ 0.0013	⁴⁰ 0.0012	³⁷ 0.0011	³⁶ 0.0011	³⁰ 0.0010	³⁹ 1.011
224	REALNETWORKS-008		²⁸ 0	¹⁵ 2	²² 0.0011	¹⁸ 0.0009	²¹ 0.0009	¹⁴ 0.0009	¹⁵ 1.009	
225	REMARKAI-000		¹⁹⁴ 2048	²⁰⁷ 691	¹⁴⁵ 0.0034	¹³⁷ 0.0021	¹³² 0.0019	¹²⁵ 0.0017	¹²⁹ 0.0015	¹⁴⁰ 1.020
226	REMARKAI-000		²⁰⁸ 2048	¹⁷ 615	²⁰³ 0.0086	¹⁹⁷ 0.0044	¹⁸⁶ 0.0036	¹⁸⁰ 0.0031	¹⁸² 0.0025	¹⁹⁵ 1.045
227	REMARKAI-002		¹⁸¹ 2048	¹³⁴ 434	²⁰¹ 0.0081	¹⁸⁸ 0.0040	¹⁷⁶ 0.0031	¹⁷⁴ 0.0026	¹⁶⁵ 0.0021	¹⁸⁹ 1.041
228	RENDIP-000		²⁰⁹ 2048	²⁸⁹ 894	⁵⁸ 0.0015	⁶¹ 0.0013	⁵⁶ 0.0012	⁵⁹ 0.0012	⁶⁶ 0.0012	⁵⁹ 1.012
229	REVEALMEDIA-000		²⁴⁸ 2052	¹¹⁴ 385	⁸³ 0.0019	⁶⁹ 0.0013	⁶⁷ 0.0013	⁶⁷ 0.0013	⁷² 0.0012	⁷¹ 1.013
230	S1-000		²⁹⁰ 4096	²⁷⁶ 865	¹¹⁸ 0.0024	¹¹⁰ 0.0018	¹¹⁴ 0.0017	¹¹⁸ 0.0016	¹²⁵ 0.0015	¹¹⁵ 1.017
231	S1-001		²⁰³ 2048	²⁵ 814	¹³⁸ 0.0031	¹⁵⁹ 0.0025	¹⁶⁵ 0.0024	¹⁶⁸ 0.0024	¹⁷⁸ 0.0023	¹⁵¹ 1.023
232	S1-002		⁶ 0	²⁷ 2	⁴⁶ 0.0014	⁶⁴ 0.0013	⁷⁰ 0.0013	⁸³ 0.0013	⁹⁶ 0.0013	⁶² 1.012
233	S1-003		¹³ 0	² 2	⁵⁰ 0.0015	⁶ 0.0013	⁶² 0.0013	⁷⁰ 0.0013	⁷⁷ 0.0013	⁶¹ 1.012
234	SCANOVATE-000		²²¹ 2048	⁷¹² 712	¹⁷⁰ 0.0050	¹⁶⁰ 0.0026	¹⁵⁶ 0.0022	¹⁴¹ 0.0018	¹³¹ 0.0015	¹⁶² 1.026
235	SCANOVATE-001		²¹⁹ 2048	¹⁹⁸ 675	¹⁷⁴ 0.0053	¹⁶⁷ 0.0027	¹⁵⁹ 0.0022	¹⁴³ 0.0018	¹²⁸ 0.0015	¹⁶⁶ 1.028
236	SENSETIME-000		³⁰¹ 4104	²²⁴ 715	¹¹⁴ 0.0023	¹³³ 0.0020	¹³⁷ 0.0019	¹⁴⁰ 0.0018	¹⁴⁶ 0.0017	¹²⁸ 1.018
237	SENSETIME-001		³⁰⁴ 4104	¹⁹ 656	¹¹⁵ 0.0023	¹³⁰ 0.0020	¹³⁴ 0.0019	¹²⁵ 0.0017	¹²⁵ 0.0016	¹²⁵ 1.018
238	SENSETIME-002		²⁵⁹ 2056	¹⁸⁶ 650	²³⁵ 0.0137	²⁵⁰ 0.0136	²⁵⁸ 0.0136	²⁶² 0.0136	²⁶⁸ 0.0136	²⁴⁹ 1.122
239	SENSETIME-003		²⁵⁷ 2056	³⁰⁴ 940	⁷⁰ 0.0010	¹⁸ 0.0010	²² 0.0010	²³ 0.0009	²⁶ 0.0009	¹¹ 1.009
240	SENSETIME-004		¹¹⁷ 1032	²²⁰ 710	⁶ 0.0010	⁸ 0.0009	¹⁰ 0.0009	¹¹ 0.0009	¹¹ 0.0009	⁷ 1.008
241	SENSETIME-005		¹¹⁴ 1032	³¹⁴ 1007	⁴ 0.0009	³ 0.0008	² 0.0008	⁷ 0.0008	⁷ 0.0008	³ 1.008
242	SENSETIME-006		¹¹⁷ 1032	³⁰ 956	³⁰ 0.0009	³ 0.0008	⁵ 0.0008	⁹ 0.0008	⁸ 0.0008	⁴ 1.008
243	SENSETIME-007		¹²⁰ 1032	³⁰⁹ 958	² 0.0008	² 0.0008	⁴ 0.0008	⁸ 0.0008	⁹ 0.0008	² 1.007
244	SENSETIME-008		³⁷ 0	⁹ 1	¹⁰ 0.0008	¹ 0.0008	³ 0.0008	³ 0.0008	⁹ 0.0008	¹ 1.007
245	SHAMAN-003		¹⁸² 2048	²¹⁵ 704	²⁸⁷ 0.1243	²⁹⁰ 0.0823	²⁸⁰ 0.0708	²⁸⁹ 0.0616	²⁸⁹ 0.0518	²⁹⁰ 1.789
246	SHAMAN-004		¹⁶ 2048	¹⁸ 642	²⁹⁸ 0.2221	²⁹⁷ 0.1473	²⁹⁵ 0.1241	²⁹⁷ 0.1049	²⁹⁴ 0.0825	²⁴¹ 2.411
247	SHAMAN-006		¹⁹⁹ 2048	²¹⁶ 706	²⁶⁷ 0.0398	²⁷⁷ 0.0344	²⁷⁸ 0.0332	²⁸⁰ 0.0323	²⁸³ 0.0315	²⁷⁴ 1.316
248	SHAMAN-007		²¹⁴ 2048	²¹⁹ 709	²⁶⁶ 0.0396	²⁷⁴ 0.0342	²⁷⁷ 0.0331	²⁷⁹ 0.0322	²⁸² 0.0314	²⁷² 1.315
249	SIAT-001		²³ 2052	²⁶ 842	⁷⁶ 0.0018	⁷⁹ 0.0014	⁶⁰ 0.0013	⁵⁷ 0.0012	⁶² 0.0012	⁷⁷ 1.013
250	SIAT-002		²⁴⁶ 2052	²⁹⁴ 906	⁷⁹ 0.0018	⁷³ 0.0014	⁷⁸ 0.0013	⁷⁴ 0.0013	⁶⁹ 0.0012	⁷⁷ 1.013
251	SMILART-004		⁷⁵ 512	⁵⁵ 167	³¹² 0.9648	³¹² 0.9641	³¹² 0.9640	³¹² 0.9639	³¹⁵ 0.9638	³¹⁴ 10.000
252	SMILART-005		¹⁶² 2048	¹⁴³ 464						
253	SQISOFT-001		²⁵ 2056	¹³⁹ 460	¹⁵⁸ 0.0042	⁸¹ 0.0014	⁵⁸ 0.0013	⁴⁹ 0.0012	⁴³ 0.0010	¹¹⁰ 1.016
254	STAQU-000		²⁸⁹ 4096	²⁵⁸ 827	¹⁹² 0.0071	²¹¹ 0.0060	²¹³ 0.0057	²²¹ 0.0055	²²⁶ 0.0053	²⁰⁸ 1.056
255	SYNESIS-003		²⁰ 2048	⁷¹ 215	²³⁹ 0.0162	²⁵ 0.0160	²⁶³ 0.0160	²⁶⁸ 0.0160	²⁷⁵ 0.0160	²⁵⁶ 1.144
256	SYNESIS-003		²⁹⁷ 4096	⁵⁰ 103	²⁹² 0.1700	²⁹³ 0.1172	²⁹³ 0.1047	²⁹⁴ 0.0953	²⁹⁵ 0.0869	²⁹³ 2.120
257	SYNESIS-005		³⁰ 4104	²⁴ 772	²⁰² 0.0085	²³⁸ 0.0085	²³⁵ 0.0085	²⁴⁷ 0.0085	²⁵⁰ 0.0085	²²⁷ 1.076
258	T4ISB-000		²¹ 0	³⁴ 2	²¹⁵ 0.0104	²⁴¹ 0.0103	²⁴⁹ 0.0103	²⁵³ 0.0103	²⁶⁰ 0.0103	²⁴⁰ 1.093
259	TECH5-001		¹⁴⁰ 1536	²⁹⁰ 898	¹⁵³ 0.0040	¹⁵⁷ 0.0024	¹⁵¹ 0.0021	¹⁴⁵ 0.0018	¹⁴¹ 0.0017	¹⁵⁴ 1.024
260	TECH5-002		⁸⁶ 513	³⁰⁵ 941	¹²⁸ 0.0027	⁷⁸ 0.0014	³⁵ 0.0012	⁴⁶ 0.0011	³⁴ 0.0010	⁸⁸ 1.014
261	TEVIAN-003		¹⁶¹ 2048	⁹⁶ 300	²³⁶ 0.0147	²²⁴ 0.0074	²¹⁴ 0.0059	²¹⁶ 0.0047	²¹⁴ 0.0037	²⁴⁶ 1.075
262	TEVIAN-004		¹⁹⁸ 2048	⁹⁴ 299	²²³ 0.0113	²⁰⁹ 0.0057	²⁰⁷ 0.0047	²⁰³ 0.0037	¹⁹⁷ 0.0030	²⁰⁹ 1.058
263	TEVIAN-005		²⁰⁷ 2048	¹²⁷ 416	¹⁹² 0.0073	¹⁸² 0.0038	¹⁷⁷ 0.0031	¹⁷⁷ 0.0027	¹⁷⁵ 0.0023	¹⁸⁴ 1.038
264	TEVIAN-006		¹¹⁷ 1032	¹⁷⁴ 599	¹²⁰ 0.0024	¹¹⁷ 0.0018	¹²³ 0.0018	¹²⁶ 0.0017	¹¹⁷ 0.0017	¹⁰⁷ 1.017
265	TEVIAN-007		¹¹⁸ 1032	²⁴⁷ 779	⁷⁵ 0.0018	⁶⁷ 0.0014	⁷³ 0.0013	⁸⁰ 0.0013	⁷⁹ 0.0013	⁶⁹ 1.013
266	TIGER-000		²³ 2052	¹³⁷ 428	²⁷ 0.0016	²⁷ 0.0010	²⁷ 0.0026	²⁷ 0.0018	²⁶⁵ 0.0120	²⁷³ 1.315
267	TIGER-002		²³⁷ 2052	¹⁴⁴ 464	¹⁷⁶ 0.0056	¹⁷⁰ 0.0029	¹⁶⁴ 0.0024	¹⁴⁸ 0.0019	¹²⁴ 0.0015	¹⁶⁹ 1.030
268	TIGER-003		²⁴ 2052	¹⁴ 464	¹⁷⁷ 0.0056	¹⁷⁷ 0.0029	¹⁶³ 0.0024	¹⁴⁷ 0.0019	¹²⁴ 0.0015	¹⁷⁰ 1.030
269	TONGYITRANS-000		²⁶¹ 2070	⁶⁴ 190	¹⁸⁸ 0.0069	¹⁸⁰ 0.0038	¹⁸¹ 0.0032	¹⁸¹ 0.0029	¹⁸⁶ 0.0026	¹⁸² 1.038
270	TONGYITRANS-001		²⁶ 2070	⁶ 189	¹⁸⁹ 0.0069	¹⁸⁰ 0.0038	¹⁸⁰ 0.0032	¹⁸² 0.0029	¹⁸⁶ 0.0026	¹⁸³ 1.038
271	TOSHIBA-000		¹⁴⁷ 1548	³⁰¹ 930	¹⁶² 0.0045	¹⁵⁹ 0.0026	¹⁵⁷ 0.0022	¹⁵⁸ 0.0020	¹⁵³ 0.0018	¹⁶⁰ 1.026
272	TOSHIBA-001		²⁹³ 2060	³⁰² 931	¹⁶⁷ 0.0048	¹⁶⁰ 0.0027	¹⁶⁰ 0.0023	¹⁵⁹ 0.0020	¹⁵³ 0.0018	¹⁶⁴ 1.027
273	TRUEFACE-000		¹⁵⁵ 2000	¹⁰⁶ 365	¹⁴² 0.0033	¹⁶⁸ 0.0028	¹⁷⁴ 0.0028	¹⁷⁶ 0.0026	¹⁸⁵ 0.0026	¹⁶¹ 1.026
274	TURINGTECHVIP-001		²⁵ 20	³² 2	²¹¹ 0.0095	²³⁸ 0.0093	²⁴² 0.0093	²⁵⁰ 0.0093	²⁵⁵ 0.0093	²³⁰ 1.084
275	VD-000		¹¹³ 1028	¹⁰⁰ 337	³⁰⁷ 0.4737	³⁰⁶ 0.3204	³⁰⁵ 0.2695	³⁰⁴ 0.2215	³⁰³ 0.1678	³⁰⁶ 4.058
276	VD-001		²³⁸ 2052	²¹⁰ 695	²⁵⁹ 0.0276	²⁶² 0.0181	²⁶⁵ 0.0162	²⁶⁴ 0.0146	²⁶⁷ 0.0130	²⁶² 1.174
277	VD-002		²⁴⁷ 2052	²⁰³ 689	²¹² 0.0095	²²⁴ 0.0077	²²⁸ 0.0073	²³⁰ 0.0070	²⁴¹ 0.0068	²²¹ 1.071
278	VD-003		²⁴⁷ 2052	²⁰⁸ 693	¹⁹⁴ 0.0076	²¹⁷ 0.0069	²²⁴ 0.0067	²³⁰ 0.0066	²³⁹ 0.0066	²¹⁵ 1.063
279	VERIDAS-001		¹⁷ 2048	²⁸ 885	¹³¹ 0.0028	¹²⁸ 0.0019	¹¹⁸ 0.0017	¹¹⁷ 0.0015	¹²⁶ 0.0015	

#	ALGORITHM	MISSES OUTSIDE RANK R		RESOURCE USAGE		ENROL MOST RECENT, N = 1.6M					
		FNIR(N, T=0, R)		TEMPLATE		FRVT 2018 MUGSHOTS					
		BYTES	MSEC	R=1	R=5	R=10	R=20	R=50	WORK-10		
289	VISIONBOX-000	²⁵⁸ 2059	¹⁴⁸ 482	⁸⁸ 0.0019	⁸⁹ 0.0015	⁹³ 0.0014	⁹⁰ 0.0013	⁸¹ 0.0013	⁸⁶	1.014	
290	VISIONLABS-004	⁶⁰ 256	⁹⁷ 315	¹²⁹ 0.0027	¹¹⁴ 0.0018	¹¹¹ 0.0016	¹¹² 0.0015	¹⁰⁷ 0.0014	¹¹⁹	1.017	
291	VISIONLABS-005	⁸⁵ 512	⁹⁵ 300	¹¹⁷ 0.0024	¹⁰⁷ 0.0017	¹⁰¹ 0.0015	⁹⁴ 0.0014	⁸⁸ 0.0013	¹⁰⁸	1.016	
292	VISIONLABS-006	⁷⁸ 512	⁹¹ 292	⁸⁰ 0.0018	⁸² 0.0015	⁸⁰ 0.0014	⁸⁷ 0.0013	⁸³ 0.0013	⁸⁰	1.014	
293	VISIONLABS-007	⁸⁴ 512	⁹² 293	⁷⁴ 0.0018	⁷⁷ 0.0014	⁶⁸ 0.0013	⁶⁶ 0.0013	⁷⁰ 0.0012	⁷⁶	1.013	
294	VISIONLABS-008	⁷² 512	⁸⁸ 277	⁹⁵ 0.0020	¹¹⁸ 0.0018	¹²⁶ 0.0018	¹³¹ 0.0018	¹⁴⁵ 0.0017	¹¹⁴	1.017	
295	VISIONLABS-009	⁷⁴ 512	¹⁵¹ 494	²⁰ 0.0011	²⁸ 0.0011	²⁹ 0.0010	³¹ 0.0010	³¹ 0.0010	²⁶	1.010	
296	VISIONLABS-010	⁷⁹ 512	²³¹ 732	⁴⁴ 0.0014	³⁷ 0.0013	⁶⁶ 0.0013	⁶⁷ 0.0013	⁷⁸ 0.0013	⁵⁶	1.012	
297	VISIONLABS-011	⁷⁷ 512	²³³ 736	²⁶ 0.0012	³⁴ 0.0011	⁴⁰ 0.0011	⁴⁰ 0.0011	⁴⁶ 0.0011	³⁴	1.010	
298	VNPIT-001	² 0	³⁰ 2	¹⁰² 0.0022	¹²³ 0.0019	¹³⁰ 0.0018	¹³⁹ 0.0018	¹⁵⁰ 0.0018	¹²⁰	1.017	
299	VNPIT-002	³³ 0	¹⁸ 2	⁸⁷ 0.0019	¹¹⁵ 0.0018	¹²⁵ 0.0018	¹³² 0.0018	¹⁴⁷ 0.0017	¹¹¹	1.016	
300	VOCORD-003	¹⁰⁴ 896	²²³ 714	¹⁸² 0.0062	¹⁷⁵ 0.0035	¹⁷⁵ 0.0030	¹⁷⁷ 0.0026	¹⁷⁷ 0.0023	¹⁷⁶	1.035	
301	VOCORD-004	¹⁰³ 896	¹⁶¹ 538	¹⁹⁷ 0.0079	¹⁹⁹ 0.0049	²⁰¹ 0.0043	²⁰⁹ 0.0038	²⁰⁸ 0.0034	¹⁹⁷	1.048	
302	VOCORD-005	¹⁰¹ 768	²⁵⁶ 822	¹⁹¹ 0.0070	¹⁹⁶ 0.0046	¹⁹⁸ 0.0041	²⁰⁵ 0.0038	²¹¹ 0.0035	¹⁹³	1.044	
303	VOCORD-006	³¹⁵ 10240	²⁵⁷ 825	³¹⁵ 1.0000	³¹⁵ 1.0000	³¹⁵ 1.0000	³¹⁴ 1.0000	³¹⁵ 1.0000	³¹⁵	10.000	
304	VTS-000	¹⁸⁰ 2048	¹⁵⁰ 492	³¹⁰ 0.5937	³¹¹ 0.5936	³¹¹ 0.5936	³¹¹ 0.5936	³¹¹ 0.5936	³¹¹	6.343	
305	VTS-001	¹⁶⁰ 2048	²⁸⁷ 891	⁵⁵ 0.0015	⁴¹ 0.0012	³⁶ 0.0011	³⁷ 0.0011	³³ 0.0010	⁴³	1.011	
306	VTS-002	¹⁶⁴ 2048	²⁹² 903	⁸⁹ 0.0019	⁷⁴ 0.0014	⁶¹ 0.0013	⁶² 0.0012	⁵⁵ 0.0011	⁷⁹	1.013	
307	VTS-003	¹⁶ 0	³⁶ 2	²¹ 0.0011	²⁰ 0.0010	¹⁷ 0.0009	¹⁸ 0.0009	¹⁶ 0.0009	¹⁷	1.009	
308	XFORWARDAI-000	²⁰⁰ 2048	²⁴⁰ 768	¹¹¹ 0.0023	¹³⁴ 0.0020	¹⁴¹ 0.0020	¹⁵³ 0.0019	¹⁵⁹ 0.0019	¹²⁹	1.018	
309	XFORWARDAI-001	¹⁶⁶ 2048	²¹⁰ 681	¹⁰⁶ 0.0020	¹²⁷ 0.0019	¹³⁸ 0.0019	¹⁵⁹ 0.0019	¹⁵⁸ 0.0019	¹²¹	1.018	
310	XFORWARDAI-002	²⁸⁷ 4096	³⁰³ 935	⁹² 0.0020	¹²⁴ 0.0019	¹³⁶ 0.0019	¹⁴⁹ 0.0019	¹⁵⁷ 0.0019	¹¹⁸	1.017	
311	YISHENG-001	²⁸³ 3704	¹¹⁶ 387	²⁵⁹ 0.0265	²⁵¹ 0.0130	²⁴⁷ 0.0102	²⁴⁴ 0.0080	²³⁴ 0.0059	²⁵²	1.134	
312	YITU-002	³⁰⁵ 4138	²⁸⁰ 870	⁸² 0.0018	⁴⁹ 0.0012	⁴³ 0.0011	³⁹ 0.0011	³⁸ 0.0010	⁵⁵	1.012	
313	YITU-003	³⁰⁶ 4138	²⁸¹ 871	¹³³ 0.0029	¹⁴⁶ 0.0023	¹³⁵ 0.0022	¹⁶³ 0.0021	¹⁶⁸ 0.0021	¹⁴³	1.021	
314	YITU-004	²⁶³ 2070	²⁹⁷ 910	³⁴ 0.0013	¹¹ 0.0009	¹¹ 0.0009	¹² 0.0009	²⁰ 0.0009	¹⁰	1.009	
315	YITU-005	²⁶⁴ 2070	²⁷⁵ 861	¹¹³ 0.0023	¹³⁶ 0.0021	¹⁴³ 0.0020	¹⁵⁵ 0.0020	¹⁶² 0.0020	¹³¹	1.019	

Table 30: **Rank-based accuracy for the FRVT 2018 mugshot sets.** In columns 3 and 4 are template size and template generation duration. Thereafter values are rank-based FNIR with $T = 0$ and FPIR = 1. This is appropriate to investigational uses but not those with higher volumes where candidates from all searches would need review. The next column is a workload statistic, a small value shows an algorithm front-loads mates into the first 10 candidates. Throughout, blue superscripts indicate the rank of the algorithm for that column, and the best value is highlighted in yellow.

MISSES BELOW THRESHOLD, T		ENROL RECENT MUGSHOT, N = 1.6M												ENROL APPLICATION PORTRAIT, N = 1.6M																			
#	ALGORITHM	ENROL: MUGSHOT			ENROL: MUGSHOT			ENROL: PROFILE			ENROL: VISA			ENROL: BORDER			PROBE: BORDER			ENROL: VISA			PROBE: KIOSK										
		FPIR=0.0003	FPIR=0.001	FPIR=0.01	FPIR=0.0003	FPIR=0.001	FPIR=0.01	FPIR=0.0003	FPIR=0.001	FPIR=0.01	FPIR=0.001	FPIR=0.003	FPIR=0.001	FPIR=0.01	FPIR=0.001	FPIR=0.003	FPIR=0.001	FPIR=0.01	FPIR=0.001	FPIR=0.003	FPIR=0.001	FPIR=0.01	FPIR=0.001	FPIR=0.003	FPIR=0.001	FPIR=0.01							
1	20FACE-000	260	0.462	270	0.348	278	0.230	273	0.763	266	0.450	267	0.301	235	1.000	230	1.000	248	1.000	203	0.424	203	0.255	114	0.772	121	0.599	196	0.938	211	0.836		
2	3DIVI-003	262	0.482	279	0.400	284	0.282	268	0.685	280	0.626	283	0.497					215	0.605	219	0.445			180	0.821	206	0.717						
3	3DIVI-004	232	0.256	249	0.169	254	0.093	235	0.400	256	0.343	261	0.237					192	0.277	196	0.172			155	0.607	181	0.485						
4	3DIVI-005	231	0.255	246	0.166	252	0.093	237	0.395	257	0.339	260	0.234	155	0.998	163	0.996	180	0.990	221	0.864	224	0.846			154	0.597	180	0.484				
5	3DIVI-006	230	0.253	248	0.168	256	0.096	238	0.403	255	0.342	262	0.238					193	0.283	197	0.174			158	0.615	182	0.490						
6	ACER-000	216	0.208	238	0.146	245	0.074	218	0.300	235	0.246	235	0.157	101	0.987	113	0.981	145	0.955	187	0.201	197	0.114			158	0.490	167	0.363				
7	ACER-001	162	0.109	180	0.056	185	0.026	153	0.136	160	0.109	166	0.069	189	1.000	201	0.999	227	0.998	145	0.068	147	0.036	101	0.406	108	0.250	137	0.479	112	0.206		
8	AIZE-001	173	0.127	200	0.077	199	0.034	183	0.187	188	0.143	189	0.087	128	0.995	141	0.994	163	0.983	159	0.101	161	0.052	94	0.364	105	0.216	117	0.387	147	0.289		
9	ALCHERA-000	223	0.231	235	0.138	237	0.070	207	0.259	217	0.216	228	0.146	168	0.999	179	0.999	209	0.996	181	0.176	190	0.111			176	0.803	178	0.456				
10	ALCHERA-001	310	1.000	310	0.999	311	0.999	310	1.000	308	1.000					309	1.000	289	1.000					307	1.000	267	1.000						
11	ALCHERA-002	288	0.807	286	0.486	287	0.302	267	0.685	277	0.591	278	0.442	209	1.000	206	1.000	232	0.999	220	0.827	221	0.770			177	0.811	197	0.705				
12	ALCHERA-003	256	0.450	240	0.155	238	0.070	219	0.304	229	0.239	233	0.152	202	1.000	192	0.999	214	0.997	180	0.172	188	0.097			133	0.464	164	0.362				
13	ALCHERA-004	267	0.520	278	0.394	27	0.211	264	0.642	272	0.529	272	0.327	129	0.995	134	0.991	105	0.813	204	0.424	209	0.232	108	0.708	116	0.515	149	0.546	173	0.398		
14	ALLGOVISION-000	182	0.138	212	0.088	219	0.045	194	0.202	204	0.166	213	0.106	114	0.993	131	0.990	167	0.982	162	0.117	169	0.066			146	0.526	172	0.396				
15	ALLGOVISION-001	191	0.155	217	0.102	222	0.053	212	0.275	22	0.221	227	0.141	119	0.993	120	0.986	126	0.933	174	0.150	178	0.081			139	0.491	171	0.389				
16	ANKE-000	202	0.184	222	0.117	234	0.063	205	0.256	220	0.220	231	0.151	125	0.995	140	0.994	178	0.990	260	1.000	249	1.000			250	1.000	312	1.000				
17	ANKE-001	200	0.183	226	0.119	235	0.063	206	0.256	219	0.220	232	0.151	131	0.995	147	0.994	189	0.992	290	1.000	279	1.000			285	1.000	259	1.000				
18	ANKE-002	126	0.062	141	0.032	141	0.014	118	0.103	125	0.079	129	0.050	79	0.975	83	0.948	100	0.795	105	0.034	109	0.018			83	0.245	108	0.190				
19	AWARE-003	199	0.174	230	0.128	248	0.082	235	0.351	24	0.298	254	0.204	98	0.987	117	0.984	16	0.977	205	0.428	209	0.378			147	0.530	174	0.443				
20	AWARE-004	248	0.355	262	0.269	273	0.175	260	0.619	271	0.509	276	0.375	206	1.000	209	1.000	236	0.999	200	0.397	205	0.279			178	0.816	192	0.631				
21	AWARE-005	273	0.608	273	0.364	248	0.085	22	0.342	25	0.253	237	0.163	203	1.000	216	1.000	239	0.999	191	0.255	196	0.122			192	0.916	197	0.714				
22	AWARE-006	261	0.475	263	0.276	274	0.175	248	0.466	259	0.398	265	0.283	185	1.000	203	0.999	228	0.999	198	0.368	202	0.254			170	0.749	189	0.623				
23	AYONIX-000	289	0.846	296	0.811	30	0.724	287	0.956	29	0.939	300	0.892	156	0.998	170	0.998	206	0.995	225	0.954	228	0.891			206	0.982	217	0.959				
24	AYONIX-001	291	0.875	300	0.824	302	0.701	282	0.946	293	0.920	296	0.845	198	1.000	198	0.999	211	0.996	230	0.999	230	0.998			203	0.969	219	0.926				
25	AYONIX-002	292	0.876	299	0.824	303	0.702	283	0.946	294	0.920	295	0.845	197	1.000	200	0.999	210	0.996	222	0.915	222	0.821			202	0.969	214	0.926				
26	CAMVI-003	151	0.094	195	0.071	230	0.058	163	0.152	180	0.132	214	0.108	85	0.979	94	0.970	152	0.940	161	0.114	181	0.100			121	0.402	168	0.377				
27	CAMVI-004	160	0.107	196	0.072	228	0.054	202	0.240	182	0.136	203	0.100	187	1.000	195	0.999	218	0.998	158	0.100	177	0.081			174	0.787	183	0.507				
28	CAMVI-005	183	0.139	216	0.099	24	0.076	21	0.451	21	0.179	222	0.132	193	1.000	207	1.000	227	0.998	175	0.156	197	0.112			214	0.999	227	0.983				
29	CANON-001	35	0.012	42	0.005	42	0.02	29	0.031	30	0.015	32	0.033	21	0.363	35	0.217	29	0.008	32	0.004	28	0.068	32	0.034	39	0.139	31	0.092				
30	CANON-002	23	0.010	35	0.005	36	0.002	25	0.027	26	0.020	19	0.013	18	0.487	24	0.407	35	0.253	52	0.013	33	0.075	45	0.046	68	0.188	45	0.106				
31	CIB-000	93	0.044	74	0.012	69	0.005	88	0.077	69	0.045	68	0.025	215	1.000	224	1.000	63	0.017	56	0.008	50	0.141	51	0.068	189	0.894	181	0.521				
32	CLEARVIEWAI-000	39	0.013	44	0.006	40	0.002	38	0.036	31	0.025	35	0.016	170	0.999	99	0.974	20	0.149	30	0.008	25	0.027	95	0.268	18	0.080						
33	CLOUDWALK-HR-000	10	0.004	13	0.002	17	0.002	10	0.015	12	0.013	15	0.012	3	0.188	3	0.133	6	0.095	15	0.005	18	0.003	10	0.033	14	0.018	20	0.099	11	0.075		
34	CLOUDWALK-MT-000	6	0.003	12	0.002	22	0.002	7	0.015	11	0.013	17	0.012	2	0.169	2	0.109	2	0.077	3	0.002	4	0.002	2	0.018	3	0.009	2	0.072	5	0.063		
35	CLOUDWALK-MT-001	3	0.003	10	0.002	20	0.002	4	0.013	14	0.011	10	0.104	1	0.070	1	0.060	1	0.001	1	0.001	1	0.015	1	0.006	1	0.056	1	0.049				
36	COGENT-000	187	0.143	171	0.053	190	0.029	174	0.175	185	0.140	207	0.100	135	0.996	154	0.995	181	0														

MISSES BELOW THRESHOLD, T		ENROL RECENT MUGSHOT, N = 1.6M												ENROL APPLICATION PORTRAIT, N = 1.6M																																																																																																																																																																																																																																																																																																																																																													
		ENROL: MUGSHOT				ENROL: MUGSHOT				ENROL: WEBCAM				ENROL: MUGSHOT				ENROL: PROFILE				ENROL: VISA		ENROL: BORDER		ENROL: BORDER 10+YR		ENROL: KIOSK																																																																																																																																																																																																																																																																																																																																															
#	ALGORITHM	FPIR=0.0003	FPIR=0.001	FPIR=0.01	FPIR=0.0003	FPIR=0.001	FPIR=0.01	FPIR=0.0003	FPIR=0.001	FPIR=0.01	FPIR=0.0003	FPIR=0.001	FPIR=0.01	FPIR=0.0003	FPIR=0.001	FPIR=0.01	FPIR=0.0003	FPIR=0.001	FPIR=0.01	FPIR=0.0003	FPIR=0.001	FPIR=0.01	FPIR=0.0003	FPIR=0.001	FPIR=0.01	FPIR=0.0003	FPIR=0.001																																																																																																																																																																																																																																																																																																																																																
47	COGNITEC-004	¹¹⁹ 0.055	¹⁴⁰ 0.031	¹⁴² 0.014	¹⁴¹ 0.127	¹⁴⁸ 0.097	¹⁴⁶ 0.058	¹²⁷ 0.995	¹²⁸ 0.990	¹²¹ 0.919	¹⁴⁴ 0.068	¹⁴⁸ 0.038	⁹² 0.316	¹⁰⁸ 0.196	⁹⁷ 0.288	¹²² 0.218	¹¹¹ 0.339	¹²⁹ 0.232	¹⁵⁰ 0.055	⁶¹ 0.010	⁵⁷ 0.004	⁶⁵ 0.058	⁵⁸ 0.022	³¹¹ 1.000	²⁶¹ 1.000	¹¹⁵ 0.878	¹¹⁶ 0.041	¹³² 0.028	⁶⁰ 0.157	⁷² 0.092	⁶³ 0.179	⁷⁶ 0.145																																																																																																																																																																																																																																																																																																																																											
49	COGNITEC-006	⁷¹ 0.029	⁵⁴ 0.008	⁵¹ 0.003	⁶⁸ 0.065	⁶¹ 0.040	⁵⁵ 0.022	²⁷⁴ 1.000	²⁹² 1.000	²²⁹ 0.999	⁹³ 0.030	⁸⁹ 0.013	⁶⁶ 0.171	⁶⁹ 0.081	¹⁶⁴ 0.681	¹¹⁹ 0.214	¹³ 0.005	²¹ 0.003	²⁴ 0.002	²⁰ 0.022	²² 0.019	²⁶ 0.014	⁸ 0.276	⁶ 0.168	¹¹ 0.104	¹¹ 0.004	¹² 0.003	⁹ 0.028	⁹ 0.014	³ 0.073	³ 0.062																																																																																																																																																																																																																																																																																																																																												
50	CUBOX-000	¹³ 0.005	²¹ 0.003	²⁴ 0.002	²⁰ 0.022	²² 0.019	²⁶ 0.014	¹⁴ 0.276	⁶ 0.168	¹¹ 0.104	¹¹ 0.004	¹² 0.003	⁹ 0.014	¹¹¹ 0.339	¹²⁹ 0.232	¹⁵² 0.055	⁶¹ 0.010	⁵⁷ 0.004	⁶⁵ 0.058	⁵⁸ 0.022	³¹¹ 1.000	²⁶¹ 1.000	¹¹⁵ 0.878	¹¹⁶ 0.041	¹³² 0.028	⁶⁰ 0.157	⁷² 0.092	⁶³ 0.179	⁷⁶ 0.145																																																																																																																																																																																																																																																																																																																																														
51	CYBERLINK-000	¹⁸¹ 0.137	¹⁸¹ 0.056	¹⁷² 0.023	¹⁶⁹ 0.162	¹⁶⁸ 0.116	¹⁶⁹ 0.070	¹⁴⁸ 0.997	¹⁵⁶ 0.995	¹⁶⁰ 0.981	¹⁴² 0.063	¹⁴⁴ 0.032	¹⁵² 0.339	¹²⁹ 0.232	¹⁵² 0.096	¹⁷⁴ 0.054	¹⁷⁰ 0.022	¹⁵⁶ 0.138	¹⁶¹ 0.109	¹⁶² 0.067	¹⁴⁶ 0.997	¹⁵¹ 0.995	¹⁶⁹ 0.984	¹³⁹ 0.062	¹³⁷ 0.031	¹⁶⁰ 0.652	¹³¹ 0.239	¹⁵³ 0.038	⁸⁴ 0.015	⁸⁰ 0.006	⁷⁸ 0.068	⁸³ 0.053	⁸⁶ 0.032	¹²¹ 0.994	¹²⁶ 0.988	¹⁴⁰ 0.957	⁸¹ 0.024	⁸⁷ 0.013	⁹⁸ 0.288	⁸⁶ 0.157																																																																																																																																																																																																																																																																																																																																			
55	CYBERLINK-004	²¹⁰ 0.188	⁵¹ 0.007	⁵⁶ 0.003	⁶⁶ 0.063	⁵⁸ 0.036	⁵⁷ 0.022	²⁴⁴ 1.000	²³⁹ 1.000	²³⁹ 0.999	⁵¹ 0.013	⁴⁹ 0.007	⁴¹ 0.100	⁴⁶ 0.051	²⁰¹ 0.954	²¹⁷ 0.208	⁶⁵ 0.010	⁶² 0.004	⁷⁰ 0.026	²¹⁰ 1.000	²¹³ 1.000	¹¹⁶ 0.888	⁵⁴ 0.014	³⁵ 0.007	³⁷ 0.089	³⁹ 0.043	¹⁹⁷ 0.926	¹⁴⁰ 0.266	¹⁵⁴ 0.045	⁵⁵ 0.008	⁵⁶ 0.004	⁵⁷ 0.054	⁵⁸ 0.026	³¹ 0.021	¹²² 0.999	¹²⁶ 0.988	¹⁴⁰ 0.957	⁸¹ 0.024	⁸⁷ 0.013	⁹⁸ 0.288	⁸⁶ 0.157																																																																																																																																																																																																																																																																																																																																		
59	DAHUA-000	¹⁷⁵ 0.128	²⁰⁸ 0.086	²¹⁰ 0.045	¹⁷² 0.179	¹⁸¹ 0.135	¹⁸⁷ 0.083	¹⁰⁰ 0.987	¹⁰⁵ 0.980	¹²⁷ 0.933	⁶⁰ 0.017	⁶¹ 0.008	⁵² 0.159	⁵⁰ 0.125	⁶⁰ 0.026	⁶¹ 0.015	¹⁶² 0.151	¹⁷² 0.122	¹⁷⁸ 0.075	⁷¹ 0.046	⁷⁵ 0.029	³⁷ 0.681	⁴⁵ 0.638	⁶⁶ 0.522	⁶⁰ 0.017	⁶¹ 0.008	⁵² 0.159	⁵⁰ 0.125	⁶⁰ 0.026	⁶¹ 0.015	¹⁵⁹ 0.073	¹⁵⁶ 0.073	¹⁴⁹ 0.077	¹⁵³ 0.041	¹⁰⁸ 0.326	¹³⁵ 0.251	¹⁵⁰ 0.073	¹⁵¹ 0.023	¹⁵² 0.073	¹⁵³ 0.041	¹⁵⁴ 0.073	¹⁵⁵ 0.023	¹⁵⁶ 0.073	¹⁵⁷ 0.041	¹⁵⁸ 0.073	¹⁵⁹ 0.023	¹⁶⁰ 0.073	¹⁶¹ 0.041	¹⁶² 0.073	¹⁶³ 0.023	¹⁶⁴ 0.073	¹⁶⁵ 0.041	¹⁶⁶ 0.073	¹⁶⁷ 0.023	¹⁶⁸ 0.073	¹⁶⁹ 0.041	¹⁷⁰ 0.073	¹⁷¹ 0.023	¹⁷² 0.073	¹⁷³ 0.041	¹⁷⁴ 0.073	¹⁷⁵ 0.023	¹⁷⁶ 0.073	¹⁷⁷ 0.041	¹⁷⁸ 0.073	¹⁷⁹ 0.023	¹⁸⁰ 0.073	¹⁸¹ 0.041	¹⁸² 0.073	¹⁸³ 0.023	¹⁸⁴ 0.073	¹⁸⁵ 0.041	¹⁸⁶ 0.073	¹⁸⁷ 0.023	¹⁸⁸ 0.073	¹⁸⁹ 0.041	¹⁹⁰ 0.073	¹⁹¹ 0.023	¹⁹² 0.073	¹⁹³ 0.041	¹⁹⁴ 0.073	¹⁹⁵ 0.023	¹⁹⁶ 0.073	¹⁹⁷ 0.041	¹⁹⁸ 0.073	¹⁹⁹ 0.023	²⁰⁰ 0.073	²⁰¹ 0.041	²⁰² 0.073	²⁰³ 0.023	²⁰⁴ 0.073	²⁰⁵ 0.041	²⁰⁶ 0.073	²⁰⁷ 0.023	²⁰⁸ 0.073	²⁰⁹ 0.041	²¹⁰ 0.073	²¹¹ 0.023	²¹² 0.073	²¹³ 0.041	²¹⁴ 0.073	²¹⁵ 0.023	²¹⁶ 0.073	²¹⁷ 0.041	²¹⁸ 0.073	²¹⁹ 0.023	²²⁰ 0.073	²²¹ 0.041	²²² 0.073	²²³ 0.023	²²⁴ 0.073	²²⁵ 0.041	²²⁶ 0.073	²²⁷ 0.023	²²⁸ 0.073	²²⁹ 0.041	²³⁰ 0.073	²³¹ 0.023	²³² 0.073	²³³ 0.041	²³⁴ 0.073	²³⁵ 0.023	²³⁶ 0.073	²³⁷ 0.041	²³⁸ 0.073	²³⁹ 0.023	²⁴⁰ 0.073	²⁴¹ 0.041	²⁴² 0.073	²⁴³ 0.023	²⁴⁴ 0.073	²⁴⁵ 0.041	²⁴⁶ 0.073	²⁴⁷ 0.023	²⁴⁸ 0.073	²⁴⁹ 0.041	²⁵⁰ 0.073	²⁵¹ 0.023	²⁵² 0.073	²⁵³ 0.041	²⁵⁴ 0.073	²⁵⁵ 0.023	²⁵⁶ 0.073	²⁵⁷ 0.041	²⁵⁸ 0.073	²⁵⁹ 0.023	²⁶⁰ 0.073	²⁶¹ 0.041	²⁶² 0.073	²⁶³ 0.023	²⁶⁴ 0.073	²⁶⁵ 0.041	²⁶⁶ 0.073	²⁶⁷ 0.023	²⁶⁸ 0.073	²⁶⁹ 0.041	²⁷⁰ 0.073	²⁷¹ 0.023	²⁷² 0.073	²⁷³ 0.041	²⁷⁴ 0.073	²⁷⁵ 0.023	²⁷⁶ 0.073	²⁷⁷ 0.041	²⁷⁸ 0.073	²⁷⁹ 0.023	²⁸⁰ 0.073	²⁸¹ 0.041	²⁸² 0.073	²⁸³ 0.023	²⁸⁴ 0.073	²⁸⁵ 0.041	²⁸⁶ 0.073	²⁸⁷ 0.023	²⁸⁸ 0.073	²⁸⁹ 0.041	²⁹⁰ 0.073	²⁹¹ 0.023	²⁹² 0.073	²⁹³ 0.041	²⁹⁴ 0.073	²⁹⁵ 0.023	²⁹⁶ 0.073	²⁹⁷ 0.041	²⁹⁸ 0.073	²⁹⁹ 0.023	³⁰⁰ 0.073	³⁰¹ 0.041	³⁰² 0.073	³⁰³ 0.023	³⁰⁴ 0.073	³⁰⁵ 0.041	³⁰⁶ 0.073	³⁰⁷ 0.023	³⁰⁸ 0.073	³⁰⁹ 0.041	³¹⁰ 0.073	³¹¹ 0.023	³¹² 0.073	³¹³ 0.041	³¹⁴ 0.073	³¹⁵ 0.023	³¹⁶ 0.073	³¹⁷ 0.041	³¹⁸ 0.073	³¹⁹ 0.023	³²⁰ 0.073	³²¹ 0.041	³²² 0.073	³²³ 0.023	³²⁴ 0.073	³²⁵ 0.041	³²⁶ 0.073	³²⁷ 0.023	³²⁸ 0.073	³²⁹ 0.041	³³⁰ 0.073	³³¹ 0.023	³³² 0.073	³³³ 0.041	³³⁴ 0.073	³³⁵ 0.023	³³⁶ 0.073	³³⁷ 0.041	³³⁸ 0.073	³³⁹ 0.023	³⁴⁰ 0.073	³⁴¹ 0.041	³⁴² 0.073	³⁴³ 0.023	³⁴⁴ 0.073	³⁴⁵ 0.041	³⁴⁶ 0.073	³⁴⁷ 0.023	³⁴⁸ 0.073	³⁴⁹ 0.041	³⁵⁰ 0.073	³⁵¹ 0.023	³⁵² 0.073	³⁵³ 0.041	³⁵⁴ 0.073	³⁵⁵ 0.023	³⁵⁶ 0.073	³⁵⁷ 0.041	³⁵⁸ 0.073	³⁵⁹ 0.023	³⁶⁰ 0.073	³⁶¹ 0.041	³⁶² 0.073	³⁶³ 0.023	³⁶⁴ 0.073	³⁶⁵ 0.041	³⁶⁶ 0.073	³⁶⁷ 0.023	³⁶⁸ 0.073	³⁶⁹ 0.041	³⁷⁰ 0.073	³⁷¹ 0.023	³⁷² 0.073	³⁷³ 0.041	³⁷⁴ 0.073	³⁷⁵ 0.023	³⁷⁶ 0.073	³⁷⁷ 0.041	³⁷⁸ 0.073	³⁷⁹ 0.023	³⁸⁰ 0.073	³⁸¹ 0.041	³⁸² 0.073	³⁸³ 0.023	³⁸⁴ 0.073	³⁸⁵ 0.041	³⁸⁶ 0.073	³⁸⁷ 0.023	³⁸⁸ 0.073	³⁸⁹ 0.041	³⁹⁰ 0.073	³⁹¹ 0.023	³⁹² 0.073	³⁹³ 0.041	³⁹⁴ 0.073	³⁹⁵ 0.023	³⁹⁶ 0.073	³⁹⁷ 0.041	³⁹⁸ 0.073	³⁹⁹ 0.023	⁴⁰⁰ 0.073	⁴⁰¹ 0.041	⁴⁰² 0.073	⁴⁰³ 0.023	⁴⁰⁴ 0.073	⁴⁰⁵ 0.041	⁴⁰⁶ 0.073	⁴⁰⁷ 0.023	⁴⁰⁸ 0.073	⁴⁰⁹ 0.041	⁴¹⁰ 0.073	⁴¹¹ 0.023	⁴¹² 0.073	⁴¹³ 0.041	⁴¹⁴ 0.073	⁴¹⁵ 0.023	⁴¹⁶ 0.073	⁴¹⁷ 0.041	⁴¹⁸ 0.073	⁴¹⁹ 0.023	⁴²⁰ 0.073	⁴²¹ 0.041	⁴²² 0.073	⁴²³ 0.023	⁴²⁴ 0.073	⁴²⁵ 0.041	⁴²⁶ 0.073	⁴²⁷ 0.023	⁴²⁸ 0.073	⁴²⁹ 0.041	⁴³⁰ 0.073	⁴³¹ 0.023	⁴³² 0.073	⁴³³ 0.041	⁴³⁴ 0.073	⁴³⁵ 0.023	⁴³⁶ 0.073	⁴³⁷ 0.041	⁴³⁸ 0.073	⁴³⁹ 0.023	⁴⁴⁰ 0.073	⁴⁴¹ 0.041	⁴⁴² 0.073	⁴⁴³ 0.023	⁴⁴⁴ 0.073	⁴⁴⁵ 0.041	⁴⁴⁶ 0.073	⁴⁴⁷ 0.023	⁴⁴⁸ 0.073	⁴⁴⁹ 0.041	⁴⁵⁰ 0.073	⁴⁵¹ 0.023	⁴⁵² 0.073	⁴⁵³ 0.041	⁴⁵⁴ 0.073	⁴⁵⁵ 0.023	⁴⁵⁶ 0.073	⁴⁵⁷ 0.041	⁴⁵⁸ 0.073	⁴⁵⁹ 0.023	⁴⁶⁰ 0.073	⁴⁶¹ 0.041	⁴⁶² 0.073	⁴⁶³ 0.023	⁴⁶⁴ 0.073	⁴⁶⁵ 0.041	⁴⁶⁶ 0.073	⁴⁶⁷ 0.023	⁴⁶⁸ 0.073	⁴⁶⁹ 0.041	⁴⁷⁰ 0.073	⁴⁷¹ 0.023	⁴⁷² 0.073	⁴⁷³ 0.041	⁴⁷⁴ 0.073	⁴⁷⁵ 0.023	

MISSES BELOW THRESHOLD, T		ENROL RECENT MUGSHOT, N = 1.6M												ENROL APPLICATION PORTRAIT, N = 1.6M															
		ENROL: MUGSHOT				ENROL: MUGSHOT				ENROL: WEBCAM				ENROL: MUGSHOT				ENROL: PROFILE				ENROL: VISA		ENROL: BORDER		ENROL: BORDER 10+YR		ENROL: VISA	
#	ALGORITHM	FPIR=0.0003	FPIR=0.001	FPIR=0.01	FPIR=0.0003	FPIR=0.001	FPIR=0.01	FPIR=0.0003	FPIR=0.001	FPIR=0.01	FPIR=0.0003	FPIR=0.001	FPIR=0.01	FPIR=0.0003	FPIR=0.001	FPIR=0.01	FPIR=0.001	FPIR=0.01	FPIR=0.001	FPIR=0.01	FPIR=0.001	FPIR=0.01	FPIR=0.001	FPIR=0.01	FPIR=0.001	FPIR=0.01			
93	HIK-004	¹⁹³ 0.156	²¹⁵ 0.099	²² 0.054	¹⁸¹ 0.182	¹⁹⁴ 0.153	²⁰⁹ 0.101	⁹⁴ 0.983	¹⁰⁰ 0.976	¹²⁶ 0.947	¹⁶⁹ 0.137	¹⁷ 0.077	²¹ 0.053	²⁴ 0.027	²³ 0.101	²¹ 0.083	¹²⁶ 0.434	¹⁶ 0.353											
94	HIK-005	¹⁵⁷ 0.102	¹⁵⁴ 0.044	¹⁵⁶ 0.019	¹¹⁰ 0.098	¹²² 0.077	¹²⁷ 0.048	¹⁹⁴ 1.000	²⁰² 0.999	²²⁰ 0.998	¹⁴³ 0.068	¹⁴⁵ 0.036																	
95	HIK-006	¹⁸⁸ 0.142	¹⁶³ 0.047	¹⁵⁹ 0.020	¹²⁵ 0.111	¹³² 0.086	¹³⁴ 0.052	²¹⁸ 1.000	²⁴⁹ 1.000	²³⁹ 0.999																			
96	HYPERVERGE-001	²² 0.009	³² 0.004	³⁷ 0.002	⁴⁰ 0.039	⁴⁷ 0.031	⁵⁰ 0.020	⁷ 0.275	¹² 0.220	¹⁸ 0.146	²⁶ 0.007	³¹ 0.004	²¹ 0.053	²⁴ 0.027	²³ 0.101	²¹ 0.083													
97	HYPERVERGE-002	²⁰ 0.008	²⁶ 0.004	²⁹ 0.002	³¹ 0.034	³⁹ 0.027	⁴² 0.018	¹⁰ 0.278	¹⁰ 0.210	¹³ 0.131	¹⁸ 0.006	¹⁸ 0.003	¹⁸ 0.048	¹⁸ 0.023	¹³ 0.093	¹⁴ 0.077													
98	HZAILU-000	⁸⁰ 0.035	¹⁰⁴ 0.020	¹⁰⁷ 0.009	⁶⁷ 0.064	⁷⁶ 0.051	⁸⁰ 0.031	⁹² 0.983	⁹⁰ 0.967	¹⁰⁶ 0.813	⁷⁰ 0.020	⁶⁷ 0.010	⁹¹ 0.316	⁶¹ 0.077	⁴⁶ 0.153	⁵⁸ 0.120													
99	HZAILU-001	⁴⁶ 0.016	⁵⁶ 0.009	⁶⁵ 0.004	²³ 0.414	²¹² 0.183	⁶⁷ 0.024	¹⁵⁹ 0.998	¹²³ 0.986	⁴⁰ 0.282	¹⁸⁶ 0.196	¹¹⁷ 0.021	¹⁶⁸ 1.000	¹² 0.997	¹⁶³ 0.679	¹⁶ 0.360													
100	IDEMIA-003	²⁷⁰ 0.552	¹⁶⁴ 0.047	¹⁶³ 0.021	³⁰⁵ 1.000	²⁰³ 0.165	¹⁸² 0.079				²⁶⁴ 1.000	¹⁶³ 0.123	¹⁶⁵ 0.061												¹⁷² 0.766	¹⁹¹ 0.630			
101	IDEMIA-004	¹¹⁸ 0.055	¹⁵⁰ 0.037	¹⁶² 0.021	¹⁵⁸ 0.144	¹⁶⁸ 0.118	¹⁸¹ 0.079	⁸² 0.976	⁹⁸ 0.973	¹⁴⁸ 0.968	¹⁶⁴ 0.123	¹⁶ 0.061													¹⁷³ 0.766	¹⁹⁶ 0.630			
102	IDEMIA-005	¹³³ 0.066	¹⁵⁶ 0.044	¹⁸³ 0.026	¹⁸⁰ 0.181	¹⁹² 0.150	²¹¹ 0.102	⁸⁶ 0.979	¹⁰³ 0.978	¹⁵⁵ 0.973	¹⁶⁵ 0.130	¹⁷¹ 0.070													¹⁸⁸ 0.879	²⁰¹ 0.743			
103	IDEMIA-006	¹³¹ 0.065	¹⁵³ 0.043	¹⁸ 0.025	²¹ 0.266	²² 0.226	²³⁶ 0.161	⁹⁷ 0.984	¹¹⁴ 0.982	¹⁶ 0.980	¹⁷² 0.144	¹⁸ 0.090													¹⁶⁸ 0.733	¹⁸⁷ 0.531			
104	IDEMIA-007	⁸¹ 0.035	⁹⁷ 0.018	⁹⁰ 0.008	⁸⁶ 0.073	⁸⁹ 0.055	⁸⁹ 0.033	³¹² 1.000	²⁶³ 1.000	³⁰⁸ 1.000	¹²⁸ 0.052	¹² 0.022	⁷¹ 0.182	⁸² 0.109	²⁶ 1.000	²² 0.982													
105	IDEMIA-008	⁸ 0.004	⁹ 0.002	¹⁰ 0.001	¹² 0.016	¹⁰ 0.013	⁶ 0.009	⁹ 0.276	⁹ 0.204	¹⁵ 0.136	¹⁴ 0.005	¹⁴ 0.003	¹⁴ 0.036	¹⁶ 0.019	²⁶ 0.106	³⁰ 0.092													
106	IDEMIA-009	⁷ 0.004	³ 0.002	⁴ 0.001	³ 0.012	³ 0.011	³ 0.008	⁴ 0.202	⁴ 0.141	⁷ 0.099	⁵ 0.003	⁵ 0.002	⁸ 0.027	⁸ 0.013	⁶ 0.074	⁶ 0.064													
107	IMAGUS-002	²⁹⁵ 0.908	²⁹⁵ 0.749	²⁹⁷ 0.564	²⁸¹ 0.944	²⁸⁹ 0.816	²⁹¹ 0.645	²³⁰ 1.000	²⁴⁰ 1.000	²⁵⁰ 1.000																			
108	IMAGUS-003	²⁹⁴ 0.898	²⁹⁷ 0.807	³⁰¹ 0.669	²⁹⁸ 0.954	²⁹² 0.909	²⁹⁴ 0.809	²³⁴ 1.000	²²⁵ 1.000	²⁴⁸ 1.000																			
109	IMAGUS-005	⁷⁸ 0.034	¹⁰¹ 0.018	¹⁰⁰ 0.008	¹⁰⁴ 0.088	¹⁰⁷ 0.040	⁶³ 0.066	⁶⁹ 0.838	⁸⁵ 0.647	⁸⁹ 0.029	¹⁰¹ 0.016	⁶³ 0.161	⁷⁷ 0.094	⁷⁸ 0.231	¹⁰⁴ 0.189														
110	IMAGUS-006	⁸⁶ 0.039	¹⁰³ 0.019	¹⁰ 0.008	¹⁰⁴ 0.093	¹¹⁰ 0.069	¹¹⁵ 0.042	⁸⁹ 0.980	⁷⁸ 0.897	⁷⁰ 0.621	⁸⁸ 0.028	⁹⁶ 0.015	⁶² 0.161	⁷⁷ 0.092	⁸⁹ 0.260	¹⁰⁶ 0.181													
111	IMAGUS-007	⁹¹ 0.044	¹¹⁶ 0.023	¹¹⁵ 0.010	¹¹⁵ 0.100	¹¹⁶ 0.073	¹¹⁹ 0.045	⁷⁶ 0.973	⁷⁶ 0.893	⁸⁶ 0.651	⁹⁶ 0.031	⁹⁸ 0.016	⁶⁵ 0.169	⁷⁹ 0.098	⁹⁴ 0.265	⁹⁹ 0.181													
112	IMAGUS-008	³⁰⁴ 0.995	³⁰⁵ 0.974	²⁹⁶ 0.523	²⁸⁸ 0.958	²⁸⁶ 0.774	²⁶⁶ 0.285	¹⁹⁵ 1.000	¹⁵⁹ 0.996	⁹¹ 0.700	²¹⁰ 0.520	¹⁷² 0.071	¹²⁶ 1.000	¹¹⁸ 0.540	¹⁴³ 0.518	¹³³ 0.246													
113	IMPERIAL-000	¹⁹⁰ 0.154	¹²³ 0.026	¹¹² 0.009	¹⁰² 0.089	¹⁰⁸ 0.068	¹¹² 0.041	²²⁶ 1.000	¹⁸³ 0.995	¹⁹⁹ 0.995	¹¹⁷ 0.042	¹¹⁸ 0.020																	
114	INCODE-000	²⁵⁴ 0.423	²⁶⁶ 0.310	²² 0.199	²⁵¹ 0.486	²⁶² 0.420	²⁶⁹ 0.304	¹⁹⁶ 1.000	¹⁷⁴ 0.998	¹⁹⁷ 0.994																			
115	INCODE-001	²⁴³ 0.319	²⁵³ 0.212	²⁶² 0.112	²²⁹ 0.348	²⁴⁵ 0.296	²⁵⁰ 0.198	²²³ 1.000	²³⁸ 1.000	²⁴³ 1.000	¹⁴¹ 0.063	¹³⁸ 0.031	⁵⁴ 0.145	⁵⁸ 0.073	⁴⁹ 0.155	⁴⁸ 0.116													
116	INCODE-002	²⁴⁸ 0.285	²⁵¹ 0.184	²⁵⁹ 0.100	²²³ 0.333	²⁴³ 0.269	²⁴⁶ 0.176	¹⁵¹ 0.998	¹³⁹ 0.993	¹⁶¹ 0.976																			
117	INCODE-003	²⁴¹ 0.286	²⁴⁷ 0.167	²⁴ 0.084	²³⁷ 0.372	²³⁹ 0.264	²³⁹ 0.164	²⁰⁵ 1.000	¹⁹⁹ 0.999	²¹¹ 0.996																			
118	INCODE-004	¹⁵⁶ 0.099	¹⁷² 0.054	¹⁷⁴ 0.023	¹⁷¹ 0.167	¹⁷¹ 0.120	¹⁷⁰ 0.070	¹⁴⁷ 0.997	¹⁴⁹ 0.995	¹²⁵ 0.929	¹⁴¹ 0.063	¹³⁸ 0.031	⁶² 0.017	⁶ 0.009	³⁹ 0.093	⁴⁸ 0.053	⁴⁷ 0.154	⁵⁷ 0.120	¹⁰³ 0.313	¹²⁵ 0.226									
119	INCODE-005	⁵² 0.021	⁶⁹ 0.011	⁶⁷ 0.005	⁵⁹ 0.055	⁶⁷ 0.043	⁷¹ 0.026	³⁰ 0.614	³⁶ 0.528	⁵¹ 0.372	⁶² 0.017	⁶ 0.009	⁵⁴ 0.145	⁵⁸ 0.073															
120	INNOVATRICS-002	²⁵² 0.379	²⁶⁰ 0.234	²⁷⁰ 0.139	²³⁷ 0.403	²⁵⁰ 0.310	²⁶⁰ 0.209	²²⁸ 1.000	²⁴³ 1.000	²⁴¹ 0.999																			
121	INNOVATRICS-003	²⁴² 0.297	²⁵⁶ 0.221	²⁶ 0.132	²⁴⁴ 0.074	²⁶⁸ 0.262	²²² 0.222	²²⁹ 0.149	⁹⁶ 0.984	¹⁰⁸ 0.980	¹⁵³ 0.973	¹²⁴ 0.047	¹²⁴ 0.022												⁸⁶ 0.251	¹⁰¹ 0.182			
122	INNOVATRICS-004	²⁰⁵ 0.184	²³² 0.132	¹⁴⁷ 0.014	¹²⁷ 0.114	¹³⁵ 0.089	¹³⁵ 0.052	⁵⁷ 0.890	⁷⁰ 0.846	⁹² 0.723	¹²⁴ 0.047	¹²⁴ 0.022																	
123	INNOVATRICS-005	¹²² 0.057	¹⁴³ 0.034	¹⁴⁷ 0.014	¹²⁷ 0.114	¹³⁵ 0.089	¹³⁵ 0.052	⁵⁷ 0.890	⁷⁰ 0.846	⁹² 0.723	¹²⁴ 0.047	¹²⁴ 0.022																	
124	INNOVATRICS-007	⁵⁷ 0.024	⁷⁵ 0.013	⁷⁴ 0.005	⁶⁹ 0.065	⁷⁷ 0.051	⁸² 0.032	⁴⁷ 0.806	⁵⁵ 0.																				

MISSES BELOW THRESHOLD, T		ENROL RECENT MUGSHOT, N = 1.6M												ENROL APPLICATION PORTRAIT, N = 1.6M							
#	ALGORITHM	ENROL: MUGSHOT			ENROL: MUGSHOT			ENROL: WEBCAM			PROBE: PROFILE			ENROL: VISA		ENROL: BORDER		PROBE: BORDER		ENROL: KIOSK	
		FPIR=0.0003	FPIR=0.001	FPIR=0.01	FPIR=0.0003	FPIR=0.001	FPIR=0.01	FPIR=0.0003	FPIR=0.001	FPIR=0.01	FPIR=0.0003	FPIR=0.001	FPIR=0.01	FPIR=0.001	FPIR=0.01	FPIR=0.001	FPIR=0.01	FPIR=0.001	FPIR=0.01	FPIR=0.001	FPIR=0.01
139	LINE-001	⁷² 0.030	³⁷ 0.005	³⁰ 0.002	⁷⁰ 0.066	³⁷ 0.027	³⁴ 0.015	²²⁷ 1.000	²⁴⁴ 1.000	²⁵⁷ 1.000	¹¹⁵ 0.992	¹¹¹ 0.981	⁷³ 0.577	¹¹⁵ 0.040	²² 0.004	¹²⁷ 1.000	¹²³ 0.690	¹⁶ 0.700	¹¹² 0.355	¹⁵⁵ 0.304	
140	LINECLOVA-002	²⁶ 0.010	²⁷ 0.004	²⁸ 0.002	²⁵³ 0.508	¹⁷⁷ 0.130	³⁷ 0.014	¹¹³ 0.992	¹¹¹ 0.981	⁷³ 0.577	¹⁵³ 0.084	¹⁶⁷ 0.061									
141	LOOKMAN-003	¹³² 0.066	¹⁵⁵ 0.044	¹⁷⁹ 0.025	¹⁴⁷ 0.131	¹⁶³ 0.112	¹⁸⁵ 0.082	⁸⁴ 0.979	¹⁰¹ 0.977	¹⁵⁹ 0.974											
142	LOOKMAN-004	¹³⁹ 0.074	¹⁵⁸ 0.045	¹⁷³ 0.024	¹³⁵ 0.123	¹⁵⁷ 0.105	¹⁷⁶ 0.075	⁸⁸ 0.980	¹⁰⁴ 0.978	¹⁵⁴ 0.973	¹⁴⁰ 0.062	¹⁵⁸ 0.047									
143	LOOKMAN-005	¹⁰⁸ 0.050	¹³⁷ 0.030	¹⁴⁹ 0.017	¹¹⁶ 0.102	¹³¹ 0.086	¹³⁸ 0.063	²⁸⁴ 1.000	²⁷⁸ 1.000	²³⁸ 0.999	⁹⁰ 0.029	⁹⁰ 0.014	⁵⁸ 0.152	⁶⁶ 0.081	²¹⁸ 1.000	⁸⁰ 0.151					
144	MANTRA-000	¹³⁴ 0.066	⁶⁶ 0.010	⁵⁸ 0.004	⁶⁴ 0.063	⁵⁶ 0.041	⁵⁰ 0.022	¹¹ 0.282	¹¹ 0.219	¹⁴ 0.136	²⁴ 0.007	¹⁶ 0.003	¹¹⁸ 0.951	¹¹⁵ 0.485	²² 0.100	¹⁵ 0.078					
145	MAXVISION-000	¹⁰⁴ 0.048	¹³⁵ 0.028	¹³⁸ 0.013	²⁴⁹ 0.468	²²⁹ 0.237	¹⁴² 0.054	⁵⁰ 0.827	⁵⁸ 0.767	⁸¹ 0.631	¹⁷³ 0.149	¹²¹ 0.022	¹²³ 0.997	¹²⁶ 0.872	¹⁵ 0.557	¹³² 0.245					
146	MAXVISION-001	²⁴ 0.010	³⁰ 0.004	²⁹ 0.002	⁴⁵ 0.044	³³ 0.025	³³ 0.015	¹¹ 0.282	¹¹ 0.219	¹⁴ 0.136	²⁴ 0.007	¹⁶ 0.003	¹¹⁸ 0.951	¹¹⁵ 0.485	²² 0.100	¹⁵ 0.078					
147	MEGVII-001	²¹⁹ 0.210	¹⁹⁷ 0.072	²⁰² 0.037	¹³³ 0.119	¹⁴⁷ 0.097	¹³¹ 0.061														
148	MEGVII-002	²³³ 0.258	²⁰¹ 0.077	²⁰⁴ 0.037	¹³⁴ 0.120	¹⁴⁷ 0.096	¹⁸⁴ 0.059	¹⁶⁷ 0.999	¹⁷⁷ 0.998	¹¹⁴ 0.872											
149	MICROFOCUS-003	²⁹⁸ 0.958	³⁰³ 0.931	³⁰⁷ 0.866	²⁹⁹ 0.988	³⁰⁵ 0.979	³⁰² 0.948				²²⁸ 0.982	²²⁸ 0.945								²¹⁰ 0.991	²²⁰ 0.977
150	MICROFOCUS-004	³⁰⁷ 0.999	³⁰⁹ 0.999	³¹³ 0.999	²⁹⁴ 0.984	³⁰⁰ 0.975	³⁰¹ 0.940				²²⁶ 0.974	²²⁷ 0.935								²⁰⁸ 0.989	²¹⁹ 0.976
151	MICROFOCUS-005	²⁹³ 0.883	³⁰¹ 0.835	³⁰⁵ 0.736	²⁸⁹ 0.951	²⁹⁶ 0.928	²⁹⁸ 0.865				²²⁴ 0.935	²²⁵ 0.848								²⁰ 0.985	²¹⁸ 0.965
152	MICROFOCUS-006	³⁰² 0.983	³⁰⁶ 0.978	³⁰⁸ 0.963	²⁸⁴ 0.950	²⁹⁹ 0.923	²⁹⁷ 0.858				²²³ 0.923	²²³ 0.843								²⁰⁴ 0.971	²¹⁵ 0.939
153	MICROSOFT-003	¹⁰⁶ 0.049	¹³² 0.028	¹³¹ 0.012	¹²⁸ 0.117	¹³⁹ 0.091	¹⁴⁵ 0.056				¹⁰⁸ 0.036	¹¹⁵ 0.019								⁸ 0.233	⁹⁶ 0.176
154	MICROSOFT-004	¹⁰⁰ 0.046	¹²⁴ 0.026	¹²² 0.011	¹²⁴ 0.111	¹³³ 0.087	¹³⁸ 0.053				¹⁰³ 0.033	¹¹⁶ 0.018								⁷⁶ 0.222	⁹³ 0.170
155	MICROSOFT-005	¹⁰² 0.047	¹²¹ 0.026	¹¹⁹ 0.010	¹⁰³ 0.090	¹¹² 0.070	¹¹³ 0.041	¹⁸⁰ 0.999	⁴¹ 0.587	⁴⁸ 0.354	⁸⁴ 0.027	⁸⁷ 0.013								⁶⁴ 0.180	⁶⁸ 0.134
156	MICROSOFT-006	⁶¹ 0.025	⁷⁰ 0.012	⁸¹ 0.006	⁵⁰ 0.048	⁵⁶ 0.037	⁶⁶ 0.024	¹⁷ 0.452	²² 0.386	³⁹ 0.281	⁹⁹ 0.032	⁹⁶ 0.015								⁶⁰ 0.178	⁷⁰ 0.138
157	MUKH-002	³⁰⁸ 0.999	²⁸⁹ 0.594	²⁶ 0.110	²²¹ 0.326	²³² 0.242	²³⁴ 0.153	²³⁷ 1.000	²²² 1.000	¹⁷² 0.987	¹⁷⁸ 0.170	¹⁸⁰ 0.089	¹¹⁰ 0.741	¹¹³ 0.382	¹¹⁸ 0.389	¹⁴⁵ 0.286					
158	NEC-000	¹⁶⁵ 0.113	²⁰⁴ 0.079	²²⁹ 0.047	¹⁷⁷ 0.171	¹⁸⁶ 0.140	¹⁹⁵ 0.093	⁹³ 0.983	¹⁰⁶ 0.979	¹⁵⁹ 0.969									¹³ 0.474	¹⁶⁹ 0.377	
159	NEC-001	¹⁸⁹ 0.148	²²¹ 0.106	²³³ 0.060	²⁰¹ 0.238	²¹⁵ 0.197	²²³ 0.133	¹⁰⁸ 0.991	¹²¹ 0.986	¹⁵² 0.972	¹⁶⁶ 0.133	¹⁷⁹ 0.082								¹³⁵ 0.468	¹⁷⁰ 0.378
160	NEC-002	⁴⁷ 0.018	¹⁸ 0.003	¹⁵ 0.002	²⁸ 0.029	²⁵ 0.020	²³ 0.013	¹⁹⁰ 1.000	¹⁹⁶ 0.999	²⁰² 0.995	³² 0.008	⁴⁷ 0.005							¹⁶ 0.676	¹⁵¹ 0.292	
161	NEC-003	¹² 0.005	¹⁵ 0.002	²¹ 0.002	¹⁸ 0.021	¹⁹ 0.017	²² 0.013	³⁹ 0.902	⁶⁶ 0.824	⁸⁰ 0.628	³⁵ 0.008	⁴⁸ 0.006	¹⁵ 0.036	¹⁷ 0.023	¹⁶¹ 0.668	¹³⁸ 0.261					
162	NEC-004	² 0.003	⁶ 0.002	¹⁴ 0.002	⁷ 0.015	⁷ 0.013	¹¹ 0.010	³⁴ 0.654	⁴⁴ 0.622	⁷² 0.575	¹² 0.004	²³ 0.004	⁷ 0.019	⁶ 0.012	² 0.100	²⁴ 0.088					
163	NEC-005	¹⁸ 0.007	⁴ 0.002	⁹ 0.001	⁵ 0.014	⁶ 0.012	⁷ 0.009	³⁸ 0.901	⁴⁹ 0.673	²⁸ 0.177	⁷ 0.003	¹⁰ 0.002	³ 0.019	⁴ 0.011	¹⁷ 0.099	²³ 0.087					
164	NEC-006	²⁵ 0.010	¹¹ 0.002	¹³ 0.002	²³ 0.024	²¹ 0.018	²⁰ 0.013	³³ 0.857	²⁹ 0.463	¹² 0.122	⁸ 0.004	¹³ 0.003	⁷ 0.026	⁷ 0.013	¹⁰ 0.094	²⁰ 0.081					
165	NEUROTECHNOLOGY-003	³⁰⁶ 0.999	²⁹³ 0.636	²⁵⁹ 0.099	²⁷⁴ 0.773	²⁴¹ 0.266	²³⁸ 0.164	³⁰¹ 1.000	²⁵⁴ 1.000	³⁰⁸ 1.000											
166	NEUROTECHNOLOGY-004	¹⁶² 0.120	¹⁹¹ 0.063	¹⁸³ 0.028	¹⁵⁹ 0.146	¹⁶³ 0.117	¹⁷² 0.073	¹³⁹ 0.996	¹⁴⁴ 0.994	¹⁷³ 0.990											
167	NEUROTECHNOLOGY-005	¹⁶⁶ 0.117	¹⁷⁸ 0.054	¹⁶⁹ 0.022	²⁰⁴ 0.252	¹⁷⁸ 0.130	¹⁷⁵ 0.074	¹⁶⁶ 0.999	¹⁶⁹ 0.998	¹⁷⁵ 0.989											
168	NEUROTECHNOLOGY-006	³⁰³ 0.987	²⁶¹ 0.249	²⁶¹ 0.121	³⁰⁹ 1.000	²⁶¹ 0.418	²⁵⁵ 0.206														
169	NEUROTECHNOLOGY-007	²²⁹ 0.252	¹⁹⁰ 0.062	¹⁶⁶ 0.021	²⁹⁶ 0.996	²⁰⁷ 0.173	¹⁶³ 0.068	²²⁹ 1.000	²²¹ 1.000	²¹⁵ 0.997	¹⁶⁷ 0.339	¹⁴⁶ 0.036							²⁷⁰ 1.000	²²⁷ 0.989	
170	NEUROTECHNOLOGY-008	²⁸⁴ 0.797	¹⁷² 0.053	¹³⁸ 0.012	¹²² 0.110	¹²⁴ 0.047	²³⁹ 1.000	²³³ 1.000	²⁵⁹ 1.000	¹⁰⁷ 0.035	¹⁰⁶ 0.017	⁸⁹ 0.293	⁹⁴ 0.149	⁷¹ 0.203	⁸¹ 0.152						
171	NEUROTECHNOLOGY-009	⁶⁵ 0.027	⁸⁸ 0.015	⁸⁰ 0.006	⁷² 0.066	⁸¹ 0.052	⁸³ 0.032	³⁵ 0.661	⁴² 0.588	⁵⁴ 0.436	⁶⁹ 0.020	⁶⁹ 0.010	⁹⁵ 0.153	⁶⁸ 0.082	⁵⁸ 0.165	⁶⁴ 0.129					
172	NEUROTECHNOLOGY-010	²⁴⁵ 0.346	⁶⁴ 0.010	⁵³ 0.003	⁴⁹ 0.047	⁵⁹ 0.037	⁶³ 0.023	¹⁵ 0.377	¹⁷ 0.277	²⁶ 0.170	⁴⁵ 0.010	⁴¹ 0.005	³⁴ 0.075	³⁷ 0.039	³³ 0.126	³⁶ 0.097					
173	NEUROTECHNOLOGY-012	¹⁵⁰ 0.092	⁴⁸ 0.007	³⁹ 0.002	⁴⁷ 0.045	⁵¹ 0.032	⁴⁶ 0.019	²⁰⁸ 1.000	⁸⁶ 0.959	¹⁷³ 0.149	³⁹ 0.008	²⁷ 0.004	²⁵ 0.061	²⁶ 0.028	¹⁹³ 0.916	²⁵ 0.088					
174	NEWLAND-002	²⁶⁸ 0.523	²⁸² 0.438	²⁸⁹ 0.294	²⁵³ 0.535	²⁶⁹ 0.466	²⁷³ 0.335	¹⁷⁶ 0.999	¹⁸⁹ 0.999	²²² 0.998											
175	NOBLIS-001	³¹¹ 1.000	³¹¹ 1.000	³¹¹ 0.991	³¹³ 1.000	³⁰⁵ 1.000	³⁰⁵														

MISSES BELOW THRESHOLD, T		ENROL RECENT MUGSHOT, N = 1.6M												ENROL APPLICATION PORTRAIT, N = 1.6M															
		ENROL: MUGSHOT				ENROL: MUGSHOT				ENROL: MUGSHOT				ENROL: VISA				ENROL: BORDER				ENROL: BORDER 10+YR				ENROL: KIOSK			
#	ALGORITHM	FPIR=0.0003	FPIR=0.001	FPIR=0.01	FPIR=0.0003	FPIR=0.001	FPIR=0.01	FPIR=0.0003	FPIR=0.001	FPIR=0.01	FPIR=0.0003	FPIR=0.001	FPIR=0.01	FPIR=0.0003	FPIR=0.001	FPIR=0.01	FPIR=0.0003	FPIR=0.001	FPIR=0.01	FPIR=0.0003	FPIR=0.001	FPIR=0.01	FPIR=0.0003	FPIR=0.001	FPIR=0.01				
185	NTECHLAB-010	¹⁴ 0.005	¹⁷ 0.003	¹² 0.002	¹⁵ 0.018	¹⁶ 0.015	¹³ 0.011	¹⁴ 0.334	¹⁶ 0.252	²⁰ 0.169	²² 0.007	³⁰ 0.004	²⁴ 0.059	²⁶ 0.031	¹⁶ 0.098	¹³ 0.077	¹¹ 0.091	¹⁰ 0.075	¹¹ 0.091	¹⁰ 0.075	²⁵ 0.105	²² 0.083	¹⁹ 0.926	²⁰ 0.779	¹⁶ 0.739	¹⁸ 0.573			
186	NTECHLAB-011	¹⁵ 0.006	²² 0.003	¹⁶ 0.002	¹⁴ 0.018	¹⁵ 0.015	¹² 0.010	¹² 0.291	¹³ 0.228	²² 0.150	⁴¹ 0.009	³⁸ 0.004	³² 0.074	³⁶ 0.038	¹¹ 0.091	¹⁰ 0.075	¹⁰ 0.296	¹² 0.232	¹⁰ 0.296	¹² 0.232	¹⁹ 0.908	¹⁷ 0.211	¹⁶ 0.132	¹⁴ 0.120					
187	PANGIAM-000	⁴¹ 0.014	⁴⁵ 0.006	⁴³ 0.003	⁴² 0.039	⁴⁵ 0.030	⁴⁴ 0.018	⁷⁸ 0.974	²⁰ 0.318	² 0.175	⁴⁴ 0.009	⁴⁰ 0.005	⁴⁸ 0.136	³¹ 0.033	²⁵ 0.105	²² 0.083	¹⁹ 0.926	²⁰ 0.779	¹⁶ 0.739	¹⁸ 0.573	¹⁴ 0.497	¹⁴ 0.268	¹⁰ 0.296	¹² 0.232					
188	PARAVISION-000	²³⁸ 0.278	²¹³ 0.089	²¹⁸ 0.045	²⁴⁴ 0.447	²⁰⁵ 0.170	²⁰⁶ 0.100	²¹⁷ 1.000	¹⁹¹ 0.999	²¹³ 0.997	²⁰⁹ 0.470	²¹⁴ 0.443	²⁰⁶ 0.444	²¹⁰ 0.428	¹⁴⁰ 0.497	¹⁴² 0.268	¹⁰⁰ 1.000	²⁸⁸ 1.000	²⁵⁴ 1.000	²⁰ 0.024	²⁸⁸ 1.000	²⁵⁴ 1.000	¹⁹¹ 0.908	¹⁷ 0.211	¹⁶ 0.132	¹⁴ 0.120			
189	PARAVISION-001	¹⁸⁴ 0.140	¹⁶³ 0.049	¹⁶¹ 0.020	¹⁹ 0.207	¹⁷⁶ 0.128	¹⁷⁴ 0.074	²³¹ 1.000	¹⁸⁰ 0.999	¹⁹⁹ 0.994	¹⁰⁶ 0.444	²¹⁰ 0.428	¹⁵⁰ 0.800	¹⁵⁷ 0.043	¹⁴⁰ 0.497	¹⁴² 0.268	¹⁰⁰ 1.000	²⁸⁸ 1.000	²⁵⁴ 1.000	²⁰ 0.024	²⁸⁸ 1.000	²⁵⁴ 1.000	¹⁹¹ 0.908	¹⁷ 0.211	¹⁶ 0.132	¹⁴ 0.120			
190	PARAVISION-002	¹⁴⁷ 0.085	¹⁶⁶ 0.050	¹⁷¹ 0.022	¹⁶⁴ 0.152	¹⁶⁹ 0.119	¹⁷⁹ 0.076	¹¹² 0.992	¹¹⁵ 0.983	⁹⁸ 0.748	¹⁴⁵ 0.997	¹⁴⁶ 0.994	⁹⁷ 0.733	¹³⁶ 0.058	¹⁴ 0.034	¹⁰ 0.015	⁴ 0.073	² 0.061	¹⁰ 0.033	¹¹ 0.033	¹⁰ 0.015								
191	PARAVISION-003	¹³⁰ 0.063	¹⁴⁴ 0.035	¹⁴⁵ 0.016	¹⁴ 0.124	¹⁴⁶ 0.096	¹⁵⁰ 0.060	¹⁴⁵ 0.997	¹⁴⁶ 0.994	⁹⁷ 0.733	¹³⁶ 0.058	¹³⁷ 0.058	¹³⁸ 0.058	¹³⁹ 0.058	¹⁴⁰ 0.058	¹⁴¹ 0.058	¹⁴² 0.058	¹⁴³ 0.058	¹⁴⁴ 0.058	¹⁴⁵ 0.058	¹⁴⁶ 0.058	¹⁴⁷ 0.058	¹⁴⁸ 0.058	¹⁴⁹ 0.058	¹⁴⁰ 0.058	¹⁴¹ 0.058	¹⁴² 0.058		
192	PARAVISION-004	⁶⁰ 0.025	⁶⁸ 0.010	⁶⁶ 0.004	⁵² 0.049	⁶⁰ 0.038	⁶⁴ 0.024	²¹⁹ 1.000	²⁴⁶ 1.000	¹⁰³ 0.797	⁶⁴ 0.018	⁷³ 0.011	¹⁹¹ 0.999	¹⁹⁰ 0.997	¹⁹¹ 0.997	¹⁹² 0.997	¹⁹³ 0.997	¹⁹⁴ 0.997	¹⁹⁵ 0.997	¹⁹⁶ 0.997	¹⁹⁷ 0.997	¹⁹⁸ 0.997	¹⁹⁹ 0.997	¹⁹⁰ 0.997	¹⁹¹ 0.997	¹⁹² 0.997	¹⁹³ 0.997		
193	PARAVISION-005	⁴⁴ 0.014	²⁹ 0.004	³⁰ 0.002	³¹ 0.031	³¹ 0.024	³⁸ 0.016	¹⁴³ 0.997	¹⁰⁷ 0.980	²¹ 0.181	⁴⁶ 0.011	⁶ 0.008	¹⁰ 0.011	¹⁰ 0.011	¹⁰ 0.011	¹⁰ 0.011	¹⁰ 0.011	¹⁰ 0.011	¹⁰ 0.011	¹⁰ 0.011	¹⁰ 0.011	¹⁰ 0.011	¹⁰ 0.011	¹⁰ 0.011	¹⁰ 0.011	¹⁰ 0.011	¹⁰ 0.011		
194	PARAVISION-007	¹⁰³ 0.048	²⁸ 0.004	²⁵ 0.002	²³⁴ 0.560	³² 0.025	³² 0.015	²³¹ 1.000	²⁵⁸ 1.000	⁴⁰ 0.009	⁵¹ 0.006	⁴⁴ 0.113	²⁰ 0.024	²⁸⁸ 1.000	²⁵⁴ 1.000	²⁰ 0.024	²⁸⁸ 1.000	²⁵⁴ 1.000	²⁰ 0.024	²⁸⁸ 1.000	²⁵⁴ 1.000	²⁰ 0.024	²⁸⁸ 1.000	²⁵⁴ 1.000	²⁰ 0.024	²⁸⁸ 1.000	²⁵⁴ 1.000	²⁰ 0.024	
195	PARAVISION-009	¹⁹ 0.007	²⁶ 0.003	⁷ 0.001	²⁴ 0.026	¹⁶ 0.019	¹⁶ 0.012	⁴⁴ 0.778	¹²⁶ 0.079	¹⁰² 0.037	¹²⁶ 0.079	¹²⁶ 0.079	¹²⁶ 0.079	¹²⁶ 0.079	¹²⁶ 0.079	¹²⁶ 0.079	¹²⁶ 0.079	¹²⁶ 0.079	¹²⁶ 0.079	¹²⁶ 0.079	¹²⁶ 0.079	¹²⁶ 0.079	¹²⁶ 0.079	¹²⁶ 0.079	¹²⁶ 0.079	¹²⁶ 0.079	¹²⁶ 0.079		
196	PIXELLALL-002	²⁷⁸ 0.664	²²⁰ 0.105	¹⁹² 0.030	²⁹¹ 0.974	²⁵⁸ 0.388	¹⁸⁶ 0.083	²³⁶ 1.000	²⁴⁹ 1.000	²¹³ 0.602	¹⁶⁰ 0.047	¹⁵⁰ 0.047	¹⁵⁰ 0.047	¹⁵⁰ 0.047	¹⁵⁰ 0.047	¹⁵⁰ 0.047	¹⁵⁰ 0.047	¹⁵⁰ 0.047	¹⁵⁰ 0.047	¹⁵⁰ 0.047	¹⁵⁰ 0.047	¹⁵⁰ 0.047	¹⁵⁰ 0.047	¹⁵⁰ 0.047	¹⁵⁰ 0.047	¹⁵⁰ 0.047	¹⁵⁰ 0.047		
197	PIXELLALL-003	¹⁰⁵ 0.049	¹¹¹ 0.022	¹⁰⁹ 0.009	¹¹⁷ 0.102	¹¹⁵ 0.073	¹¹⁶ 0.043	¹⁰⁸ 0.009	¹¹⁷ 0.102	¹¹⁶ 0.043	²⁰⁸ 1.000	²²¹ 0.998	¹¹¹ 0.037	¹¹⁸ 0.020	¹⁵⁰ 0.554														
198	PIXELLALL-004	¹⁶⁸ 0.120	¹⁰⁰ 0.018	⁹³ 0.007	²⁷⁹ 0.783	¹²⁶ 0.079	¹⁰² 0.037	²²⁹ 1.000	²³¹ 0.999	¹²⁶ 0.051	¹²⁶ 0.051	¹²⁶ 0.051	¹²⁶ 0.051	¹²⁶ 0.051	¹²⁶ 0.051	¹²⁶ 0.051	¹²⁶ 0.051	¹²⁶ 0.051	¹²⁶ 0.051	¹²⁶ 0.051	¹²⁶ 0.051	¹²⁶ 0.051							
199	PIXELLALL-005	¹⁴¹ 0.079	⁷² 0.012	⁶⁸ 0.005	²⁴⁶ 0.456	⁷⁴ 0.050	⁷³ 0.027	²³⁷ 1.000	²⁴⁰ 0.999	⁸⁵ 0.027	¹⁰³ 0.017	⁷⁵ 0.203	⁵⁵ 0.071	²¹⁷ 1.000	²²⁹ 0.998														
200	PTAKURATSATU-000	¹²³ 0.057	¹⁴⁵ 0.037	¹⁵⁰ 0.017	¹⁷⁰ 0.165	¹⁷⁴ 0.124	¹⁷¹ 0.071	⁷² 0.947	⁸⁰ 0.924	¹¹² 0.868	¹²³ 0.046	¹²² 0.022	⁷⁷ 0.206	⁸⁰ 0.120	⁷⁹ 0.232	¹⁰⁹ 0.328	¹¹³ 0.206	¹⁰⁵ 0.194											
201	QNAP-000	³⁰¹ 0.972	²³¹ 0.129	²³⁴ 0.052	³⁰⁰ 0.998	²²⁸ 0.238	²¹⁷ 0.117	²⁴² 1.000	²⁵² 1.000	²⁵² 1.000	¹⁸³ 0.191	¹⁷⁰ 0.068	¹⁰⁵ 0.539	¹¹⁰ 0.263	²¹³ 0.998	²²⁵ 0.985													
202	QNAP-001	¹⁴⁶ 0.083	¹⁷⁵ 0.054	¹⁷⁶ 0.024	¹⁷⁶ 0.176	¹⁸³ 0.137	¹⁸⁸ 0.085	⁶⁸ 0.943	⁸¹ 0.228	¹¹⁵ 0.870	¹⁵¹ 0.081	¹⁵¹ 0.081	¹⁵¹ 0.081	¹⁵¹ 0.081	¹⁵¹ 0.081	¹⁵¹ 0.081	¹⁵¹ 0.081	¹⁵¹ 0.081	¹⁵¹ 0.081	¹⁵¹ 0.081	¹⁵¹ 0.081	¹⁵¹ 0.081	¹⁵¹ 0.081	¹⁵¹ 0.081	¹⁵¹ 0.081	¹⁵¹ 0.081			
203	QNAP-002	⁹⁶ 0.045	¹²⁵ 0.026	¹³⁹ 0.013	¹⁵⁴ 0.136	¹⁵⁸ 0.106	¹⁶⁵ 0.068	⁴⁹ 0.820	⁶⁰ 0.772	⁷⁷ 0.622	¹³⁰ 0.052	¹²⁹ 0.025	⁸⁷ 0.281	⁹⁹ 0.171	⁹⁶ 0.272	¹²⁰ 0.214													
204	QUANTASOFT-001	²⁸² 0.713	²⁹⁴ 0.639	²⁹⁵ 0.493	²⁴⁰ 0.071	²³⁰ 0.308	²³⁷ 0.261	²⁴⁹ 0.190	²⁰⁵ 0.097	²¹⁰ 0.077	¹²⁹ 0.937	¹²⁹ 0.937	¹²⁹ 0.937	¹²⁹ 0.937	¹²⁹ 0.937	¹²⁹ 0.937	¹²⁹ 0.937	¹²⁹ 0.937	¹²⁹ 0.937	¹²⁹ 0.937	¹²⁹ 0.937	¹²⁹ 0.937	¹²⁹ 0.937	¹²⁹ 0.937	¹²⁹ 0.937	¹²⁹ 0.937			
205	RANKONE-002	²⁰³ 0.184	²²⁴ 0.118	^{240</sup}																									

MISSSES BELOW THRESHOLD, T		ENROL RECENT MUGSHOT, N = 1.6M												ENROL APPLICATION PORTRAIT, N = 1.6M														
		ENROL: MUGSHOT				ENROL: MUGSHOT				ENROL: MUGSHOT				ENROL: BORDER				ENROL: BORDER		ENROL: BORDER 10+YR		ENROL: KIOSK						
#	ALGORITHM	FPIR=0.0003	FPIR=0.001	FPIR=0.01	FPIR=0.0003	FPIR=0.001	FPIR=0.01	FPIR=0.0003	FPIR=0.001	FPIR=0.01	FPIR=0.0003	FPIR=0.001	FPIR=0.01	FPIR=0.001	FPIR=0.01	FPIR=0.001	FPIR=0.01	FPIR=0.001	FPIR=0.01	FPIR=0.001	FPIR=0.01	FPIR=0.001	FPIR=0.01	FPIR=0.001	FPIR=0.01			
231	s1-001	11 ⁰ .054	48 ⁰ .016	91 ⁰ .007	71 ⁰ .066	80 ⁰ .052	92 ⁰ .033	111 ⁰ .992	117 ⁰ .985	141 ⁰ .952	68 ⁰ .019	68 ⁰ .010	136 ⁰ .	60 ⁰ .075	40 ⁰ .148	51 ⁰ .119												
232	s1-002	124 ⁰ .060	45 ⁰ .006	41 ⁰ .002	98 ⁰ .085	46 ⁰ .031	41 ⁰ .018	62 ⁰ .924	8 ⁰ .196	5 ⁰ .095	27 ⁰ .007	19 ⁰ .003	116 ⁰ .792	97 ⁰ .151	184 ⁰ .841	75 ⁰ .144												
233	s1-003	110 ⁰ .050	58 ⁰ .009	54 ⁰ .003	55 ⁰ .052	57 ⁰ .037	54 ⁰ .022	238 ⁰ .1000	219 ⁰ .1000	176 ⁰ .989	55 ⁰ .014	49 ⁰ .006	99 ⁰ .396	35 ⁰ .037	31 ⁰ .1000	116 ⁰ .209												
234	SCANOVATE-000	158 ⁰ .103	194 ⁰ .067	193 ⁰ .030	216 ⁰ .296	231 ⁰ .240	230 ⁰ .150	66 ⁰ .931	75 ⁰ .893	104 ⁰ .803	188 ⁰ .215	193 ⁰ .	118 ⁰ .	120 ⁰ .400	153 ⁰ .299													
235	SCANOVATE-001	174 ⁰ .128	205 ⁰ .081	205 ⁰ .037	215 ⁰ .281	224 ⁰ .227	226 ⁰ .140	67 ⁰ .935	79 ⁰ .911	107 ⁰ .834	184 ⁰ .192	187 ⁰ .	103 ⁰ .	123 ⁰ .404	149 ⁰ .290													
236	SENSETIME-000	8 ⁰ .036	10 ⁰ .021	110 ⁰ .009	90 ⁰ .078	101 ⁰ .063	108 ⁰ .040	303 ⁰ .1000	266 ⁰ .1000	173 ⁰ .988																		
237	SENSETIME-001	83 ⁰ .036	112 ⁰ .022	114 ⁰ .010	94 ⁰ .080	103 ⁰ .064	114 ⁰ .041																					
238	SENSETIME-002	8 ⁰ .037	83 ⁰ .015	144 ⁰ .014	139 ⁰ .124	42 ⁰ .028	6 ⁰ .023	142 ⁰ .997	143 ⁰ .994	163 ⁰ .979	98 ⁰ .032	105 ⁰ .	017											145 ⁰ .523	88 ⁰ .160			
239	SENSETIME-003	9 ⁰ .004	8 ⁰ .002	7 ⁰ .001	6 ⁰ .014	6 ⁰ .012	5 ⁰ .009	29 ⁰ .607	31 ⁰ .477	43 ⁰ .311	33 ⁰ .	008	45 ⁰ .	005									37 ⁰ .133	46 ⁰ .115				
240	SENSETIME-004	7 ⁰ .003	7 ⁰ .002	6 ⁰ .001	8 ⁰ .015	8 ⁰ .013	10 ⁰ .010	13 ⁰ .301	14 ⁰ .229	21 ⁰ .149	19 ⁰ .	006	25 ⁰ .	004									2 ⁰ .113	38 ⁰ .100				
241	SENSETIME-005	32 ⁰ .011	14 ⁰ .002	5 ⁰ .001	17 ⁰ .018	14 ⁰ .014	8 ⁰ .010	6 ⁰ .259	7 ⁰ .173	10 ⁰ .103	23 ⁰ .	007	28 ⁰ .	004	20 ⁰ .051	19 ⁰ .	023	24 ⁰ .104	32 ⁰ .093									
242	SENSETIME-006	11 ⁰ .005	7 ⁰ .002	3 ⁰ .001	11 ⁰ .016	7 ⁰ .012	4 ⁰ .009	164 ⁰ .999	178 ⁰ .998	89 ⁰ .680	9 ⁰ .	004	7 ⁰ .	002	12 ⁰ .034	12 ⁰ .	016	12 ⁰ .093	17 ⁰ .079									
243	SENSETIME-007	1 ⁰ .003	1 ⁰ .001	2 ⁰ .001	2 ⁰ .012	2 ⁰ .009	2 ⁰ .007	192 ⁰ .1000	197 ⁰ .999	67 ⁰ .538	4 ⁰ .	003	3 ⁰ .	001	6 ⁰ .	024	5 ⁰ .	011	085 ⁰ .	074								
244	SENSETIME-008	1 ⁰ .002	1 ⁰ .001	1 ⁰ .001	1 ⁰ .011	1 ⁰ .009	1 ⁰ .007	108 ⁰ .990	23 ⁰ .405	3 ⁰ .086	2 ⁰ .	002	2 ⁰ .	001	5 ⁰ .	021	2 ⁰ .	009	7 ⁰ .	080	8 ⁰ .	074						
245	SHAMAN-003	26 ⁰ .506	283 ⁰ .451	288 ⁰ .347	265 ⁰ .650	278 ⁰ .597	282 ⁰ .472																					
246	SHAMAN-004	279 ⁰ .679	292 ⁰ .615	293 ⁰ .488	276 ⁰ .812	285 ⁰ .754	290 ⁰ .639																					
247	SHAMAN-006	20 ⁰ .185	23 ⁰ .141	252 ⁰ .092	213 ⁰ .278	227 ⁰ .237	240 ⁰ .168	83 ⁰ .978	96 ⁰ .972	146 ⁰ .960																		
248	SHAMAN-007	20 ⁰ .183	237 ⁰ .141	251 ⁰ .092	230 ⁰ .240	242 ⁰ .242	242 ⁰ .169																					
249	SIAT-001	17 ⁰ .132	93 ⁰ .018	90 ⁰ .007	26 ⁰ .641	27 ⁰ .365	274 ⁰ .348																					
250	SIAT-002	25 ⁰ .417	110 ⁰ .022	95 ⁰ .007	280 ⁰ .942	269 ⁰ .478	280 ⁰ .460																		195 ⁰ .	923	92 ⁰ .169	
251	SMILARIT-004	300 ⁰ .970	304 ⁰ .968	309 ⁰ .965	292 ⁰ .977	301 ⁰ .976	303 ⁰ .973																					
252	SMILARIT-005																											
253	SQISOFT-001	22 ⁰ .226	233 ⁰ .132	215 ⁰ .044	224 ⁰ .340	234 ⁰ .252	215 ⁰ .111	74 ⁰ .956	62 ⁰ .797	75 ⁰ .608	114 ⁰ .040	114 ⁰ .	019	93 ⁰ .	317	95 ⁰ .	150	125 ⁰ .	420	105 ⁰ .	189							
254	STAQU-000	24 ⁰ .334	188 ⁰ .062	167 ⁰ .022	277 ⁰ .848	265 ⁰ .443	153 ⁰ .061	211 ⁰ .1000	217 ⁰ .1000	233 ⁰ .999	211 ⁰ .	035	151 ⁰ .	039	120 ⁰ .	961	101 ⁰ .	183	240 ⁰ .	1000	228 ⁰ .	999						
255	SYNESIS-003	164 ⁰ .111	192 ⁰ .065	194 ⁰ .032	165 ⁰ .155	173 ⁰ .123	180 ⁰ .078	77 ⁰ .973	87 ⁰ .960	119 ⁰ .911	148 ⁰ .	075	149 ⁰ .	039									104 ⁰ .	314	130 ⁰ .	235		
256	SYNESIS-003	27 ⁰ .648	28 ⁰ .582	292 ⁰ .443	269 ⁰ .708	281 ⁰ .646	28 ⁰ .524																					
257	SYNESIS-005	10 ⁰ .050	119 ⁰ .025	130 ⁰ .011	101 ⁰ .088	112 ⁰ .072	117 ⁰ .043	126 ⁰ .995	116 ⁰ .984	101 ⁰ .795	101 ⁰ .	032	99 ⁰ .	016									73 ⁰ .	214	87 ⁰ .	158		
258	T41SB-000	66 ⁰ .027	90 ⁰ .016	125 ⁰ .011	77 ⁰ .068	83 ⁰ .053	94 ⁰ .034	24 ⁰ .566	34 ⁰ .510	56 ⁰ .463	71 ⁰ .	021	70 ⁰ .	010	112 ⁰ .	759	100 ⁰ .	177	53 ⁰ .	161	60 ⁰ .	125						
259	TECH5-001	28 ⁰ .807	182 ⁰ .057	153 ⁰ .018	29 ⁰ .994	29 ⁰ .935	144 ⁰ .055	293 ⁰ .1000	250 ⁰ .1000	247 ⁰ .1000	189 ⁰ .	244	134 ⁰ .	028									217 ⁰ .	0994	210 ⁰ .	817		
260	TECH5-002	116 ⁰ .053	128 ⁰ .027	133 ⁰ .012	105 ⁰ .094	111 ⁰ .070	110 ⁰ .040	56 ⁰ .874	65 ⁰ .805	79 ⁰ .627	113 ⁰ .	039	113 ⁰ .	019	76 ⁰ .	205	83 ⁰ .	111	128 ⁰ .	440	102 ⁰ .	182						
261	TEVIAN-003	22 ⁰ .239	250 ⁰ .177	257 ⁰ .096	228 ⁰ .346	247 ⁰ .298	251 ⁰ .198																					
262	TEVIAN-004	198 ⁰ .170	223 ⁰ .117	236 ⁰ .063	197 ⁰ .216	209 ⁰ .176	216 ⁰ .115																					
263	TEVIAN-005	17 ⁰ .019	21 ⁰ .087	217 ⁰ .045	179 ⁰ .180	189 ⁰ .144	192 ⁰ .089	102 ⁰ .988	88 ⁰ .962	102 ⁰ .796																		
264	TEVIAN-006	38 ⁰ .024	63 ⁰ .010	71 ⁰ .005	44 ⁰ .041	49 ⁰ .032	53 ⁰ .021	25 ⁰ .562	25 ⁰ .425	41 ⁰ .291	38 ⁰ .	016	63 ⁰ .	009	38 ⁰ .	093	44 ⁰ .	050	20 ⁰ .	951	49 ⁰ .	117						
265	TEVIAN-007	3 ⁰ .011	41 ⁰ .005	45 ⁰ .003	26 ⁰ .028	27 ⁰ .022	29 ⁰ .015	19 ⁰ .504	19 ⁰ .301	30 ⁰ .183	43 ⁰ .	009	42 ⁰ .	005	27 ⁰ .	065	30 ⁰ .	033	31 ⁰ .	122	41 ⁰ .	102						
266	TIGER-000	259 ⁰ .462	277 ⁰ .390	281 ⁰ .261	255 ⁰ .565	270 ⁰ .500	275 ⁰ .366																					
267	TIGER-002	194 ⁰ .158	206 ⁰ .086	208 ⁰ .039	193 ⁰ .202	198 ⁰ .158	199 ⁰ .095	183 ⁰ .999	185 ⁰ .999	160 ⁰ .975																		
268	TIGER-003	19 ⁰ .158	20 ⁰ .086	207 ⁰ .039	192 ⁰ .202	199 ⁰ .158	198 ⁰ .095																					
269	TONGYITRANS-000	161 ⁰ .107	199 ⁰ .074	206 ⁰ .038	157 ⁰ .141	162 ⁰ .112	167 ⁰ .069																					
270	TONGYITRANS-001	17 ⁰ .124	19 ⁰ .066	195 ⁰ .032	142 ⁰ .128	153 ⁰ .101	150 ⁰ .062																					
271	TOSHIBA-000	170 ⁰ .123	189 ⁰ .062	187 ⁰ .027	161 ⁰ .150	167 ⁰ .118	173 ⁰ .074	144 ⁰ .997	155 ⁰ .995	174 ⁰ .988																		

Table 36: Threshold-based accuracy. Values are $FNIR(N, T, L)$ with $N = 1.6$ million with thresholds set to produce $FPIR = 0.0003, 0.001$, and 0.01 in non-mate searches. Throughout blue superscripts indicate the rank of the algorithm for that column. Caution: The Power-low models are mostly intended to draw attention to the kind of behavior, not as a model to be used for prediction.

18:02:21
2022/11/09

$\text{FNIR}(N, R, I) =$ False neg. identification rate
 $\text{FPIR}(N, T) =$ False pos. identification rate

N = Num. enrolled subjects
 R = Num. candidates examined

T = Threshold

$T = 0 \rightarrow$ Investigation
 $T > 0 \rightarrow$ Identification

MISSES BELOW THRESHOLD, T			ENROL RECENT MUGSHOT, N = 1.6M												ENROL APPLICATION PORTRAIT, N = 1.6M												
			ENROL: MUGSHOT				ENROL: MUGSHOT				ENROL: WEBCAM				PROBE: PROFILE				ENROL: VISA			ENROL: BORDER			ENROL: KIOSK		
#	ALGORITHM	FPIR=0.0003	FPIR=0.001	FPIR=0.01	FPIR=0.0003	FPIR=0.001	FPIR=0.01	FPIR=0.0003	FPIR=0.001	FPIR=0.01	FPIR=0.0003	FPIR=0.001	FPIR=0.01	FPIR=0.0003	FPIR=0.001	FPIR=0.01	FPIR=0.0001	FPIR=0.01	FPIR=0.001	FPIR=0.01	FPIR=0.0001	FPIR=0.01	FPIR=0.001	FPIR=0.01	FPIR=0.0001	FPIR=0.01	
277	VD-002	¹⁸⁸ 0.144	²⁰³ 0.079	²⁰⁷ 0.036	¹⁸⁹ 0.188	¹⁹⁷ 0.148	¹⁹³ 0.092	¹⁸³ 0.998	¹⁵⁸ 0.996	¹⁷⁴ 0.987	¹⁵⁶ 0.095	¹⁶¹ 0.048	⁹⁵ 0.367	¹⁰⁴ 0.220	¹¹⁵ 0.372	¹⁴⁴ 0.280											
278	VD-003	²²⁴ 0.234	¹⁶⁰ 0.046	¹⁵⁸ 0.020	¹⁴⁹ 0.133	¹⁵¹ 0.100	¹⁷⁹ 0.999	¹⁸⁷ 0.999	¹⁹⁴ 0.994	¹²⁷ 0.051	¹³¹ 0.027	⁸² 0.244	⁸⁹ 0.133	¹⁰⁶ 0.315	¹⁰⁹ 0.203												
279	VERIDAS-001	¹⁴³ 0.080	¹⁴⁸ 0.037	¹⁴⁶ 0.016	¹²¹ 0.106	¹²⁹ 0.082	¹³⁰ 0.051	¹¹⁷ 0.993	¹²⁴ 0.987	¹³⁰ 0.938	¹¹⁹ 0.044	¹²² 0.023	⁸⁴ 0.266	⁹² 0.146	⁹³ 0.264	¹¹⁰ 0.204											
280	VERIDAS-002	¹⁴⁴ 0.080	¹⁴⁹ 0.037	¹⁴⁷ 0.016	¹²⁰ 0.106	¹²⁹ 0.082	¹³¹ 0.051	¹¹⁶ 0.993	¹²⁵ 0.987	¹³¹ 0.938	¹¹⁸ 0.044	¹²⁶ 0.023	⁸⁵ 0.266	⁹³ 0.146	⁹² 0.264	¹¹¹ 0.204											
281	VERIDAS-003	¹³⁶ 0.072	⁹¹ 0.017	⁸⁷ 0.006	⁸² 0.071	⁹⁶ 0.055	⁹⁰ 0.033	¹⁶¹ 0.998	¹⁶⁴ 0.997	¹²³ 0.927	⁶⁸ 0.020	⁷² 0.011	⁸⁶ 0.150	⁶² 0.078	⁶² 0.178	⁷⁴ 0.142											
282	VERIJELAS-000	²⁸⁸ 0.846	²⁹⁶ 0.799	³⁰¹ 0.681	²⁷⁹ 0.868	²⁸⁸ 0.813	²⁹² 0.697	¹⁷⁵ 0.999	¹⁸² 0.999	²⁰⁸ 0.995	¹⁹⁵ 0.324	¹⁹⁹ 0.216	¹¹⁷ 0.933	¹¹⁹ 0.561	¹⁵³ 0.589	¹⁷⁷ 0.462											
283	VIGILANTSOLUTIONS-003	²⁶³ 0.482	²⁸¹ 0.408	²⁸⁷ 0.282	²⁷⁷ 0.730	²⁸⁷ 0.660	²⁸⁶ 0.526	¹⁷⁷ 0.999	¹⁸¹ 0.999	²⁰⁷ 0.995																	
284	VIGILANTSOLUTIONS-004	²⁷⁵ 0.624	²⁸⁷ 0.549	²⁹¹ 0.422	²⁷⁸ 0.858	²⁹⁰ 0.817	²⁹³ 0.709	¹⁵⁸ 0.998	¹⁶¹ 0.996	¹⁸⁶ 0.991																	
285	VIGILANTSOLUTIONS-005	²⁹⁶ 0.936	²⁷⁶ 0.388	²¹⁰ 0.043				²²⁵ 1.000	²⁴² 1.000	²⁵⁹ 1.000																	
286	VIGILANTSOLUTIONS-006	²⁹⁹ 0.959	²⁷¹ 0.353	²¹³ 0.043				²⁴⁰ 1.000	²³⁵ 1.000	²⁶⁰ 1.000																	
287	VIGILANTSOLUTIONS-007	¹⁴⁰ 0.076	¹³⁶ 0.028	¹²⁷ 0.011	¹²⁶ 0.113	¹³⁴ 0.088	¹³⁷ 0.053	¹⁴⁹ 0.997	¹⁶⁰ 0.996	¹⁸⁷ 0.991	¹⁵² 0.081	¹⁵⁹ 0.047	⁹⁷ 0.371	¹⁰⁷ 0.242	¹¹⁹ 0.391	¹⁵² 0.295											
288	VIGILANTSOLUTIONS-008	¹¹¹ 0.051	¹⁰⁶ 0.021	¹¹¹ 0.010	¹¹⁷ 0.105	¹²¹ 0.077	¹²¹ 0.046	¹³⁶ 1.000	¹⁸⁴ 0.999	¹⁸⁹ 0.991	¹⁶⁰ 0.104	¹⁶⁴ 0.054	¹⁰⁰ 0.398	¹⁰⁹ 0.259	¹⁴² 0.511	¹⁵⁸ 0.316											
289	VISIONBOX-000	¹³⁷ 0.073	⁹⁶ 0.018	⁹² 0.007	⁸³ 0.071	⁹³ 0.057	⁹⁸ 0.035	¹²² 0.995	¹³² 0.990	¹³⁸ 0.974	⁷⁸ 0.023	⁸¹ 0.012	⁸⁵ 0.146	⁶⁴ 0.081	⁵⁴ 0.162	⁶¹ 0.126											
290	VISIONLABS-004	¹⁴⁹ 0.091	¹⁸³ 0.058	¹⁷⁶ 0.024	¹⁸⁸ 0.199	²⁰⁹ 0.159	²⁰¹ 0.097	⁶⁹ 0.944	⁷⁴ 0.890	⁹⁹ 0.742																	
291	VISIONLABS-005	¹⁴⁵ 0.080	¹⁶⁷ 0.050	¹⁶⁰ 0.020	¹⁸² 0.183	¹⁹⁰ 0.147	¹⁹⁰ 0.087	⁷⁰ 0.945	⁷³ 0.888	⁹⁴ 0.736																	
292	VISIONLABS-006	⁹⁵ 0.044	¹²⁷ 0.027	¹¹⁸ 0.010	¹³⁰ 0.117	¹³⁸ 0.090	¹³³ 0.051	⁴² 0.764	⁴⁷ 0.672	⁶⁹ 0.511																	
293	VISIONLABS-007	⁹⁴ 0.044	¹²⁶ 0.027	¹¹⁷ 0.010	¹²⁹ 0.117	¹³⁷ 0.090	¹³² 0.051	⁴¹ 0.764	⁴⁸ 0.672	⁶¹ 0.511	⁹⁷ 0.031	⁹⁴ 0.014	⁶⁶ 0.185	⁷⁸ 0.145													
294	VISIONLABS-008	⁶⁸ 0.028	⁷⁶ 0.013	⁷⁸ 0.006	⁷⁹ 0.068	⁷⁷ 0.051	⁸⁵ 0.032	²⁶ 0.574	³² 0.481	⁴⁴ 0.317	⁷⁹ 0.017	⁸⁸ 0.008	⁴⁰ 0.151	⁵² 0.119													
295	VISIONLABS-009	³⁶ 0.012	³⁴ 0.005	²⁷ 0.002	³¹ 0.032	³⁵ 0.025	³⁹ 0.017	⁶⁵ 0.930	⁶³ 0.799	³² 0.196	³⁸ 0.008	³⁷ 0.004	²⁸ 0.113	³³ 0.093													
296	VISIONLABS-010	⁴³ 0.014	⁴⁰ 0.005	³⁶ 0.002	³⁶ 0.034	⁴⁰ 0.027	⁴⁵ 0.019		²⁴ 0.169	³¹ 0.008	²⁹ 0.027	²⁷ 0.109	²⁷ 0.089														
297	VISIONLABS-011	³⁴ 0.011	²⁴ 0.003	¹⁸ 0.002	²² 0.024	²⁹ 0.020	²⁵ 0.014		³¹ 0.194	¹³ 0.004	¹¹ 0.002	¹⁵ 0.034	¹³ 0.017	¹⁰ 0.090	¹⁶ 0.079												
298	VNPPT-001	⁶⁷ 0.027	⁸⁰ 0.014	⁸⁷ 0.006	¹⁶⁶ 0.158	¹⁰⁹ 0.068	⁹⁹ 0.036	⁶¹ 0.922	⁵³ 0.718	⁵² 0.373	¹⁰⁶ 0.035	⁷⁶ 0.011	¹²¹ 0.990	¹¹⁷ 0.537	¹¹³ 0.362	⁶⁶ 0.134											
299	VNPPT-002	⁴⁰ 0.013	⁴⁷ 0.007	⁵⁰ 0.003	⁴³ 0.040	⁴⁵ 0.032	⁵² 0.021	²⁵ 0.568	¹⁸ 0.292	²³ 0.154	²⁸ 0.007	²⁴ 0.004	³¹ 0.072	²⁹ 0.031	¹⁵ 0.096	¹² 0.075											
300	VOCORD-003	²⁴⁶ 0.354	²²⁷ 0.122	²²¹ 0.048	¹⁸⁷ 0.195	¹⁹⁶ 0.155	¹⁹⁶ 0.093	¹⁶⁵ 0.999	¹⁷³ 0.998	¹⁸¹ 0.991	¹⁷⁶ 0.157	¹⁸⁸ 0.105															
301	VOCORD-004	²⁸⁷ 0.826	²⁷² 0.355	²²² 0.051	²³⁹ 0.401	²⁰⁹ 0.173	¹⁹⁴ 0.093	²²² 1.000	²²⁰ 1.000	²³⁹ 0.999	¹⁸⁵ 0.193	¹⁶⁸ 0.065	²⁰⁷ 0.991	²⁰⁵ 0.776													
302	VOCORD-005	²⁸⁰ 0.689	²⁴¹ 0.158	²¹⁴ 0.044	¹⁶⁸ 0.161	¹⁷⁹ 0.130	¹⁸³ 0.080	¹⁷¹ 0.999	¹⁶⁵ 0.997	¹⁴⁹ 0.968	¹⁷⁰ 0.138	¹⁸² 0.090	¹¹⁶ 0.381	¹⁴⁶ 0.287													
303	VOCORD-006	³¹⁵ 1.000	³¹⁴ 1.000	³¹⁴ 1.000	³⁰⁵ 1.000	³¹¹ 1.000	²⁸⁸ 1.000	²⁸⁸ 1.000	²⁸⁹ 1.000	²⁸⁷ 1.000	²⁸⁹ 1.000	²⁸⁷ 1.000	²²⁷ 1.000	²⁹¹ 1.000													
304	VTS-000	²⁷² 0.605	²⁹⁸ 0.598	²⁹⁸ 0.595	²⁶¹ 0.624	²⁷⁹ 0.619	²⁸⁹ 0.613	¹⁸¹ 0.999	¹⁹⁴ 0.999	²²⁶ 0.998	²¹⁶ 0.613	²¹⁸ 0.609	¹¹³ 0.760	¹²⁷ 0.739	¹⁷¹ 0.761	²⁰² 0.749											
305	VTS-001	⁷⁹ 0.035	⁷⁷ 0.013	⁷⁸ 0.006	⁷⁵ 0.067	⁷⁸ 0.051	⁷⁹ 0.031	¹⁵² 0.998	¹⁴² 0.994	⁶⁷ 0.510	⁷⁶ 0.022	⁸² 0.012	⁸² 0.141	⁶³ 0.079	⁶⁷ 0.192	⁶² 0.126											
306	VTS-002	¹¹⁵ 0.053	¹²² 0.026	¹²¹ 0.010	¹¹¹ 0.098	¹¹⁸ 0.075	¹²² 0.046	¹⁹⁹ 1.000	²⁰⁴ 1.000	¹⁴² 0.953	¹²¹ 0.045	¹³⁰ 0.026	⁸⁸ 0.231	⁹⁰ 0.133	¹²⁴ 0.417	¹⁰³ 0.187											
307	VTS-003	⁴⁵ 0.015	⁵² 0.007	⁴⁹ 0.003	⁵¹ 0.048	⁵⁶ 0.033	⁴⁷ 0.019	²²⁴ 1.000	²²⁸ 1.000	⁸² 0.632	⁵³ 0.014	⁴⁵ 0.005	¹⁷ 0.954	⁴⁹ 0.060	¹⁵ 0.635	²⁸ 0.089											
308	XFORWARDAI-000	⁷⁰ 0.029	⁸⁶ 0.015	⁸⁷ 0.006	⁸⁰ 0.070	⁸⁷ 0.053	⁹⁶ 0.034	³⁸ 0.698	²⁷ 0.440	³⁶ 0.250	⁷² 0.021	⁷¹ 0.011	⁶¹ 0.159	⁶⁷ 0.082	⁵⁷ 0.169	⁶⁷ 0.134											

Appendices

Appendix A Accuracy on large-population FRVT 2018 mugshots

2022/11/09
18:02:21

$\text{FNIR}(N, R, T) =$	False neg. identification rate	$N =$ Num. enrolled subjects	$T =$ Threshold	$T = 0 \rightarrow$ Investigation
$\text{FPTR}(N, T) =$	False pos. identification rate	$R =$ Num. candidates examined	$T > 0 \rightarrow$ Identification	

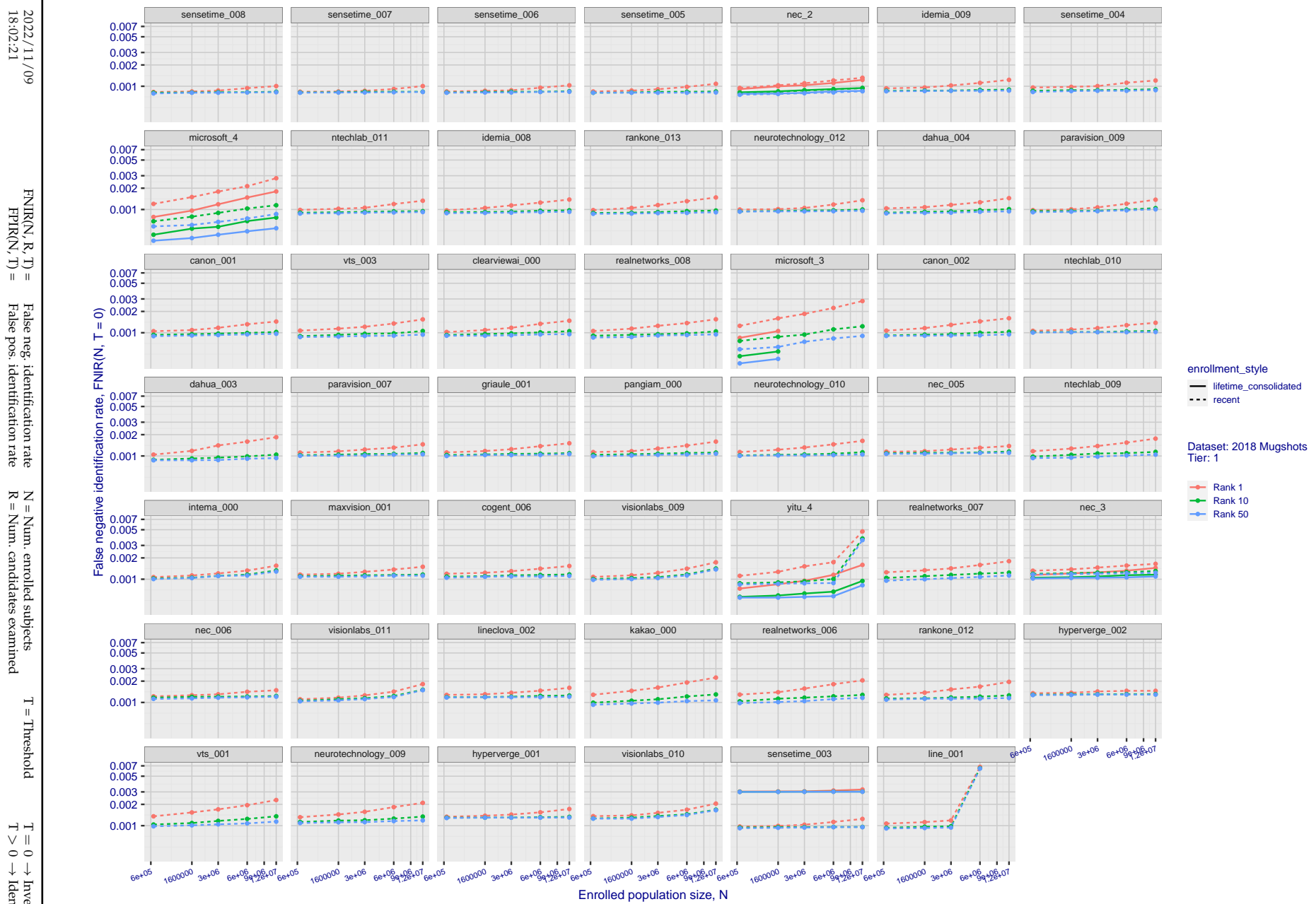


Figure 20: [FRVT-2018 Mugshot Dataset] Rank-based identification miss rates vs. number of enrolled subjects. The figure shows false negative identification rates, $\text{FNIR}(N, R)$, across various gallery sizes and ranks 1, 10 and 50. The threshold is set to zero, so this metric rewards even weak scoring rank 1 mates. This also means $\text{FPIR} = 1$, so any search without an enrolled mate will return non-mated candidates. For clarity, results are sorted and reported into tiers spanning multiple pages, the tiering criteria being rank 1 hit rate on a gallery size of 640 000.

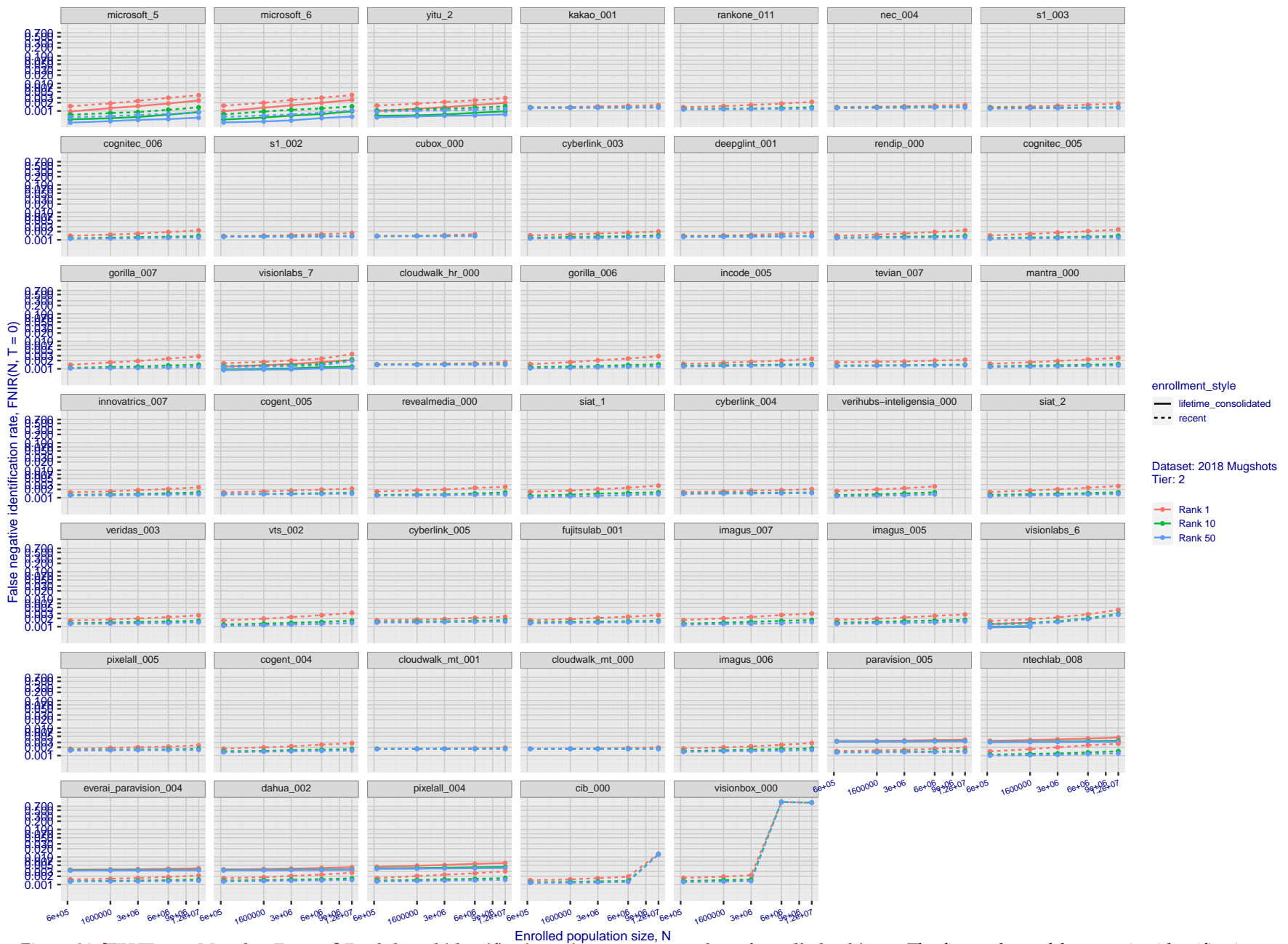


Figure 21: [FRVT-2018 Mugshot Dataset] Rank-based identification miss rates vs. number of enrolled subjects. The figure shows false negative identification rates, $\text{FNIR}(N, R)$, across various gallery sizes and ranks 1, 10 and 50. The threshold is set to zero, so this metric rewards even weak scoring rank 1 mates. This also means $\text{FPIR} = 1$, so any search without an enrolled mate will return non-mated candidates. For clarity, results are sorted and reported into tiers spanning multiple pages, the tiering criteria being rank 1 hit rate on a gallery size of 640 000.

2022/11/09
18:02:21

 $\text{FNIR}(N, R, T) =$
 False neg. identification rate
 $\text{FPIR}(N, T) =$
 False pos. identification rate

 $N =$ Num. enrolled subjects
 $R =$ Num. candidates examined
 $T =$ Threshold
 $T = 0 \rightarrow$ Investigation
 $T > 0 \rightarrow$ Identification

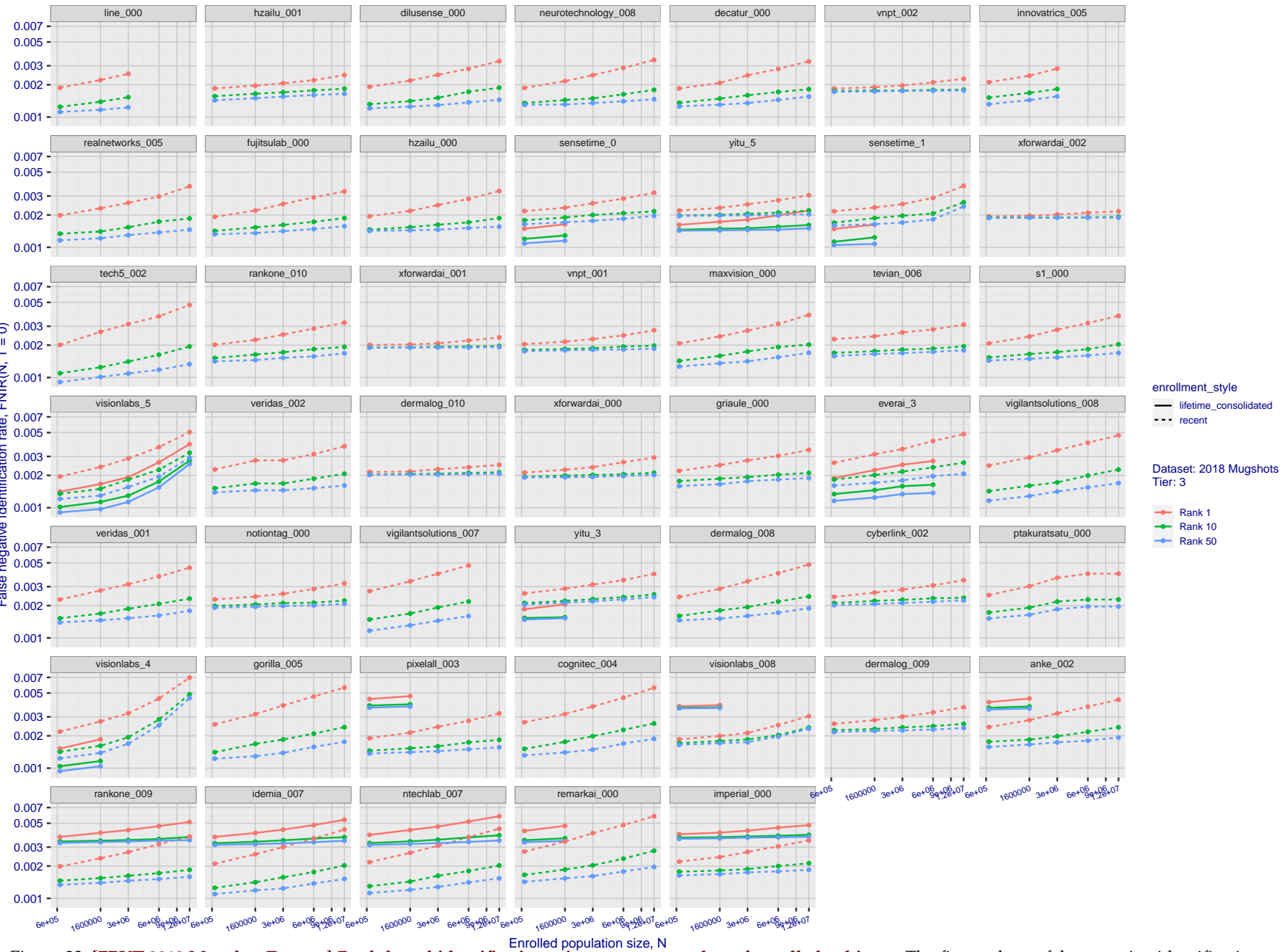


Figure 22: [FRVT-2018 Mugshot Dataset] Rank-based identification miss rates vs. number of enrolled subjects. The figure shows false negative identification rates, $\text{FNIR}(N, R)$, across various gallery sizes and ranks 1, 10 and 50. The threshold is set to zero, so this metric rewards even weak scoring rank 1 mates. This also means $\text{FPIR} = 1$, so any search without an enrolled mate will return non-mated candidates. For clarity, results are sorted and reported into tiers spanning multiple pages, the tiering criteria being rank 1 hit rate on a gallery size of 640 000.

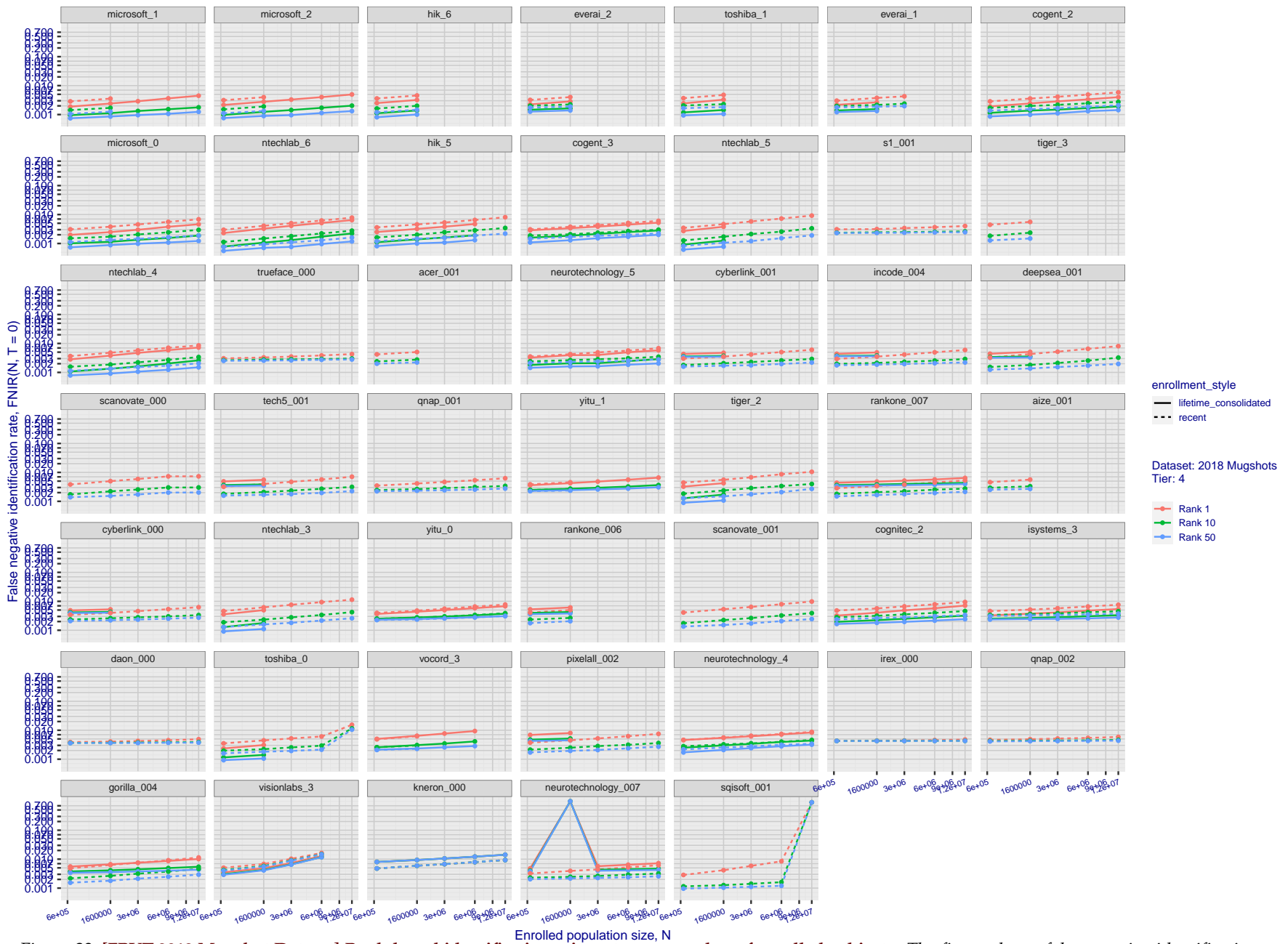


Figure 23: [FRVT-2018 Mugshot Dataset] Rank-based identification miss rates vs. number of enrolled subjects. The figure shows false negative identification rates, $\text{FNIR}(N, R)$, across various gallery sizes and ranks 1, 10 and 50. The threshold is set to zero, so this metric rewards even weak scoring rank 1 mates. This also means $\text{FPIR} = 1$, so any search without an enrolled mate will return non-mated candidates. For clarity, results are sorted and reported into tiers spanning multiple pages, the tiering criteria being rank 1 hit rate on a gallery size of 640 000.

2022/11/09
18:02:21FNIR(N, R, T) = False neg. identification rate
FPIR(N, T) = False pos. identification rateN = Num. enrolled subjects
R = Num. candidates examined

T = Threshold

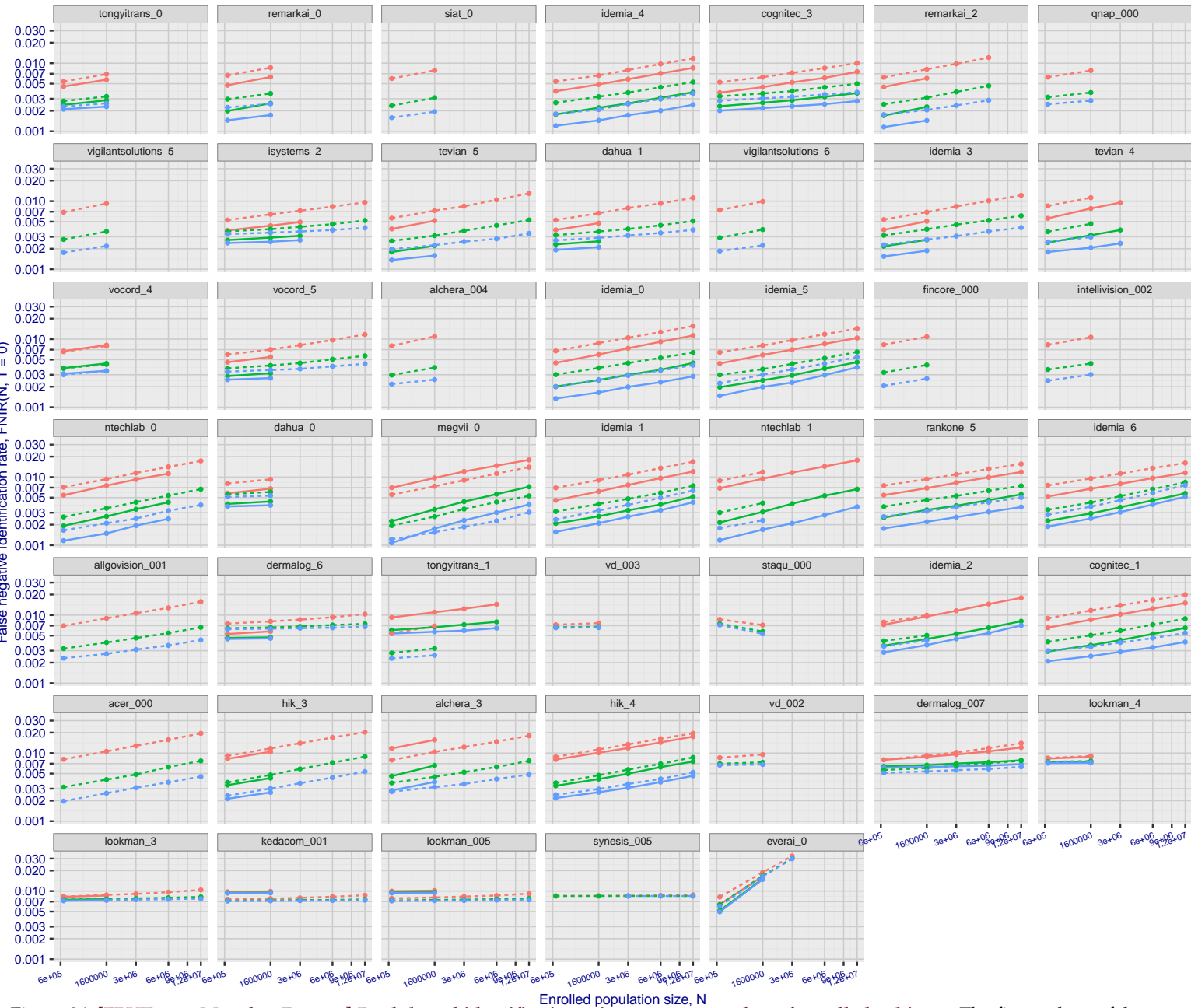
T = 0 → Investigation
T > 0 → Identification

Figure 24: [FRVT-2018 Mugshot Dataset] Rank-based identification miss rates vs. number of enrolled subjects. The figure shows false negative identification rates, $\text{FNIR}(N, R)$, across various gallery sizes and ranks 1, 10 and 50. The threshold is set to zero, so this metric rewards even weak scoring rank 1 mates. This also means $\text{FPIR} = 1$, so any search without an enrolled mate will return non-mated candidates. For clarity, results are sorted and reported into tiers spanning multiple pages, the tiering criteria being rank 1 hit rate on a gallery size of 640 000.

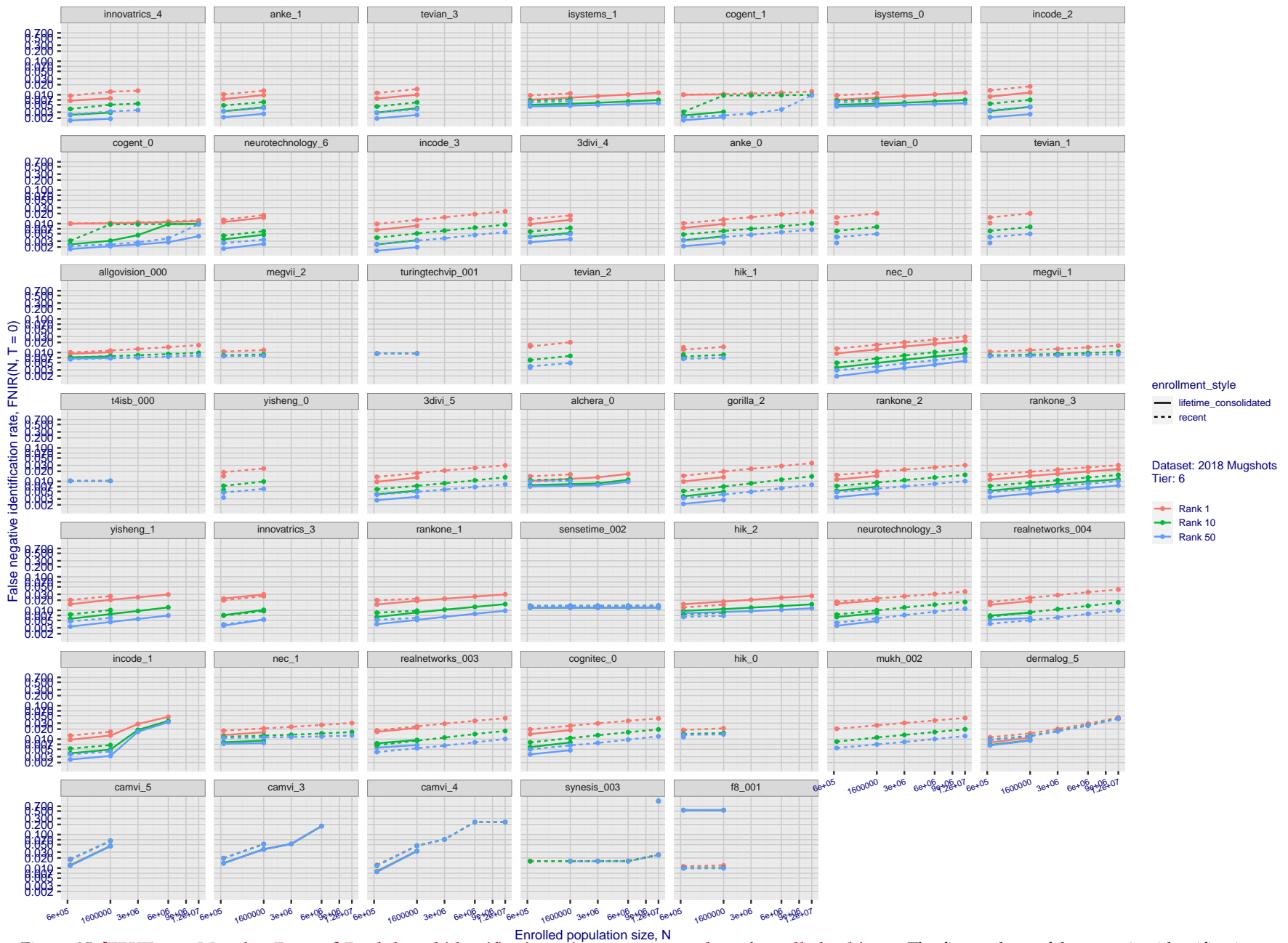


Figure 25: [FRVT-2018 Mugshot Dataset] Rank-based identification miss rates vs. number of enrolled subjects. The figure shows false negative identification rates, $\text{FNIR}(N, R)$, across various gallery sizes and ranks 1, 10 and 50. The threshold is set to zero, so this metric rewards even weak scoring rank 1 mates. This also means $\text{FPIR} = 1$, so any search without an enrolled mate will return non-mated candidates. For clarity, results are sorted and reported into tiers spanning multiple pages, the tiering criteria being rank 1 hit rate on a gallery size of 640 000.

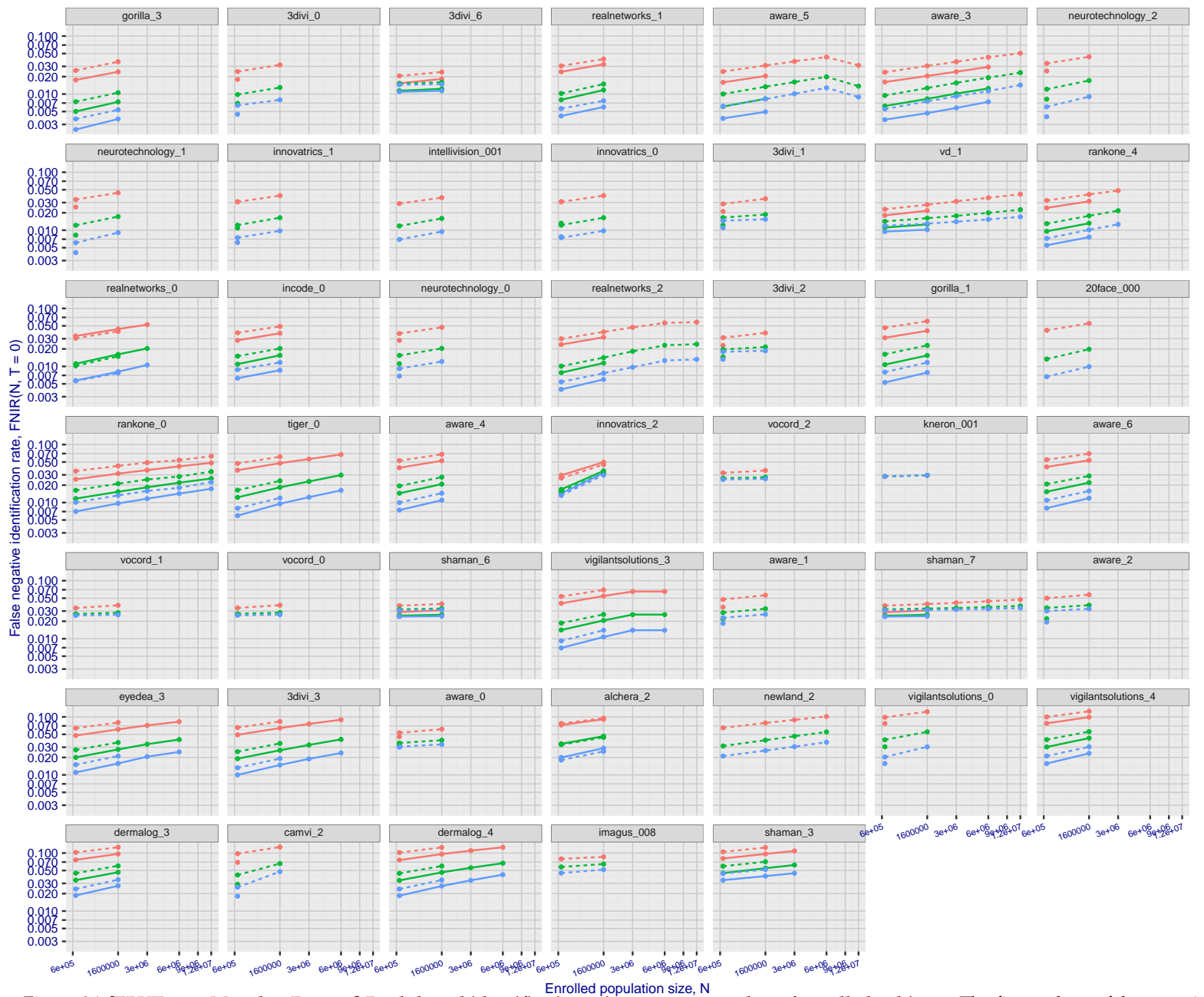


Figure 26: [FRVT-2018 Mugshot Dataset] Rank-based identification miss rates vs. number of enrolled subjects. The figure shows false negative identification rates, $\text{FNIR}(N, R)$, across various gallery sizes and ranks 1, 10 and 50. The threshold is set to zero, so this metric rewards even weak scoring rank 1 mates. This also means $\text{FPIR} = 1$, so any search without an enrolled mate will return non-mated candidates. For clarity, results are sorted and reported into tiers spanning multiple pages, the tiering criteria being rank 1 hit rate on a gallery size of 640 000.

2022/11/09
18:02:21FNIR(N, R, T) = False neg. identification rate
FPIR(N, T) = False pos. identification rateN = Num. enrolled subjects
R = Num. candidates examinedT = Threshold
 $T = 0 \rightarrow$ Investigation
 $T > 0 \rightarrow$ Identification

2022/11/09
18:02:21

$\text{FNIR}(N, K, T) =$ False neg. identification rate
 $\text{FPIR}(N, T) =$ False pos. identification rate

N = Null, enrolled subjects
R = Num. candidates examined

1
Introduction

$I = 0 \rightarrow$ Investigation
 $T > 0 \rightarrow$ Identification

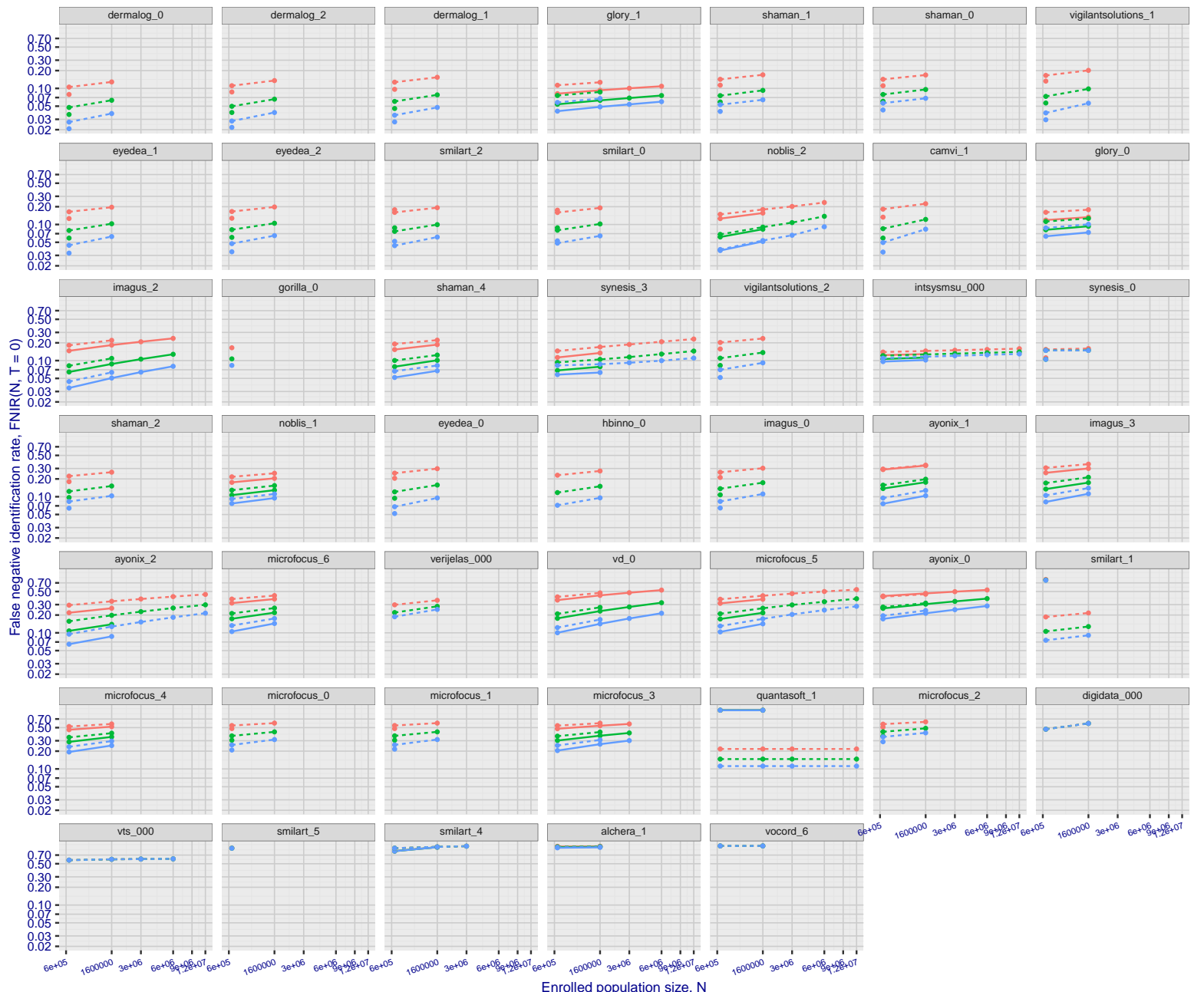


Figure 27: [FRVT-2018 Mugshot Dataset] Rank-based identification miss rates vs. number of enrolled subjects. The figure shows false negative identification rates, FNIR(N, R), across various gallery sizes and ranks 1, 10 and 50. The threshold is set to zero, so this metric rewards even weak scoring rank 1 mates. This also means FPIR = 1, so any search without an enrolled mate will return non-mated candidates. For clarity, results are sorted and reported into tiers spanning multiple pages, the tiering criteria being rank 1 hit rate on a gallery size of 640 000.

2022/11/09
18:02:21

FNIR(N, R, T) = False neg. identification rate
FPTR(N, T) = False pos. identification rate

N = Num. enrolled subjects
R = Num. candidates examined

T = Threshold
T > 0 → Identification

T = 0 → Investigation

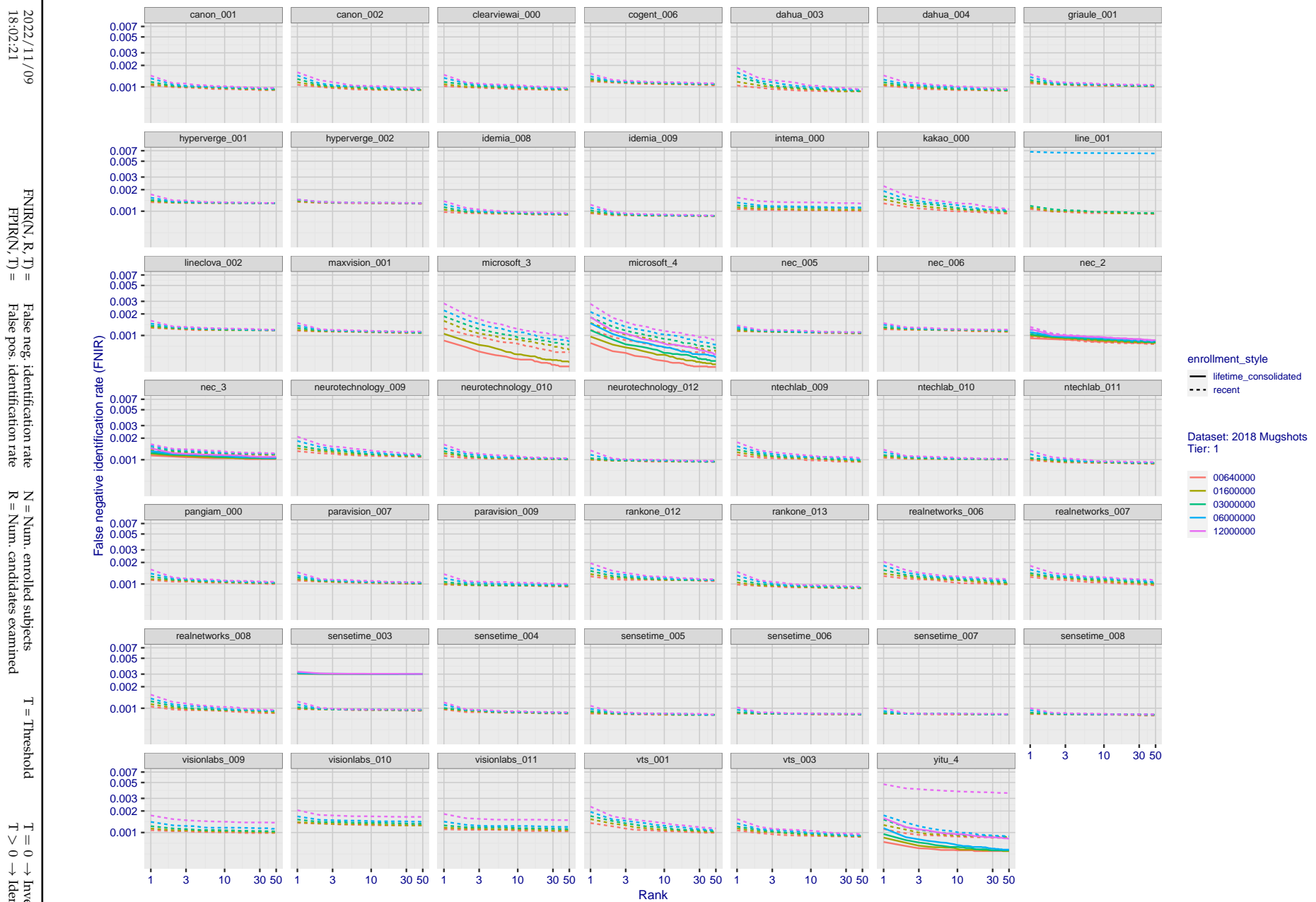


Figure 28: [FRVT-2018 Mugshot Dataset] Rank-based identification miss rates vs. rank. The figure shows false negative identification rates (FNIR) for ranks up to 50. This metric is appropriate to investigational applications where human reviewers will adjudicate sorted candidate lists. Note that with threshold set to zero, FPIR = 1, i.e. any search without an enrolled mate will return non-mated candidates. Results are sorted and reported into tiers for clarity, with the tiering criteria being rank 1 hit rate on a gallery size of N = 640 000 subjects.

2022/11/09
18:02:21

 $\text{FNIR}(N, R, T) =$
False neg. identification rate
 $\text{FPIR}(N, T) =$
False pos. identification rate

 $N =$ Num. enrolled subjects
 $R =$ Num. candidates examined
 $T =$ Threshold
 $T = 0 \rightarrow$ Investigation
 $T > 0 \rightarrow$ Identification

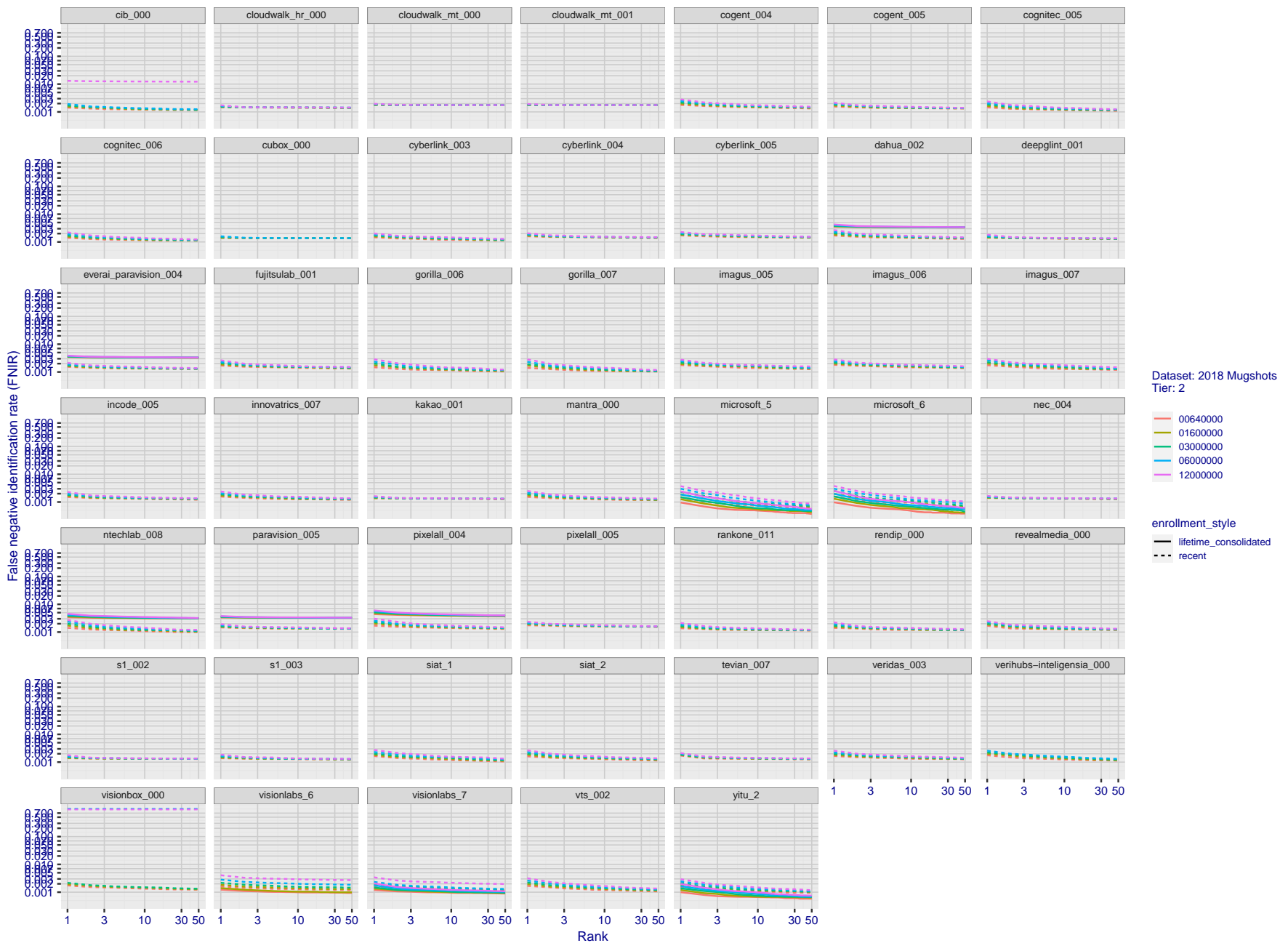


Figure 29: [FRVT-2018 Mugshot Dataset] Rank-based identification miss rates vs. rank. The figure shows false negative identification rates (FNIR) for ranks up to 50. This metric is appropriate to investigational applications where human reviewers will adjudicate sorted candidate lists. Note that with threshold set to zero, FPIR = 1, i.e. any search without an enrolled mate will return non-mated candidates. Results are sorted and reported into tiers for clarity, with the tiering criteria being rank 1 hit rate on a gallery size of $N = 640\,000$ subjects.

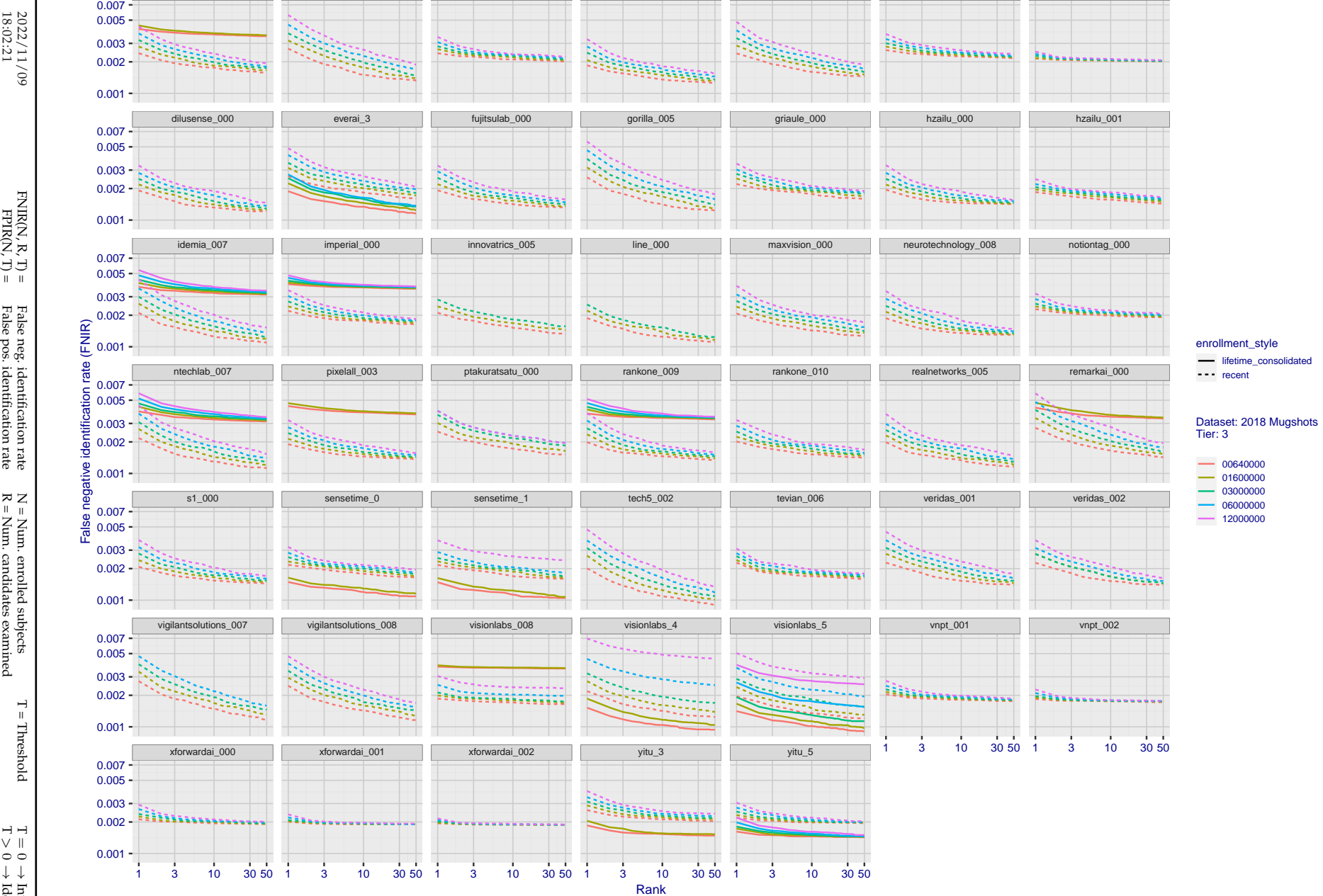


Figure 30: [FRVT-2018 Mugshot Dataset] Rank-based identification miss rates vs. rank. The figure shows false negative identification rates (FNIR) for ranks up to 50. This metric is appropriate to investigational applications where human reviewers will adjudicate sorted candidate lists. Note that with threshold set to zero, FPIR = 1, i.e. any search without an enrolled mate will return non-mated candidates. Results are sorted and reported into tiers for clarity, with the tiering criteria being rank 1 hit rate on a gallery size of N = 640 000 subjects.

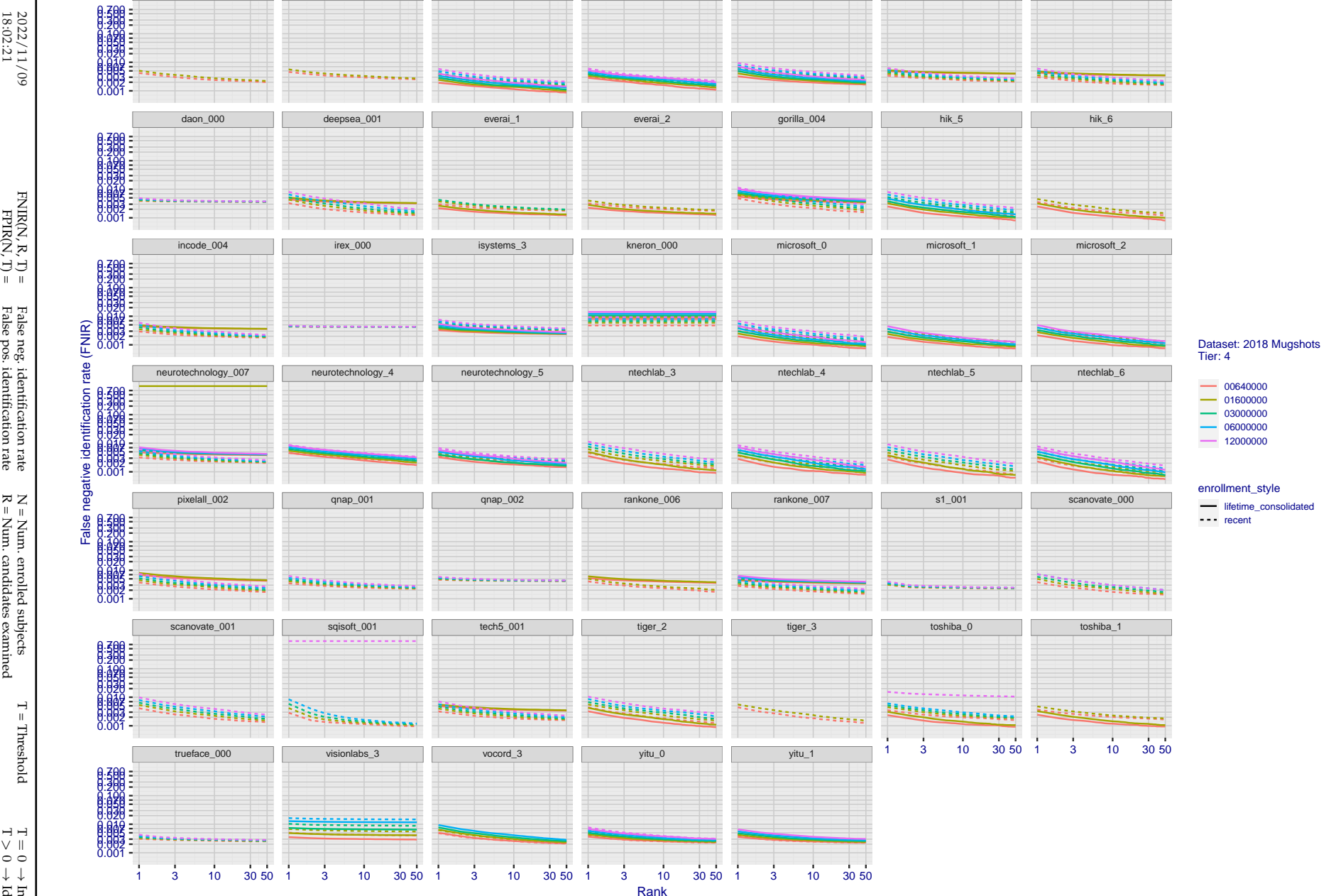


Figure 31: [FRVT-2018 Mugshot Dataset] Rank-based identification miss rates vs. rank. The figure shows false negative identification rates (FNIR) for ranks up to 50. This metric is appropriate to investigational applications where human reviewers will adjudicate sorted candidate lists. Note that with threshold set to zero, FPIR = 1, i.e. any search without an enrolled mate will return non-mated candidates. Results are sorted and reported into tiers for clarity, with the tiering criteria being rank 1 hit rate on a gallery size of N = 640 000 subjects.

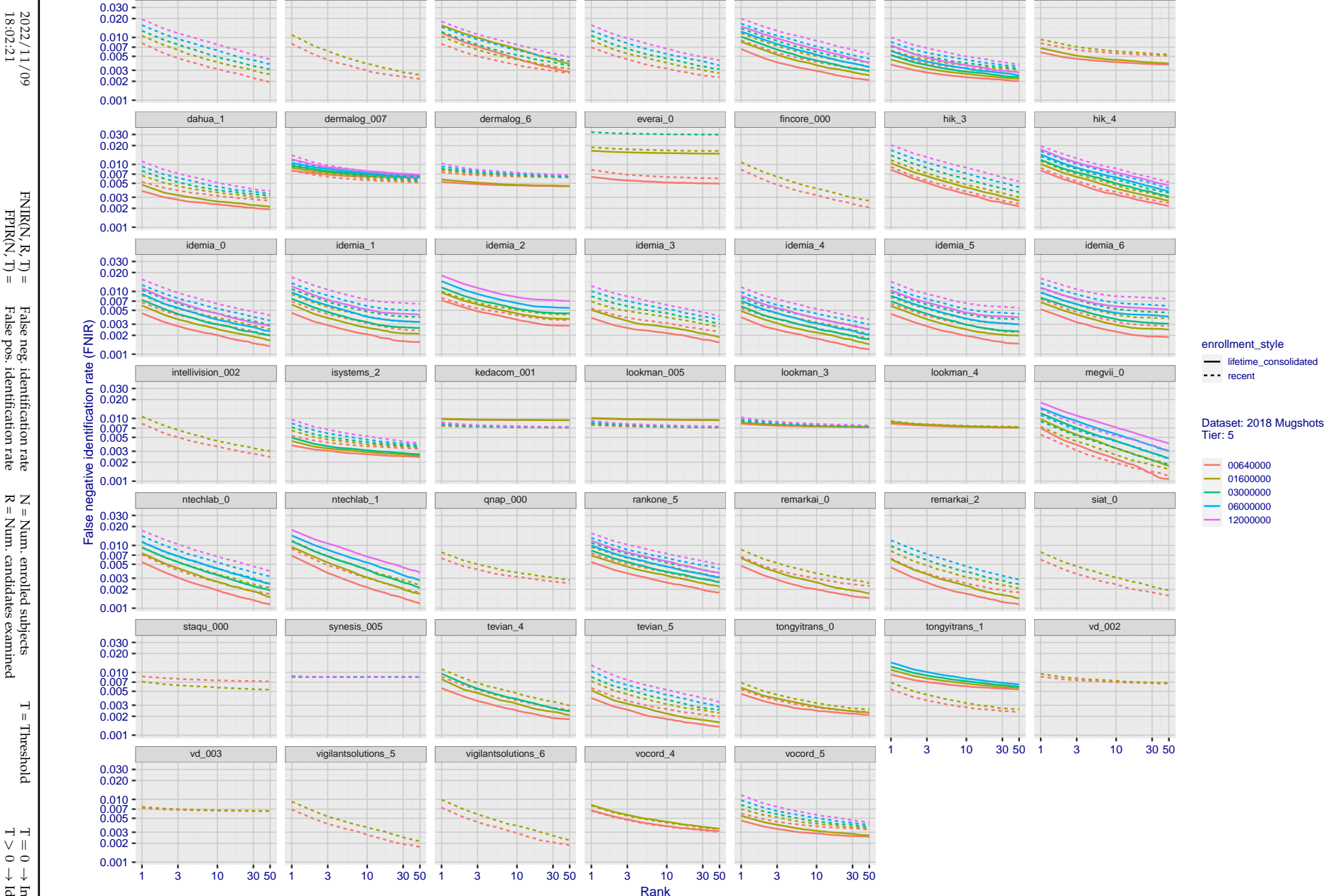


Figure 32: [FRVT-2018 Mugshot Dataset] Rank-based identification miss rates vs. rank. The figure shows false negative identification rates (FNIR) for ranks up to 50. This metric is appropriate to investigational applications where human reviewers will adjudicate sorted candidate lists. Note that with threshold set to zero, FPIR = 1, i.e. any search without an enrolled mate will return non-mated candidates. Results are sorted and reported into tiers for clarity, with the tiering criteria being rank 1 hit rate on a gallery size of N = 640 000 subjects.

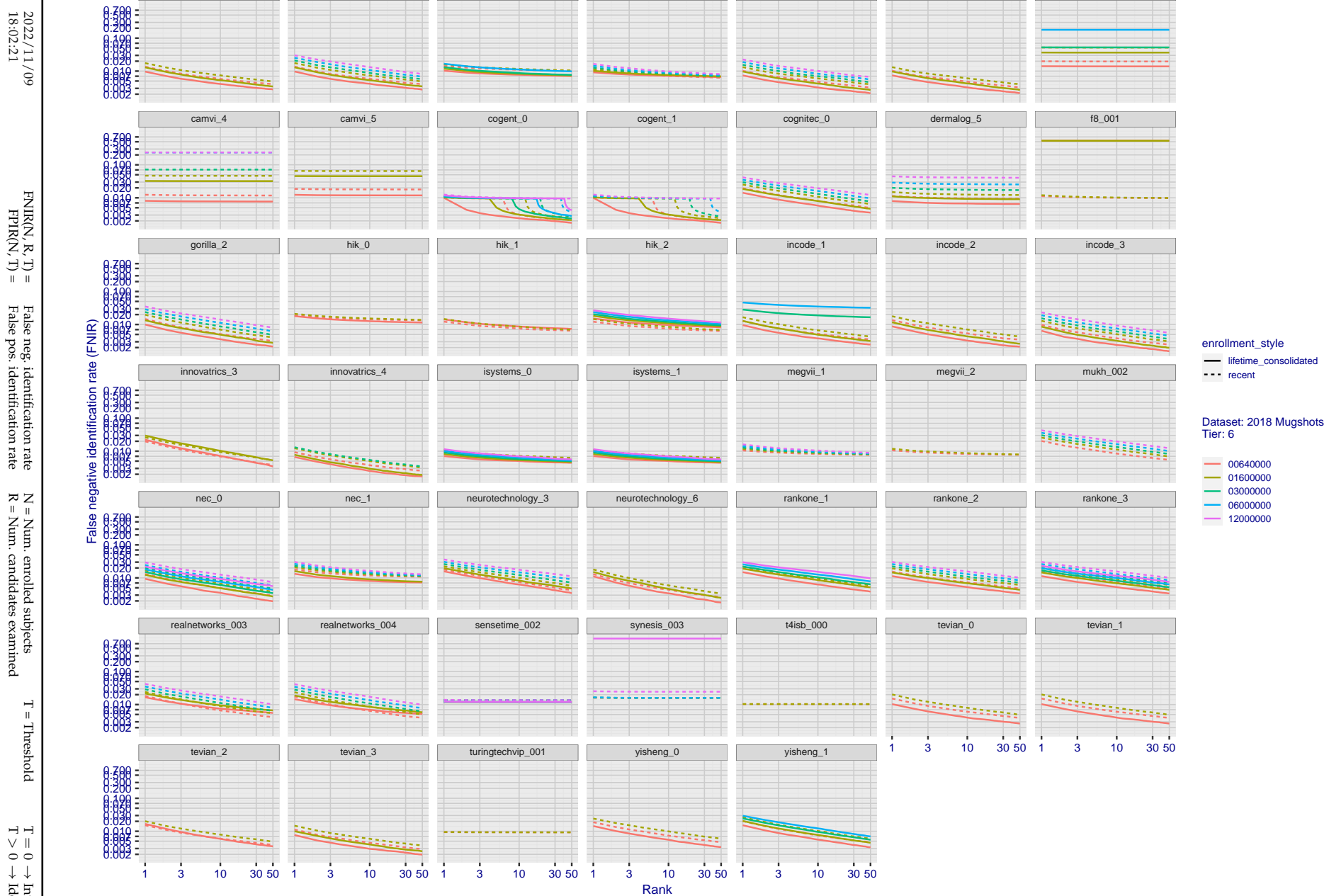


Figure 33: [FRVT-2018 Mugshot Dataset] Rank-based identification miss rates vs. rank. The figure shows false negative identification rates (FNIR) for ranks up to 50. This metric is appropriate to investigational applications where human reviewers will adjudicate sorted candidate lists. Note that with threshold set to zero, FPIR = 1, i.e. any search without an enrolled mate will return non-mated candidates. Results are sorted and reported into tiers for clarity, with the tiering criteria being rank 1 hit rate on a gallery size of N = 640 000 subjects.

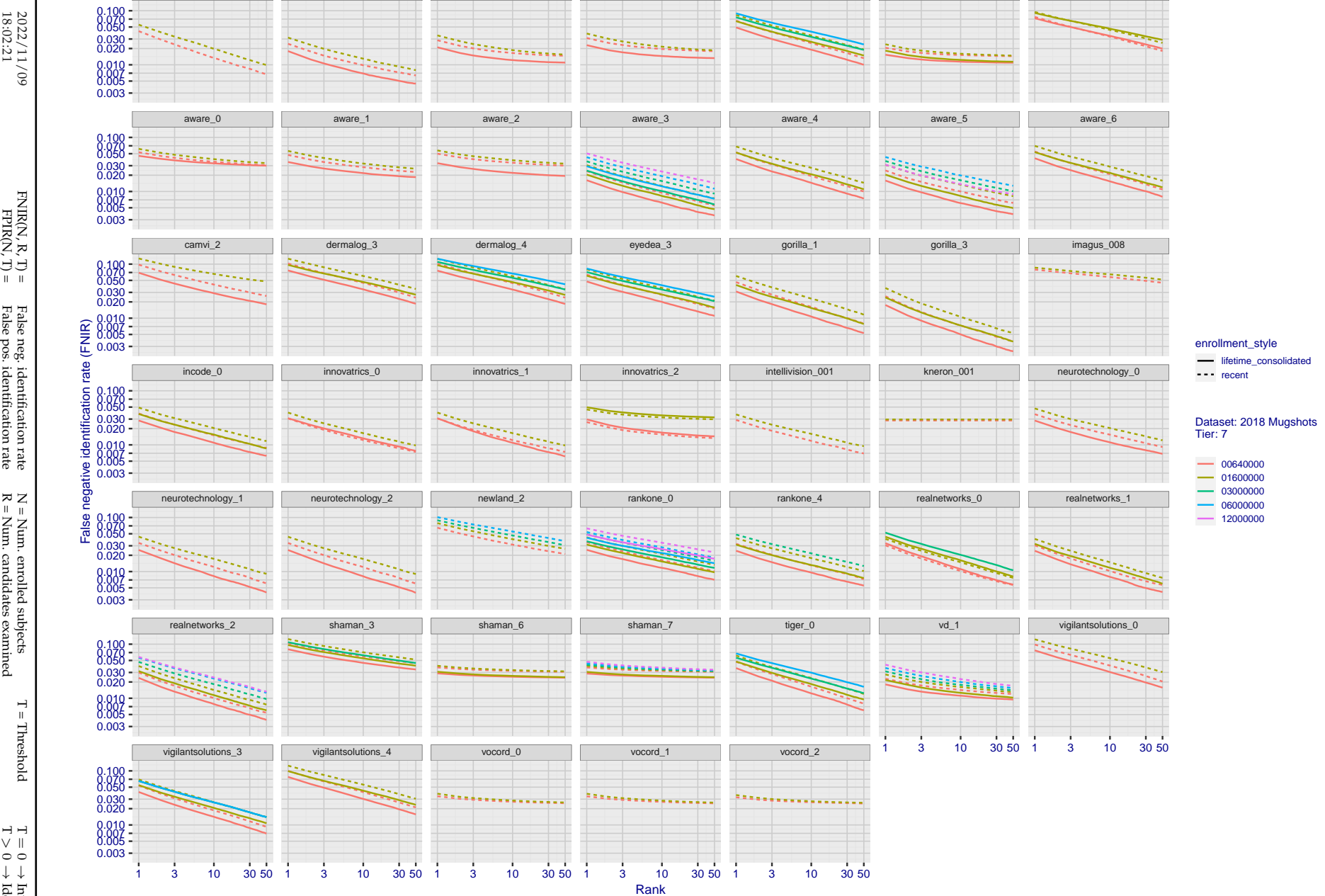


Figure 34: [FRVT-2018 Mugshot Dataset] Rank-based identification miss rates vs. rank. The figure shows false negative identification rates (FNIR) for ranks up to 50. This metric is appropriate to investigational applications where human reviewers will adjudicate sorted candidate lists. Note that with threshold set to zero, FPIR = 1, i.e. any search without an enrolled mate will return non-mated candidates. Results are sorted and reported into tiers for clarity, with the tiering criteria being rank 1 hit rate on a gallery size of N = 640 000 subjects.

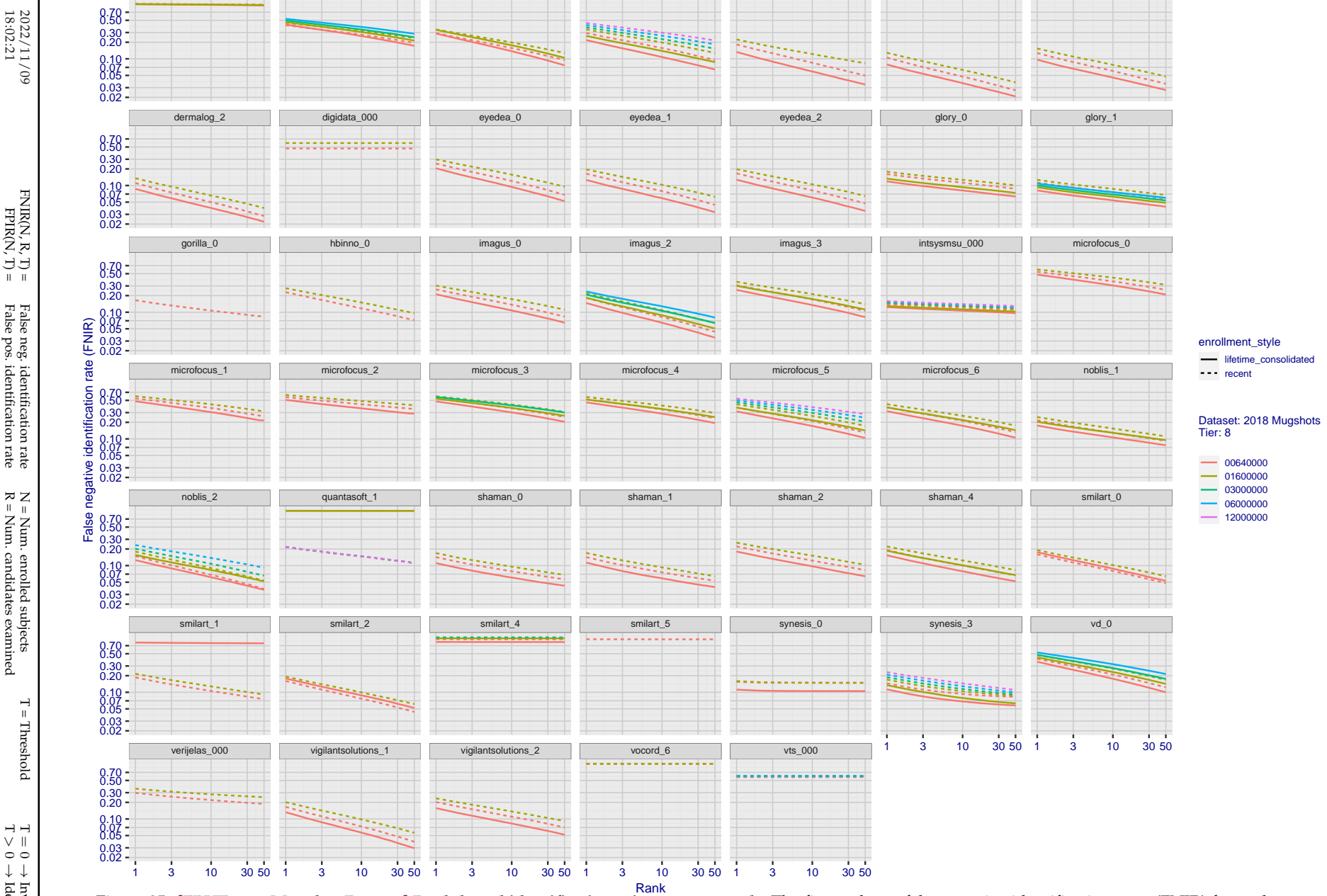


Figure 35: [FRVT-2018 Mugshot Dataset] Rank-based identification miss rates vs. rank. The figure shows false negative identification rates (FNIR) for ranks up to 50. This metric is appropriate to investigational applications where human reviewers will adjudicate sorted candidate lists. Note that with threshold set to zero, FPIR = 1, i.e. any search without an enrolled mate will return non-mated candidates. Results are sorted and reported into tiers for clarity, with the tiering criteria being rank 1 hit rate on a gallery size of N = 640 000 subjects.

2022/11/09
18:02:21

FNIR(N, R, T) = False neg. identification rate
FPTR(N, T) = False pos. identification rate

N = Num. enrolled subjects
R = Num. candidates examined

T = Threshold
T > 0 → Identification

T = 0 → Investigation

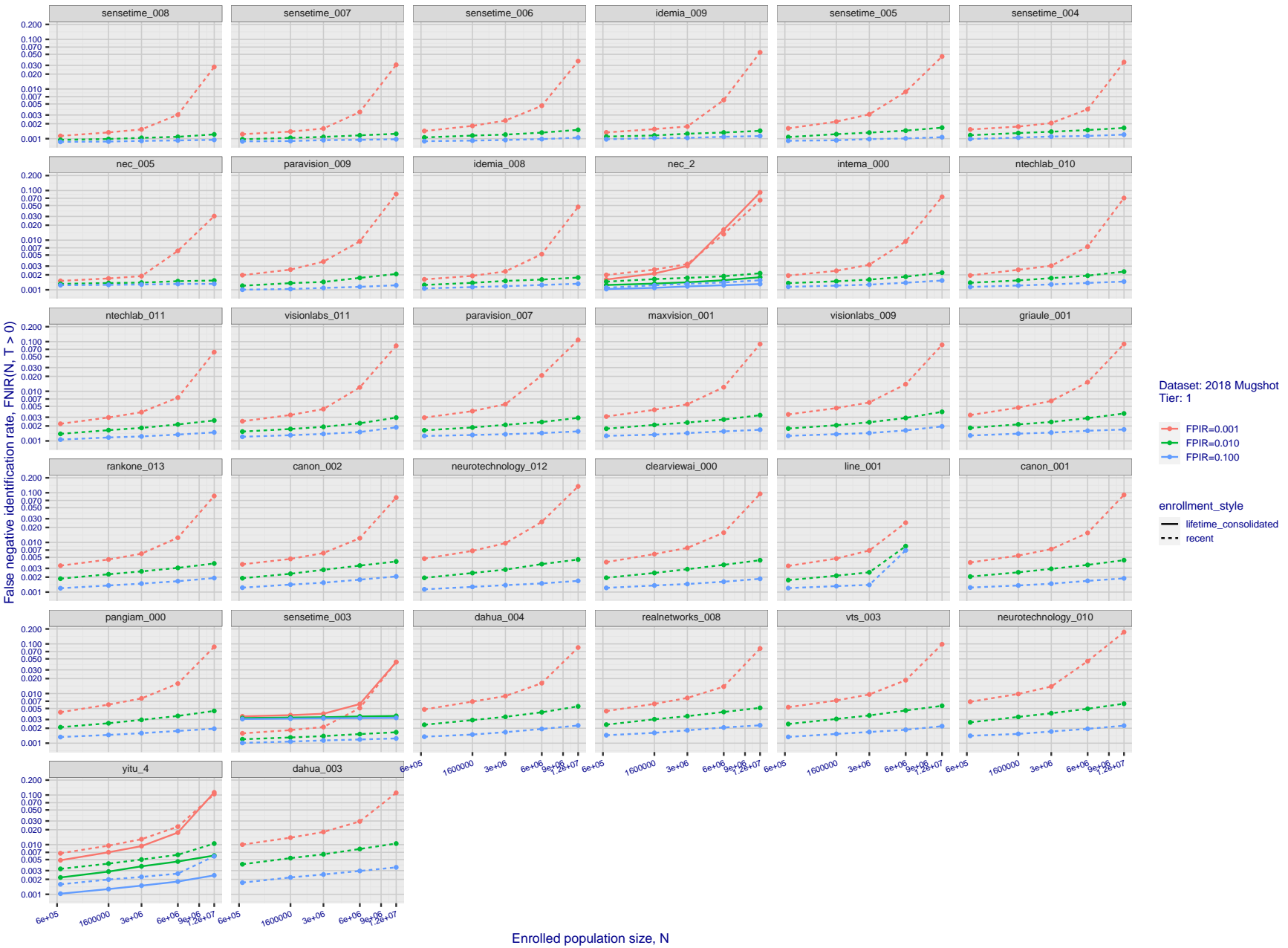
2022/11/09
18:02:21FNIR(N, R, T) = False neg. identification rate
FPIR(N, T) = False pos. identification rateN = Num. enrolled subjects
R = Num. candidates examined
T = ThresholdT = 0 → Investigation
T > 0 → Identification

Figure 36: [FRVT-2018 Mugshot Dataset] Threshold-based identification miss rates vs. number of enrolled subjects. The figure shows FNIR(N, T) across various gallery sizes when the threshold is set to achieve the given FPIRs. The rank criterion is irrelevant at high thresholds as mates are always at rank 1. The results are computed from the trials listed in rows 1-10 of Table 1. Less accurate algorithms were not run on large N , so results are missing. For clarity, results are sorted and reported into tiers spanning multiple pages. The tiering criteria is complicated: First paging by $\text{FNIR}(N_b, 1, 0)$, then sorting by median $\text{FNIR}(N_b, T)$, $N_b = 640\,000$.

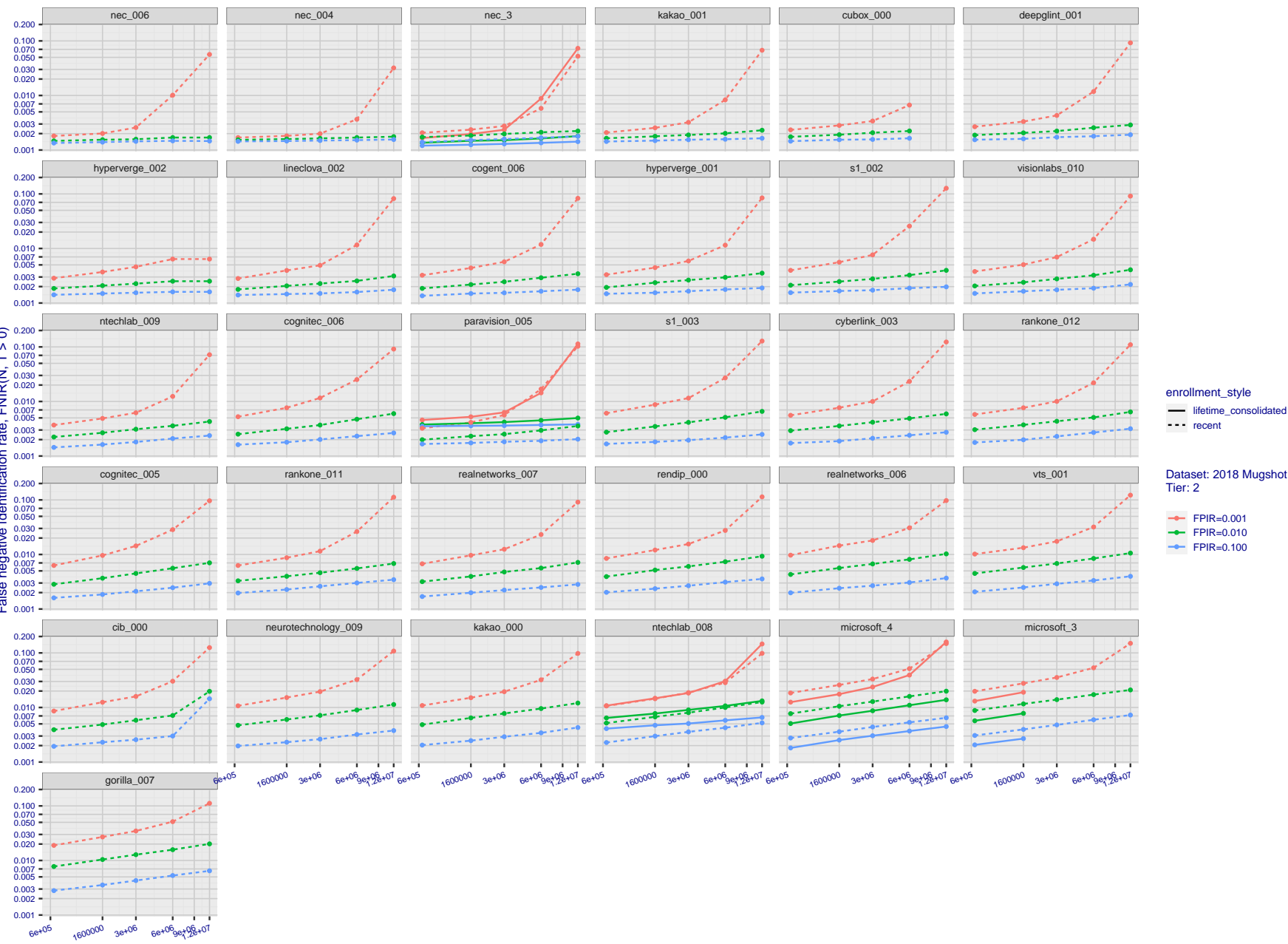
2022/11/09
18:02:21

Figure 37: [FRVT-2018 Mugshot Dataset] Threshold-based identification miss rates vs. number of enrolled subjects. The figure shows $\text{FNIR}(N, T)$ across various gallery sizes when the threshold is set to achieve the given FPIRs. The rank criterion is irrelevant at high thresholds as mates are always at rank 1. The results are computed from the trials listed in rows 1-10 of Table 1. Less accurate algorithms were not run on large N , so results are missing. For clarity, results are sorted and reported into tiers spanning multiple pages. The tiering criteria is complicated: First paging by $\text{FNIR}(N_b, 1, 0)$, then sorting by median $\text{FNIR}(N_b, T)$, $N_b = 640\,000$.

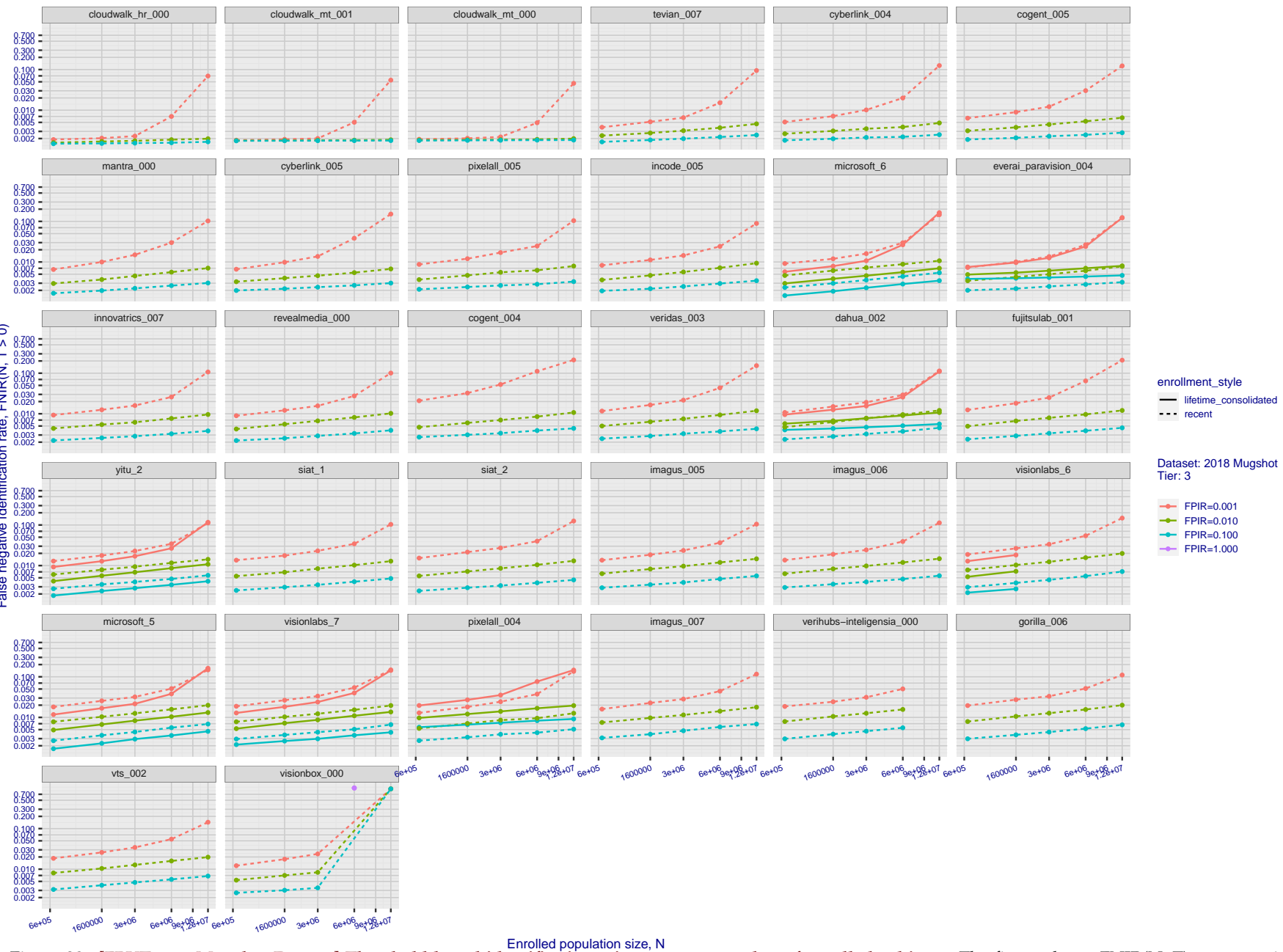
2022/11/09
18:02:21

Figure 38: [FRVT-2018 Mugshot Dataset] Threshold-based identification miss rates vs. number of enrolled subjects. The figure shows FNIR(N, T) across various gallery sizes when the threshold is set to achieve the given FPIRs. The rank criterion is irrelevant at high thresholds as mates are always at rank 1. The results are computed from the trials listed in rows 1-10 of Table 1. Less accurate algorithms were not run on large N , so results are missing. For clarity, results are sorted and reported into tiers spanning multiple pages. The tiering criteria is complicated: First paging by FNIR($N_b, 1, 0$), then sorting by median FNIR(N_b, T), $N_b = 640\,000$.

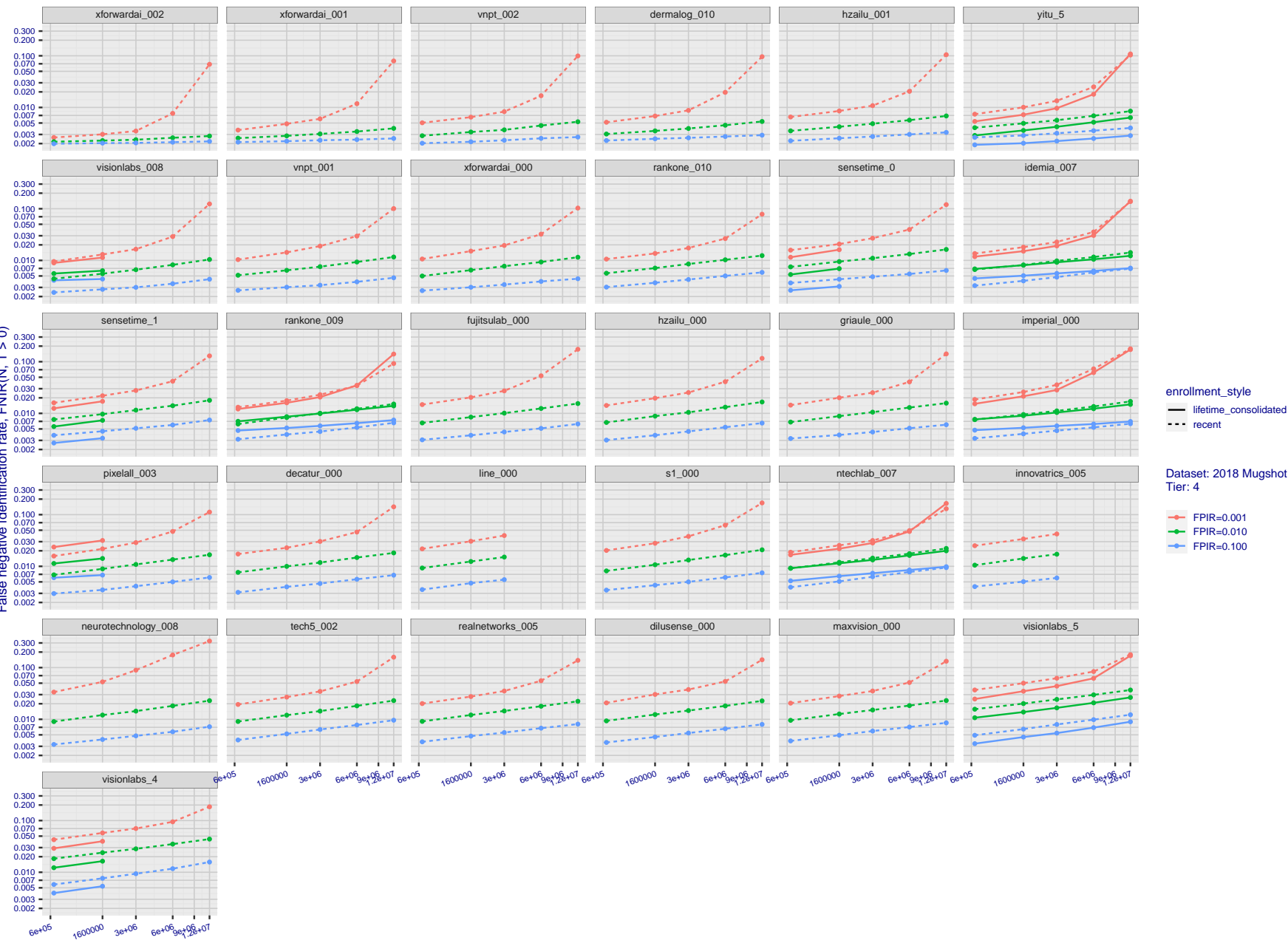
2022/11/09
18:02:21

Figure 39: [FRVT-2018 Mugshot Dataset] Threshold-based identification miss rates vs. number of enrolled subjects. The figure shows $\text{FNIR}(N, T)$ across various gallery sizes when the threshold is set to achieve the given FPIRs. The rank criterion is irrelevant at high thresholds as mates are always at rank 1. The results are computed from the trials listed in rows 1-10 of Table 1. Less accurate algorithms were not run on large N , so results are missing. For clarity, results are sorted and reported into tiers spanning multiple pages. The tiering criteria is complicated: First paging by $\text{FNIR}(N_b, 1, 0)$, then sorting by median $\text{FNIR}(N_b, T)$, $N_b = 640\,000$.

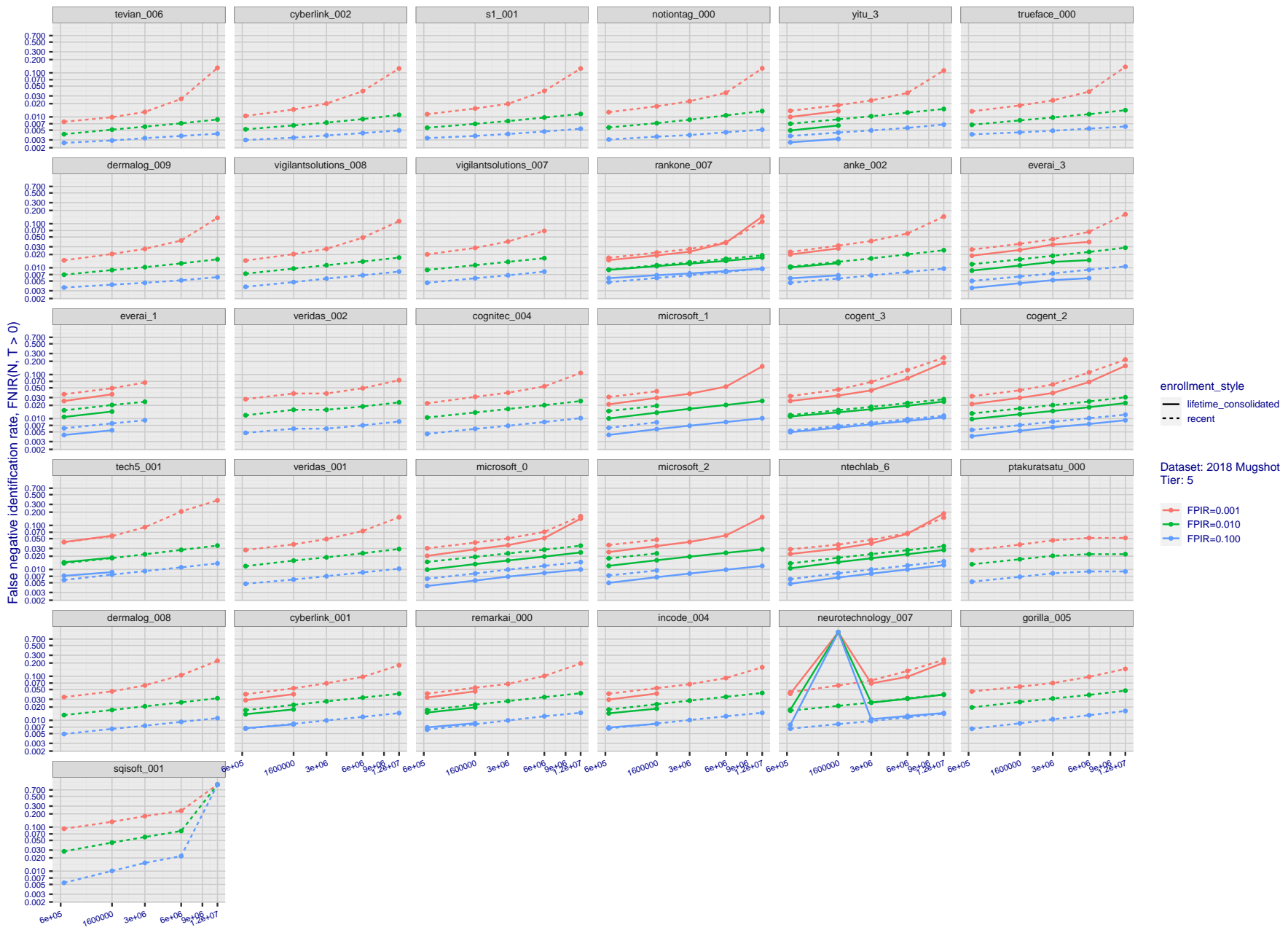


Figure 40: [FRVT-2018 Mugshot Dataset] Threshold-based identification miss rates vs. number of enrolled subjects. The figure shows FNIR(N, T) across various gallery sizes when the threshold is set to achieve the given FPIRs. The rank criterion is irrelevant at high thresholds as mates are always at rank 1. The results are computed from the trials listed in rows 1-10 of Table 1. Less accurate algorithms were not run on large N , so results are missing. For clarity, results are sorted and reported into tiers spanning multiple pages. The tiering criteria is complicated: First paging by $\text{FNIR}(N_b, 1, 0)$, then sorting by median $\text{FNIR}(N_b, T)$, $N_b = 640\,000$.

2022/11/09
18:02:21FNIR(N, R, T) = False neg. identification rate
FPFR(N, T) = False pos. identification rateN = Num. enrolled subjects
R = Num. candidates examined

T = Threshold

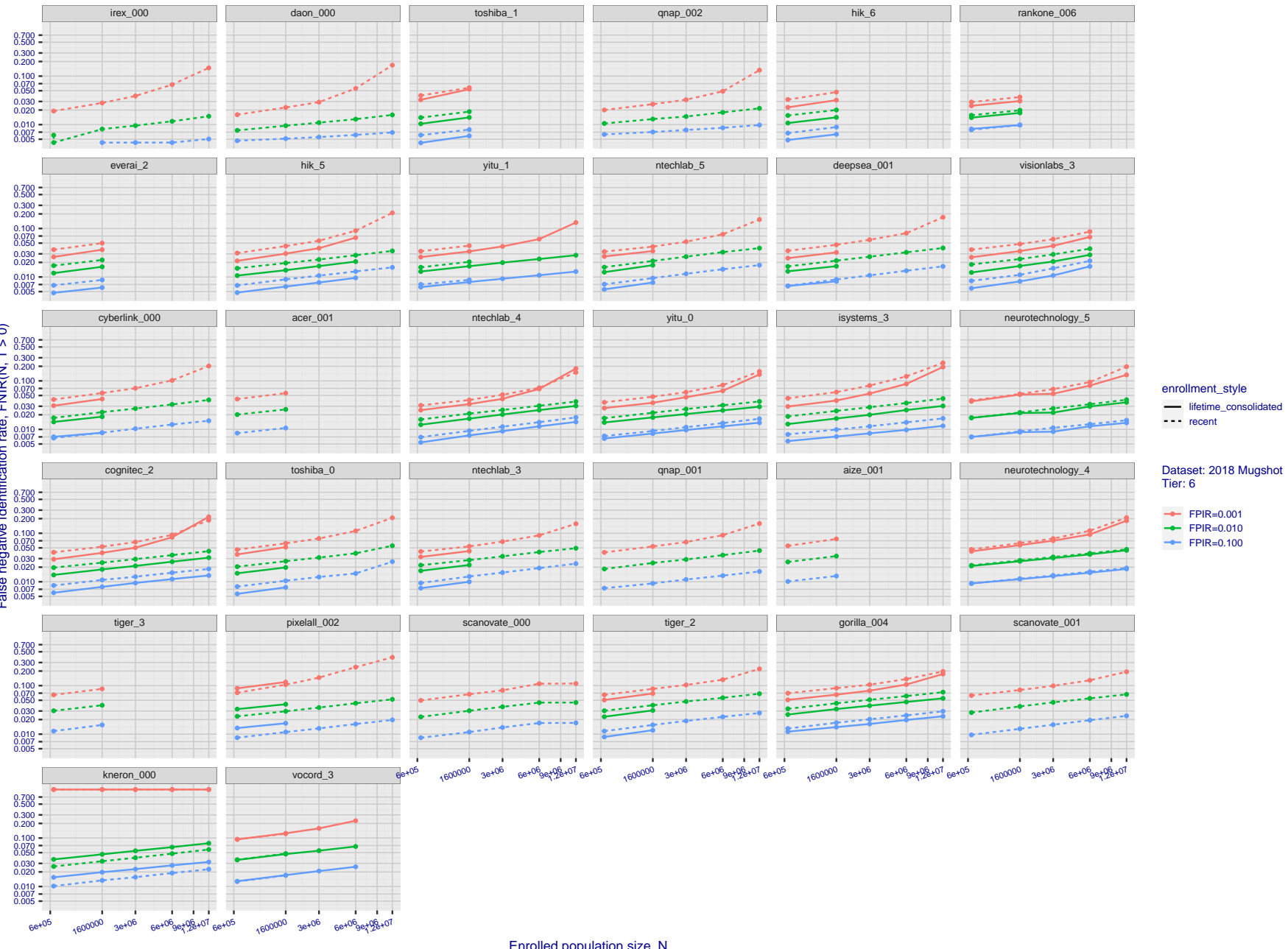
T = 0 → Investigation
T > 0 → Identification

Figure 41: [FRVT-2018 Mugshot Dataset] Threshold-based identification miss rates vs. number of enrolled subjects. The figure shows FNIR(N, T) across various gallery sizes when the threshold is set to achieve the given FPIRs. The rank criterion is irrelevant at high thresholds as mates are always at rank 1. The results are computed from the trials listed in rows 1-10 of Table 1. Less accurate algorithms were not run on large N, so results are missing. For clarity, results are sorted and reported into tiers spanning multiple pages. The tiering criteria is complicated: First paging by FNIR(N_b , 1, 0), then sorting by median FNIR(N_b , T), $N_b = 640\,000$.

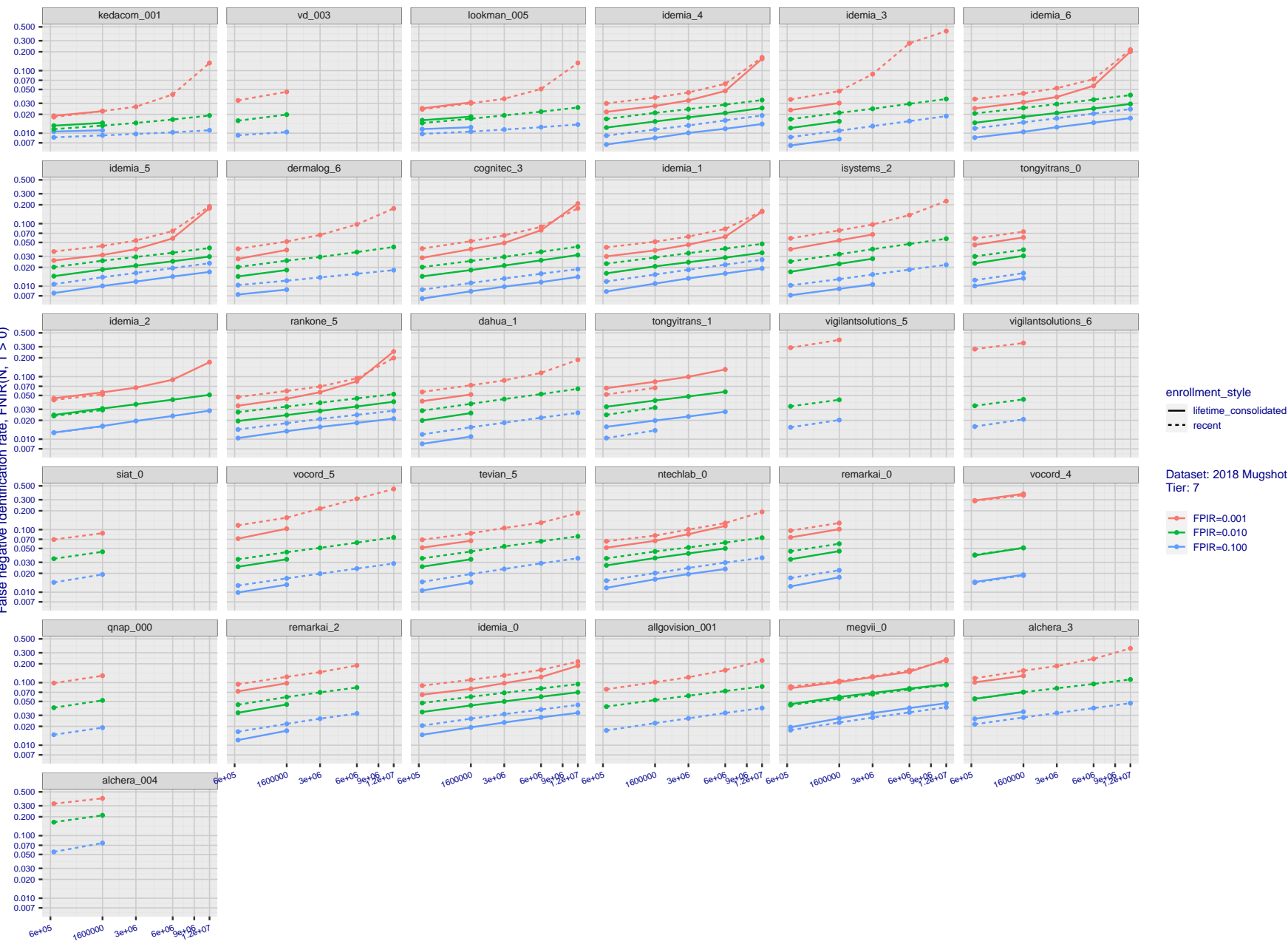
2022/11/09
18:02:21

Figure 42: [FRVT-2018 Mugshot Dataset] Threshold-based identification miss rates vs. number of enrolled subjects. The figure shows FNIR(N, T) across various gallery sizes when the threshold is set to achieve the given FPIRs. The rank criterion is irrelevant at high thresholds as mates are always at rank 1. The results are computed from the trials listed in rows 1-10 of Table 1. Less accurate algorithms were not run on large N , so results are missing. For clarity, results are sorted and reported into tiers spanning multiple pages. The tiering criteria is complicated: First paging by $\text{FNIR}(N_b, 1, 0)$, then sorting by median $\text{FNIR}(N_b, T)$, $N_b = 640\,000$.

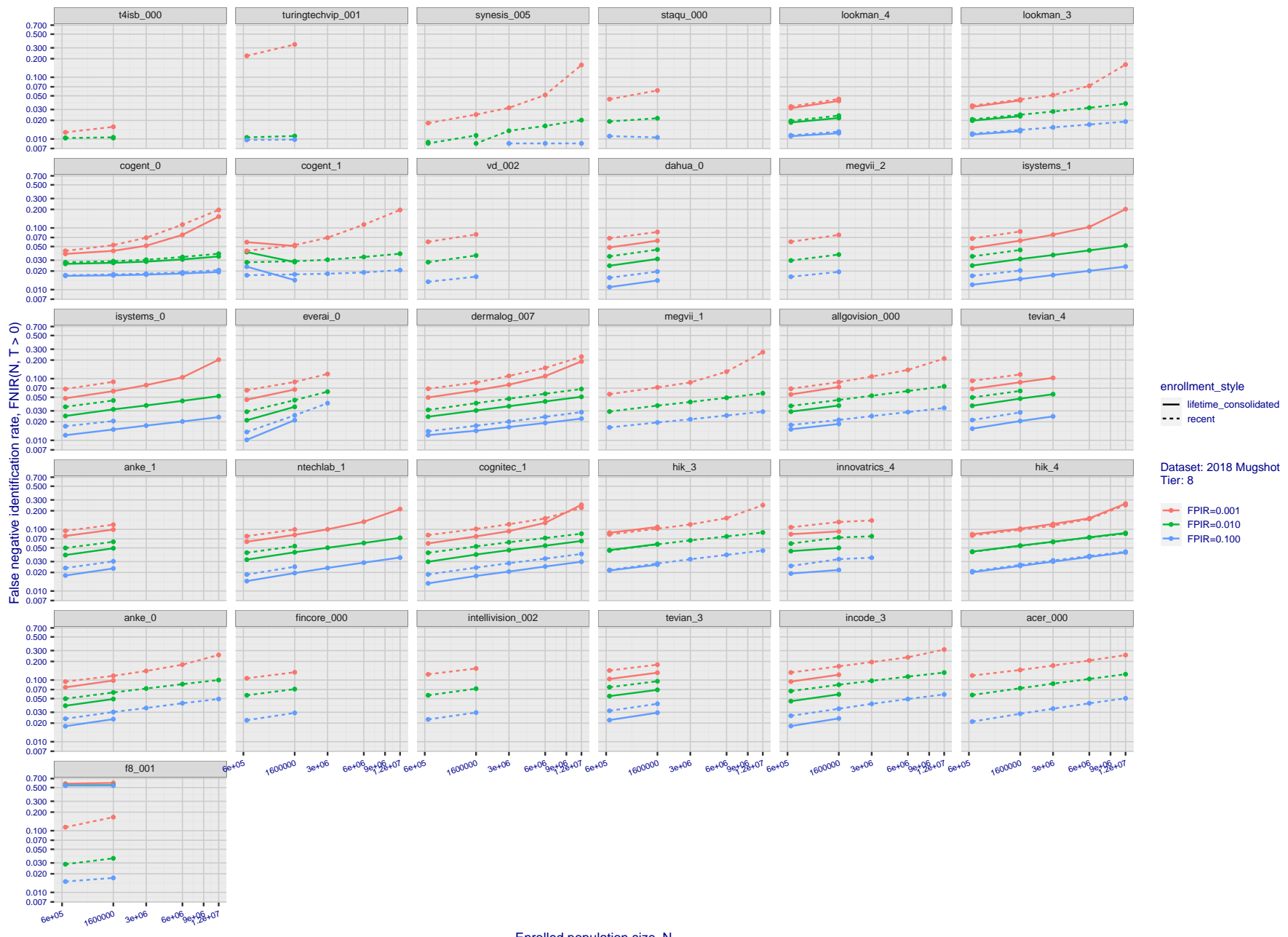


Figure 43: [FRVT-2018 Mugshot Dataset] Threshold-based identification miss rates vs. number of enrolled subjects. The figure shows $\text{FNIR}(N, T)$ across various gallery sizes when the threshold is set to achieve the given FPIRs. The rank criterion is irrelevant at high thresholds as mates are always at rank 1. The results are computed from the trials listed in rows 1-10 of Table 1. Less accurate algorithms were not run on large N , so results are missing. For clarity, results are sorted and reported into tiers spanning multiple pages. The tiering criteria is complicated: First paging by $\text{FNIR}(N_b, 1, 0)$, then sorting by median $\text{FNIR}(N_b, T)$, $N_b = 640\,000$.

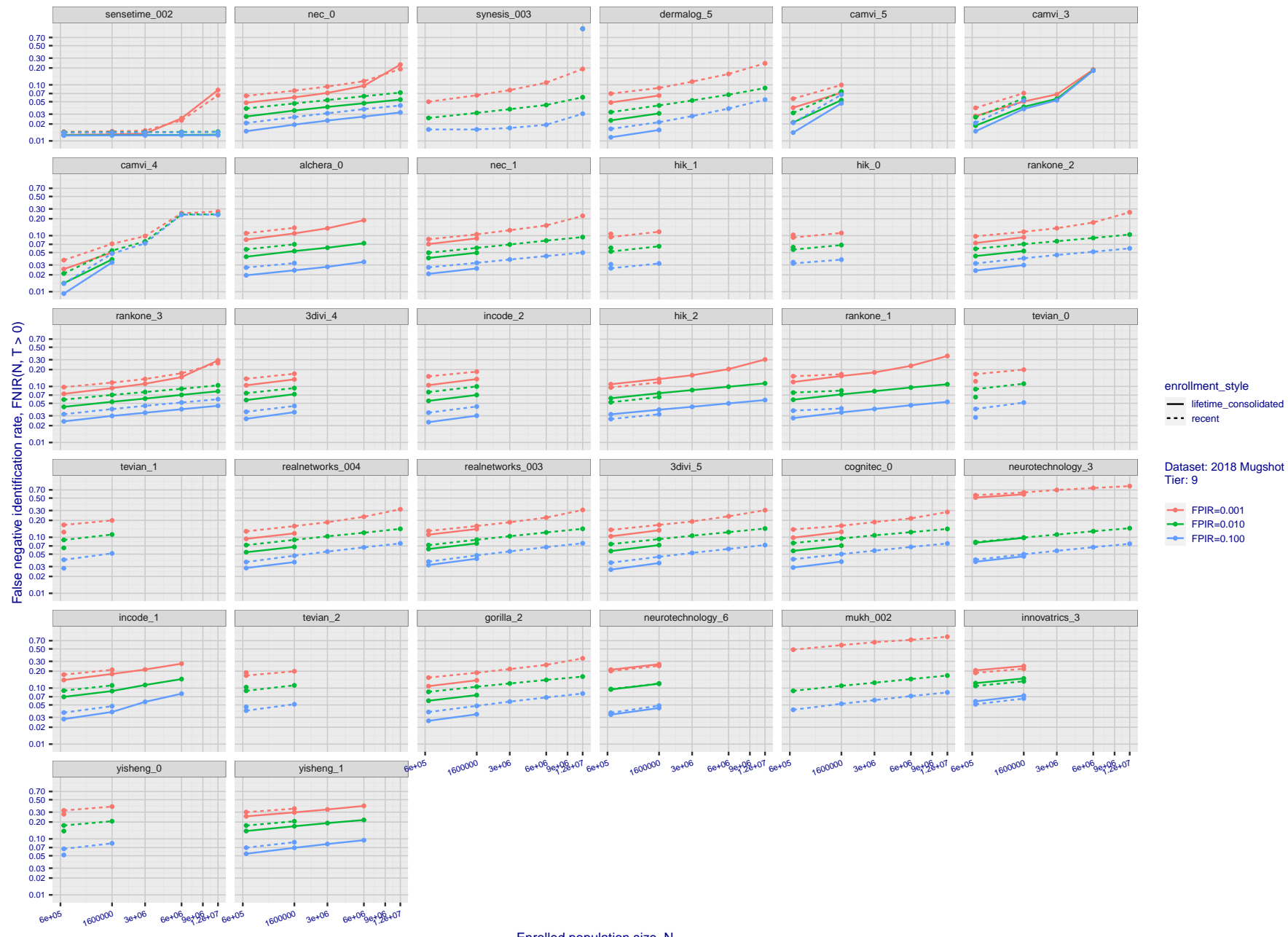
2022/11/09
18:02:21

Figure 44: [FRVT-2018 Mugshot Dataset] Threshold-based identification miss rates vs. number of enrolled subjects. The figure shows $\text{FNIR}(N, T)$ across various gallery sizes when the threshold is set to achieve the given FPIRs. The rank criterion is irrelevant at high thresholds as mates are always at rank 1. The results are computed from the trials listed in rows 1-10 of Table 1. Less accurate algorithms were not run on large N , so results are missing. For clarity, results are sorted and reported into tiers spanning multiple pages. The tiering criteria is complicated: First paging by $\text{FNIR}(N_b, 1, 0)$, then sorting by median $\text{FNIR}(N_b, T)$, $N_b = 640\,000$.

2022/11/09
18:02:21FNIR(N, R, T) = False neg. identification rate
FPFR(N, T) = False pos. identification rateN = Num. enrolled subjects
R = Num. candidates examined

T = Threshold

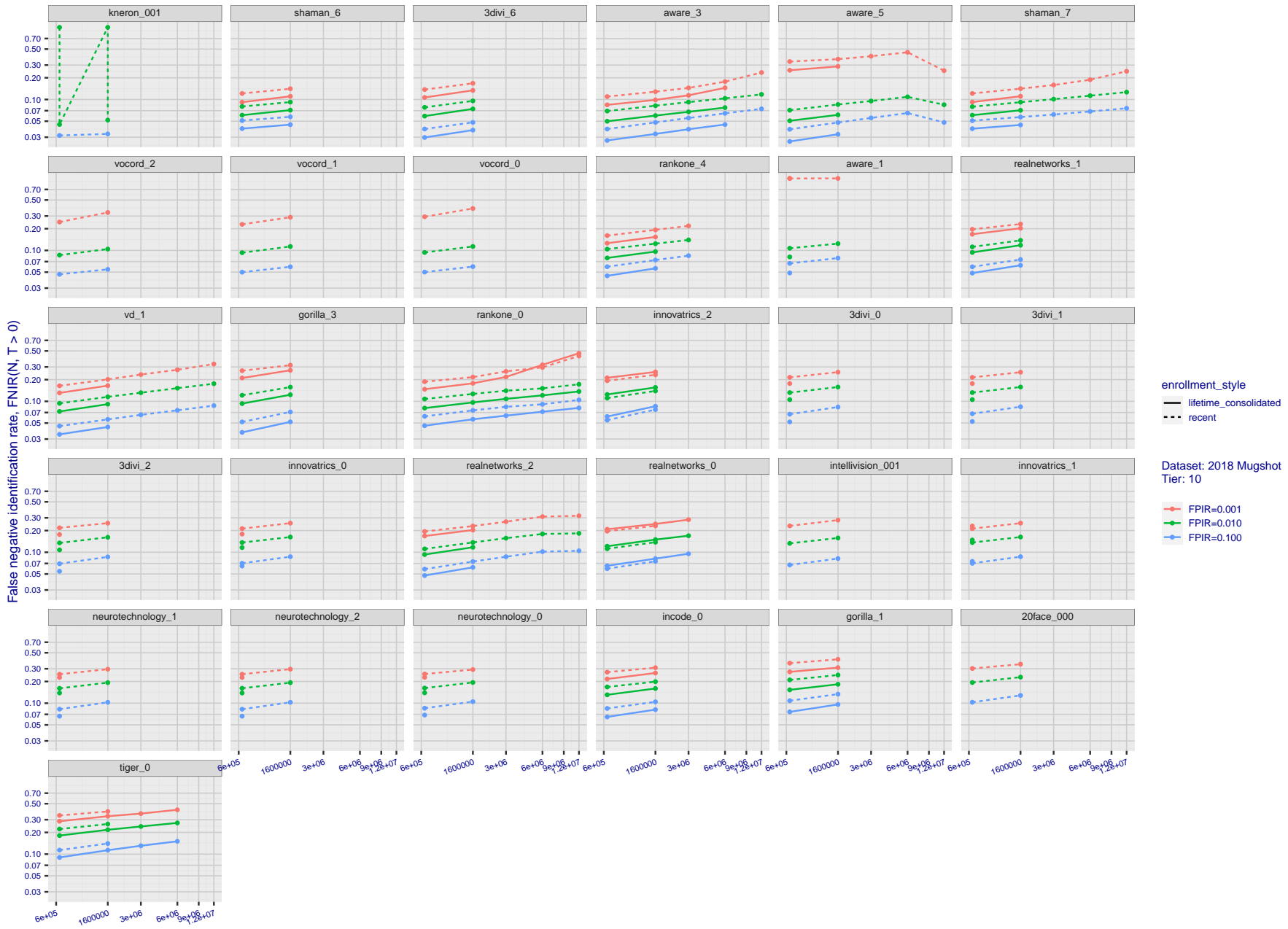
T = 0 → Investigation
T > 0 → Identification

Figure 45: [FRVT-2018 Mugshot Dataset] Threshold-based identification miss rates vs. number of enrolled subjects. The figure shows $\text{FNIR}(N, T)$ across various gallery sizes when the threshold is set to achieve the given FPIRs. The rank criterion is irrelevant at high thresholds as mates are always at rank 1. The results are computed from the trials listed in rows 1-10 of Table 1. Less accurate algorithms were not run on large N , so results are missing. For clarity, results are sorted and reported into tiers spanning multiple pages. The tiering criteria is complicated: First paging by $\text{FNIR}(N_b, 1, 0)$, then sorting by median $\text{FNIR}(N_b, T)$, $N_b = 640\,000$.

2022/11/09
18:02:21FNIR(N, R, T) = False neg. identification rate
FPFR(N, T) = False pos. identification rateN = Num. enrolled subjects
R = Num. candidates examined

T = Threshold

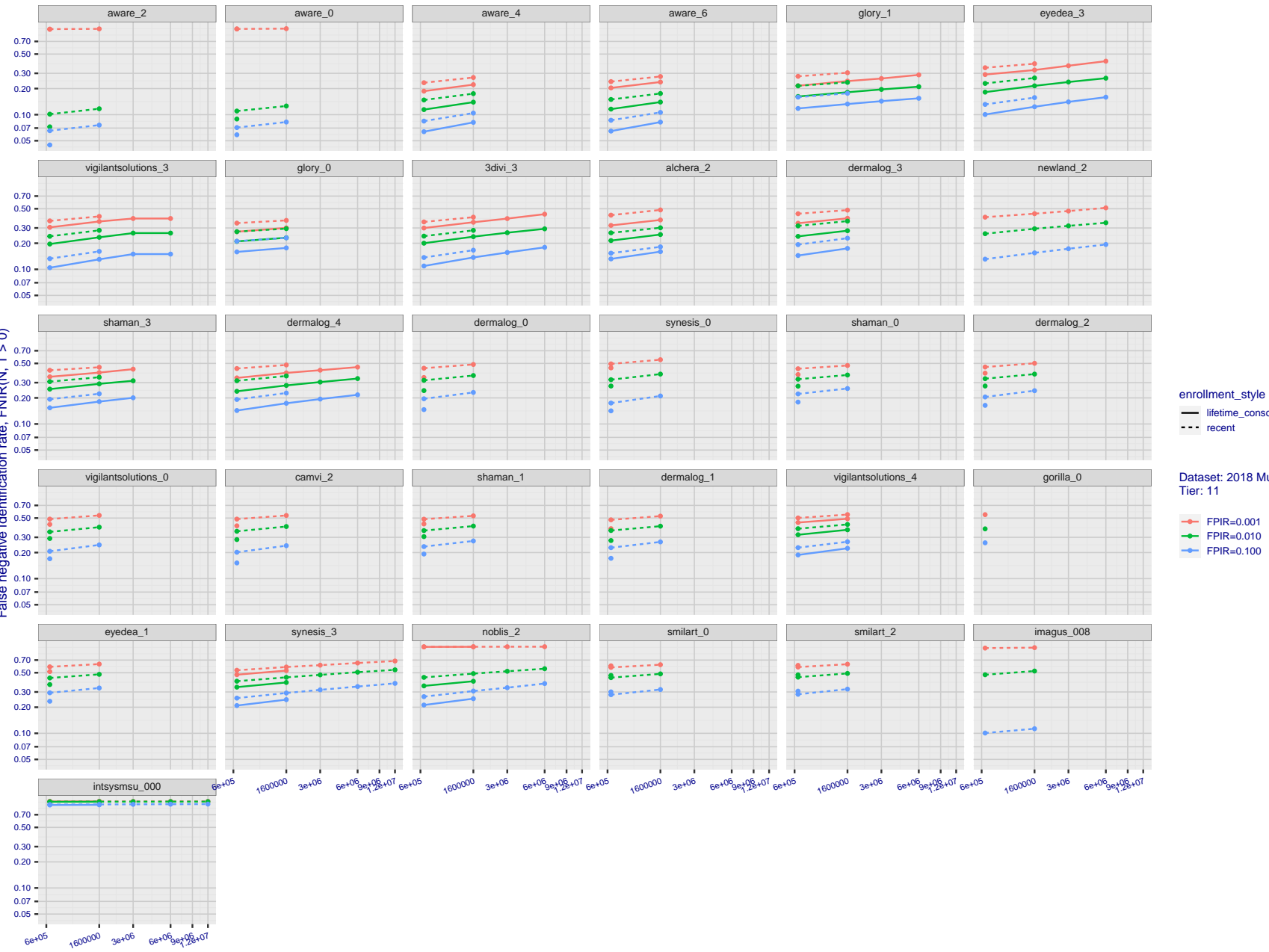
T = 0 → Investigation
T > 0 → Identification

Figure 46: [FRVT-2018 Mugshot Dataset] Threshold-based identification miss rates vs. number of enrolled subjects. The figure shows $\text{FNIR}(N, T)$ across various gallery sizes when the threshold is set to achieve the given FPIRs. The rank criterion is irrelevant at high thresholds as mates are always at rank 1. The results are computed from the trials listed in rows 1-10 of Table 1. Less accurate algorithms were not run on large N , so results are missing. For clarity, results are sorted and reported into tiers spanning multiple pages. The tiering criteria is complicated: First paging by $\text{FNIR}(N_b, 1, 0)$, then sorting by median $\text{FNIR}(N_b, T)$, $N_b = 640\,000$.

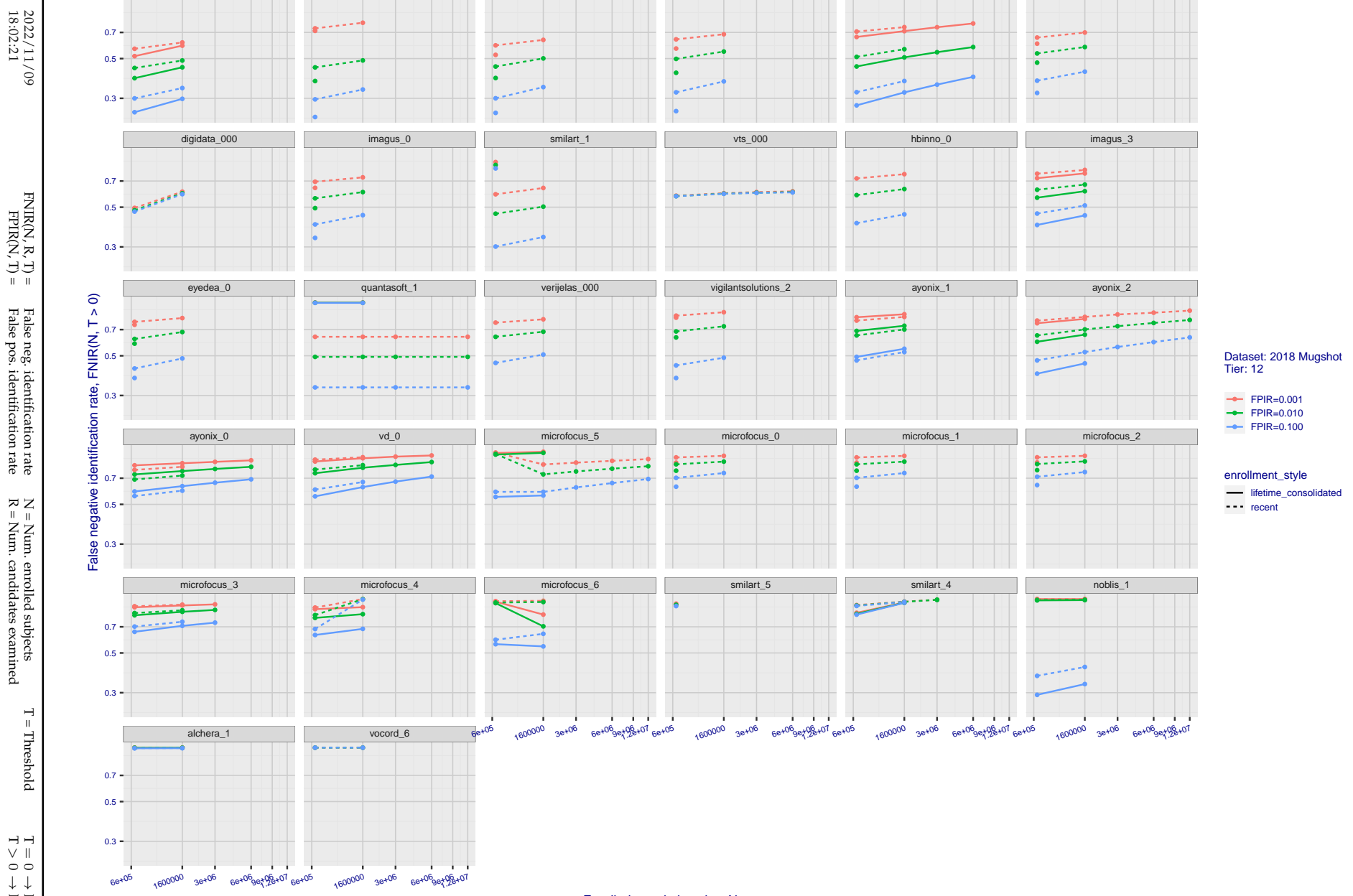


Figure 47: [FRVT-2018 Mugshot Dataset] Threshold-based identification miss rates vs. number of enrolled subjects. The figure shows FNIR(N, T) across various gallery sizes when the threshold is set to achieve the given FPIRs. The rank criterion is irrelevant at high thresholds as mates are always at rank 1. The results are computed from the trials listed in rows 1-10 of Table 1. Less accurate algorithms were not run on large N, so results are missing. For clarity, results are sorted and reported into tiers spanning multiple pages. The tiering criteria is complicated: First paging by $\text{FNIR}(N_b, 1, 0)$, then sorting by median $\text{FNIR}(N_b, T)$, $N_b = 640\,000$.

2022/11/09
18:02:21

$\text{FNIR}(N, R, T) =$	False neg. identification rate	$N =$ Num. enrolled subjects	$T =$ Threshold	$T = 0 \rightarrow$ Investigation
$\text{FPIR}(N, T) =$	False pos. identification rate	$R =$ Num. candidates examined	$T > 0 \rightarrow$ Identification	

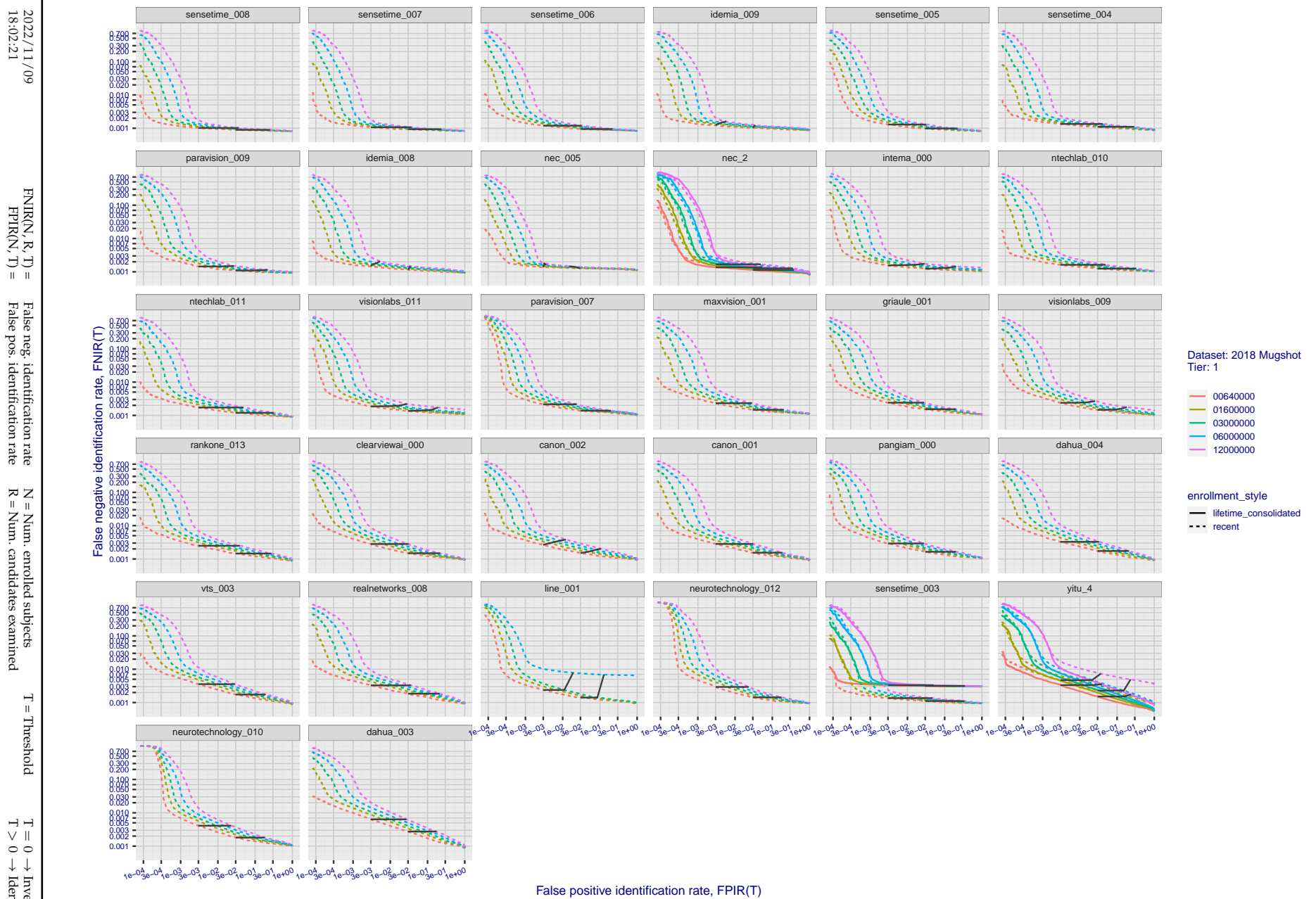


Figure 48: [FRVT-2018 Mugshot Dataset] Identification miss rates vs. false positive rates. The figure shows miss rates $\text{FNIR}(N, L, T)$ as a function of $\text{FPIR}(N, T)$, with N ranging from 640 000 to 12 000 000 as noted in rows 1-10 of Table 1. These error tradeoff characteristics are useful for applications where a threshold must be elevated to limit false positives, such as when human reviewer labor is not matched to the volume of searches. Dark lines join points of equal threshold: If horizontal, $\text{FPIR}(T)$ rises with N , and mate scores are independent of N . Other algorithms adjust scores in an attempt to make FPIR independent of N .

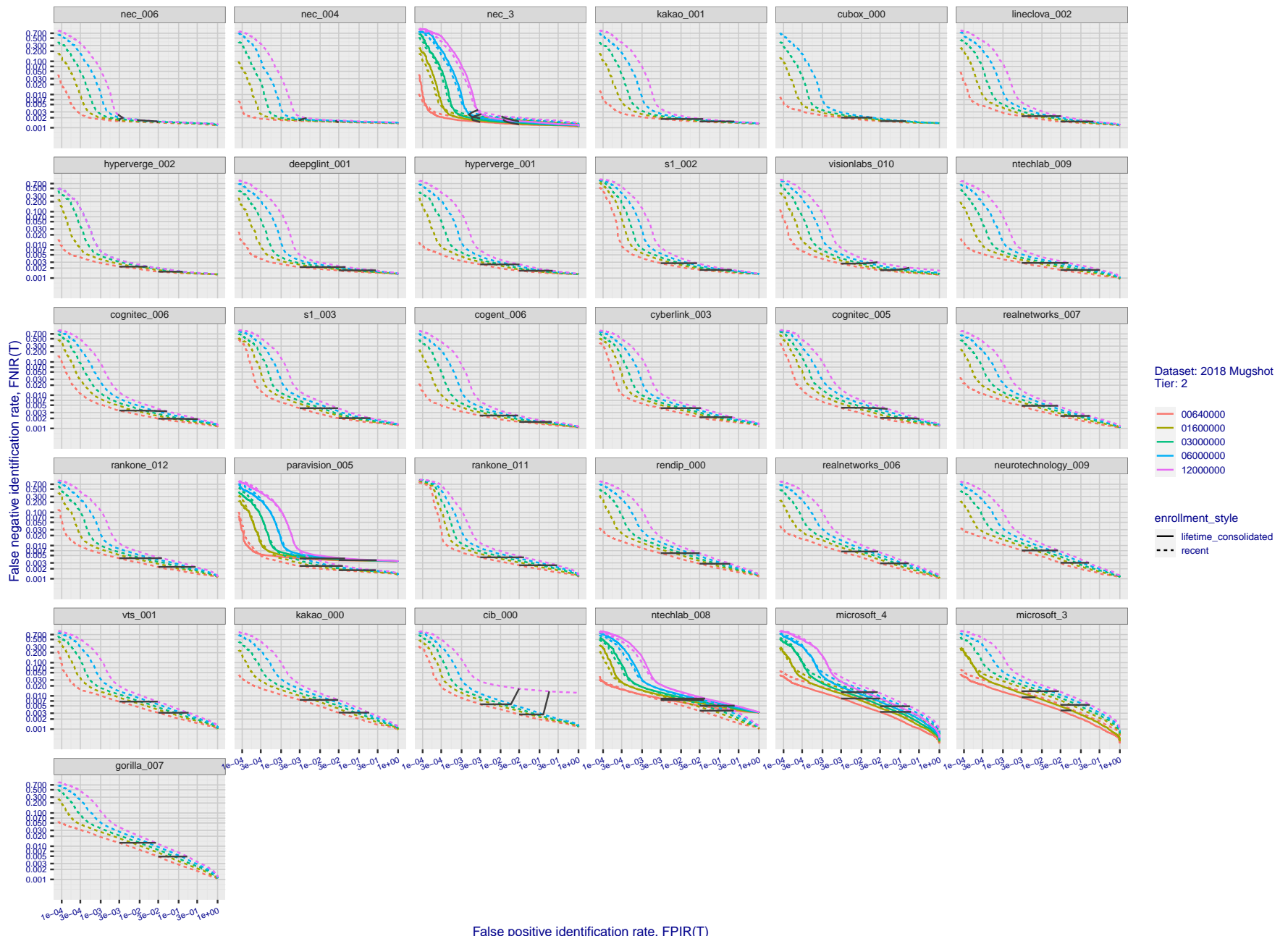


Figure 49: [FRVT-2018 Mugshot Dataset] Identification miss rates vs. false positive rates. The figure shows miss rates $\text{FNIR}(N, L, T)$ as a function of $\text{FPIR}(N, T)$, with N ranging from 640 000 to 12 000 000 as noted in rows 1-10 of Table 1. These error tradeoff characteristics are useful for applications where a threshold must be elevated to limit false positives, such as when human reviewer labor is not matched to the volume of searches. Dark lines join points of equal threshold: If horizontal, $\text{FPIR}(T)$ rises with N , and mate scores are independent of N . Other algorithms adjust scores in an attempt to make FPIR independent of N .

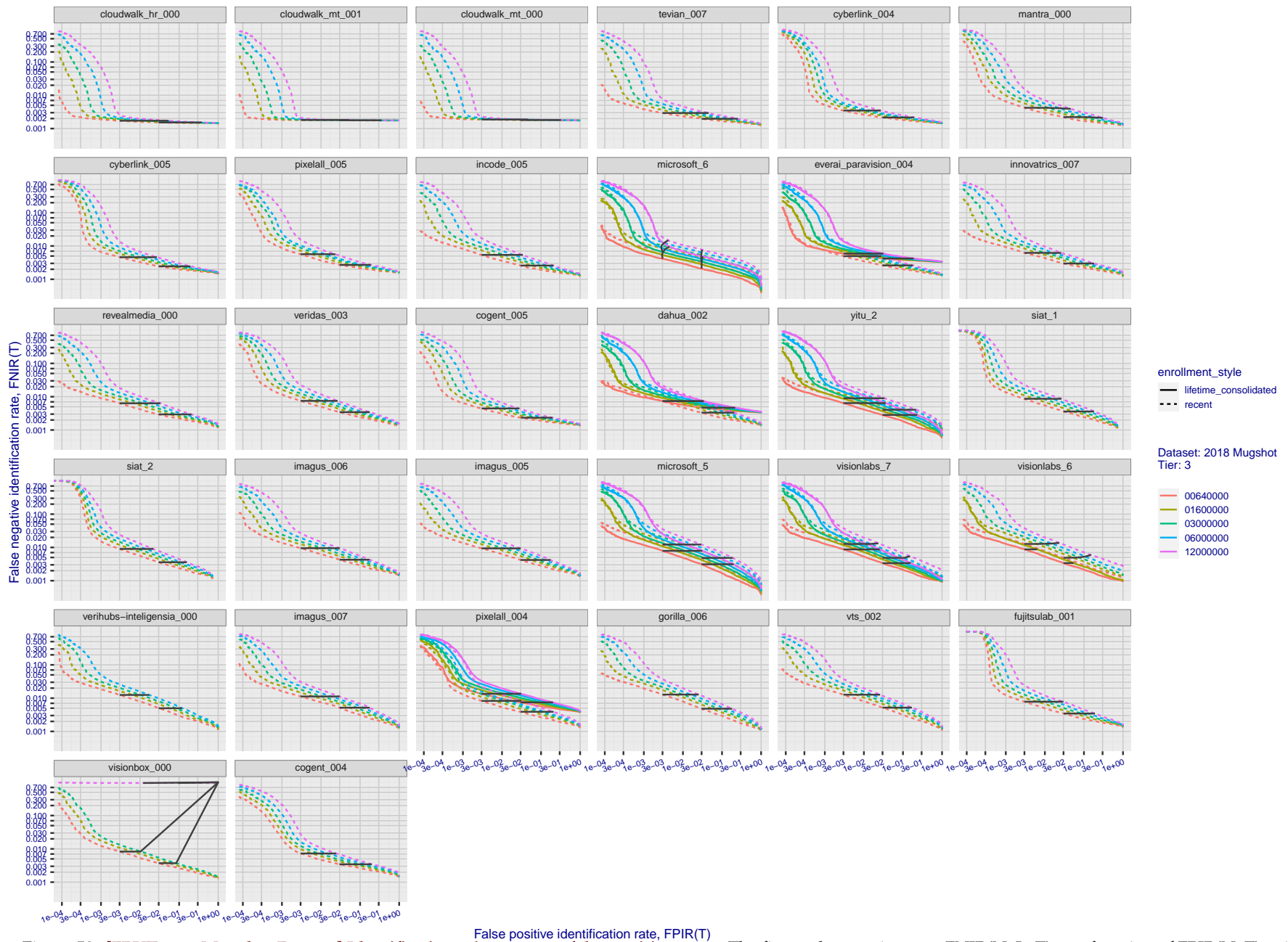


Figure 50: [FRVT-2018 Mugshot Dataset] Identification miss rates vs. false positive rates. The figure shows miss rates $\text{FNIR}(N, L, T)$ as a function of $\text{FPIR}(N, T)$, with N ranging from 640 000 to 12 000 000 as noted in rows 1-10 of Table 1. These error tradeoff characteristics are useful for applications where a threshold must be elevated to limit false positives, such as when human reviewer labor is not matched to the volume of searches. Dark lines join points of equal threshold: If horizontal, $\text{FPIR}(T)$ rises with N , and mate scores are independent of N . Other algorithms adjust scores in an attempt to make FPIR independent of N .

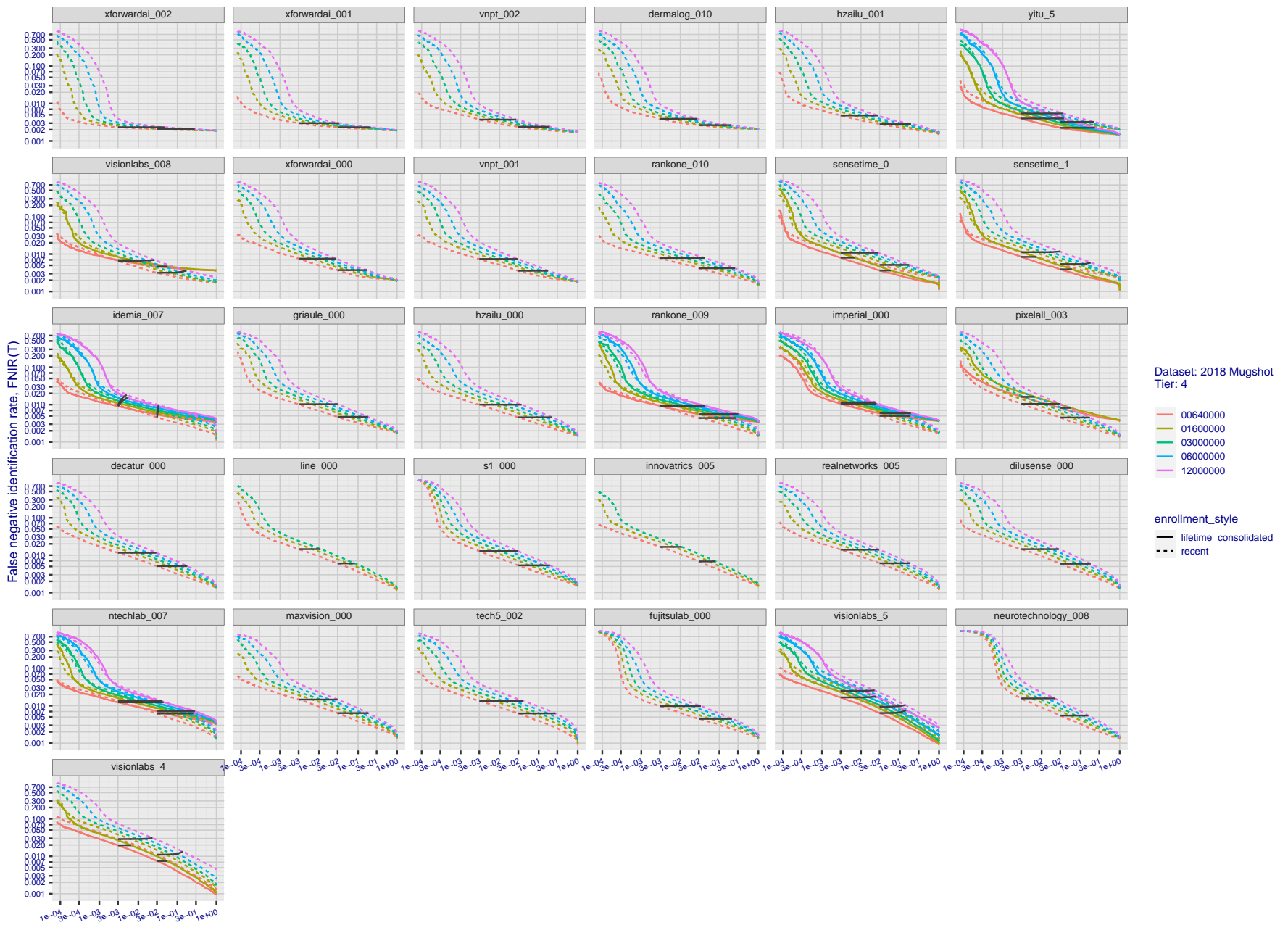


Figure 51: [FRVT-2018 Mugshot Dataset] Identification miss rates vs. false positive rates. The figure shows miss rates $\text{FNIR}(N, L, T)$ as a function of $\text{FPIR}(N, T)$, with N ranging from 640 000 to 12 000 000 as noted in rows 1-10 of Table 1. These error tradeoff characteristics are useful for applications where a threshold must be elevated to limit false positives, such as when human reviewer labor is not matched to the volume of searches. Dark lines join points of equal threshold: If horizontal, $\text{FPIR}(T)$ rises with N , and mate scores are independent of N . Other algorithms adjust scores in an attempt to make FPIR independent of N .

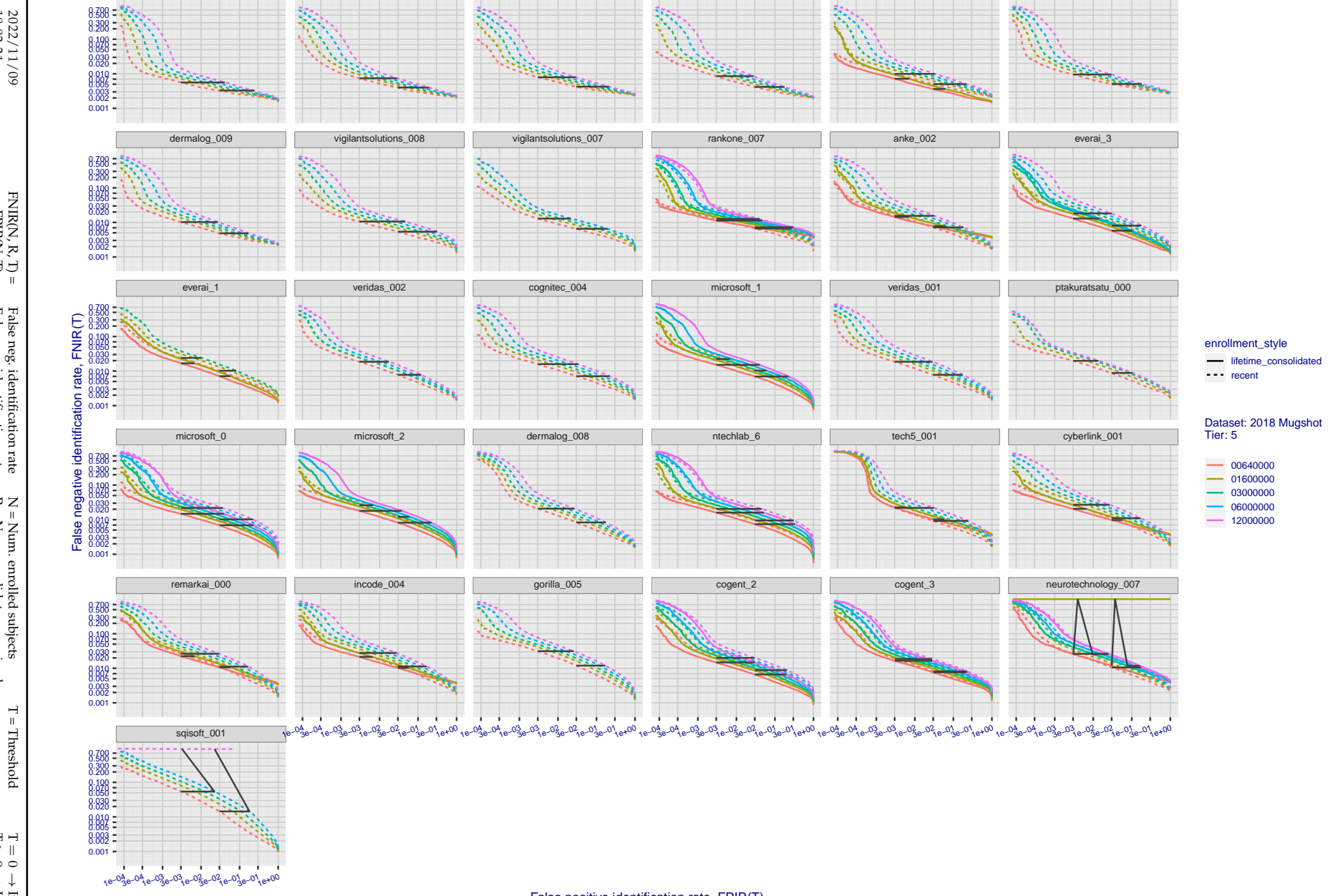


Figure 52: [FRVT-2018 Mugshot Dataset] Identification miss rates vs. false positive rates. The figure shows miss rates $\text{FNIR}(N, L, T)$ as a function of $\text{FPIR}(N, T)$, with N ranging from 640 000 to 12 000 000 as noted in rows 1-10 of Table 1. These error tradeoff characteristics are useful for applications where a threshold must be elevated to limit false positives, such as when human reviewer labor is not matched to the volume of searches. Dark lines join points of equal threshold: If horizontal, $\text{FPIR}(T)$ rises with N , and mate scores are independent of N . Other algorithms adjust scores in an attempt to make FPIR independent of N .

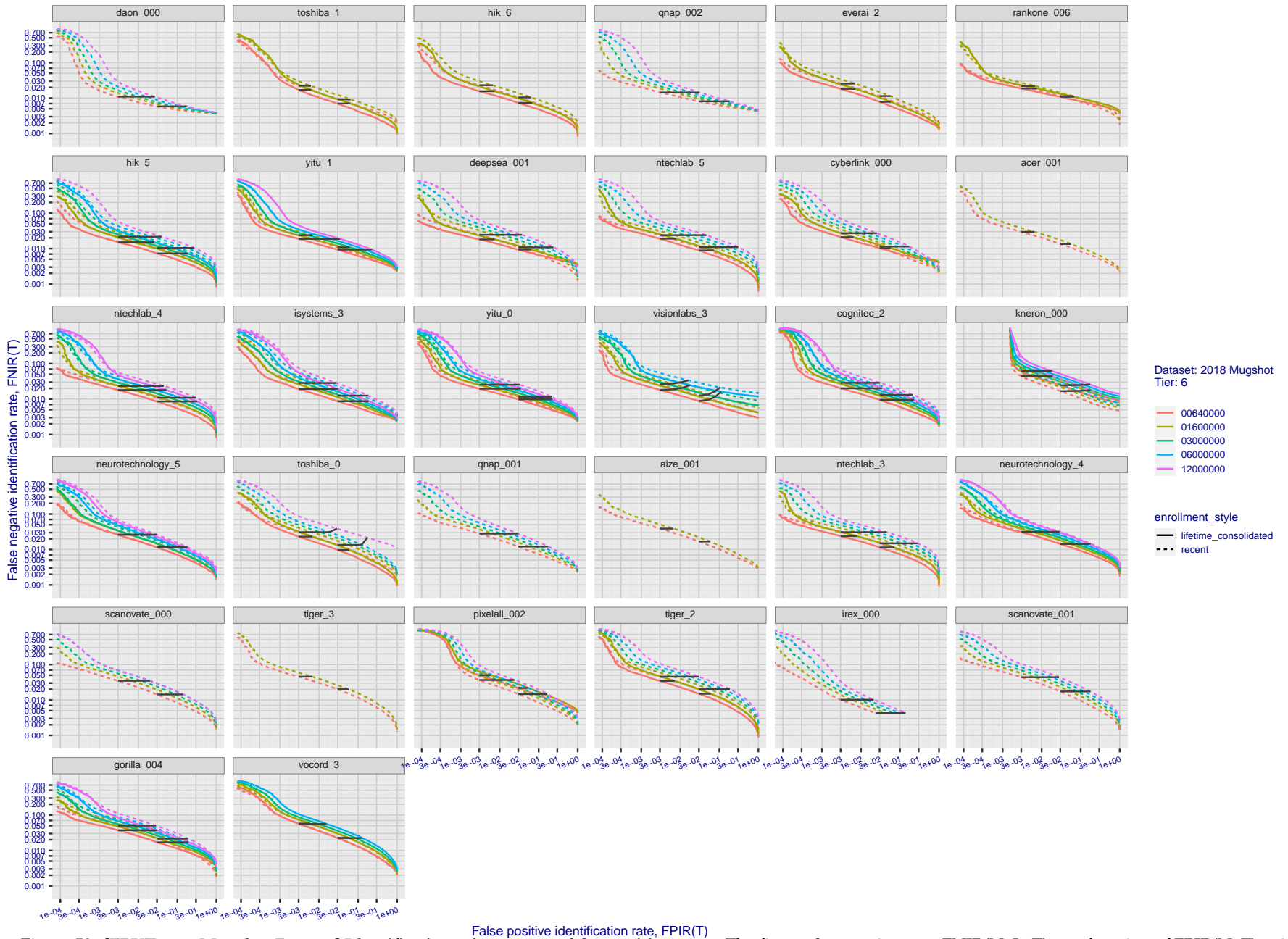


Figure 53: [FRVT-2018 Mugshot Dataset] Identification miss rates vs. false positive rates. The figure shows miss rates $\text{FNIR}(N, L, T)$ as a function of $\text{FPIR}(N, T)$, with N ranging from 640 000 to 12 000 000 as noted in rows 1-10 of Table 1. These error tradeoff characteristics are useful for applications where a threshold must be elevated to limit false positives, such as when human reviewer labor is not matched to the volume of searches. Dark lines join points of equal threshold: If horizontal, $\text{FPIR}(T)$ rises with N , and mate scores are independent of N . Other algorithms adjust scores in an attempt to make FPIR independent of N .

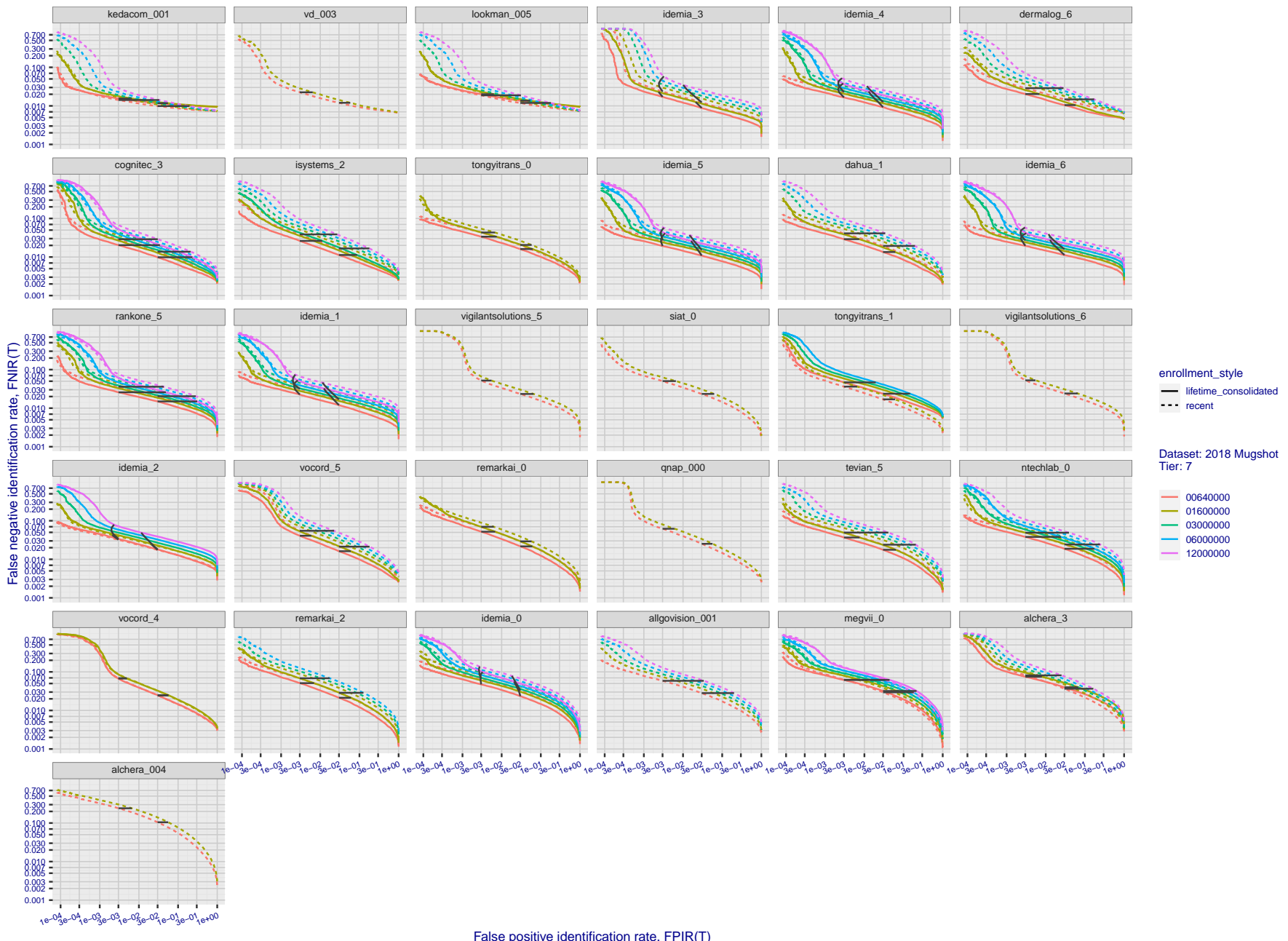


Figure 54: [FRVT-2018 Mugshot Dataset] Identification miss rates vs. false positive rates. The figure shows miss rates $\text{FNIR}(N, L, T)$ as a function of $\text{FPIR}(N, T)$, with N ranging from 640 000 to 12 000 000 as noted in rows 1-10 of Table 1. These error tradeoff characteristics are useful for applications where a threshold must be elevated to limit false positives, such as when human reviewer labor is not matched to the volume of searches. Dark lines join points of equal threshold: If horizontal, $\text{FPIR}(T)$ rises with N , and mate scores are independent of N . Other algorithms adjust scores in an attempt to make FPIR independent of N .

2022/11/09
18:02:21FNIR(N, R, T) = False neg. identification rate
FPIR(N, T) = False pos. identification rate N = Num. enrolled subjects
 R = Num. candidates examined
 T = Threshold $T = 0 \rightarrow$ Investigation
 $T > 0 \rightarrow$ Identification

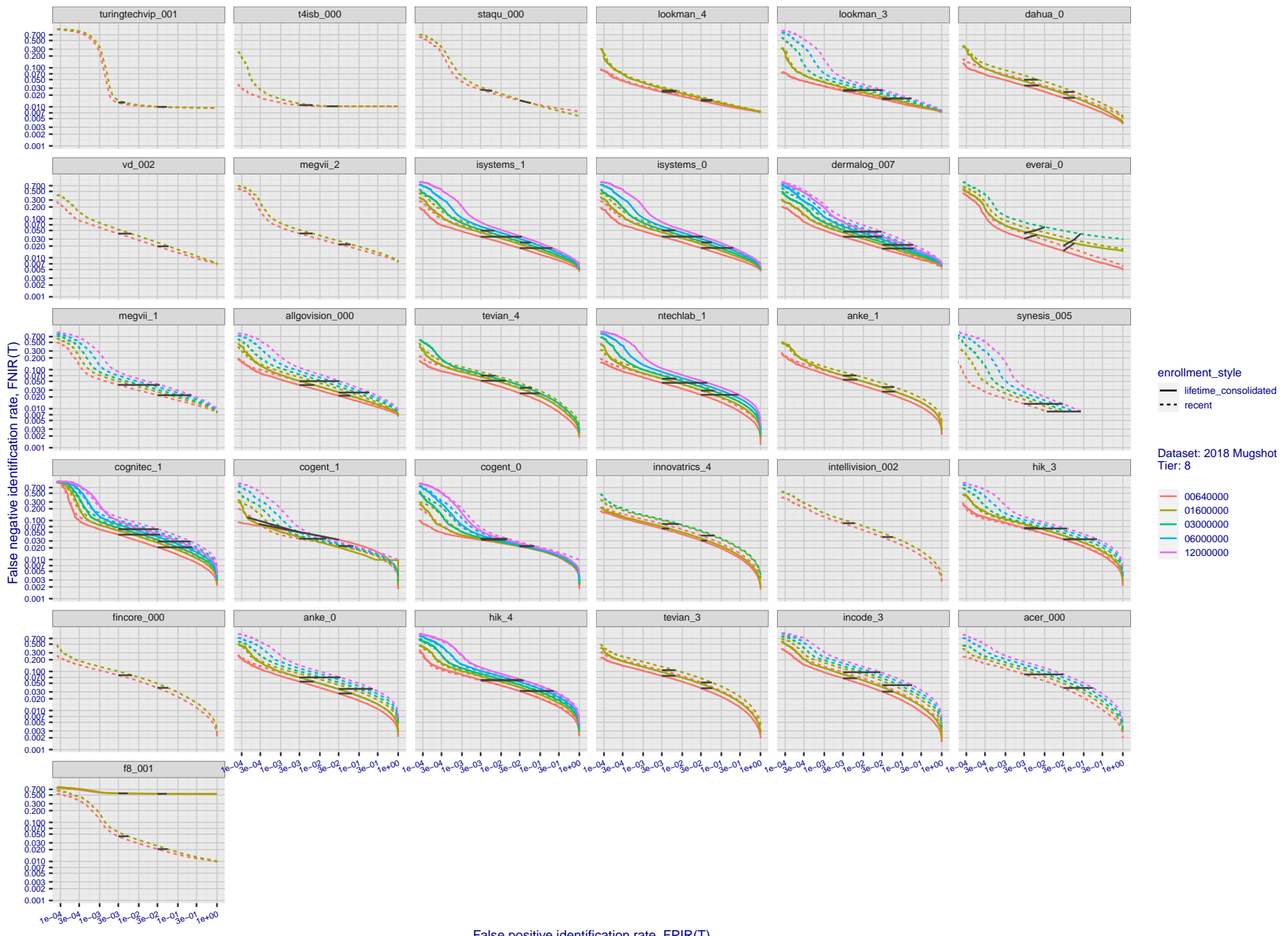


Figure 55: [FRVT-2018 Mugshot Dataset] Identification miss rates vs. false positive rates. The figure shows miss rates $\text{FNIR}(N, L, T)$ as a function of $\text{FPIR}(N, T)$, with N ranging from 640 000 to 12 000 000 as noted in rows 1-10 of Table 1. These error tradeoff characteristics are useful for applications where a threshold must be elevated to limit false positives, such as when human reviewer labor is not matched to the volume of searches. Dark lines join points of equal threshold: If horizontal, $\text{FPIR}(T)$ rises with N , and mate scores are independent of N . Other algorithms adjust scores in an attempt to make FPIR independent of N .

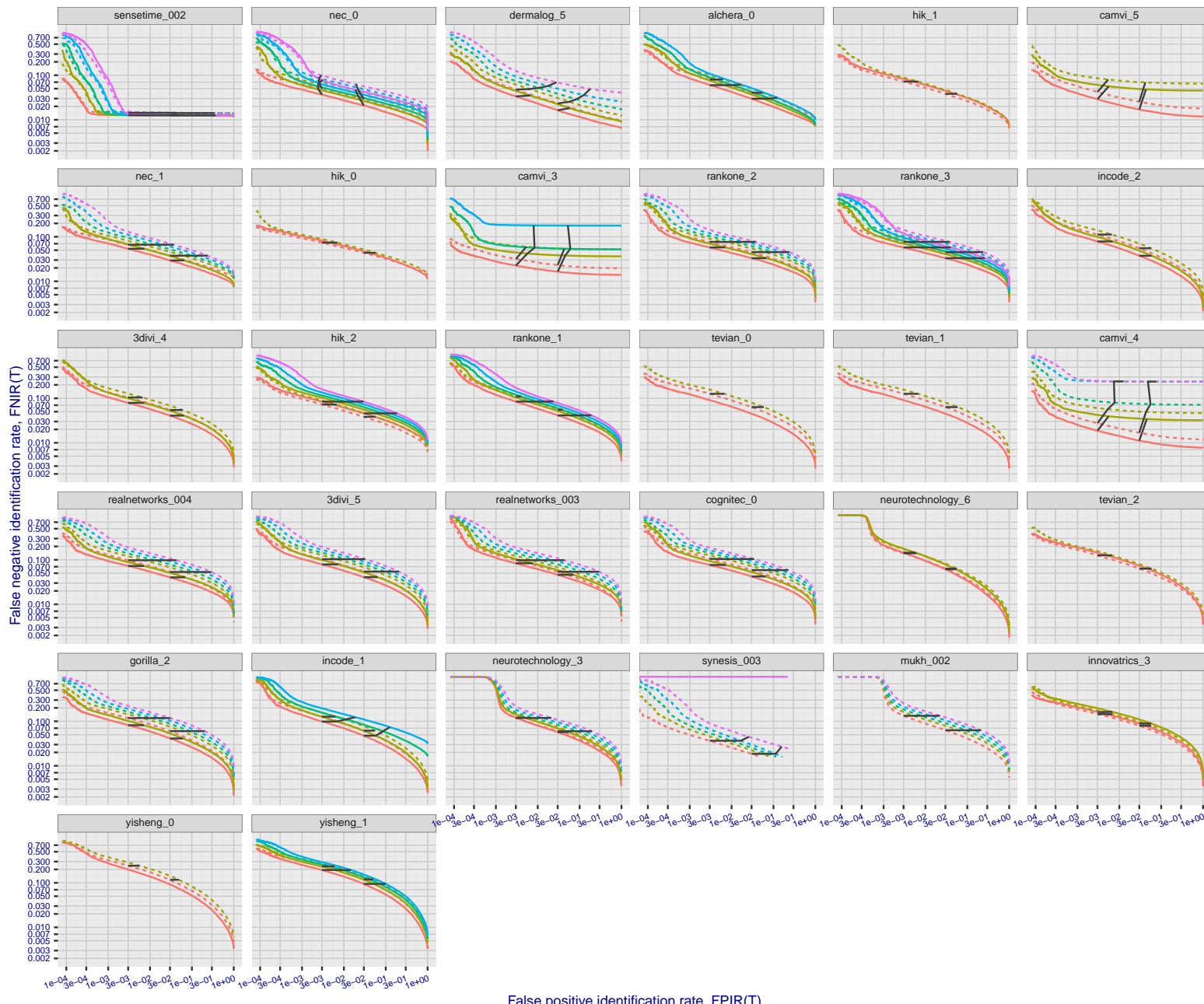


Figure 56: [FRVT-2018 Mugshot Dataset] Identification miss rates vs. false positive rates. The figure shows miss rates $\text{FNIR}(N, L, T)$ as a function of $\text{FPIR}(N, T)$, with N ranging from 640 000 to 12 000 000 as noted in rows 1-10 of Table 1. These error tradeoff characteristics are useful for applications where a threshold must be elevated to limit false positives, such as when human reviewer labor is not matched to the volume of searches. Dark lines join points of equal threshold: If horizontal, $\text{FPIR}(T)$ rises with N , and mate scores are independent of N . Other algorithms adjust scores in an attempt to make FPIR independent of N .

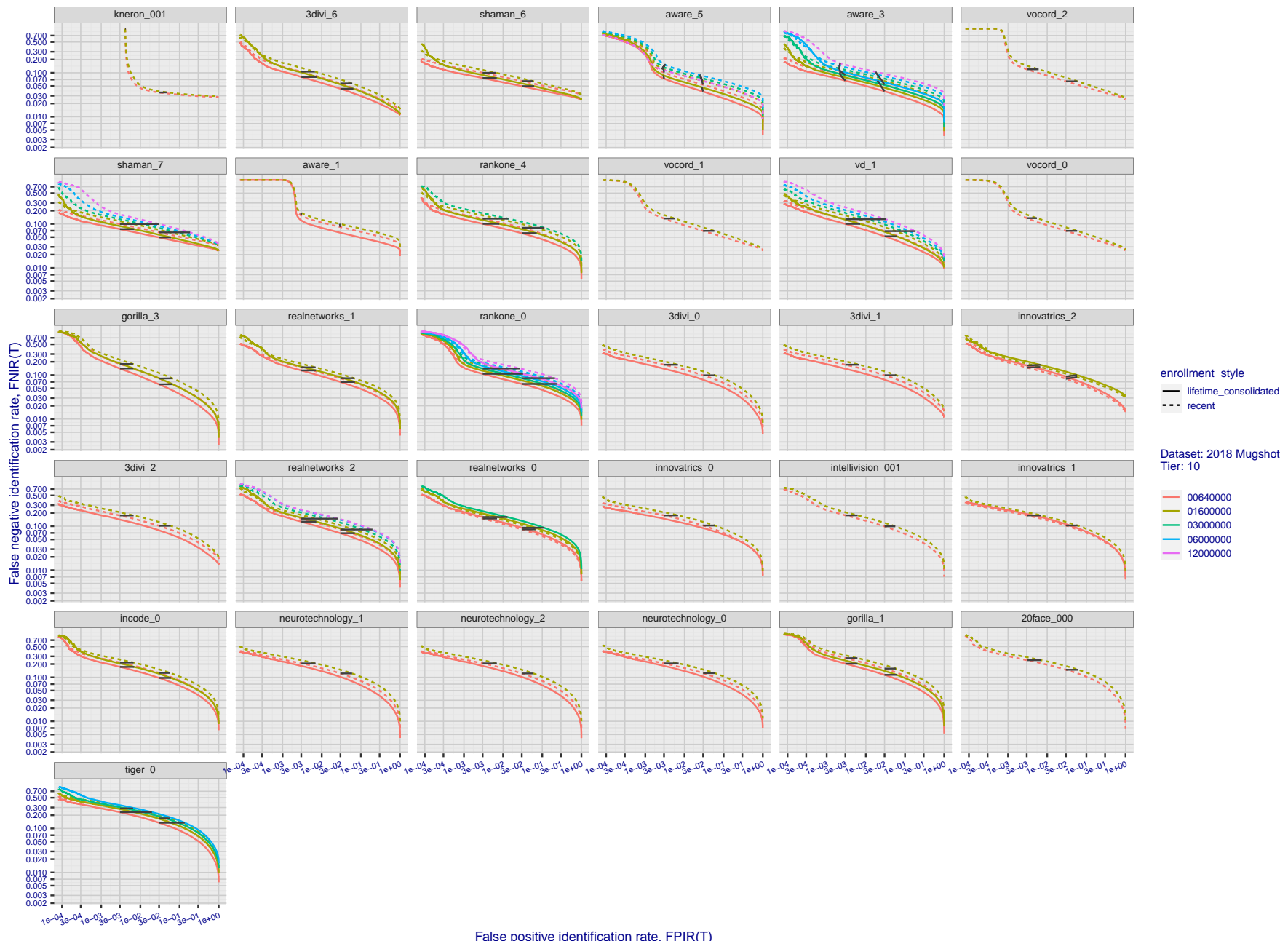


Figure 57: [FRVT-2018 Mugshot Dataset] Identification miss rates vs. false positive rates. The figure shows miss rates $\text{FNIR}(N, L, T)$ as a function of $\text{FPIR}(N, T)$, with N ranging from 640 000 to 12 000 000 as noted in rows 1-10 of Table 1. These error tradeoff characteristics are useful for applications where a threshold must be elevated to limit false positives, such as when human reviewer labor is not matched to the volume of searches. Dark lines join points of equal threshold: If horizontal, $\text{FPIR}(T)$ rises with N , and mate scores are independent of N . Other algorithms adjust scores in an attempt to make FPIR independent of N .

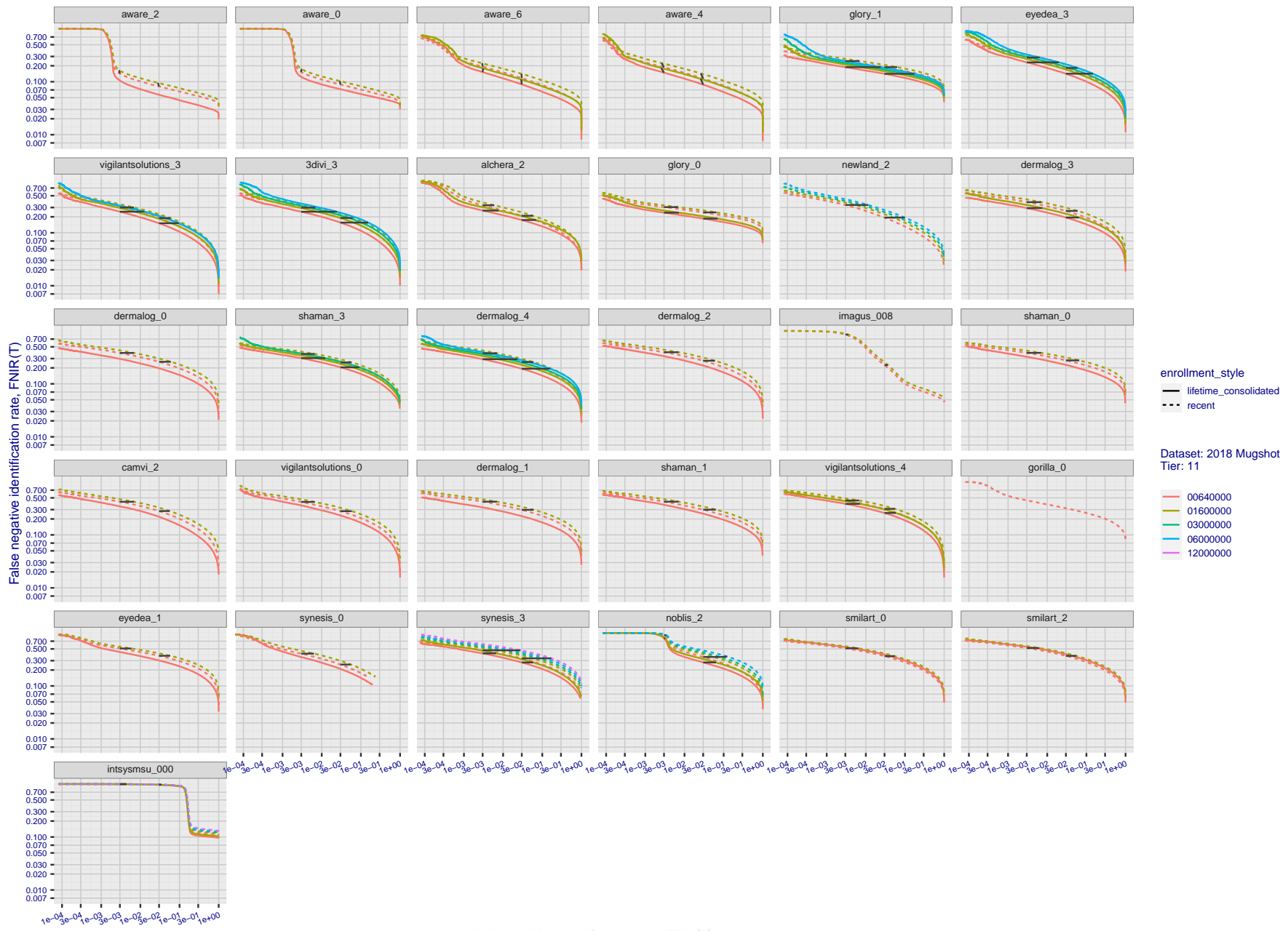


Figure 58: [FRVT-2018 Mugshot Dataset] Identification miss rates vs. false positive rates. The figure shows miss rates $\text{FNIR}(N, L, T)$ as a function of $\text{FPIR}(N, T)$, with N ranging from 640 000 to 12 000 000 as noted in rows 1-10 of Table 1. These error tradeoff characteristics are useful for applications where a threshold must be elevated to limit false positives, such as when human reviewer labor is not matched to the volume of searches. Dark lines join points of equal threshold: If horizontal, $\text{FPIR}(T)$ rises with N , and mate scores are independent of N . Other algorithms adjust scores in an attempt to make FPIR independent of N .

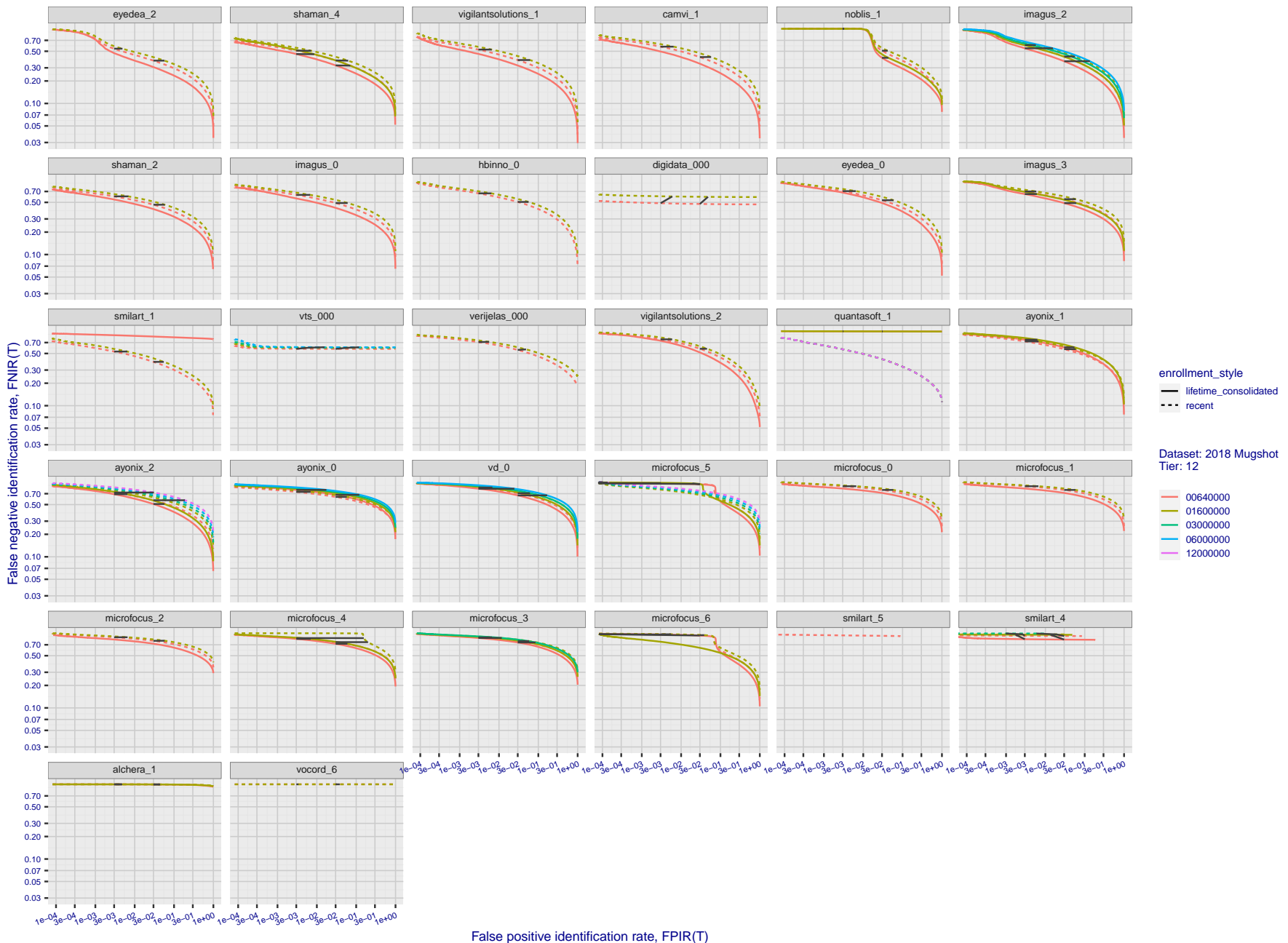


Figure 59: [FRVT-2018 Mugshot Dataset] Identification miss rates vs. false positive rates. The figure shows miss rates $\text{FNIR}(N, L, T)$ as a function of $\text{FPIR}(N, T)$, with N ranging from 640 000 to 12 000 000 as noted in rows 1-10 of Table 1. These error tradeoff characteristics are useful for applications where a threshold must be elevated to limit false positives, such as when human reviewer labor is not matched to the volume of searches. Dark lines join points of equal threshold: If horizontal, $\text{FPIR}(T)$ rises with N , and mate scores are independent of N . Other algorithms adjust scores in an attempt to make FPIR independent of N .

2022/11/09
18:02:21FNIR(N, R, T) = False neg. identification rate
FPIR(N, T) = False pos. identification rateN = Num. enrolled subjects
R = Num. candidates examined

T = Threshold

T = 0 → Investigation
 $T > 0 \rightarrow$ Identification

Appendix B Effect of time-lapse: Accuracy after face ageing

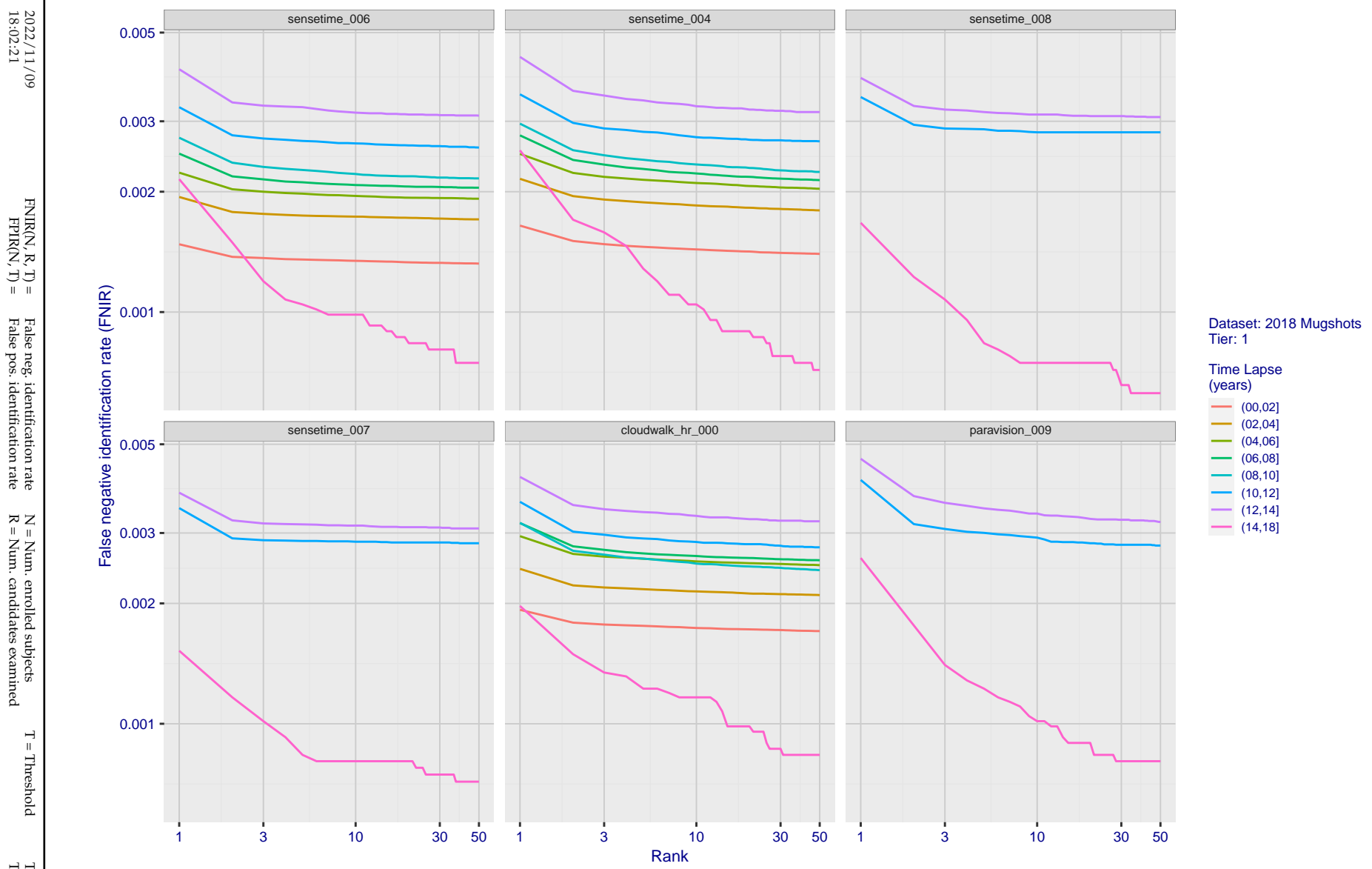


Figure 60: [FRVT-2018 Mugshot Ageing Dataset] Identification miss rates vs. rank by time-elapsed. The oldest image of each individual is enrolled. Thereafter, all more recent images are searched. Miss rates are computed over all searches noted in row 17 of Table 1 and binned by number of years between search and initial enrollment.

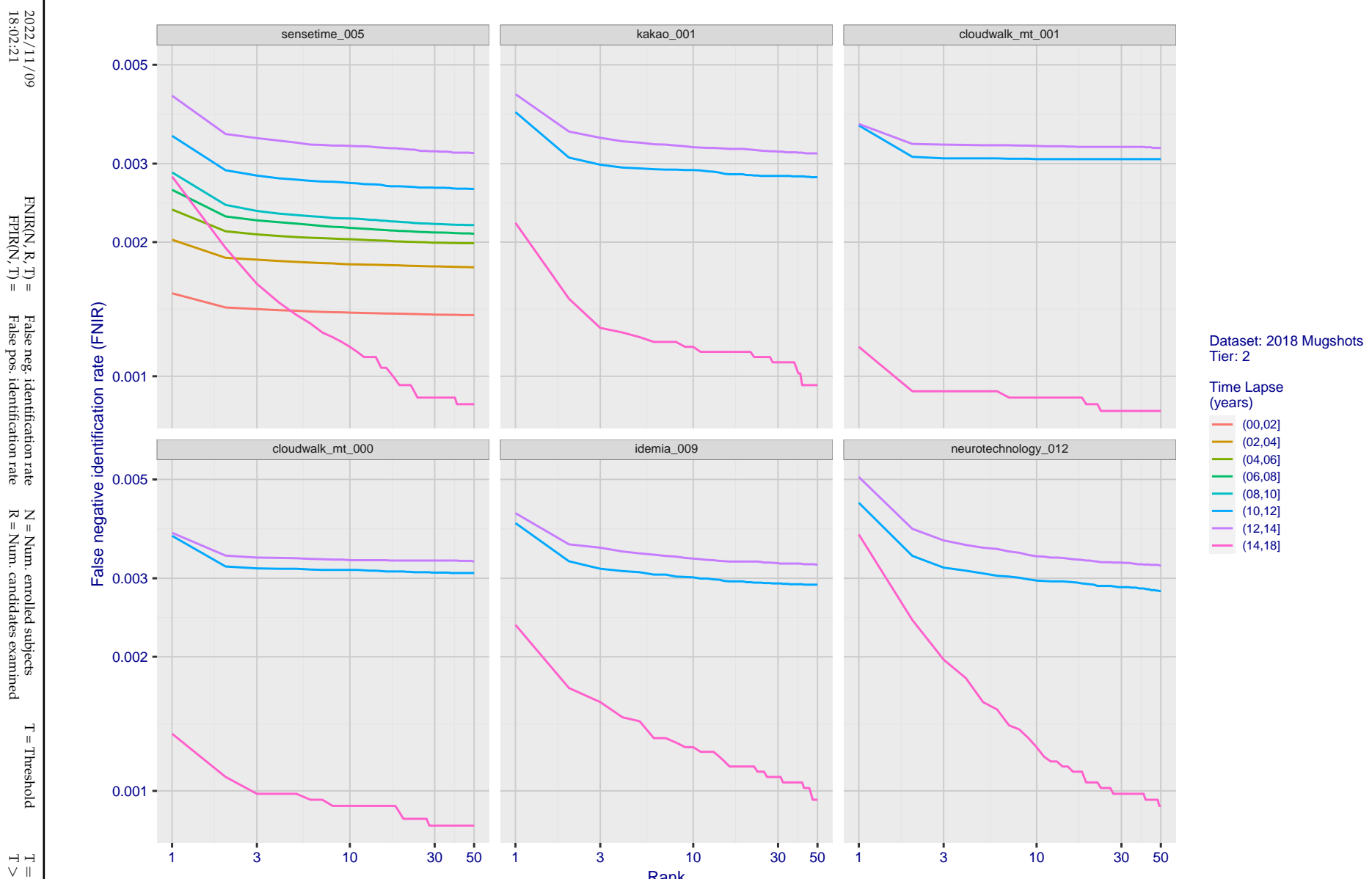


Figure 61: [FRVT-2018 Mugshot Ageing Dataset] Identification miss rates vs. rank by time-elapsed. The oldest image of each individual is enrolled. Thereafter, all more recent images are searched. Miss rates are computed over all searches noted in row 17 of Table 1 and binned by number of years between search and initial enrollment.

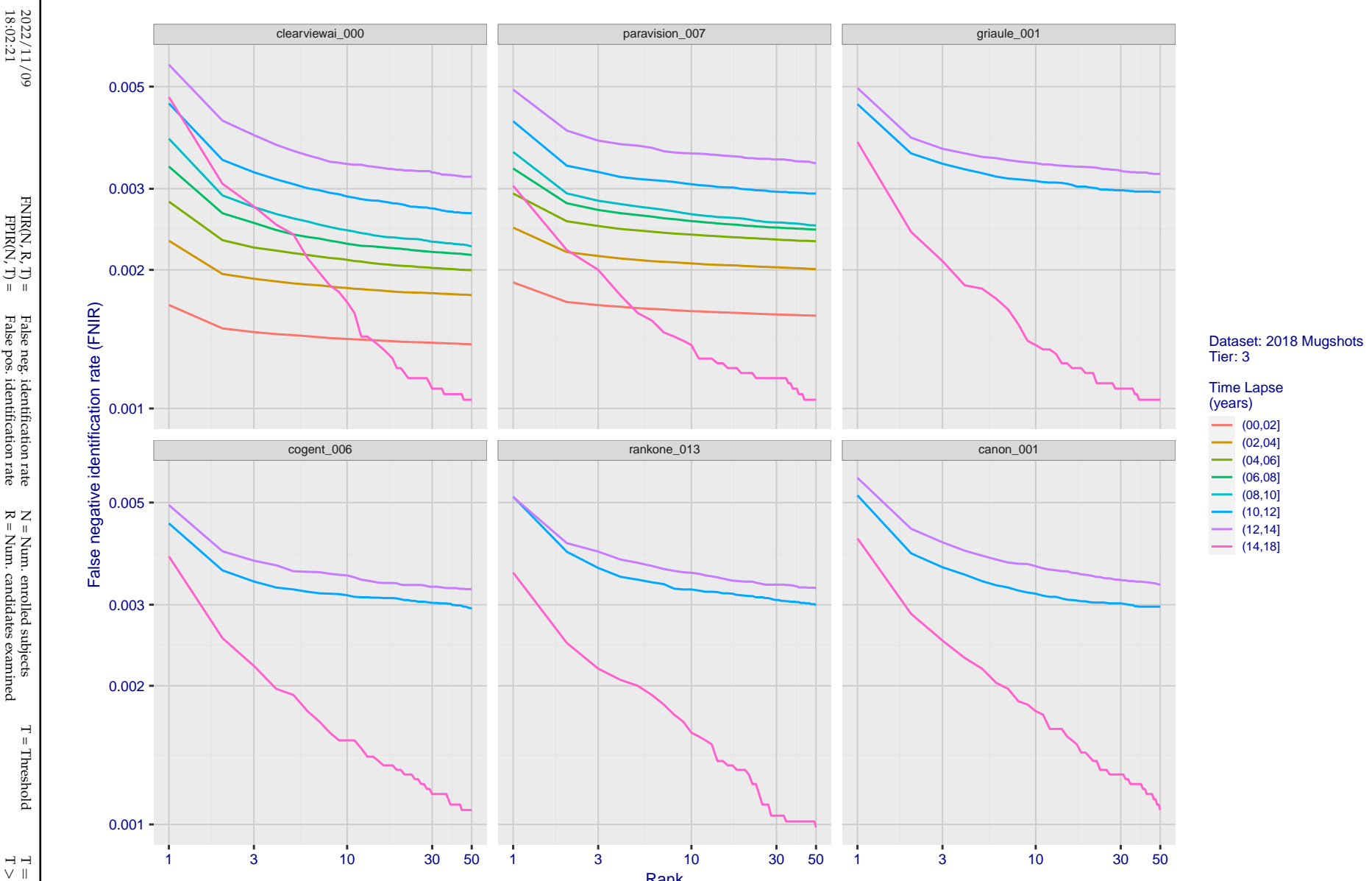


Figure 62: [FRVT-2018 Mugshot Ageing Dataset] Identification miss rates vs. rank by time elapsed. The oldest image of each individual is enrolled. Thereafter, all more recent images are searched. Miss rates are computed over all searches noted in row 17 of Table 1 and binned by number of years between search and initial enrollment.

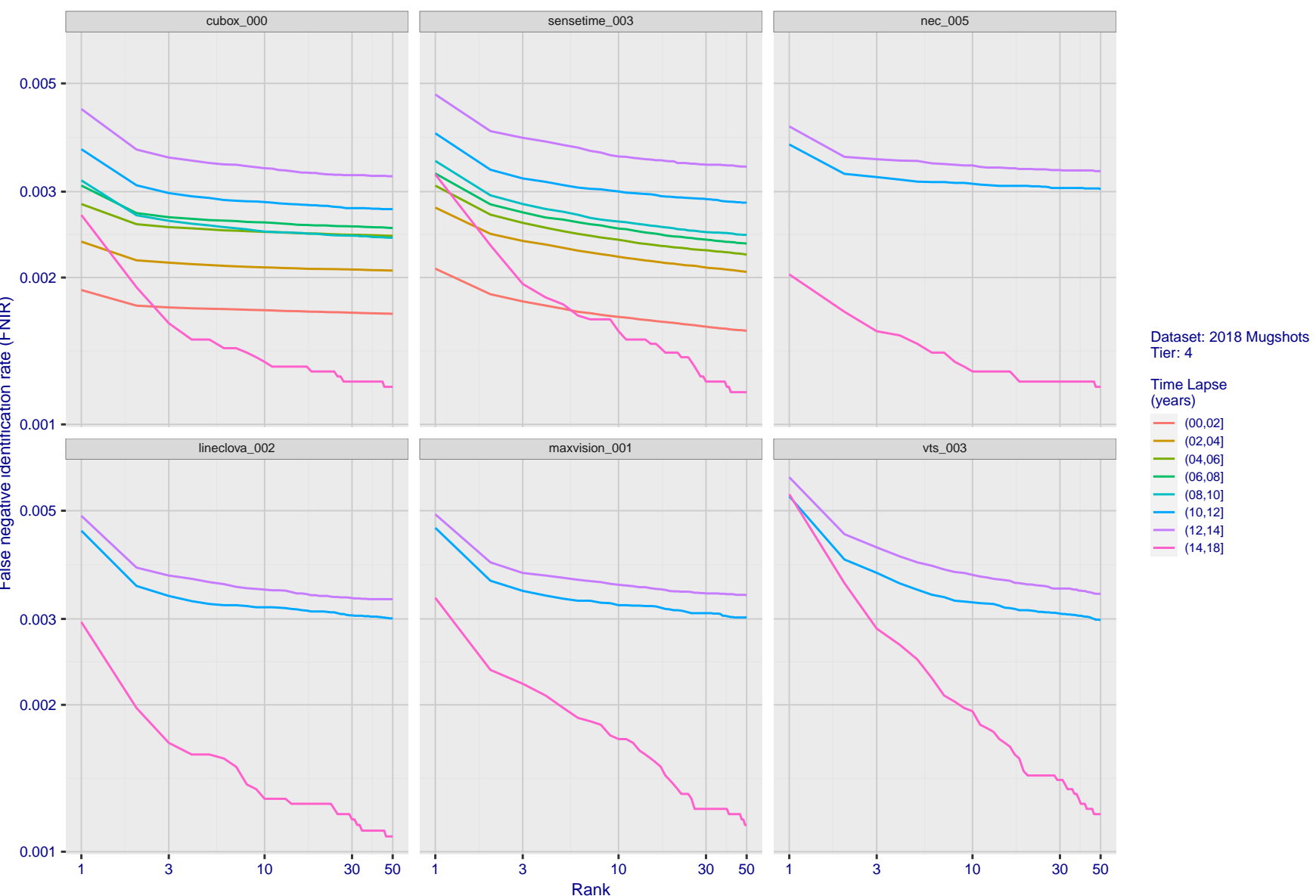
2022/11/09
18:02:21

Figure 63: [FRVT-2018 Mugshot Ageing Dataset] Identification miss rates vs. rank by time-elapsed. The oldest image of each individual is enrolled. Thereafter, all more recent images are searched. Miss rates are computed over all searches noted in row 17 of Table 1 and binned by number of years between search and initial enrollment.

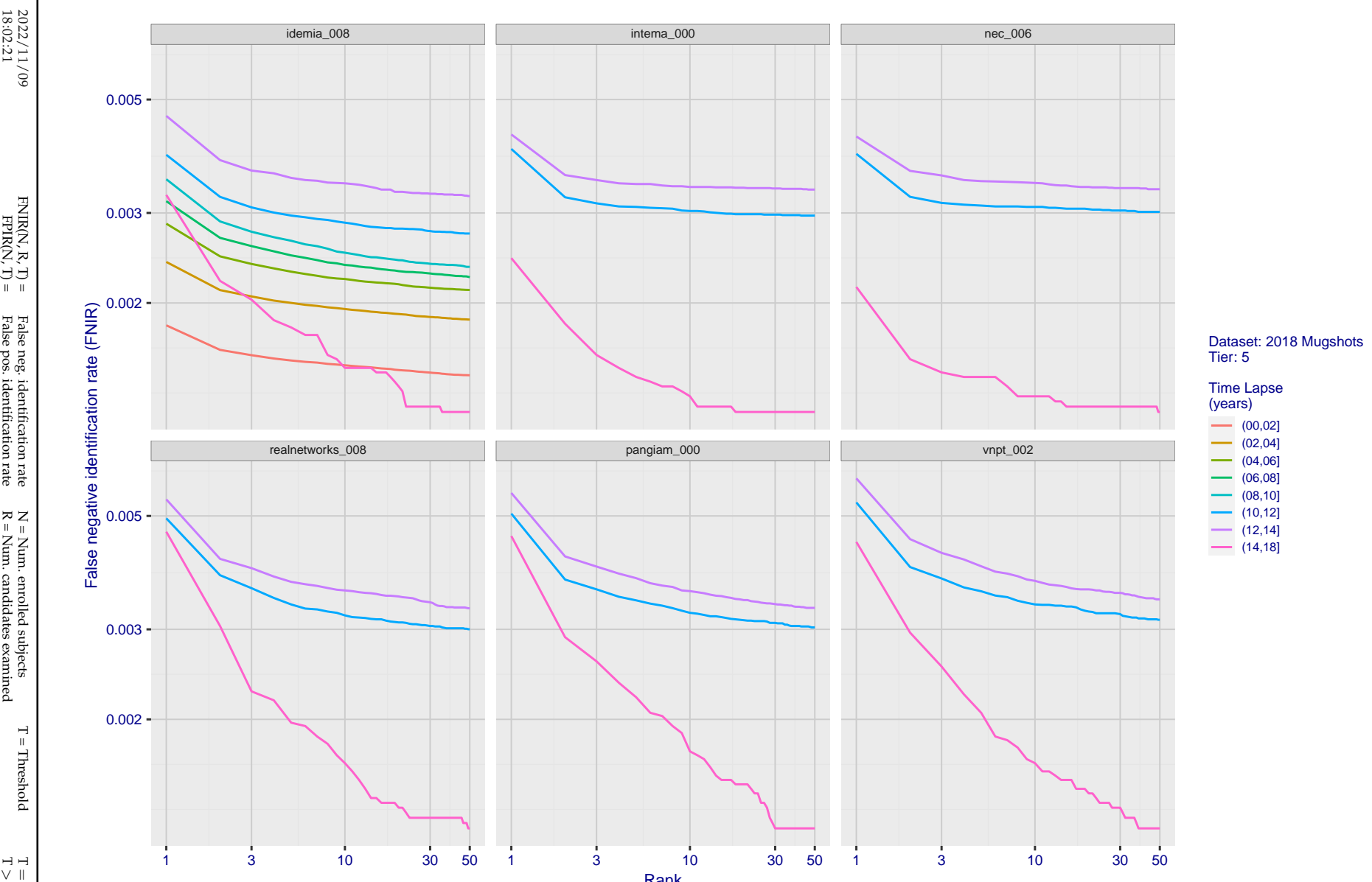


Figure 64: [FRVT-2018 Mugshot Ageing Dataset] Identification miss rates vs. rank by time elapsed. The oldest image of each individual is enrolled. Thereafter, all more recent images are searched. Miss rates are computed over all searches noted in row 17 of Table 1 and binned by number of years between search and initial enrollment.

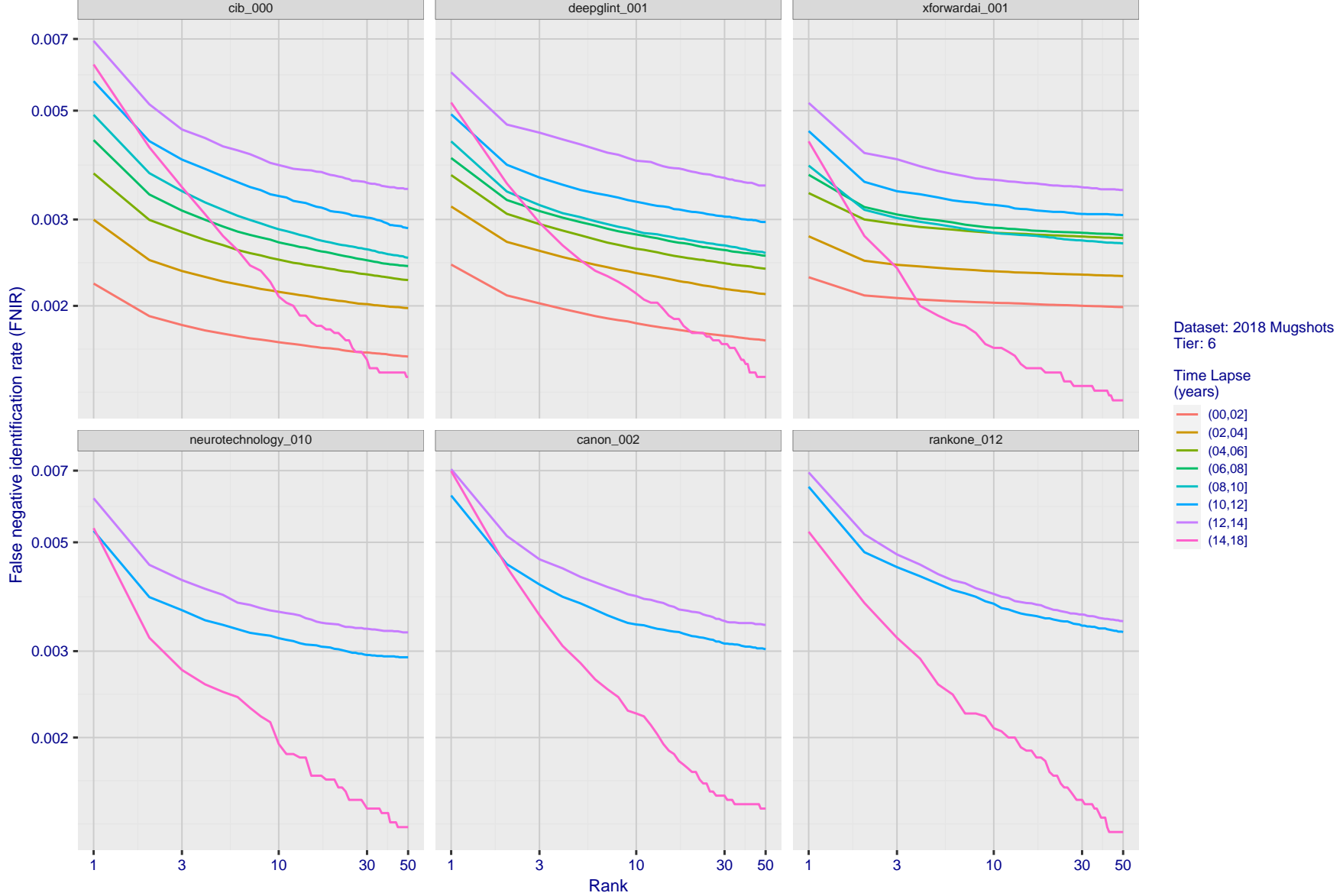


Figure 65: [FRVT-2018 Mugshot Ageing Dataset] Identification miss rates vs. rank by time-elapsed. The oldest image of each individual is enrolled. Thereafter, all more recent images are searched. Miss rates are computed over all searches noted in row 17 of Table 1 and binned by number of years between search and initial enrollment.

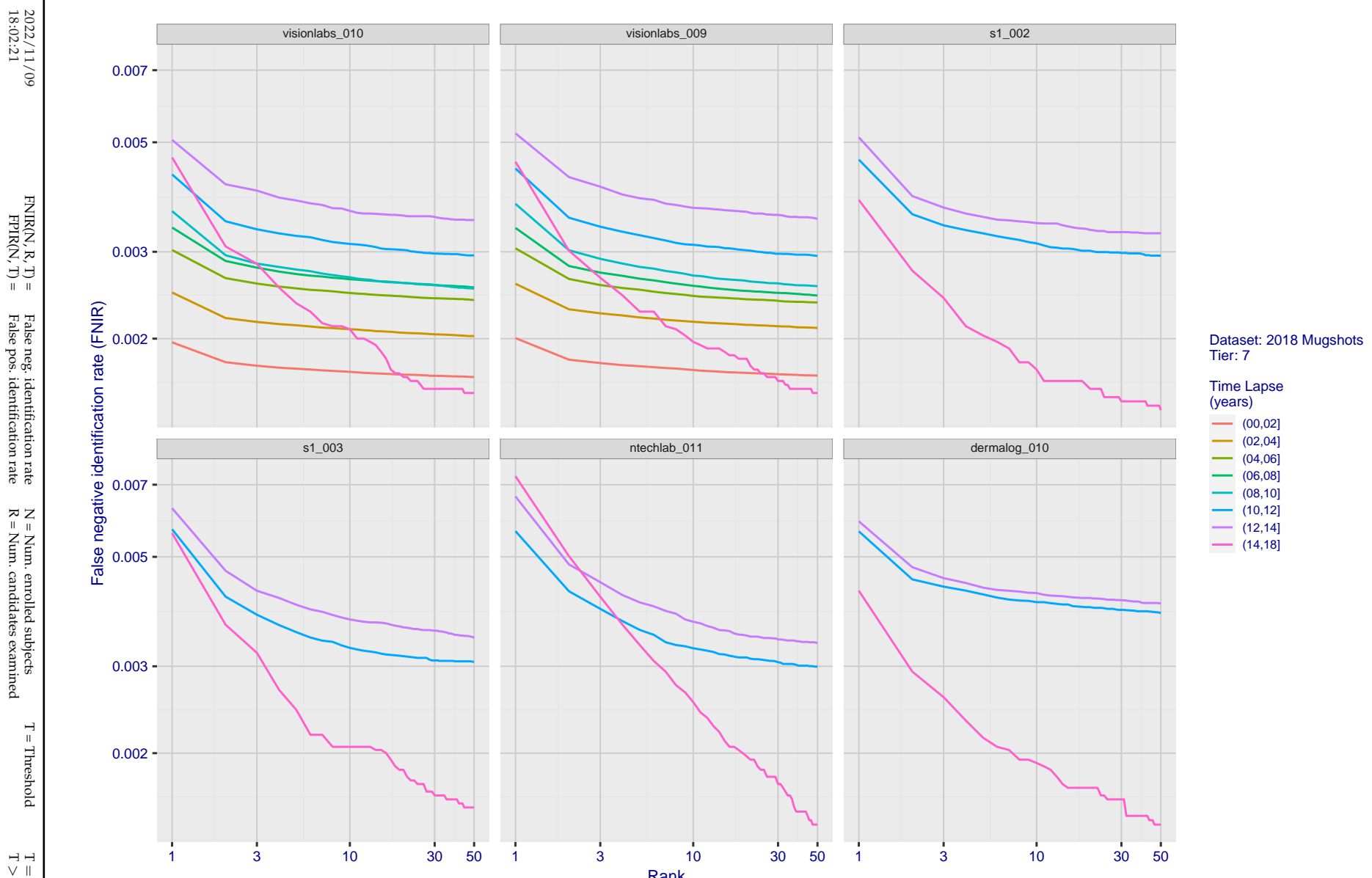


Figure 66: [FRVT-2018 Mugshot Ageing Dataset] Identification miss rates vs. rank by time-elapsed. The oldest image of each individual is enrolled. Thereafter, all more recent images are searched. Miss rates are computed over all searches noted in row 17 of Table 1 and binned by number of years between search and initial enrollment.

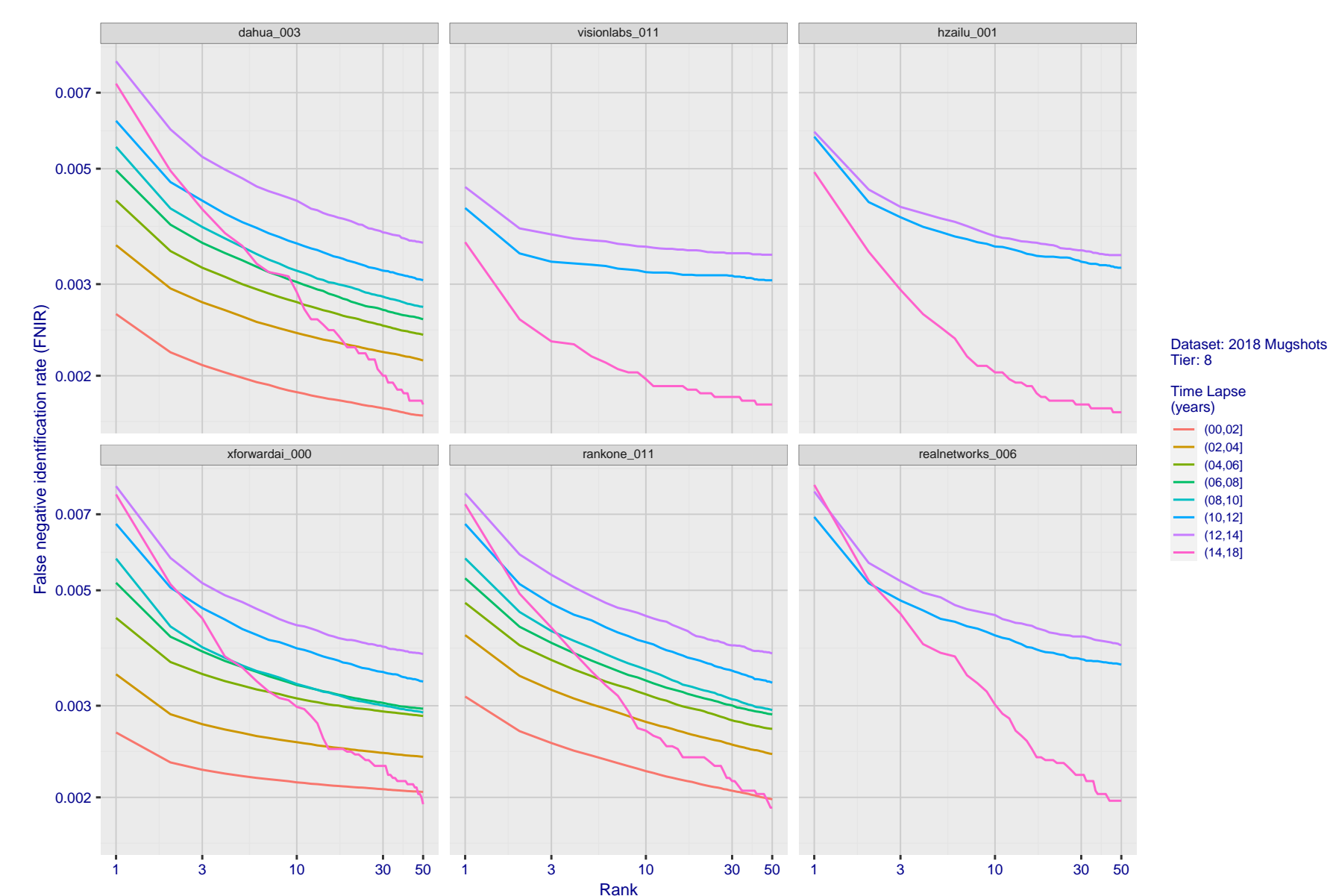
2022/11/09
18:02:21

Figure 67: [FRVT-2018 Mugshot Ageing Dataset] Identification miss rates vs. rank by time-elapsed. The oldest image of each individual is enrolled. Thereafter, all more recent images are searched. Miss rates are computed over all searches noted in row 17 of Table 1 and binned by number of years between search and initial enrollment.

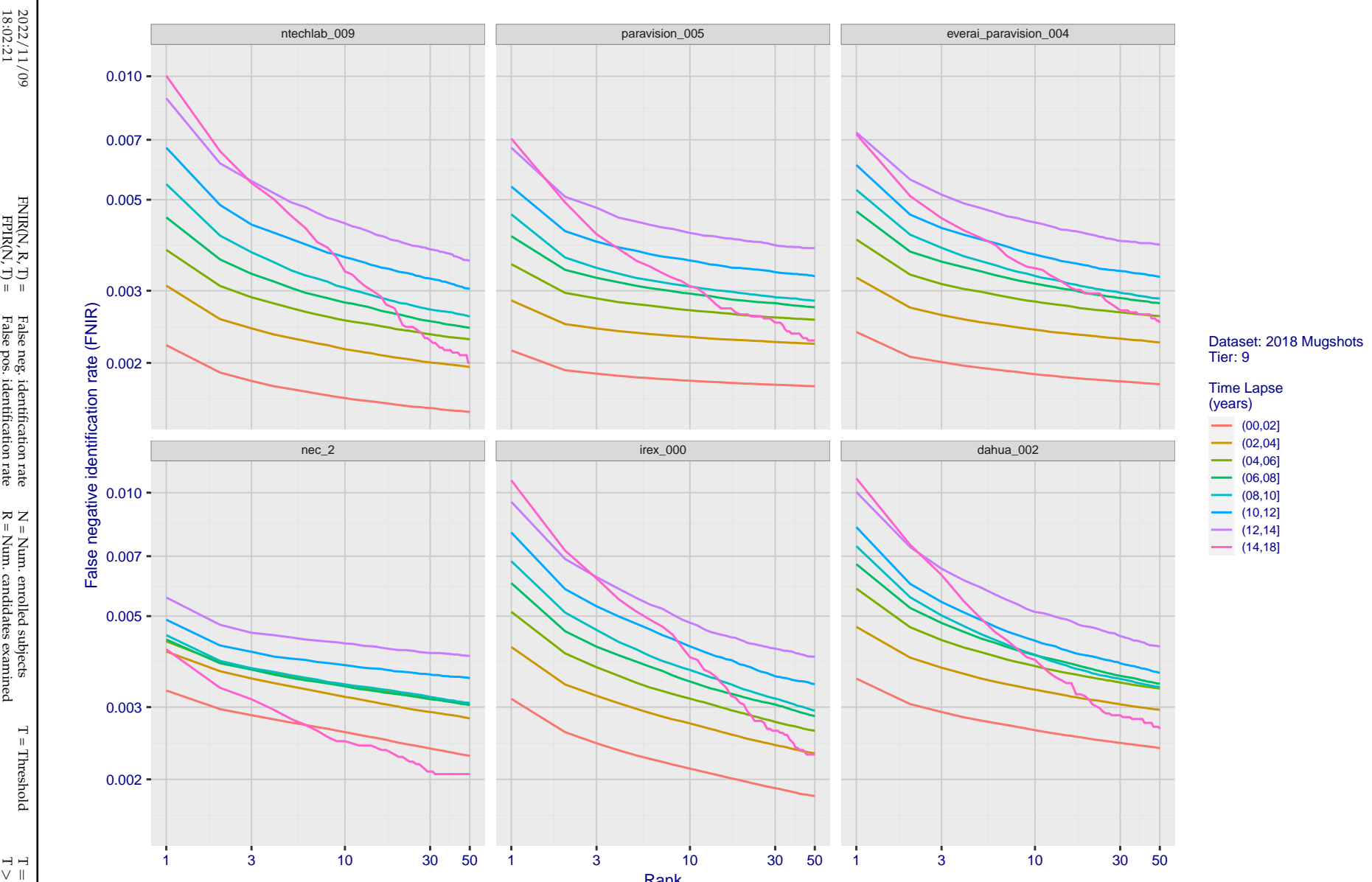


Figure 68: [FRVT-2018 Mugshot Ageing Dataset] Identification miss rates vs. rank by time-elapsed. The oldest image of each individual is enrolled. Thereafter, all more recent images are searched. Miss rates are computed over all searches noted in row 17 of Table 1 and binned by number of years between search and initial enrollment.

2022/11/09
18:02:21FNIR(N, R, T) = False neg. identification rate
FPIR(N, T) = False pos. identification rateN = Num. enrolled subjects
R = Num. candidates examinedT = Threshold
T = 0 → Investigation

T > 0 → Identification

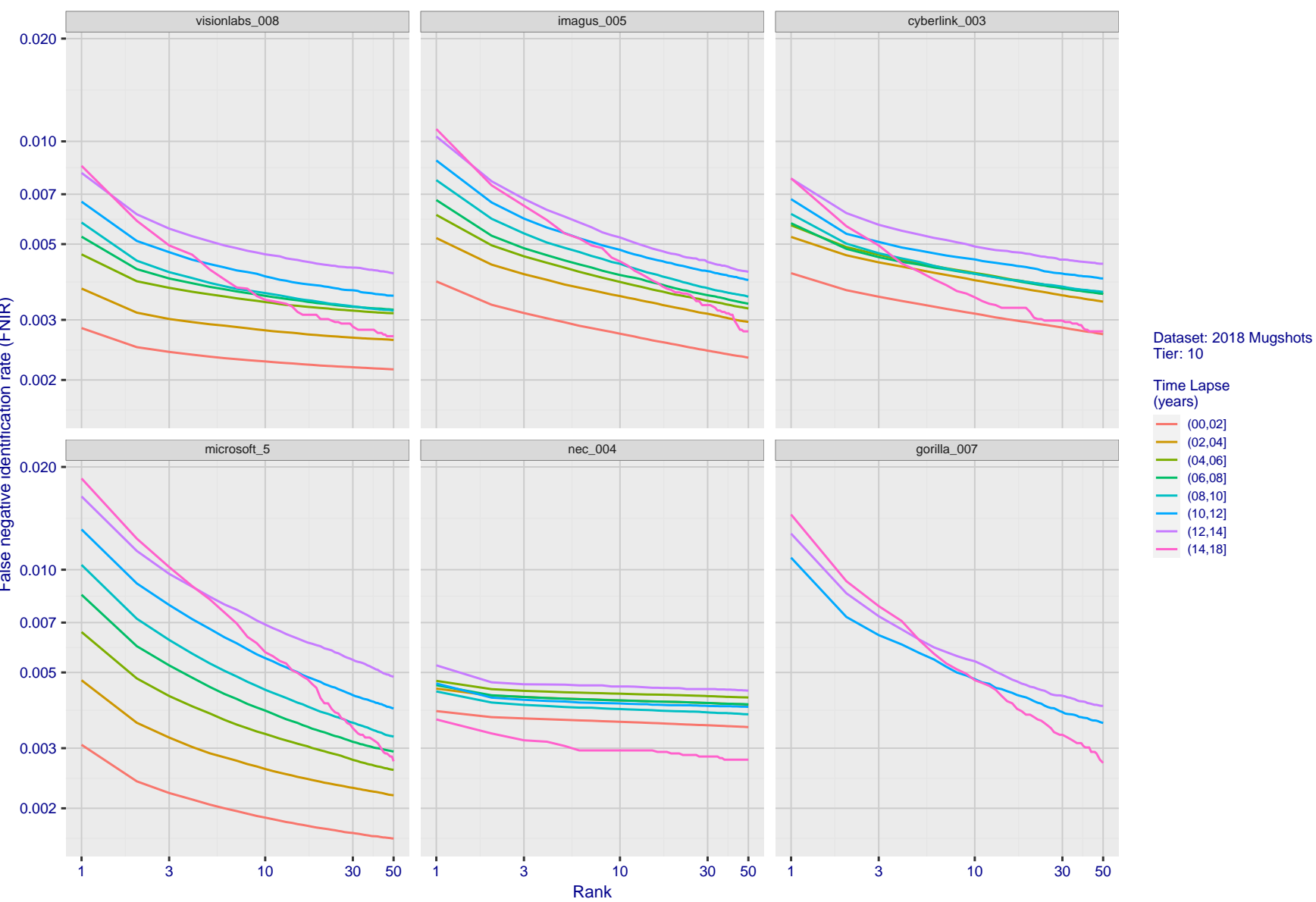


Figure 69: [FRVT-2018 Mugshot Ageing Dataset] Identification miss rates vs. rank by time-elapsed. The oldest image of each individual is enrolled. Thereafter, all more recent images are searched. Miss rates are computed over all searches noted in row 17 of Table 1 and binned by number of years between search and initial enrollment.

2022/11/09
18:02:21FNIR(N, R, T) = False neg. identification rate
FPTR(N, T) = False pos. identification rateN = Num. enrolled subjects
R = Num. candidates examinedT = Threshold
T = 0 → Investigation

T > 0 → Identification

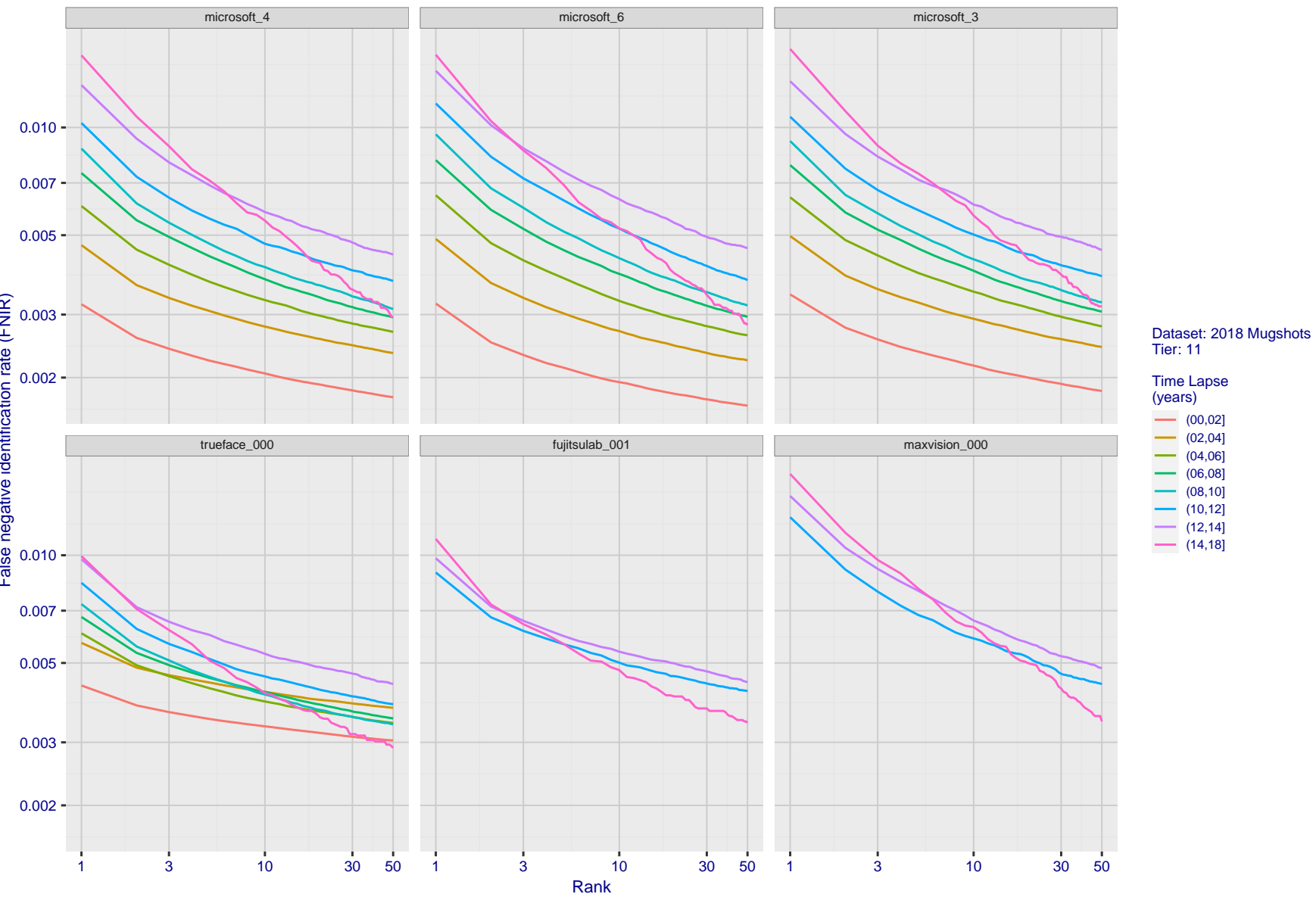


Figure 70: [FRVT-2018 Mugshot Ageing Dataset] Identification miss rates vs. rank by time-elapsed. The oldest image of each individual is enrolled. Thereafter, all more recent images are searched. Miss rates are computed over all searches noted in row 17 of Table 1 and binned by number of years between search and initial enrollment.

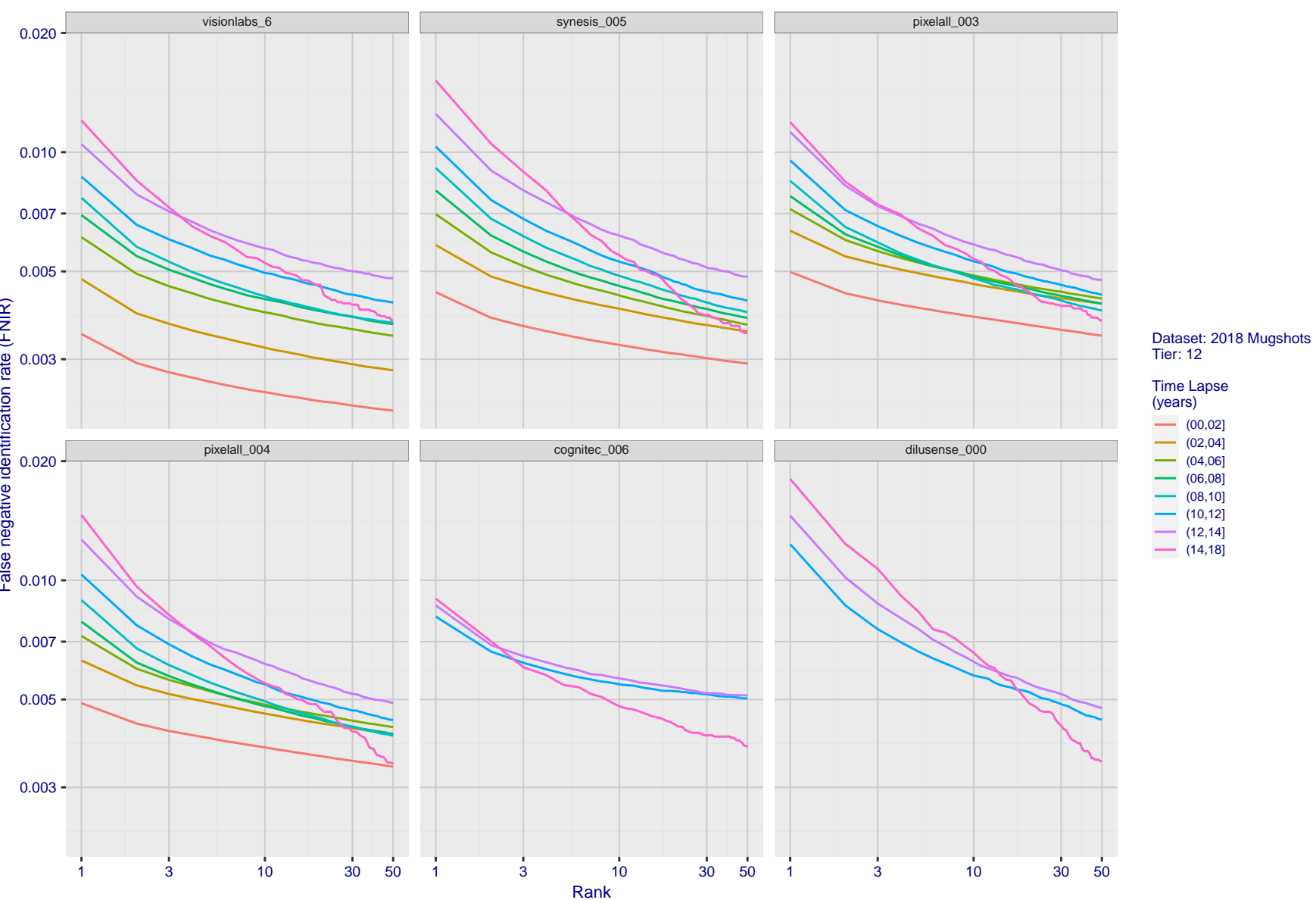
2022/11/09
18:02:21

Figure 71: [FRVT-2018 Mugshot Ageing Dataset] Identification miss rates vs. rank by time-elapsed. The oldest image of each individual is enrolled. Thereafter, all more recent images are searched. Miss rates are computed over all searches noted in row 17 of Table 1 and binned by number of years between search and initial enrollment.

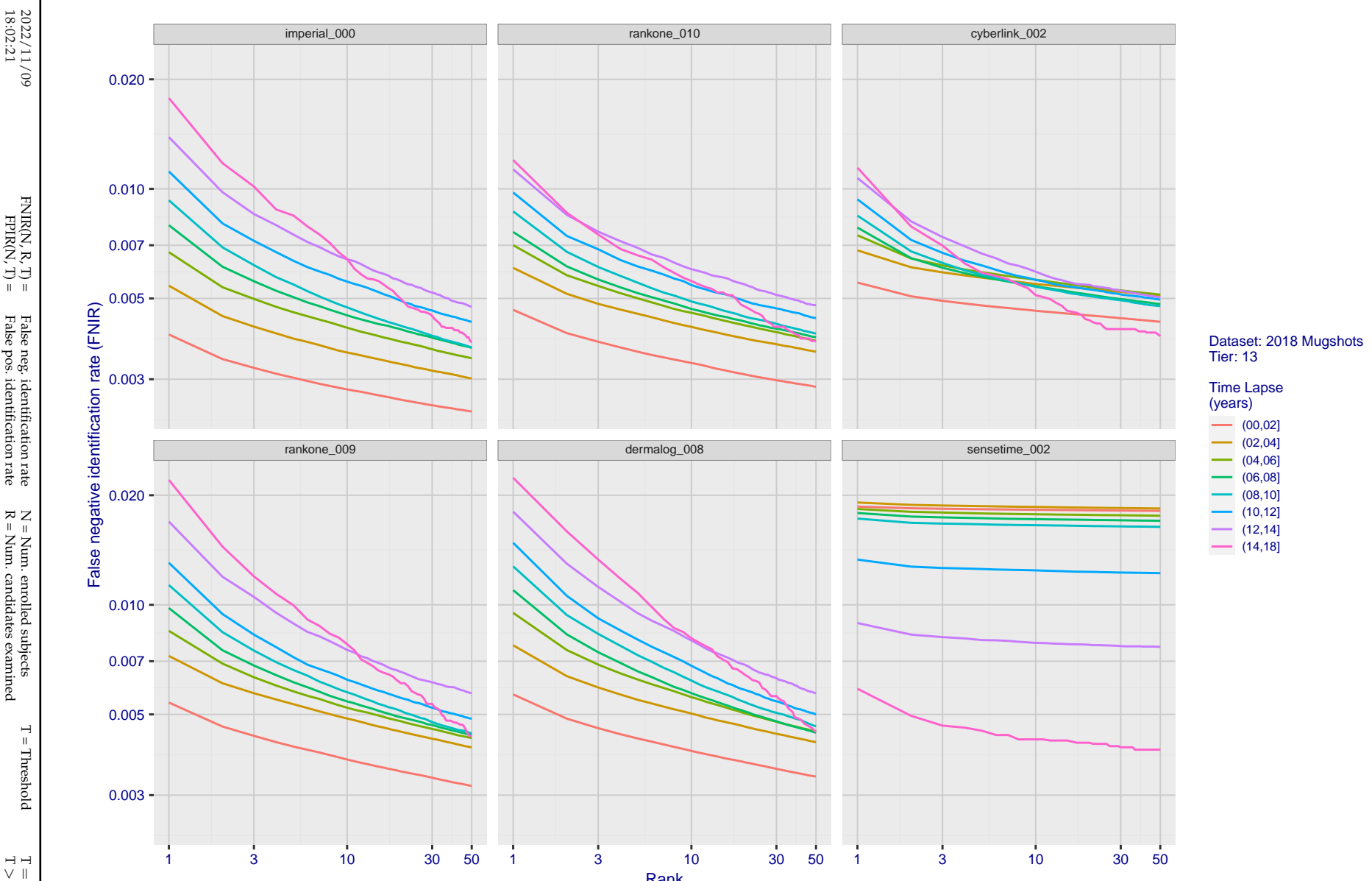


Figure 72: [FRVT-2018 Mugshot Ageing Dataset] Identification miss rates vs. rank by time-elapsed. The oldest image of each individual is enrolled. Thereafter, all more recent images are searched. Miss rates are computed over all searches noted in row 17 of Table 1 and binned by number of years between search and initial enrollment.

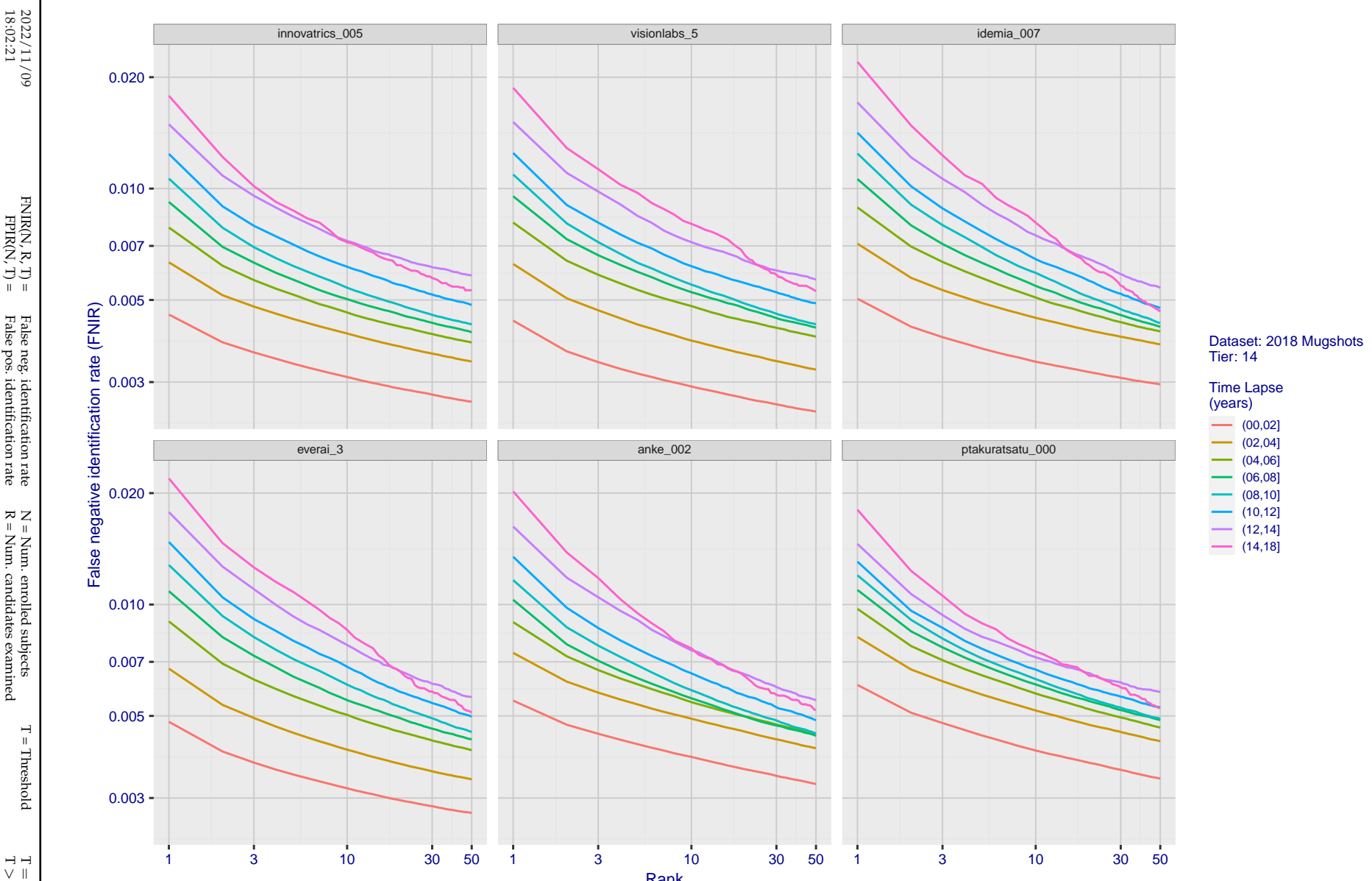


Figure 73: [FRVT-2018 Mugshot Ageing Dataset] Identification miss rates vs. rank by time-elapsed. The oldest image of each individual is enrolled. Thereafter, all more recent images are searched. Miss rates are computed over all searches noted in row 17 of Table 1 and binned by number of years between search and initial enrollment.

2022/11/09
18:02:21FNIR(N, R, T) = False neg. identification rate
FPFR(N, T) = False pos. identification rateN = Num. enrolled subjects
R = Num. candidates examinedT = Threshold
T = 0 → Investigation

T > 0 → Identification

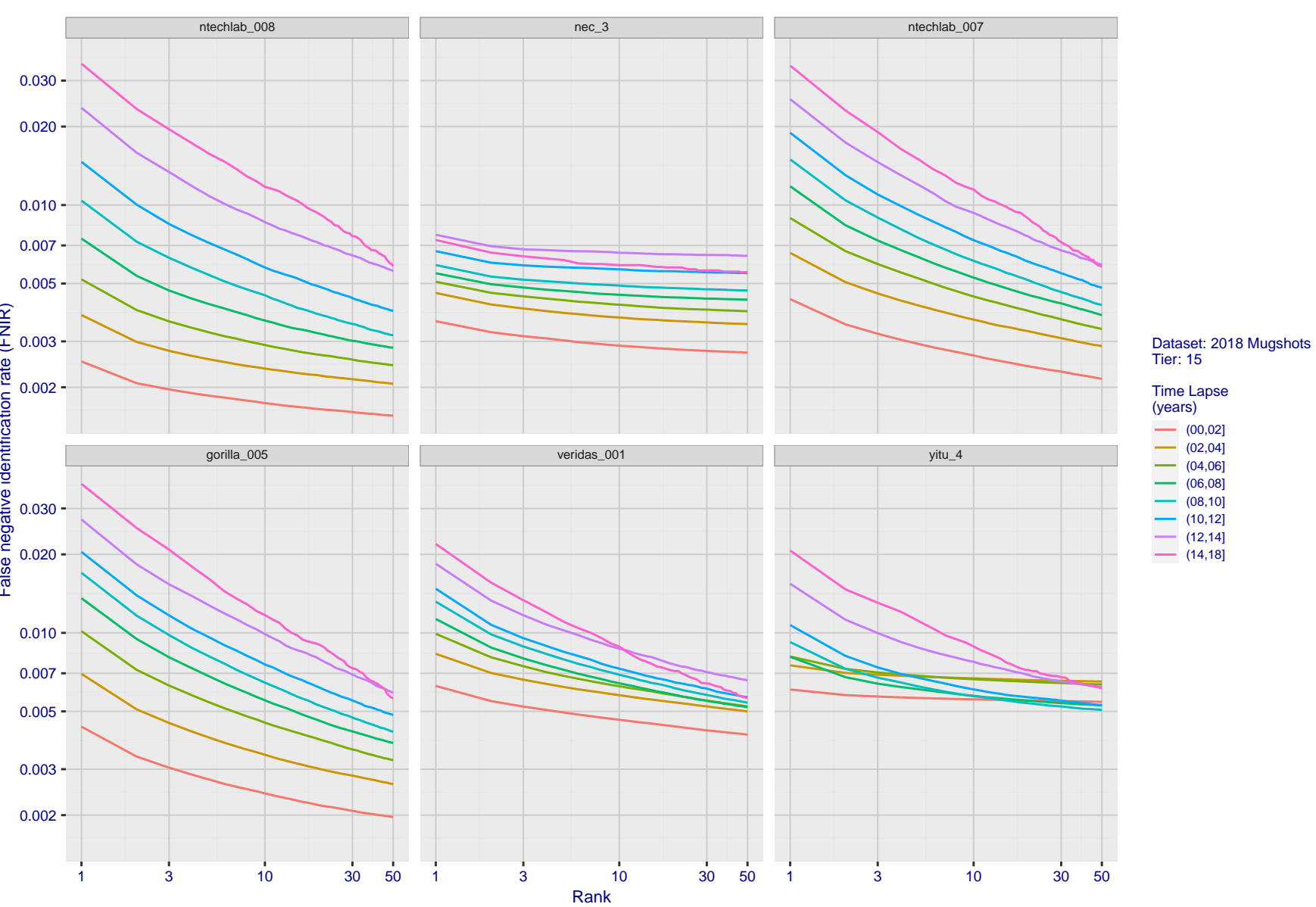


Figure 74: [FRVT-2018 Mugshot Ageing Dataset] Identification miss rates vs. rank by time-elapsed. The oldest image of each individual is enrolled. Thereafter, all more recent images are searched. Miss rates are computed over all searches noted in row 17 of Table 1 and binned by number of years between search and initial enrollment.

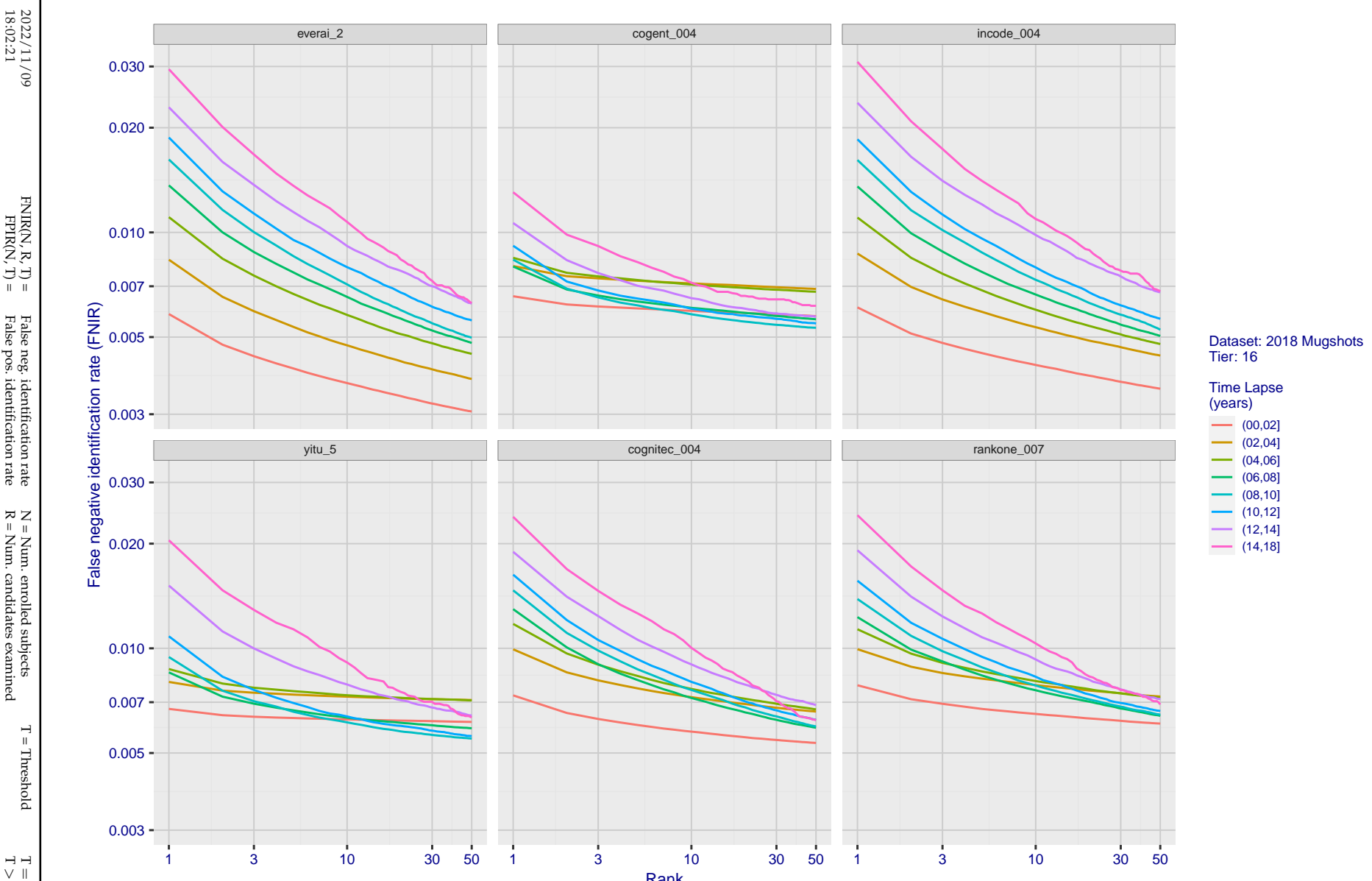


Figure 75: [FRVT-2018 Mugshot Ageing Dataset] Identification miss rates vs. rank by time-elapsed. The oldest image of each individual is enrolled. Thereafter, all more recent images are searched. Miss rates are computed over all searches noted in row 17 of Table 1 and binned by number of years between search and initial enrollment.

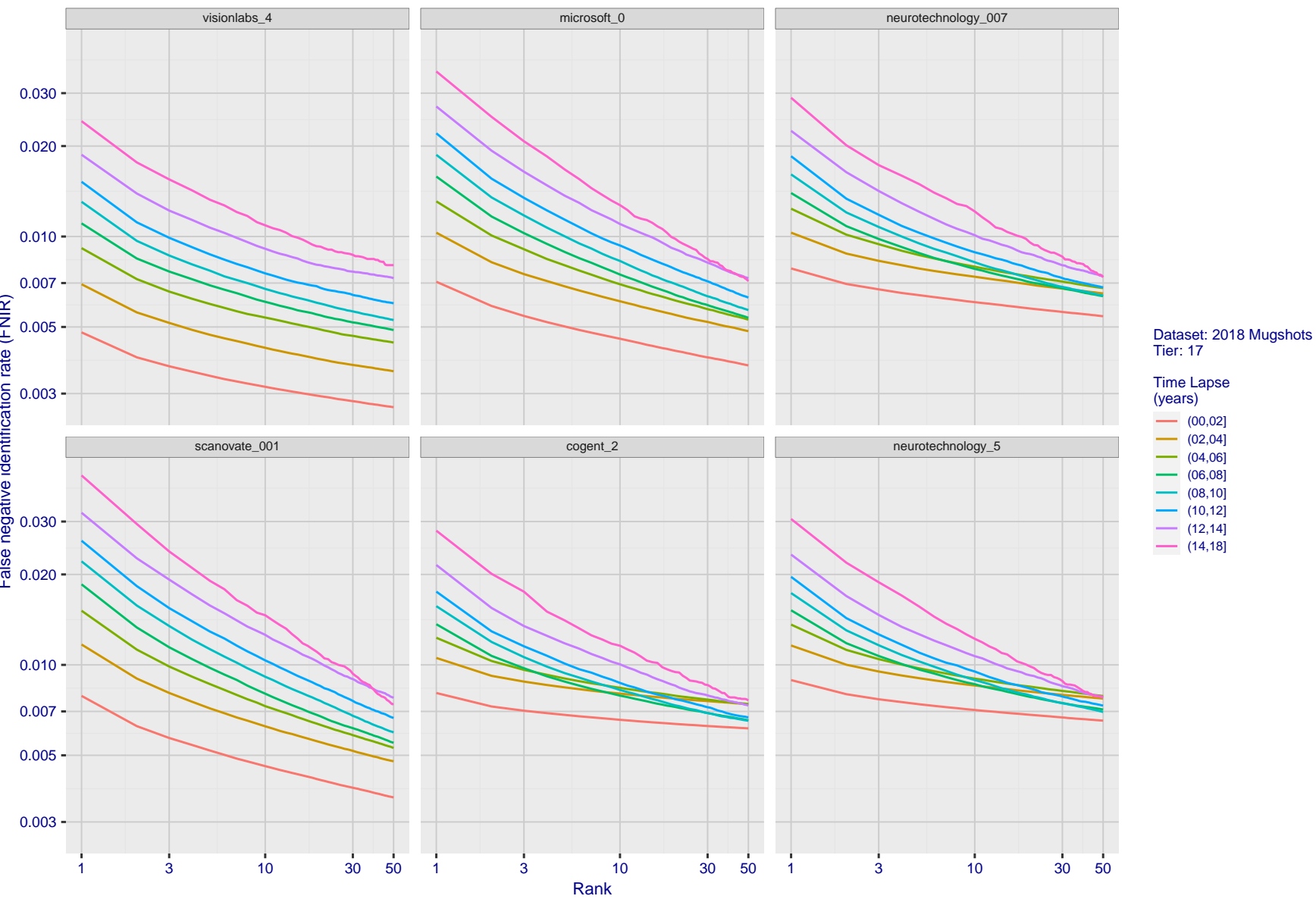
2022/11/09
18:02:21

Figure 76: [FRVT-2018 Mugshot Ageing Dataset] Identification miss rates vs. rank by time-elapsed. The oldest image of each individual is enrolled. Thereafter, all more recent images are searched. Miss rates are computed over all searches noted in row 17 of Table 1 and binned by number of years between search and initial enrollment.

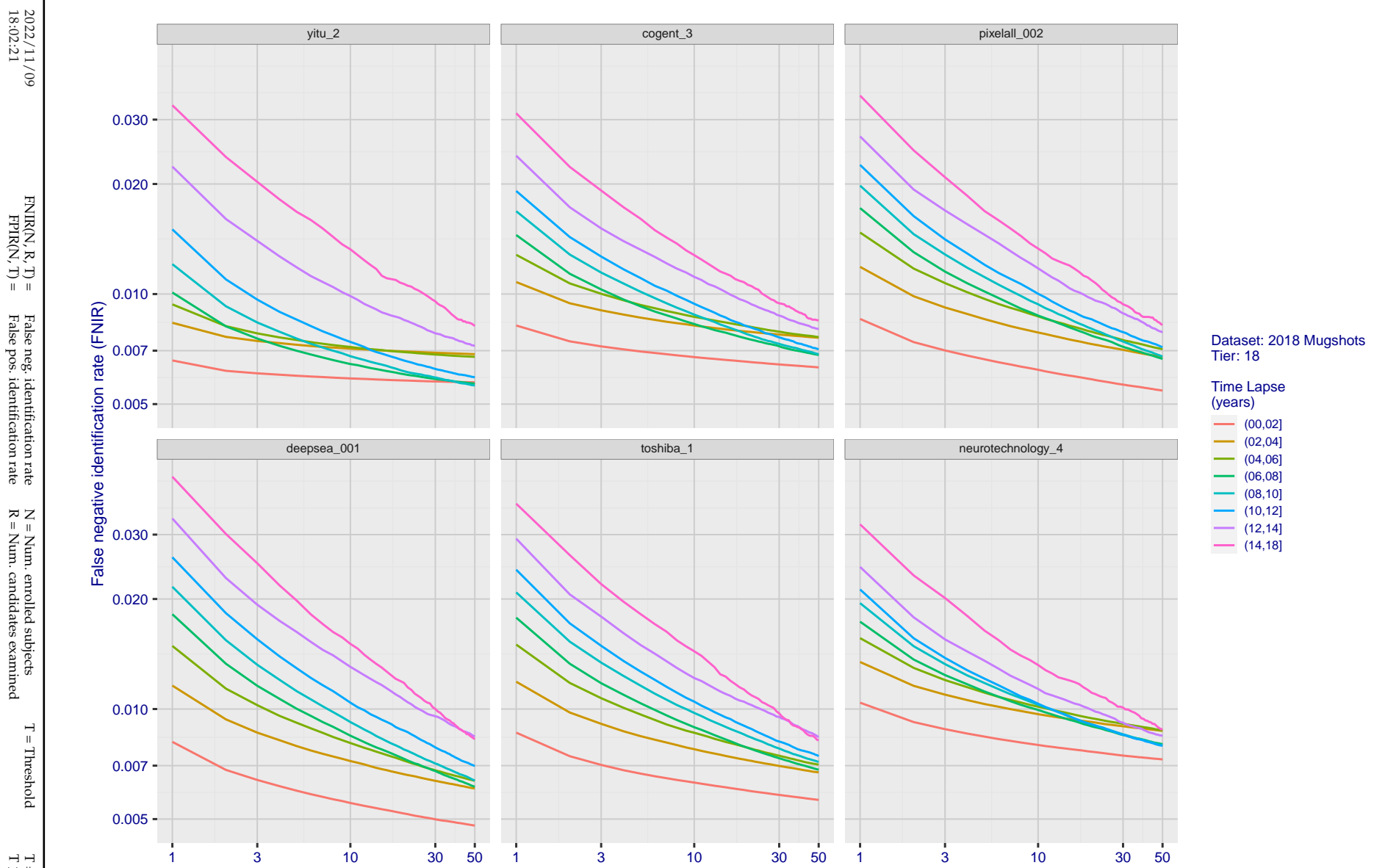


Figure 77: [FRVT-2018 Mugshot Ageing Dataset] Identification miss rates vs. rank by time elapsed. The oldest image of each individual is enrolled. Thereafter, all more recent images are searched. Miss rates are computed over all searches noted in row 17 of Table 1 and binned by number of years between search and initial enrollment.

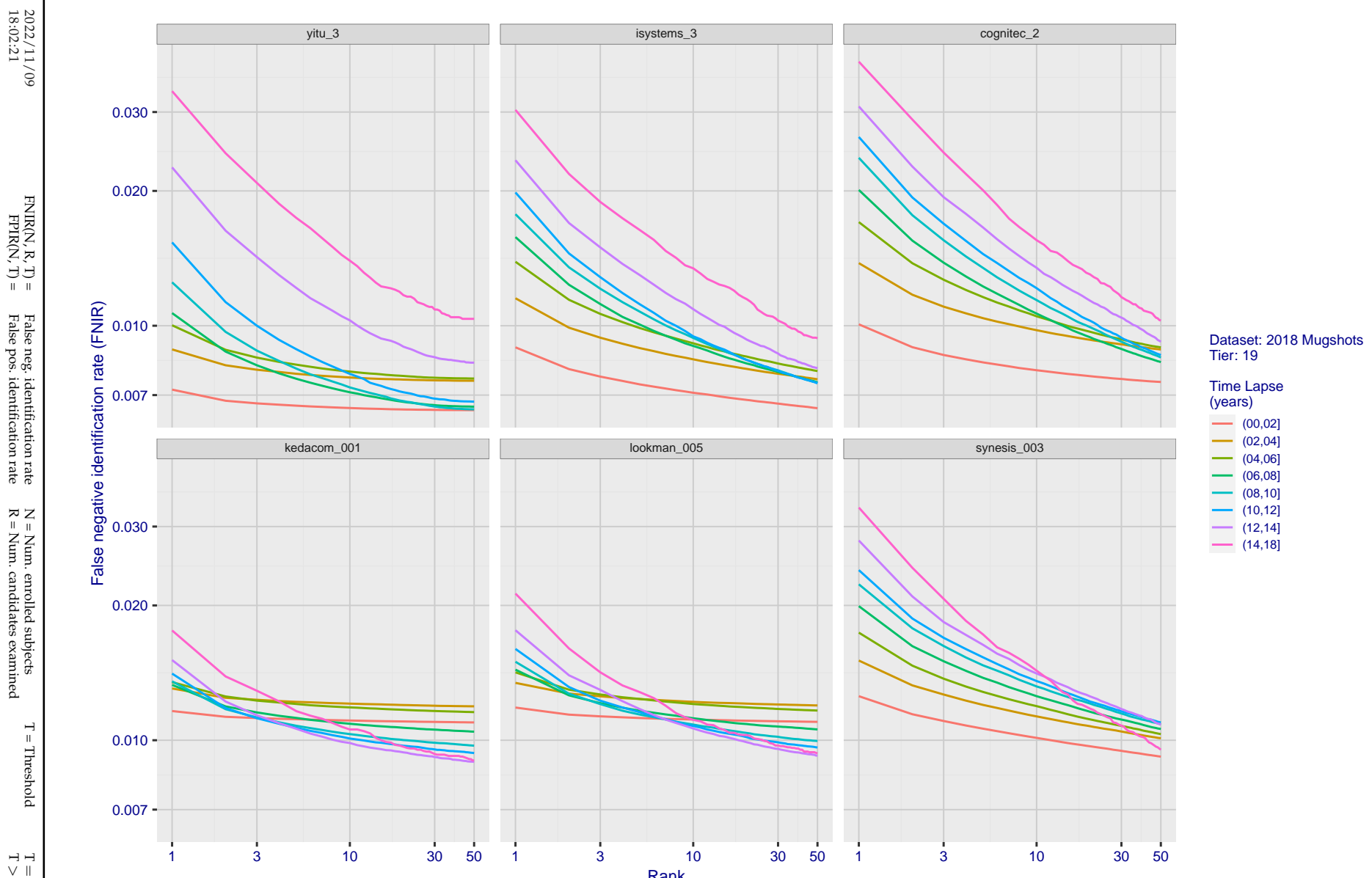


Figure 78: [FRVT-2018 Mugshot Ageing Dataset] Identification miss rates vs. rank by time-elapsed. The oldest image of each individual is enrolled. Thereafter, all more recent images are searched. Miss rates are computed over all searches noted in row 17 of Table 1 and binned by number of years between search and initial enrollment.

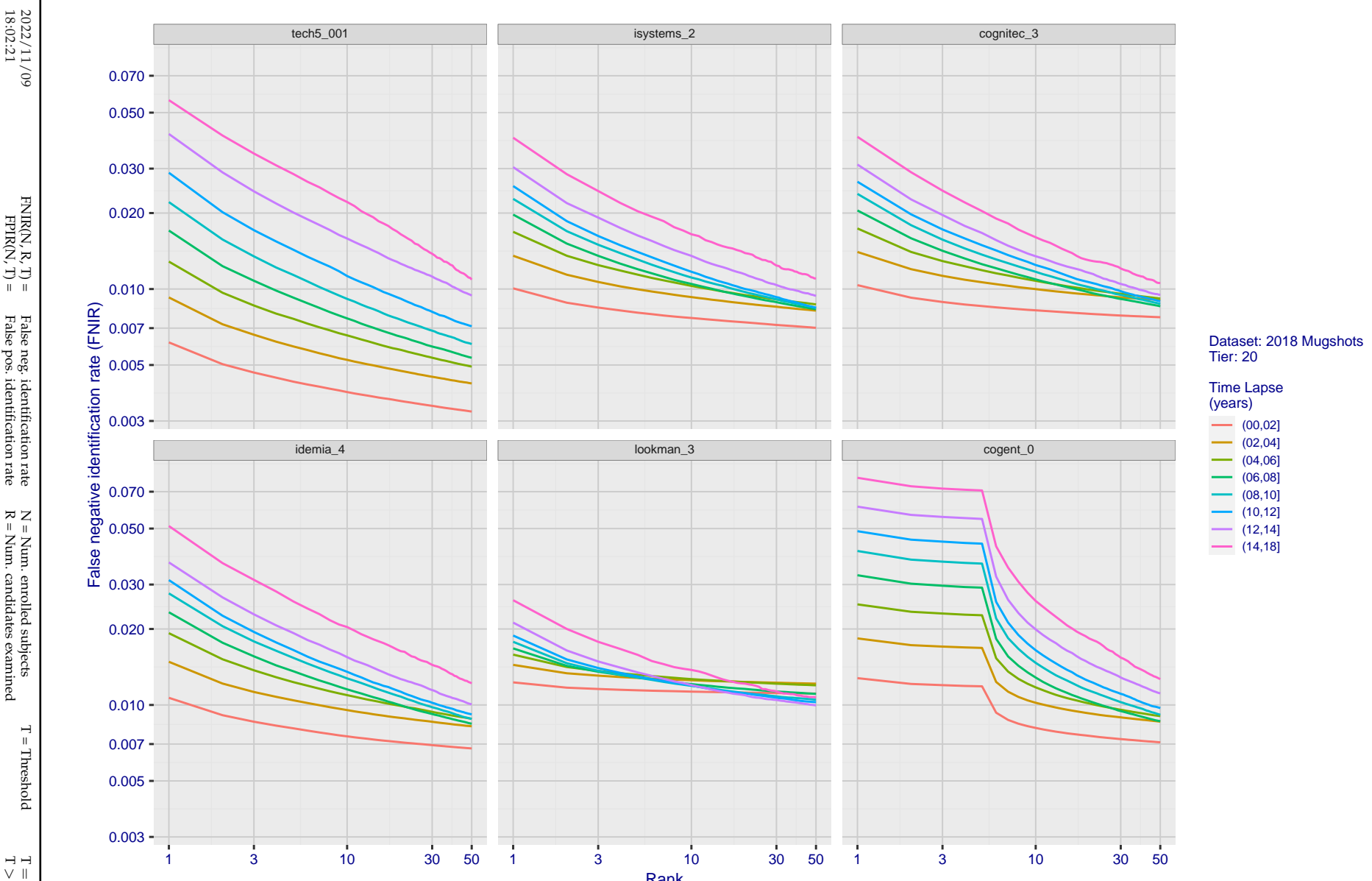


Figure 79: [FRVT-2018 Mugshot Ageing Dataset] Identification miss rates vs. rank by time-elapsed. The oldest image of each individual is enrolled. Thereafter, all more recent images are searched. Miss rates are computed over all searches noted in row 17 of Table 1 and binned by number of years between search and initial enrollment.

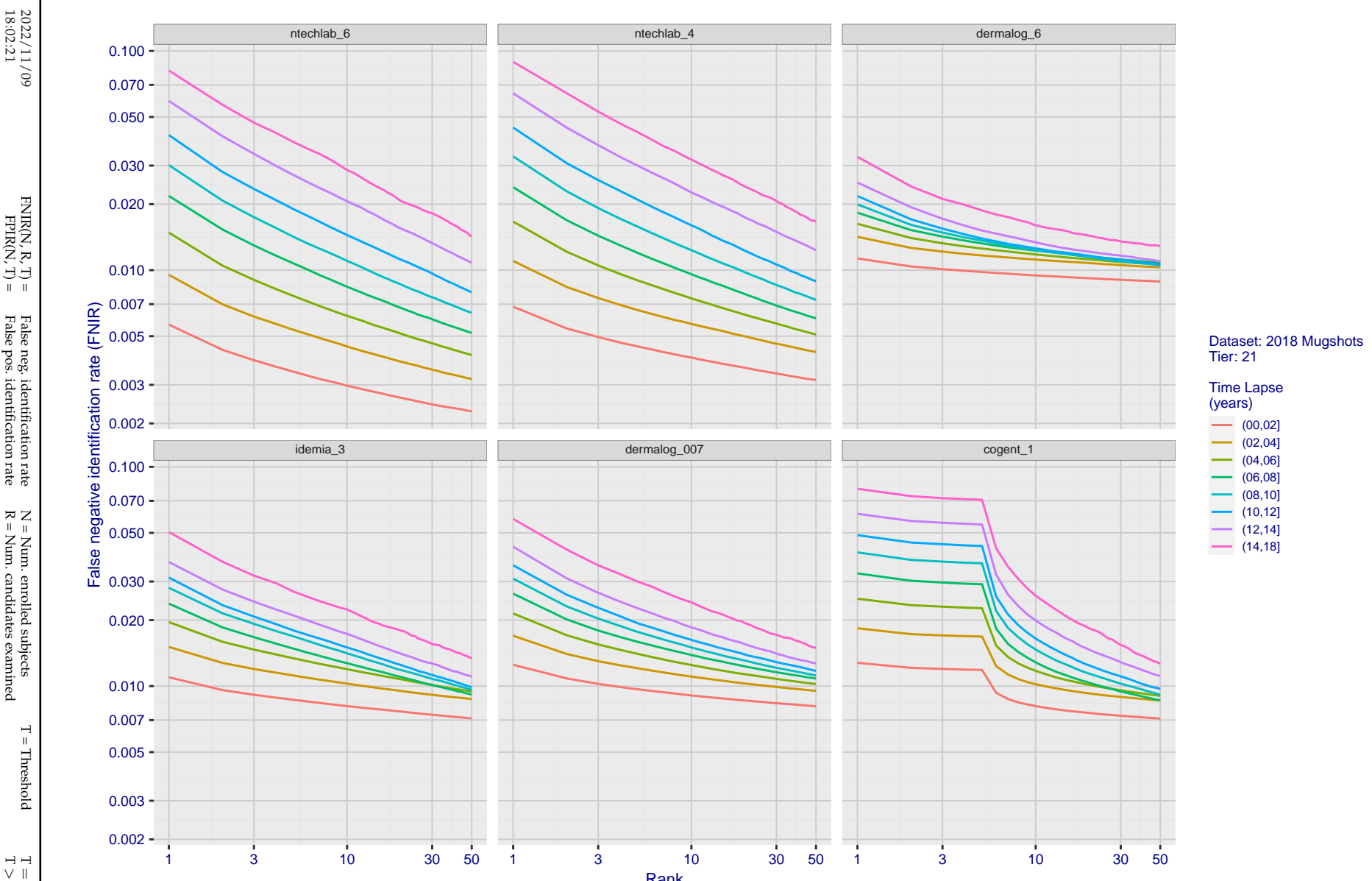


Figure 80: [FRVT-2018 Mugshot Ageing Dataset] Identification miss rates vs. rank by time-elapsed. The oldest image of each individual is enrolled. Thereafter, all more recent images are searched. Miss rates are computed over all searches noted in row 17 of Table 1 and binned by number of years between search and initial enrollment.

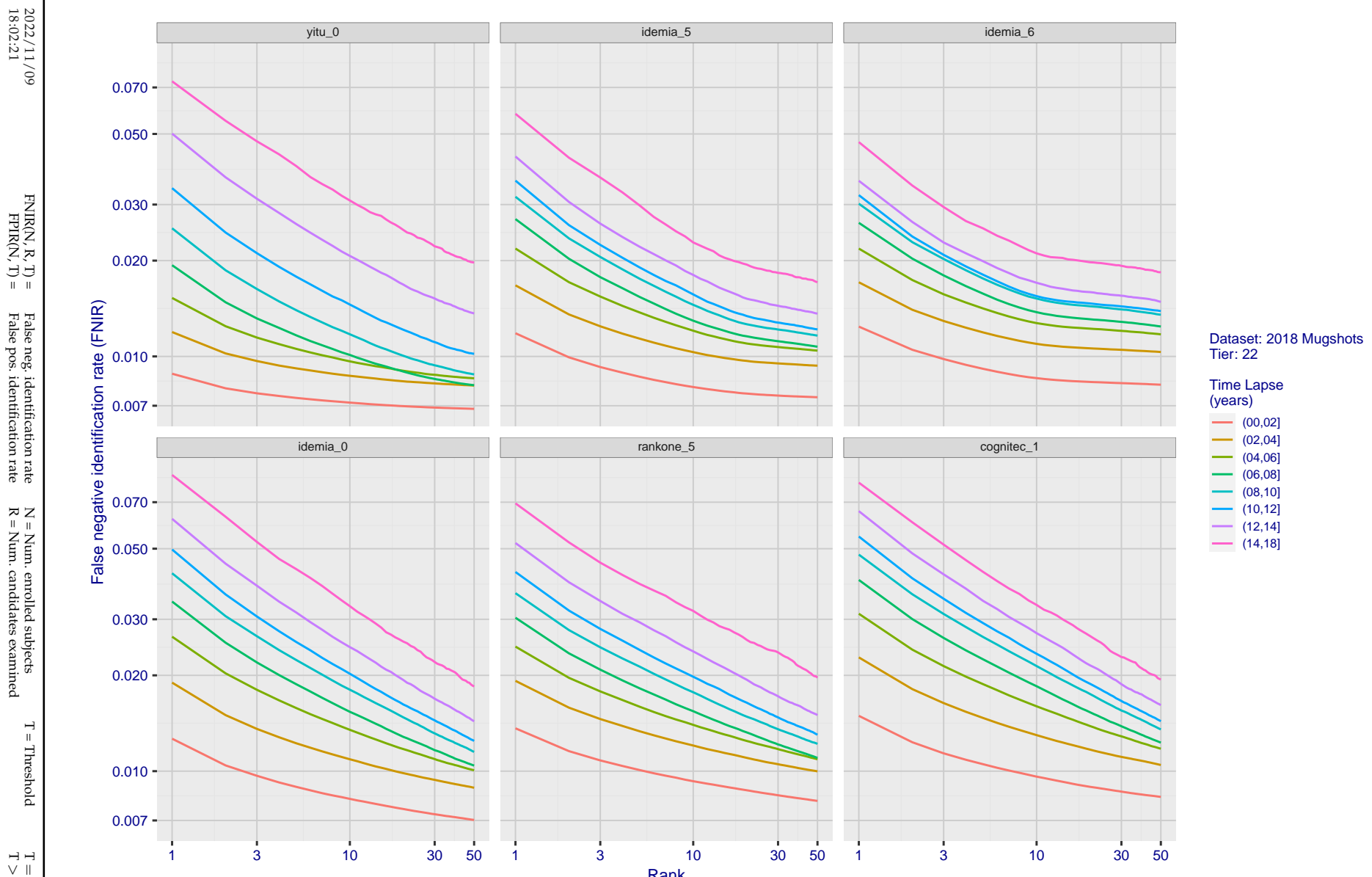


Figure 81: [FRVT-2018 Mugshot Ageing Dataset] Identification miss rates vs. rank by time-elapsed. The oldest image of each individual is enrolled. Thereafter, all more recent images are searched. Miss rates are computed over all searches noted in row 17 of Table 1 and binned by number of years between search and initial enrollment.

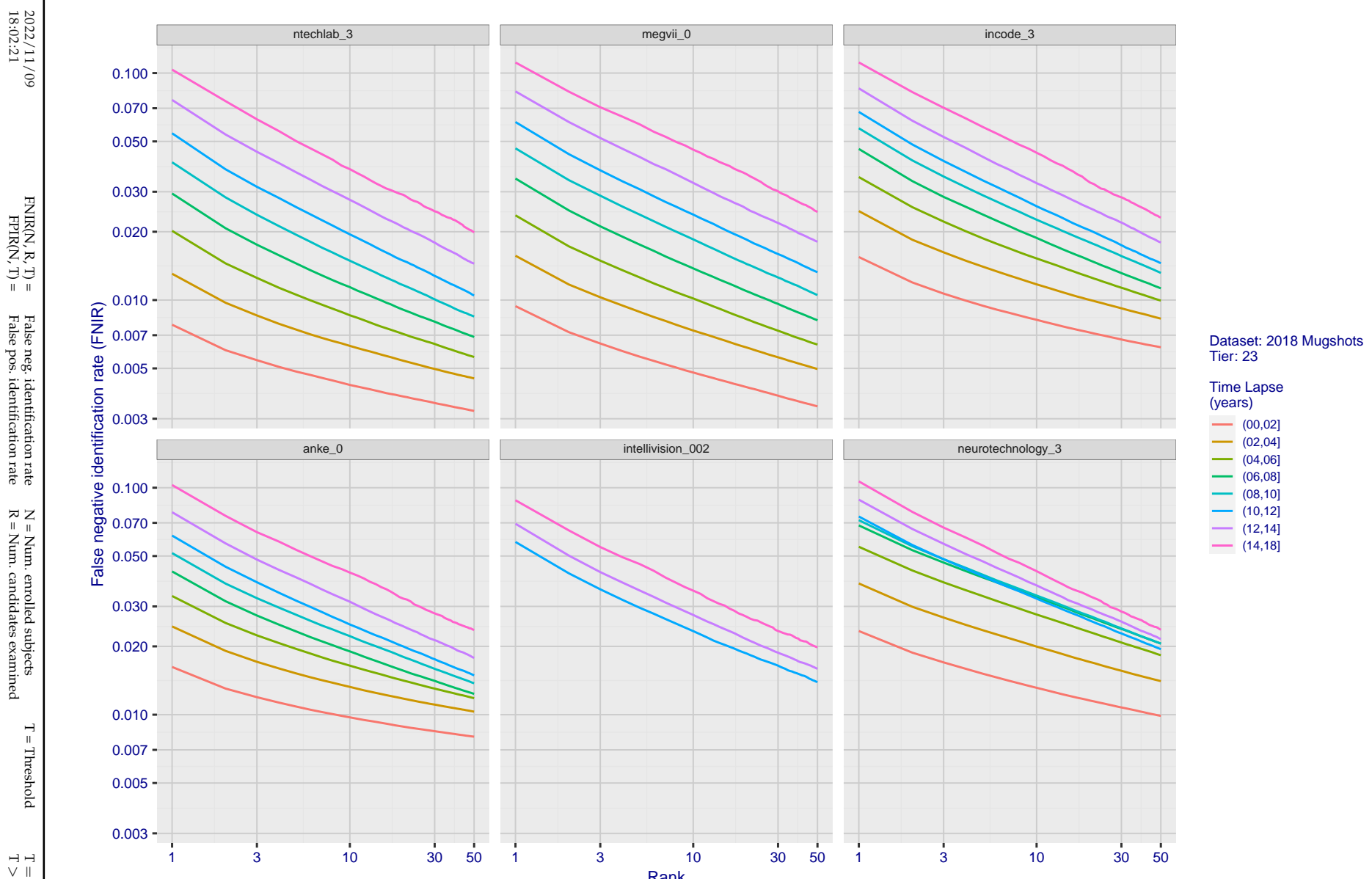


Figure 82: [FRVT-2018 Mugshot Ageing Dataset] Identification miss rates vs. rank by time-elapsed. The oldest image of each individual is enrolled. Thereafter, all more recent images are searched. Miss rates are computed over all searches noted in row 17 of Table 1 and binned by number of years between search and initial enrollment.

2022/11/09
18:02:21FNIR(N, R, T) = False neg. identification rate
FPIR(N, T) = False pos. identification rateN = Num. enrolled subjects
R = Num. candidates examinedT = Threshold
T = 0 → Investigation

T > 0 → Identification

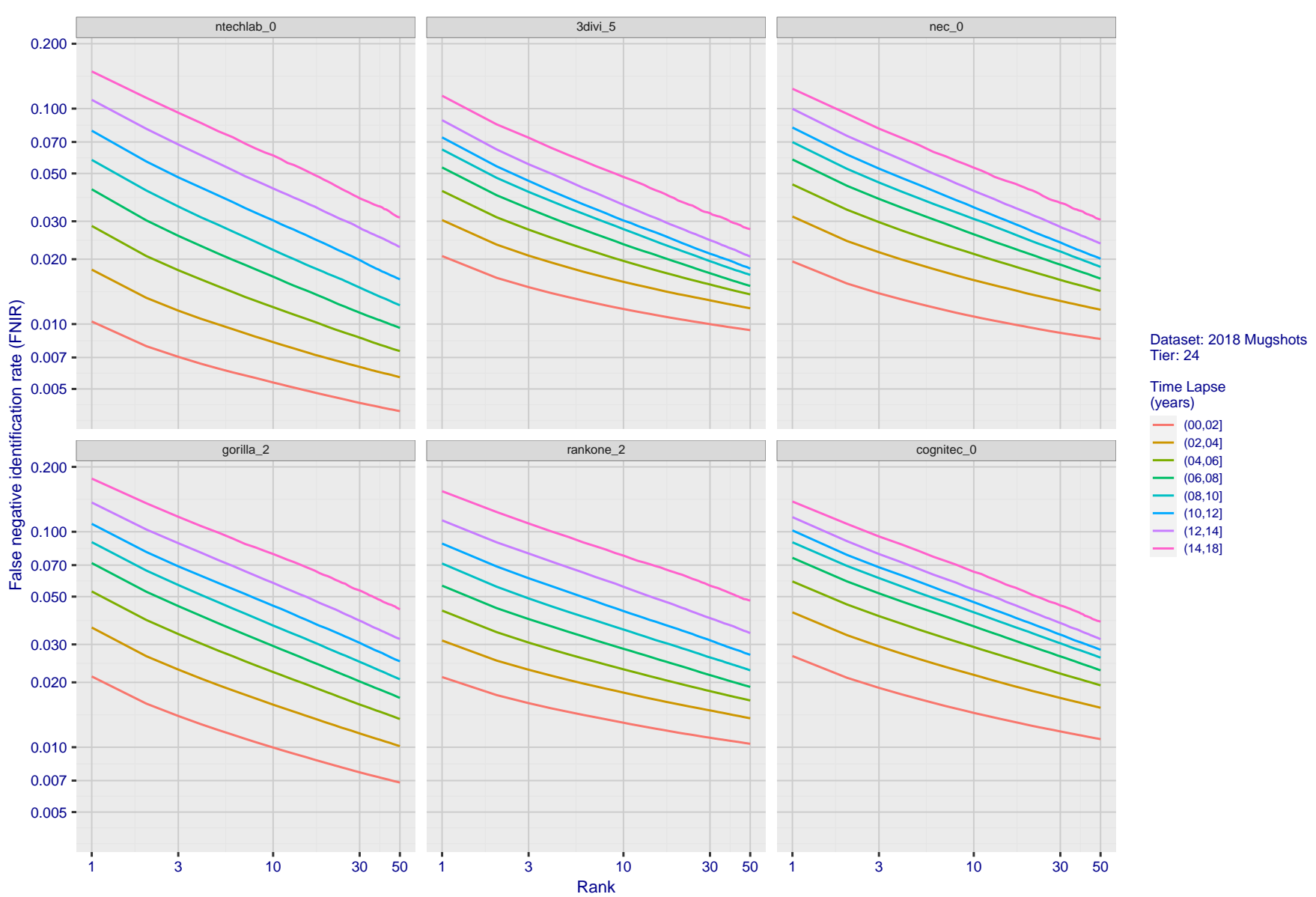


Figure 83: [FRVT-2018 Mugshot Ageing Dataset] Identification miss rates vs. rank by time-elapsed. The oldest image of each individual is enrolled. Thereafter, all more recent images are searched. Miss rates are computed over all searches noted in row 17 of Table 1 and binned by number of years between search and initial enrollment.

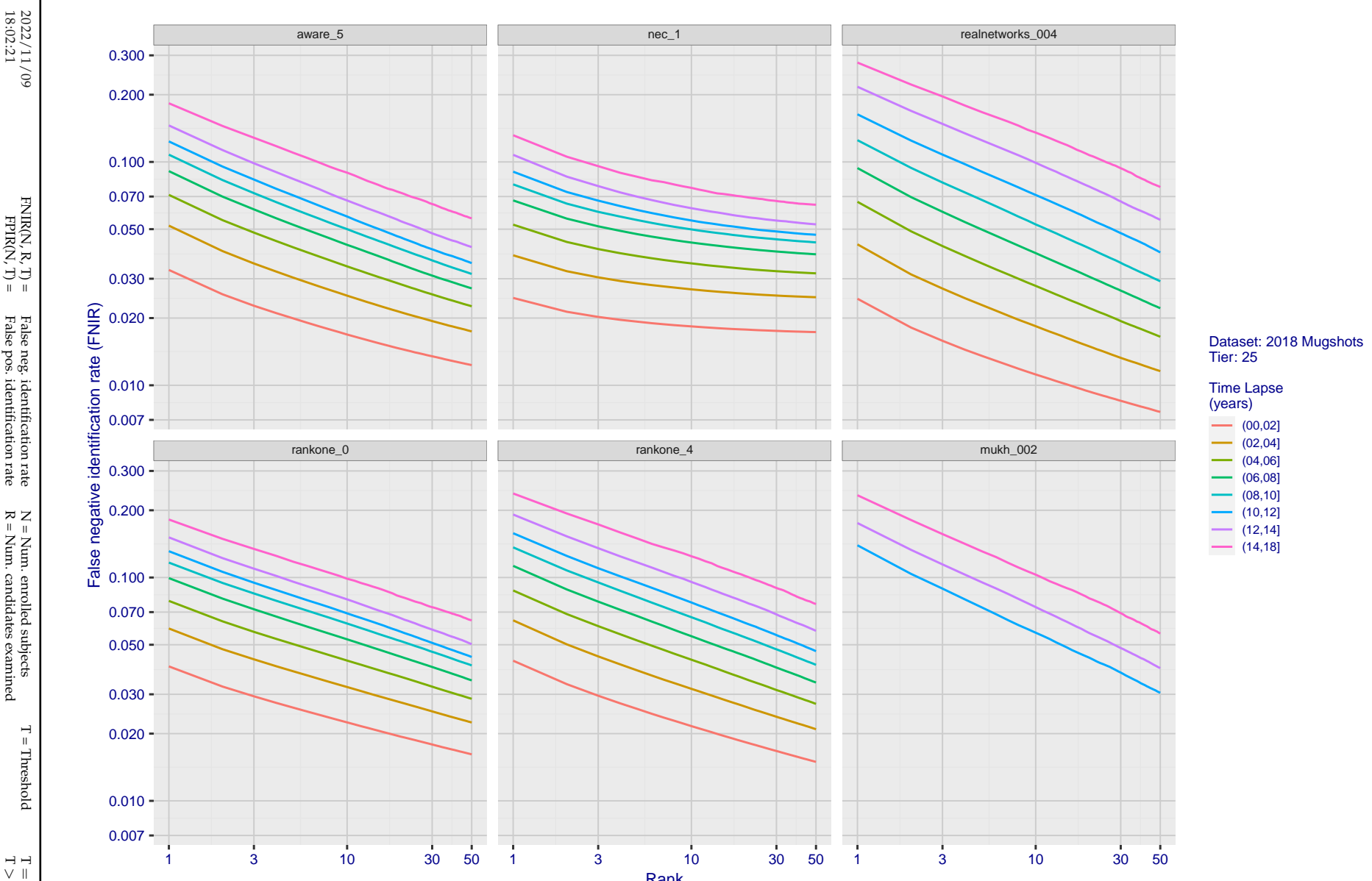


Figure 84: [FRVT-2018 Mugshot Ageing Dataset] Identification miss rates vs. rank by time-elapsed. The oldest image of each individual is enrolled. Thereafter, all more recent images are searched. Miss rates are computed over all searches noted in row 17 of Table 1 and binned by number of years between search and initial enrollment.

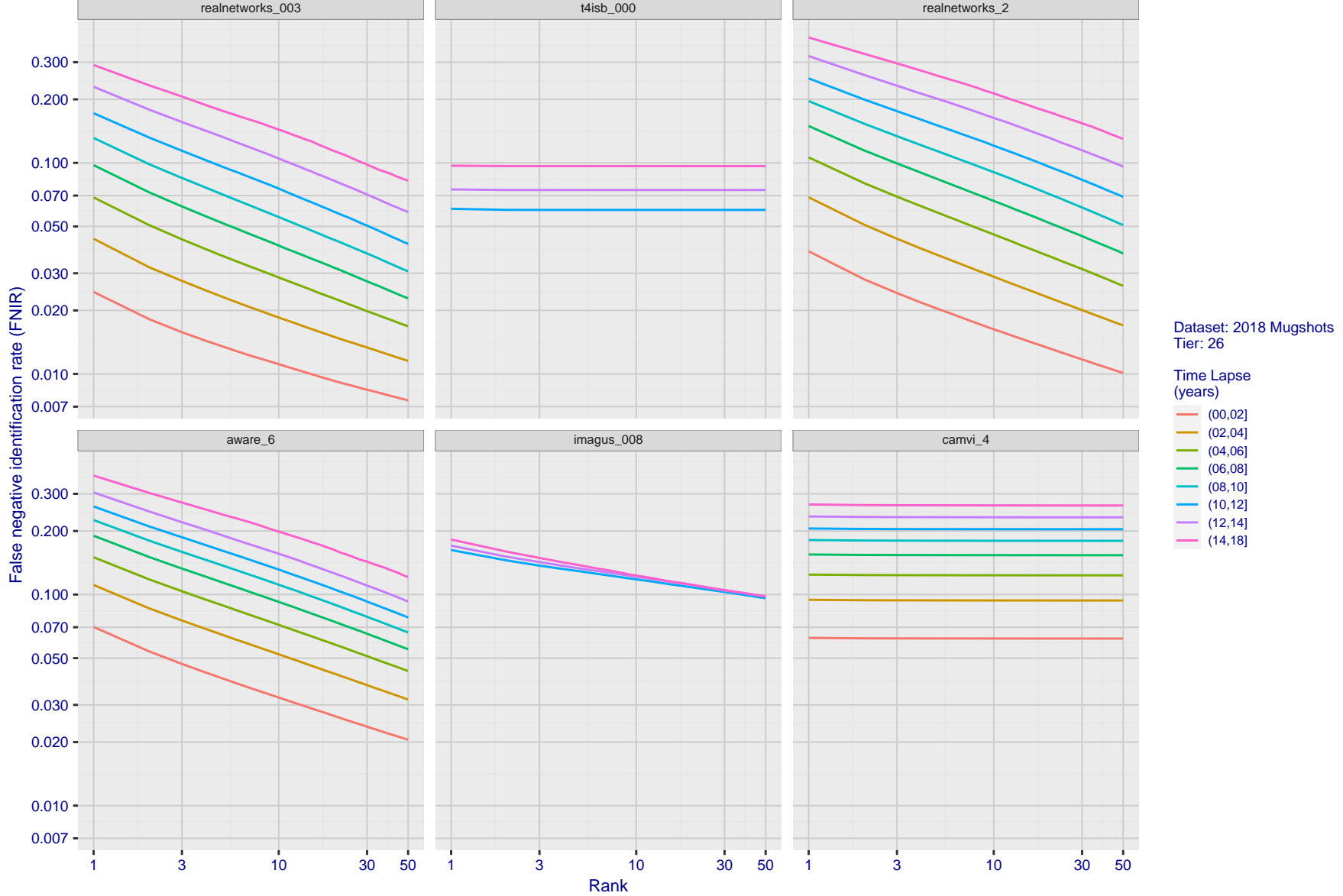


Figure 85: [FRVT-2018 Mugshot Ageing Dataset] Identification miss rates vs. rank by time-elapsed. The oldest image of each individual is enrolled. Thereafter, all more recent images are searched. Miss rates are computed over all searches noted in row 17 of Table 1 and binned by number of years between search and initial enrollment.

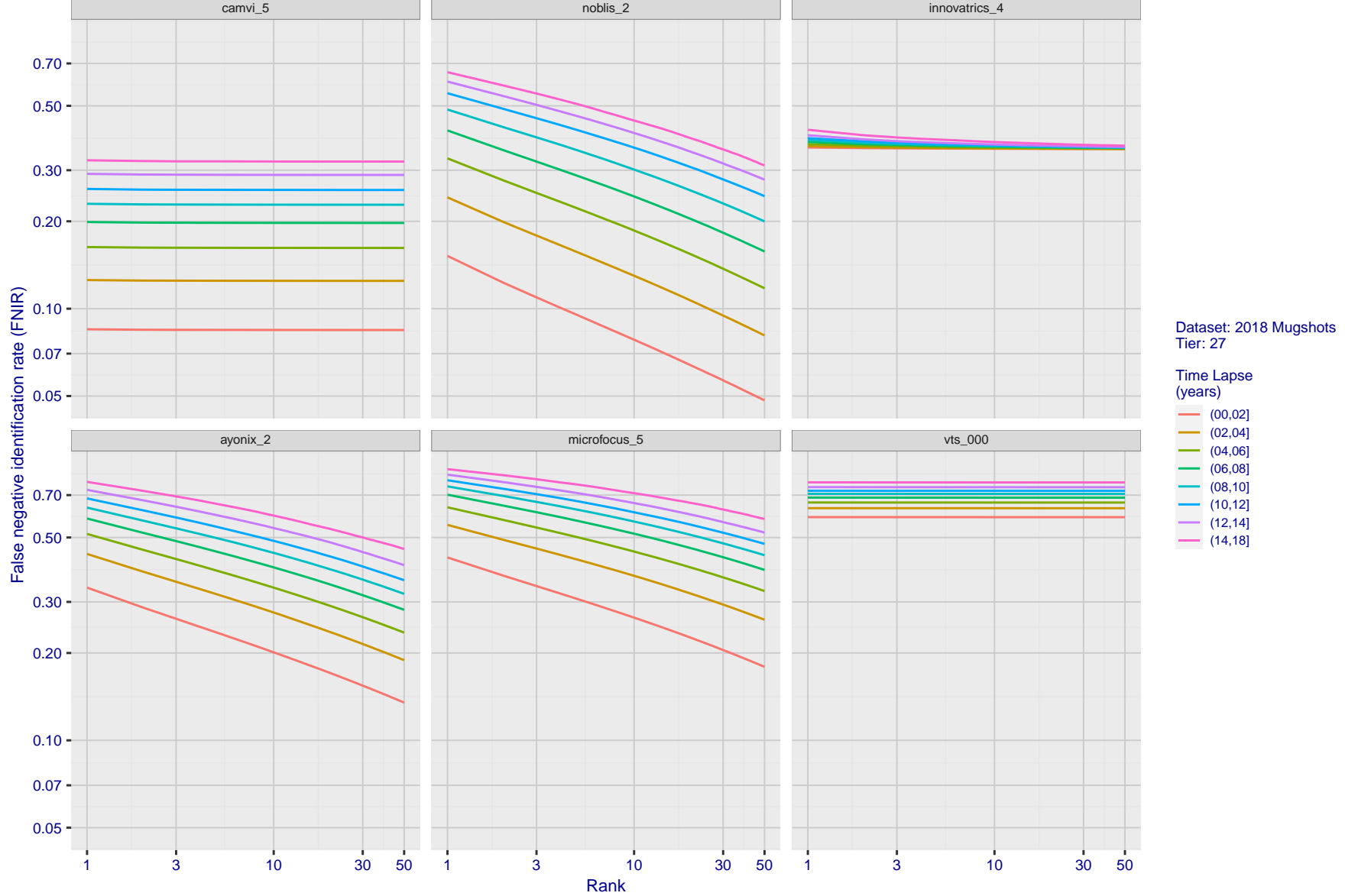


Figure 86: [FRVT-2018 Mugshot Ageing Dataset] Identification miss rates vs. rank by time-elapsed. The oldest image of each individual is enrolled. Thereafter, all more recent images are searched. Miss rates are computed over all searches noted in row 17 of Table 1 and binned by number of years between search and initial enrollment.

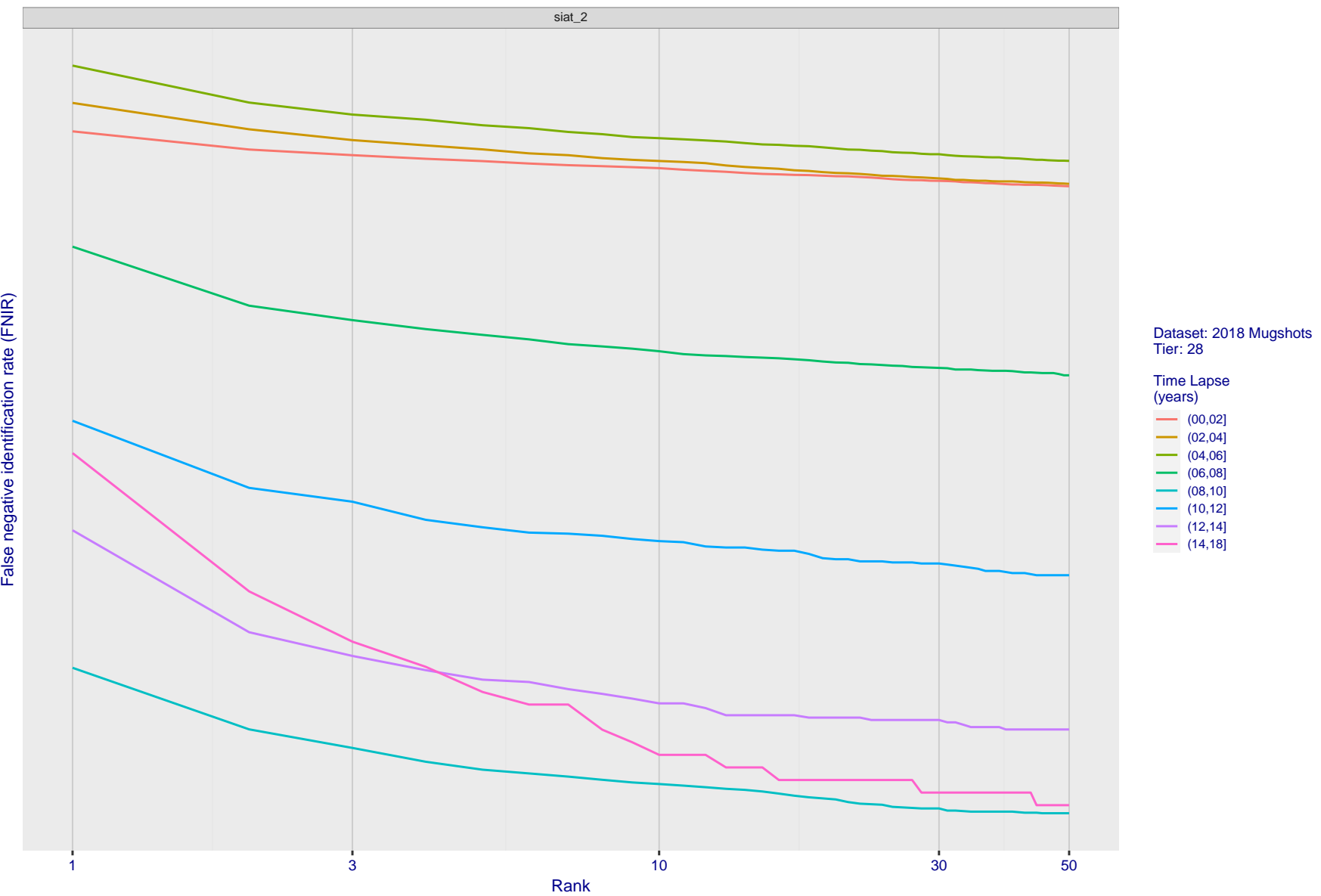


Figure 87: [FRVT-2018 Mugshot Ageing Dataset] Identification miss rates vs. rank by time-elapsed. The oldest image of each individual is enrolled. Thereafter, all more recent images are searched. Miss rates are computed over all searches noted in row 17 of Table 1 and binned by number of years between search and initial enrollment.

2022/11/09
18:02:21

$\text{FNIR}(N, R, T) =$ False neg. identification rate
 $\text{FPTR}(N, T) =$ False pos. identification rate

$N =$ Num. enrolled subjects
 $R =$ Num. candidates examined
 $T =$ Threshold
 $T = 0 \rightarrow$ Investigation
 $T > 0 \rightarrow$ Identification

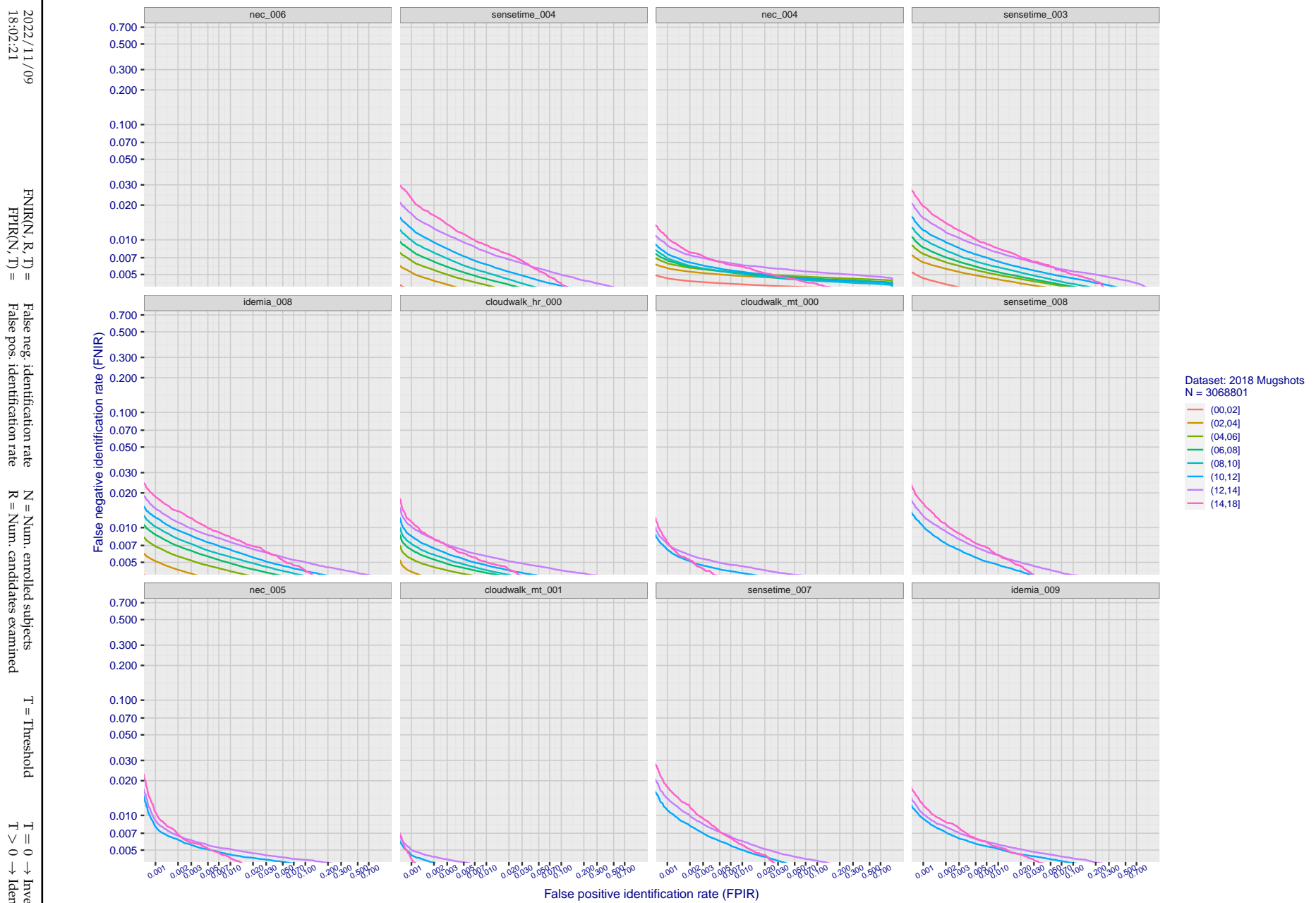


Figure 88: [FRVT-2018 Mugshot Ageing Dataset] Identification miss rates vs. FPIR by time-elapsed. The oldest image of each individual is enrolled. Thereafter, all more recent images are searched. Miss rates are computed over all searches noted in row 17 of Table 1 and binned by number of years between search and initial enrollment. FPIR is computed from the same FRVT 2018 non-mates noted in row 3 of Table 1 with $N = 3000000$.

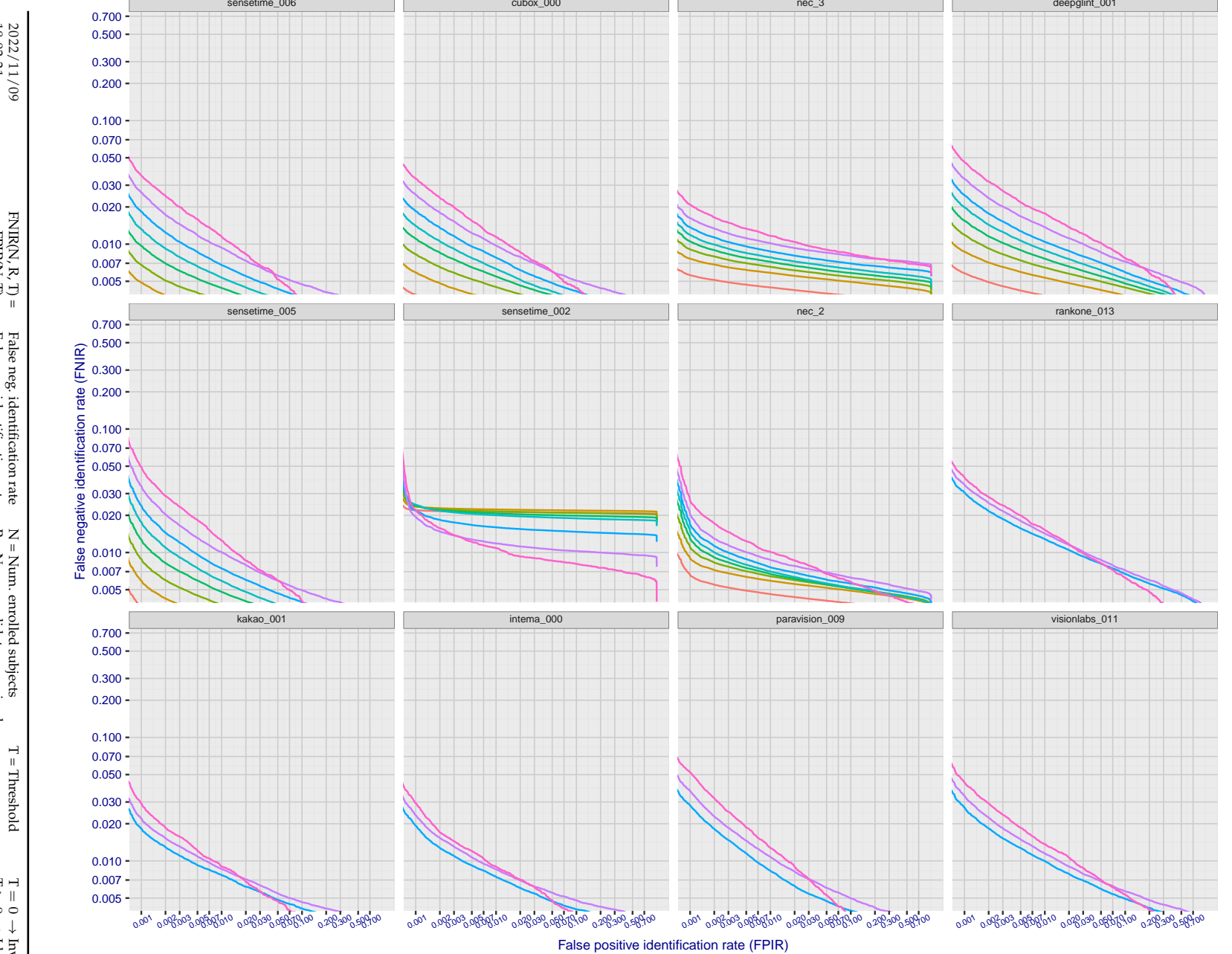


Figure 89: [FRVT-2018 Mugshot Ageing Dataset] Identification miss rates vs. FPIR by time elapsed. The oldest image of each individual is enrolled. Thereafter, all more recent images are searched. Miss rates are computed over all searches noted in row 17 of Table 1 and binned by number of years between search and initial enrollment. FPIR is computed from the same FRVT 2018 non-mates noted in row 3 of Table 1 with $N = 3\,000\,000$.

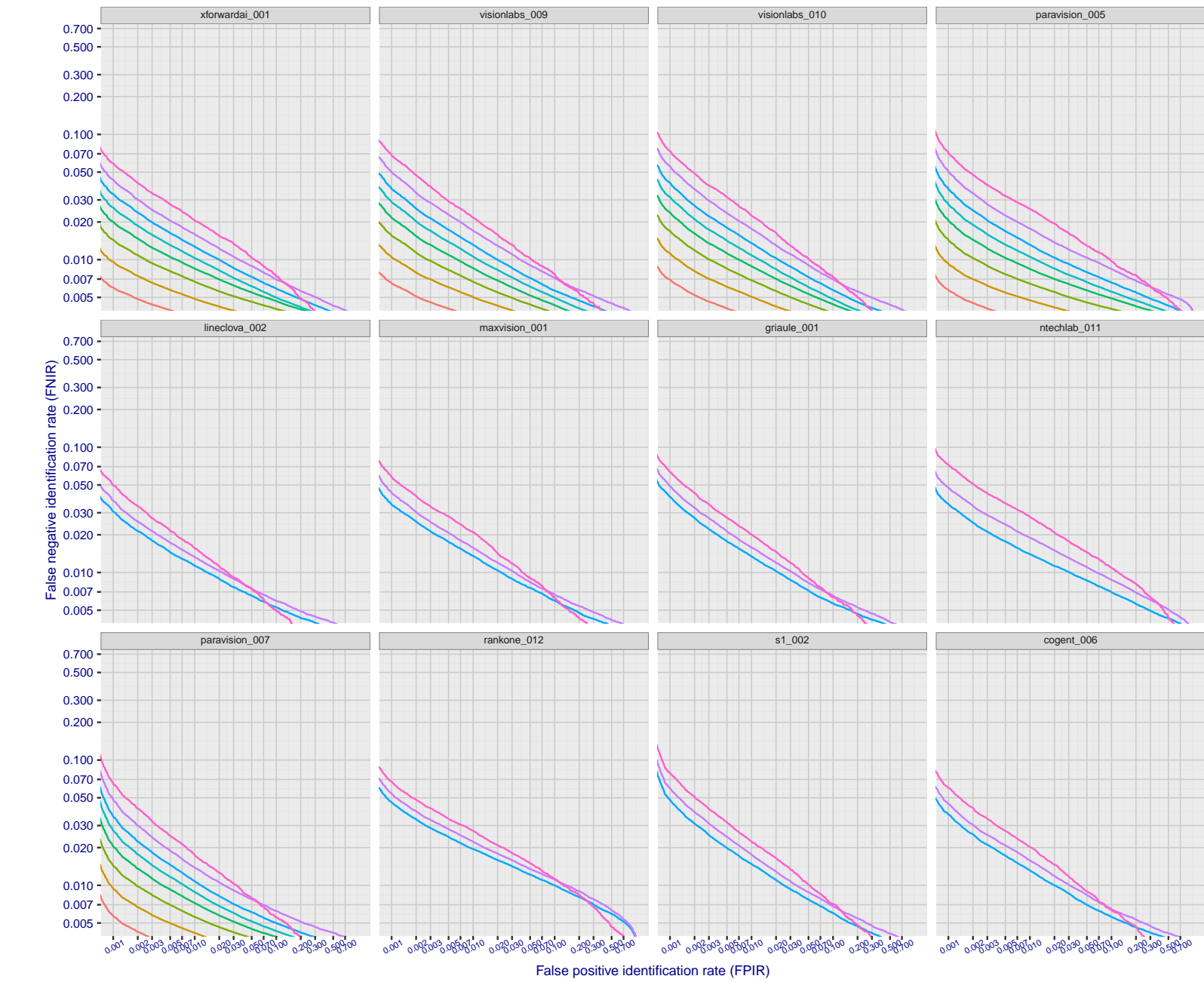


Figure 90: [FRVT-2018 Mugshot Ageing Dataset] Identification miss rates vs. FPIR by time-elapsed. The oldest image of each individual is enrolled. Thereafter, all more recent images are searched. Miss rates are computed over all searches noted in row 17 of Table 1 and binned by number of years between search and initial enrollment. FPIR is computed from the same FRVT 2018 non-mates noted in row 3 of Table 1 with $N = 3\,000\,000$.

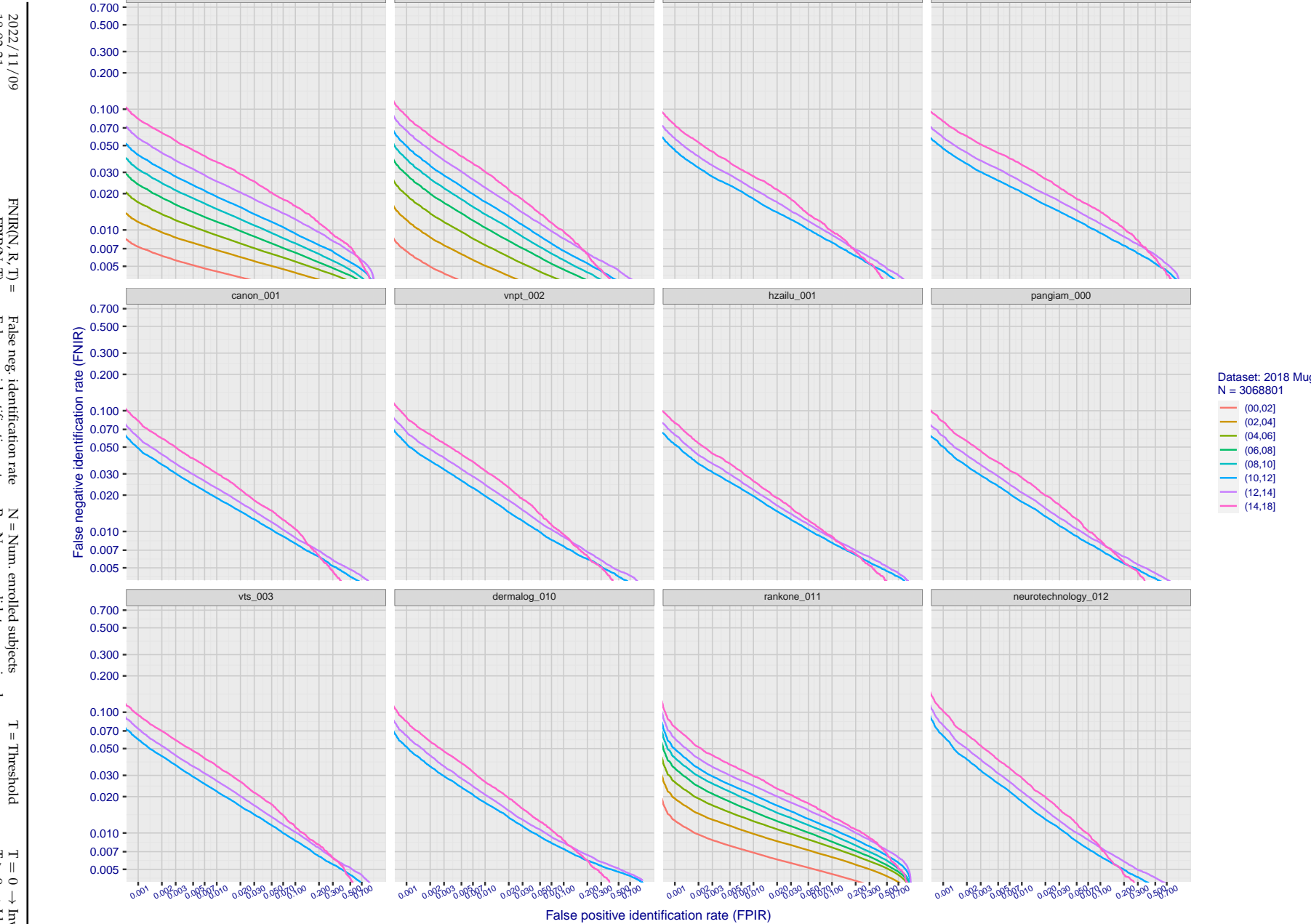


Figure 91: [FRVT-2018 Mugshot Ageing Dataset] Identification miss rates vs. FPIR by time elapsed. The oldest image of each individual is enrolled. Thereafter, all more recent images are searched. Miss rates are computed over all searches noted in row 17 of Table 1 and binned by number of years between search and initial enrollment. FPIR is computed from the same FRVT 2018 non-mates noted in row 3 of Table 1 with $N = 3000\,000$.

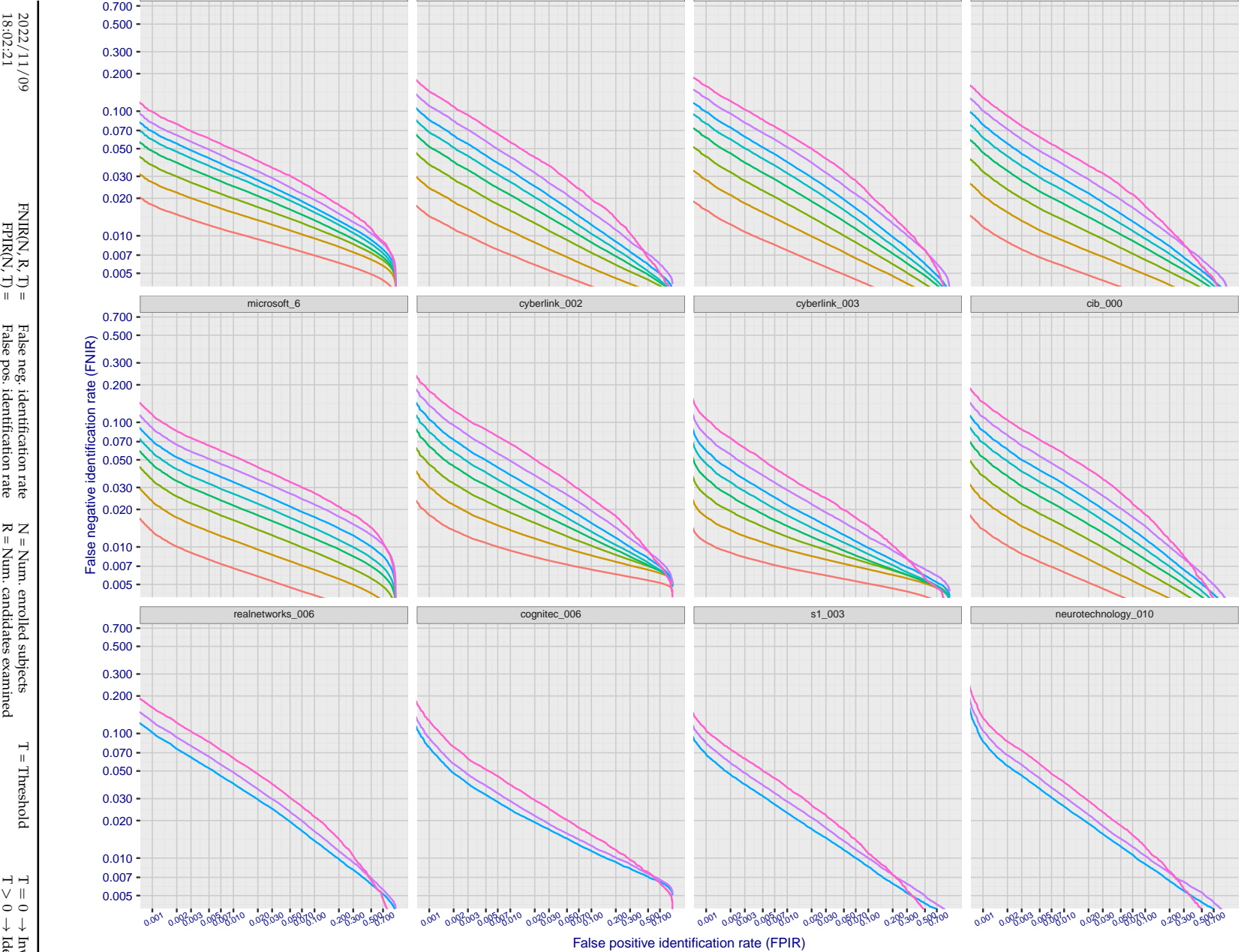


Figure 92: [FRVT-2018 Mugshot Ageing Dataset] Identification miss rates vs. FPIR by time-elapsed. The oldest image of each individual is enrolled. Thereafter, all more recent images are searched. Miss rates are computed over all searches noted in row 17 of Table 1 and binned by number of years between search and initial enrollment. FPIR is computed from the same FRVT 2018 non-mates noted in row 3 of Table 1 with $N = 3\,000\,000$.

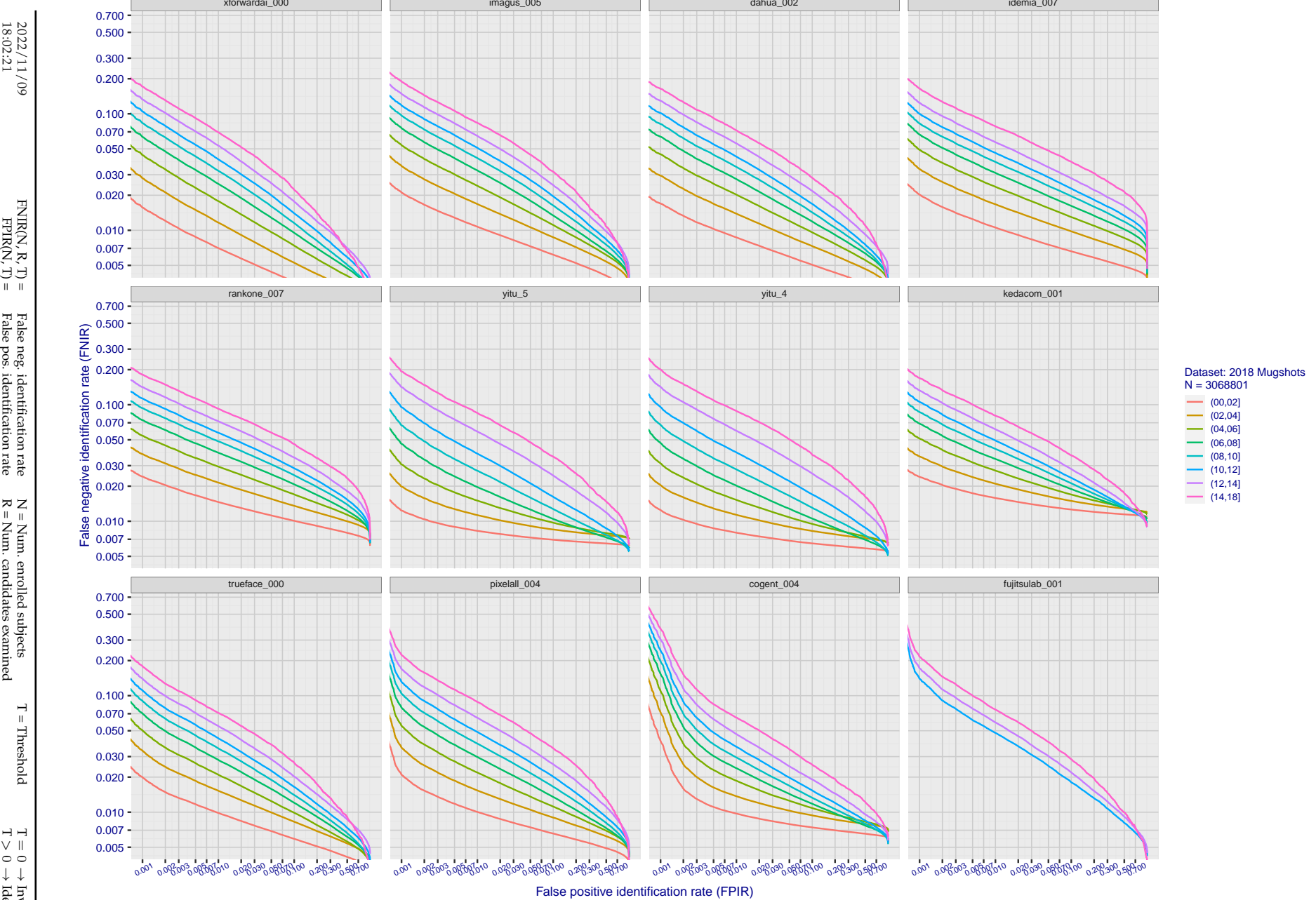


Figure 93: [FRVT-2018 Mugshot Ageing Dataset] Identification miss rates vs. FPIR by time-elapsed. The oldest image of each individual is enrolled. Thereafter, all more recent images are searched. Miss rates are computed over all searches noted in row 17 of Table 1 and binned by number of years between search and initial enrollment. FPIR is computed from the same FRVT 2018 non-mates noted in row 3 of Table 1 with $N = 3\,000\,000$.

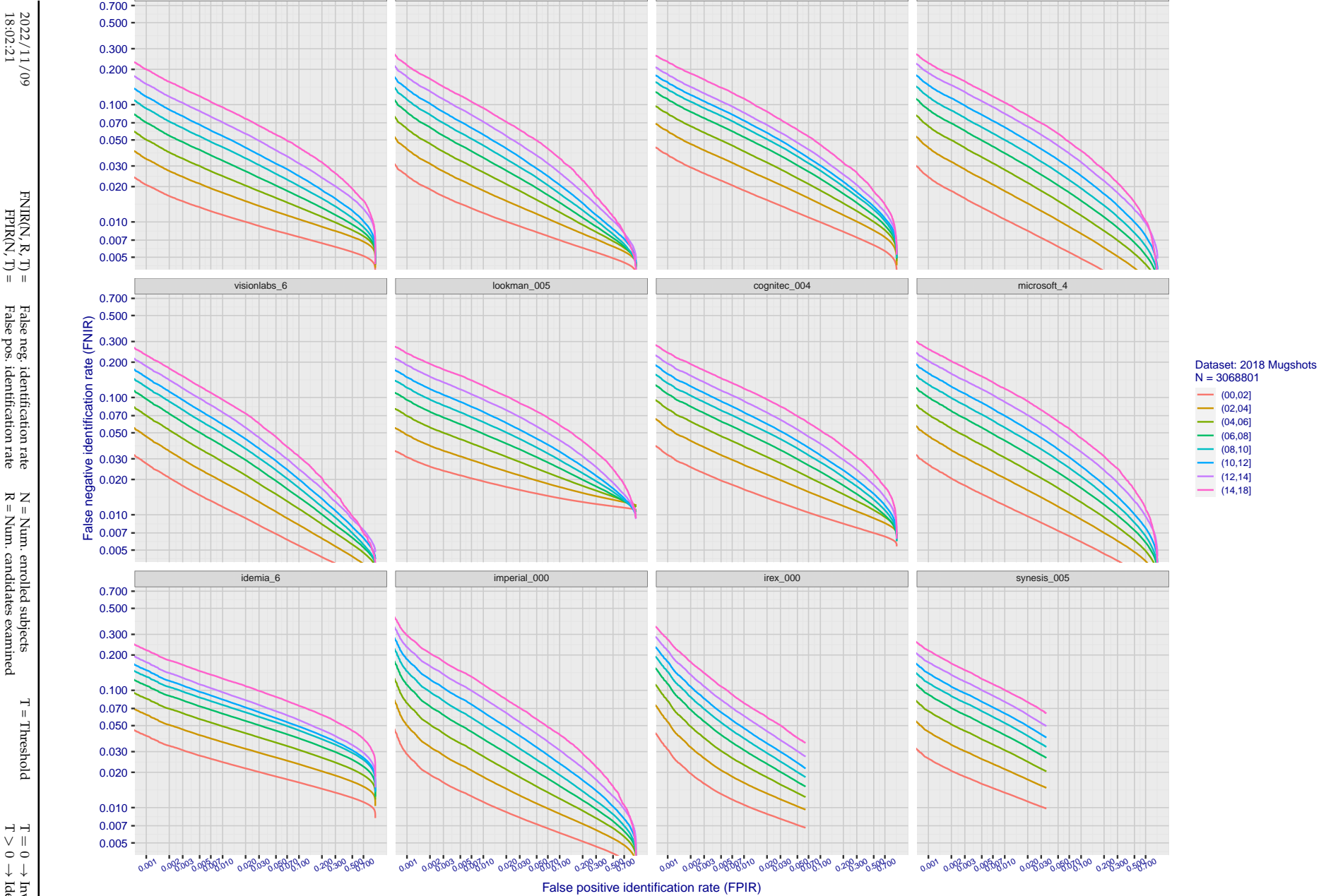


Figure 94: [FRVT-2018 Mugshot Ageing Dataset] Identification miss rates vs. FPIR by time-elapsed. The oldest image of each individual is enrolled. Thereafter, all more recent images are searched. Miss rates are computed over all searches noted in row 17 of Table 1 and binned by number of years between search and initial enrollment. FPIR is computed from the same FRVT 2018 non-mates noted in row 3 of Table 1 with N = 3 000 000.

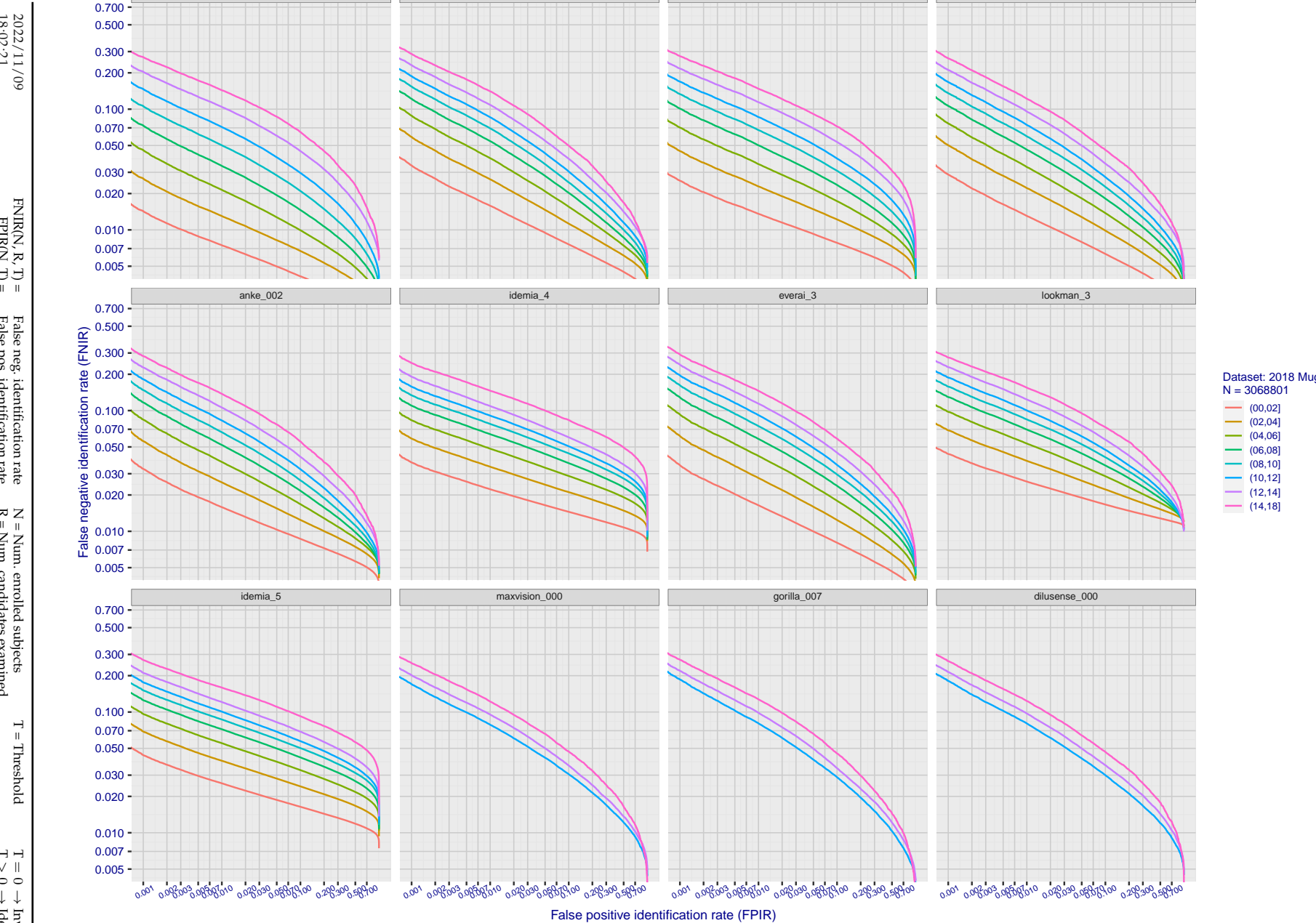


Figure 95: [FRVT-2018 Mugshot Ageing Dataset] Identification miss rates vs. FPIR by time-elapsed. The oldest image of each individual is enrolled. Thereafter, all more recent images are searched. Miss rates are computed over all searches noted in row 17 of Table 1 and binned by number of years between search and initial enrollment. FPIR is computed from the same FRVT 2018 non-mates noted in row 3 of Table 1 with N = 3 000 000.

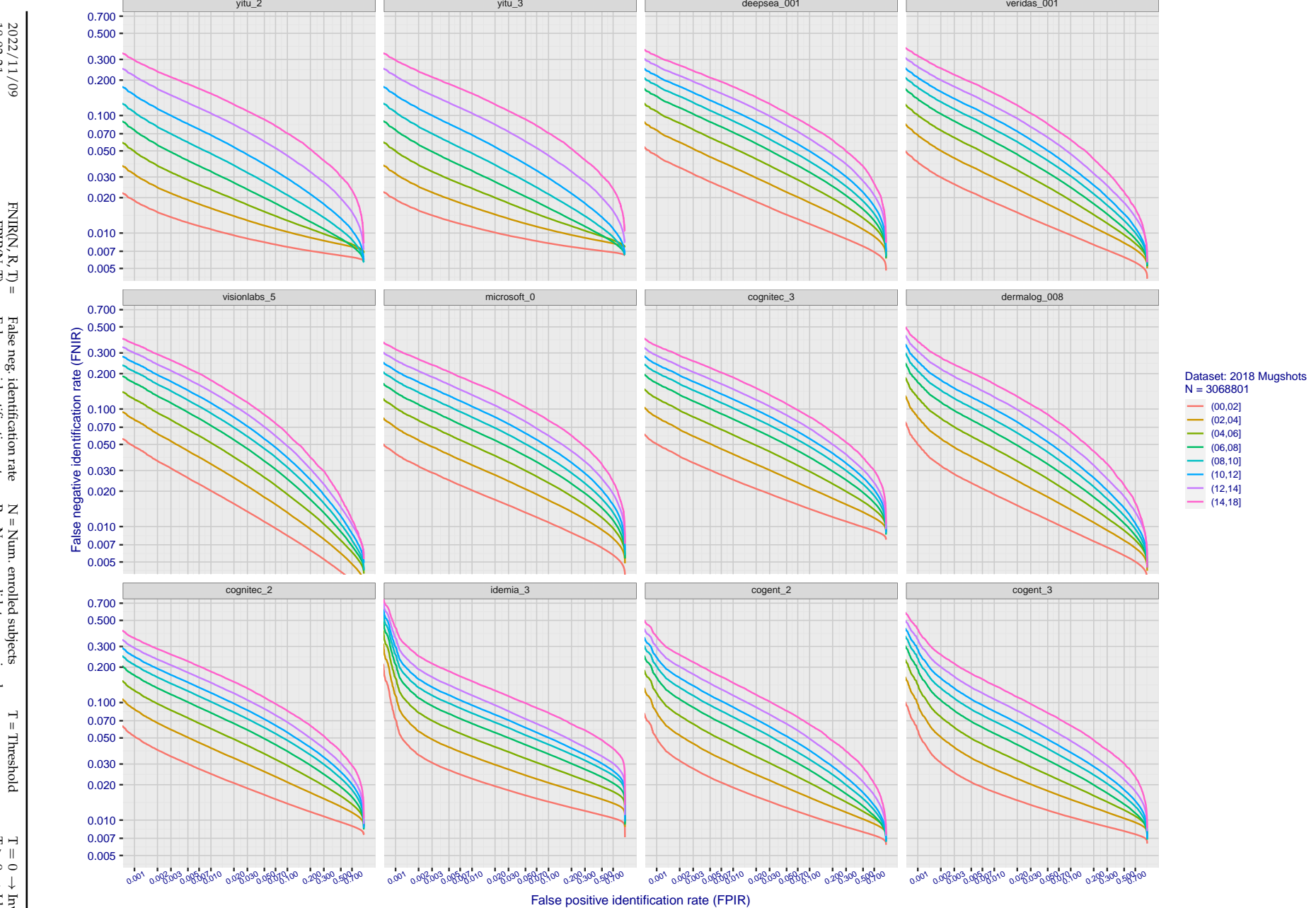


Figure 96: [FRVT-2018 Mugshot Ageing Dataset] Identification miss rates vs. FPIR by time-elapsed. The oldest image of each individual is enrolled. Thereafter, all more recent images are searched. Miss rates are computed over all searches noted in row 17 of Table 1 and binned by number of years between search and initial enrollment. FPIR is computed from the same FRVT 2018 non-mates noted in row 3 of Table 1 with $N = 3\,000\,000$.

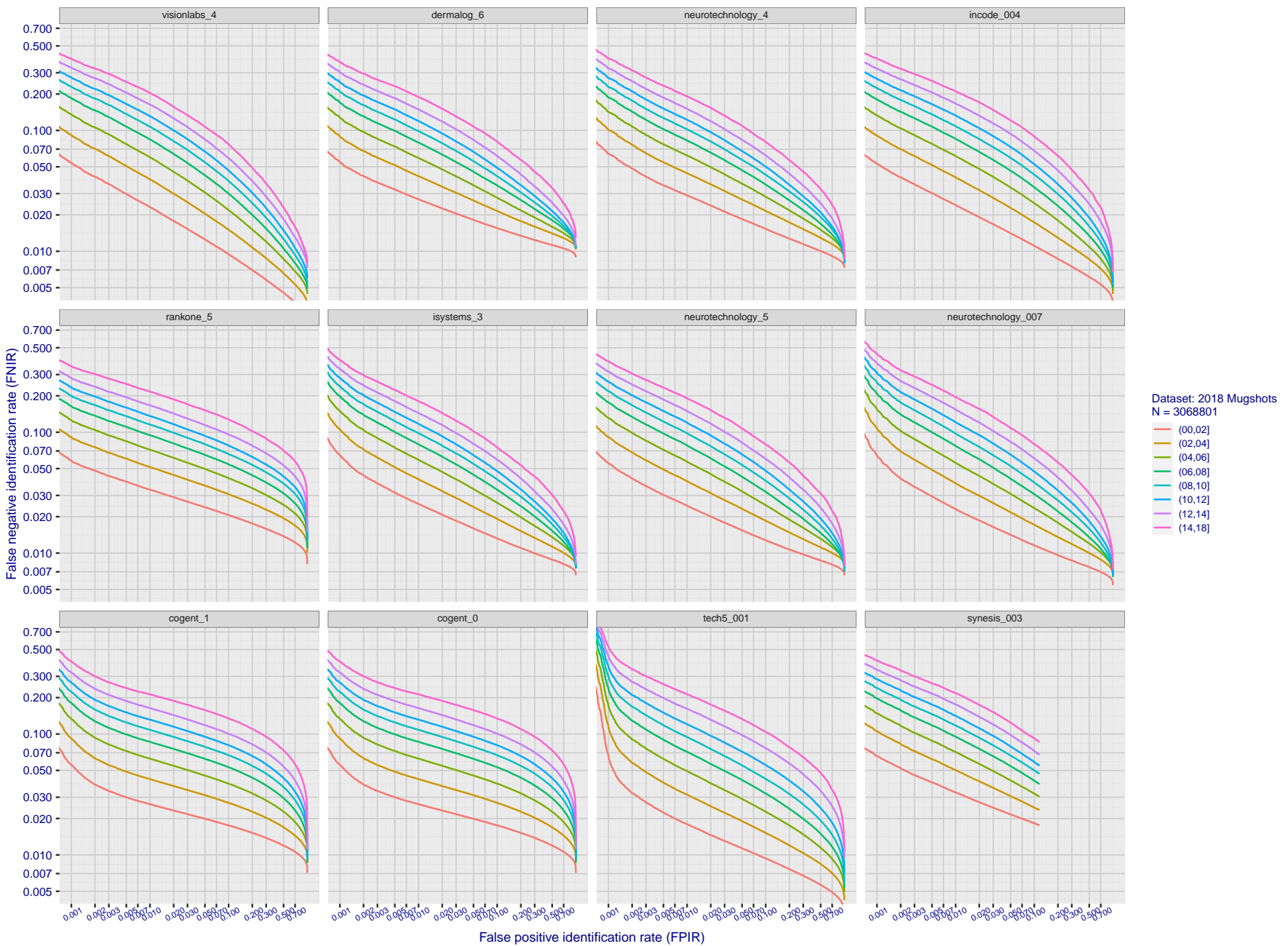


Figure 97: [FRVT-2018 Mugshot Ageing Dataset] Identification miss rates vs. FPIR by time-elapsed. The oldest image of each individual is enrolled. Thereafter, all more recent images are searched. Miss rates are computed over all searches noted in row 17 of Table 1 and binned by number of years between search and initial enrollment. FPIR is computed from the same FRVT 2018 non-mates noted in row 3 of Table 1 with $N = 3000\,000$.

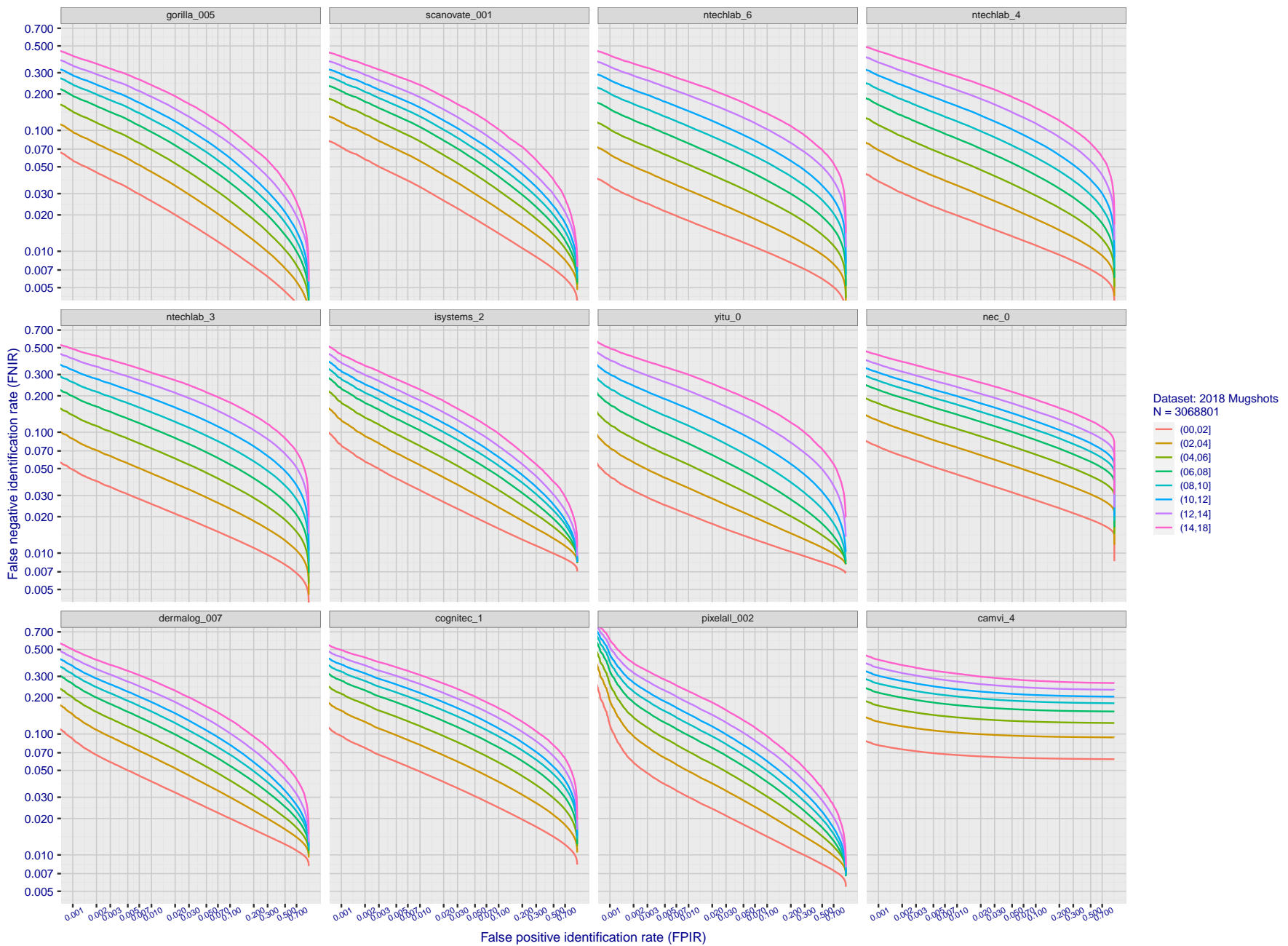


Figure 98: [FRVT-2018 Mugshot Ageing Dataset] Identification miss rates vs. FPIR by time-elapsed. The oldest image of each individual is enrolled. Thereafter, all more recent images are searched. Miss rates are computed over all searches noted in row 17 of Table 1 and binned by number of years between search and initial enrollment. FPIR is computed from the same FRVT 2018 non-mates noted in row 3 of Table 1 with $N = 3\,000\,000$.

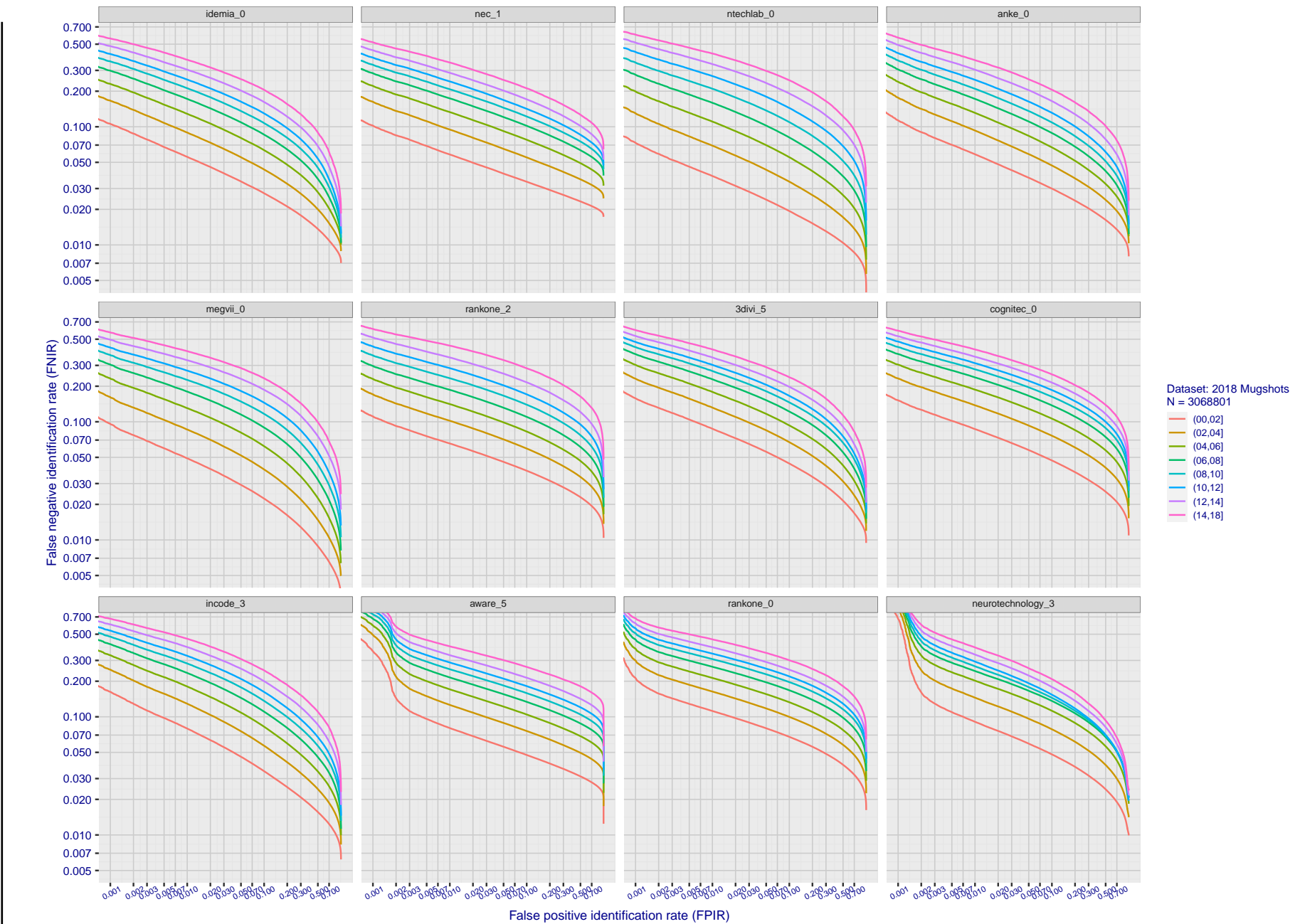


Figure 99: [FRVT-2018 Mugshot Ageing Dataset] Identification miss rates vs. FPIR by time-elapsed. The oldest image of each individual is enrolled. Thereafter, all more recent images are searched. Miss rates are computed over all searches noted in row 17 of Table 1 and binned by number of years between search and initial enrollment. FPIR is computed from the same FRVT 2018 non-mates noted in row 3 of Table 1 with $N = 3000\,000$.

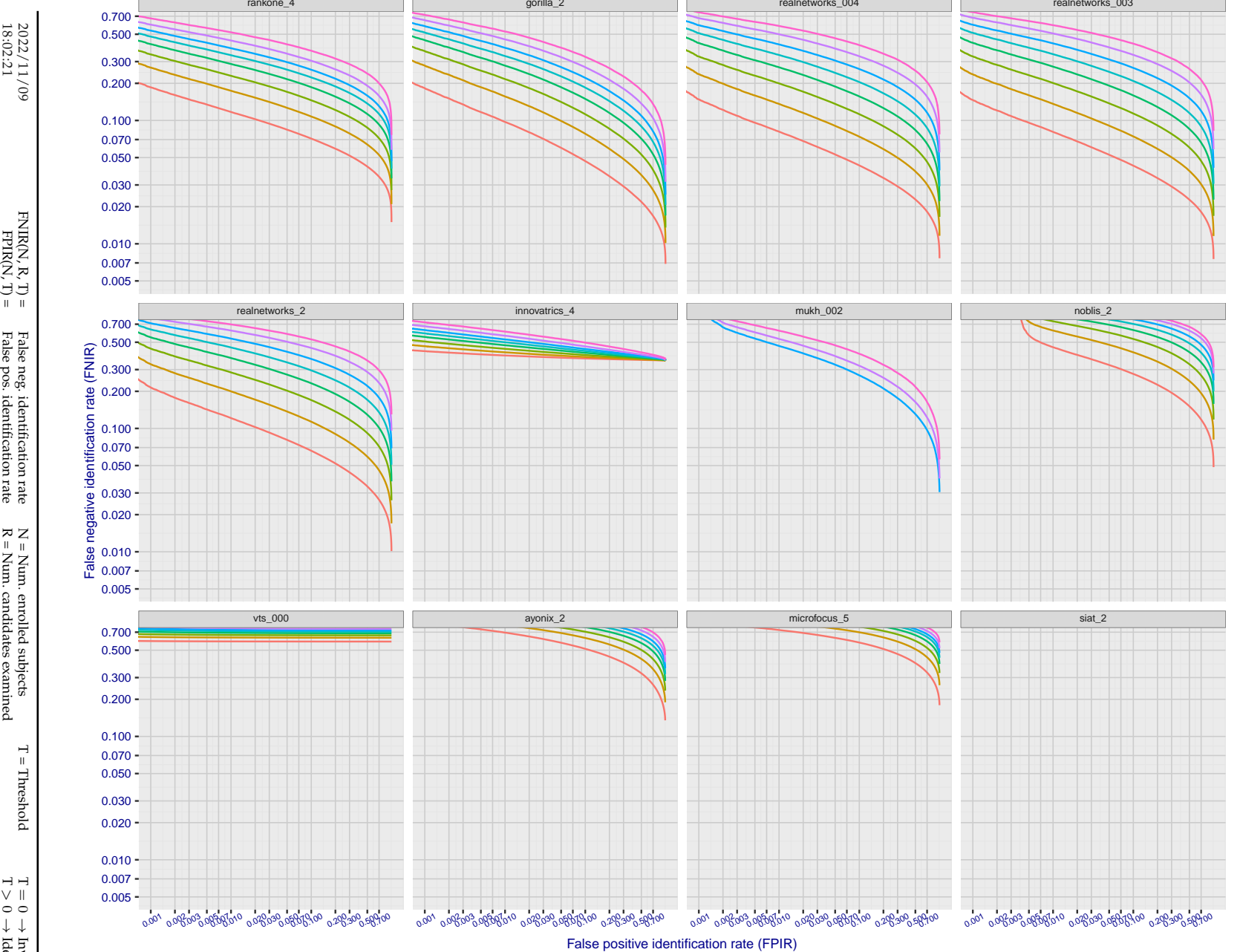


Figure 100: [FRVT-2018 Mugshot Ageing Dataset] Identification miss rates vs. FPIR by time-elapsed. The oldest image of each individual is enrolled. Thereafter, all more recent images are searched. Miss rates are computed over all searches noted in row 17 of Table 1 and binned by number of years between search and initial enrollment. FPIR is computed from the same FRVT 2018 non-mates noted in row 3 of Table 1 with $N = 3000\,000$.

2022/11/09
18:02:21

FNIR(N, R, T) = False neg. identification rate
FPTR(N, T) = False pos. identification rate

N = Num. enrolled subjects
R = Num. candidates examined

T = Threshold
T > 0 → Identification

T = 0 → Investigation

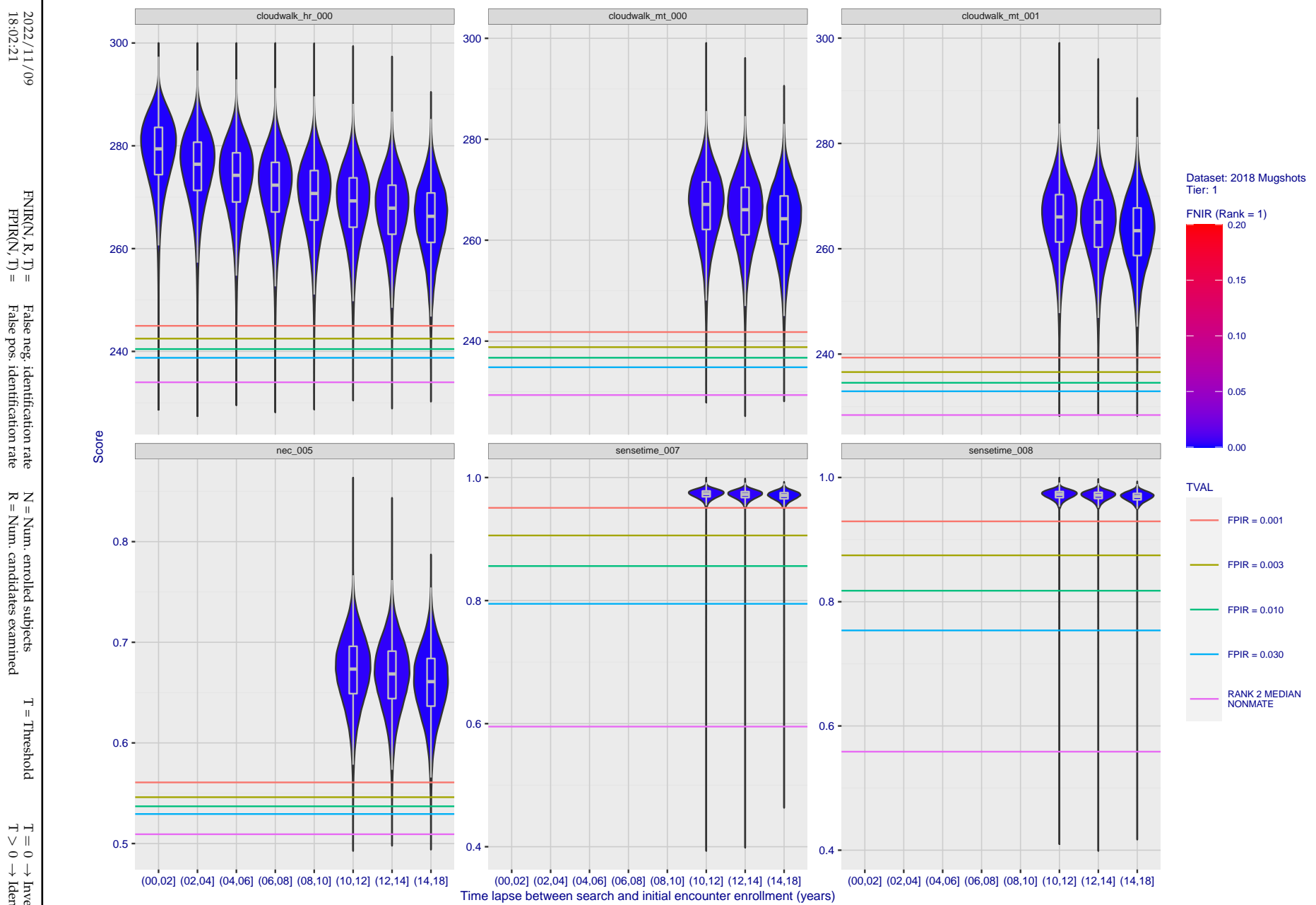


Figure 101: [FRVT-2018 Mugshot Ageing Dataset] Native mate scores vs. time-elapsed. The oldest image of each individual is enrolled. Thereafter, all more recent images are searched. Mated score distributions are computed over all searches noted in row 17 of Table 1 binned by number of years between search and initial enrollment.

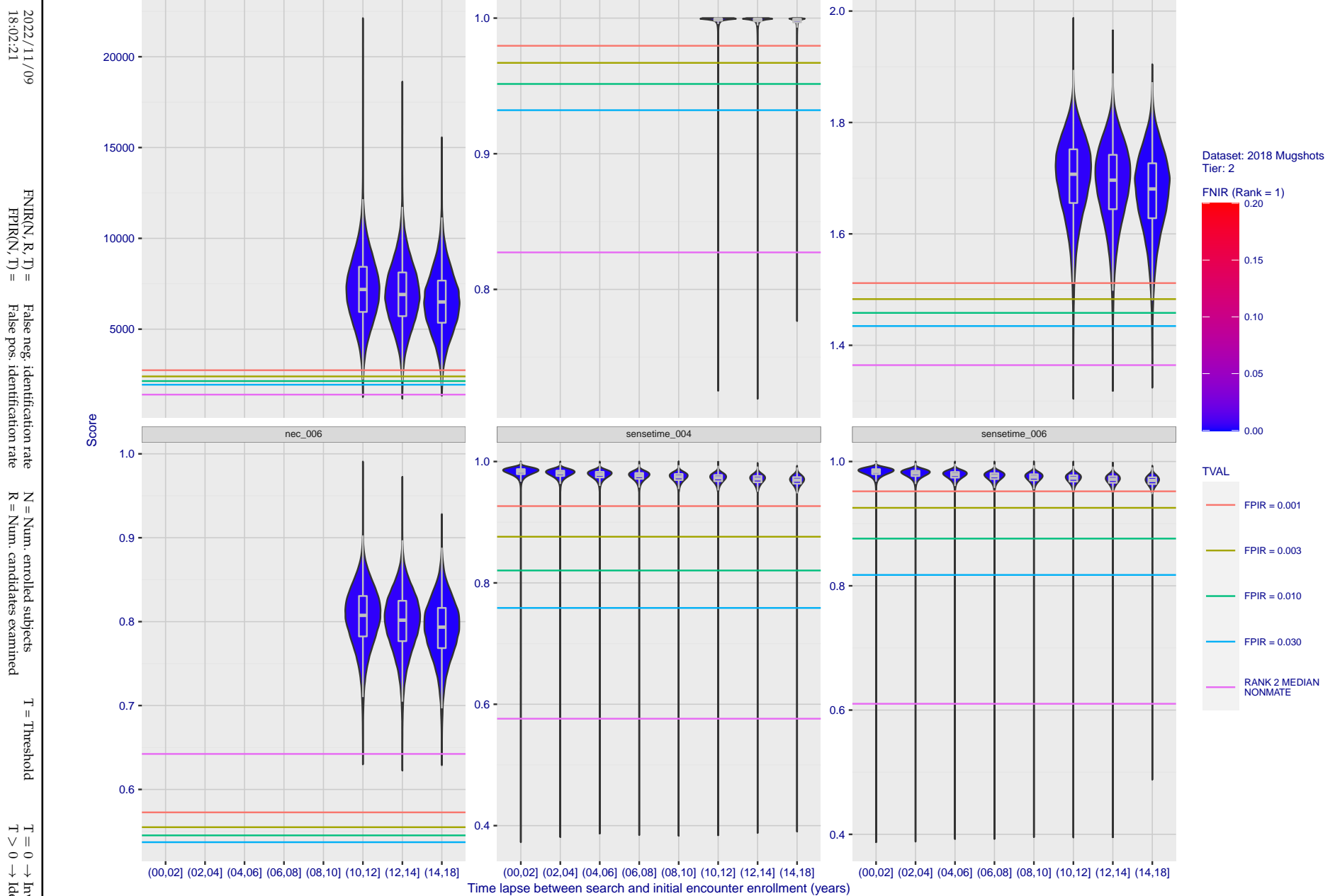


Figure 102: [FRVT-2018 Mugshot Ageing Dataset] Native mate scores vs. time-elapsed. The oldest image of each individual is enrolled. Thereafter, all more recent images are searched. Mated score distributions are computed over all searches noted in row 17 of Table 1 binned by number of years between search and initial enrollment.

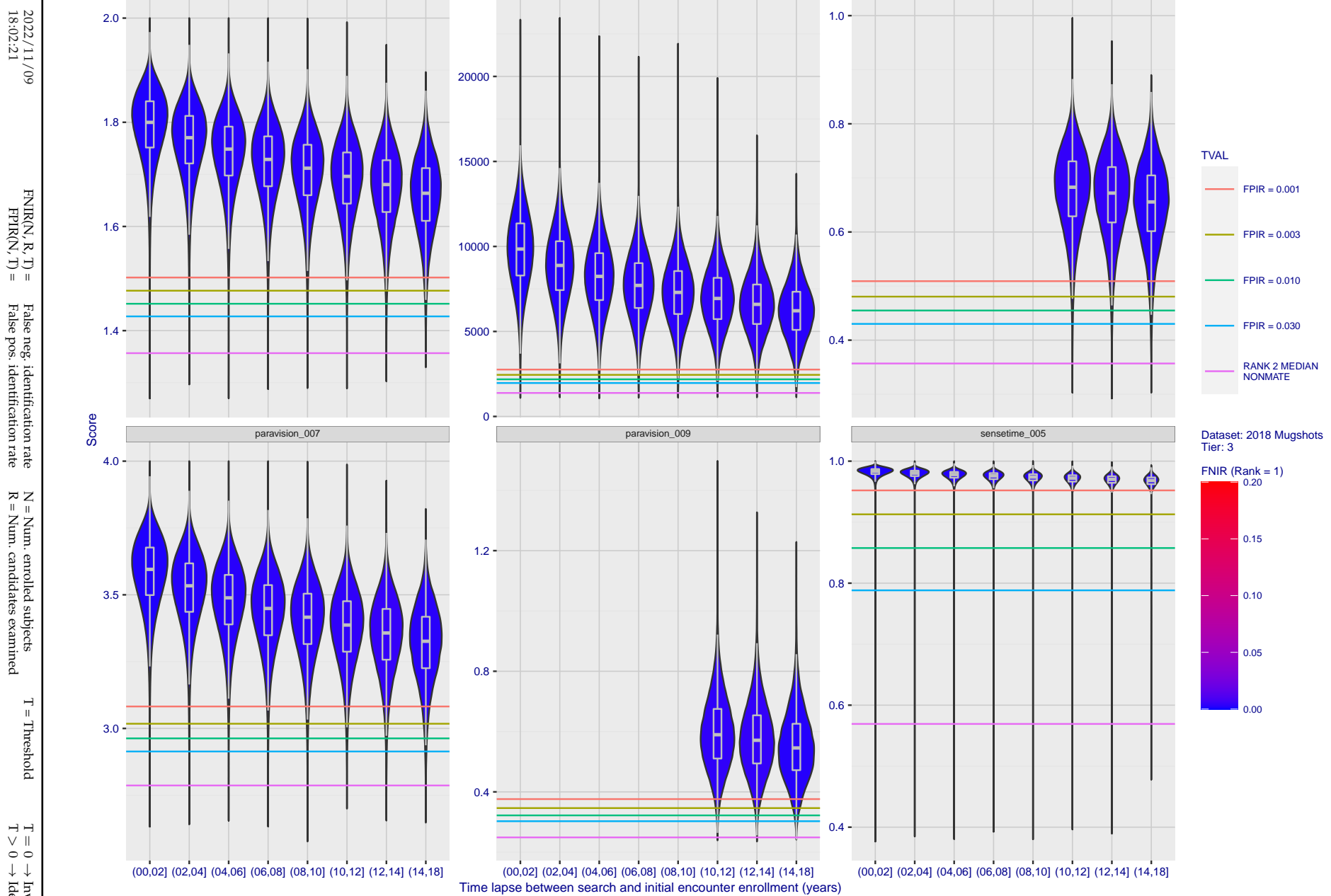


Figure 103: [FRVT-2018 Mugshot Ageing Dataset] Native mate scores vs. time-elapsed. The oldest image of each individual is enrolled. Thereafter, all more recent images are searched. Mated score distributions are computed over all searches noted in row 17 of Table 1 binned by number of years between search and initial enrollment.

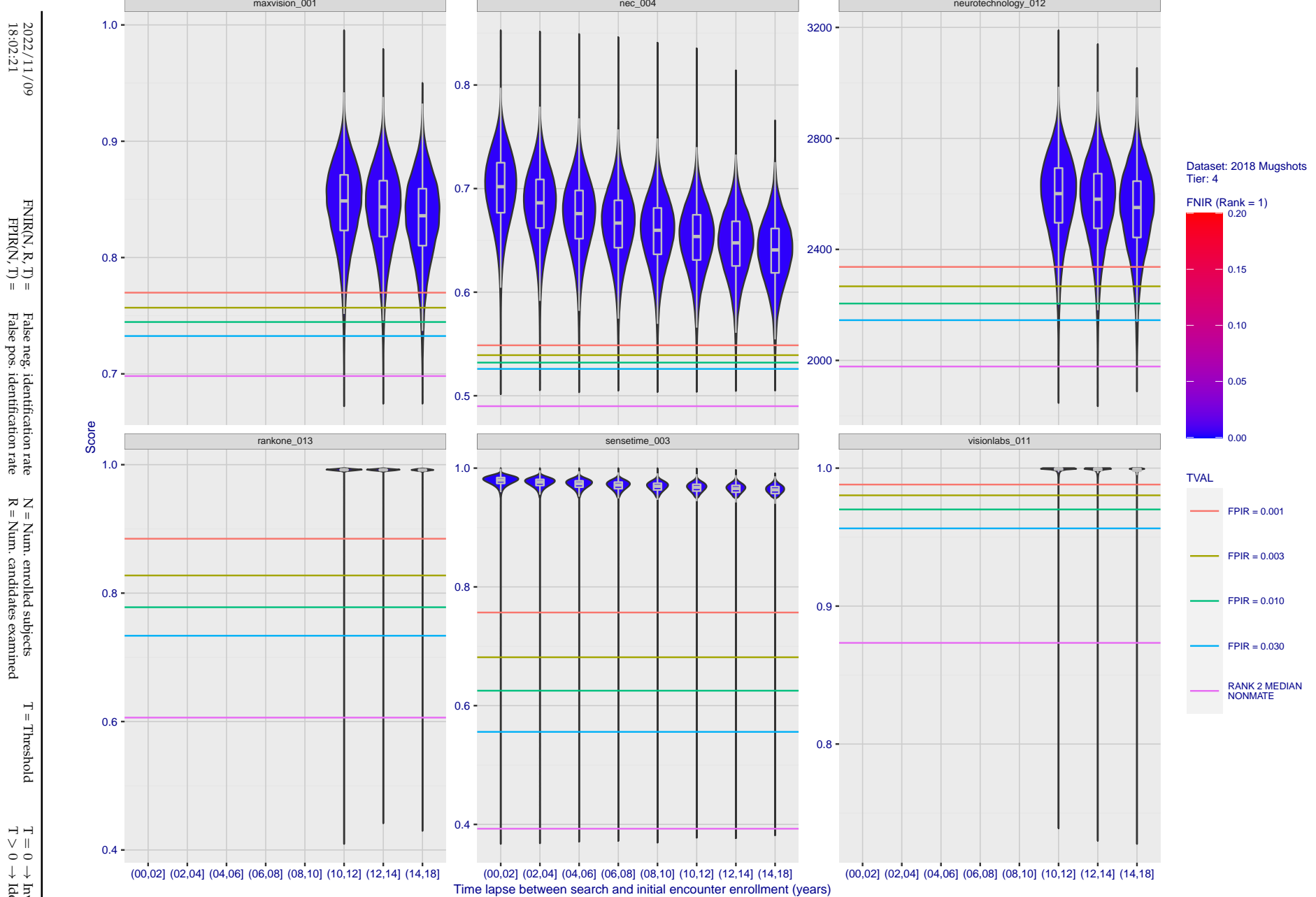


Figure 104: [FRVT-2018 Mugshot Ageing Dataset] Native mate scores vs. time-elapsed. The oldest image of each individual is enrolled. Thereafter, all more recent images are searched. Mated score distributions are computed over all searches noted in row 17 of Table 1 binned by number of years between search and initial enrollment.

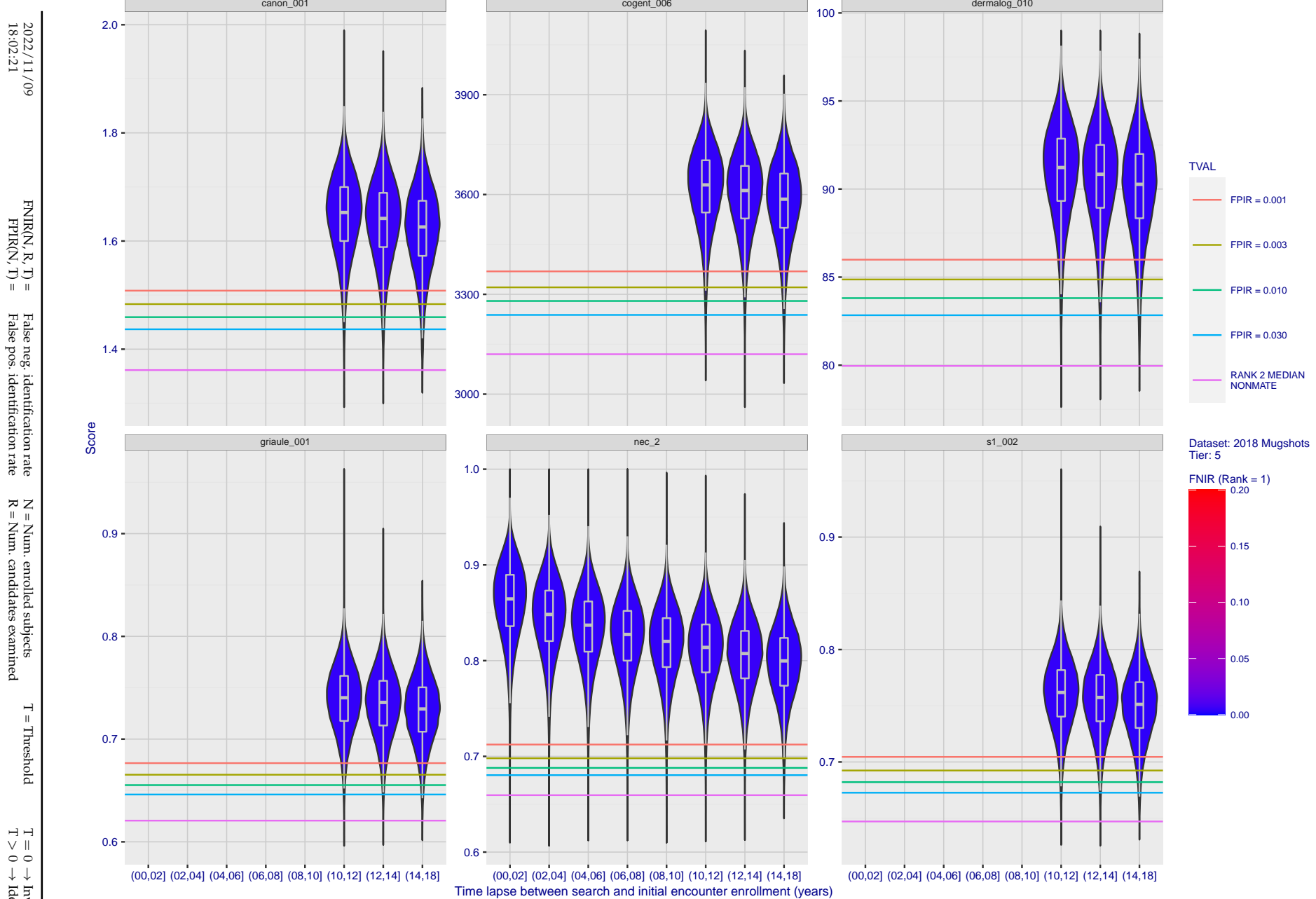


Figure 105: [FRVT-2018 Mugshot Ageing Dataset] Native mate scores vs. time-elapsed. The oldest image of each individual is enrolled. Thereafter, all more recent images are searched. Mated score distributions are computed over all searches noted in row 17 of Table 1 binned by number of years between search and initial enrollment.

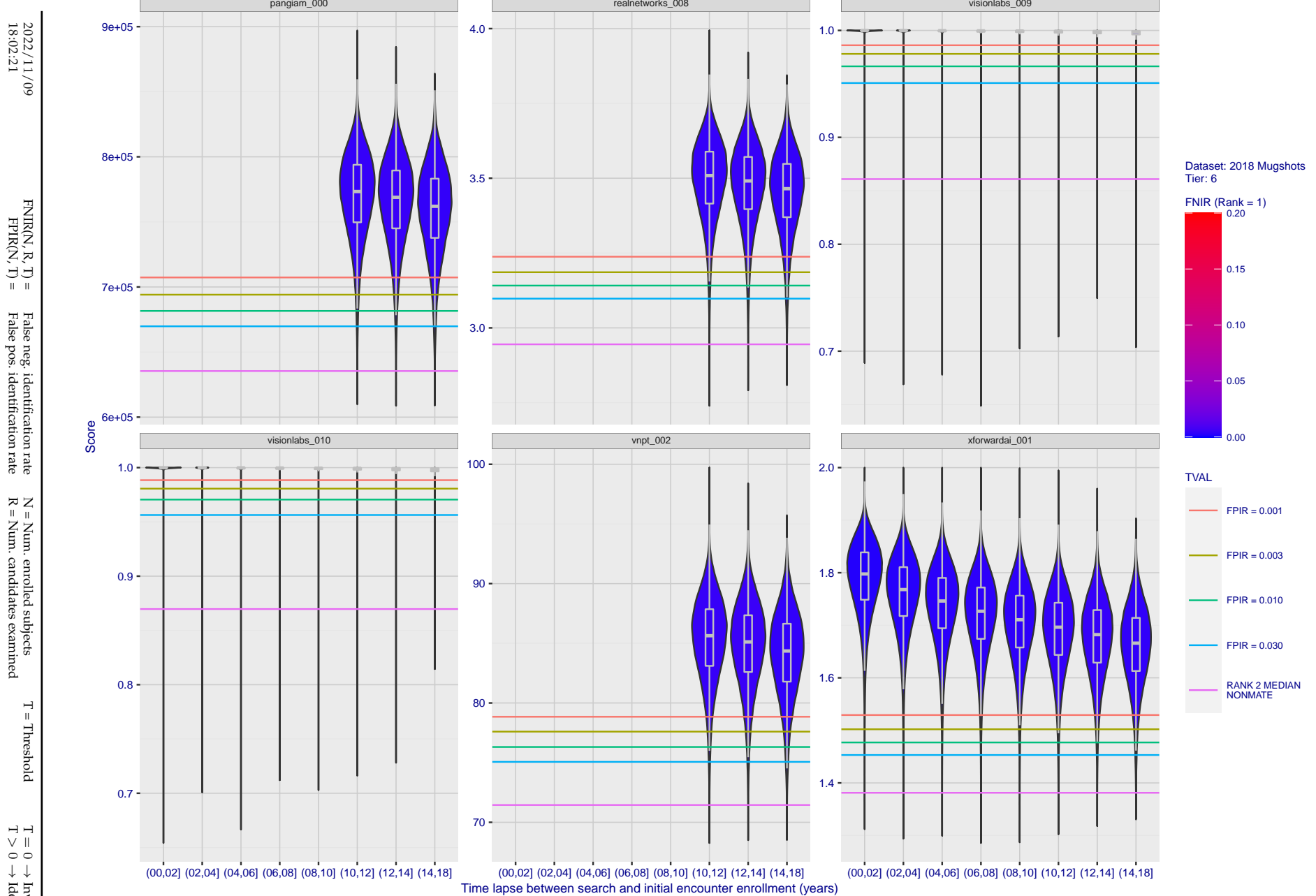


Figure 106: [FRVT-2018 Mugshot Ageing Dataset] Native mate scores vs. time-elapsed. The oldest image of each individual is enrolled. Thereafter, all more recent images are searched. Mated score distributions are computed over all searches noted in row 17 of Table 1 binned by number of years between search and initial enrollment.

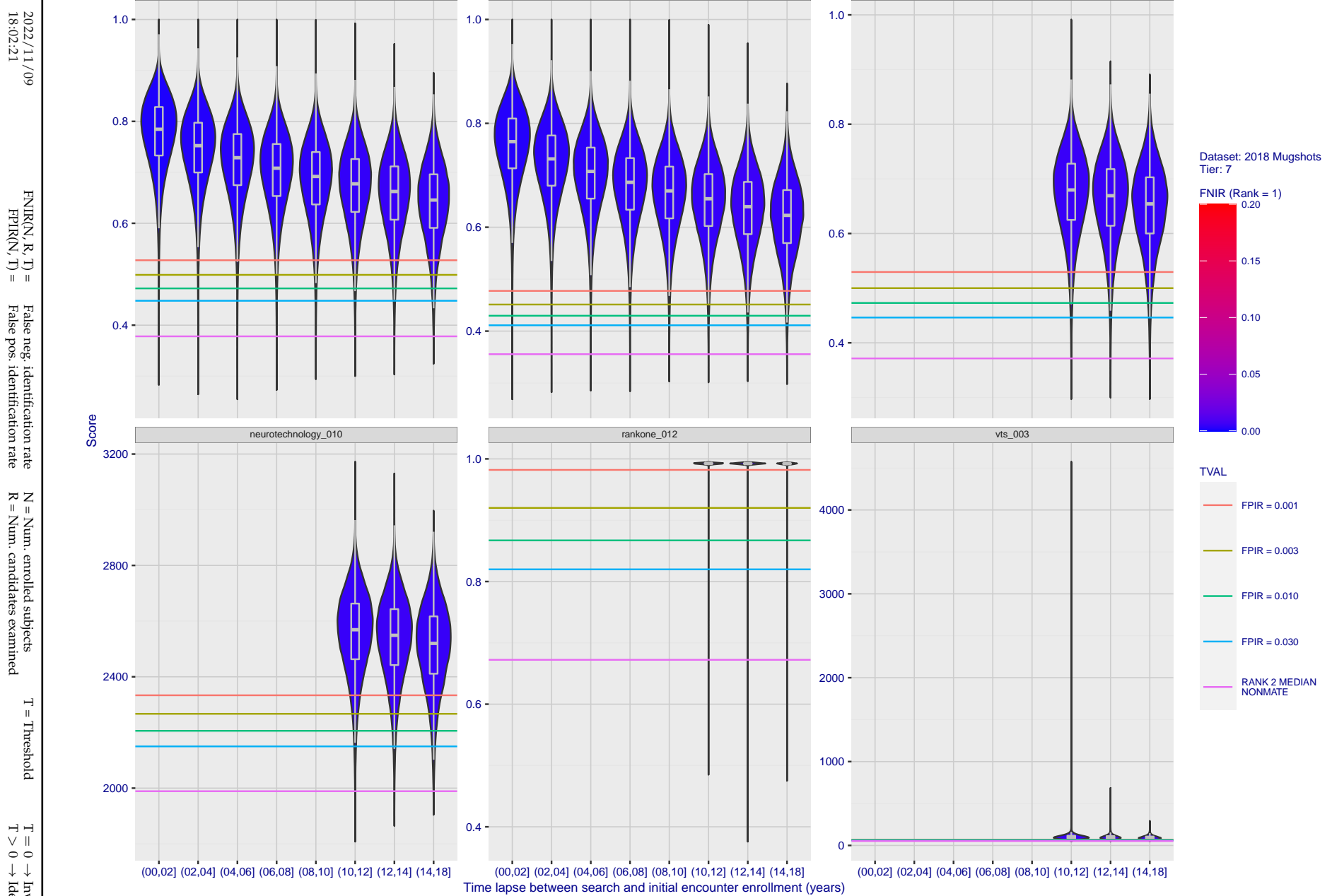


Figure 107: [FRVT-2018 Mugshot Ageing Dataset] Native mate scores vs. time-elapsed. The oldest image of each individual is enrolled. Thereafter, all more recent images are searched. Mated score distributions are computed over all searches noted in row 17 of Table 1 binned by number of years between search and initial enrollment.

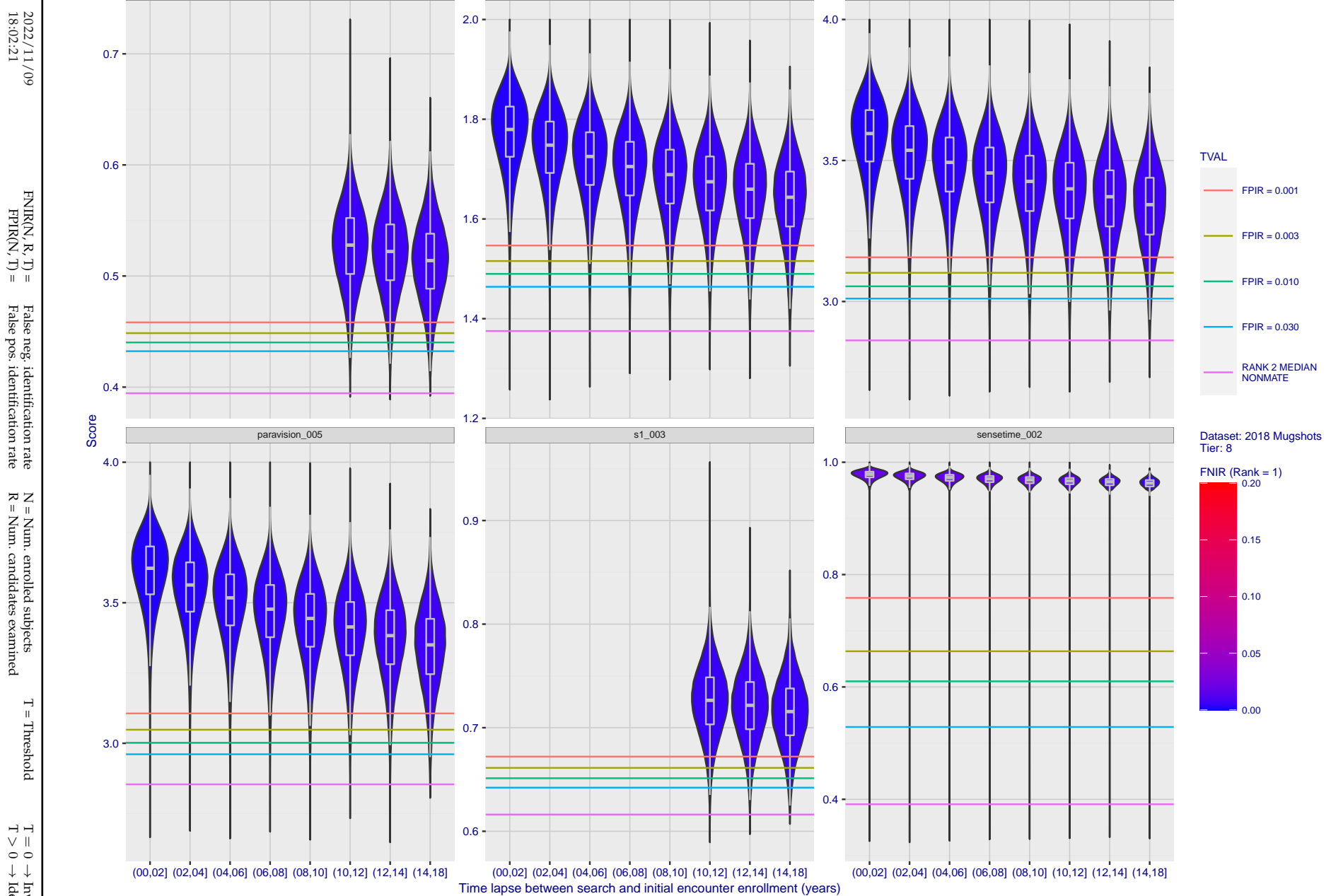


Figure 108: [FRVT-2018 Mugshot Ageing Dataset] Native mate scores vs. time-elapsed. The oldest image of each individual is enrolled. Thereafter, all more recent images are searched. Mated score distributions are computed over all searches noted in row 17 of Table 1 binned by number of years between search and initial enrollment.

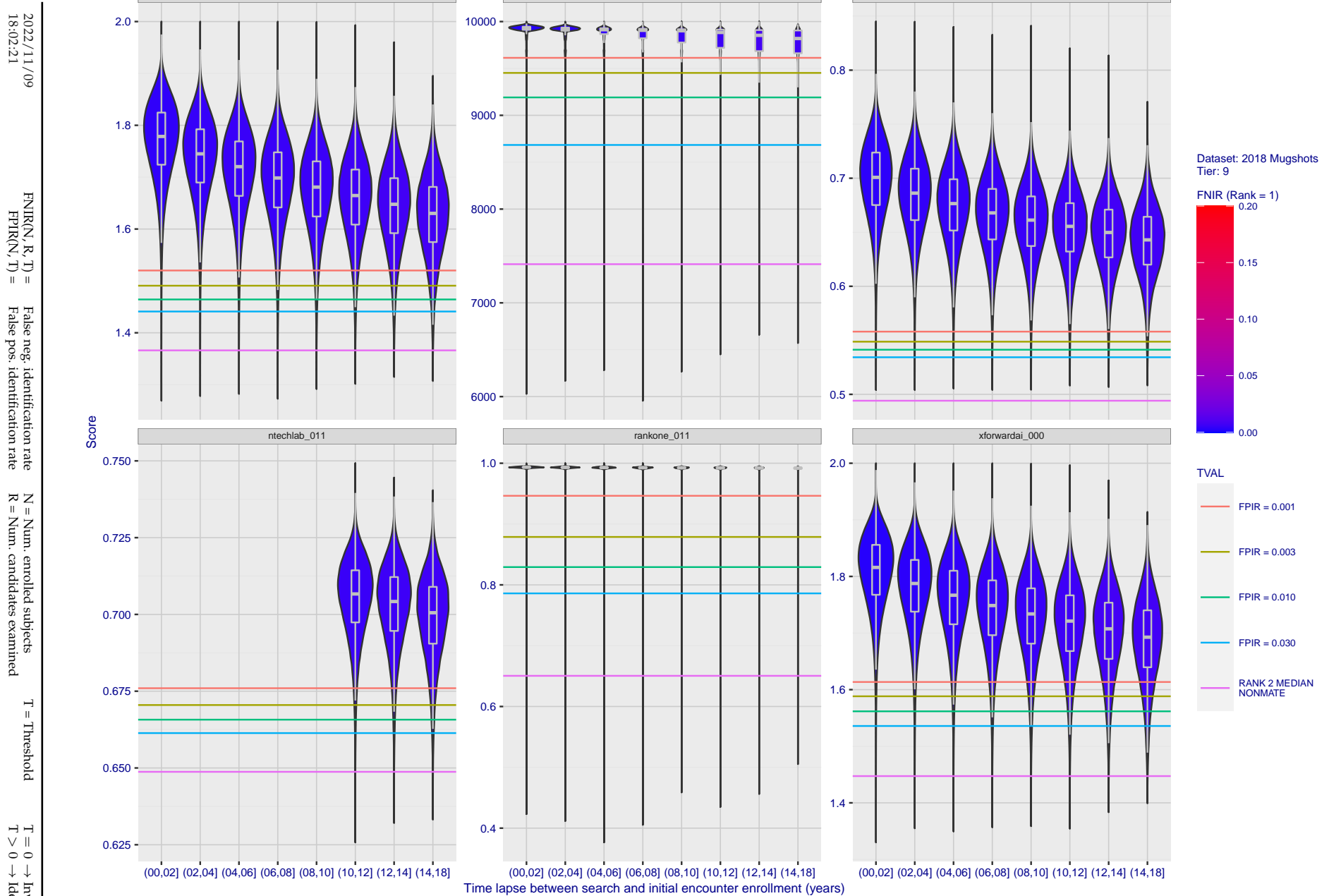


Figure 109: [FRVT-2018 Mugshot Ageing Dataset] Native mate scores vs. time-elapsed. The oldest image of each individual is enrolled. Thereafter, all more recent images are searched. Mated score distributions are computed over all searches noted in row 17 of Table 1 binned by number of years between search and initial enrollment.

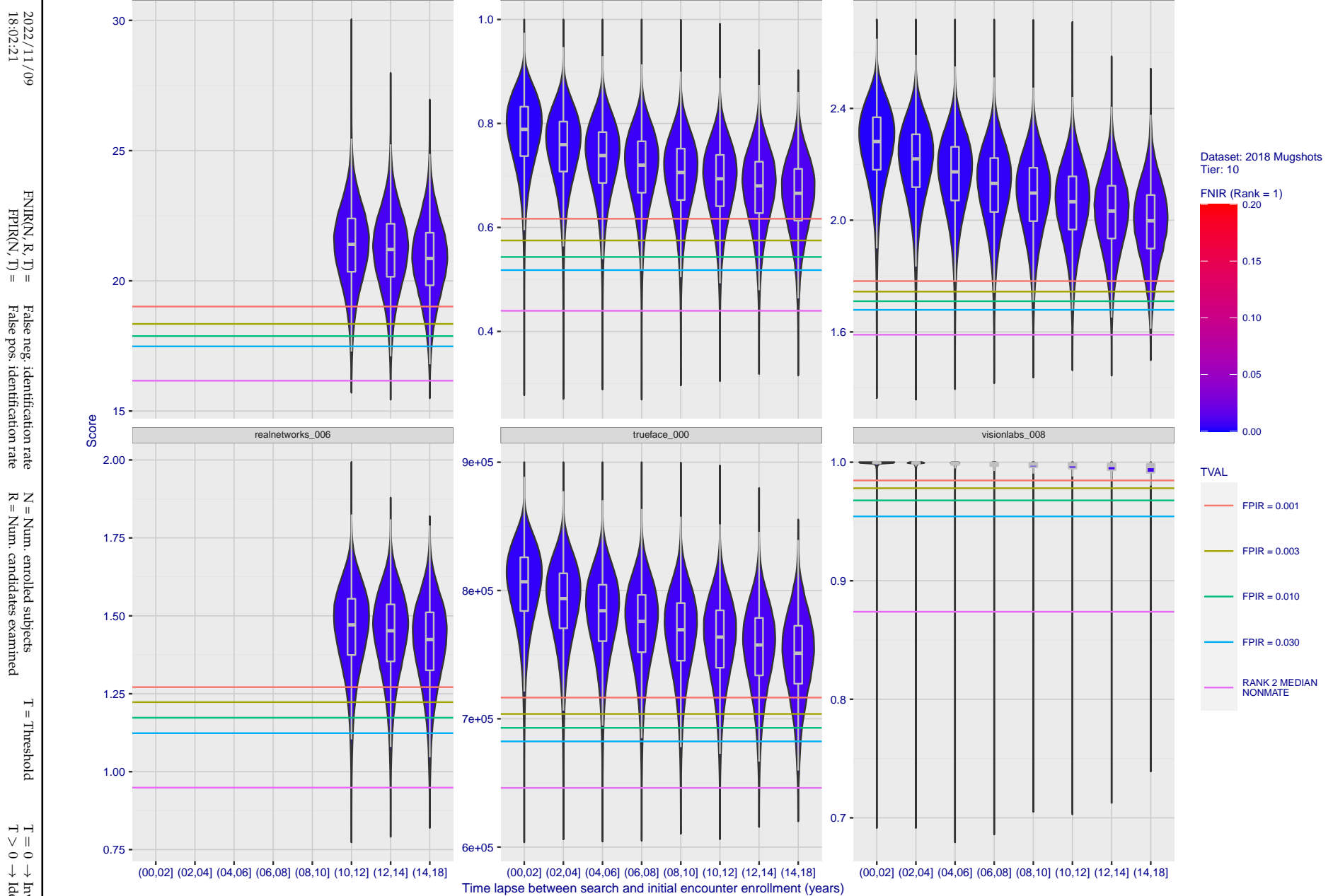


Figure 110: [FRVT-2018 Mugshot Ageing Dataset] Native mate scores vs. time-elapsed. The oldest image of each individual is enrolled. Thereafter, all more recent images are searched. Mated score distributions are computed over all searches noted in row 17 of Table 1 binned by number of years between search and initial enrollment.

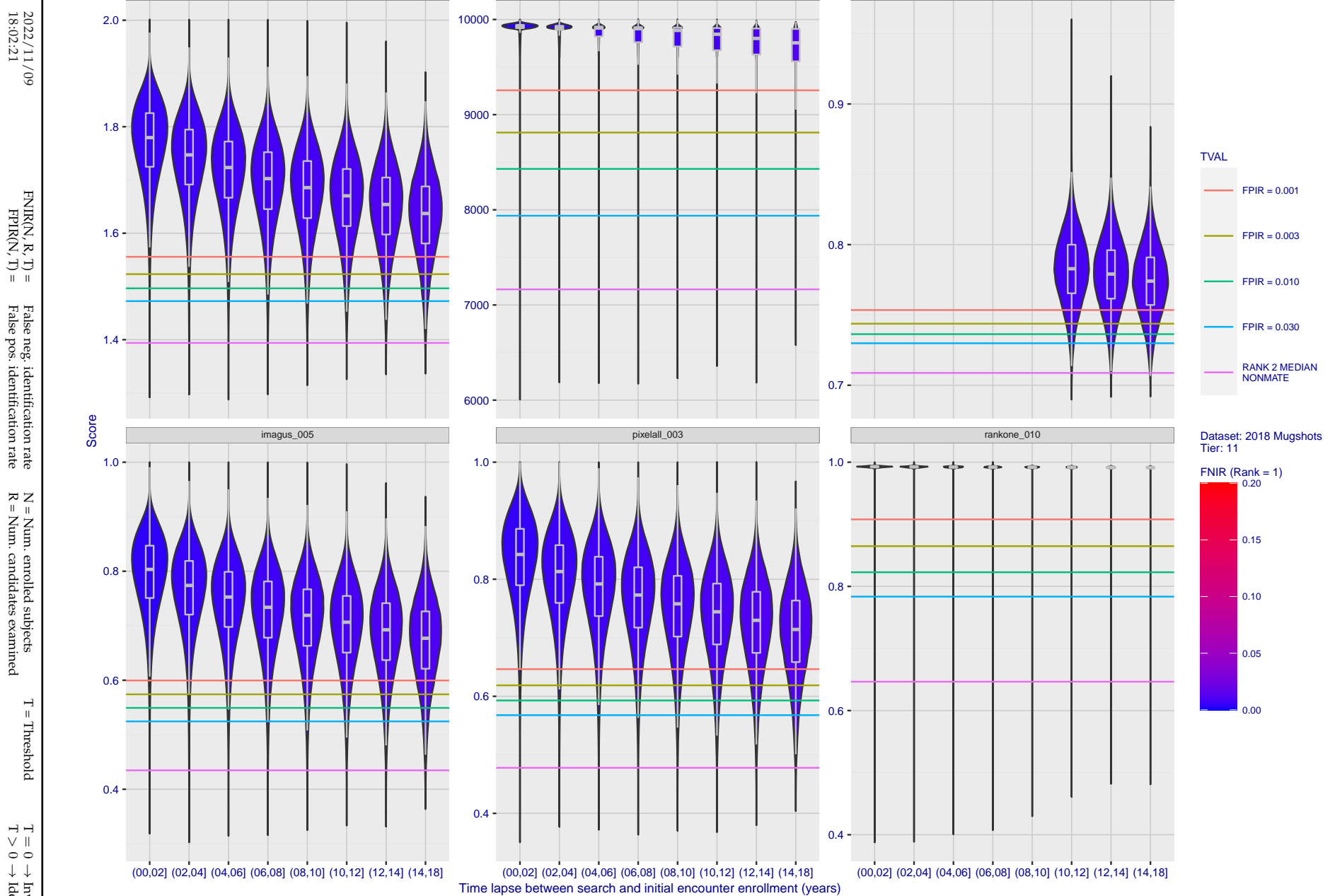


Figure 111: [FRVT-2018 Mugshot Ageing Dataset] Native mate scores vs. time-elapsed. The oldest image of each individual is enrolled. Thereafter, all more recent images are searched. Mated score distributions are computed over all searches noted in row 17 of Table 1 binned by number of years between search and initial enrollment.

2022/11/1
18:02:21

$\text{FPIR}(N, T) = \text{False pos. identification rate}$

R = Num. candidates examined

1 - 110

$T > 0 \rightarrow$ Identification

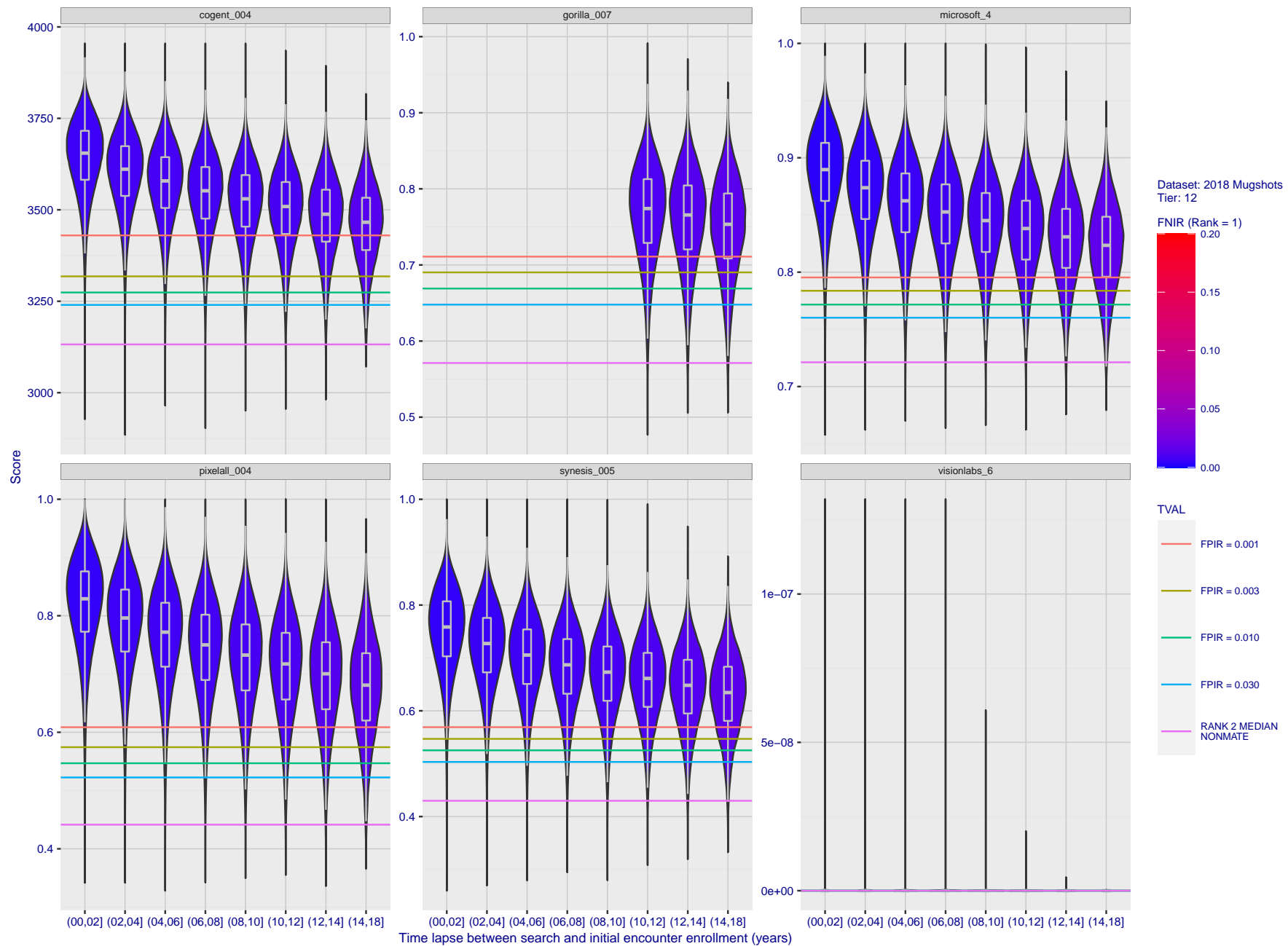


Figure 112: [FRVT-2018 Mugshot Ageing Dataset] Native mate scores vs. time-elapsed. The oldest image of each individual is enrolled. Thereafter, all more recent images are searched. Mated score distributions are computed over all searches noted in row 17 of Table 1 binned by number of years between search and initial enrollment.

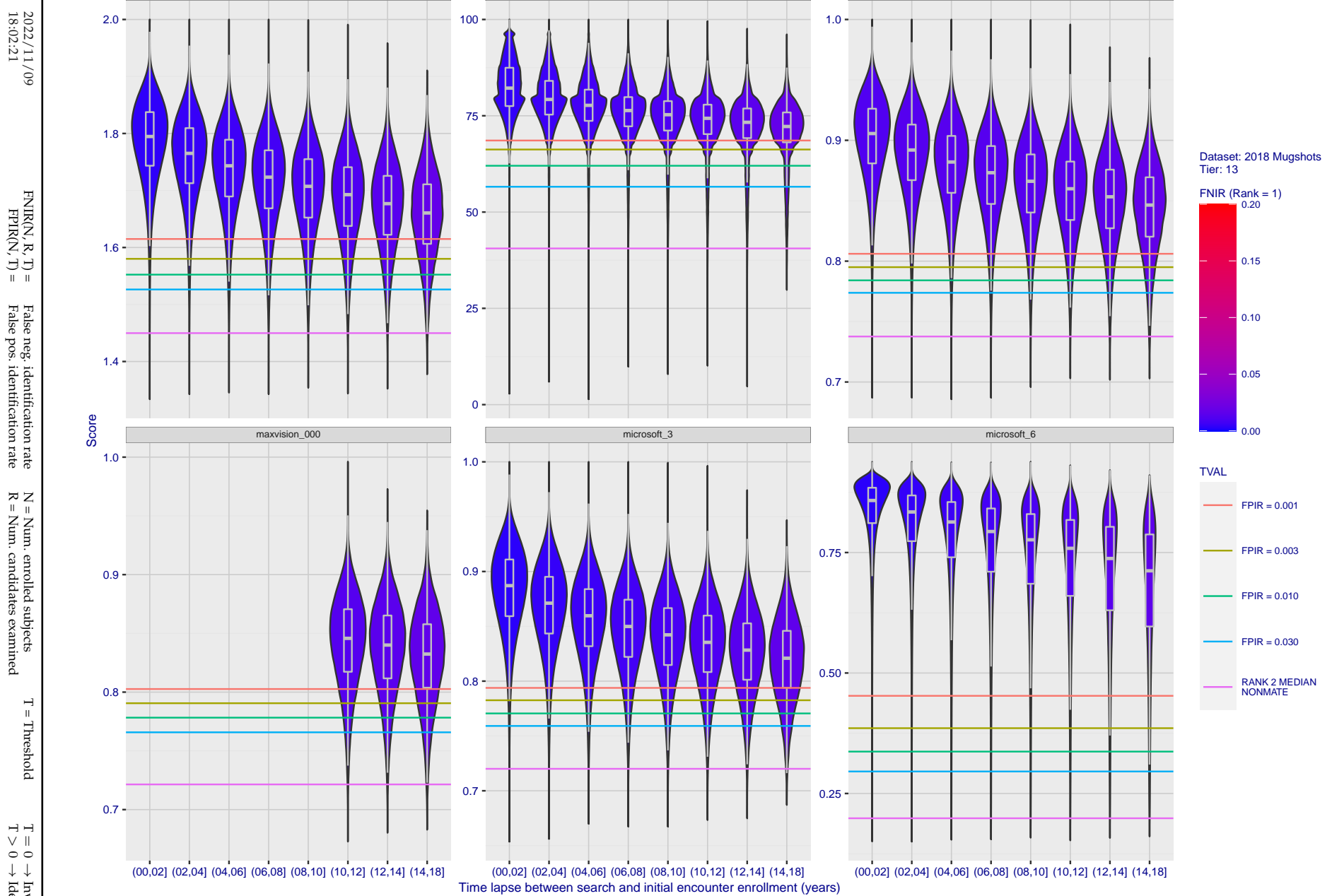


Figure 113: [FRVT-2018 Mugshot Ageing Dataset] Native mate scores vs. time-elapsed. The oldest image of each individual is enrolled. Thereafter, all more recent images are searched. Mated score distributions are computed over all searches noted in row 17 of Table 1 binned by number of years between search and initial enrollment.

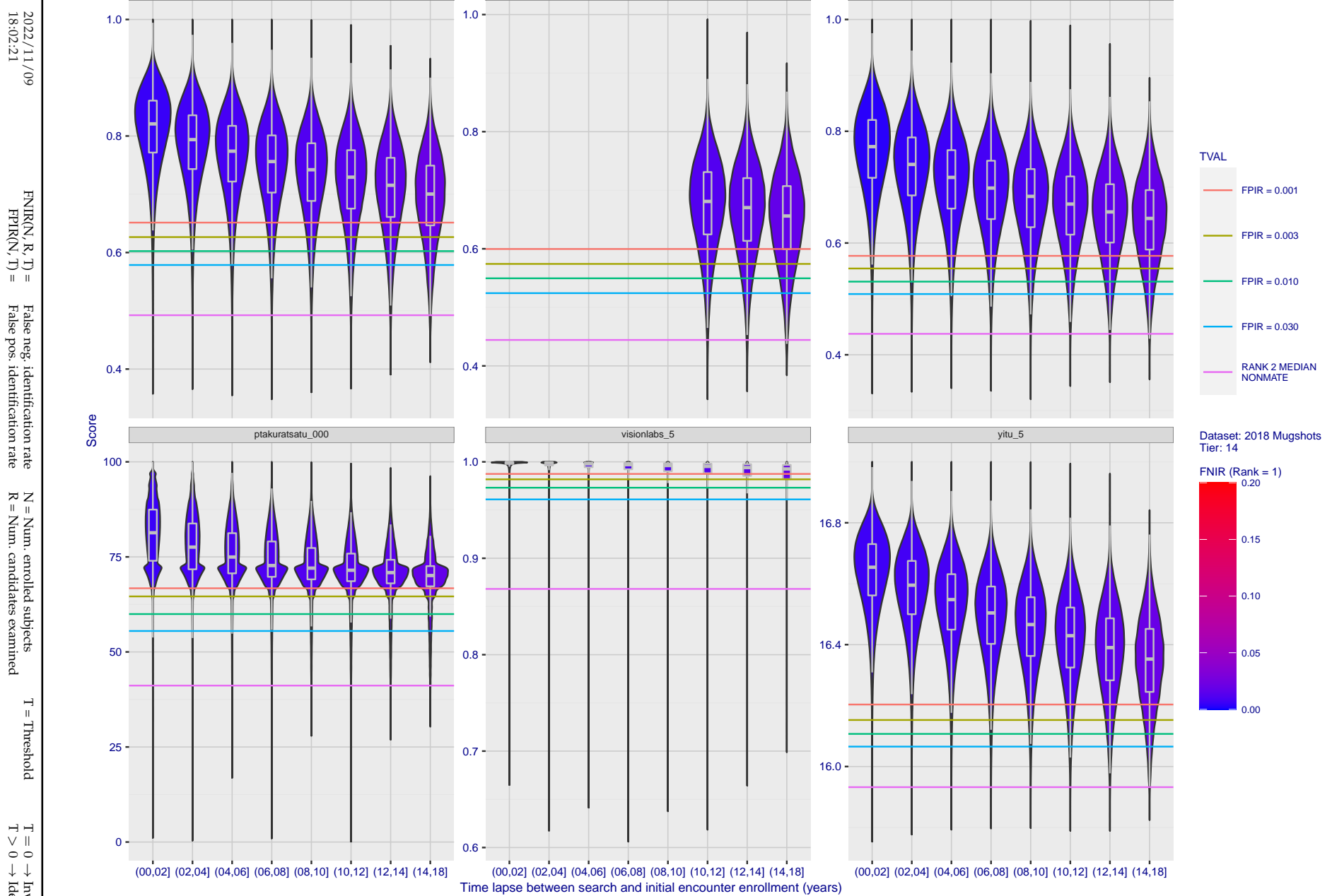


Figure 114: [FRVT-2018 Mugshot Ageing Dataset] Native mate scores vs. time-elapsed. The oldest image of each individual is enrolled. Thereafter, all more recent images are searched. Mated score distributions are computed over all searches noted in row 17 of Table 1 binned by number of years between search and initial enrollment.

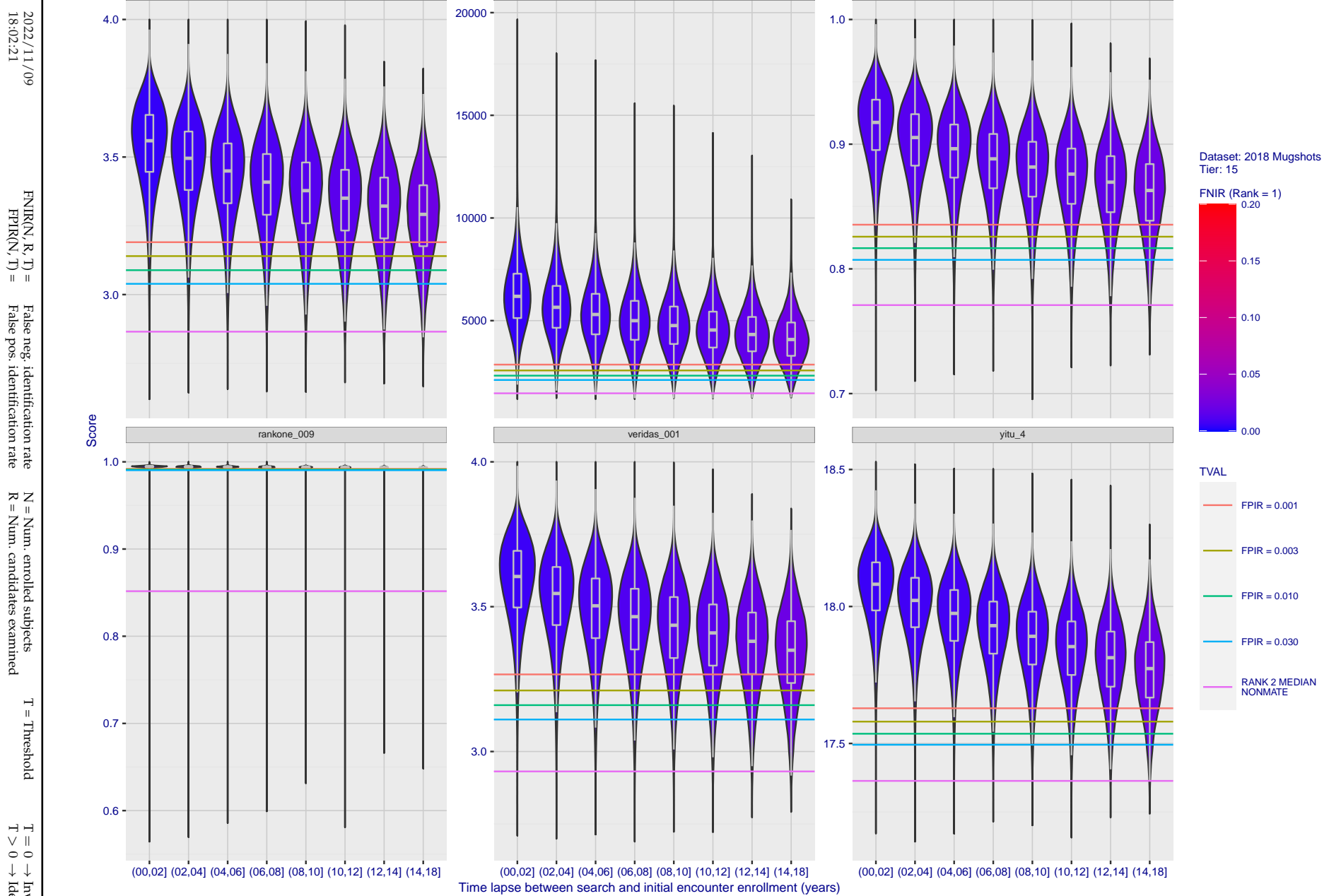


Figure 115: [FRVT-2018 Mugshot Ageing Dataset] Native mate scores vs. time-elapsed. The oldest image of each individual is enrolled. Thereafter, all more recent images are searched. Mated score distributions are computed over all searches noted in row 17 of Table 1 binned by number of years between search and initial enrollment.

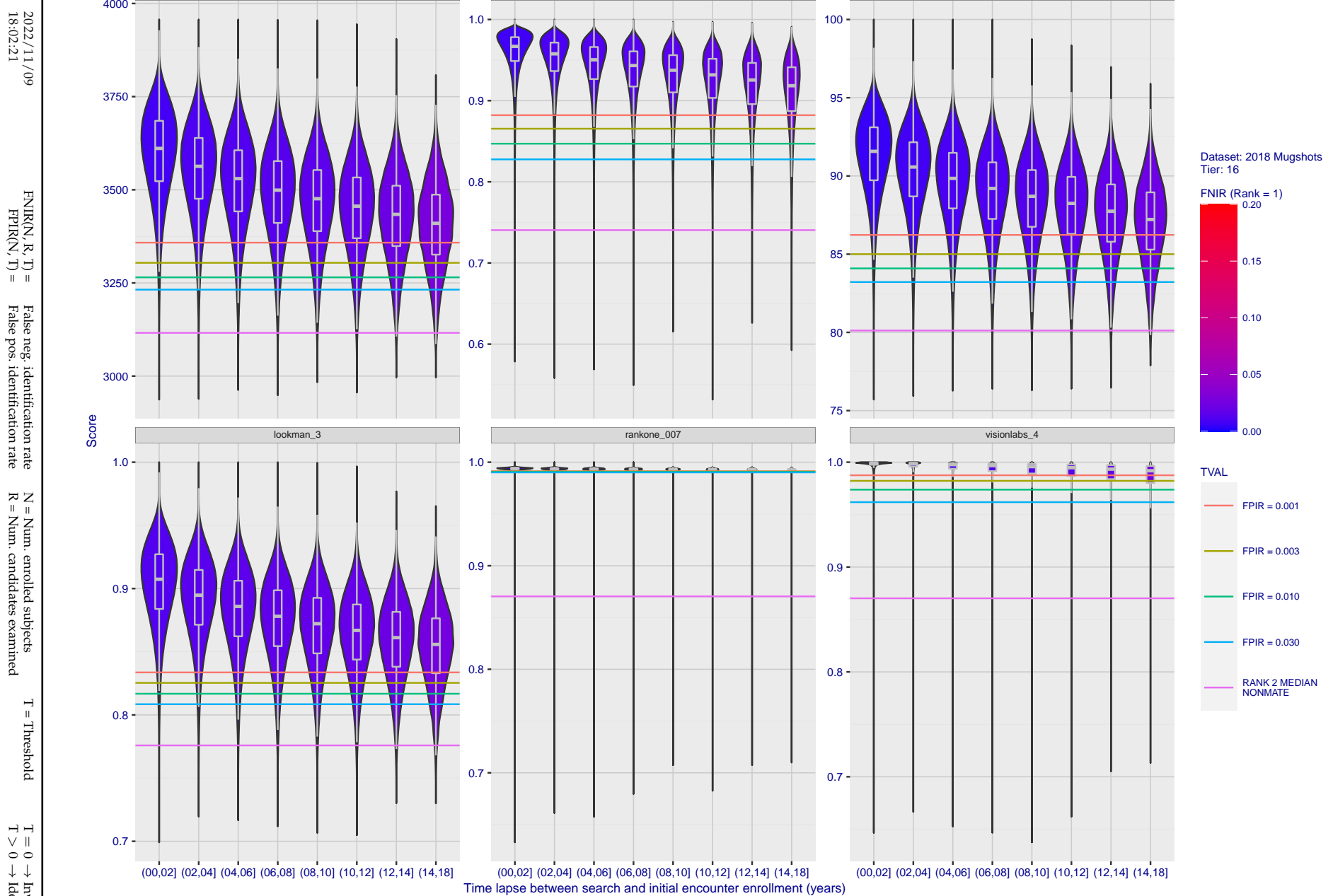


Figure 116: [FRVT-2018 Mugshot Ageing Dataset] Native mate scores vs. time-elapsed. The oldest image of each individual is enrolled. Thereafter, all more recent images are searched. Mated score distributions are computed over all searches noted in row 17 of Table 1 binned by number of years between search and initial enrollment.

2022/11/18:02:21

$\text{FNIR}(N, K, 1) =$ False neg. identification rate
 $\text{FPIR}(N, T) =$ False pos. identification rate

R = Num. candidates examined

I = I_{max}

$I = 0 \rightarrow$ Investigation
 $T > 0 \rightarrow$ Identification

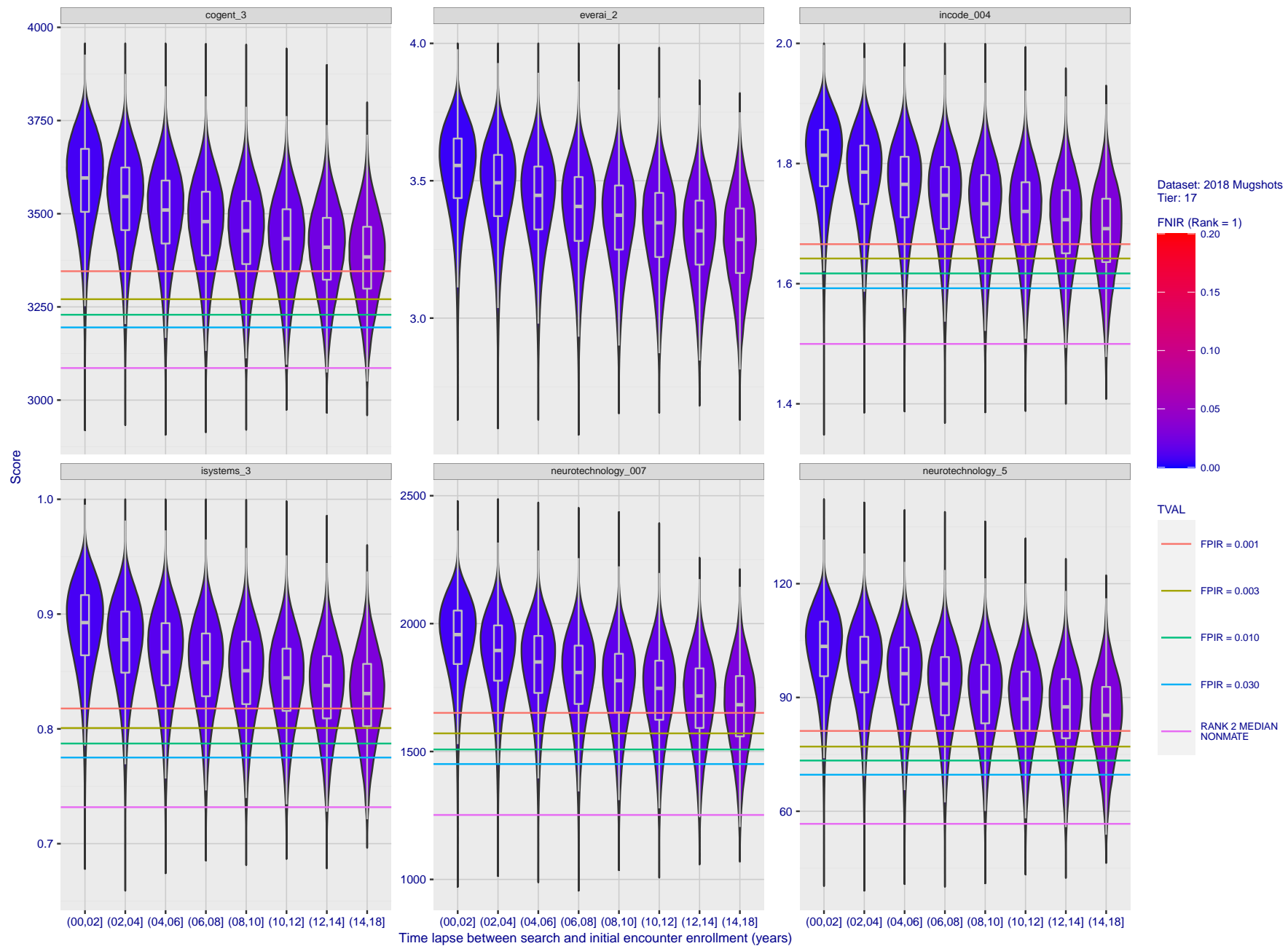


Figure 117: [FRVT-2018 Mugshot Ageing Dataset] Native mate scores vs. time-elapsed. The oldest image of each individual is enrolled. Thereafter, all more recent images are searched. Mated score distributions are computed over all searches noted in row 17 of Table 1 binned by number of years between search and initial enrollment.

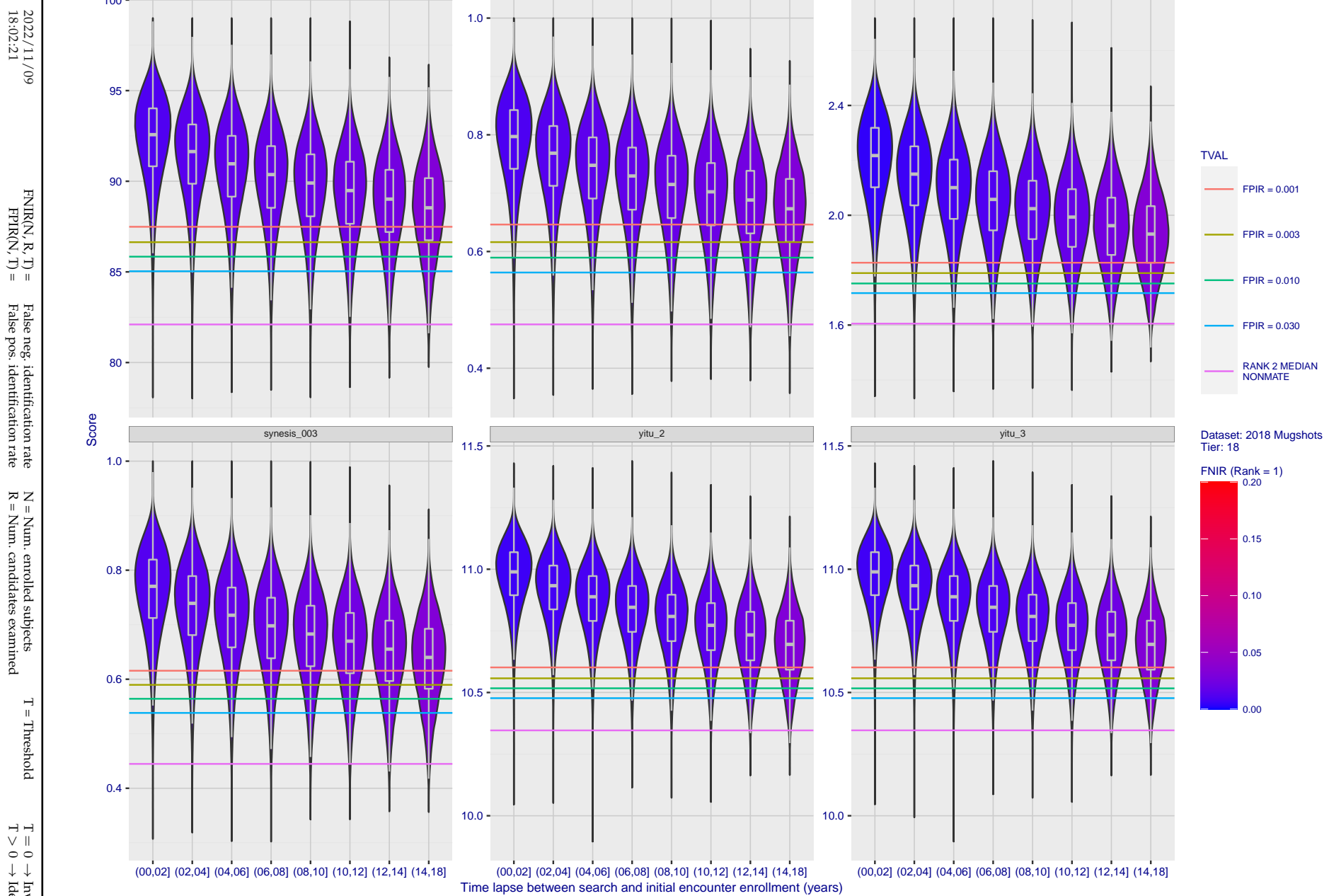


Figure 118: [FRVT-2018 Mugshot Ageing Dataset] Native mate scores vs. time-elapsed. The oldest image of each individual is enrolled. Thereafter, all more recent images are searched. Mated score distributions are computed over all searches noted in row 17 of Table 1 binned by number of years between search and initial enrollment.

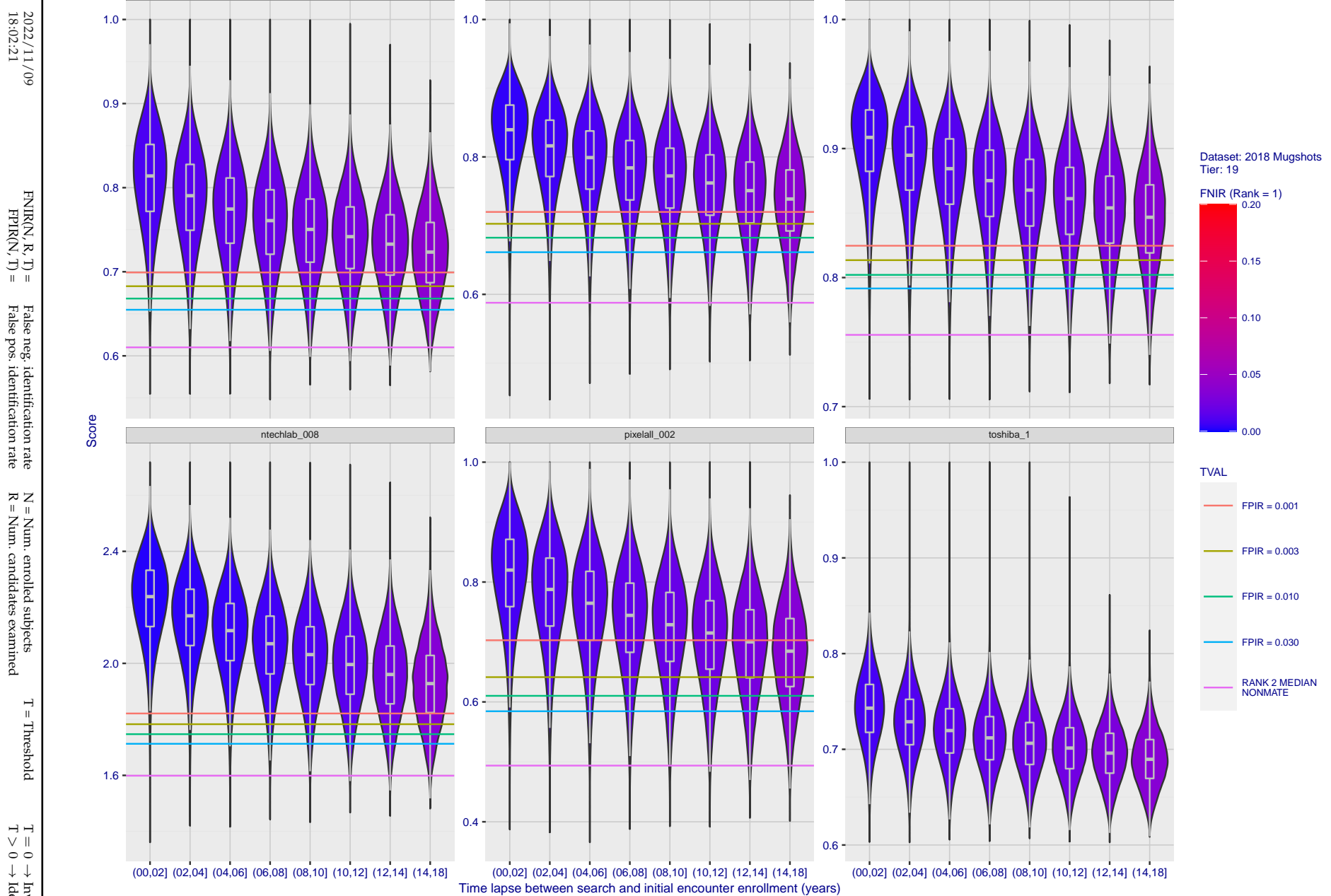


Figure 119: [FRVT-2018 Mugshot Ageing Dataset] Native mate scores vs. time-elapsed. The oldest image of each individual is enrolled. Thereafter, all more recent images are searched. Mated score distributions are computed over all searches noted in row 17 of Table 1 binned by number of years between search and initial enrollment.

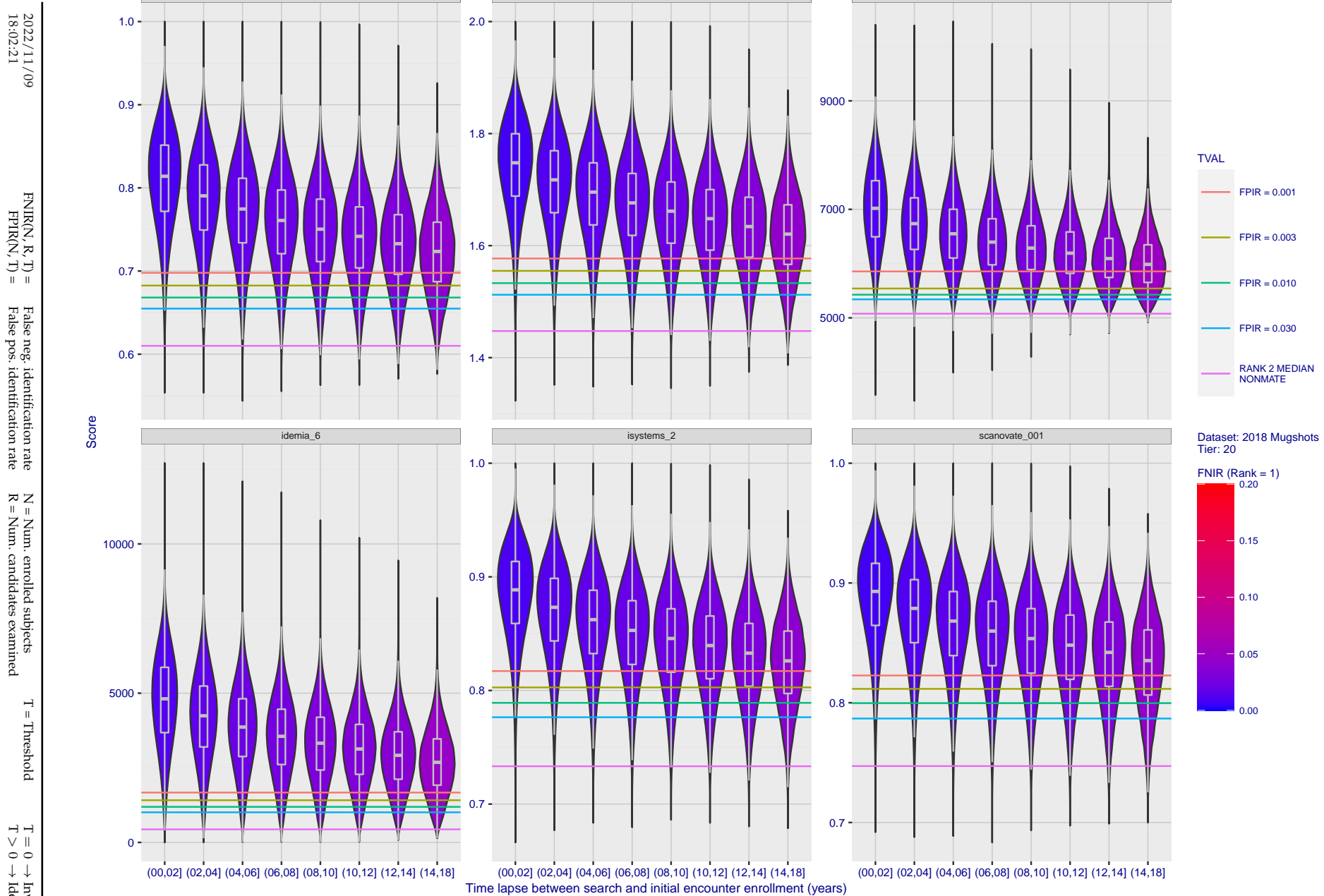


Figure 120: [FRVT-2018 Mugshot Ageing Dataset] Native mate scores vs. time-elapsed. The oldest image of each individual is enrolled. Thereafter, all more recent images are searched. Mated score distributions are computed over all searches noted in row 17 of Table 1 binned by number of years between search and initial enrollment.

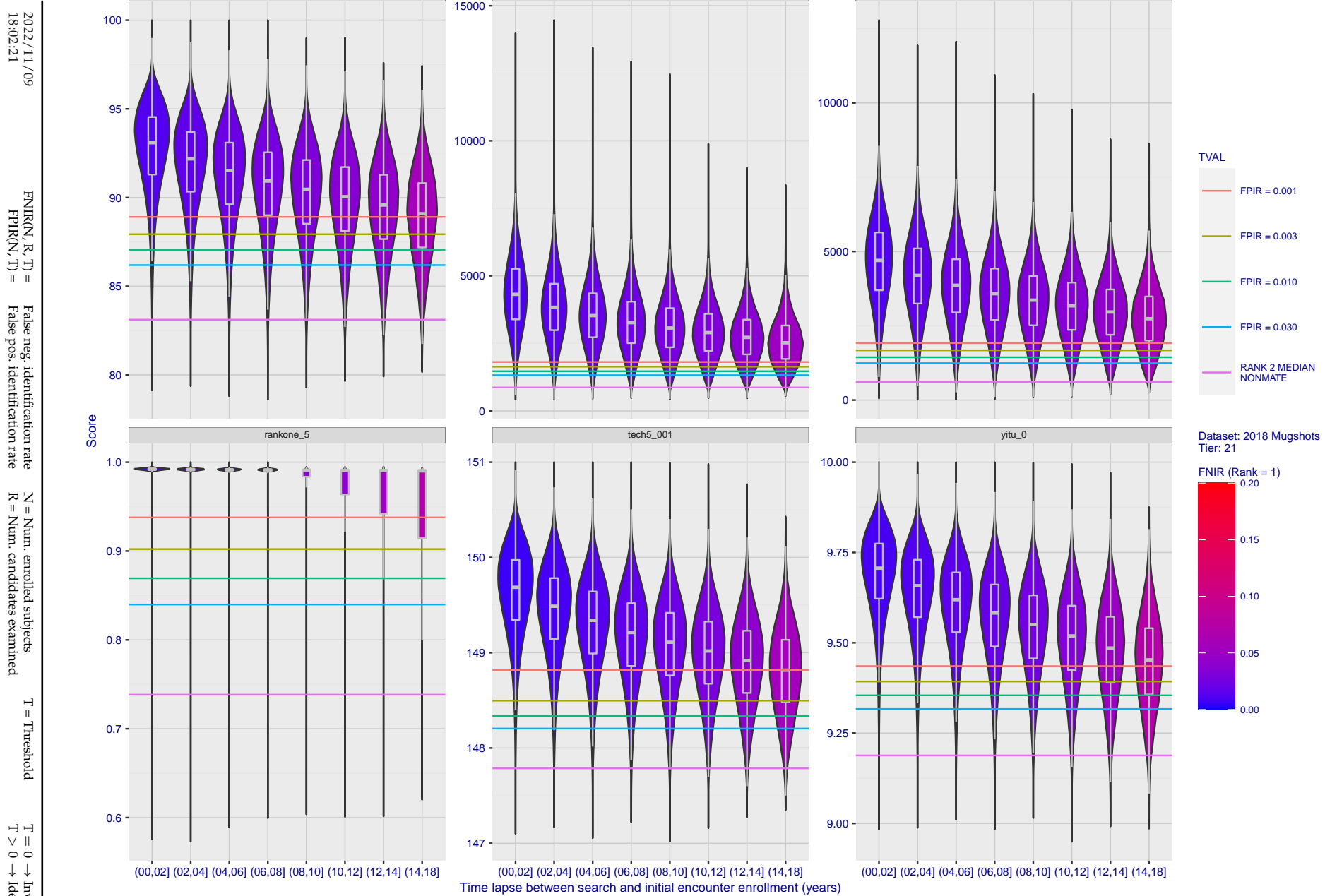


Figure 121: [FRVT-2018 Mugshot Ageing Dataset] Native mate scores vs. time-elapsed. The oldest image of each individual is enrolled. Thereafter, all more recent images are searched. Mated score distributions are computed over all searches noted in row 17 of Table 1 binned by number of years between search and initial enrollment.

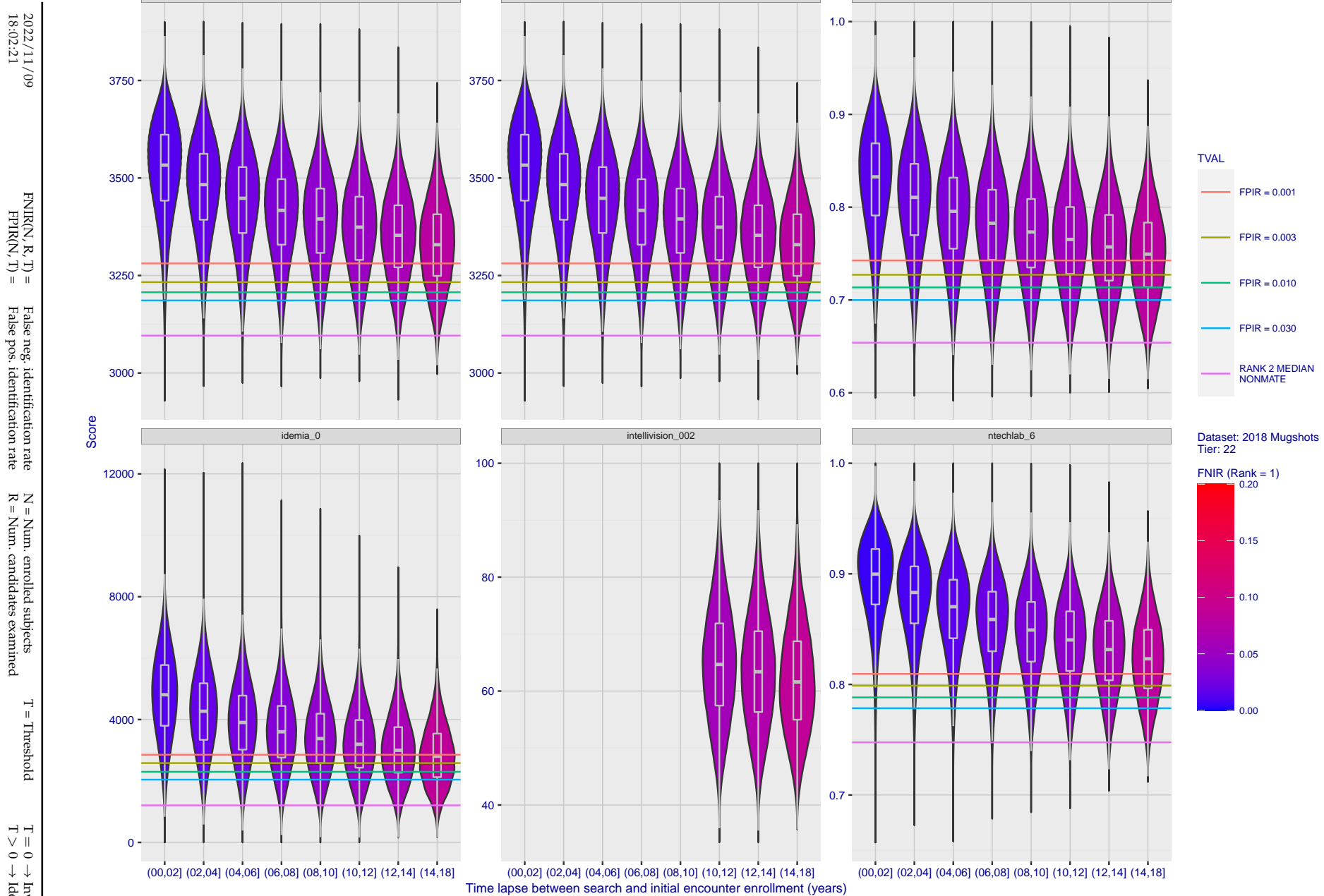


Figure 122: [FRVT-2018 Mugshot Ageing Dataset] Native mate scores vs. time-elapsed. The oldest image of each individual is enrolled. Thereafter, all more recent images are searched. Mated score distributions are computed over all searches noted in row 17 of Table 1 binned by number of years between search and initial enrollment.

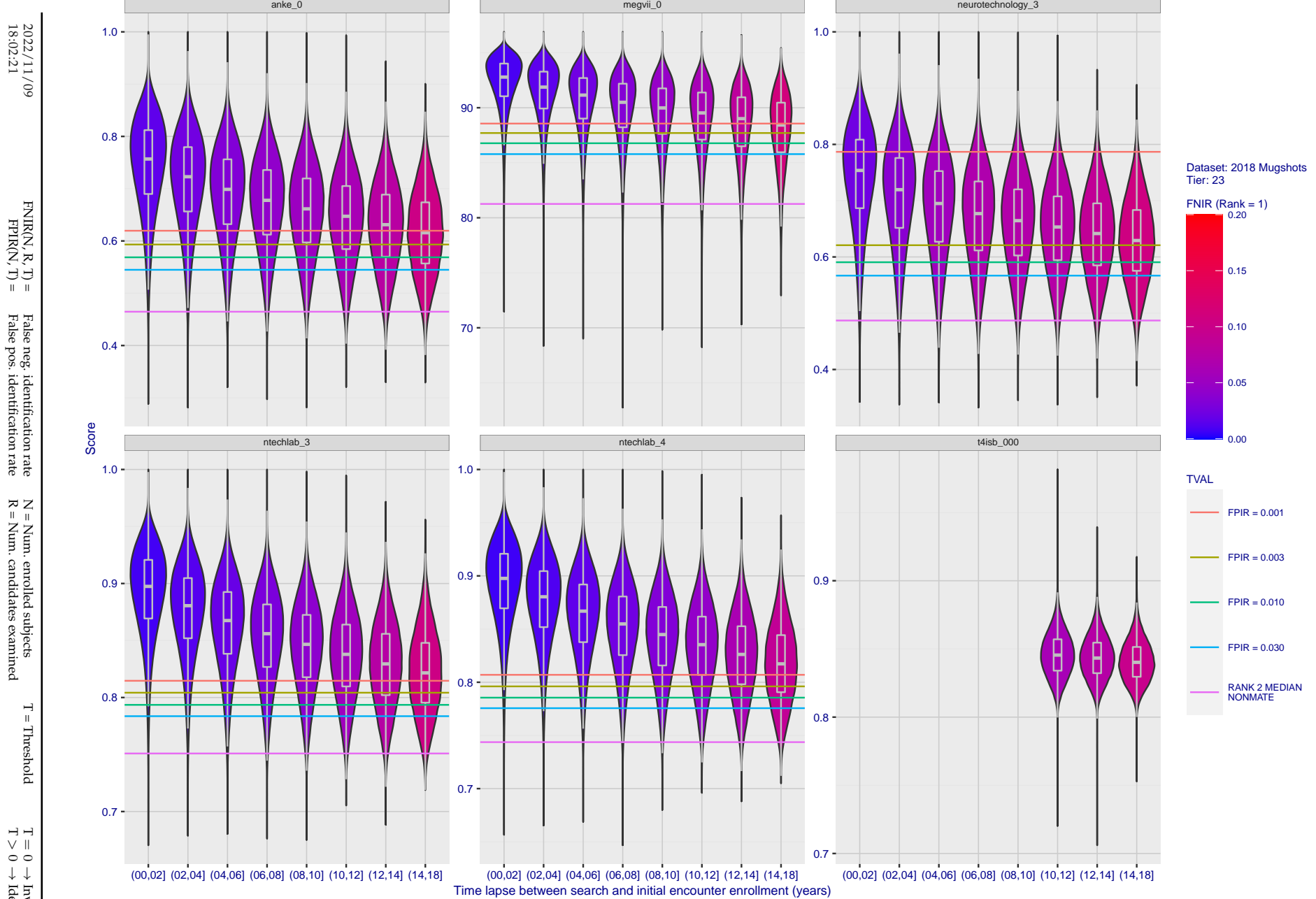


Figure 123: [FRVT-2018 Mugshot Ageing Dataset] Native mate scores vs. time-elapsed. The oldest image of each individual is enrolled. Thereafter, all more recent images are searched. Mated score distributions are computed over all searches noted in row 17 of Table 1 binned by number of years between search and initial enrollment.

2022/11/18:02:21

$\text{FN}(\text{N}, \text{R}, \text{T}) =$ false neg. identification rate
 $\text{FPIR}(\text{N}, \text{T}) =$ False pos. identification rate

N = Num. elicited subjects
 R = Num. candidates examined

1 - 115

$T > 0 \rightarrow$ Identification

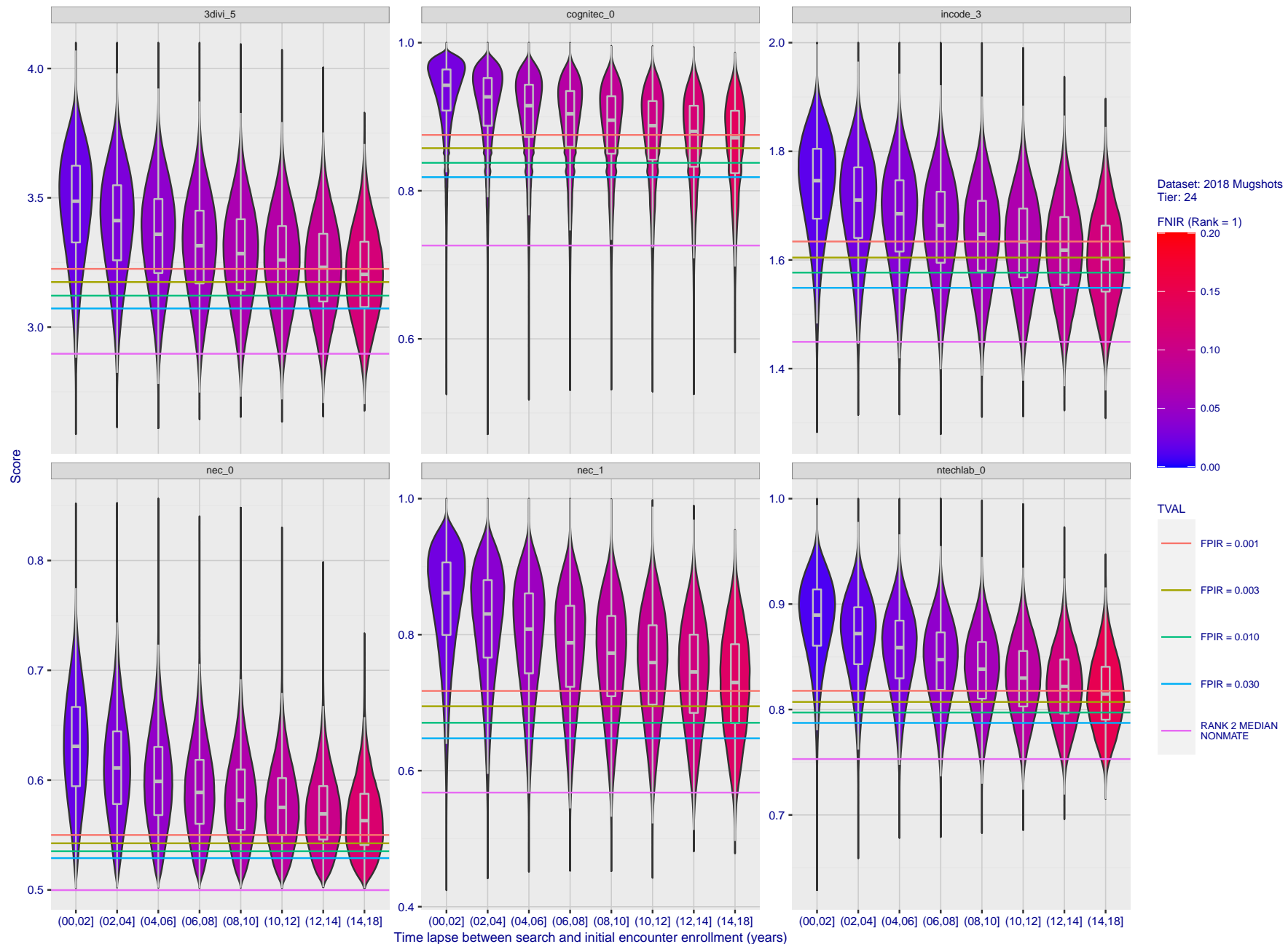


Figure 124: [FRVT-2018 Mugshot Ageing Dataset] Native mate scores vs. time elapsed. The oldest image of each individual is enrolled. Thereafter, all more recent images are searched. Mated score distributions are computed over all searches noted in row 17 of Table 1 binned by number of years between search and initial enrollment.

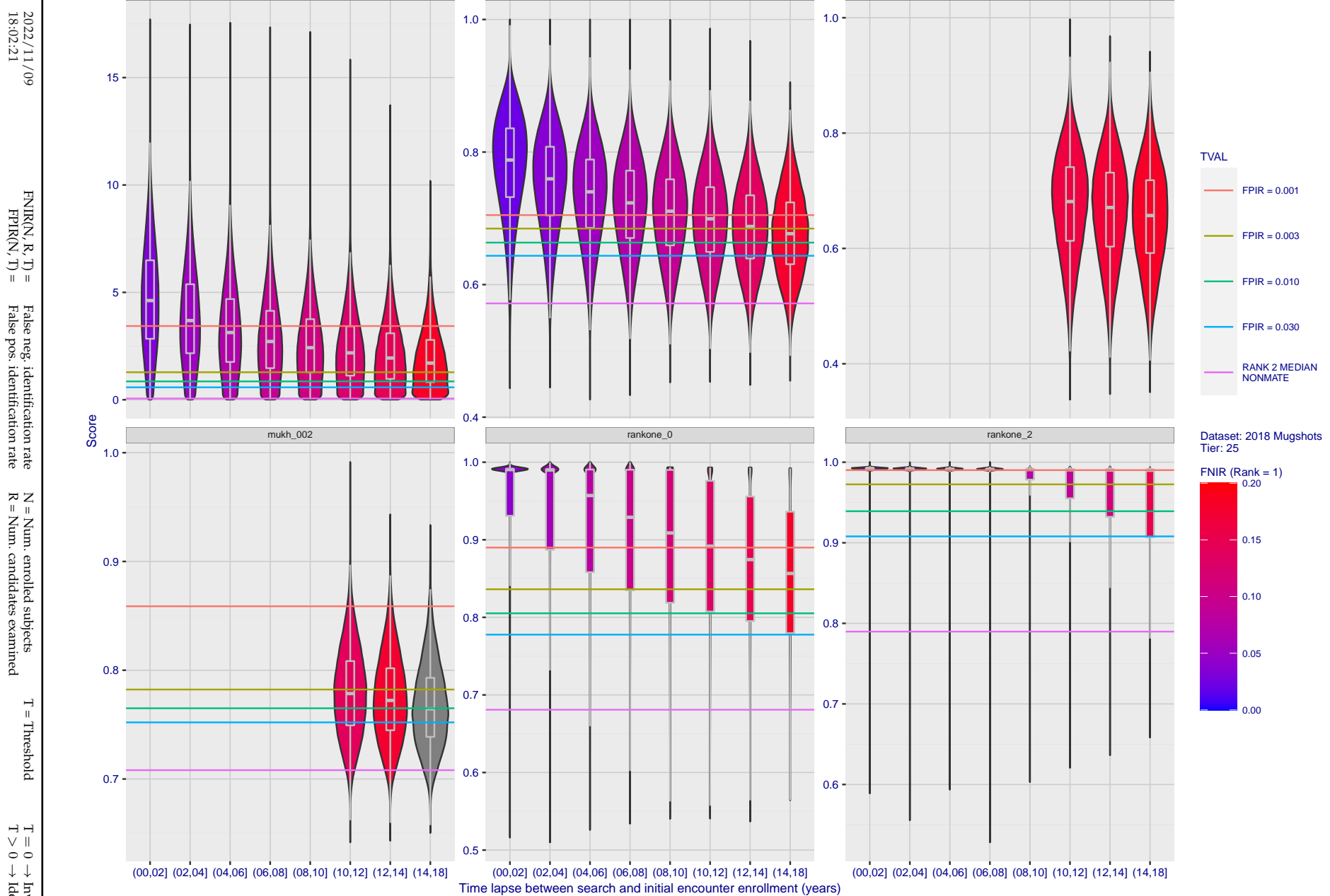


Figure 125: [FRVT-2018 Mugshot Ageing Dataset] Native mate scores vs. time-elapsed. The oldest image of each individual is enrolled. Thereafter, all more recent images are searched. Mated score distributions are computed over all searches noted in row 17 of Table 1 binned by number of years between search and initial enrollment.

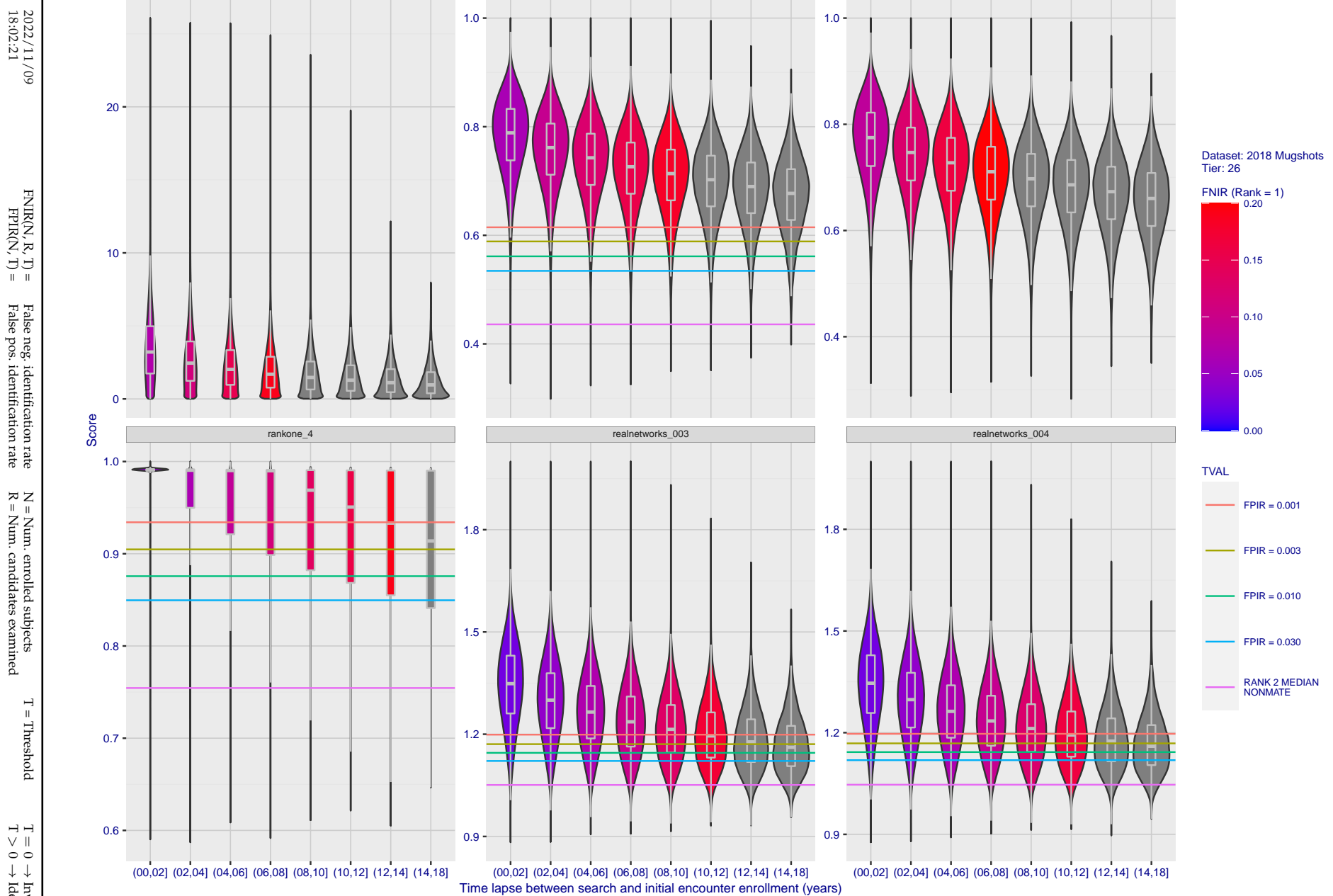


Figure 126: [FRVT-2018 Mugshot Ageing Dataset] Native mate scores vs. time-elapsed. The oldest image of each individual is enrolled. Thereafter, all more recent images are searched. Mated score distributions are computed over all searches noted in row 17 of Table 1 binned by number of years between search and initial enrollment.

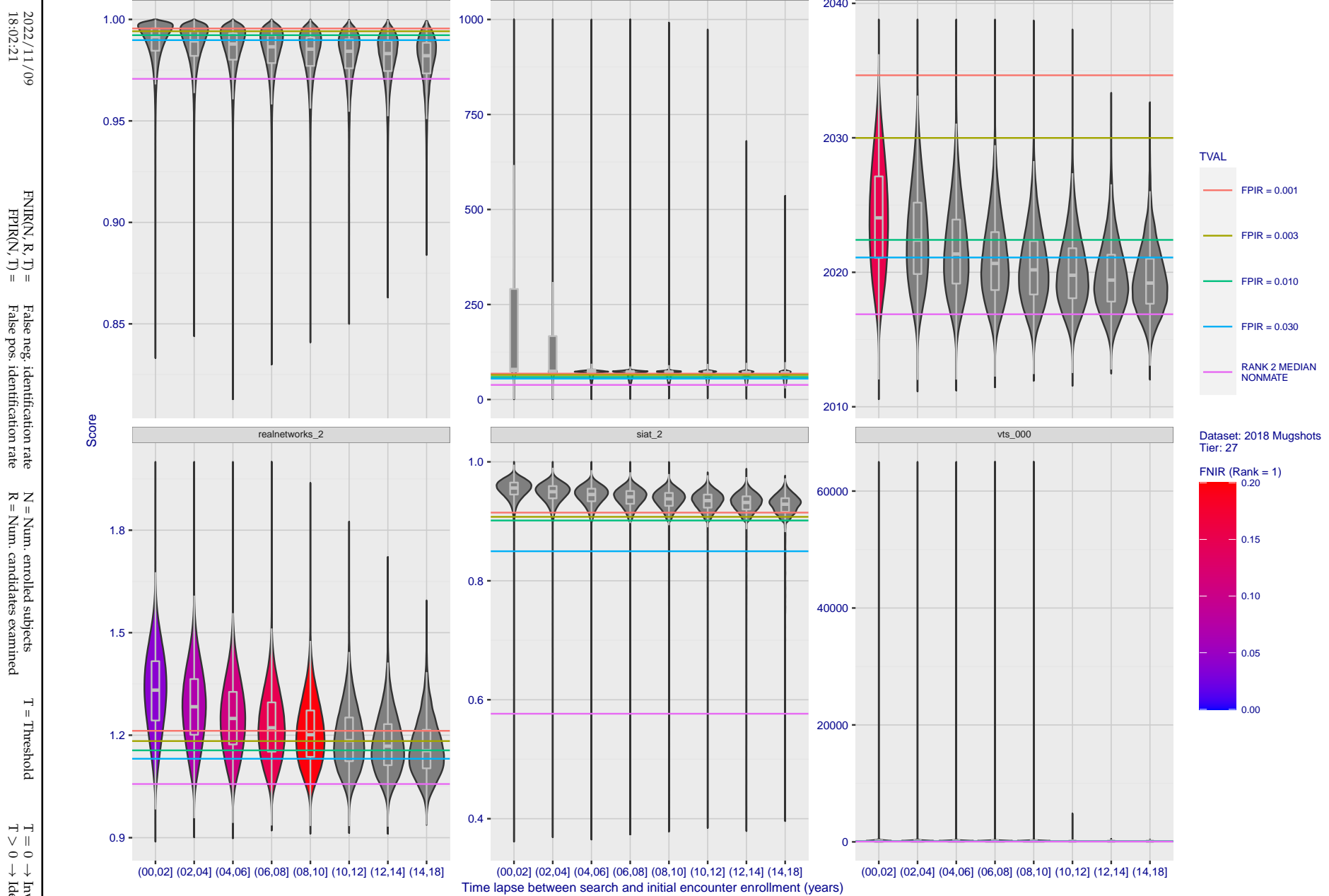


Figure 127: [FRVT-2018 Mugshot Ageing Dataset] Native mate scores vs. time-elapsed. The oldest image of each individual is enrolled. Thereafter, all more recent images are searched. Mated score distributions are computed over all searches noted in row 17 of Table 1 binned by number of years between search and initial enrollment.

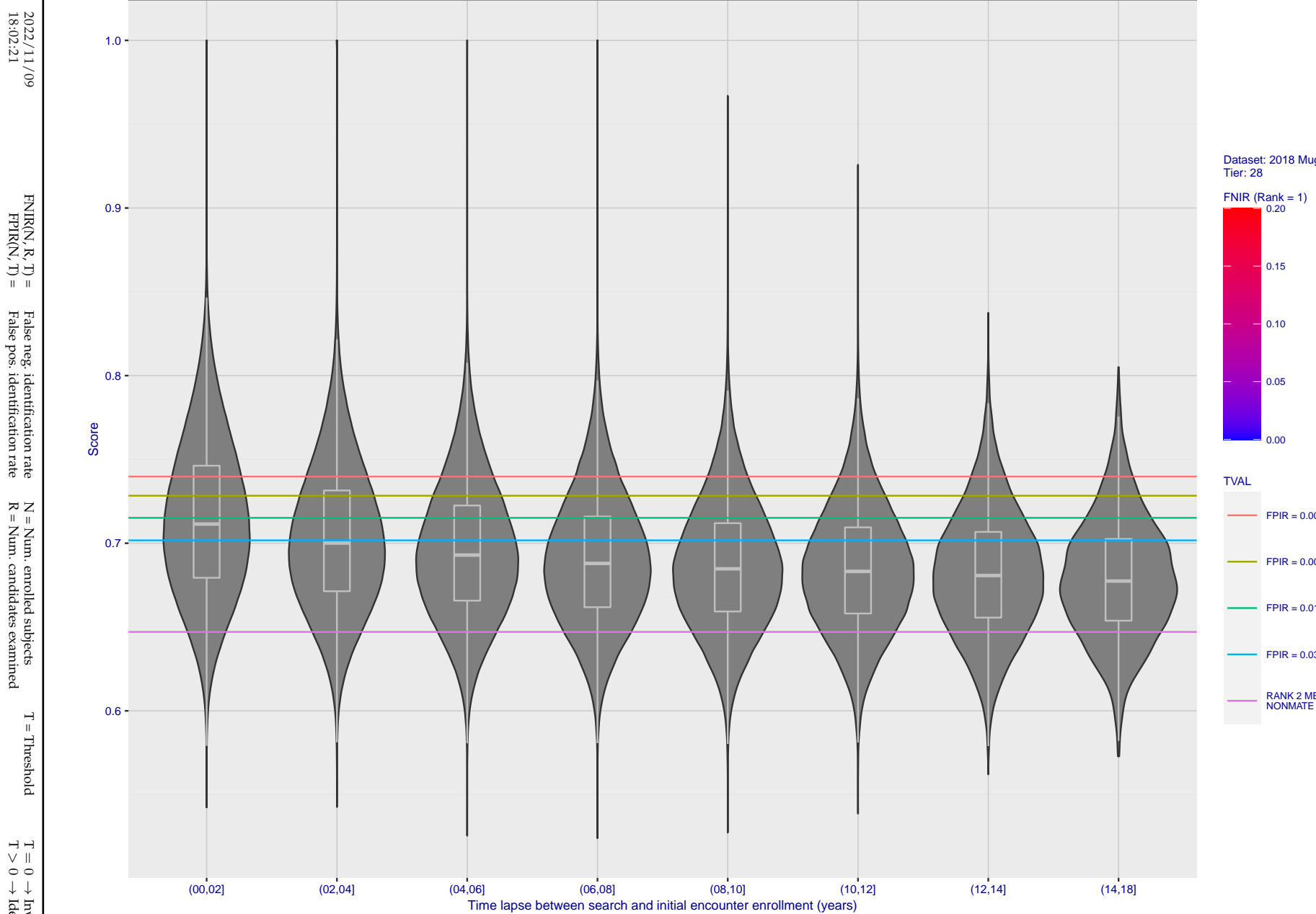


Figure 128: [FRVT-2018 Mugshot Ageing Dataset] Native mate scores vs. time-elapsed. The oldest image of each individual is enrolled. Thereafter, all more recent images are searched. Mated score distributions are computed over all searches noted in row 17 of Table 1 binned by number of years between search and initial enrollment.

Appendix C Effect of enrolling multiple images

2022/11/09
18:02:21FNIR(N, R, T) = False neg. identification rate
FPIR(N, T) = False pos. identification rateN = Num. enrolled subjects
R = Num. candidates examined

T = Threshold

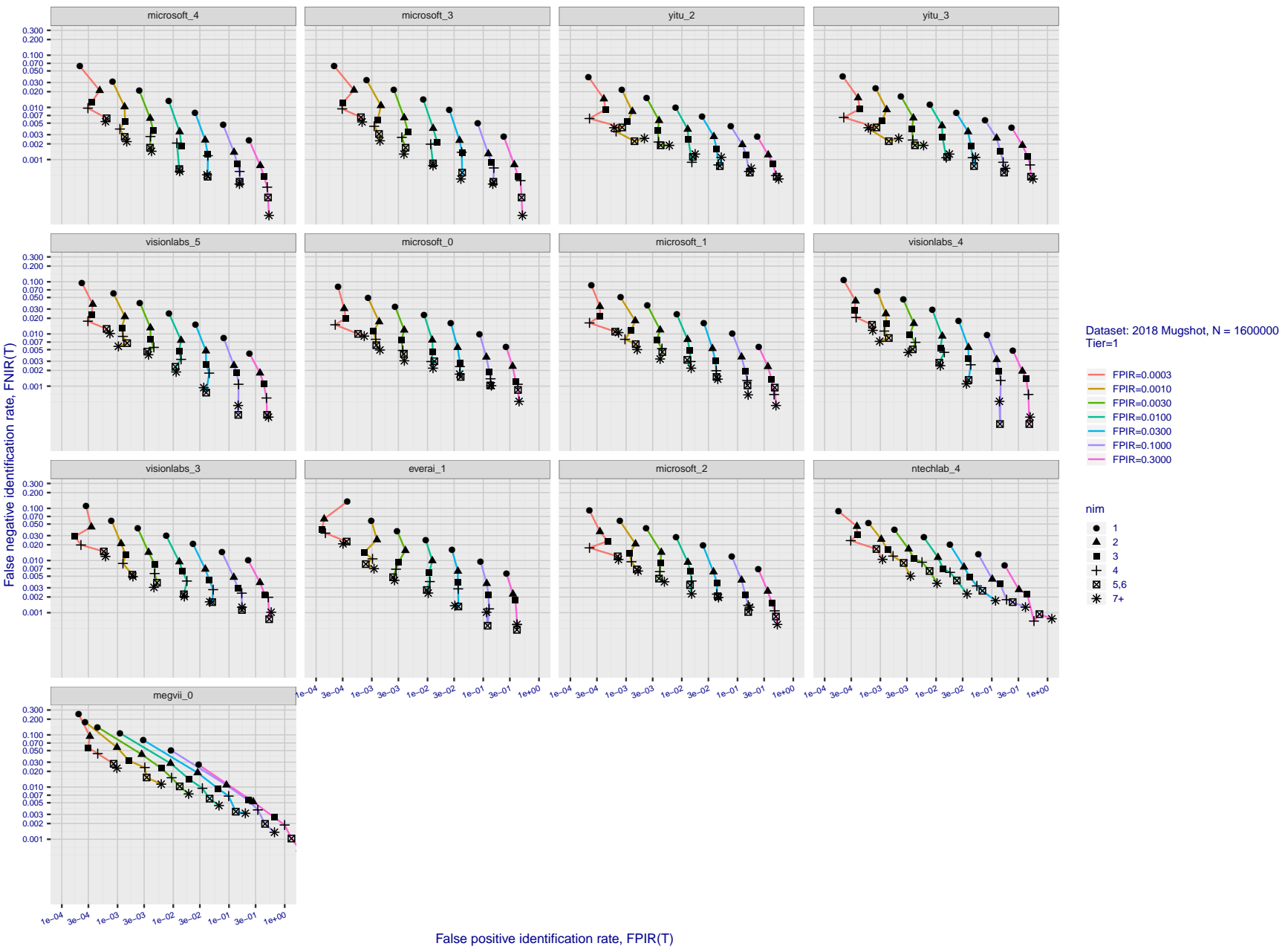
T = 0 → Investigation
T > 0 → Identification

Figure 129: [FRVT-2018 Mugshot Dataset] Effect of enrolling multiple images for each identity. The plot shows an identification miss rates vs. false positive rates, at seven operating thresholds. The enrolled population size is fixed. The images are enrolled with lifetime-consolidation - see section 2.3.

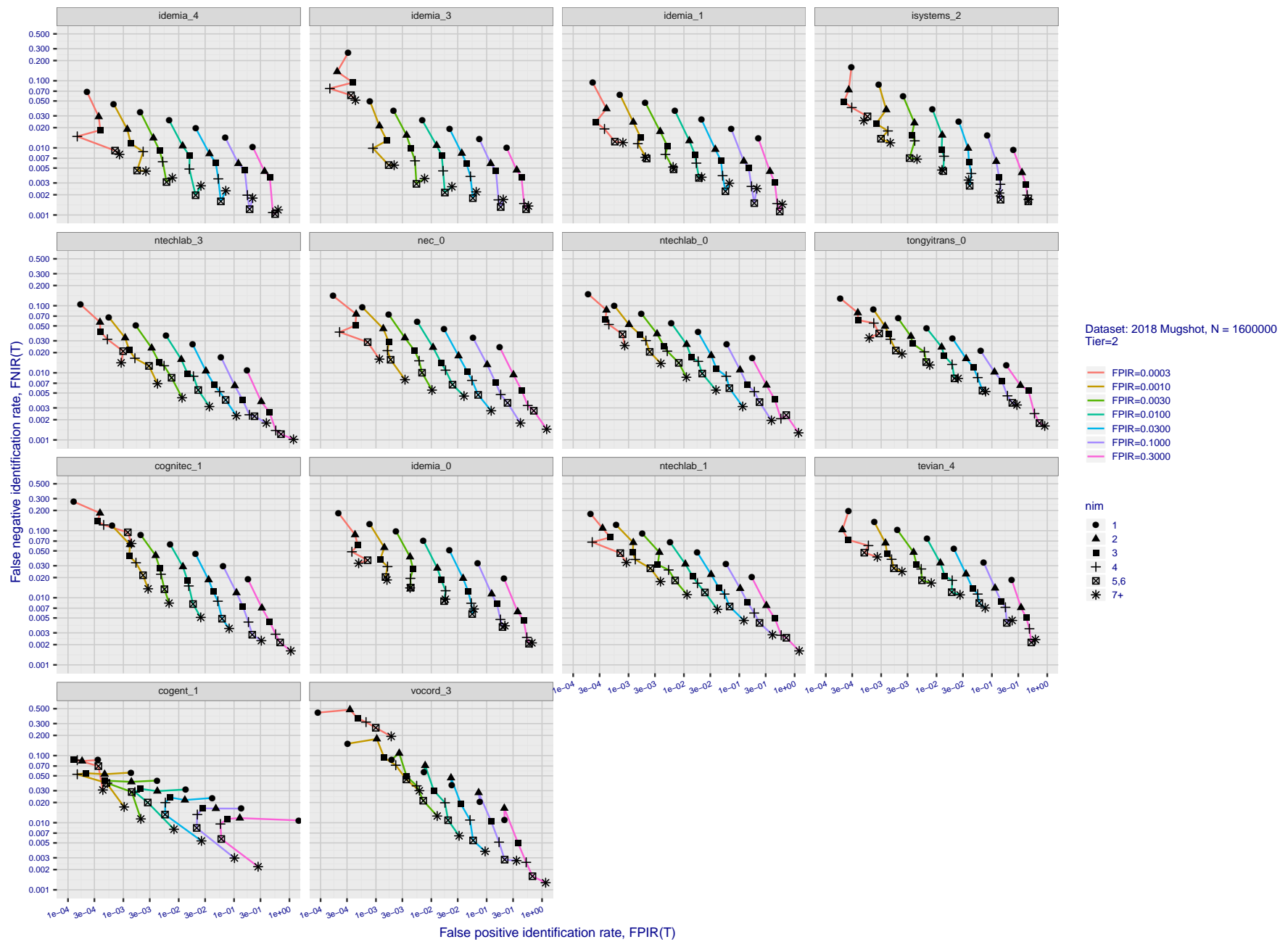


Figure 130: [FRVT-2018 Mugshot Dataset] Effect of enrolling multiple images for each identity. The plot shows an identification miss rates vs. false positive rates, at seven operating thresholds. The enrolled population size is fixed. The images are enrolled with lifetime-consolidation - see section 2.3.

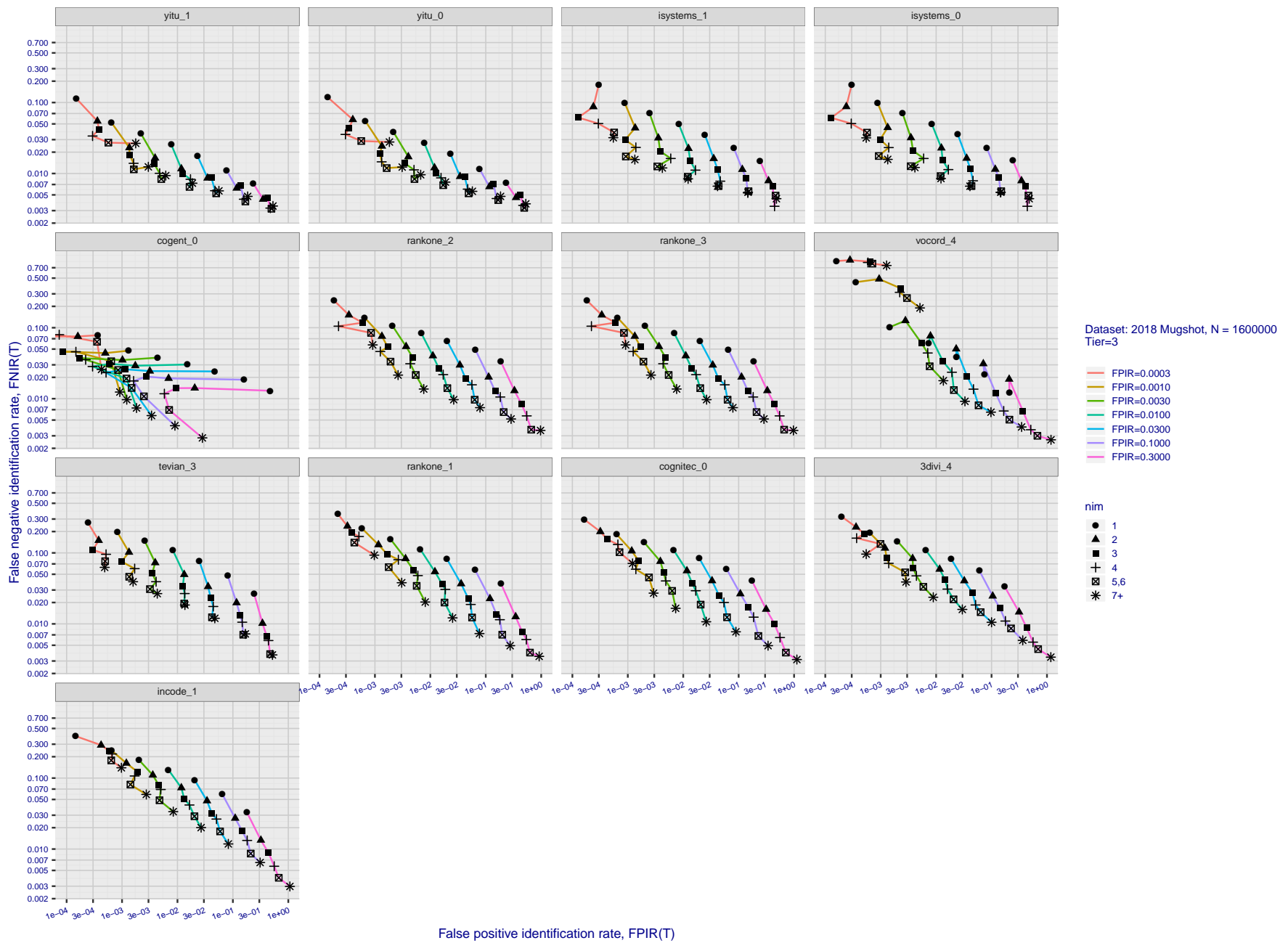


Figure 131: [FRVT-2018 Mugshot Dataset] Effect of enrolling multiple images for each identity. The plot shows an identification miss rates vs. false positive rates, at seven operating thresholds. The enrolled population size is fixed. The images are enrolled with lifetime-consolidation - see section 2.3.

2022/11/09
18:02:21

 $FNIR(N, R, T)$ = False neg. identification rate
 $FPIR(N, T) =$ False pos. identification rate

 N = Num. enrolled subjects
 R = Num. candidates examined

 T = Threshold
 $T = 0 \rightarrow$ Investigation
 $T > 0 \rightarrow$ Identification

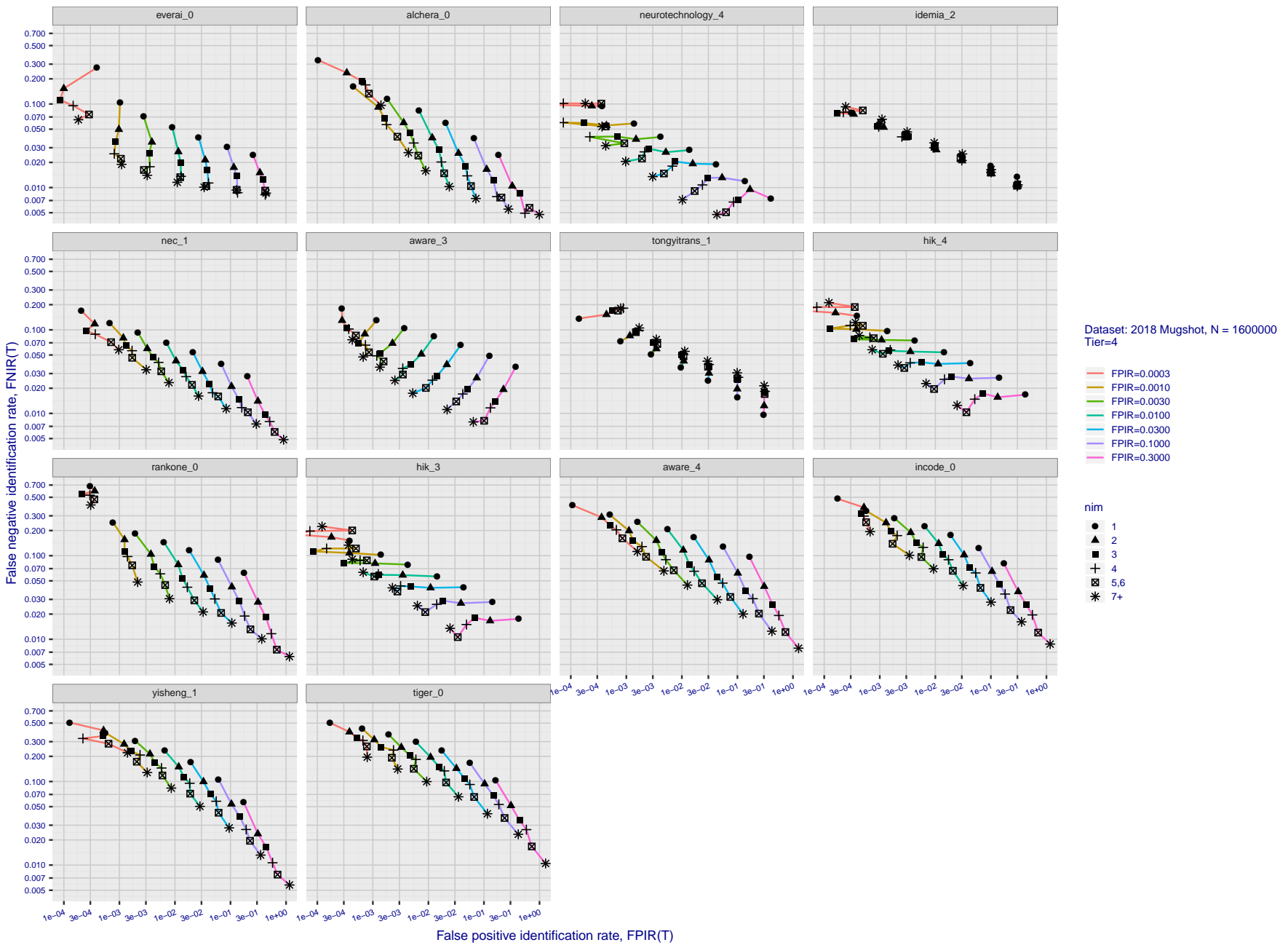


Figure 132: [FRVT-2018 Mugshot Dataset] Effect of enrolling multiple images for each identity. The plot shows an identification miss rates vs. false positive rates, at seven operating thresholds. The enrolled population size is fixed. The images are enrolled with lifetime-consolidation - see section 2.3.

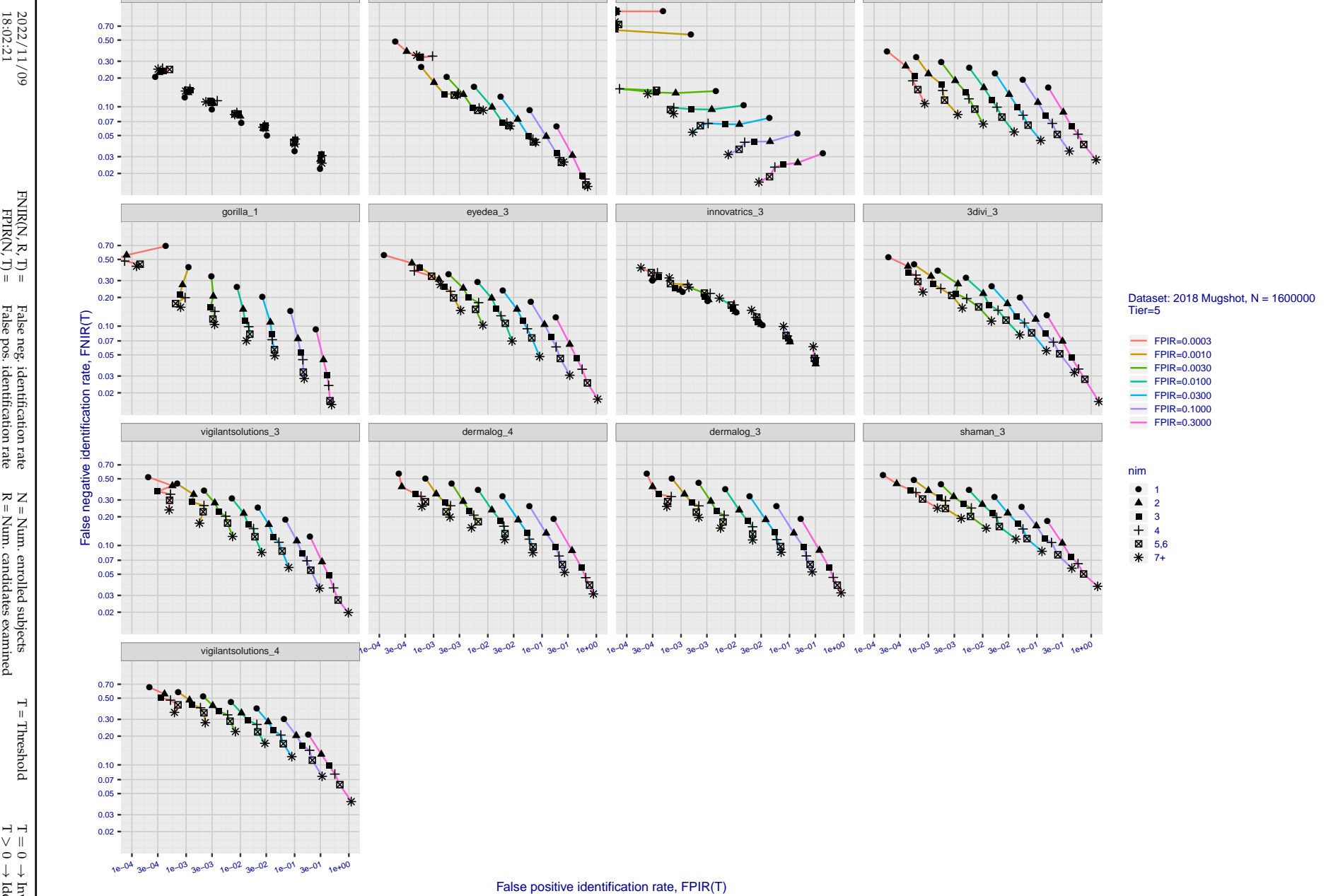


Figure 133: [FRVT-2018 Mugshot Dataset] Effect of enrolling multiple images for each identity. The plot shows an identification miss rates vs. false positive rates, at seven operating thresholds. The enrolled population size is fixed. The images are enrolled with lifetime-consolidation - see section 2.3.

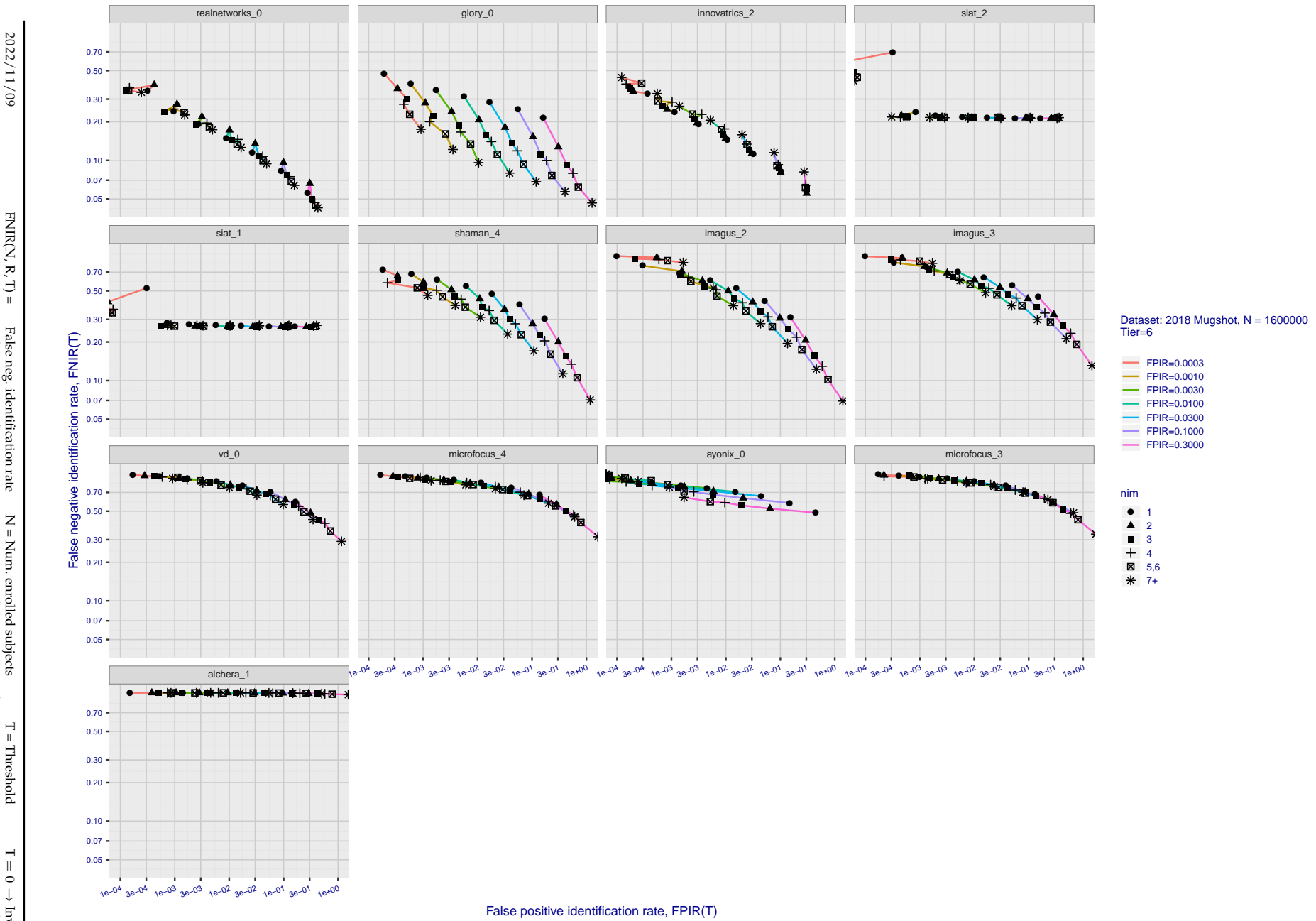


Figure 134: [FRVT-2018 Mugshot Dataset] Effect of enrolling multiple images for each identity. The plot shows an identification miss rates vs. false positive rates, at seven operating thresholds. The enrolled population size is fixed. The images are enrolled with lifetime-consolidation - see section 2.3.

Appendix D Accuracy with poor quality webcam images

2022/11/09
18:02:21

FNIR(N, R, T) = False neg. identification rate
FPTR(N, T) = False pos. identification rate

N = Num. enrolled subjects
R = Num. candidates examined

T = Threshold
T > 0 → Identification

T = 0 → Investigation

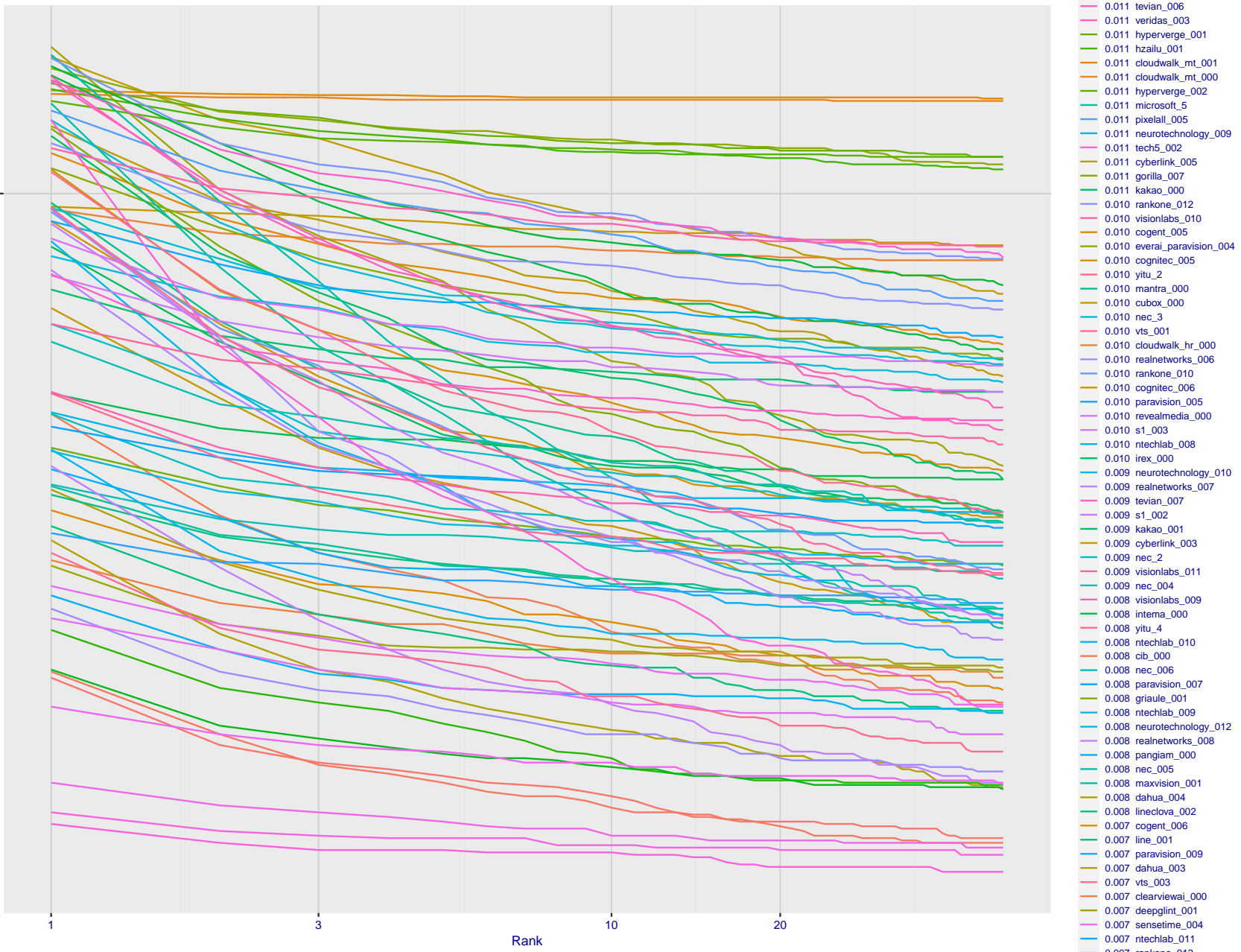


Figure 135: [Webcam Dataset] Identification miss rates vs. rank. The results apply to cross-domain recognition in which webcams are searched against enrolled mugshots. The FNIR values are higher than those for mugshot-mugshot identification due to low image resolution, lighting and less constrained subject pose in webcam images - see Figure 6.

2022/11/09

18:02:21

FNIR(N, R, T) = False neg. identification rate
FPTR(N, T) = False pos. identification rateN = Num. enrolled subjects
R = Num. candidates examined

T = Threshold

T = 0 → Investigation
T > 0 → Identification

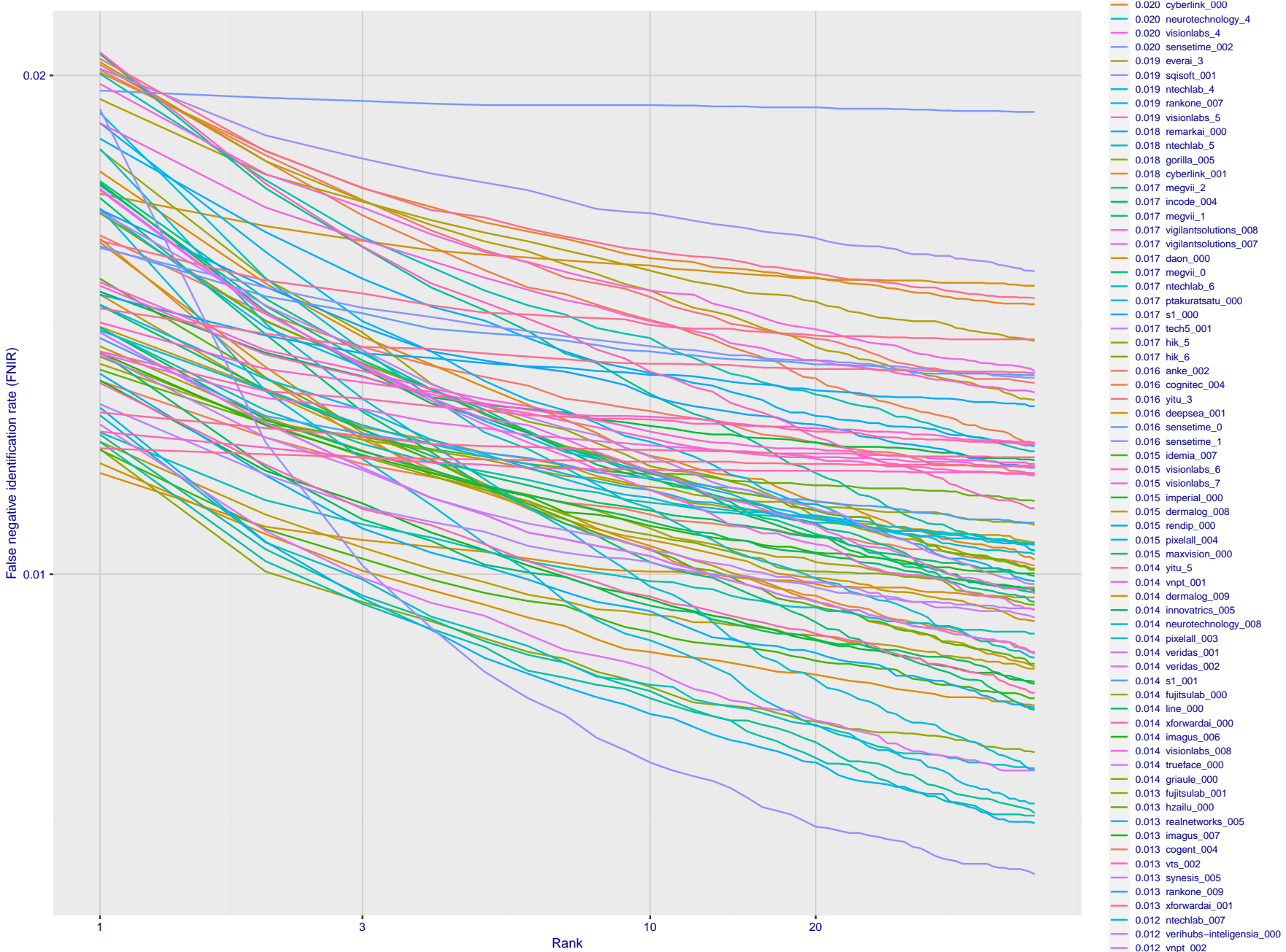


Figure 136: [Webcam Dataset] Identification miss rates vs. rank. The results apply to cross-domain recognition in which webcams are searched against enrolled mugshots. The FNIR values are higher than those for mugshot-mugshot identification due to low image resolution, lighting and less constrained subject pose in webcam images - see Figure 6.

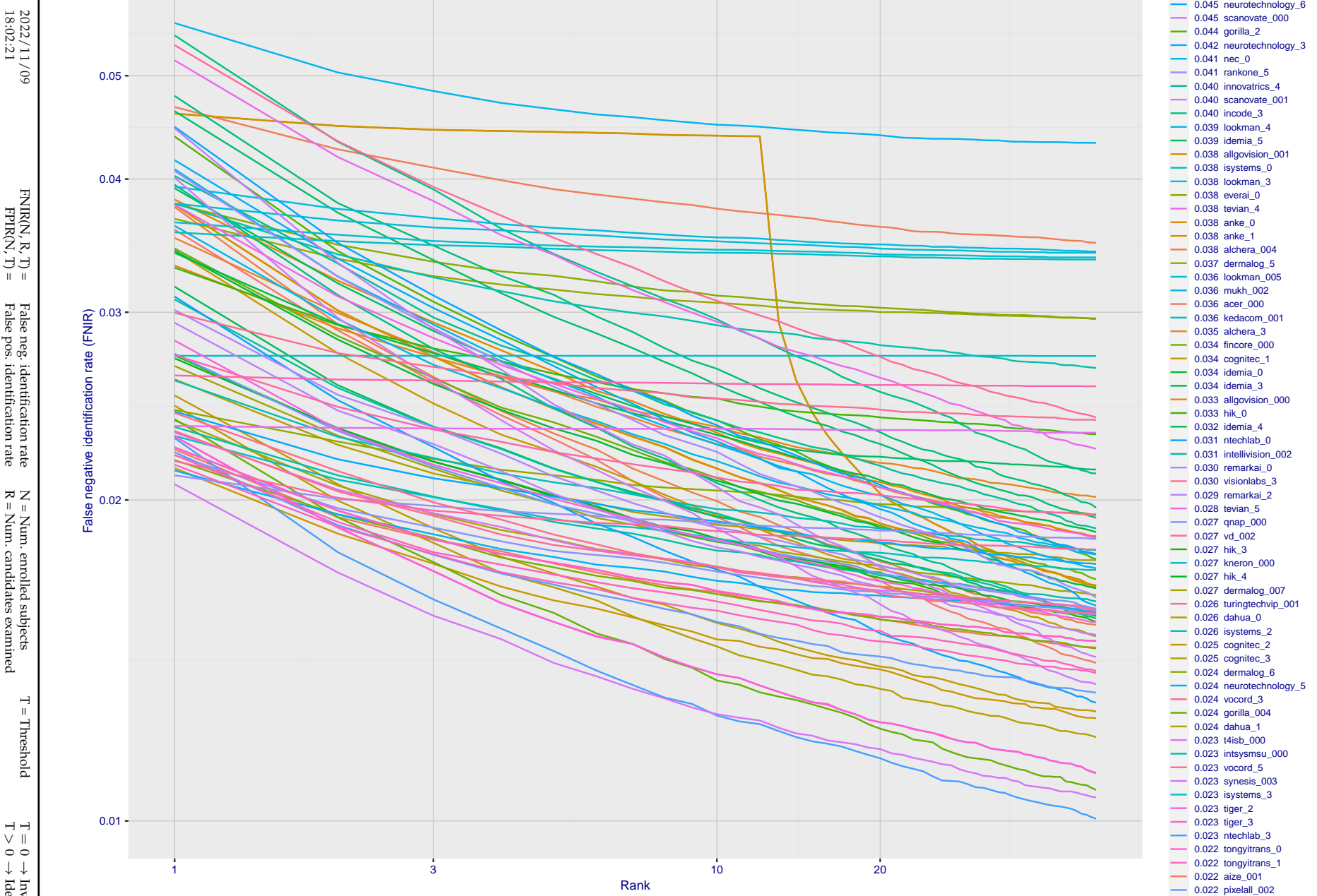


Figure 137: [Webcam Dataset] Identification miss rates vs. rank. The results apply to cross-domain recognition in which webcams are searched against enrolled mugshots. The FNIR values are higher than those for mugshot-mugshot identification due to low image resolution, lighting and less constrained subject pose in webcam images - see Figure 6.

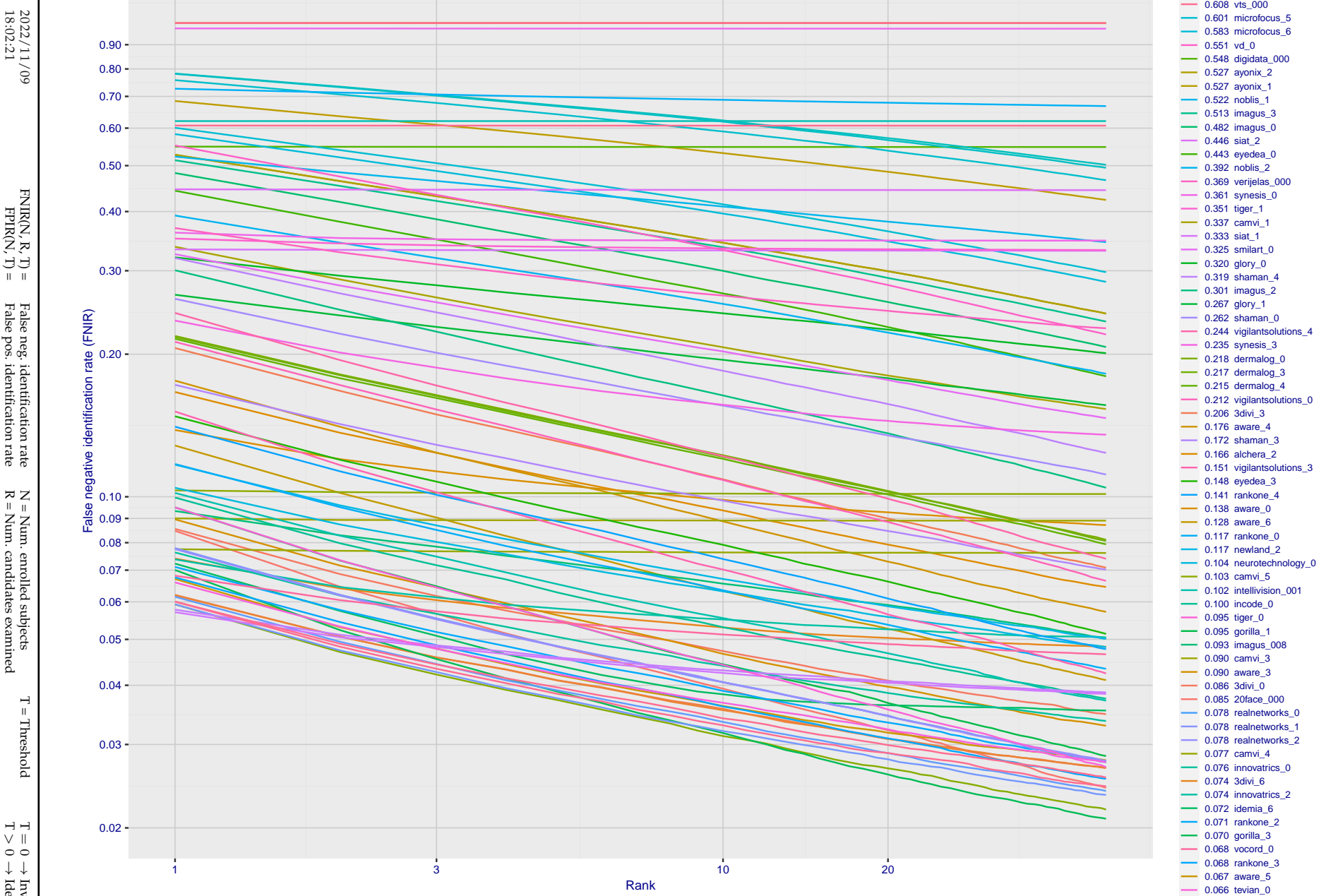


Figure 138: [Webcam Dataset] Identification miss rates vs. rank. The results apply to cross-domain recognition in which webcams are searched against enrolled mugshots. The FNIR values are higher than those for mugshot-mugshot identification due to low image resolution, lighting and less constrained subject pose in webcam images - see Figure 6.

2022/11/09
18:02:21

$\text{FNIR}(N, R, T) =$	False neg. identification rate	$N =$ Num. enrolled subjects	$T =$ Threshold	$T = 0 \rightarrow$ Investigation
$\text{FPTR}(N, T) =$	False pos. identification rate	$R =$ Num. candidates examined	$T > 0 \rightarrow$ Identification	

2022/11/09
18:02:21FNIR(N, R, T) = False neg. identification rate
FPIR(N, T) = False pos. identification rateN = Num. enrolled subjects
R = Num. candidates examined

T = Threshold

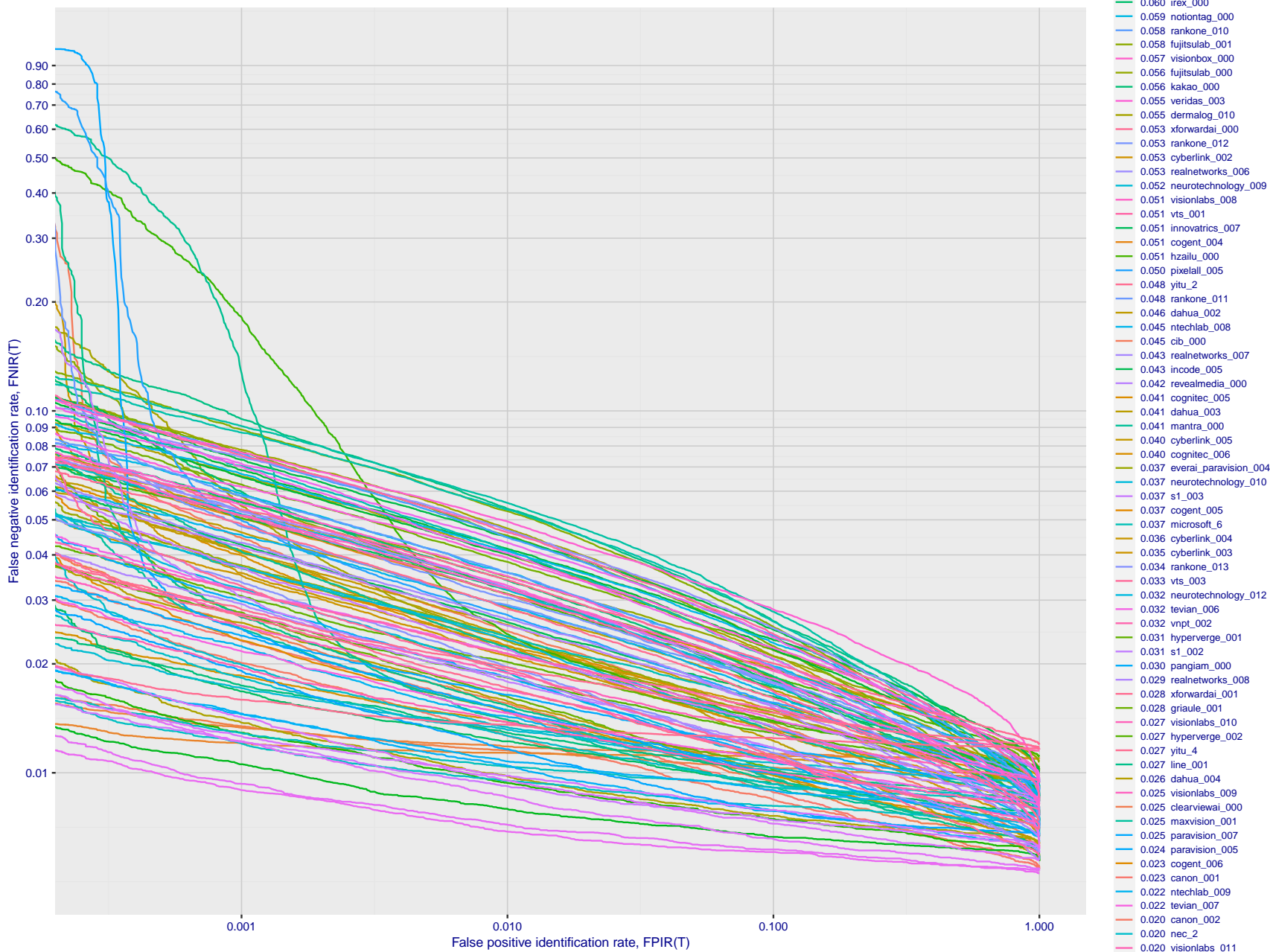
T = 0 → Investigation
T > 0 → Identification

Figure 139: [Webcam Dataset] Identification miss rates vs. false positive rates. The results apply to cross-domain recognition in which webcams are searched against enrolled mugshots. The FNIR values are higher than those for mugshot-mugshot identification due to low image resolution, lighting and less constrained subject pose in webcam images - see Figure 6.

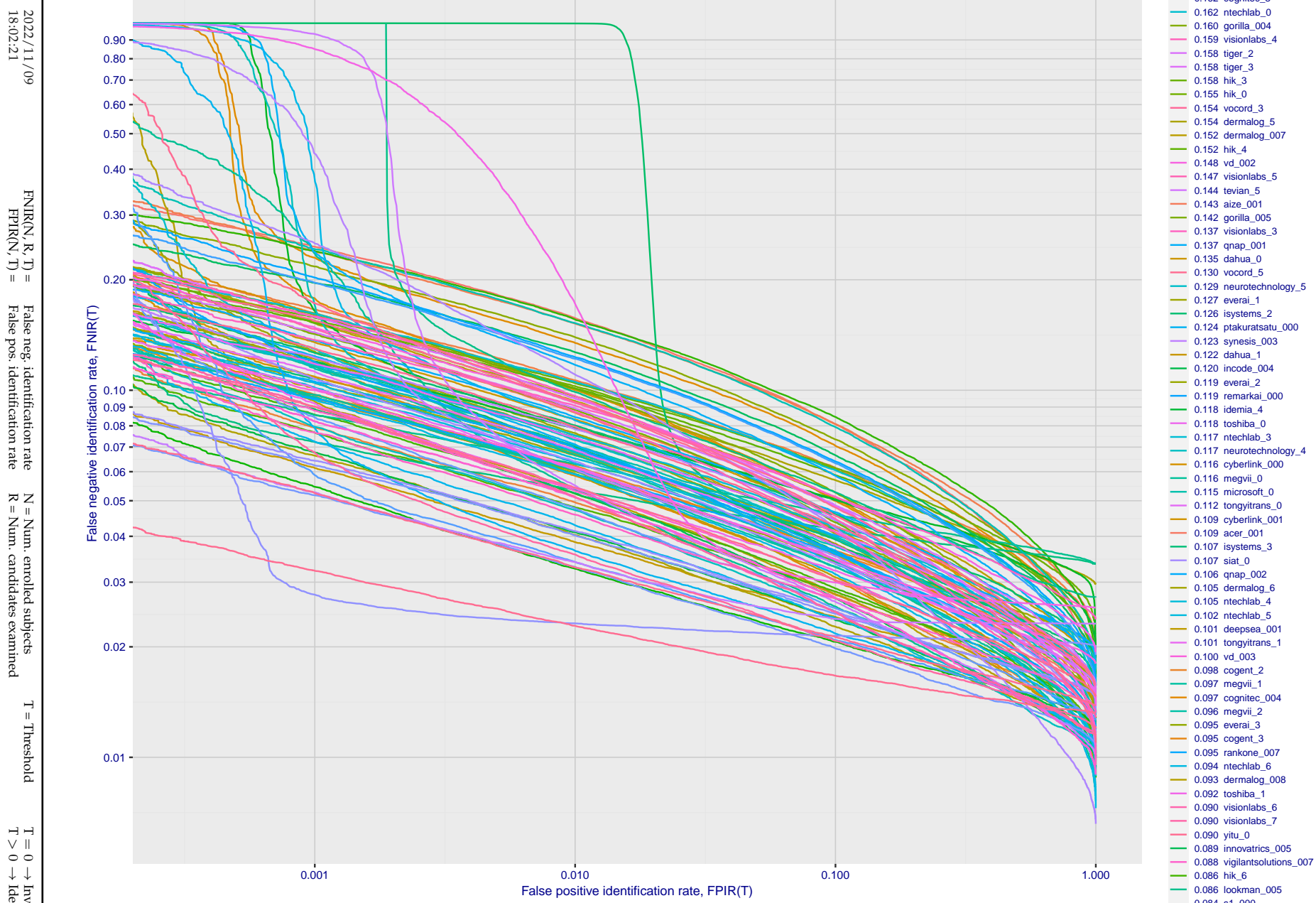


Figure 140: [Webcam Dataset] Identification miss rates vs. false positive rates. The results apply to cross-domain recognition in which webcams are searched against enrolled mugshots. The FNIR values are higher than those for mugshot-mugshot identification due to low image resolution, lighting and less constrained subject pose in webcam images - see Figure 6.

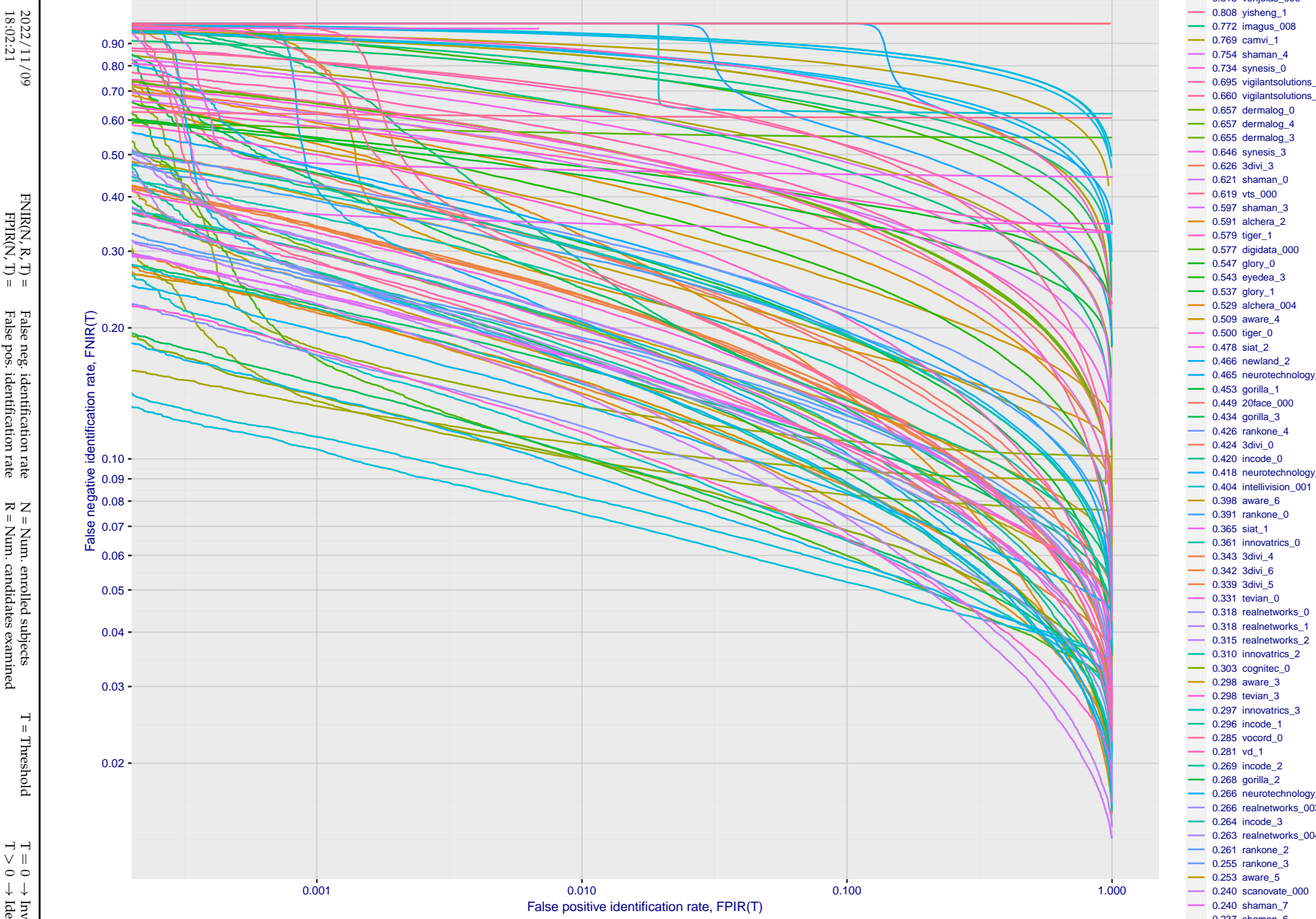


Figure 141: [Webcam Dataset] Identification miss rates vs. false positive rates. The results apply to cross-domain recognition in which webcams are searched against enrolled mugshots. The FNIR values are higher than those for mugshot-mugshot identification due to low image resolution, lighting and less constrained subject pose in webcam images - see Figure 6.

Appendix E Accuracy for profile-view to frontal recognition

Figures 142 - 144 gives accuracy results for searching 100 000 mated and 100 000 non-mated profile-view images against the same FRVT 2018 frontal enrollment dataset, $N = 1\,600\,000$, used in the main mugshot trials. This experiment corresponds to row-13 of Table 1. An example of profile-view image is given in Figure 7.

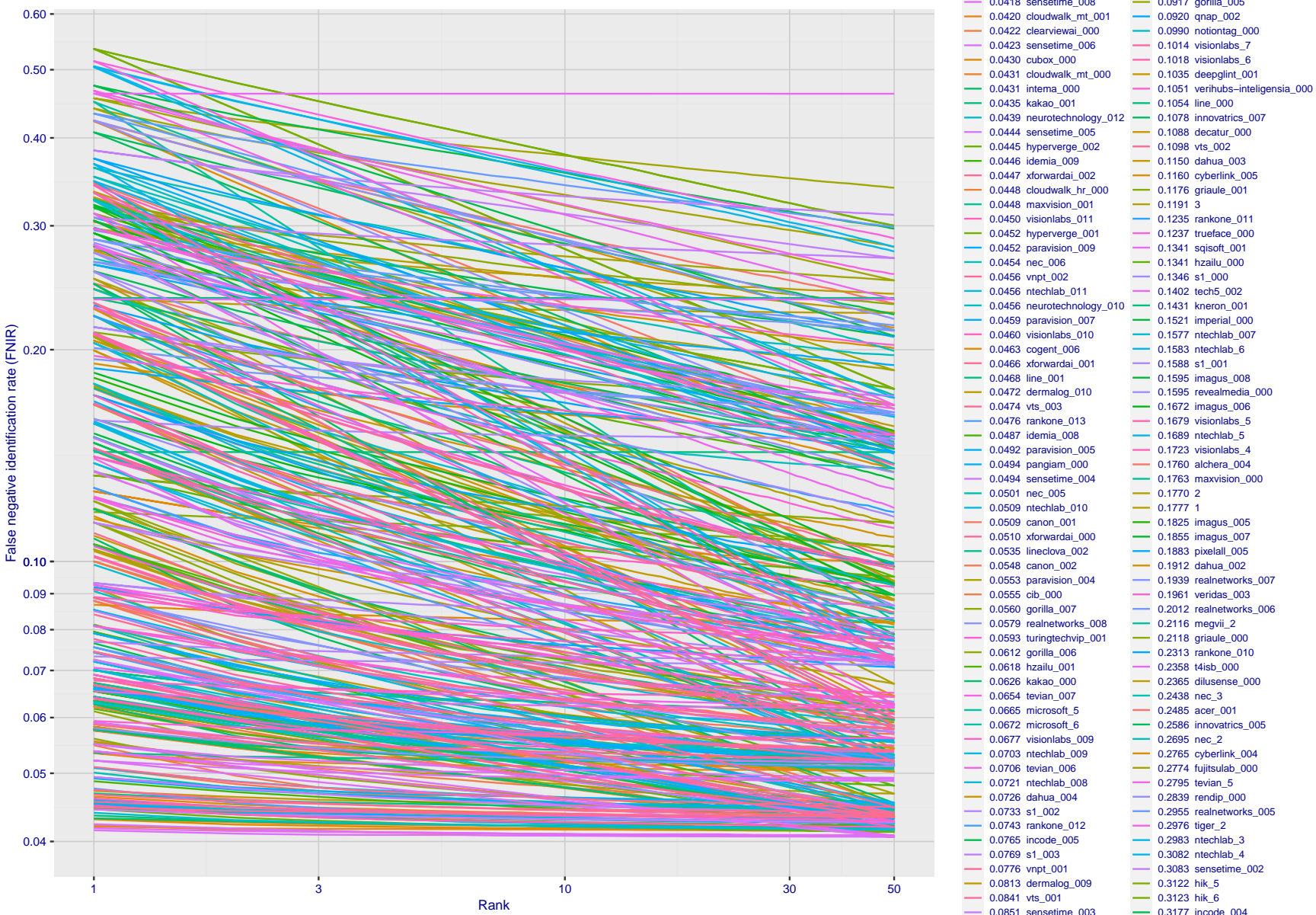


Figure 142: [Mugshot and profile-view dataset] Rank-based accuracy. For some of the more accurate Phase 3 algorithms the figure plots error tradeoff characteristics for frontal and profile-view searches into an enrolled set of $N = 1\,600\,000$ frontal images. Note that some algorithms fail on profile-view images with $\text{FNIR} \rightarrow 1$ - this evaluation did not ask developers to provide profile-view capability. Some algorithms, on the other hand, give FNIR approaching that for frontal-view searches using c. 2010 algorithms. The best result is that 91% of profile-view searches yield the correct mate at rank 1, and better than 94% in the top-50 candidates.

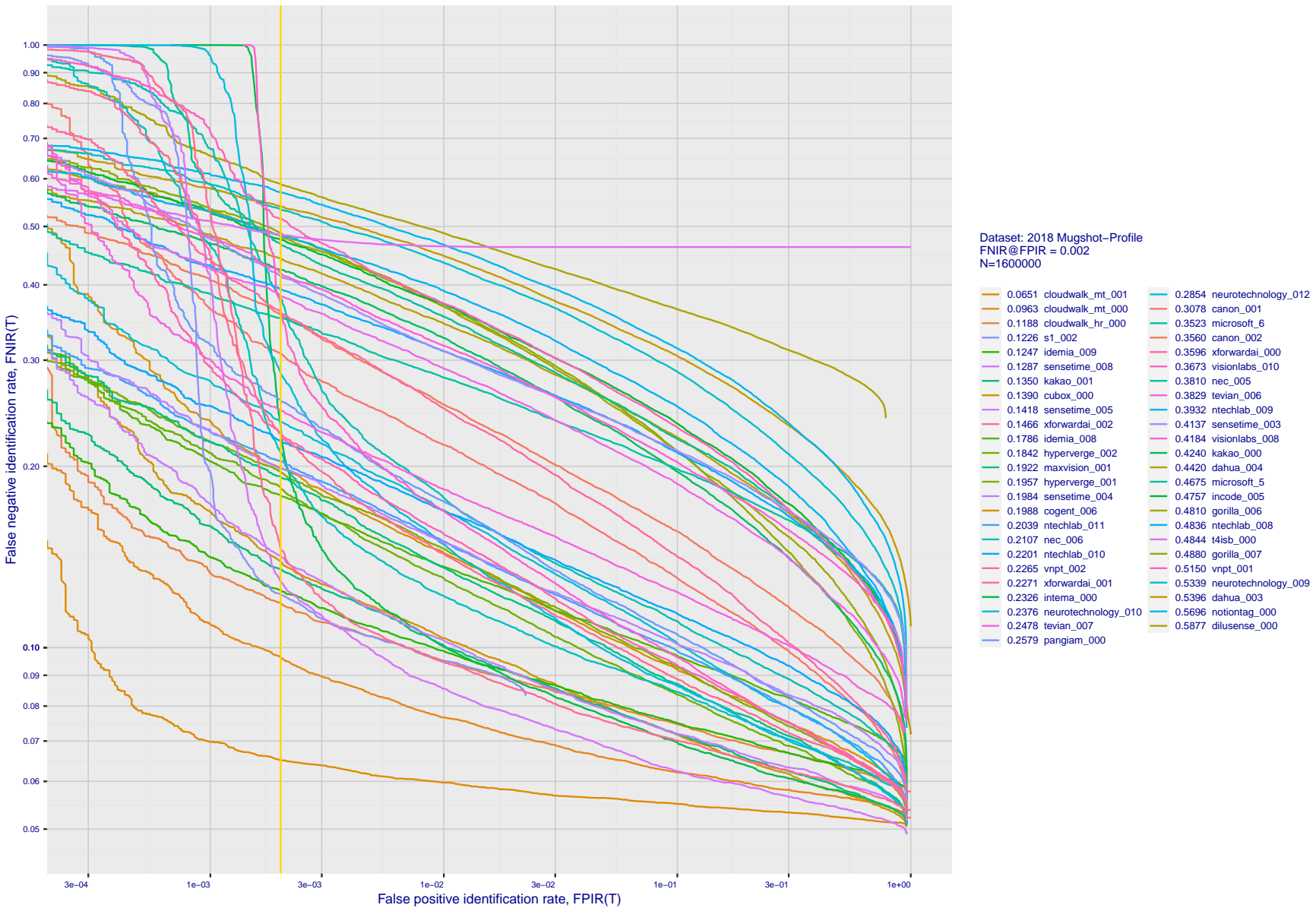


Figure 143: [Mugshot and profile-view dataset] Threshold-based accuracy. For some of the more accurate Phase 3 algorithms the figure plots error tradeoff characteristics for frontal and profile-view searches into an enrolled set of $N = 1\,600\,000$ frontal images. Note that some algorithms fail on profile-view images with $\text{FNIR} \rightarrow 1$ - this evaluation did not ask developers to provide profile-view capability. Some algorithms, on the other hand, give FNIR approaching that for frontal-view searches using c. 2010 algorithms.

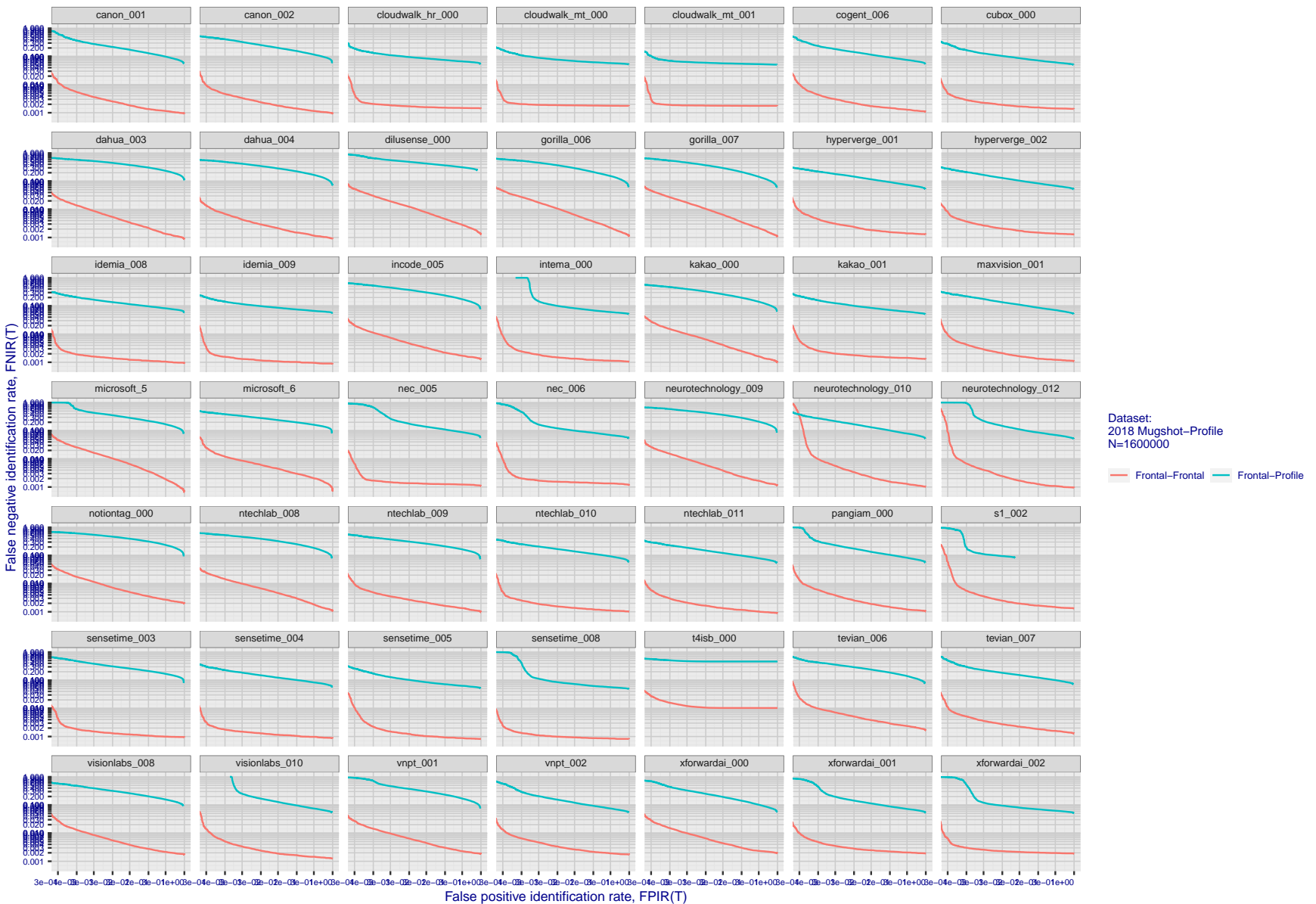


Figure 144: [Mugshot and profile-view dataset] Speed-accuracy tradeoff. For some of the more accurate Phase 3 algorithms the figure plots error tradeoff characteristics for frontal and profile-view searches into an enrolled set of $N = 1\,600\,000$ frontal images. Some algorithms fail on profile-view images with $\text{FNIR} \rightarrow 1$ - this evaluation did not ask developers to provide profile-view capability. Some algorithms, on the other hand, give FNIR approaching that for frontal-view searches using c. 2010 algorithms. Blue lines connect points of equal threshold from which it is evident that some algorithms would give markedly higher false positive outcomes if profile-view images were searched in a system configured for frontal searches. This would be a vulnerability in an access control system.

Appendix F Search duration

As in and prior tests, this section documents search speeds spanning three orders of magnitude. In applications where search volumes are high enough, this will have implications for hardware requirements especially for large N or when search duration is appreciably larger than the time it takes to prepare a template from the search image(s). Further, given very large (and growing) operational databases, the scalability of algorithms is important. It has been reported previously [8] that search duration can scale sublinearly with enrolled population size N. Further there has been considerable recent research on indexing, exact [13] and approximate nearest neighbor search [1,13] and fast-search [14,16].

Figure 145 charts the search duration measurements presented earlier in Tables 2 - 4.

- ▷ Most algorithms scale linearly. For those in that category, there is a wide range in speed with search durations ranging from 82 milliseconds for a 12 million gallery (for NEC-3) to more than 40 seconds (for Yitu-3, Toshiba-2) and even higher for less accurate algorithms.
- ▷ Some developers (Camvi, Dermalog, EverAI, Innovatrics, and Visionlabs) provide algorithms whose template search durations grow approximately logarithmically i.e. $T(N) \sim \log N$ with the constant a varying between implementations. In the figure this model is fit using the point $T(1) = 0$, and $T(640\,000)$. This very sublinear behaviour affords extremely fast search times in very large galleries. One caveat for the sublinear algorithms is that their fast-search data structures can require considerable computation time - on the order of hours - for N in the millions, and this scales mildly super-linearly, i.e. $O(N^b)$, $b > 1$. There are exceptions: the Camvi algorithms take minutes; and Innovatrics' scale sublinearly.

2022/11/09
18:02:21

FNIR(N, R, T) = False neg. identification rate
FPTR(N, T) = False pos. identification rate

N = Num. enrolled subjects
R = Num. candidates examined

T = Threshold
T > 0 → Identification

T = 0 → Investigation

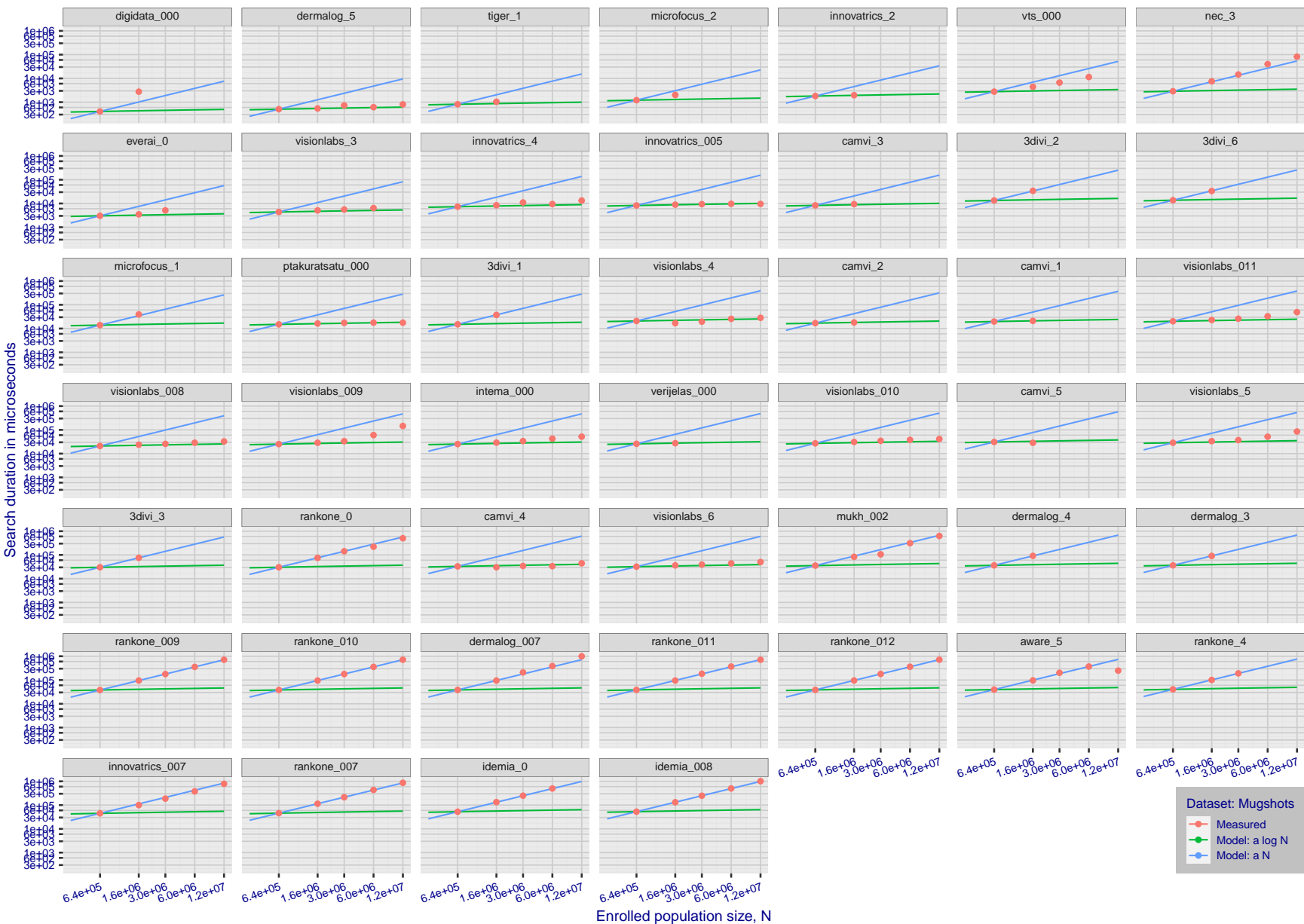
2022/11/09
18:02:21FNIR(N, R, T) = False neg. identification rate
FPFR(N, T) = False pos. identification rateN = Num. enrolled subjects
R = Num. candidates examinedT = Threshold
T = 0 → Investigation
T > 0 → Identification

Figure 145: [Mugshot Dataset] Search duration vs. enrolled population size. In red are the actual point durations measured on a single c. 2016 core. The blue shows linear growth from $N = 640\,000$. The green line shows logarithmic growth from that point to $N = 1\,600\,000$. Note the sublinear growth from algorithms from Camvi, Dermalog, EverAI, Innovatrics, and Visionlabs. The tiger_1 algorithm is also sublinear, but inaccurate and inoperable at $N \geq 3000000$. This capability sometimes comes at the additional expense of converting a linear gallery data structure into whatever fast-search data structure is used. Note that search times are sometimes dominated by the template generation times shown in Table 26.

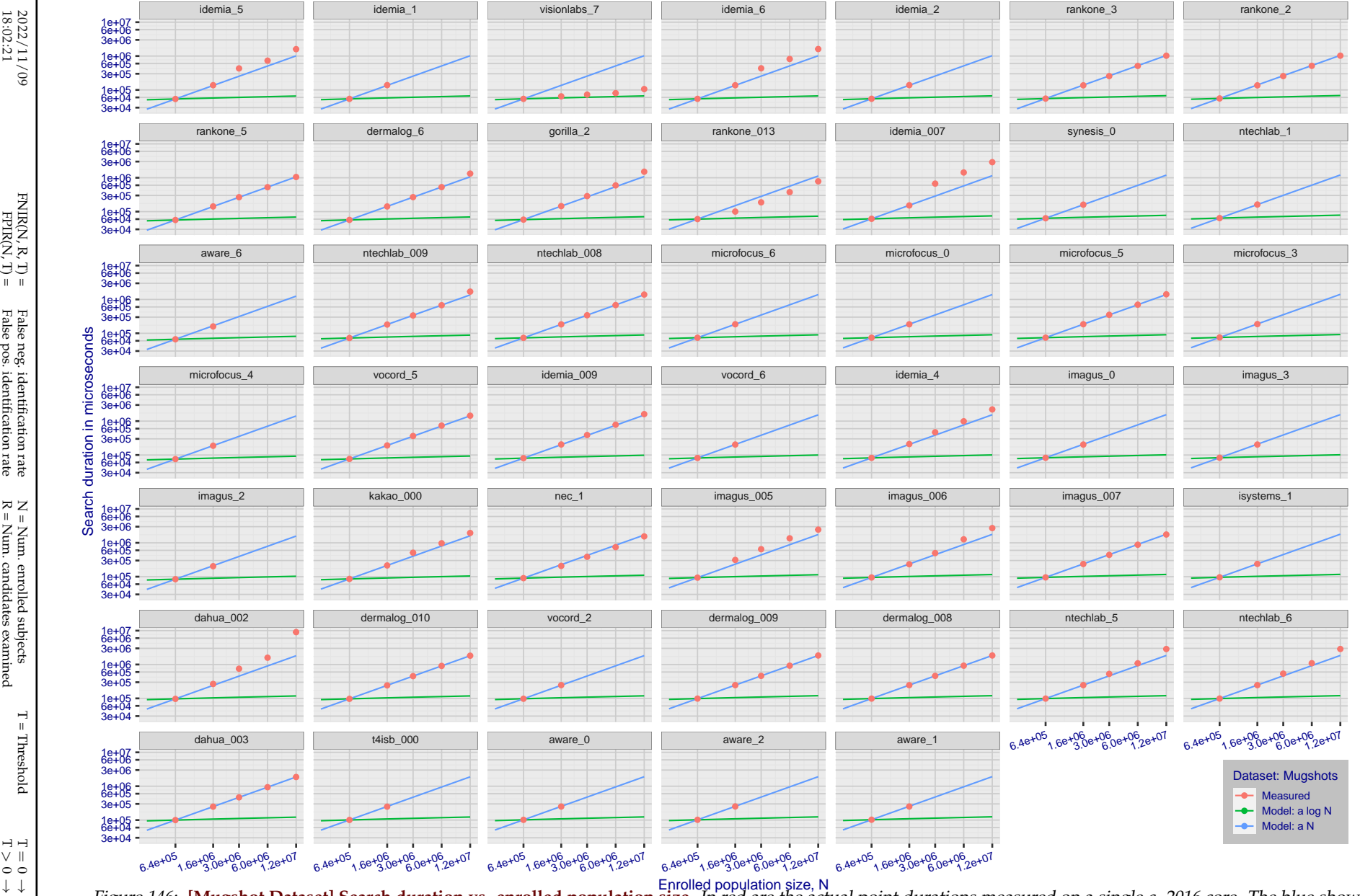


Figure 146: [Mugshot Dataset] Search duration vs. enrolled population size. In red are the actual point durations measured on a single c. 2016 core. The blue shows linear growth from $N = 640\,000$. The green line shows logarithmic growth from that point to $N = 1\,600\,000$. Note the sublinear growth from algorithms from Camvi, Dermalog, EverAI, Innovatrics, and Visionlabs. The tiger_1 algorithm is also sublinear, but inaccurate and inoperable at $N \geq 3000000$. This capability sometimes comes at the additional expense of converting a linear gallery data structure into whatever fast-search data structure is used. Note that search times are sometimes dominated by the template generation times shown in Table 26.

2022/11/09
18:02:21FNIR(N, R, T) = False neg. identification rate
FPFR(N, T) = False pos. identification rateN = Num. enrolled subjects
R = Num. candidates examined

T = Threshold

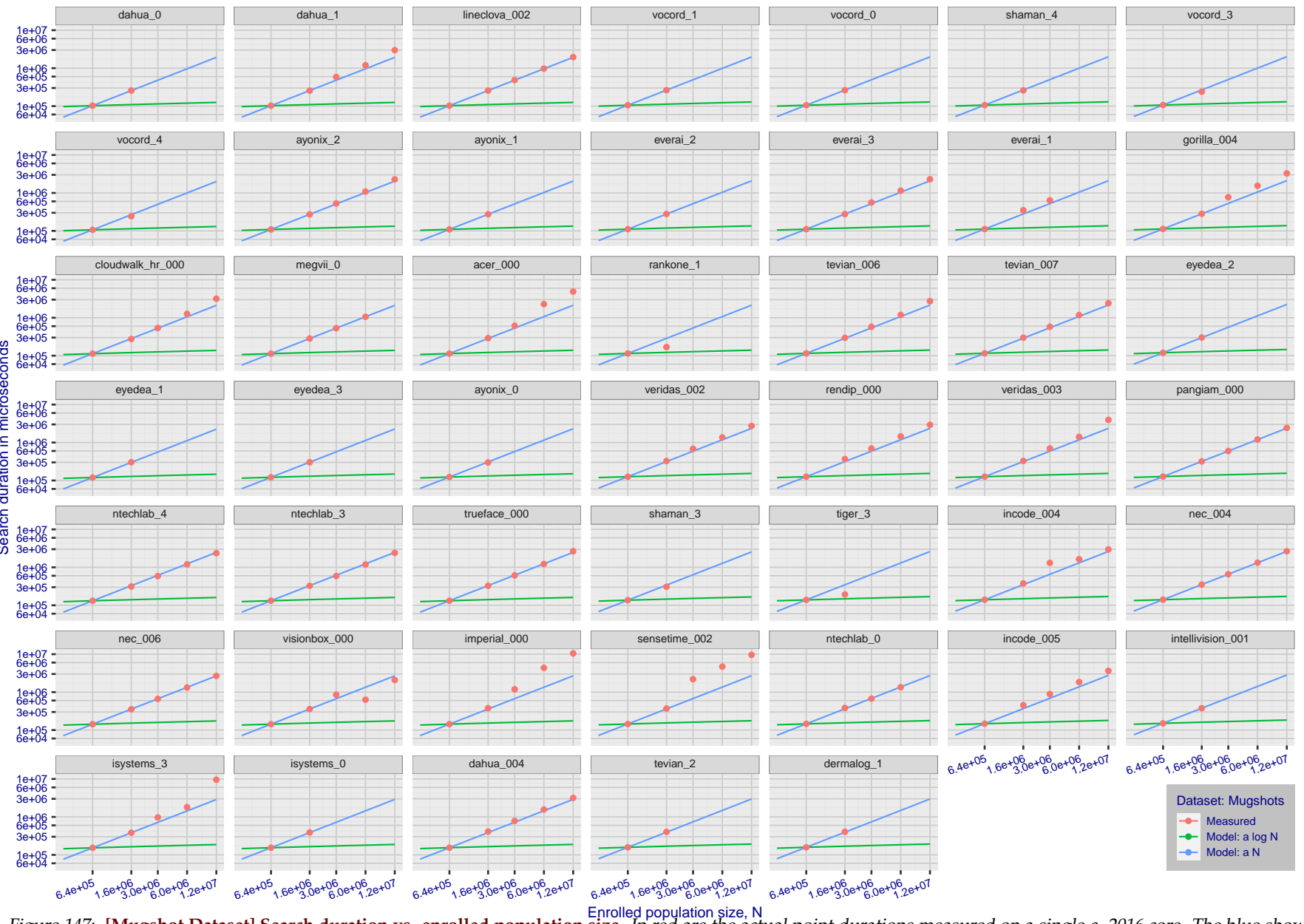
T = 0 → Investigation
T > 0 → Identification

Figure 147: [Mugshot Dataset] Search duration vs. enrolled population size. In red are the actual point durations measured on a single c. 2016 core. The blue shows linear growth from $N = 640\,000$. The green line shows logarithmic growth from that point to $N = 1\,600\,000$. Note the sublinear growth from algorithms from Camvi, Dermalog, EverAI, Innovatrics, and Visionlabs. The tiger_1 algorithm is also sublinear, but inaccurate and inoperable at $N \geq 3000000$. This capability sometimes comes at the additional expense of converting a linear gallery data structure into whatever fast-search data structure is used. Note that search times are sometimes dominated by the template generation times shown in Table 26.

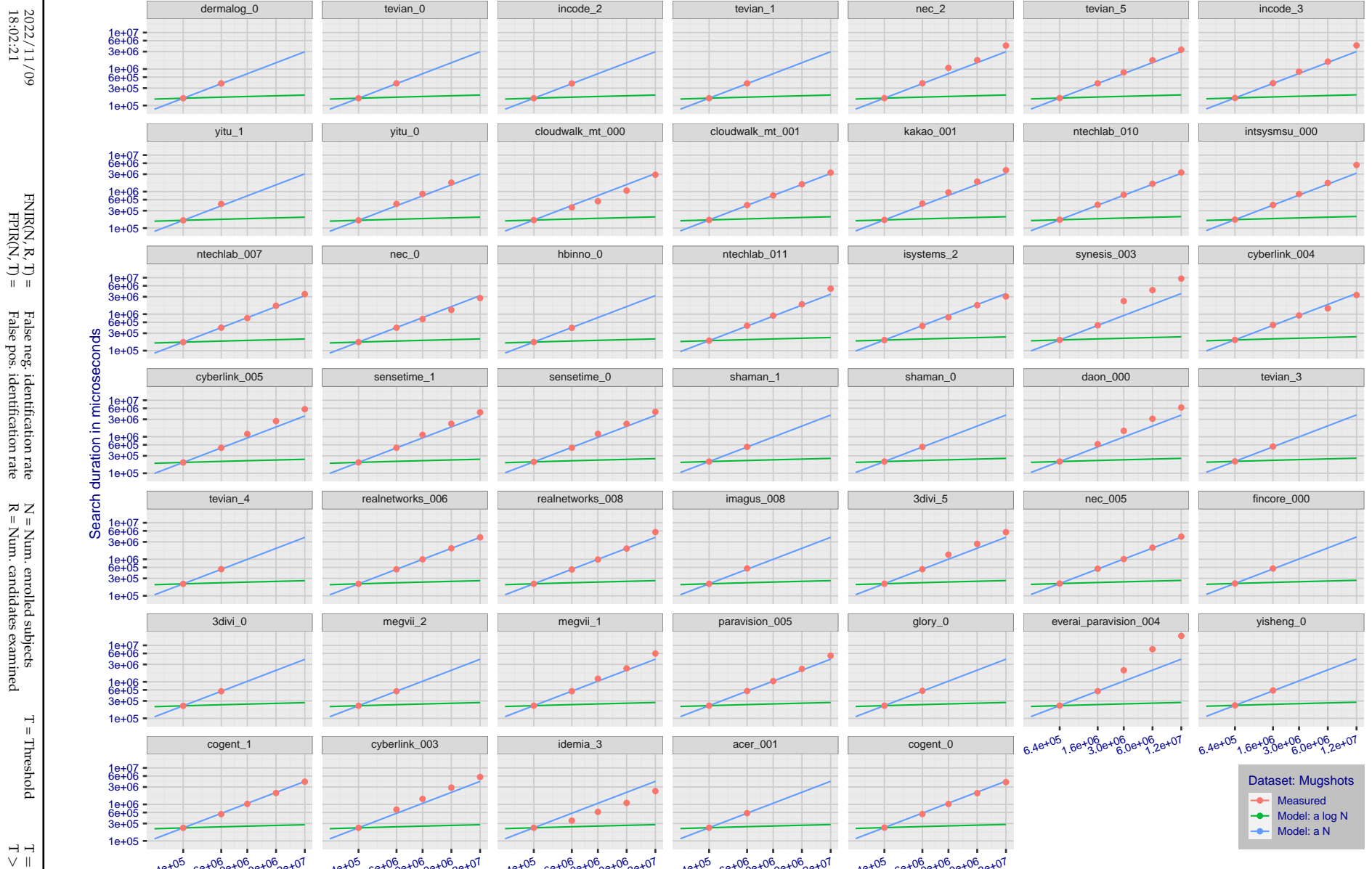


Figure 148: [Mugshot Dataset] Search duration vs. enrolled population size. In red are the actual point durations measured on a single c. 2016 core. The blue shows linear growth from $N = 640\,000$. The green line shows logarithmic growth from that point to $N = 1\,600\,000$. Note the sublinear growth from algorithms from Camvi, Dermalog, EverAI, Innovatrics, and Visionlabs. The tiger_1 algorithm is also sublinear, but inaccurate and inoperable at $N \geq 3000000$. This capability sometimes comes at the additional expense of converting a linear gallery data structure into whatever fast-search data structure is used. Note that search times are sometimes dominated by the template generation times shown in Table 26.

2022/11/09
18:02:21FNIR(N, R, T) = False neg. identification rate
FPFR(N, T) = False pos. identification rateN = Num. enrolled subjects
R = Num. candidates examined

T = Threshold

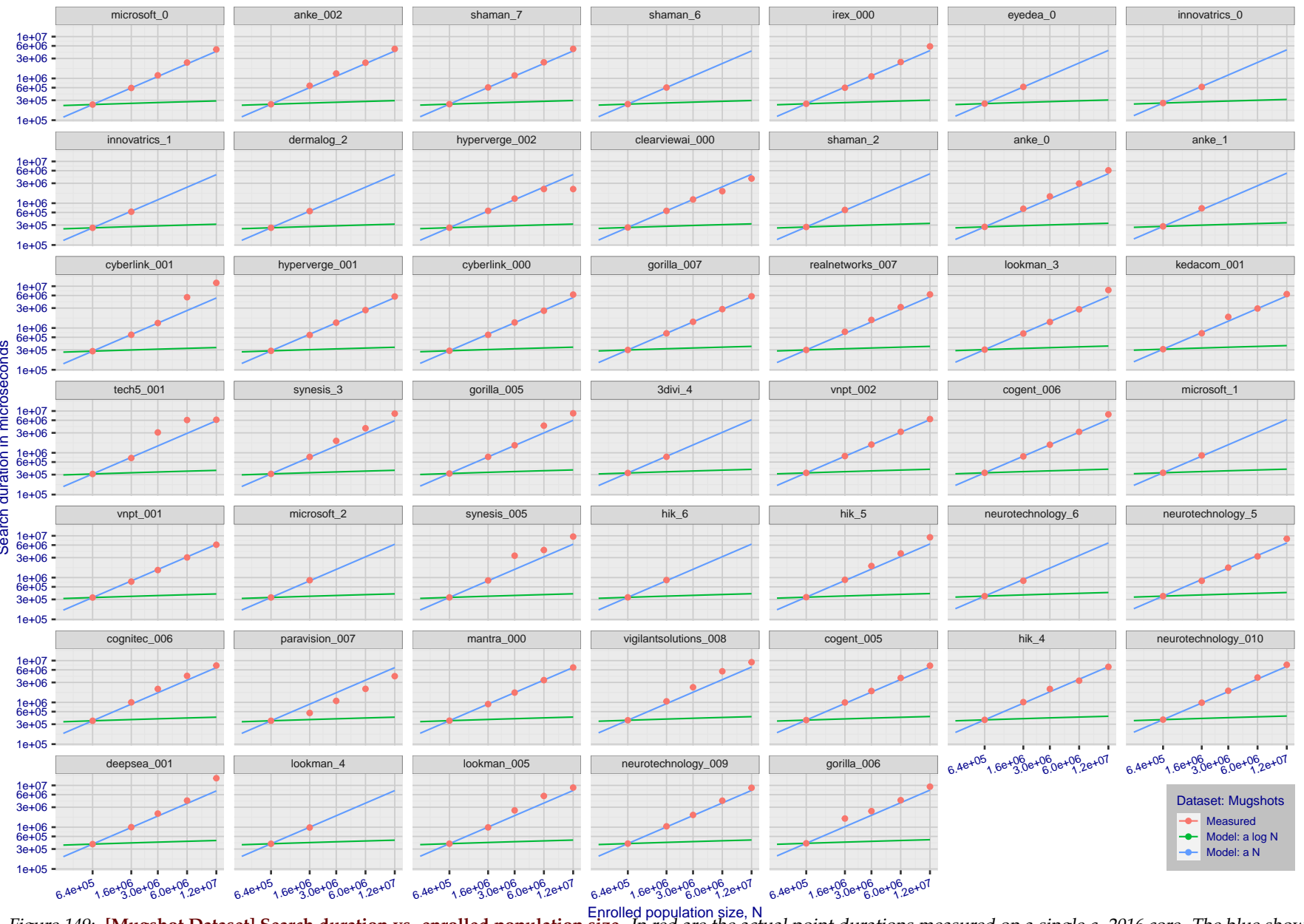
T = 0 → Investigation
T > 0 → Identification

Figure 149: [Mugshot Dataset] Search duration vs. enrolled population size. In red are the actual point durations measured on a single c. 2016 core. The blue shows linear growth from $N = 640\,000$. The green line shows logarithmic growth from that point to $N = 1\,600\,000$. Note the sublinear growth from algorithms from Camvi, Dermalog, EverAI, Innovatrics, and Visionlabs. The tiger_1 algorithm is also sublinear, but inaccurate and inoperable at $N \geq 3000000$. This capability sometimes comes at the additional expense of converting a linear gallery data structure into whatever fast-search data structure is used. Note that search times are sometimes dominated by the template generation times shown in Table 26.

2022/11/09
18:02:21FNIR(N, R, T) = False neg. identification rate
FPFR(N, T) = False pos. identification rateN = Num. enrolled subjects
R = Num. candidates examined

T = Threshold

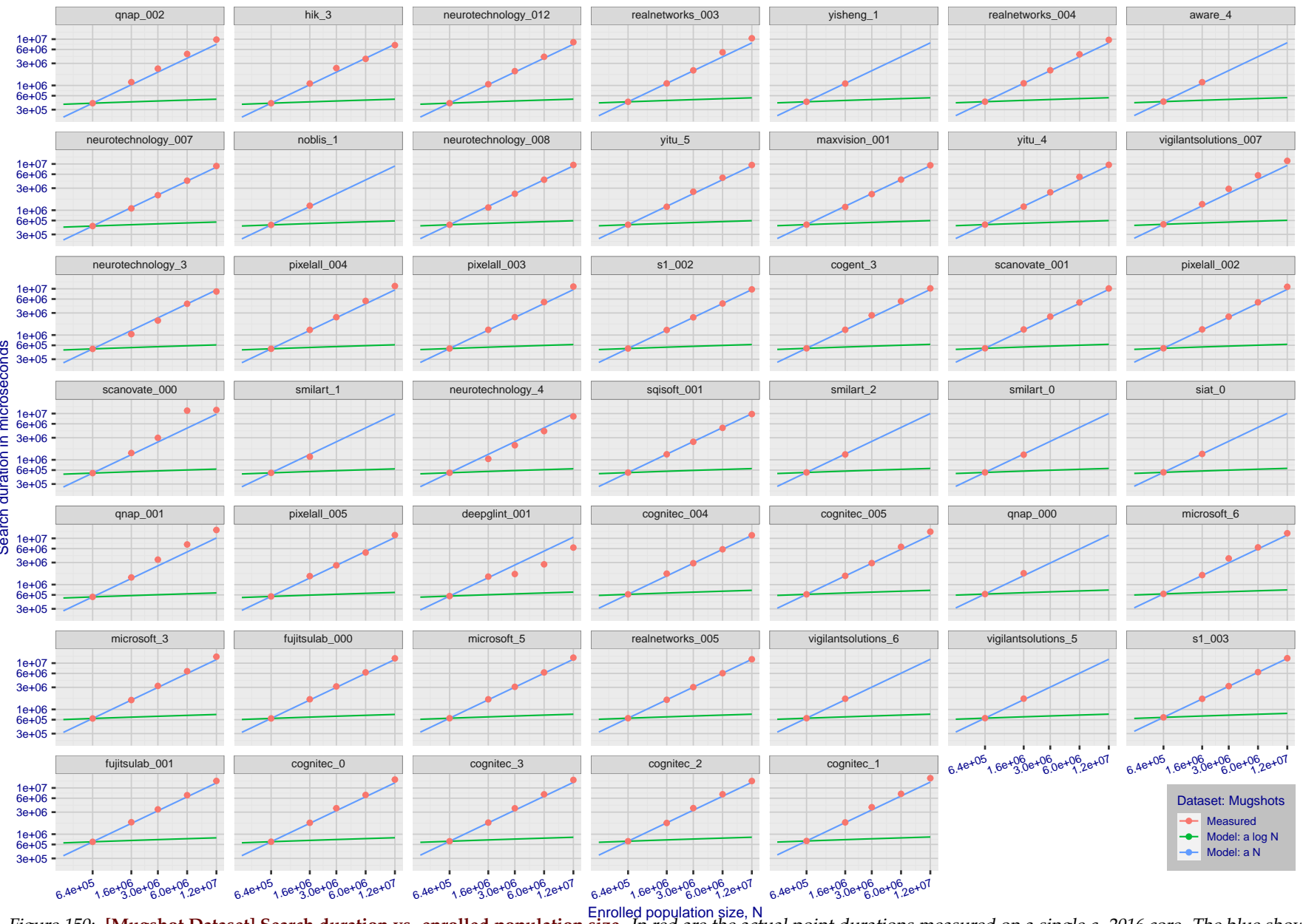
T = 0 → Investigation
 $T > 0 \rightarrow$ Identification

Figure 150: [Mugshot Dataset] Search duration vs. enrolled population size. In red are the actual point durations measured on a single c. 2016 core. The blue shows linear growth from $N = 640\,000$. The green line shows logarithmic growth from that point to $N = 1\,600\,000$. Note the sublinear growth from algorithms from Camvi, Dermalog, EverAI, Innovatronics, and Visionlabs. The tiger_1 algorithm is also sublinear, but inaccurate and inoperable at $N \geq 3000000$. This capability sometimes comes at the additional expense of converting a linear gallery data structure into whatever fast-search data structure is used. Note that search times are sometimes dominated by the template generation times shown in Table 26.

2022/11/09
18:02:21FNIR(N, R, T) = False neg. identification rate
FPFR(N, T) = False pos. identification rateN = Num. enrolled subjects
R = Num. candidates examined

T = Threshold

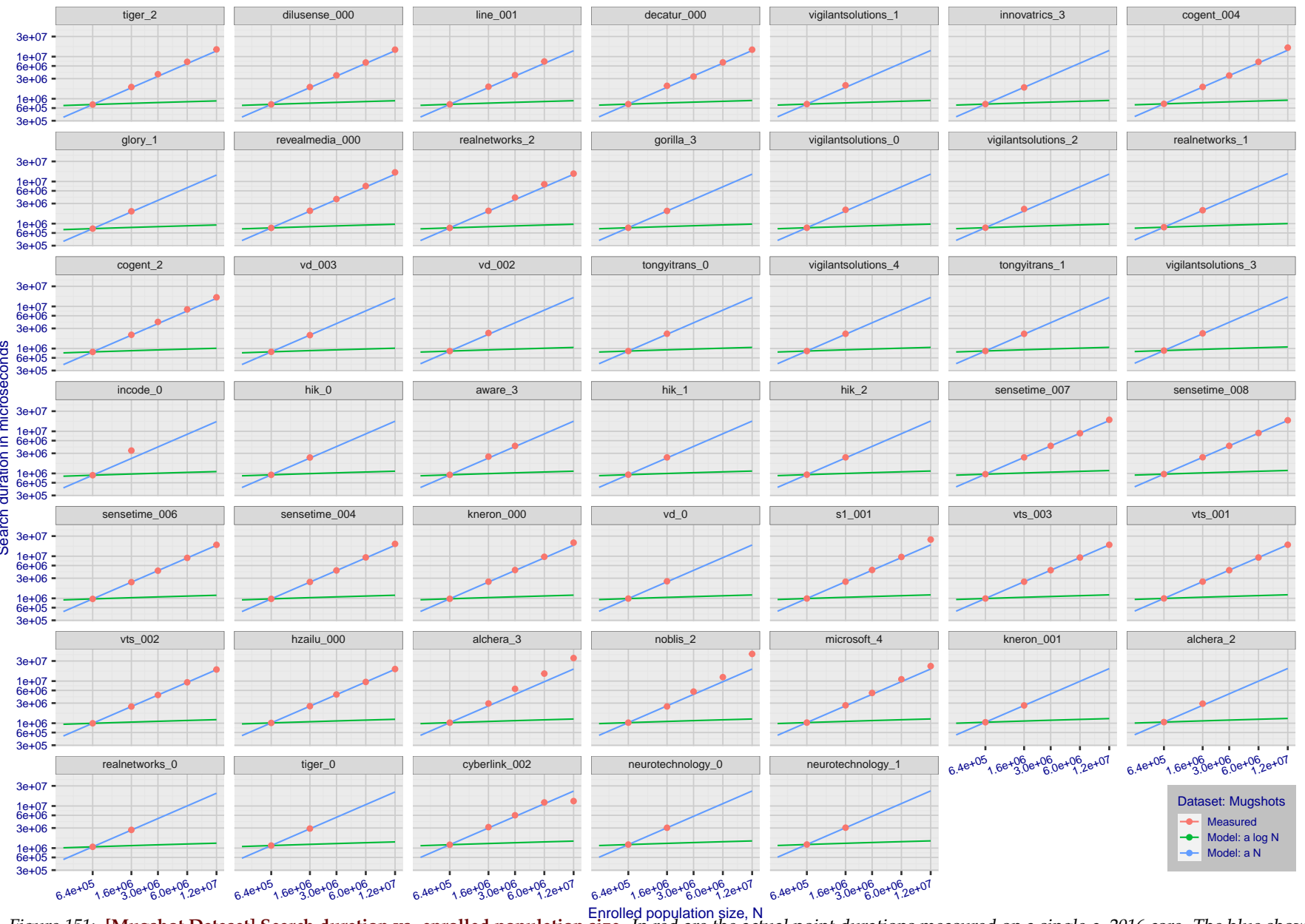
T = 0 → Investigation
T > 0 → Identification

Figure 151: [Mugshot Dataset] Search duration vs. enrolled population size. In red are the actual point durations measured on a single c. 2016 core. The blue shows linear growth from $N = 640\,000$. The green line shows logarithmic growth from that point to $N = 1\,600\,000$. Note the sublinear growth from algorithms from Camvi, Dermalog, EverAI, Innovatrics, and Visionlabs. The tiger_1 algorithm is also sublinear, but inaccurate and inoperable at $N \geq 3000000$. This capability sometimes comes at the additional expense of converting a linear gallery data structure into whatever fast-search data structure is used. Note that search times are sometimes dominated by the template generation times shown in Table 26.

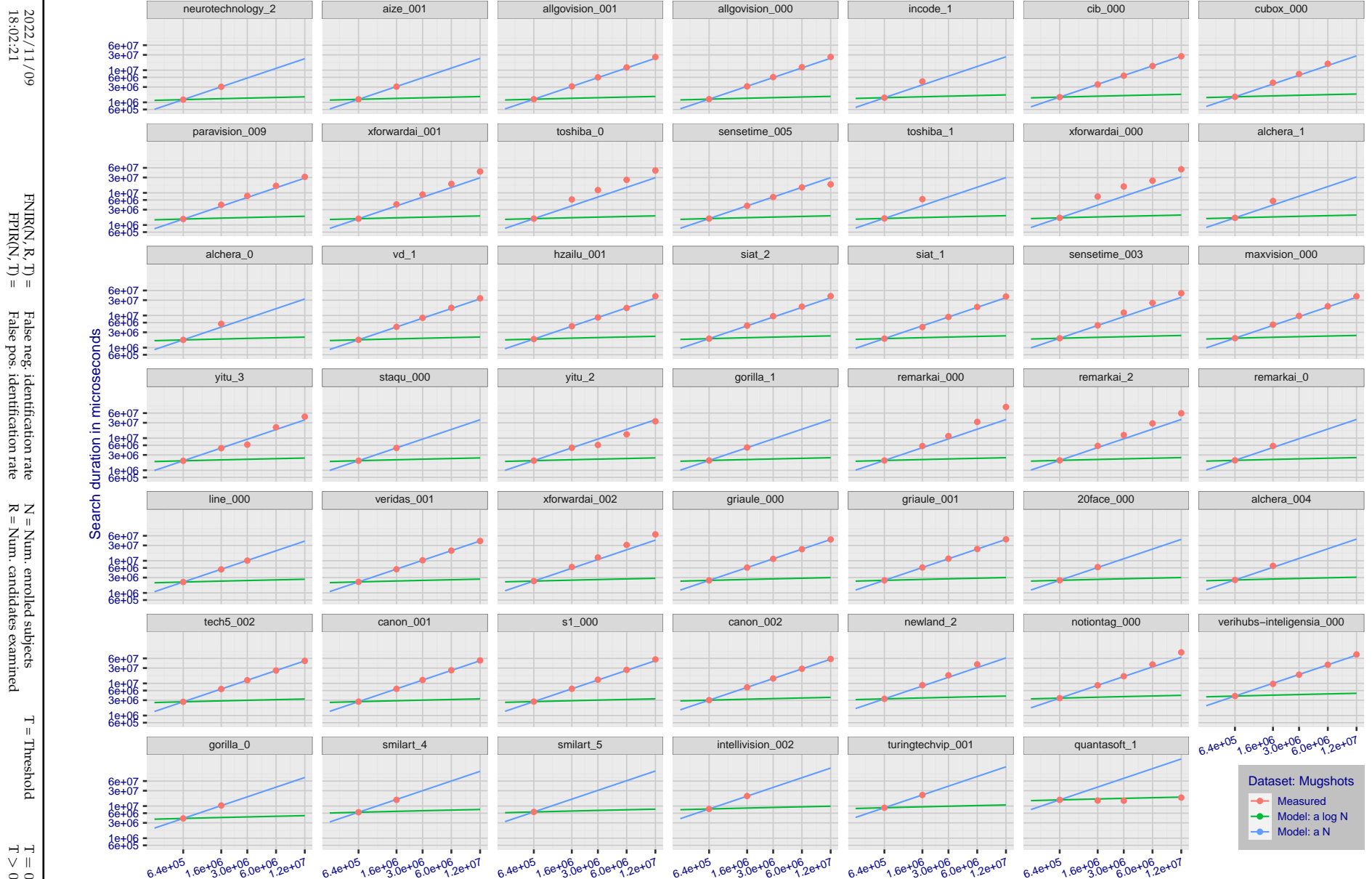


Figure 152: [Mugshot Dataset] Search duration vs. enrolled population size. In red are the actual point durations measured on a single c. 2016 core. The blue shows linear growth from $N = 640\,000$. The green line shows logarithmic growth from that point to $N = 1\,600\,000$. Note the sublinear growth from algorithms from Camvi, Dermalog, EverAI, Innovatrics, and Visionlabs. The tiger_1 algorithm is also sublinear, but inaccurate and inoperable at $N \geq 3000000$. This capability sometimes comes at the additional expense of converting a linear gallery data structure into whatever fast-search data structure is used. Note that search times are sometimes dominated by the template generation times shown in Table 26.

Appendix G Gallery Insertion Timing

2022/11/09
18:02:21FNIR(N, R, T) = False neg. identification rate
FPIR(N, T) = False pos. identification rateN = Num. enrolled subjects
R = Num. candidates examined

T = Threshold

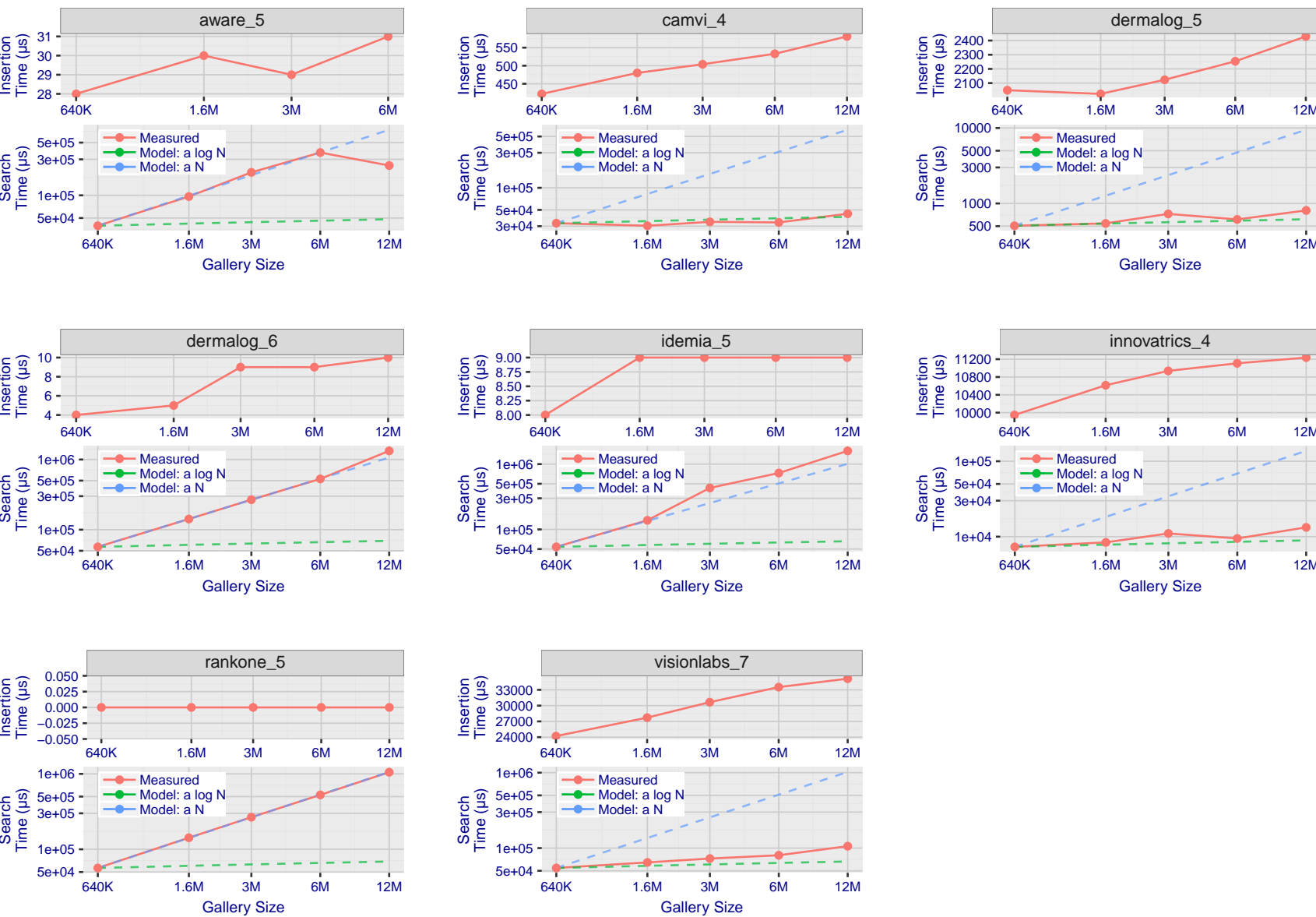
T = 0 → Investigation
T > 0 → Identification

Figure 153: [Mugshot Dataset] Gallery insertion duration vs. enrolled population size. This chart plots the time it takes to insert a single template into a finalized gallery, illustrated over increasing gallery sizes. For reference, search times on finalized galleries of corresponding sizes are plotted right underneath. Gallery insertion time plots were generated on algorithms that 1) successfully implemented gallery insertion with no errors and 2) that were run on galleries with N up to 12 000 000. Generally, only the more accurate algorithms were run on galleries with N up to 12 000 000.

2022/11/09
18:02:21FNIR(N, R, T) = False neg. identification rate
FPFR(N, T) = False pos. identification rateN = Num. enrolled subjects
R = Num. candidates examinedT = Threshold
T = 0 → Investigation

T > 0 → Identification

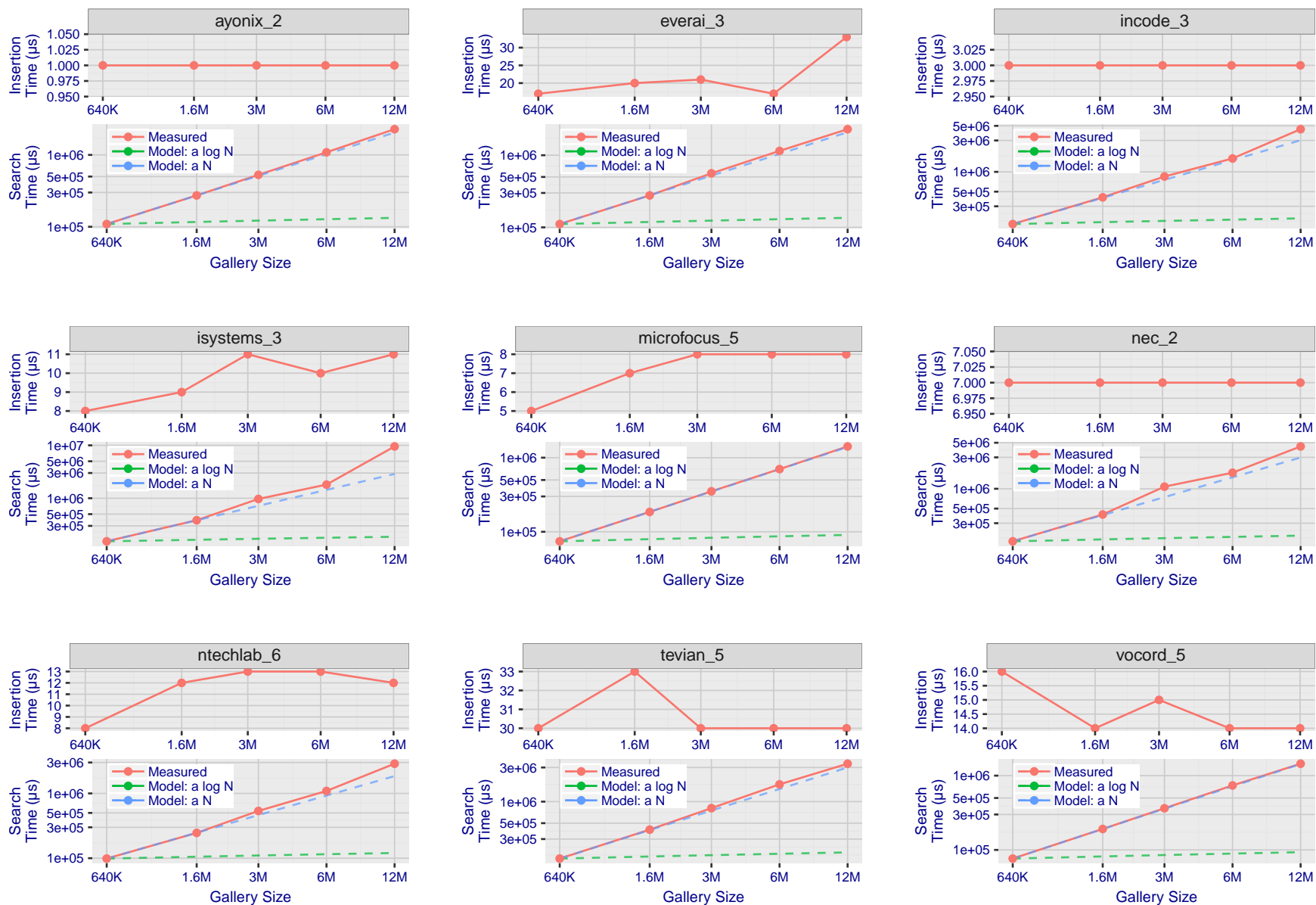


Figure 154: [Mugshot Dataset] Gallery insertion duration vs. enrolled population size. This chart plots the time it takes to insert a single template into a finalized gallery, illustrated over increasing gallery sizes. For reference, search times on finalized galleries of corresponding sizes are plotted right underneath. Gallery insertion time plots were generated on algorithms that 1) successfully implemented gallery insertion with no errors and 2) that were run on galleries with N up to 12 000 000. Generally, only the more accurate algorithms were run on galleries with N up to 12 000 000.

2022/11/09
18:02:21FNIR(N, R, T) = False neg. identification rate
FPTR(N, T) = False pos. identification rateN = Num. enrolled subjects
R = Num. candidates examined

T = Threshold

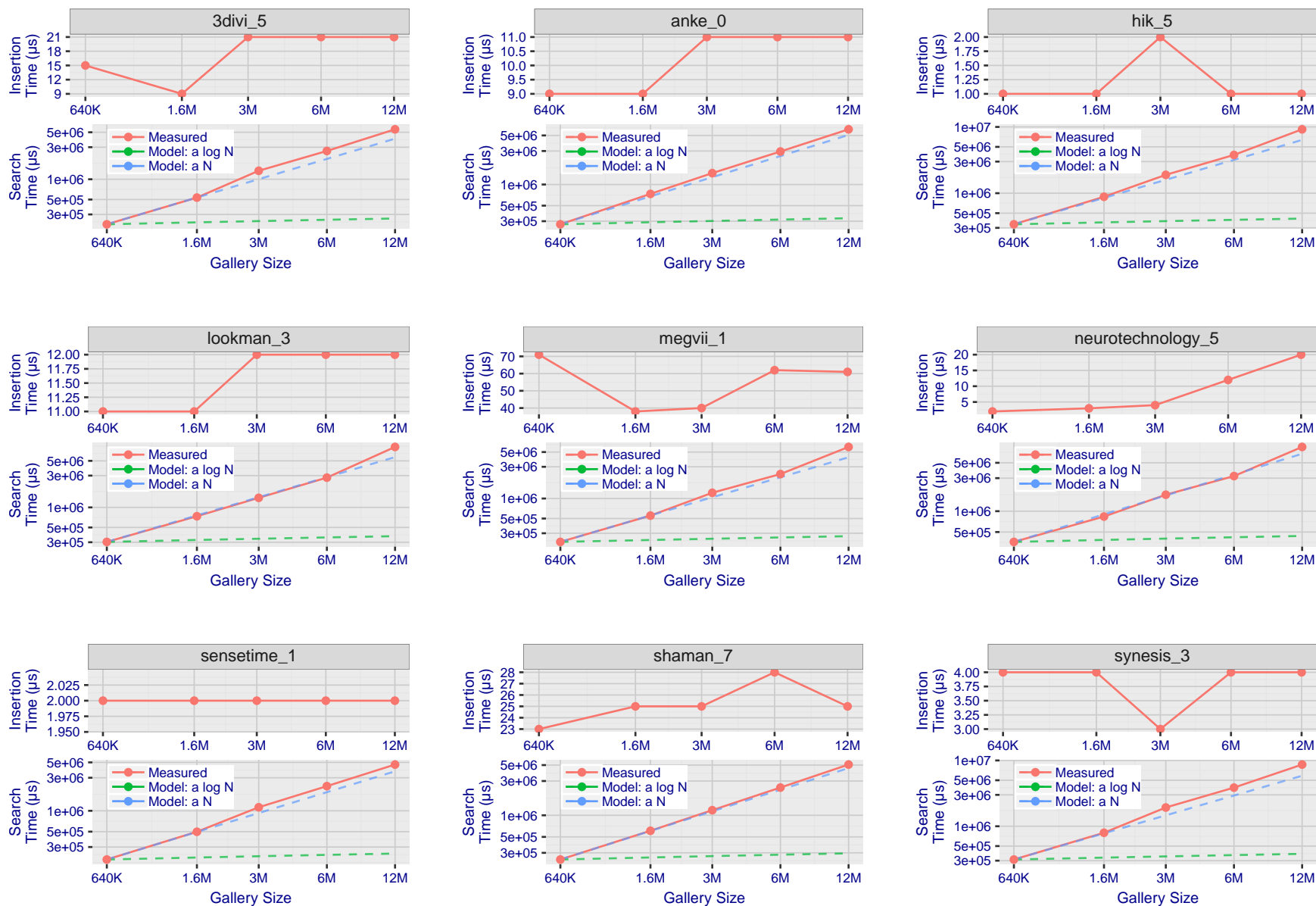
T = 0 → Investigation
 $T > 0 \rightarrow$ Identification

Figure 155: [Mugshot Dataset] Gallery insertion duration vs. enrolled population size. This chart plots the time it takes to insert a single template into a finalized gallery, illustrated over increasing gallery sizes. For reference, search times on finalized galleries of corresponding sizes are plotted right underneath. Gallery insertion time plots were generated on algorithms that 1) successfully implemented gallery insertion with no errors and 2) that were run on galleries with N up to 12 000 000. Generally, only the more accurate algorithms were run on galleries with N up to 12 000 000.

2022/11/09
18:02:21FNIR(N, R, T) = False neg. identification rate
FPTR(N, T) = False pos. identification rateN = Num. enrolled subjects
R = Num. candidates examinedT = Threshold
T = 0 → Investigation

T > 0 → Identification

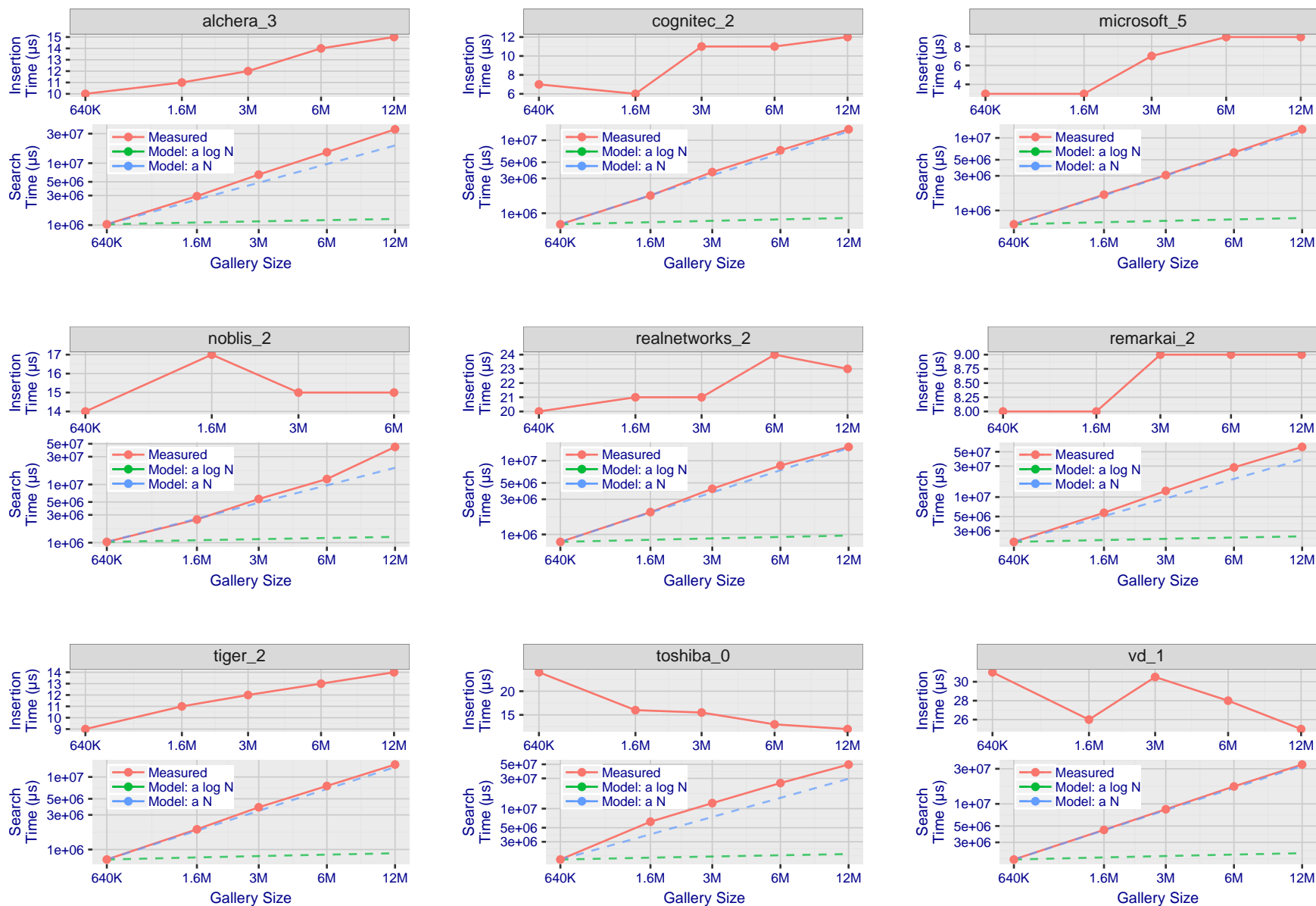


Figure 156: [Mugshot Dataset] Gallery insertion duration vs. enrolled population size. This chart plots the time it takes to insert a single template into a finalized gallery, illustrated over increasing gallery sizes. For reference, search times on finalized galleries of corresponding sizes are plotted right underneath. Gallery insertion time plots were generated on algorithms that 1) successfully implemented gallery insertion with no errors and 2) that were run on galleries with N up to 12 000 000. Generally, only the more accurate algorithms were run on galleries with N up to 12 000 000.

References

- [1] Artem Babenko and Victor Lempitsky. Efficient indexing of billion-scale datasets of deep descriptors. In *The IEEE Conference on Computer Vision and Pattern Recognition (CVPR)*, June 2016.
- [2] L. Best-Rowden and A. K. Jain. Longitudinal study of automatic face recognition. *IEEE Transactions on Pattern Analysis and Machine Intelligence*, 40(1):148–162, Jan 2018.
- [3] Blumstein, Cohen, Roth, and Visher, editors. *Random parameter stochastic models of criminal careers*. National Academy of Sciences Press, 1986.
- [4] Thomas P. Bonczar and Lauren E. Glaze. Probation and parole in the united statesm 2007, statistical tables. Technical report, Bureau of Justice Statistics, December 2008.
- [5] White D., Kemp R. I., Jenkins R., Matheson M, and Burton A. M. Passport officers' errors in face matching. *PLoS ONE*, 9(8), 2014. e103510. doi:10.1371/journal.pone.0103510.
- [6] P. Grother, G. W. Quinn, and P. J. Phillips. Evaluation of 2d still-image face recognition algorithms. NIST Interagency Report 7709, National Institute of Standards and Technology, 8 2010. <http://face.nist.gov/mbe> as MBE2010 FRVT2010.
- [7] P. J. Grother, R. J. Micheals, and P. J. Phillips. Performance metrics for the frvt 2002 evaluation. In *Proceedings of Audio and Video Based Person Authentication Conference (AVBPA)*, June 2003.
- [8] Patrick Grother and Mei Ngan. Interagency report 8009, performance of face identification algorithms. *Face Recognition Vendor Test (FRVT)*, May 2014.
- [9] Patrick Grother, George Quinn, and Mei Ngan. Face in video evaluation (five) face recognition of non-cooperative subjects. Interagency Report 8173, National Institute of Standards and Technology, March 2017. <https://doi.org/10.6028/NIST.IR.8173>.
- [10] Patrick Grother, George W. Quinn, and Mei Ngan. Face recognition vendor test - still face image and video concept, evaluation plan and api. Technical report, National Institute of Standards and Technology, 7 2013. http://biometrics.nist.gov/cs.links/face/frvt/frvt2012/NIST_FRVT2012.api_Aug15.pdf.
- [11] K. He, X. Zhang, S. Ren, and J. Sun. Deep residual learning for image recognition. In *2016 IEEE Conference on Computer Vision and Pattern Recognition (CVPR)*, pages 770–778, June 2016.
- [12] Gary B. Huang, Manu Ramesh, Tamara Berg, and Erik Learned-Miller. Labeled faces in the wild: A database for studying face recognition in unconstrained environments. Technical Report 07-49, University of Massachusetts, Amherst, October 2007.
- [13] Masato Ishii, Hitoshi Imaoka, and Atsushi Sato. Fast k-nearest neighbor search for face identification using bounds of residual score. In *2017 12th IEEE International Conference on Automatic Face & Gesture Recognition (FG 2017)*, pages 194–199, Los Alamitos, CA, USA, May 2017. IEEE Computer Society.
- [14] Jeff Johnson, Matthijs Douze, and Hervé Jégou. Billion-scale similarity search with gpus. *CoRR*, abs/1702.08734, 2017.

- [15] Ira Kemelmacher-Shlizerman, Steven M. Seitz, Daniel Miller, and Evan Brossard. The megaface benchmark: 1 million faces for recognition at scale. *CoRR*, abs/1512.00596, 2015.
- [16] Yury A. Malkov and D. A. Yashunin. Efficient and robust approximate nearest neighbor search using hierarchical navigable small world graphs. *CoRR*, abs/1603.09320, 2016.
- [17] Joyce A. Martin, Brady E. Hamilton, Michelle J.K. Osterman, Anne K. Driscoll, , and Patrick Drake. National vital statistics reports. Technical Report 8, Centers for Disease Control and Prevention, National Center for Health Statistics, National Vital Statistics System, Division of Vital Statistics, November 2018.
- [18] O. M. Parkhi, A. Vedaldi, and A. Zisserman. Deep face recognition. In *British Machine Vision Conference*, 2015.
- [19] P. Jonathon Phillips, Amy N. Yates, Ying Hu, Carina A. Hahn, Eilidh Noyes, Kelsey Jackson, Jacqueline G. Cava-zos, Géraldine Jeckeln, Rajeev Ranjan, Swami Sankaranarayanan, Jun-Cheng Chen, Carlos D. Castillo, Rama Chellappa, David White, and Alice J. O'Toole. Face recognition accuracy of forensic examiners, superrecognitioners, and face recognition algorithms. *Proceedings of the National Academy of Sciences*, 115(24):6171–6176, 2018.
- [20] Florian Schroff, Dmitry Kalenichenko, and James Philbin. Facenet: A unified embedding for face recognition and clustering. *CoRR*, abs/1503.03832, 2015.
- [21] Jeroen Smits and Christiaan Monden. Twinning across the developing world. *PLOS ONE*, 6(9):1–5, 09 2011.
- [22] Yaniv Taigman, Ming Yang, Marc'Aurelio Ranzato, and Lior Wolf. Deepface: Closing the gap to human-level performance in face verification. In *Proceedings of the 2014 IEEE Conference on Computer Vision and Pattern Recognition, CVPR '14*, pages 1701–1708, Washington, DC, USA, 2014. IEEE Computer Society.
- [23] A. Towler, R. I. Kemp, and D White. *Unfamiliar face matching systems in applied settings*. Nova Science, 2017.
- [24] Working Group 3. Ed. M. Werner. *ISO/IEC 19794-5 Information Technology - Biometric Data Interchange Formats - Part 5: Face image data*. JTC1 :: SC37, 2 edition, 2011. <http://webstore.ansi.org>.
- [25] David White, James D. Dunn, Alexandra C. Schmid, and Richard I. Kemp. Error rates in users of automatic face recognition software. *PLoS ONE*, 10:1–14, October 2015.
- [26] Bradford Wing and R. Michael McCabe. Special publication 500-271: American national standard for information systems data format for the interchange of fingerprint, facial, and other biometric information part 1. Technical report, NIST, September 2015. ANSI/NIST ITL 1-2015.
- [27] Andreas Wolf. Portrait quality - (reference facial images for mrtd). Technical report, ICAO, April 2018.
- [28] D. Yadav, N. Kohli, P. Pandey, R. Singh, M. Vatsa, and A. Noore. Effect of illicit drug abuse on face recognition. In *2016 IEEE Winter Conference on Applications of Computer Vision (WACV)*, pages 1–7, Los Alamitos, CA, USA, mar 2016. IEEE Computer Society.